frontiers | Research Topics

Biomarkers of perioperative stroke in older patients

Edited by
Li Li, Yujie Chen, Anwen Shao, Gaiqing Wang, Weifeng Yao, John Zhang and Yang Zhang

Published in
Frontiers in Aging Neuroscience

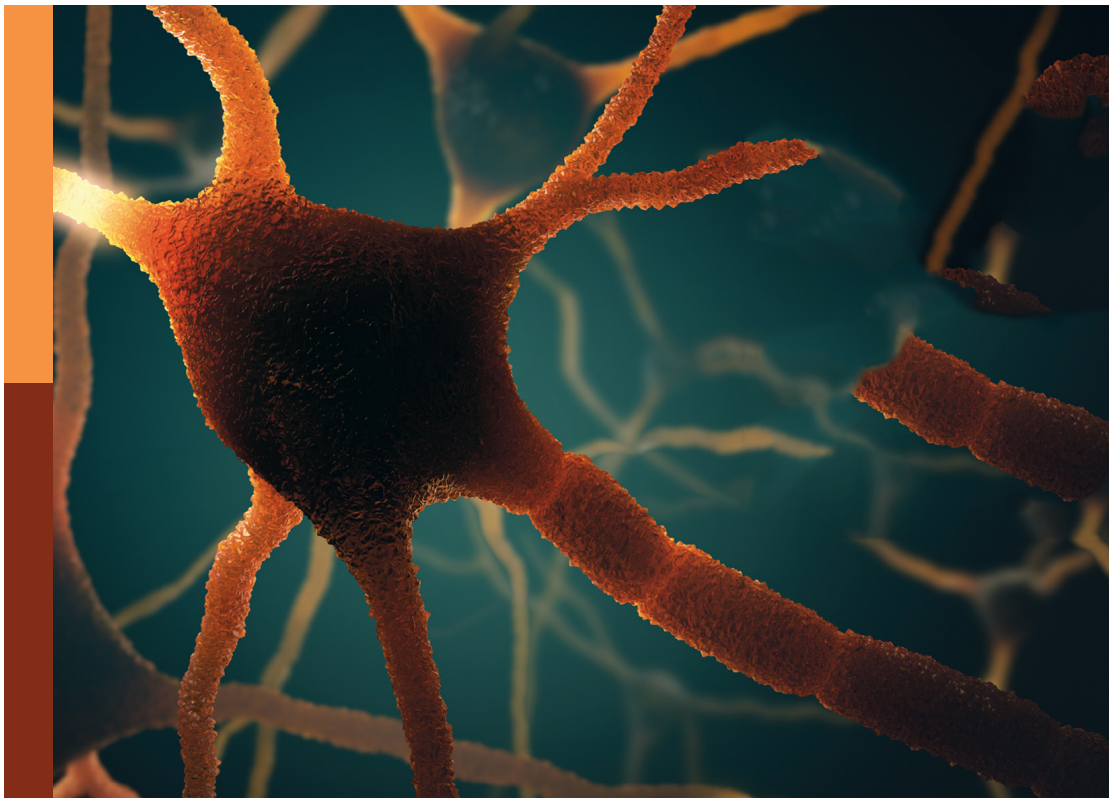

ISSN 1664-8714
ISBN 978-2-8325-2298-1
DOI 10.3389/978-2-8325-2298-1

About Frontiers

Frontiers is more than just an open access publisher of scholarly articles: it is a pioneering approach to the world of academia, radically improving the way scholarly research is managed. The grand vision of Frontiers is a world where all people have an equal opportunity to seek, share and generate knowledge. Frontiers provides immediate and permanent online open access to all its publications, but this alone is not enough to realize our grand goals.

Frontiers journal series

The Frontiers journal series is a multi-tier and interdisciplinary set of open-access, online journals, promising a paradigm shift from the current review, selection and dissemination processes in academic publishing. All Frontiers journals are driven by researchers for researchers; therefore, they constitute a service to the scholarly community. At the same time, the *Frontiers journal series* operates on a revolutionary invention, the tiered publishing system, initially addressing specific communities of scholars, and gradually climbing up to broader public understanding, thus serving the interests of the lay society, too.

Dedication to quality

Each Frontiers article is a landmark of the highest quality, thanks to genuinely collaborative interactions between authors and review editors, who include some of the world's best academicians. Research must be certified by peers before entering a stream of knowledge that may eventually reach the public - and shape society; therefore, Frontiers only applies the most rigorous and unbiased reviews. Frontiers revolutionizes research publishing by freely delivering the most outstanding research, evaluated with no bias from both the academic and social point of view. By applying the most advanced information technologies, Frontiers is catapulting scholarly publishing into a new generation.

What are Frontiers Research Topics?

Frontiers Research Topics are very popular trademarks of the *Frontiers journals series*: they are collections of at least ten articles, all centered on a particular subject. With their unique mix of varied contributions from Original Research to Review Articles, Frontiers Research Topics unify the most influential researchers, the latest key findings and historical advances in a hot research area.

Find out more on how to host your own Frontiers Research Topic or contribute to one as an author by contacting the Frontiers editorial office: frontiersin.org/about/contact

Biomarkers of perioperative stroke in older patients

Topic editors

Li Li — Capital Medical University, China
Yujie Chen — Army Medical University, China
Anwen Shao — Zhejiang University, China
Gaiqing Wang — Department of Neurology, The Third People's Hospital of Hainan Province, China
Weifeng Yao — Third Affiliated Hospital of Sun Yat-sen University, China
John Zhang — Loma Linda University, United States
Yang Zhang — Chongqing University, China

Citation

Li, L., Chen, Y., Shao, A., Wang, G., Yao, W., Zhang, J., Zhang, Y., eds. (2023). *Biomarkers of perioperative stroke in older patients*. Lausanne: Frontiers Media SA. doi: 10.3389/978-2-8325-2298-1

Table of contents

frontiers in Aging Neuroscience

REVIEW
published: 19 November 2021
doi: 10.3389/fnagi.2021.780489

Emerging Impact of Non-coding RNAs in the Pathology of Stroke

Soudeh Ghafouri-Fard[1], Zeinab Shirvani-Farsani[2], Bashdar Mahmud Hussen[3], Mohammad Taheri[4] and Noormohammad Arefian[5]**

[1] Department of Medical Genetics, School of Medicine, Shahid Beheshti University of Medical Sciences, Tehran, Iran, [2] Department of Cell and Molecular Biology, Faculty of Life Sciences and Technology, Shahid Beheshti University, Tehran, Iran, [3] Department of Pharmacognosy, College of Pharmacy, Hawler Medical University, Erbil, Iraq, [4] Institute of Human Genetics, Jena University Hospital, Jena, Germany, [5] Skull Base Research Center, Loghman Hakim Hospital, Shahid Beheshti University Hospital, Tehra, Iran

Ischemic stroke (IS) is an acute cerebral vascular event with high mortality and morbidity. Though the precise pathophysiologic routes leading to this condition are not entirely clarified, growing evidence from animal and human experiments has exhibited the impact of non-coding RNAs in the pathogenesis of IS. Various lncRNAs namely MALAT1, linc-SLC22A2, linc-OBP2B-1, linc_luo_1172, linc-DHFRL1-4, SNHG15, linc-FAM98A-3, H19, MEG3, ANRIL, MIAT, and GAS5 are possibly involved in the pathogenesis of IS. Meanwhile, lots of miRNAs contribute in this process. Differential expression of lncRNAs and miRNAs in the sera of IS patients versus unaffected individuals has endowed these transcripts the aptitude to distinguish at risk patients. Despite conduction of comprehensive assays for evaluation of the influence of lncRNAs/miRNAs in the pathogenesis of IS, therapeutic impacts of these transcripts in IS have not been clarified. In the present paper, we review the impact of lncRNAs/miRNAs in the pathobiology of IS through assessment of evidence provided by human and animal studies.

Keywords: lncRNA, miRNA, stroke, expression, biomarker

OPEN ACCESS

Edited by:
Li Li,
Capital Medical University, China

Reviewed by:
Laurent Metzinger,
University of Picardie Jules Verne, France
Atefe Abak,
Tabriz University of Medical Sciences, Iran
Ilgiz Fanilevich Gareev,
First Affiliated Hospital of Harbin Medical University, China
Hazha Hidayat,
Salahaddin University, Iraq
Reyhane Eghtedarian,
Shahid Beheshti University, Iran

***Correspondence:**
Mohammad Taheri
Mohammad_823@yahoo.com
Noormohammad Arefian
narefian@yahoo.com

Received: *21 September 2021*
Accepted: *28 October 2021*
Published: *19 November 2021*

Citation:
Ghafouri-Fard S, Shirvani-Farsani Z, Hussen BM, Taheri M and Arefian N (2021) Emerging Impact of Non-coding RNAs in the Pathology of Stroke. Front. Aging Neurosci. 13:780489. doi: 10.3389/fnagi.2021.780489

INTRODUCTION

Ischemic stroke (IS) is an acute cerebrovascular event with high mortality and morbidity. This disorder is the third most frequent cause of mortality in Western regions of the world (Feigin et al., 2015). Current treatments for IS include thrombolysis, mechanical thromboectomy and neuroprotective therapies (Liaw and Liebeskind, 2020). Although the exact pathophysiologic routes leading to this condition are not entirely clarified, growing evidence from animal and human experiments has exhibited the impact of non-coding transcripts in the pathogenesis of IS (Zhu et al., 2019). These transcripts are highly variable in the terms of size, function, genomic location and conservation, yet in a broad classification they can be categorized based on their size to small versus long non-coding RNAs (lncRNAs). Small non-coding RNAs have some subclasses among them are microRNAs (miRNAs). Both lncRNAs and miRNAs have regulatory impacts on gene expression but via different routes. Being firstly discovered in 1993 in *C. elegans* (Lee et al., 1993),

Abbreviations: AF, atrial fibrillation; AUC, area under curve; ceRNAs, competing endogenous RNAs; GO, gene ontology; HS, hemorrhagic stroke; hs-CRP, high-sensitivity C-reactive protein; IS, Ischemic stroke; LAA, large-artery atherosclerosis; lncRNAs, long non-coding RNAs; MCAO, middle cerebral artery occlusion; miRNAs, microRNAs; NIHSS, NIH Stroke Scale; PBMCs, peripheral blood mononuclear cells; ROC, receiver operating characteristic; TIA, transient ischemic attack.

miRNAs comprise an ever-growing type of non-coding RNAs that target specific sequences in the 3′ untranslated regions of genes, then decreasing their expression via mRNA degradation or translation blocking (O'Brien et al., 2018). These transcripts are about 22 nucleotides in length. They can hypothetically target almost any gene in the human genome. However, the extent of miRNA response elements complementarity defines their route of action, i.e., AGO2-dependent cleavage of target transcript or RISC-associated translational suppression (Jo et al., 2015). Besides, a number of miRNAs might influence gene expression at transcriptional and post-transcriptional stages within the nucleus (O'Brien et al., 2018). However, this mode of action has not been fully discovered. The dynamic nature of miRNA-associated gene regulation potentiates them as tools for regulation of gene expression in a cell type/situation-specific mode since several events such as alternative splicing events, polyadenylation state and the presence of cell type-specific RNA binding proteins affect miRNA response elements (O'Brien et al., 2018). LncRNAs are another group of transcripts with fundamental roles in the regulation of gene transcription via several modes including acting as signal, decoy molecules, scaffolds, guide and enhancer transcripts. The chief mode action of lncRNAs is their role in the regulation of transcription in reaction to numerous stimuli through acting as molecular signals (Fang and Fullwood, 2016). Although they generally do not have open reading frame, many of them have similar characteristics with protein-coding genes among them are the presence of 5′ cap, poly A tail and alternative splicing events (Cheng et al., 2005; Derrien et al., 2012). Through participating in chromatin configuration alteration, interaction with chromatin structures, acting as competing endogenous RNAs (ceRNAs) or natural antisense lncRNAs, lncRNAs contribute in the pathogenesis of human disorders (Fang and Fullwood, 2016). **Figure 1** depicts the role of a number of non-coding RNAs in the pathobiology of IS through different signaling pathways particularly PI3K/AKT and NF-κ β .

HUMAN STUDIES

Long Non-coding RNAs and Ischemic Stroke

Assessment of expression of lncRNAs has been the focus of numerous studies conducted in human subjects. For instance, a high throughput study has been performed on blood specimens of patients with IS and controls who have been matched with cases in terms of vascular risk factors. The study has revealed differential expression of approximately 300 lncRNAs between IS group and male controls, while 97 lncRNAs have been differentially expressed between IS group and female controls. Notably, some of differentially expressed lncRNAs have been shown to reside in genomic regions formerly recognized as IS risk loci namely lipoprotein, lipoprotein(a)-like 2, ABO blood group, prostaglandin 12 synthase, and α-adducins (Dykstra-Aiello et al., 2016). Another study has reported distinct lncRNAs signatures in peripheral blood mononuclear cells (PBMCs) among patients with IS, transient ischemic attack (TIA) and healthy subjects. Notably, expressions of linc-DHFRL1-4, SNHG15, and linc-FAM98A-3 have been substantially increased in IS patients versus healthy controls and TIA patients. Expression of linc-FAM98A-3 has been returned to normal level by day 7, whereas SNHG15 levels have been continued to be high during the follow-up period, demonstrating the capability of lncRNAs to observe IS dynamics (Deng et al., 2018). Another microarray-based assay has reported up-regulation of 560 and down-regulation of 690 lncRNAs in IS patients versus controls among them have been lncRNAs ENST00000568297, ENST00000568243, and NR_046084. Dysregulated lncRNAs have been predicted to partake in IS pathology by modulating central miRNAs, mRNAs, or IS-associated pathways (Guo et al., 2018). Assessment of lncRNA signature at two time points after IS has revealed differential expression of 3,009 and 2,034 lncRNAs 24 h and 7 days after IS, respectively. These results have shown the impact of IS on lncRNA signature at both the acute and subacute phases. Notably, expression of lncRNAs in the processing and presentation processes of antigens have been increased at 24 h and returned to basal amounts on day 7 following IS. Besides, expressions of inflammatory mediator regulation of TRP channels and GABAergic synapses have been decreased on day 7 following IS (Zhu et al., 2018). Levels of H19 in the circulation of patients with IS have been positively correlated with the National Institute of Health Stroke Scale Scores of the patients in in three time points following stroke attack. Mechanistically, H19 silencing could reduce expression of neurogenesis related proteins. In addition, H19 precludes the development of neurogenesis after IS via p53/Notch1 pathway (Wang et al., 2019a). Another experiment has reported association between H19 and Acute Stroke Treatment (TOAST) subclasses of atherosclerotic patients. Forced over-expression of H19 has enhanced ACP5 expression, increased cell proliferation and blocked cell apoptosis. Up-regulation of H19 has increased the plaque size in the animal model, thus H19 participates in the atherosclerotic processes and surges the risk of IS through increasing ACP5 levels (Huang et al., 2019). RMST is another up-regulated lncRNA in the plasma specimens of IS patients (Hou and Cheng, 2018). A previous study in Chinese Han population has shown over-expression of ANRIL in IS patients parallel with down-regulation of CDKN2A. The rs2383207 and rs1333049 SNPs have been associated with risk of IS in male subjects (Yang et al., 2018). Another study has reported higher levels of ANRIL in patients with the atrial fibrillation (AF) and ischemic stroke compared with AF patients without IS. Serum levels of ANRIL have been correlated with the NIHSS and the mRS scores (Zeng and Jin, 2020). **Table 1** gives a summary of human studies reporting elevation of lncRNAs in IS.

Contrary to two mentioned studies in the previous section, Feng et al. have demonstrated decreased levels of ANRIL in plasma specimens of patients with acute IS patients versus controls (Feng et al., 2019). ZFAS1 is another down-regulated lncRNA in IS patients. Moreover, expression of ZFAS1 in patients with large-artery atherosclerosis (LAA) stroke has been lower compared with those with non-LAA stroke and controls. In addition, ZFAS1 expression has been lower in the small vessel occlusion group compared with cardioembolism

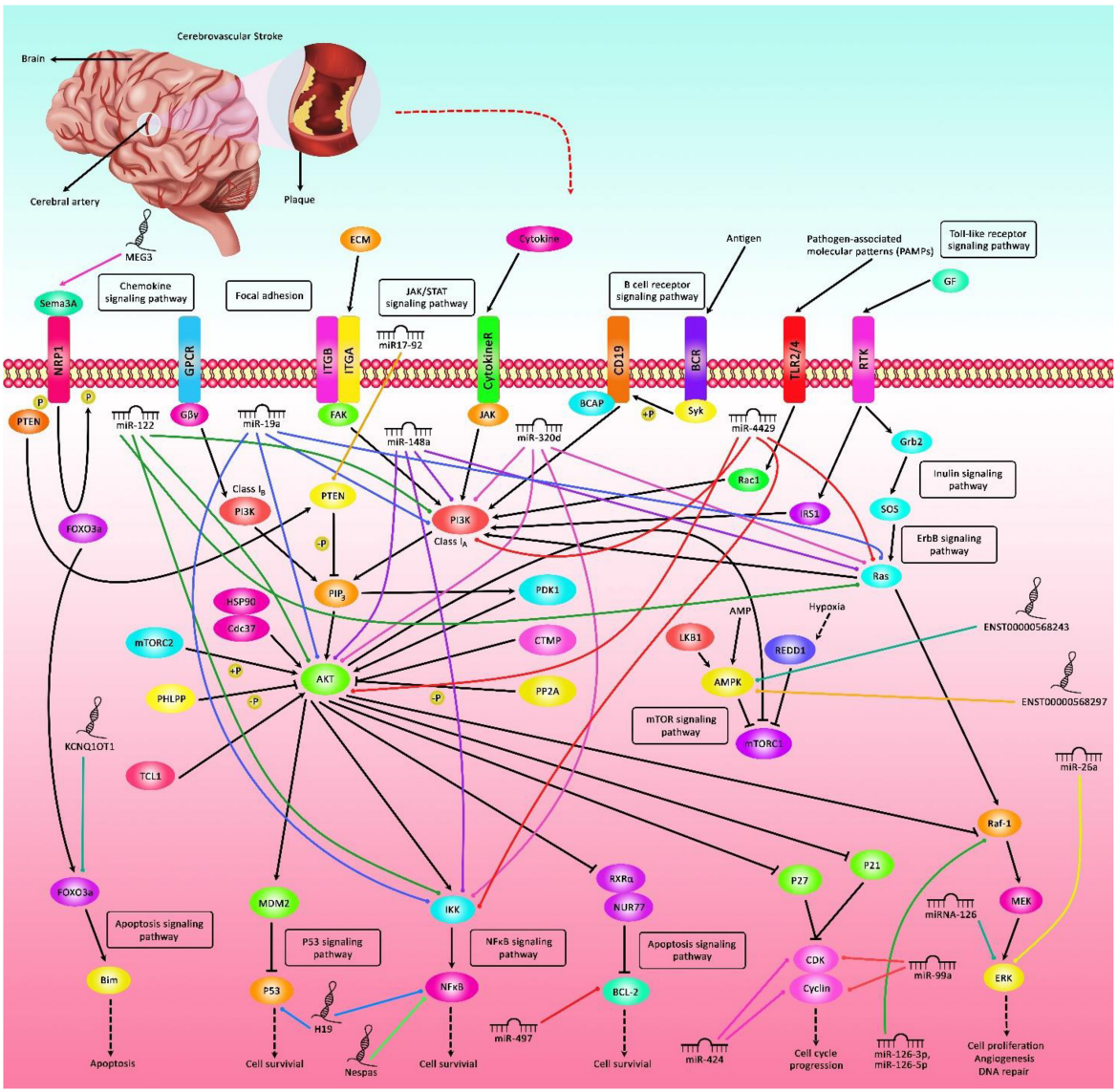

FIGURE 1 | A schematic representation of the interaction between non-coding RNAs and various signaling cascades in ischemic stroke (IS). Differential expression of lncRNAs as well as miRNAs could have an important role in the pathogenesis of IS. Various miRNAs such as miR-19a, miR-122, miR-148a, miR-320d, and miR-4429 via targeting Akt, PI3K, Ras, and IKK could modulate expression of genes leukocytes, thus affecting the course of IS. In addition, miR-497 by regulating the expression levels of Bcl-2 and Bcl-w could induce ischemic neuronal death. Additionally, lncRNA H19 via directly targeting P53 could suppress neurogenesis following IS through p53/Notch1 axis. Furthermore, MEG3 could promote cell survival and reduce cell apoptosis via modulating the expression of Sema3A. Besides, KCNQ1OT1 through modulating the expression of FOXO3 could enhance brain injury and induce autophagy in IS.

(Wang et al., 2019b). FLJ23867, H3F3AP6, TNPO1P1 are also among lncRNAs which are down-regulated in IS PBMCs compared with control PBMCs (Zhu et al., 2019). An lncRNA profiling using RNA-seq method and subsequent KEGG pathway and gene ontology (GO) enrichment assays have shown down-regulation of RPS6KA2-AS1 and lnc-CALM1-7 in exosomes retrieved from sera of patients with acute minor IS (Xu et al., 2020). **Table 2** gives a summary of human studies that displayed under-expression of lncRNAs in IS.

ANRIL low-expression has been determined as a marker of better recurrence-free survival in of AF patients with IS. Based on the outcomes of Cox regression model, serum levels of ANRIL, NIH Stroke Scale (NIHSS) score, infarct volume, and smoking have been the risk factors for AF with IS (Zeng and Jin, 2020). Another study has reported that down-regulation of ANRIL in acute IS can differentiate these patients from healthy subjects with area under curve (AUC) of 0.759. Besides, expression levels of this lncRNA has been negatively correlated with NIHSS score and high-sensitivity C-reactive protein (hs-CRP), TNF-α and IL-6 concentrations, while being positively correlated with IL-10 concentrations (Feng et al., 2019). Down-regulation of ZFAS1 could predict risk of LAA strokes. Based on the results of receiver

TABLE 1 | Human studies showing elevation of lncRNAs in IS.

lncRNAs	The specimen types	Numbers of clinical specimens	Cell models	Targets/ Regulators	Signaling pathways	Function	References
ANRIL	Blood	71 IS patients and 71 normal controls.	–	CDKN2A	–	ANRIL has a role in pathology of IS.	Yang et al., 2018
ANRIL	Serum	132 AF patients with IS and 254 AF without IS	–	–	–	Serum ANRIL is a marker in AF with IS.	Zeng and Jin, 2020
GAS5	Blood	509 IS patients and 668 healthy controls	–	–	–	GAS5 overexpression is associated with increased IS risk.	Zheng et al., 2018
H19		85 IS patients and 85 healthy controls	VSMC and HUVECs	ACP5	–	H19 has enhanced ACP5 expression, increased cell proliferation and blocked cell apoptosis.	Huang et al., 2019
H19	plasma	40 patients with acute ischemic stroke and 25 controls	–	p53	p53/Notch1 pathway	H19 represses neurogenesis following IS via p53/Notch1 axis.	Wang et al., 2019a
H19	Plasma, neutrophils, and lymphocytes	36 patients with anterior circulation ischemia, and 25 normal subjects	BV2 cells	HDAC1	–	H19 induces neuroinflammatory responses.	Wang et al., 2017
KCNQ1OT1	Blood	42 IS patients and 40 healthy controls	N2a	FOXO3	miR−200a/ FOXO3/ ATG7 pathway	KCNQ1OT1 expression enhanced brain injury and induced autophagy in IS.	Wang et al., 2019a
linc-SLC22A2, linc-OBP2B-1, linc_luo_1172	Blood	133 IS patients and 133 controls	–	–	–	–	Dykstra-Aiello et al., 2016
linc-DHFRL1-4, SNHG15 and linc-FAM98A-3	Blood	206 IS patients, 55 TIA patients and 179 controls	–	–	–	–	Deng et al., 2018
lncRNA-ENST00000568297, lncRNA-ENST00000568243, NR_046084	Blood	50 IS patients and 50 controls	–	BCG5, FOXJ3, MAP3K5	PI3K-Akt, p53 pathway, AMPK pathway	LncRNA-ENST00000568297 and lncRNA-ENST00000568243 Are possible diagnostic biomarkers for IS.	Guo et al., 2018
lnc-CRKL-2, lnc-NTRK3-4	serum	100 AMS patients and 100 healthy controls	–	–	–	These new lncRNAs are markers for the detection of AMS.	Xu et al., 2020
MALAT1	Serum	40 CIS patients and 40 healthy controls	HBMECs	VEGFA	miR-205-5p/VEGFA Pathway	MALAT1 preserves angiogenic properties of HBMECs under OGD/R circumstances.	Gao et al., 2020
MEG3	PBMCs	20 IS patients and 20 controls.	mouse brain neuroma cell line, N2a	miR-424-5p, Sema3A	MAPK	MEG3 enhances cell survival and decreased cell apoptosis.	Xiang et al., 2020
MIAT	Blood	189 IS patients and 189 healthy controls	–	–	–	MIAT is a biomarker for discriminating IS patients from healthy persons.	Zhu et al., 2018
RMST	plasma	10 AIS patients and 10 controls	hippocampal cells	–	–	RMST induces ischemic brain injury and disrupts neurological function.	Hou and Cheng, 2018
SCARNA10, TERC, LINC01481	Blood	10 IS and 5 controls	–	–	–	These LncRNAs play an important role in peripheral immune system changes after IS.	Zhu et al., 2019

TABLE 2 | Summary of clinical investigations reporting under-expression of lncRNAs in IS.

lncRNAs	The specimen types	Numbers of clinical specimens	Function	References
ANRIL	Blood	126 AIS patients and 125 controls	The reduced expression of ANRIL was related with higher risk of IS, higher disease severity and high inflammatory responses in acute IS patients.	Feng et al., 2019
NR_036641, ENST00000079667, ENST00000507442	Blood	133 IS patients and 133 controls	–	Dykstra-Aiello et al., 2016
ZFAS1		176 IS patients and 111 controls	ZFAS1 had an appropriate diagnostic value for large-artery atherosclerosis stroke	Wang et al., 2019b
FLJ23867, H3F3AP6, TNPO1P1	Blood	10 ischemic stroke and 5 controls	These LncRNAs play an important role in peripheral immune system alterations after IS.	Zhu et al., 2019
RPS6KA2-AS1, lnc-CALM1-7	serum	100 AMS patients and 100 healthy controls	These new lncRNAs are biomarkers AMS.	Xu et al., 2020

operating characteristic curve, ZFAS1 has 89.39% sensitivity in distinguishing LAA stroke patients from controls (Wang et al., 2019b). Another biomarker discovery study in PBMCs of IS patients has demonstrated AUC values of 0.73, 0.74, and 0.69 for ENST00000568297, ENST00000568243 and NR_046084, respectively (Deng et al., 2018). Moreover, MIAT levels in IS patients have been remarkably increased in correlation with NIHSS scores, mRS, hs-CRP and infarct size. Based on the results of ROC (receiver operating characteristic) curves, MIAT has been suggested as a possible marker for distinguishing IS patients from the healthy subjects with AUC value of 0.842. Moreover, patients with over-expression of MIAT had a comparatively poor prognosis. Multivariate analysis has shown the potential of MIAT as an independent prognostic biomarker of functional outcome and mortality of IS (Zhu et al., 2018). **Table 3** gives a brief review of investigations that reported diagnostic/prognostic role of lncRNAs in IS.

MicroRNAs and Stroke

Expression of miR-205-5p has been surged in the serum specimens of CIS patients and human brain microvascular endothelial cells under oxygen glucose deprivation/re-oxygenation. Besides, this condition has interfered with the tube formation of human brain microvascular endothelial cells. miR-205-5p knock-down has enhanced proliferation and angiogenic capacity of endothelial cells to resist oxygen glucose deprivation/re-oxygenation injury (Gao et al., 2020). The relationship between upper limb recovery after IS and miRNA signature has been assessed by another group. Authors have discovered lower levels of miR-371-3p, miR-524, miR-520g, miR-1255A, miR-453, and miR-583, while upper levels of miR-941, miR-449b, and miR-581 in good recover group compared with poor recovery group. These miRNAs have been shown to congregate on pathways related with axon guidance, developmental processes and carcinogenesis (Edwardson et al., 2018b). Expression of let-7e-5p has also been shown to be elevated in IS patients compared with control subjects. Over-expression of let-7e-5p has been associated with elevated probability of IS. This miRNA has been suggested to influence expression of four genes enriched in the MAPK pathway including CASP3 and NLK (Huang et al., 2016). miRNA levels might also distinguish IS patients from those with hemorrhagic stroke (HS). Leung et al. have demonstrated higher median plasma levels of miR-124-3p in acute phase of HS patients compared with similar phase of IS, while miR-16 had the opposite trend. Both miRNAs have been suggested as diagnostic markers for discrimination of HS from IS (Leung et al., 2014). A high throughput miRNA profiling in IS has reported differential expression of 115 miRNAs between IS cases and healthy controls. These transcripts have been linked with axon guidance, glioma, MAPK, mTOR and Erb-B signaling pathways. miR-32-3p, miR-106-5p, and miR-532-5p have been the first ranked ones (Li et al., 2015). **Table 4** provides the summary of researches which reported elevation of miRNAs in IS.

Blood amounts of miR-30a and miR-126 have been substantially decreased in all assessed patients with IS until 24 weeks. Circulating let-7b has been decreased in patients

TABLE 3 | Diagnostic/prognostic role of lncRNAs in stroke.

Samples	Area under curve	Sensitivity	Specificity	Kaplan-Meier analysis	Univariate cox regression	Multivariate cox regression	References
Blood specimens from 126 AIS patients and 125 controls	0.759 for ANRIL	72.2% for ANRIL	71.2% for ANRIL	–	–	–	Feng et al., 2019
Blood specimens from 206 Ischemic stroke patients in the acute phase, 55 transient ischemic attack patients and 179 healthy controls	0.711 for linc-DHFRL1-4, 0.756 for SNHG15, 0.659 for linc-FAM98A-3	0.687 for linc-DHFRL1-4, 0.594 for SNHG15, 0.594 for linc-FAM98A-3	0.719 for linc-DHFRL1-4, 0.844 for SNHG15, 0.688 for linc-FAM98A-3	–	–	–	Deng et al., 2018
Blood specimens from 50 patients with IS and 50 controls	0.733 for ENST00000568297, 0.743 for ENST00000568243, 0.690 for NR_046084	64.8% for ENST00000568297, 70.5% for ENST00000568243, 61.5% for NR_046084	63.6% for ENST00000568297, 69.5% for ENST00000568243, 69.2% for NR_046084	–	–	–	Guo et al., 2018
176 IS patients and 111 controls	0.727 for ZFAS1	89.39 for ZFAS1	48.65 for ZFAS1	–	–	ZFAS1 low expression was associated with risk of LAA strokes.	Wang et al., 2019b
Blood specimens from 71 IS patients and 71 normal controls.	0.642 for ANRIL	0.663 for ANRIL	0.538 for ANRIL	–	–	–	Yang et al., 2018
Blood specimens from 189 IS patients and 189 healthy controls	0.842 for MIAT	74.1% for MIAT	80.4% for MIAT	Patients with over-expression of MIAT had a higher mortality compared with the low-MIAT patients. High MIAT was associated with poor prognosis.	Elevated MIAT Has been associated with IS.	MIAT was an independent prognostic indicator of functional consequences and mortality.	Zhu et al., 2018
Serum specimens from 132 AF patients with IS and 254 AF without IS	0.826 for ANRIL	76.6% for ANRIL	81.4% for ANRIL	Patients with lower lncRNA ANRIL expression had higher relapse-free survival compared with the high−expression group.	Serum ANRIL expression, NIHSS score, infarct size, and smoking were the risk factors for AF with IS.	Serum ANRIL expression and smoking were independent risk factors for AF with IS.	Zeng and Jin, 2020

TABLE 4 | Summary of human studies reporting elevation of miRNAs in IS.

microRNA	The specimen types	Numbers of clinical specimens	Cells	Targets/ Regulators	Signaling pathways	Function	References
let-7e-5p	Blood	302 IS patients and 302 healthy controls	U937 cell line	CASP3 and NLK	MAPK signaling pathway	Let-7e-5p might be a useful noninvasive marker for the diagnosis of IS.	Huang et al., 2016
miR-145	Blood	32 IS patients and 18 healthy controls	–	KLF4/5	–	MiR-145 might serve as a useful biomarker and therapy for IS.	Gan et al., 2012
miR-363, miR-487b	Blood	24 AIS patients and 24 control	–	MAP2K4	toll-like receptor signaling pathway	These miRNA may regulate leukocyte gene expression.	Jickling et al., 2014
miR-125b-2, miR-27a, miR-422a, miR-488 and miR-627	Blood	169 stroke patients, 24 healthy controls, and 94 individuals with metabolic syndrome	–	–	–	These miRNAs may serve as potential diagnostic biomarkers for IS.	Sepramaniam et al., 2014
miR-9-5p, miR-9-3p, miR-107, miR-124-3p, and miR-128-3p	CSF	21 IS patients and 21 controls	–	–	–	These miRNAs show the ischemia-related brain damage.	Sørensen et al., 2017
miR-17-5p, miR-20b-5p, miR-27b-3p, miR-93-5p	Extracellular Vesicle in blood	34 non-stroke and 139 stroke patients	–	–	stress/hypoxia and repair pathways	These miRNAs profile shows the development of cerebral SVD.	van Kralingen et al., 2019
hsa-miR-4656, hsa-miR-432, hsa-miR-503, hsa-miR-376c, hsa-miR-130a-3p and hsa-miR-487b	PBMCs	20 IS patients and 19 healthy controls	–	TGFB3, CELSR2 and ITM2C	–	These miRNAs regulate immune responses.	Bam et al., 2018
let-7b	Plasma	197 IS patients and 50 controls	–	–	–	Let-7b might serve as a useful noninvasive marker for the diagnosis of IS.	Long et al., 2013
miR-124-3p and miR-16	Plasma	74 IS and 19 HS	–	–	–	miR-124-3p and miR-16 Expression levels may be the potential circulating biomarker to distinguish hemorrhagic stroke and IS.	Leung et al., 2014
miR-222, miR-218, and miR-185	Plasma	106 AIS patients and 110 controls	–	–	–	These miRNAs might serve as promising and independent biomarkers for risk of AIS.	Jin and Xing, 2017
hsa-miR-106b-5P, hsa-miR-4306	Plasma	136 AIS patients and 116 healthy controls	–	–	–	Enhanced expression of hsa-miR-106b-5P and hsa-miR-4306 in plasma may be novel biomarkers for the early detection of AIS.	Wang et al., 2014
miR-16	Plasma	40 HACI patients and 30 healthy controls.	–	–	–	The high expression of miR-16 in plasma were related to TOAST and OCSP criteria.	Tian et al., 2016
miR-143-3p, miR-125b-5p, miR-125a-5p	Plasma	200 IS patients and 100 healthy controls	–	–	–	A combination of miR-125a-5p, miR-125b-5p, and miR-143-3p might have clinical utility as an early diagnostic biomarker.	Tiedt et al., 2017
miR-125b-5p and miR-206	Plasma	94 AIS patients with or without endovascular treatment	–	–	–	miR-125b-5p and miR-206 levels are related with stroke severity.	van Kralingen et al., 2019
miR-371-3p and miR-520g	Plasma	27 IS patients	–	–	–	These miRNAs are markers of neural repair.	Edwardson et al., 2018a

(Continued)

TABLE 4 | (Continued)

microRNA	The specimen types	Numbers of clinical specimens	Cells	Targets/ Regulators	Signaling pathways	Function	References
miR-205-5p	Serum	40 CIS patients and 40 healthy controls	HBMECs	MALAT1	-	miR-205-5p inhibits proliferation of endothelial cells.	Gao et al., 2020
miR-15a, miR-16, and miR-17-5p	Serum	106 AIS patients and 120 healthy controls	–	–	–	Combination of miR-15a, miR-16, and miR-17-5p may be a potential AIS biomarker.	Wu et al., 2015
miR-15a and miR-16	Serum	20 CLI patients, 122 T2D+ CLI patients, and 43 healthy controls	Circulating proangiogenic cells (PACs), VSMCs, and pericytes	VEGF-A and AKT3	AKT signaling pathway	miR-15a/16 induces PAC survival and migration, and increases migratory capacity of PACs	Spinetti et al., 2013
miR-145	Serum	146 AIS patients and 96 control	–	–	–	MiR-145 might serve as a useful biomarker and therapy for IS.	Jia et al., 2015
miR-9 and miR-124	Serum	65 AIS patients and 66 control	–	–	–	Serum exosomal miR-9 and miR-124 are markers for AIS.	Ji et al., 2016
miR-223	Serum	50 AIS patients and 33 control	–	–	–	Exosomal miR-223 levels are associated with acute IS.	Chen et al., 2017
miR-146b	Serum	128 AIS patients and 102 control	–	–	–	Elevated serum miR-146b expression might be a potential biomarker for AIS evaluation.	Chen et al., 2018b
miR32-3p, miR-106b-5p, miR-423-5p, miR-451a, miR-1246, miR-1299, miR-3149, and miR-4739	Serum	117 AIS patients and 82 healthy controls	–	–	–	These miRNAs may serve as potential diagnostic biomarkers for IS.	Li et al., 2015
miR-23b-3p, miR-29b-3p, miR-181a-5p and miR-21-5p	Serum	177 IS, 81 TIA patients and 42 controls.	–	–	–	Enhanced expression of miR-23b-3p, miR-29b-3p and miR-21–5p might distinguish between IS and TIA.	Wu et al., 2017
PC-3p-57664, PC-5p-12969, hsa-miR-122-5p and hsa-miR-211-5p	Serum	34 IS patients and 11 healthy controls. postmortem specimens from 10 IS brains and 10 control brains	lymphoblastoid cell line	–	–	These miRNAs are biomarkers for IS.	Vijayan et al., 2018
let-7e	serum and cerebral spinal fluid	72 IS patients and 51 healthy controls	–	–	–	let-7e Expression levels in serum may be the potential circulating biomarker for the acute stage of ischemic stroke.	Peng et al., 2015

TABLE 5 | Summary of human studies reporting down-regulation of miRNAs in IS.

microRNA	The specimen types	Numbers of clinical specimens	Cell line	Targets/ Regulators	Signaling pathways	Function	References
miR-145		–	Primary astrocytes from rats	AQP4	–	miR-145 protects astrocytes from damage.	Zheng et al., 2017
miR-122, miR-148a, let-7i, miR-19a, miR-320d, miR-4429	Blood	24 AIS patients and 24 control	–	GFR, RAS, PI3K, AKT, IKK	NF-κβ signaling	These miRNA may regulate leukocyte gene expression in IS.	Jickling et al., 2014
miR-574-3p	Blood	55 chronic stroke patients and 2360 controls	–	DBNDD2 and ELOVL1	neurometabolic and chronic neuronal injury response pathways	miR-574-3p has a role in regulating chronic brain and systemic cellular response to stroke	Salinas et al., 2019
miRNA-660-5p	Extracellular Vesicle in blood	34 non-stroke and 139 stroke patients	–	–	–	This miRNA associated with pathophysiology of IS	van Kralingen et al., 2019
hsa-miR-874-3p	PBMCs	20 IS patients and 19 healthy controls	–	IL12A and IL12B	–	hsa-miR-874-3p involves in the immune system alteration during IS pathophysiology	Bam et al., 2018
miR-30a and miR-126	Plasma	197 IS patients and 50 controls	–	–	–	miR-30a and miR-126 are markers of IS.	Long et al., 2013
miR-126, miR-130a, and miR-378	Plasma	106 AIS patients and 110 controls	–	–	–	These miRNAs might serve as promising and independent biomarkers for risk of AIS.	Jin and Xing, 2017
hsa-miR-320e, hsa-miR-320d	Plasma	136 AIS patients and 116 healthy controls	–	–	–	Reduced expression of hsa-miR-320e and hsa-miR-320d is marker for early detection of AIS.	Wang et al., 2014
let-7i-3p and miR-23a-3p	Plasma	10 AIS patients and 10 healthy controls	–	–	–	These miRNAs associated with the peculiarities of clinical manifestations of IS	Zhanin et al., 2018
miR-195	Plasma	96 AIS patients	C57BL/6 mice, BV2 microglial cells and HEK293T cells	CX3CL1 and CX3CR1	CX3CL1/CX3CR1 signaling pathway	miR-195 has neuroprotective roles.	Guang et al., 2019
miR-449b, miR-519b, miR-581, miR-616, miR-892b, miR-941, miR-1179, miR-1292, and miR-1296	Plasma	27 IS patients	–	–	–	These miRNAs show neural repair.	Edwardson et al., 2018a
miR23a and miR-221	Serum	146 AIS patients and 96 control	–	–	–		Jia et al., 2015
miR-124, miR-9	Serum	31 AIS patients and 11 control	–	MMP-9	–	Serum miR-124, miR-9 inhibit neuroinflammation and brain injury.	Liu et al., 2015

(Continued)

TABLE 5 | (Continued)

microRNA	The specimen types	Numbers of clinical specimens	Cell line	Targets/ Regulators	Signaling pathways	Function	References
miR-224-3p, miR377-5p, miR-518b, miR-532-5p, and miR-1913	Serum	117 AIS patients and 82 healthy controls	–	–	–	These miRNAs in serum may be markers for IS.	Li et al., 2015
miR-146a	Serum	44 IS patients and 22 controls	–	–	–	miR-146a was decreased in patients with more severe conditions.	Kotb et al., 2019
miR-1228-5p, miR-1268a, miR-1268b, miR-4433b-3p, miR-6090, miR-6752-5p, and miR6803-5p	Serum	86 IS patients and 45 controls	–	–	–	These miRNAs forecast the risk of cerebrovascular disorder before the onset of IS.	Sonoda et al., 2019
hsa-miR-22–3p, PC-3p-32463, hsa-miR-30d-5p and hsa-miR-23a-3p	Serum	34 IS patients and 11 healthy controls. postmortem specimens from 10 IS brains and 10 control brains	lymphoblastoid cell line	–	–	These miRNAs could be used as biomarkers for IS.	Vijayan et al., 2018

with LAA compared with healthy subjects, while circulating let-7b have been higher in patients with other kinds of IS until 24 weeks. Notably, aberrant miRNAs levels have been resolved 48 weeks after IS onset in all patients. Authors have suggested that miR-30a might affect IS through modulation of RhoB and beclin-1. Moreover, miR-126 and let-7 can contribute in this process through modulation of VCAM-1 and inflammatory responses, respectively (Long et al., 2013). Another investigation has demonstrated that miRNA signature reveal not only the chronological development of IS but also the specific reasons for development of IS. Authors have suggested a 32-miRNA panel that can distinguish stroke etiologies during the acute phase. Moreover, miR-125b-2*, miR-27a*, miR-422a, miR-488, and miR-627 have been constantly dysregulated in acute stroke independent of age or severity or underlying metabolic background (Sepramaniam et al., 2014). **Table 5** provides outcome of human studies reporting down-regulation of miRNAs in IS.

Diagnostic and prognostic role of miRNAs have been appraised in IS. Elevated serum amounts of miR-15a, miR-16, and miR-17-5p in acute IS patients could be used as diagnostic markers. Based on the multivariate logistic regression analysis, serum miR-17-5p levels could discriminate the presence of acute IS. miR-15a, miR-16, and miR-17-5p had AUC values of 0.698, 0.82, and 0.784, respectively. Combination of three miRNAs increased the AUC value to 0.845 (Wu et al., 2015). ROC curve analysis has revealed AUC values of 0.91, 0.91, 0.92, and 0.93 for plasma miR-30a levels, at 24 h, 1, 4, and 24 weeks, respectively. These values have been 0.93, 0.92, 0.92, and 0.91 for miR-126 at these time points, respectively. Taken together, miR-30a, miR-126 and let-7b can be suitable biomarkers for IS (Long et al., 2013). Expression levels of miR-145 and miR-210 have been remarkably elevated in IS patients with robust AUC values of 0.90 and 1.0, respectively. Yet, dysregulation of miR-145 and miR-210 has not been exclusive for the acute phase as they have been also up-regulated in recovery phase (Sepramaniam et al., 2014). **Table 6** provides summary of studies reporting diagnostic/prognostic role of miRNAs in IS.

Animal Studies

Investigations in animal models of IS have provided valuable data about the mechanisms of involvement of lncRNAs/miRNAs in IS and possible application of targeted therapies against these transcripts. For instance, expression of RMST has been elevated in primary hippocampal neurons exposed with oxygen-glucose deprivation and in animal models of IS induced by middle cerebral artery occlusion (MCAO). RMST silencing has amended brain injury in the mentioned animal model and attenuated hippocampal neuron defects (Hou and Cheng, 2018). H19 is another up-regulated lncRNA in animal models of IS whose silencing has diminished the size of brain tissue damage following middle cerebral artery obstruction and reperfusion and ameliorated the neurological defects. Mechanistically, H19 silencing could reduce expression of neurogenesis related proteins. Taken together, H19 precludes the development of neurogenesis after IS via p53/Notch1 pathway (Wang et al., 2019a). A throughput miRNA sequencing in infarcted brain

TABLE 6 | Diagnostic/prognostic role of miRNAs in IS.

Sample number	Area under curve	Sensitivity	Specificity	Kaplan-Meier analysis	Univariate cox regression	Multivariate cox regression	References
Plasma specimens from 197 IS patients and 50 controls	0.91 for miR-30 0.92 for miR-126 0.93 for let-7b	80% for miR-30, 84% for miR-126, 84% for let-7b	94% for miR-30, 92% for miR-126, 92% for let-7b	–	–	–	Long et al., 2013
serum and cerebral spinal fluid specimens from 72 IS patients and 51 healthy controls	0.86 for let-7e	82.8%	73.4%	–	–	–	Peng et al., 2015
Blood specimens from 302 IS patients and 302 healthy controls	0.82 for let-7e-5p	–	–	–	–	–	Huang et al., 2016
Serum specimens from 106 AIS patients and 120 healthy controls	0.698 for miR-15a, 0.82 for miR-16, and 0.784 for miR-17-5p	–	–	–	–	Serum miR-17-5p is an independent marker for AIS.	Wu et al., 2015
Plasma specimens from 74 IS and 19 HS	0.70 for miR-124-3p, 0.59 for miR-16	68.4% for miR-124-3p, 94.7% for miR-16	71.2% for miR-124-3p, 35.1% for miR-16	–	–	NIHSS, platelet count and the plasma levels of miR-124-3p were significant predictors of HS.	Leung et al., 2014
Plasma specimens from 106 AIS patients and 110 controls	0.767 for combined miRNAs	87.7% for combined miRNAs	54.5% for combined miRNAs	–	miR-126, miR-130a, miR-378, miR-222, miR-218, and miR-185 were predicting factors for risk of AIS.	miR-126 and miR-130a were protective factors for AIS. miR-222, miR-218, and miR-185 were risk factors for AIS.	Jin and Xing, 2017
Serum specimens from 146 AIS patients and 96 control	0.896 for miR-145, 0.816 for miR-23a, 0.819 for miR-221	–	–	–	–	–	Jia et al., 2015
Serum specimens from 65 AIS patients and 66 control	0.8026 for miR-9, 0.6976 for miR-124	–	–	–	–	–	Ji et al., 2016
Serum specimens from 50 AIS patients and 33 control	0.859 for miR-223	84.0% for miR-223	78.8% for miR-223	–	–	Circulating exosomal miR-223 is risk factor for IS.	Chen et al., 2017
Serum specimens from 128 AIS patients and 102 control	0.863 for combination of hs-CRP and miR-146b	–	–	–	–	–	Chen et al., 2018b
Blood specimens from 169 stroke patients, 24 healthy controls, and 94 individuals with metabolic syndrome	0.95 for miR-125b-2, 0.89 for miR-27a, 0.92 for miR-422a, 0.87 for miR-488, 0.84 for miR-627	–	–	–	–	–	Sepramaniam et al., 2014

(Continued)

TABLE 6 | (Continued)

Sample number	Area under curve	Sensitivity	Specificity	Kaplan-Meier analysis	Univariate cox regression	Multivariate cox regression	References
Plasma specimens from 136 AIS patients and 116 healthy controls	0.962 for hsa-miR-106b-5P; 0.952 for hsa-miR-4306; 0.981 for hsa-miR-320e; 0.987 for hsa-miR-320d	–	–	–	–	–	Wang et al., 2014
Plasma specimens from 40 HACI patients and 30 healthy controls.	0.775 for miR-16	69.7% for miR-16	87% for miR-16	–	–	Patients with higher expression of MiR-16 were associated with poor prognosis.	Tian et al., 2016
Plasma specimens from 200 IS patients and 100 healthy controls.	0.93 for combination of miR-143-3p, miR-125b-5p, and miR-125a-5p	85.6% for combination of miR-143-3p, miR-125b-5p, and miR-125a-5p	76.3% for combination of miR-143-3p, miR-125b-5p, and miR-125a-5p	–	–	–	Tiedt et al., 2017
Serum specimens from 177 IS, 81 TIA patients and 42 controls.	0.883 for combination of miR-23b-3p, miR-29b-3p, miR-181a-5p and miR-21–5p	–	–	–	miR-23b-3p, miR-29b-3p and miR-21–5p levels were independently associated with IS. miR-23b-3p, miR-29b-3p and miR-181a-5p levels were associated with TIA.	Enhanced miR-23b-3p, miR-29b-3p, miR-181a-5p and miR-21–5p levels were closely associated with IS, and enhanced miR23b-3p, miR-29b-3p and miR-181a-5p levels were associated with TIA.	Wu et al., 2017
Serum specimens from 86 IS patients and 45 controls	0.95 for combination of miR-1268b, miR-4433b-3p, and miR-6803-5p	84% for combination of miR-1268b, miR-4433b-3p, and miR-6803-5p	98% for combination of miR-1268b, miR-4433b-3p, and miR-6803-5p	–	–	–	Sonoda et al., 2019
Plasma specimens from 94 AIS patients with or without endovascular treatment	0.735 for miR125b-5p	86.36% for miR125b-5p	55.36% for miR125b-5p	–	–	Higher expression of miR125b-5p associated with an unfavorable outcome.	van Kralingen et al., 2019

TABLE 7 | Summary of animal studies which displayed elevation of lncRNAs and miRNAs in stroke.

lncRNAs/miRNAs	Animal models	Cells	Targets/ Regulators	Signaling	Function	References
RMST	MCAO mouse model	hippocampal cells	–	–	RMST induces ischemic brain injury and disrupts neurological function.	Hou and Cheng, 2018
GAS5	brain tissues of C57BL/6 J mice	–	miR-137	Notch1 signaling pathway	GAS5 is a ceRNA for miR-137 to control Notch1.	Chen et al., 2018a
Nespas	brain tissues of C57BL/6 J mice	Mouse BV2 microglial cells	TAK1	NF-κB signaling	Nespas induces Neuroinflammation Through inhibiting NF-κB Activation	Deng et al., 2019
MALAT1	brain cortex of C57BL/6 J mice	cortical neurons of mice	Beclin1, miR-30a	–	MALAT1 induces ischemic injury and autophagy.	Guo et al., 2017
H19	C57BL/6 J mice	–	miR-675, IGF1R, pS6 kinase	IGF1 signaling pathway, mTOR pathway	H19 knockdown mice indicated amelioration on the performance of a skilled, cortical dependent motor task.	Wang et al., 2020b
Maclpil	C57BL/6 mice	–	LCP1	–	Maclpil regulates the migration of macrophage and phagocytosis by LCP1.	Wang et al., 2020b
MEG3	C57BL/6 J mice	N2a cell	miR-21	miR-21/PDCD4 pathway	MEG3 promotes ischemic damage and disrupts overall neurological levels.	Zheng et al., 2017
MALAT1	C57BL/6J mice	Mouse BMECs and N2A cells	Bim and E-selectin	apoptotic pathways	Malat1 expression reduced ischemia-induced endothelial cell death *in vitro*	Zhang et al., 2017b
MEG3	SD rats	–	BDNF, NGF and bFGF	Wnt/β-catenin signaling pathway	MEG3 reduced nerve growth and enhanced neurological damage.	You and You, 2019
MEG3	SD rats	rat brain microvascular endothelial cells	NOX4	p53/NOX4 pathway	MEG3 was an important regulator of apoptosis.	Zhan et al., 2017
ANRIL	Wistar rats	neural cells	VEGF	NF-κB signaling pathway	ANRIL increases VEGF and induces angiogenesis.	Zhang et al., 2017a
H19	Wistar rats	Neural stem cell (NSC)	SUZ12, EZH2, miR-675	oxidative response, NF-κβ signaling	H19 expression induces the proliferation and neuronal differentiation of NSCs.	Wang et al., 2020b
H19	C57BL/6J mice	–	p53	p53/Notch1 pathway	H19 represses neurogenesis after IS.	Wang et al., 2019a
MALAT1	C57BL/6 J mice	Primary astrocytes	AQP4, miR-145	–	MALAT1 induced cerebral ischemia-reperfusion damage.	Wang et al., 2020a
H19, Lnc-EF094477 and LncBC090003	Wistar rats	Neural progenitor cells (NPCs)	–	–	H19 regulated post-stroke neurogenesis.	Liu et al., 2019
GAS5	C57BL/6 mice	293 T	MAP4K4	–	GAS5 induses neuron cell apoptosis and nerve injury in ischemic stroke through inhibiting DNMT3B-dependent MAP4K4 methylation	Deng et al., 2020b

(Continued)

TABLE 7 | (Continued)

lncRNAs/miRNAs	Animal models	Cells	Targets/ Regulators	Signaling	Function	References
MEG3	MCAO rats	OGD/R-treated neurocytes	miR-485 and AIM2	MEG3/miR-485/AIM2 axis	MEG3 induces cerebral ischemia reperfusion injury through elevating pyroptosis by targeting miR-485/AIM2 axis	Liang et al., 2020
miR-211-5p, miR-183-5p, miR-182 and miR-96-5p	Brain of 10 Rat MCAO model and 10 controls	–	PPFIA1, SLC7A1, NTRK2, KDM48	Ras, cGMP-PKG and phospholipase D signaling pathways	These miRNAs may control cell proliferation and apoptosis via the cGMP-PKG signaling pathway.	Duan et al., 2019
miR-669c-3p	Primary cortical neuron cultures and Primary microglial cultures from C57BL/6 J neonatal mice	N2a cell line	MyD88	toll-like receptor signaling pathway	miR-669c overexpression modulates the inflammatory responses.	Kolosowska et al., 2020
miR-3473b	brain tissues from CD-1 mice	BV2 microglial cells	SOCS3	–	The expression of miR-3473b activates microglial and the inflammation and induces neuroinflammation.	Wang et al., 2018
miR-26a	Brain tissues from 48 SD rats	–	HIF-1a and VEGF	PI3K/AKT and MAPK/ERK pathway	miR-26a controls cell proliferation and angiogenesis.	Liang et al., 2018b
miR17-92	C57BL/6J mice	SVZ neural progenitor cells	PTEN	Shh signaling pathway	miR17-92 induces the proliferation and viability of SVZ neural progenitor cells.	Liu et al., 2013
miR-92a	mice	human endothelial cells	integrin subunit alpha5	–	miR-92a increased angiogenesis and functional recovery of injured tissue.	Bonauer et al., 2009
miR-497	C57/B6 mice	mouse neuroblastoma (N2A) cells	bcl-2 and bcl-w	ischemia-induced cell death signaling pathway	miR-497 induces ischemic neuronal death.	Yin et al., 2010
miR-130a	Brain tissue from SD rats	neurons	XIAP	–	miR−130a inhibits the proliferation, viability, and differentiation of NSCs.	Deng et al., 2020a
miR-125b	plasma and brain tissue specimens from 50 SD rats	PC-12 cell line	CK2α	CK2α/NADPH Oxidase Signaling pathway	miRNA-125b increases cerebral ischemia injury.	Liang et al., 2018b
miR-223-5p	primary cortical neurons from Wistar rat, SD rats	cortical neurons	NCKX2	–	miR-223-5p amended ischemic damage and enhanced neurological function.	Cuomo et al., 2019
miR-155	C57BL/6 mice	endothelial cells	Dhx40, Dync1i1, Zfp652, Agtr1a	proangiogenic signaling pathway	miR-155 reduces blood flow and cerebral microvasculature.	Caballero-Garrido et al., 2015
miR-155	C57BL/6 mice	–	–	–	Mir-155 promotes ischemia/reperfusion induced brain injury and hemorrhagic transformation	Suofu et al., 2020

TABLE 8 | Summary of animal studies which displayed down-regulation of lncRNAs and miRNAs in stroke.

lncRNAs/miRNAs	Animal models	Cells	Targets/ Regulators	Signaling pathways	Function	References
Meg3	268 adult male Sprague–Dawley rats	HMEC-1	NICD, Hes-1, and Hey-1	Notch Pathway	Meg3 inhibits brain lesions, promotes neurological outcomes and induces angiogenesis after IS	Liu et al., 2017
LncRNA-1810034E14Rik	C57BL/6 mice	primary microglial cells	–	NF-κB pathway	1810034E14Rik upregulation decreased the expression of inflammatory cytokines in IS animal and inhibited the microglial cells	Qu et al., 2019
HOTTIP	C57BL/6 mice	Primary cortical neurons	miR-143	miR-143/hexokinase 2 pathway	HOTTIP expression reduced ischemic injury and attenuated glycolytic metabolism in neurons	Liang et al., 2018a
Lnc-M64384, Lnc-MRAK013682, Lnc-MRAK051099	Wistar rats	Neural progenitor cells (NPCs)	–	–	Theses lncRNA may use as an therapy for amelioration of neurological functions.	Liu et al., 2019
lncRNA Rian	C57BL/6 mice	N2a cell line (mouse)	miR-144-3p	Rian/miR-144-3p/GATA3 signaling	Rian inhibits cell apoptosis from cerebral ischemia-reperfusion injury by Rian/miR-144-3p/GATA3 signaling	Yao et al., 2020
miR-10b-3p and miR-217-5p	Brain of 10 Rat MCAO model and 10 controls	–	PPFIA1, SLC7A1, NTRK2, KDM48	Ras signaling pathway, cGMP-PKG signaling pathway, phospholipase D signaling pathway	These miRNAs may control cell proliferation and apoptosis via the cGMP-PKG signaling pathway	Duan et al., 2019
miR-424	plasma and ipsilateral brain tissue from C57/BL6 mice	BV2 microglial cell	CDC25A, cyclin D1, and CDK6	–	miR-424 suppresses neuronal apoptosis and microglia activation	Zhao et al., 2013
miR-126-3p and miR-126-5p	ICR mice	–	SPRED1, VEGFA, and p-Raf-1	MAP kinase pathway, VEGFA/SPRED1/raf-1 signaling pathway	miR-126-3p reduces the OGD/R-induced apoptosis and enhances cell survival.	Xiao et al., 2020
miRNA-126	60 ICR mice	HUVECs	PTPN9	AKT and ERK signaling pathways	miRNA-126 reduces brain atrophy size and enhances neurobehavioral function.	Qu et al., 2019
miR-22	16 SD rats	rat pheochromo-cytoma cell line	TNF-α, IL-1β, IL-6, IL-18, MIP-2 and PGE2	p38 MAPK pathway	miRNA-22 inhibits the inflammatory factors *in vitro*.	Dong et al., 2019
miR-652	SD rats	SH-SY5Y cell lin	NOX2	ROS pathway	miR-652 inhibited NOX2 expression, reduced NOX activity and ROS level and enhanced apoptosis	Zuo et al., 2020

(Continued)

TABLE 8 | (Continued)

lncRNAs/miRNAs	Animal models	Cells	Targets/ Regulators	Signaling pathways	Function	References
miR-3552	blood and brain specimens from 7 brain specimens from MCAO rats and 5 brain specimens from sham-operated rats	–	CASP3	apoptosis pathway	miR-3552 might regulate apoptosis by CASP3	Li et al., 2020
miR-103	SD rats	HUVECs	VEGF	–	miR-103 inhibits the increase of tube length and the migration of cells and ischemic stroke angiogenesis, and enhances infarction volume	Shi et al., 2018
miR-195	SD rats	cerebral cortex cells RCCNC	KLF5	JNK signaling pathway	miR-195 upregulation suppresses cerebral infarction, loss of neuronal cells, and induces synaptic plasticity	Chang et al., 2020
miR-122	Blood specimens from SD rats	–	Vcam1, Nos2, Pla2g2a	granulocyte/ agranulocyte adhesion and diapedesis, leukocyte extravasation, eicosanoid signaling and atherosclerosis signaling	miR-122 upregulation enhances stroke outcomes.	Liu da et al., 2016
miR-579-3p	brain tissue from SD rats	neurons	NRIP1	NF-êB pathway	miR-579-3p has neuroprotective effect and reduces inflammation and apoptosis.	Jia et al., 2020
miR-7a-5p	spontaneously hypertensive rats, C57BL/6 mice	PC12 cells	α-Syn	–	miR-7a-5p improved ischemic brain damage.	Kim et al., 2018
miR-219	Serum and brain tissue from Wistar rats	–	NMDA	–	miR-219 modulated ischemia by NMDA.	Silva et al., 2017
miR-99a	C57BL/6 mice	neuro-2a cells	cyclin D1 and CDK6	–	miR-99a decreased neuronal injury after cerebral I/R.	Tao et al., 2015
miR-126	SD rats	adipose derived stem cells (ADSCs)	–	–	miR-126 induced neurogenesis and vasculogenesis, and suppresses microglial activation and inflammatory response after ischemic stroke.	Geng et al., 2019
miR-130a-3p	MCAO/R mice	SH-SY5Y and N2a cells	DAPK1	H19/miR-130a-3p/DAPK1 axis	miR-130a-3p controls apoptosis in SH-SY5Y and N2a cells as well as on cerebral damage by I/R.	Feng et al., 2021

regions after regional cerebral ischemia has shown up-regulation of 20 miRNAs while down-regulation of 17 miRNAs in the infarct area among them have been miR-211-5p, miR-183-5p, miR-182, and miR-96-5p which have been functionally related with some important pathways in the neurons (Duan et al., 2019). **Table 7** summarizes the data regarding the roles of up-regulated non-coding RNAs in the pathogenesis of IS as revealed by animal studies.

Meg3 is a down-regulated lncRNA after IS. Up-regulation of Meg3 has inhibited functional recovery and diminished capillary mass after IS. On the other hand, its silencing has amended brain lesions and enhanced angiogenesis after IS. Meg3 exerts these functions through inhibiting notch pathway (Liu et al., 2017). Expression of lncRNA-1810034E14Rik has also been down-regulated in LPS-exposed or oxygen-glucose deprivation-induced microglial cells. Up-regulation of 1810034E14Rik has reduced the infarct volume, ameliorated brain injury in MCAO model and decreased production of inflammatory cytokines both in the animal model and in microglial cells. Besides, 1810034E14Rik up-regulation could block the induction of microglial cells and suppress p65 phosphorylation of p65 (Qu et al., 2019). The above-mentioned examples indicate that down-regulation of lncRNAs in IS might be a compensative mechanism for amelioration of neuron damage or can be directly participate in the pathogenic mechanisms during IS. **Table 8** summarizes the data regarding the roles of down-regulated non-coding RNAs in the pathogenesis of IS as revealed by animal studies.

DISCUSSION

A wealth of information about the role of non-coding RNAs in the development of IS has been obtained from combination of RNA-sequencing assays and bioinformatics assays such as GO, KEGG pathway enrichment assays and network analyses. These kinds of studies not only exhibited dysregulation of these transcripts, but also provided mechanistical insights about their route of actions. Generally, non-coding RNAs might participate in the pathophysiology of IS through different routes. As a number of differentially expressed lncRNAs between IS patients and healthy controls map to genomic loci near IS-associated genes, regulation of gene expression through *cis*-acting modes is a possible route. Another possible mechanism of contribution of lncRNAs in the pathology of IS is their ceRNA role. MEG3/miR-424-5p, KCNQ1OT1/miR-200a and MALAT1/miR-205-5p are few examples of interplay between lncRNAs and miRNAs in the context of IS.

Aberrant expression of non-coding RNAs in IS patients might be due to the presence of a number of genomic variants within the coding genes as demonstrated for ANRIL lncRNA. This lncRNA is among the mostly assessed lncRNAs in IS. However, the results of all studies are not consistent in this regard. Such inconsistency might be due to phase of sampling during the course of IS or the presence of other confounding parameters. The presence of lncRNAs in the serum specimens and exosomes extracted from these specimens facilitates diagnosis of IS and its clinical variants using this noninvasive route of sampling.

MicroRNAs contribute in the pathogenesis of IS through modulation of genes implicated in the atherosclerosis or inflammatory responses. Exosomal miRNAs might affect communication between several types of cells including endothelial and smooth muscle cells. IS-related circulating miRNAs might hypothetically exert similar functions. Yet, this hypothesis should be judged in upcoming studies. Peripheral expression of miRNAs can be used to differentiate IS patients from healthy subjects or IS patients from other related conditions such as HS. Moreover, their signature might predict recovery from IS-related clinical signs.

The observed sex-biased pattern of differentially expression of lncRNAs (Dykstra-Aiello et al., 2016) might determine different pathogenic processes for the evolution of IS among men and women which should be further examined. Moreover, a number of investigations have displayed specific lncRNA signatures at certain time points following IS, demonstrating the specific roles of lncRNAs in each step of pathogenic processes following IS.

In spite of conduction of various functional studies to unravel the role of non-coding RNAs in IS, therapeutic application of these transcripts have not been clarified. Therefore, future investigation should appraise the possibility of using these transcripts as therapeutic targets in IS. Another limitation of most of mentioned studies is their relatively small sample sizes and lack of simultaneous appraisal of exposures and outcomes in cross-sectional studies. Application of non-coding RNAs as therapeutic targets for IS has faced some challenges in terms of safe delivery of the drug to specific targets, avoidance of off-target effects and determination of best time for intervention. This filed is still in its infancy.

AUTHOR CONTRIBUTIONS

SG-F wrote the manuscript and revised it. MT designed the study and supervised it. NA, ZS-F, and BH collected the data and designed the figures and the tables. All authors approved the manuscript.

REFERENCES

Bam, M., Yang, X., Sen, S., Zumbrun, E. E., Dennis, L., Zhang, J., et al. (2018). Characterization of dysregulated miRNA in Peripheral blood mononuclear cells from ischemic stroke patients. *Mol. Neurobiol.* 55, 1419–1429. doi: 10.1007/s12035-016-0347-8

Bonauer, A., Carmona, G., Iwasaki, M., Mione, M., Koyanagi, M., Fischer, A., et al. (2009). MicroRNA-92a controls angiogenesis and functional recovery of ischemic tissues in mice. *Science* 324, 1710–1713. doi: 10.1126/science.1174381

Caballero-Garrido, E., Pena-Philippides, J. C., Lordkipanidze, T., Bragin, D., Yang, Y., Erhardt, E. B., et al. (2015). In vivo inhibition of miR-155 promotes recovery after experimental mouse stroke. *J. Neurosci.* 35, 12446–12464. doi: 10.1523/jneurosci.1641-15.2015

Chang, L., Zhang, W., Shi, S., Peng, Y., Wang, D., Zhang, L., et al. (2020). microRNA-195 attenuates neuronal apoptosis in rats with ischemic stroke through inhibiting KLF5-mediated activation of the JNK signaling pathway. *Mol. Med.* 26:31. doi: 10.1186/s10020-020-00150-w

Chen, F., Zhang, L., Wang, E., Zhang, C., and Li, X. (2018a). LncRNA GAS5 regulates ischemic stroke as a competing endogenous RNA for miR-137 to regulate the Notch1 signaling pathway. *Biochem. Biophys. Res. Commun.* 496, 184–190. doi: 10.1016/j.bbrc.2018.01.022

Chen, Y., Song, Y., Huang, J., Qu, M., Zhang, Y., Geng, J., et al. (2017). Increased circulating exosomal miRNA-223 is associated with acute ischemic stroke. *Front. Neurol.* 8:57. doi: 10.3389/fneur.2017.00057

Chen, Z., Wang, K., Huang, J., Zheng, G., Lv, Y., Luo, N., et al. (2018b). Upregulated serum MiR-146b serves as a biomarker for acute ischemic stroke. *Cell. Physiol. Biochem.* 45, 397–405. doi: 10.1159/000486916

Cheng, J., Kapranov, P., Drenkow, J., Dike, S., Brubaker, S., Patel, S., et al. (2005). Transcriptional maps of 10 human chromosomes at 5-nucleotide resolution. *Science* 308, 1149–1154. doi: 10.1126/science.1108625

Cuomo, O., Cepparulo, P., Anzilotti, S., Serani, A., Sirabella, R., Brancaccio, P., et al. (2019). Anti-miR-223-5p ameliorates ischemic damage and improves neurological function by preventing NCKX2 downregulation after ischemia in rats. *Mol. Therapy Nucleic Acids* 18, 1063–1071. doi: 10.1016/j.omtn.2019.10.022

Deng, Q.-W., Li, S., Wang, H., Sun, H.-L., Zuo, L., Gu, Z.-T., et al. (2018). Differential long noncoding RNA expressions in peripheral blood mononuclear cells for detection of acute ischemic stroke. *Clin. Sci.* 132, 1597–1614. doi: 10.1042/cs20180411

Deng, W., Fan, C., Zhao, Y., Mao, Y., Li, J., Zhang, Y., et al. (2020a)). MicroRNA-130a regulates neurological deficit and angiogenesis in rats with ischaemic stroke by targeting XIAP. *J. Cell Mol. Med.* 24, 10987–11000. doi: 10.1111/jcmm.15732

Deng, Y., Chen, D., Gao, F., Lv, H., Zhang, G., Sun, X., et al. (2020b). Silencing of long non-coding RNA GAS5 suppresses neuron cell apoptosis and nerve injury in ischemic stroke through inhibiting DNMT3B-Dependent MAP4K4 methylation. *Trans. Stroke Res.* 11, 950–966. doi: 10.1007/s12975-019-00770-3

Deng, Y., Chen, D., Wang, L., Gao, F., Jin, B., Lv, H., et al. (2019). Silencing of long noncoding RNA nespas aggravates microglial cell death and neuroinflammation in ischemic stroke. *Stroke* 50, 1850–1858. doi: 10.1161/STROKEAHA.118.023376

Derrien, T., Johnson, R., Bussotti, G., Tanzer, A., Djebali, S., Tilgner, H., et al. (2012). The GENCODE v7 catalog of human long noncoding RNAs: analysis of their gene structure, evolution, and expression. *Genome Res.* 22, 1775–1789. doi: 10.1101/gr.132159.111

Dong, H., Cui, B., and Hao, X. (2019). MicroRNA-22 alleviates inflammation in ischemic stroke via p38 MAPK pathways. *Mol. Med. Rep.* 20, 735–744. doi: 10.3892/mmr.2019.10269

Duan, X., Gan, J., Peng, D. Y., Bao, Q., Xiao, L., Wei, L., et al. (2019). Identification and functional analysis of microRNAs in rats following focal cerebral ischemia injury. *Mol. Med. Rep.* 19, 4175–4184. doi: 10.3892/mmr.2019.10073

Dykstra-Aiello, C., Jickling, G. C., Ander, B. P., Shroff, N., Zhan, X., Liu, D., et al. (2016). Altered expression of long noncoding RNAs in blood after ischemic stroke and proximity to putative stroke risk loci. *Stroke* 47, 2896–2903. doi: 10.1161/STROKEAHA.116.013869

Edwardson, M. A., Zhong, X., Cheema, A., and Dromerick, A. (2018a). Plasma microRNA markers of upper limb recovery following human stroke. *J. Clin. Trans. Sci.* 2:45. doi: 10.1017/cts.2018.176

Edwardson, M. A., Zhong, X., Fiandaca, M. S., Federoff, H. J., Cheema, A. K., and Dromerick, A. W. (2018b). Plasma microRNA markers of upper limb recovery following human stroke. *Sci. Rep.* 8:12558.

Fang, Y., and Fullwood, M. J. (2016). Roles, functions, and mechanisms of long non-coding RNAs in cancer. *Genom. Proteom. Bioinform.* 14, 42–54. doi: 10.1016/j.gpb.2015.09.006

Feigin, V. L., Krishnamurthi, R. V., Parmar, P., Norrving, B., Mensah, G. A., Bennett, D. A., et al. (2015). Update on the global burden of ischemic and hemorrhagic stroke in 1990-2013: the GBD 2013 study. *Neuroepidemiology* 45, 161–176. doi: 10.1159/000441085

Feng, L., Guo, J., and Ai, F. (2019). Circulating long noncoding RNA ANRIL downregulation correlates with increased risk, higher disease severity and elevated pro-inflammatory cytokines in patients with acute ischemic stroke. *J. Clin. Lab. Anal.* 33:e22629. doi: 10.1002/jcla.22629

Feng, M., Zhu, X., and Zhuo, C. (2021). H19/miR-130a-3p/DAPK1 axis regulates the pathophysiology of neonatal hypoxic-ischemia encephalopathy. *Neurosci. Res.* 163, 52–62. doi: 10.1016/j.neures.2020.03.005

Gan, C., Wang, C., and Tan, K. (2012). Circulatory microRNA-145 expression is increased in cerebral ischemia. *Genet. Mol. Res.* 11, 147–152. doi: 10.4238/2012.January.27.1

Gao, C., Zhang, C.-C., Yang, H.-X., and Hao, Y.-N. (2020). MALAT1 protected the angiogenesis function of human brain microvascular endothelial cells (HBMECs) under oxygen glucose deprivation/re-oxygenation (OGD/R) challenge by interacting with miR-205-5p/VEGFA pathway. *Neuroscience* 435, 135–145. doi: 10.1016/j.neuroscience.2020.03.027

Geng, W., Tang, H., Luo, S., Lv, Y., Liang, D., Kang, X., et al. (2019). Exosomes from miRNA-126-modified ADSCs promotes functional recovery after stroke in rats by improving neurogenesis and suppressing microglia activation. *Am. J. Transl. Res.* 11, 780–792.

Guang, Y., Zhendong, L., Lu, W., Xin, C., Xiaoxiong, W., Qi, D., et al. (2019). MicroRNA-195 protection against focal cerebral ischemia by targeting CX3CR1. *J. Neurosurg. JNS* 131, 1445–1454. doi: 10.3171/2018.5.JNS173061

Guo, D., Ma, J., Yan, L., Li, T., Li, Z., Han, X., et al. (2017). Down-Regulation of lncrna MALAT1 attenuates neuronal cell death through suppressing beclin1-dependent autophagy by regulating Mir-30a in cerebral ischemic stroke. *Cell. Physiol. Biochem.* 43, 182–194. doi: 10.1159/000480337

Guo, X., Yang, J., Liang, B., Shen, T., Yan, Y., Huang, S., et al. (2018). Identification of novel LncRNA biomarkers and construction of LncRNA-Related networks in han chinese patients with ischemic stroke. *Cell. Physiol. Biochem.* 50, 2157–2175. doi: 10.1159/000495058

Hou, X.-X., and Cheng, H. (2018). Long non-coding RNA RMST silencing protects against middle cerebral artery occlusion (MCAO)-induced ischemic stroke. *Biochem. Biophys. Res. Commun.* 495, 2602–2608. doi: 10.1016/j.bbrc.2017.12.087

Huang, S., Lv, Z., Guo, Y., Li, L., Zhang, Y., Zhou, L., et al. (2016). Identification of blood Let-7e-5p as a biomarker for ischemic stroke. *PLoS One* 11:e0163951. doi: 10.1371/journal.pone.0163951

Huang, Y., Wang, L., Mao, Y., and Nan, G. (2019). Long noncoding RNA-H19 contributes to atherosclerosis and induces ischemic stroke via the upregulation of acid phosphatase 5. *Front. Neurol.* 10:32. doi: 10.3389/fneur.2019.00032

Ji, Q., Ji, Y., Peng, J., Zhou, X., Chen, X., Zhao, H., et al. (2016). Increased brain-specific MiR-9 and MiR-124 in the serum exosomes of acute ischemic stroke patients. *PLoS One* 11:e0163645. doi: 10.1371/journal.pone.0163645

Jia, J., Cui, Y., Tan, Z., Ma, W., and Jiang, Y. (2020). MicroRNA-579-3p exerts neuroprotective effects against ischemic stroke via anti-inflammation and anti-apoptosis. *Neuropsychiatric Dis. Treatment* 16, 1229–1238. doi: 10.2147/ndt.s240698

Jia, L., Hao, F., Wang, W., and Qu, Y. (2015). Circulating miR-145 is associated with plasma high-sensitivity C-reactive protein in acute ischemic stroke patients. *Cell Biochem. Funct.* 33, 314–319. doi: 10.1002/cbf.3116

Jickling, G. C., Ander, B. P., Zhan, X., Noblett, D., Stamova, B., and Liu, D. (2014). microRNA expression in peripheral blood cells following acute ischemic stroke and their predicted gene targets. *PLoS One* 9:e99283. doi: 10.1371/journal.pone.0099283

Jin, F., and Xing, J. (2017). Circulating pro-angiogenic and anti-angiogenic microRNA expressions in patients with acute ischemic stroke and their association with disease severity. *Neurol. Sci.* 38, 2015–2023. doi: 10.1007/s10072-017-3071-x

Jo, M. H., Shin, S., Jung, S.-R., Kim, E., Song, J.-J., and Hohng, S. (2015). Human Argonaute 2 has diverse reaction pathways on target RNAs. *Mol. Cell* 59, 117–124. doi: 10.1016/j.molcel.2015.04.027

Kim, T., Mehta, S. L., Morris-Blanco, K. C., Chokkalla, A. K., Chelluboina, B., Lopez, M., et al. (2018). The microRNA miR-7a-5p ameliorates ischemic brain damage by repressing α-synuclein. *Sci. Signal.* 11:eaat4285. doi: 10.1126/scisignal.aat4285

Kolosowska, N., Gotkiewicz, M., Dhungana, H., Giudice, L., Giugno, R., Box, D., et al. (2020). Intracerebral overexpression of miR-669c is protective in mouse ischemic stroke model by targeting MyD88 and inducing alternative microglial/macrophage activation. *J. Neuroinflamm.* 17:194. doi: 10.1186/s12974-020-01870-w

Kotb, H. G., Ibrahim, A. H., Mohamed, E. F., Ali, O. M., Hassanein, N., Badawy, D., et al. (2019). The expression of microRNA 146a in patients with ischemic stroke: an observational study. *Int. J. Gen. Med.* 12, 273–278. doi: 10.2147/IJGM.S213535

Lee, R. C., Feinbaum, R. L., and Ambros, V. (1993). The *C. elegans* heterochronic gene lin-4 encodes small RNAs with antisense complementarity to lin-14. *Cell* 75, 843–854. doi: 10.1016/0092-8674(93)90529-y

Leung, L. Y., Chan, C. P., Leung, Y. K., Jiang, H. L., Abrigo, J. M., Wang de, F., et al. (2014). Comparison of miR-124-3p and miR-16 for early diagnosis of hemorrhagic and ischemic stroke. *Clin. Chim. Acta* 433, 139–144. doi: 10.1016/j.cca.2014.03.007

Li, L., Dong, L., Zhao, J., He, W., Chu, B., Zhang, J., et al. (2020). Circulating miRNA-3552 as a potential biomarker for ischemic stroke in rats. *BioMed. Res. Int.* 2020:4501393. doi: 10.1155/2020/4501393

Li, P., Teng, F., Gao, F., Zhang, M., Wu, J., and Zhang, C. (2015). Identification of circulating MicroRNAs as potential biomarkers for detecting acute ischemic stroke. *Cell Mol. Neurobiol.* 35, 433–447.

Liang, J., Wang, Q., Li, J.-Q., Guo, T., and Yu, D. (2020). Long non-coding RNA MEG3 promotes cerebral ischemia-reperfusion injury through increasing pyroptosis by targeting miR-485/AIM2 axis. *Exp. Neurol.* 325:113139. doi: 10.1016/j.expneurol.2019.113139

Liang, Y., Xu, J., Wang, Y., Tang, J. Y., Yang, S. L., Xiang, H. G., et al. (2018a). Inhibition of MiRNA-125b decreases cerebral ischemia/reperfusion injury by targeting CK2α/NADPH oxidase signaling. *Cell. Physiol. Biochem.* 45, 1818–1826. doi: 10.1159/000487873

Liang, Z., Chi, Y. J., Lin, G. Q., Luo, S. H., Jiang, Q. Y., and Chen, Y. K. (2018b). MiRNA-26a promotes angiogenesis in a rat model of cerebral infarction via PI3K/AKT and MAPK/ERK pathway. *Eur. Rev. Med. Pharmacol. Sci.* 22, 3485–3492. doi: 10.26355/eurrev_201806_15175

Liaw, N., and Liebeskind, D. (2020). Emerging therapies in acute ischemic stroke. *F1000Res* 9:F1000 Faculty Rev-546.

Liu, J., Li, Q., Zhang, K.-S., Hu, B., Niu, X., Zhou, S.-M., et al. (2017). Downregulation of the long non-coding RNA Meg3 promotes angiogenesis after ischemic brain injury by activating notch signaling. *Mol. Neurobiol.* 54, 8179–8190. doi: 10.1007/s12035-016-0270-z

Liu, X. S., Chopp, M., Wang, X. L., Zhang, L., Hozeska-Solgot, A., Tang, T., et al. (2013). MicroRNA-17-92 cluster mediates the proliferation and survival of neural progenitor cells after stroke. *J. Biol. Chem.* 288, 12478–12488. doi: 10.1074/jbc.M112.449025

Liu, X. S., Fan, B., Wang, X., Chopp, M., and Zhang, Z. G. (2019). "Differential long noncoding RNA and messenger RNA expression profiling and functional network analysis in stroke-induced neurogenesis," in *Proceedings of the 2019 IEEE International Conference on Bioinformatics and Biomedicine (BIBM)*, (Piscataway, NJ: IEEE).

Liu, Y., Zhang, J., Han, R., Liu, H., Sun, D., and Liu, X. (2015). Downregulation of serum brain specific microRNA is associated with inflammation and infarct volume in acute ischemic stroke. *J. Clin. Neurosci.* 22, 291–295. doi: 10.1016/j.jocn.2014.05.042

Liu da, Z., Jickling, G. C., Ander, B. P., Hull, H., Zhan, X., Cox, C., et al. (2016). Elevating microRNA-122 in blood improves outcomes after temporary middle cerebral artery occlusion in rats. *J. Cereb. Blood Flow Metab.* 36, 1374–1383. doi: 10.1177/0271678X15610786

Long, G., Wang, F., Li, H., Yin, Z., Sandip, C., Lou, Y., et al. (2013). Circulating miR-30a, miR-126 and let-7b as biomarker for ischemic stroke in humans. *BMC Neurol.* 13:178. doi: 10.1186/1471-2377-13-178

O'Brien, J., Hayder, H., Zayed, Y., and Peng, C. (2018). Overview of microRNA biogenesis, mechanisms of actions, and circulation. *Front. Endocrin.* 9:402. doi: 10.3389/fendo.2018.00402

Peng, G., Yuan, Y., Wu, S., He, F., Hu, Y., and Luo, B. (2015). MicroRNA let-7e is a potential circulating biomarker of acute stage ischemic stroke. *Trans. Stroke Res.* 6, 437–445. doi: 10.1007/s12975-015-0422-x

Qu, M., Pan, J., Wang, L., Zhou, P., Song, Y., Wang, S., et al. (2019). MicroRNA-126 regulates angiogenesis and neurogenesis in a mouse model of focal cerebral ischemia. *Mol. Therapy Nucleic Acids* 16, 15–25. doi: 10.1016/j.omtn.2019.02.002

Salinas, J., Lin, H., Aparico, H. J., Huan, T., Liu, C., Rong, J., et al. (2019). Whole blood microRNA expression associated with stroke: results from the framingham heart study. *PLoS One* 14:e0219261. doi: 10.1371/journal.pone.0219261

Sepramaniam, S., Tan, J.-R., Tan, K.-S., DeSilva, D. A., Tavintharan, S., Woon, F.-P., et al. (2014). Circulating microRNAs as biomarkers of acute stroke. *Int. J. Mol. Sci.* 15, 1418–1432.

Shi, F.-P., Wang, X.-H., Zhang, H.-X., Shang, M.-M., Liu, X.-X., Sun, H.-M., et al. (2018). MiR-103 regulates the angiogenesis of ischemic stroke rats by targeting vascular endothelial growth factor (VEGF). *Iran. J. Basic Med. Sci.* 21, 318–324. doi: 10.22038/IJBMS.2018.27267.6657

Silva, C. I., Novais, P. C., Rodrigues, A. R., Carvalho, C. A. M., Colli, B. O., Carlotti, C. G. Jr., et al. (2017). Expression of NMDA receptor and microRNA-219 in rats submitted to cerebral ischemia associated with alcoholism. *Arquivos de Neuro-Psiquiatria* 75, 30–35. doi: 10.1590/0004-282X20160188

Sonoda, T., Matsuzaki, J., Yamamoto, Y., Sakurai, T., Aoki, Y., Takizawa, S., et al. (2019). Serum MicroRNA-Based risk prediction for stroke. *Stroke* 50, 1510–1518. doi: 10.1161/STROKEAHA.118.023648

Sørensen, S. S., Nygaard, A.-B., Carlsen, A. L., Heegaard, N. H. H., Bak, M., and Christensen, T. (2017). Elevation of brain-enriched miRNAs in cerebrospinal fluid of patients with acute ischemic stroke. *Biomarker Res.* 5:24. doi: 10.1186/s40364-017-0104-9

Spinetti, G., Fortunato, O., Caporali, A., Shantikumar, S., Marchetti, M., Meloni, M., et al. (2013). MicroRNA-15a and microRNA-16 impair human circulating proangiogenic cell functions and are increased in the proangiogenic cells and serum of patients with critical limb ischemia. *Circ. Res.* 112, 335–346. doi: 10.1161/CIRCRESAHA.111.300418

Suofu, Y., Wang, X., He, Y., Li, F., Zhang, Y., Carlisle, D. L., et al. (2020). Mir-155 knockout protects against ischemia/reperfusion-induced brain injury and hemorrhagic transformation. *NeuroReport* 31, 235–239. doi: 10.1097/WNR.0000000000001382

Tao, Z., Zhao, H., Wang, R., Liu, P., Yan, F., Zhang, C., et al. (2015). Neuroprotective effect of microRNA-99a against focal cerebral ischemia-reperfusion injury in mice. *J. Neurol. Sci.* 355, 113–119. doi: 10.1016/j.jns.2015.05.036

Tian, C., Li, Z., Yang, Z., Huang, Q., Liu, J., and Hong, B. (2016). Plasma MicroRNA-16 is a biomarker for diagnosis, stratification, and prognosis of hyperacute cerebral infarction. *PLoS One* 11:e0166688. doi: 10.1371/journal.pone.0166688

Tiedt, S., Prestel, M., Malik, R., Schieferdecker, N., Duering, M., Kautzky, V., et al. (2017). RNA-Seq identifies circulating miR-125a-5p, miR-125b-5p, and miR-143-3p as potential biomarkers for acute ischemic stroke. *Circ. Res.* 121, 970–980. doi: 10.1161/CIRCRESAHA.117.311572

van Kralingen, J. C., McFall, A., Ord, E. N. J., Coyle, T. F., Bissett, M., McClure, J. D., et al. (2019). Altered extracellular vesicle microRNA expression in ischemic stroke and small vessel disease. *Trans. Stroke Res.* 10, 495–508. doi: 10.1007/s12975-018-0682-3

Vijayan, M., Kumar, S., Yin, X., Zafer, D., Chanana, V., Cengiz, P., et al. (2018). Identification of novel circulatory microRNA signatures linked to patients with ischemic stroke. *Hum. Mol. Genet.* 27, 2318–2329. doi: 10.1093/hmg/ddy136

Wang, H., Zheng, X., Jin, J., Zheng, L., Guan, T., Huo, Y., et al. (2020a). LncRNA MALAT1 silencing protects against cerebral ischemia-reperfusion injury through miR-145 to regulate AQP4. *J. Biomed. Sci.* 27:40. doi: 10.1186/s12929-020-00635-0

Wang, J., Cao, B., Zhao, H., Gao, Y., Luo, Y., Chen, Y., et al. (2019a). Long noncoding RNA H19 prevents neurogenesis in ischemic stroke through p53/Notch1 pathway. *Brain Res. Bull.* 150, 111–117. doi: 10.1016/j.brainresbull.2019.05.009

Wang, J., Ruan, J., Zhu, M., Yang, J., Du, S., Xu, P., et al. (2019b). Predictive value of long noncoding RNA ZFAS1 in patients with ischemic stroke. *Clin. Exp. Hypertens* 41, 615–621. doi: 10.1080/10641963.2018.1529774

Wang, J., Zhao, H., Fan, Z., Li, G., Ma, Q., Tao, Z., et al. (2017). Long noncoding RNA H19 promotes neuroinflammation in ischemic stroke by driving histone deacetylase 1-Dependent M1 microglial polarization. *Stroke* 48, 2211–2221. doi: 10.1161/STROKEAHA.117.017387

Wang, W., Sun, G., Zhang, L., Shi, L., and Zeng, Y. (2014). Circulating microRNAs as novel potential biomarkers for early diagnosis of acute stroke in humans. *J. Stroke Cereb. Dis.* 23, 2607–2613. doi: 10.1016/j.jstrokecerebrovasdis.2014.06.002

Wang, X., Chen, S., Ni, J., Cheng, J., Jia, J., and Zhen, X. (2018). miRNA-3473b contributes to neuroinflammation following cerebral ischemia. *Cell Death Dis.* 9:11. doi: 10.1038/s41419-017-0014-7

Wang, Y., Luo, Y., Yao, Y., Ji, Y., Feng, L., Du, F., et al. (2020b). Silencing the lncRNA Maclpil in pro-inflammatory macrophages attenuates acute experimental ischemic stroke via LCP1 in mice. *J. Cereb. Blood Flow Metab.* 40, 747–759. doi: 10.1177/0271678X19836118

Wu, J., Du, K., and Lu, X. (2015). Elevated expressions of serum miR-15a, miR-16, and miR-17-5p are associated with acute ischemic stroke. *Int. J. Clin. Exp. Med.* 8, 21071–21079.

Wu, J., Fan, C. L., Ma, L. J., Liu, T., Wang, C., Song, J. X., et al. (2017). Distinctive expression signatures of serum microRNAs in ischaemic stroke and transient ischaemic attack patients. *Thrombosis Haemostasis* 117, 992–1001. doi: 10.1160/TH16-08-0606

Xiang, Y., Zhang, Y., Xia, Y., Zhao, H., Liu, A., and Chen, Y. (2020). LncRNA MEG3 targeting miR-424-5p via MAPK signaling pathway mediates neuronal apoptosis in ischemic stroke. *Aging* 12, 3156–3174. doi: 10.18632/aging.102790

Xiao, Z. H., Wang, L., Gan, P., He, J., Yan, B. C., and Ding, L. D. (2020). Dynamic changes in miR-126 expression in the hippocampus and penumbra following experimental transient global and focal cerebral ischemia–reperfusion. *Neurochem. Res.* 45, 1107–1119. doi: 10.1007/s11064-020-02986-4

Xu, X., Zhuang, C., and Chen, L. (2020). Exosomal long non-coding RNA expression from serum of patients with acute minor stroke. *Neuropsychiatric Dis. Treatment* 16:153. doi: 10.2147/NDT.S230332

Yang, J., Gu, L., Guo, X., Huang, J., Chen, Z., Huang, G., et al. (2018). LncRNA ANRIL expression and ANRIL gene polymorphisms contribute to the risk of ischemic stroke in the chinese han population. *Cell Mol. Neurobiol.* 38, 1253–1269. doi: 10.1007/s10571-018-0593-6

Yao, P., Li, Y.-L., Chen, Y., Shen, W., Wu, K.-Y., and Xu, W.-H. (2020). Overexpression of long non-coding RNA Rian attenuates cell apoptosis from cerebral ischemia-reperfusion injury via Rian/miR-144-3p/GATA3 signaling. *Gene* 737:144411. doi: 10.1016/j.gene.2020.144411

Yin, K.-J., Deng, Z., Huang, H., Hamblin, M., Xie, C., Zhang, J., et al. (2010). miR-497 regulates neuronal death in mouse brain after transient focal cerebral ischemia. *Neurobiol. Dis.* 38, 17–26. doi: 10.1016/j.nbd.2009.12.021

You, D., and You, H. (2019). Repression of long non-coding RNA MEG3 restores nerve growth and alleviates neurological impairment after cerebral ischemia-reperfusion injury in a rat model. *Biomed. Pharmacotherapy* 111, 1447–1457. doi: 10.1016/j.biopha.2018.12.067

Zeng, W., and Jin, J. (2020). The correlation of serum long non-coding RNA ANRIL with risk factors, functional outcome, and prognosis in atrial fibrillation patients with ischemic stroke. *J. Clin. Lab. Anal.* 34:e23352. doi: 10.1002/jcla.23352

Zhan, R., Xu, K., Pan, J., Xu, Q., Xu, S., and Shen, J. (2017). Long noncoding RNA MEG3 mediated angiogenesis after cerebral infarction through regulating p53/NOX4 axis. *Biochem. Biophys. Res. Commun.* 490, 700–706. doi: 10.1016/j.bbrc.2017.06.104

Zhang, B., Wang, D., Ji, T.-F., Shi, L., and Yu, J.-L. (2017a). Overexpression of lncRNA ANRIL up-regulates VEGF expression and promotes angiogenesis of diabetes mellitus combined with cerebral infarction by activating NF-κB signaling pathway in a rat model. *Oncotarget* 8, 17347–17359. doi: 10.18632/oncotarget.14468

Zhang, X., Tang, X., Liu, K., Hamblin, M. H., and Yin, K.-J. (2017b). Long noncoding RNA Malat1 regulates cerebrovascular pathologies in ischemic stroke. *J. Neurosci.* 37, 1797–1806. doi: 10.1523/jneurosci.3389-16.2017

Zhanin, I. S., Gusar, V. A., Timofeeva, A. T., Pinelis, V. G., and Asanov, A. Y. (2018). MicroRNA expression profile in patients in the early stages of ischemic stroke. *Neurol. Neuropsychiatry Psychosomat.* 10, 72–78. doi: 10.1016/j.jpsychires.2019.05.018

Zhao, H., Wang, J., Gao, L., Wang, R., Liu, X., Gao, Z., et al. (2013). MiRNA-424 protects against permanent focal cerebral ischemia injury in mice involving suppressing microglia activation. *Stroke* 44, 1706–1713. doi: 10.1161/STROKEAHA.111.000504

Zheng, L., Cheng, W., Wang, X., Yang, Z., Zhou, X., and Pan, C. (2017). Overexpression of MicroRNA-145 ameliorates astrocyte injury by targeting aquaporin 4 in cerebral ischemic stroke. *BioMed. Res. Int.* 2017:9530951. doi: 10.1155/2017/9530951

Zheng, Z., Liu, S., Wang, C., and Han, X. (2018). A functional polymorphism rs145204276 in the promoter of long noncoding RNA GAS5 is associated with an increased risk of ischemic stroke. *J. Stroke Cereb. Dis.* 27, 3535–3541. doi: 10.1016/j.jstrokecerebrovasdis.2018.08.016

Zhu, M., Li, N., Luo, P., Jing, W., Wen, X., Liang, C., et al. (2018). Peripheral blood leukocyte expression of lncRNA MIAT and its diagnostic and prognostic value in ischemic stroke. *J. Stroke Cereb. Dis.* 27, 326–337. doi: 10.1016/j.jstrokecerebrovasdis.2017.09.009

Zhu, W., Tian, L., Yue, X., Liu, J., Fu, Y., and Yan, Y. (2019). LncRNA expression profiling of ischemic stroke during the transition from the acute to subacute stage. *Front. Neurol.* 10:36. doi: 10.3389/fneur.2019.00036

Zuo, M.-L., Wang, A.-P., Song, G.-L., and Yang, Z.-B. (2020). miR-652 protects rats from cerebral ischemia/reperfusion oxidative stress injury by directly targeting NOX2. *Biomed. Pharmacotherapy.* 124:109860. doi: 10.1016/j.biopha.2020.109860

Conflict of Interest: The authors declare that the research was conducted in the absence of any commercial or financial relationships that could be construed as a potential conflict of interest.

The reviewer RE declared a shared affiliation with several of the authors, SG-F, ZS-F, and NA, to the handling editor at the time of the review.

Publisher's Note: All claims expressed in this article are solely those of the authors and do not necessarily represent those of their affiliated organizations, or those of the publisher, the editors and the reviewers. Any product that may be evaluated in this article, or claim that may be made by its manufacturer, is not guaranteed or endorsed by the publisher.

frontiers in Aging Neuroscience

REVIEW
published: 06 December 2021
doi: 10.3389/fnagi.2021.772036

An Update on Antioxidative Stress Therapy Research for Early Brain Injury After Subarachnoid Hemorrhage

Fa Lin[1,2,3,4†], *Runting Li*[1,2,3,4†], *Wen-Jun Tu*[1,5,6], *Yu Chen*[1,2,3,4], *Ke Wang*[1,2,3,4], *Xiaolin Chen*[1,2,3,4*] *and Jizong Zhao*[1,2,3,4,7*]

[1] Department of Neurosurgery, Beijing Tiantan Hospital, Capital Medical University, Beijing, China, [2] China National Clinical Research Center for Neurological Diseases, Beijing, China, [3] Center of Stroke, Beijing Institute for Brain Disorders, Beijing, China, [4] Beijing Key Laboratory of Translational Medicine for Cerebrovascular Disease, Beijing, China, [5] The General Office of Stroke Prevention Project Committee, National Health Commission of the People's Republic of China, Beijing, China, [6] Institute of Radiation Medicine, Chinese Academy of Medical Sciences, Peking Union Medical College, Tianjin, China, [7] Savaid Medical School, University of Chinese Academy of Sciences, Beijing, China

OPEN ACCESS

Edited by:
Li Li,
Capital Medical University, China

Reviewed by:
Christian Scheiwe,
University Hospital Freiburg, Germany
Ming Feng,
Peking Union Medical College Hospital (CAMS), China
Zongjian Liu,
Capital Medical University, China

***Correspondence:**
Xiaolin Chen
cxl_bjtth@163.com
Jizong Zhao
zhaojizong@bjtth.org

[†] *These authors have contributed equally to this work*

Specialty section:
This article was submitted to Cellular and Molecular Mechanisms of Brain-Aging, a section of the journal Frontiers in Aging Neuroscience

Received: *07 September 2021*
Accepted: *08 November 2021*
Published: *06 December 2021*

Citation:
Lin F, Li R, Tu W-J, Chen Y, Wang K, Chen X and Zhao J (2021) An Update on Antioxidative Stress Therapy Research for Early Brain Injury After Subarachnoid Hemorrhage. Front. Aging Neurosci. 13:772036. doi: 10.3389/fnagi.2021.772036

The main reasons for disability and death in aneurysmal subarachnoid hemorrhage (aSAH) may be early brain injury (EBI) and delayed cerebral ischemia (DCI). Despite studies reporting and progressing when DCI is well-treated clinically, the prognosis is not well-improved. According to the present situation, we regard EBI as the main target of future studies, and one of the key phenotype-oxidative stresses may be called for attention in EBI after laboratory subarachnoid hemorrhage (SAH). We summarized the research progress and updated the literature that has been published about the relationship between experimental and clinical SAH-induced EBI and oxidative stress (OS) in PubMed from January 2016 to June 2021. Many signaling pathways are related to the mechanism of OS in EBI after SAH. Several antioxidative stress drugs were studied and showed a protective response against EBI after SAH. The systematical study of antioxidative stress in EBI after laboratory and clinical SAH may supply us with new therapies about SAH.

Keywords: oxidative stress, subarachnoid hemorrhage, early brain injury, delayed cerebral ischemia, experimental – animal models

INTRODUCTION

Aneurysmal subarachnoid hemorrhage (aSAH) is a devastating disease, mainly induced by the rupture of an intracranial aneurysm and linked to high levels of morbidity and mortality (Bor et al., 2008; Connolly et al., 2012; Macdonald and Schweizer, 2017; Chao et al., 2021). Although we have progressed in treatment, 40% of aSAH survivors remain dependent as a consequence of neurological disability and behavioral and cognitive impairments (Brathwaite and Macdonald, 2014; Etminan and Macdonald, 2017). Clinical studies have shown that cerebral vasospasm (CVS) is not the single contributor to delayed cerebral ischemia (DCI) and poor prognosis in patients with aSAH (Naraoka et al., 2018; Mayer et al., 2019; Schupper et al., 2020; Post et al., 2021; Takeuchi et al., 2021). At present, amassing laboratory evidence demonstrates that early brain injury (EBI), which happens within 72 h after aSAH, causes subsequently pathophysiological changes and poor

outcomes (Kusaka et al., 2004). The pathological changes and mechanisms of EBI collectively contain increased intracranial pressure (ICP), oxidative stress (OS), neuroinflammation, blood–brain barrier (BBB) disruption, brain edema, and cell death. Among them, the OS responses include a wide variety of active and inactive substances, which play a substantial role in EBI after aSAH and may be associated with DCI and long-term outcomes (Cahill et al., 2006; Rowland et al., 2012; Sehba et al., 2012; Shao et al., 2020). Therefore, we should pay more attention to strategies targeting cerebral redox responses to some extent. In this review, we update the impact of OS in the occurrence and development of SAH and several major oxidative pathways and biomarkers related to EBI after SAH. Additionally, we also take an overlook for the potential therapeutic drugs.

Although widely accepted than other pathogenic mechanisms, DCI has not reached further improvement clinically. By the same token, the failure of clazosentan, despite mitigating moderate and severe vasospasm, has shifted the focus of preclinical and clinical research from DCI to EBI toward a more multifactorial etiology in recent times (Macdonald et al., 2008, 2011; Cahill and Zhang, 2009; Caner et al., 2012).

MECHANISMS OF EARLY BRAIN INJURY

The topic raised in 2004, EBI is a designation that refers to the damage occurring to the brain in the first 72 h ensuing the initial aneurysmal bleeding and preceding vasospasm, including the primary injury and its direct consequences (Kusaka et al., 2004). The mechanisms resulting in EBI after aSAH are multifactorial and complicated. Conventionally, they are partitioned into the following parts (Rowland et al., 2012): (1) mechanical: acute or chronic hydrocephalus (Asada et al., 2021; Toyota et al., 2021); (2) physiological: raised ICP, decreased cerebral perfusion pressure (CPP) and cerebral blood flow (CBF), impaired cerebral autoregulation (CA), vasoconstriction, global ischemia, and delayed edema; (3) ionic: impaired ionic homeostasis, Ca^{2++} overload, K^{+} efflux, and cortical spreading depression (CSD); (4) inflammatory: NO (nitric oxide)/NOS (nitric oxide synthase) pathway activation, endothelin-1 (ET-1) release, platelet activation; and (5) cell death: endothelial cells, neurons, and astrocytes.

Aside from the aforementioned classical mechanisms, atypical mechanisms are newly proposed. Diverse factors, such as micro-spasm rather than macro-spasm (Fumoto et al., 2019), microthrombosis (Fumoto et al., 2019), early cortical infarction (Hartings et al., 2017; Eriksen et al., 2019), white matter injury (WMI) (Wu Y. et al., 2017; Pang et al., 2019; Peng et al., 2019; Ru et al., 2021), endoplasmic reticulum (ER) stress (Xie et al., 2019; Xu et al., 2019; Xiong et al., 2020), and immune inflammation (Ju et al., 2020; Rubio-Perez et al., 2021; Zeyu et al., 2021), are involved in cell death-relevant mechanisms in EBI after aSAH. Admittedly, various mechanisms or contributors to early injury will consequently result in cell death of the catastrophic ictus. Nowadays, the cell death processes in study include apoptosis, necrosis, autophagy (Dou et al., 2017; Sun C. et al., 2019; Sun C. M. et al., 2019), necroptosis (Kooijman et al., 2014; Chen et al., 2017, 2018, 2019; Xie et al., 2017; Yang C. et al., 2018; Yuan et al., 2019; Fang et al., 2020; Xu H. et al., 2021), pyroptosis (Yuan et al., 2020; Xu P. et al., 2021; Zhang C. S. et al., 2021), and ferroptosis (Lee et al., 2010; Zhao et al., 2018; Fang et al., 2020; Sq et al., 2020; Cao et al., 2021; Li et al., 2021; Qu et al., 2021). All but the former two well-known cell death mechanisms remain novel types and cutting-edge hot topics. For example, autophagy is an important protective mechanism against apoptosis, and recombinant osteopontin (rOPN) inhibits neuronal apoptosis by activating autophagy and regulating autophagy-apoptosis interactions (Sun C. M. et al., 2019). Necroptosis, a caspase-independent mechanism, plays a crucial part in the pathophysiological process by reducing the number of abnormal cells in brain tissue. Recently, SAH-induced synaptic impairments mitigated by NEC-1 in the hippocampus that inhibits necroptosis in relation to the CREB-BDNF pathway were verified (Yang C. et al., 2018). Moreover, another type of cell death, SAH-induced neuronal pyroptosis, is ameliorated in part by postconditioning with hydrogen gas through the mitoK_{ATP}/ERK1/2/p38 MAPK signaling pathway (Zhang C. S. et al., 2021). Unlike other types of cell death, such as necrosis and apoptosis, ferroptosis is a regulated process caused by an imbalance of the redox system. Cell death results in damaged structure and function of vessels and nerves, causing ultimately post-SAH dysfunction.

Typically, the elementary changes after SAH can be segmented into two periods: EBI and DCI. Pathological changes occurring in the initial stage of hemorrhage propagate and lead to inflammation, OS, and apoptosis. Studies showed that OS plays a key role in the pathogenesis of EBI after SAH.

OXIDATIVE STRESS IN SUBARACHNOID HEMORRHAGE

Although progress is made in cell death, the actual pathogenesis of EBI after SAH is still rarely understood. Several pieces of research demonstrate that OS is one of the basic drivers of EBI (Zhang et al., 2016c; Fumoto et al., 2019).

Relying on the activity of the producer and removal systems, OS has its yin and yang faces, but those covered in this review are the result of the dysregulation of reduction-oxidation (redox) reactions. Sies and Jones (2020) also defined the elevated constitution of various reactive oxygen species (ROS) resulting in all classes of molecular damage as "oxidative distress." OS, a relative extra of ROS compared with antioxidants, has been associated with cardiovascular, neurodegenerative, and many other diseases. ROS is an overall term for derivatives of dioxygen not chemically precise, which serve as a normal character of aerobic life. Hydrogen peroxide (H_2O_2) and the $O_2^{\bullet -}$ are pivotal agents produced by greater than 40 enzymes (Murphy, 2009; Go et al., 2015). Additionally, many other reactive categories are contained in redox signaling, for example, hydrogen sulfide and oxidized lipids (Fujii et al., 2010; Yu et al., 2014; Jarocka-Karpowicz et al., 2020).

After SAH, exhibiting aberrant redox hemostasis, the production of oxidants mainly comes from the disruption of

mitochondria (Yan et al., 2015; Fan et al., 2021; Xu W. et al., 2021), extravascular hemolyzed blood (Vecchione et al., 2009; Deng et al., 2018), and enzymatic sources of free radicals (Sies et al., 2017; Yang et al., 2017; Sies and Jones, 2020). Intrinsic antioxidant activity can be exhausted by excessive free radicals, resulting in lipid peroxidation, protein breakdown, and DNA damage. Mention must be made that beyond the biology of H_2O_2 and $O_2^{\bullet -}$, a significant area of ROS research is lipid-derived ROS. Oxidative DNA damage has also been widely distinguished by mutagenesis, DNA methylation, and chromatin structure. Although substantiation is also gathered about oxidative damage to RNA, the underlying functional effect has not yet been fully illustrated.

OXIDATIVE STRESS IN EARLY BRAIN INJURY

For decades, the treatment of CVS and DCI has always been the focus of clinical practice. However, mounting evidence showed that even angiographic vasospasm is reversed, and clinical outcomes remain frustrating (Macdonald et al., 2008; Gomis et al., 2010). So far, nimodipine remains the only medication proven to lessen DCI and unfavorable outcomes. Therefore, new therapeutic regimens are promising (Hänggi et al., 2015).

Previously, the aspecific erasure of ROS using antioxidant compounds was unsuccessful in offsetting SAH initiation. However, regulating specific ROS-mediated signaling pathways offers a viewpoint, mainly containing enzymatic defense systems like those regulated by the nuclear factor erythroid 2 (NF-E2)-related factor 2 (Nrf2) (Zolnourian et al., 2019; Sies and Jones, 2020) and PI3K/Akt, the role of key molecules such as melatonin, sirtuins, and hydrogen sulfide, and the modifiable factors that are corporately thought as the exposome [by way of illustration, nutrition (Liu et al., 2015), lifestyle, and irradiation] (see overview in **Table 1** and **Figure 1**). Discovering strategies for effectively detoxifying free radicals has become a theme of great interest from both practical and academic viewpoints.

KEAP1-NRF2-ARE Pathway

An important "sensors" protein that captures specific metabolic information after SAH and transforms it into an appropriate response is Kelch-like ECH-associated protein 1 (Keap1), which contains reactive cysteine residues that collectively respond to ROS resulting from heme. Covalent modification of Keap1 leads to reduce ubiquitination and accumulates Nrf2 (Bollong et al., 2018). It is combined with a given DNA site, the antioxidant response element, modulating the transcription of a series of antioxidant enzymes (Zolnourian et al., 2019). Lots of researches on stroke models have substantiated that Nrf2 levels lift soon after the stroke. It first appears within 3 h and peaks within 24 h post insult, with the peri-infarct area markedly increasing (Yang et al., 2009; Tanaka et al., 2011). The study indicated that Nrf2 expression is significantly activated in neurons, astrocytes, leukocytes, microglia, endothelin cells, smooth muscle cells, and adventitial cells after SAH-induced brain insult (Wang et al., 2010). Wang et al., found that the Nrf2-ARE pathway is upregulated in rat models with experimental SAH in the time course at 12, 24, and 48 h (Chen et al., 2011). Since then, lots of known activators of the Keap1-Nrf2-ARE pathway were overwhelmingly carried out in the study. Although controversial conclusions are sometimes achieved due to pleiotropic and primary mechanisms, more effective inducers with less crossing activation of other pathways are identified and reach favorable outcomes.

In addition to the agents summarized by former researchers, such as sulforaphane, astaxanthin, curcumin, lycopene, tetrabutyl hydroquinone, dimethyl fumarate, melatonin, and erythropoietin, there are also many other experimental studies conducted more recently. Efforts to target the Nrf2 signaling pathway therapeutically have largely focused on covalent small molecule agonists of Keap1. Mitoquinone (MitoQ), effective in the prevention of mitochondrial dysfunction, restrained OS-related neuronal death by stimulating mitophagy through Keap1/Nrf2/PHB2 pathway after SAH in rats (Zhang T. et al., 2019). In the endovascular perforation mice SAH model, MitoQ treatment reduced OS, both short term and long term. Another activator of Nrf2, RTA 408, a new second-generation semisynthetic oleanane triterpenoid, manifested an antioxidant and anti-inflammatory phenotype (Reisman et al., 2014). After administrated intraperitoneally, vasospasm was reversed by RTA 408 through growth in Nrf2 and reduction in NF-κB (Tsai et al., 2020).

Intriguingly, performing as a downstream molecule in the Keap1-Nrf2-ARE pathway, heme oxygenase-1 (HO-1), also known as HSP32, could be induced by upregulating expression of Nrf2 (Wang and Doré, 2007; Jiang et al., 2020). After SAH, vasospasm and lipid peroxidation can be weakened by HO-1 through the improvement of clearance. Post-hemorrhagic administration of Nrf2 activator, tetramethylpyrazine nitrone (Wu et al., 2019), aloperine (Song et al., 2018), milk fat globule-epidermal growth factor 8 (MFGE8) (Liu et al., 2014, 2015), tumor necrosis factor-alpha stimulated gene-6 (Li et al., 2020), ursolic acid (UA) (Zhang et al., 2014a,b; Ding et al., 2017), gastrodin (Wang et al., 2019), tert-Butylhydroquinone (Wang et al., 2014), promotes posttranscriptional augment of both Nrf2 and HO-1, attenuates OS, and then reduces early brain damage, including brain edema, BBB damage, and cognitive impairment following SAH in animal models. Moreover, an additional NRF family member, namely, Nrf1 (Qian et al., 2019), responsible for ROS detoxification, participates in an effective treatment to moderate SAH-elicited EBI. Researchers concluded that HSP22 played a part in neuroprotective effects by regulating TFAM/Nrf1-triggered mitochondrial biogenesis with positive feedback, further attenuating OS and EBI (Fan et al., 2021).

Mitochondrial Pathways

Shortly after the induction of SAH, EBI triggers mitochondrial disorder, in which many signaling molecules communicate with each other to control OS (Prentice et al., 2015). Thus, another pivotal key in alleviating EBI is discovering new options to keep normal mitochondrial activity by attenuating OS. The mechanisms for ROS generated by mitochondria are

TABLE 1 | Clinical and experimental studies overview of OS in EBI after SAH.

	Method/animal	Numbers (all/groups)	Drug/agent	Pathway	Effect	References
KEAP1-NRF2-ARE pathway	Injection/rat	30/2	–	Nrf2-ARE	Nrf2 expression is upregulated in the cerebral artery of rats after experimental SAH	Wang et al., 2010
	Injection/rat	72/4	Sulforaphane	Nrf2-ARE	Nrf2-ARE pathway is activated in the brain after SAH, playing a beneficial role in EBI development, possibly through inhibiting cerebral oxidative stress by inducing antioxidant and detoxifying enzymes	Chen et al., 2011
	Perforation/rat	163/5	MitoQ/ML385	Keap1/Nrf2/PHB2	MitoQ inhibited oxidative stress related neuronal death by activating mitophagy via Keap1/Nrf2/PHB2 pathway	Zhang T. et al., 2019
	Injection/rat	60/5	RTA 408	Nrf2 and NF-κB	RTA 408 attenuated SAH-induced vasospasm through its reversal of SAH-induced changes in Nrf2, NF-κB, and iNOS	Tsai et al., 2020
	Injection/rabbit Perforation /rabbit	40/6	Tetramethyl-pyrazine nitrone (TBN)	Nrf2/HO-1	TBN ameliorated SAH-induced cerebral vasospasm and neuronal damage, attributed to its anti-oxidative stress effect and upregulation of Nrf2/HO-1	Wu et al., 2019
	Injection/rat	150/5	Aloperine (ALO)	Nrf2-ARE	ALO can ameliorate oxidative damage against EBI following SAH, most likely via the Nrf2-ARE survival pathway	Song et al., 2018
	Perforation/rat	210/4	Recombinant MFGE8	Integrinβ3/Nrf2/HO	Recombinant MFGE8 attenuated oxidative stress that may be mediated by integrin β3/nuclear factor erythroid 2–related factor 2/HO pathway after SAH	Liu et al., 2014
	Perforation/rat	221/4	TSG-6	NF-κB and HO-1	TSG-6 attenuated oxidative stress and apoptosis in EBI after SAH partly by inhibiting NF-κB and activating HO-1 pathway in brain tissue	Li et al., 2020
	Perforation/rat	96/4	Ursolic acid	TLR4/NF-κB	UA alleviated EBI by its anti-inflammatory properties, and the therapeutic benefit of post-SAH UA administration is due to its effect on inhibiting the activation of the TLR4/NF-κB signaling pathway	Zhang et al., 2014a
	Perforation/rat	132/3	Gastrodin	Nrf2/HO-1	The administration of gastrodin provides neuroprotection against early brain injury after experimental SAH	Wang et al., 2019
	Injection/rat	160/4	tert-Butylhy-droquinone (tBHQ)	Keap1/Nrf2/ARE	The administration of tBHQ abated the development of EBI and cognitive dysfunction in this SAH model for activation of the Keap1/Nrf2/ARE pathway	Wang et al., 2014
Mitochondrial pathway	Perforation/rat	76/4	–	–	Enhanced autophagy plays a protective role in early brain injury after SAH	Jing et al., 2012
	Perforation/rat	93/5	TT01001	–	mitoNEET activation with TT01001 reduced oxidative stress injury and neuronal apoptosis by improving mitochondrial dysfunction in EBI after SAH	Shi et al., 2020
	Perforation/rat	132/5	Docosahexaenoic acid	–	Prevent oxidative stress-based apoptosis after SAH, further improve mitochondrial dynamics-related signaling pathways	Zhang T. et al., 2018
	Perforation/rat	135/8	Resolvin D2	RvD2/GPR18	Upregulating GPR18 by RvD2 may improve neurological functions in different brain regions via multiple mechanisms	Zhang T. et al., 2021

(Continued)

TABLE 1 | (Continued)

	Method/animal	Numbers (all/groups)	Drug/agent	Pathway	Effect	References
	Perforation/rat	238/4	Lipoxin A4 (LXA4)	FPR2/p38	Exogenous LXA4 inhibited inflammation by activating FPR2 and inhibiting p38 after SAH	Guo et al., 2016
	Perforation/rat	32/4	Naringin	MAPK	Reduced the oxidant damage and apoptosis by inhibiting the activation of MAPK signaling pathway	Han et al., 2017a
	Injection/rat	232/4	Peroxiredoxin 1/2	ASK1/p38	Early expression of Prx1/2 may protect the brain from oxidative damage after SAH and may provide a novel target for treating SAH	Lu et al., 2019
	Perforation/rat	275/3	Mdivi-1	PERK/eIF2α/CHOP	Inhibition of Drp1 by Mdivi-1 attenuated early brain injury after SAH probably via the suppression of inflammation-related blood–brain barrier disruption and endoplasmic reticulum stress-based apoptosis	Fan et al., 2017
	Injection/rat	192/4	SS31	Mitochondrial apoptotic	SS31 could alleviate EBI after SAH through its antioxidant property and ability in inhibiting neuronal apoptosis, likely by modulating the mitochondrial apoptotic pathway	Shen et al., 2020
Other Pathway	Perforation/rat	165/10	ReOX40	OX40-OX40L/PI3K/AKT	ReOX40 attenuates neuronal apoptosis through OX40-OX40L/PI3K/AKT pathway in EBI after SAH	Wu et al., 2020
	Perforation/rat	249/5	Aggf1	PI3K/Akt/NF-κB	Exogenous Aggf1 treatment attenuated neuroinflammation and BBB disruption, improved neurological deficits after SAH in rats, at least in part through the PI3K/Akt/NF-κB pathway	Zhu et al., 2018
	Perforation/rat	196/11	Kisspeptin-54 (KP54)	GPR54/ARRB2/AKT/GSK3β	Administration of KP54 attenuated oxidative stress, neuronal apoptosis and neurobehavioral impairments through GPR54/ARRB2/AKT/GSK3β signaling pathway after SAH in rat	Huang et al., 2021
	Perforation/mouse	168/4	Apolipoprotein E	JAK2/STAT3/NOX2	apoE and apoE-mimetic peptide have whole-brain protective effects that may reduce EBI after SAH via M1 microglial quiescence	Pang et al., 2018
	Injection/rat	32/4	SC79	Iron accumulation	Disrupted iron homeostasis could contribute to EBI and Akt activation may regulate iron metabolism to relieve iron toxicity, further protecting neurons from EBI after SAH	Hao et al., 2016
	Injection/rat	319/4	SC79	Akt/GSK3β	SC79 exerts its neuroprotective effect likely through the dual activities of anti-oxidation and antiapoptosis	Zhang et al., 2016a
	Perforation/rat	84/4	Scutellarin (SCU)	Erk5-KLF2-eNOS	SCU could attenuate vasospasm and neurological deficits via modulating the Erk5-KLF2-eNOS pathway after SAH	Li Q. et al., 2016
	Injection/rat	120/3	Purmorphamine (PUR)	Sonic hedgehog	PUR exerts neuroprotection against SAH-evoked injury in rats, mediated in part by antiapoptotic and antioxidant mechanism, upregulating phospho-ERK levels, mediating Shh signaling molecules in the PFC	Hu et al., 2016
	Perforation/rat	199/5	TGR5/INT-777	cAMP/PKCε/ALDH2	The activation of TGR5 with INT-777 attenuated oxidative stress and neuronal apoptosis via the cAMP/PKCε/ALDH2 signaling pathway	Zuo G. et al., 2019
	Perforation/rat	196/5	AVE 0991	Mas/PKA/p-CREB/UCP-2	Mas activation with AVE reduces oxidative stress injury and neuronal apoptosis through Mas/PKA/p-CREB/UCP-2 pathway after SAH	Mo et al., 2019

(Continued)

TABLE 1 | (Continued)

	Method/animal	Numbers (all/groups)	Drug/agent	Pathway	Effect	References
Melatonin	Injection/rabbit	48/4	Melatonin	–	Post-SAH melatonin administration may attenuate inflammatory response and oxidative stress in the spasmodic artery	Fang et al., 2009
	Human	169/2	Melatonin	–	Patients with higher serum melatonin concentrations are more likely to have a poor prognosis	Zhan et al., 2021
	Perforation/mouse	–/3	Melatonin	Sirt3/SOD2 and Bax/Bcl-2/CC3	Melatonin provided protection from the effects of EBI following SAH by regulating the expression of murine SIRT3	Yang S. et al., 2018
	Perforation/mouse	–/3	Melatonin	NRF2 and mitophagy	By increasing the expression of NRF2, the mitophagy induced by melatonin provided protection against brain injury post-SAH	Sun et al., 2018
	Injection/rat	72/4	Melatonin	Nrf2-ARE	Through activating Nrf2-ARE pathway and modulating cerebral oxidative stress by inducing antioxidant and detoxifying enzymes	Wang et al., 2012
	Injection/rat	80/4	Melatonin	TLR4	Post-SAH melatonin administration might be due to its salutary effect on modulating TLR4 signaling pathway	Dong et al., 2016
	Perforation/rat	56/3	Melatonin	Mitochondrial	The mechanism of these antiapoptosis effects was related to the enhancement of autophagy, which ameliorated cell apoptosis via a mitochondrial pathway	Chen et al., 2014b
	Perforation/rat	77/3	Melatonin	Tight junction and pro-inflammatory	Melatonin prevents disruption of tight junction proteins which might play a role in attenuating brain edema secondary to BBB dysfunctions by repressing the inflammatory response in EBI after SAH	Chen et al., 2014a
Sirtuins	Injection/rat	262/4	Activator 3	SIRT1	SIRT1 plays an important role in endogenous neuroprotection by deacetylation and subsequent inhibition of FoxOs-, NF-κ B-, and p53-induced oxidative, inflammatory and apoptotic pathways	Zhang et al., 2016
	Injection/rat Injection/mouse	422/8	Astaxanthin (ATX)	SIRT1/TLR4	ATX treatment inhibits TLR4-mediated inflammatory injury by increasing SIRT1 expression after SAH	Zhang X. et al., 2019
	Injection/rat	96/4	Astaxanthin (ATX)	Nrf2-ARE	ATX treatment alleviated EBI in SAH model, possibly through activating the Nrf2-ARE pathway by inducing antioxidant and detoxifying enzymes	Wu et al., 2014
	Injection/rat Injection/rabbit	325/8 20/4	Astaxanthin (ATX)	–	ATX administration could alleviate EBI after SAH, potentially through its powerful antioxidant property	Zhang et al., 2014
	Injection/rat Injection /mouse	213/5 –	Fucoxanthin (Fx)/EX527	Sirt1	Fx provided protection against SAH-induced oxidative insults by inducing Sirt1 signaling	Zhang X. S. et al., 2020
	Injection/rat Injection /mouse	159/6 57/2	Salvianolic acid B	SIRT1 and Nrf2	SalB provides protection against SAH-triggered oxidative damage by upregulating the Nrf2 antioxidant signaling pathway, which may be modulated by SIRT1 activation	Zhang X. et al., 2018
	Perforation/rat	68/4	Salvianolic acid A	ERK/P38/Nrf2	SalA also modulated Nrf2 signaling, and the phosphorylation of ERK and P38 MAPK signaling in SAH rats	Gu et al., 2017
	Injection /mouse	132/4	LV-shPGC-1a	PGC-1a/SIRT3	The detrimental PGC-1a/SIRT3 pathway, involving regulation of the endogenous antioxidant activity against neuronal damage	Zhang K. et al., 2020
	Perforation/rat	200/5	Bexarotene	PPARγ/SIRT6/FoxO3a	The anti-neuroinflammatory effect was at least partially through regulating PPARγ/SIRT6/FoxO3a pathway	Zuo Y. et al., 2019

(Continued)

TABLE 1 | (Continued)

	Method/animal	Numbers (all/groups)	Drug/agent	Pathway	Effect	References
Hydrogen sulfide	Injection/rat	96/4	Hydrogen sulfide	–	NaSH as an exogenous H_2S donor could significantly reduce EBI induced by SAH	Cui et al., 2016
	Injection/rat	134/5	L-cysteine	CBS/H_2S	L-cysteine may play a neuroprotective role in SAH by inhibiting cell apoptosis, upregulating CREB-BDNF expression, and promoting synaptic structure via the CBS/H_2S pathway	Li et al., 2017
	Perforation/rat	35/3	Hydrogen gas	–	The first report demonstrating that high dose hydrogen gas therapy reduces mortality and improves outcome after SAH	Camara et al., 2019
	Perforation/rat	182/5	Hydrogen gas	ROS/NLRP3	Hydrogen inhalation can ameliorate oxidative stress related endothelial cells injury in the brain and improve neurobehavioral outcomes in rats following SAH related to the inhibition of activation of ROS/NLRP3 axis	Zhuang et al., 2019
	Injection/rabbit	72/4	Hydrogen-rich saline (HS)	–	Treatment with hydrogen in experimental SAH rabbits could alleviate brain injury via decreasing the oxidative stress injury and brain edema	Zhuang et al., 2012
	Perforation/rat	129/4	Hydrogen-rich saline (HS)	NF-κB	HS may inhibit inflammation in EBI and improve neurobehavioral outcome after SAH, partially via inactivation of NF-κB pathway and NLRP3 inflammasome	Shao et al., 2016
	Injection/rat	244/8	Sodium/hydrogen exchanger 1 (NHE1)	–	NHE1 participates in EBI induced by SAH through mediating inflammation, oxidative stress, behavioral and cognitive dysfunction, BBB injury, brain edema, and promoting neuronal degeneration and apoptosis	Song et al., 2019
	Perforation/mouse	–/5	CO	–	First report to demonstrate that CO minimizes delayed SAH-induced neurobehavioral deficits	Kamat et al., 2019
Modifiable factors	Injection/rat	120/5	Gp91ds-tat/GKT137831/apocynin	–	Nox4 should contribute to the pathological processes in SAH-induced EBI, and there was not an overlay effect of Nox2 inhibition and Nox4 inhibition on preventing SAH-induced EBI	Zhang L. et al., 2017
	Injection/rabbit	40/5	Telmisartan	Trx/TrxR	Downregulation of TXNIP and upregulation of Trx/TrxR	Erdi et al., 2016
	Injection/rat	24/3	Verapamil	Antioxidant and antiapoptotic	Intrathecal verapamil can prevent vasospasm, oxidative stress, and apoptosis after experimental subarachnoid hemorrhage	Akkaya et al., 2019
	Perforation/rat	21/3	3,4-dihydroxyphenylethanol (DOPET)	–	Free radical scavenging capacity	Zhong et al., 2016
	Perforation/rat	40/4	3,4-dihydroxyphenylethanol (DOPET)	Akt and NF-κB	DOPET attenuates apoptosis in a rat SAH model through modulating oxidative stress and Akt and NF-κB signaling pathways	Fu and Hu, 2016
	Perforation/rat	80/4	Propofol/LY294002	PI3K/Akt	Propofol attenuates SAH-induced EBI by inhibiting inflammatory reaction and oxidative stress, which might be associated with the activation of PI3K/Akt signaling pathway	Zhang H. B. et al., 2019
	Perforation/rat	248/10	Wnt-3a	Frz-1/aldolase C/PPAN	Intranasal administration of wnt-3a alleviates neuronal apoptosis through Frz-1/aldolase C/PPAN pathway in the EBI of SAH rats	Ruan et al., 2020
	Perforation/rat	48/3	Preconditioning exercise	Nrf2/HO-1 14–3-3γ/p-β-catenin Ser37/Bax/caspase-3	Preconditioning exercise ameliorates EBI after SAH	Otsuka et al., 2021

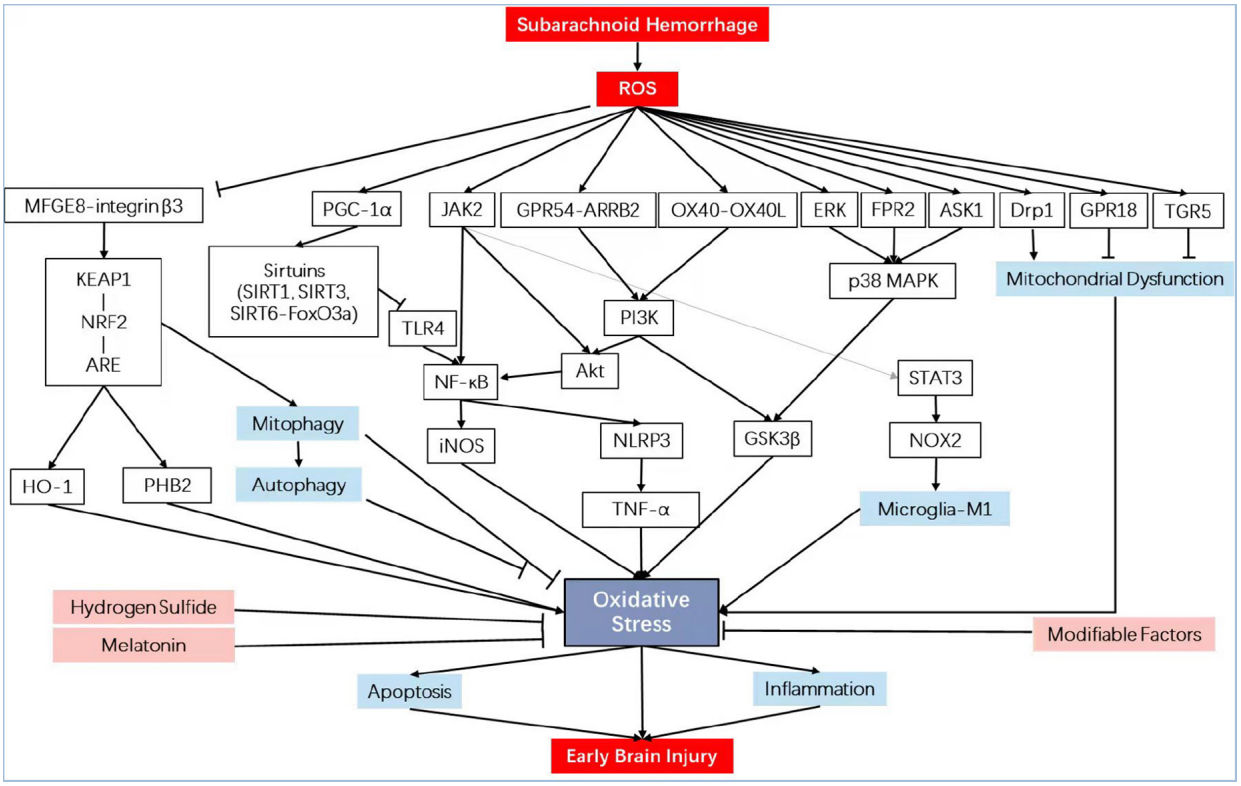

FIGURE 1 | Schematic diagram illustrating the signaling pathways involved in oxidative stress in early brain injury. iNOS, inducible nitric oxide synthase; PHB2, prohibitin 2; NRF2, nuclear factor erythroid 2-related factor 2; HO-1, heme oxygenase-1; NF-κB, nuclear factor kappa-B; KEAP1, Kelch-like epichlorohydrin-associated protein 1; ARE, antioxidant response element; MFGE8, milk fat globule–EGF factor-8; TLR4, toll-like receptor 4; TNF-α, tumor necrosis factor-α; GPR18, G protein-coupled receptor 18; p38 MAPK, mitogen-activated protein kinase; FPR2, formyl peptide receptor 2; ASK1, apoptosis signal-regulating kinase 1; Drp1, dynamin-related protein 1; OX40L, OX40 cognate ligand-protein; GPR54, G protein-coupled receptor 54; ARRB2, β-arrestin 2; GSK3β, glycogen synthase kinase-3β; PI3K, phosphatidylinositol 3-kinase; TGR5, trans-membrane G protein-coupled receptor-5; PGC-1α, peroxisome proliferators-activated receptor-γ coactivator-1α; NLRP3, NLR family, pyrin domain containing 3.

under the consensus that the production of ROS is maximal when the ingredients of the electron transport chains (ETCs) are superlatively impaired (Murphy et al., 1999; Moro et al., 2005). Particularly interacting with autophagy and apoptosis, activation of autophagic pathways attenuates EBI after SAH in rats (Jing et al., 2012; Shi et al., 2020; Xu W. et al., 2021). Among the mounts of antioxidant agents, docosahexaenoic acid (DHA), the so-called omega-3 fatty acid, reduces OS through enhancing mitochondrial dynamics in EBI (Zhang T. et al., 2018). Concretely, DHA reduced the number of ROC-positive cells, improved cell viability, attenuated malondialdehyde levels, and superoxide dismutase (SOD) stress. Furthermore, a metabolite of DHA, namely, resolvin D2 (RvD2), helps to defend EBI, especially in the cortex and hypothalamus (Zhang T. et al., 2021). The p38 mitogen-activated protein kinase (MAPK) is a major player in mitochondrial dysfunction after SAH (Sasaki et al., 2004; Yatsushige et al., 2007; Guo et al., 2016; Han et al., 2017a; Tomar et al., 2017; Lu et al., 2019). Recently, a p38 inhibitor, DJ-1, protects mitochondrial dysfunction by induction of translocation (Huang et al., 2018). Another selective inhibitor of Drp1, Mdivi-1, exerts neuroprotective effects against mitochondrial fission and OS (Fan et al., 2017; Wu P. et al., 2017). More recently, SS31 cell-membrane permeating mitochondria has been shown to exert potential neuroprotective effects (Petri et al., 2006). Via suppressing Bax translocation and cytochrome c release, SS31 ameliorated OS by inhibiting the mitochondrial pathway (Shen et al., 2020).

Other Pathways

PI3K/Akt Pathway

The PI3K/Akt pathway is one of the important pathways that inhibit cell apoptosis and, therefore, plays a protective role against SAH. In recent years, antiapoptosis agents targeting this pathway generated the cross-talk with antioxidative effect (Wu et al., 2020). For example, Aggf1, also known as an angiogenic factor with G, patch, and FHA domain 1, in a recombinant human form, reduces BBB disruption and neuroinflammation through PI3K/Akt/NF-κB pathway after SAH in rats by significantly decreasing the level of myeloperoxidase (Zhu et al., 2018). For the first time, John H. Zhang et al., found that KISS1 siRNA knockdown (KD) aggravated neurological deficits and the brain expression of markers for OS in rats both 24 h and 28 days after SAH, suggesting that KP54 attenuated OS through activating

GPR54/ARRB2/AKT/GSK3β pathway after SAH in rats (Mead et al., 2007; Huang et al., 2021). Another frontier hotspot involved in the PI3K/Akt pathway is the microglial polarization-mediated WMI (Xue et al., 2021). Additionally proposed by the John H. Zhang research group, low-density lipoprotein receptor-related protein-1 (LRP1), a scavenger receptor of apolipoprotein E (apoE), is validated for microglia polarization toward pro-antioxidative M2 phenotypes via Shc1/PI3K/Akt pathway after SAH in rats (Wu Y. et al., 2017; Rojo et al., 2018; Peng et al., 2019). Uniformly, apoE and apoE-mimetic peptides possess whole-brain protective effects that may reduce EBI after mice SAH via M1 microglial quiescence through the attenuation of the JAK2/STAT3/NOX2 signaling pathway axis (Pang et al., 2018). A shred of direct evidence presented by Kuanyu Li and his colleagues is that pAkt effectively inhibits iron accumulation, defense against OS, and ameliorates EBI in a model of experimental SAH in the temporal lobe (Jo et al., 2012; Hao et al., 2016; Zhang et al., 2016a). Interestingly, SC79 is an absorptive permeability without reported side effects, indicating a novel and promising delivery drug in patients with EBI after SAH.

More Recently Progressed Pathway

In addition to the Keap-Nrf2-ARE pathway and PI3K/Akt pathway, there are many other pathways that are oxidative related and proved to be effective. For instance, Scutellarin, a flavonoid from the Chinese herb *Erigeron breviscapus*, reduces vasospasm via the Erk5-KLF2-eNOS pathway after SAH (Li Q. et al., 2016). An agonist of the Shh co-receptor plays a part in neuroprotection against SAH-induced damage, mediated in part by antioxidant mechanisms, upregulating phospho-ERK levels, and mediating Shh signaling molecules in the prefrontal cortex (Hu et al., 2016). Benefitting from a broad distribution in neurons, astrocytes, and microglia, activation of TGR5 with INT-777 significantly attenuates OS through cAMP/PKCε/ALDH2 pathway after SAH in rats (Zuo G. et al., 2019). Recognized as a new component of the brain renin-angiotensin system, Mas is selectively target-activated by AVE 0991 and reduces OS through Mas/PKA/CREB/UCP-2 pathway (Mo et al., 2019). Moreover, 12/15-LOX is overexpressed in macrophages after SAH in mice, and restraint of the pathway attenuates brain injury and ameliorates unfavorable neurological outcomes. Progressing data support that various pathways may participate in the redox balance in EBI after SAH and needs to be added with a new insight of other underlying pathways.

Melatonin

The number of data accumulated till now concerning the protective action of melatonin against OS is preponderant (Galano et al., 2011; Wu H. J. et al., 2017; Luo et al., 2019; Shao et al., 2020). Melatonin, a lipophilic amino acid that originated from tryptophan, N-acetyl-5-methoxytryptamine, is synthesized in the pineal gland and other organs and exhibits both direct and indirect antioxidant effects. Melatonin first reported the antioxidative function in preventing focal regions of injury via inducing HO-1 expression following a rat SAH model in 2002 (Martinez-Cruz et al., 2002). Before the post-clazosentan era, studies regarding the EBI experiments were still broadly focused on delayed brain injury, such as setting the assessment point at day 5 (Fang et al., 2009). Although melatonin shows no improvement in neurologic scores, the phenomenon is settled by large doses with immensely lessened mortality (Ayer et al., 2008a,b). However, the latest study shows that patients with higher serum melatonin concentrations are more likely to have a poor prognosis (Zhan et al., 2021). The increased concentrations of serum melatonin correlate with admission WFNS scores and mFS and serum melatonin appears as an independent predictor for poor 6-month prognosis after aSAH, with a high discriminatory ability for the risk of the poor outcome under the ROC curve, indicating that serum melatonin might serve as a promising prognostic biomarker for aSAH (Zhan et al., 2021). *In vivo* experiments exhibit that melatonin supplied protection from the effects of EBI after SAH by adjusting the expression of murine SIRT3 (one of the members of the sirtuin family) (Yang S. et al., 2018). Another two recent studies also denoted that melatonin plays a neuroprotective role by increasing the expression of NRF2-mitophagy and ER stress via inducing antioxidant, LC3-II/LC3-I, and Atg 5-mediated autophagy, NLRP3 inflammasome-mediated anti-inflammatory effects, and detoxifying enzymes post-SAH (Wang et al., 2012; Dong et al., 2016; Wu H. J. et al., 2017; Sun et al., 2018). Melatonin may reduce neurobehavioral dysfunction in the SAH model through the TRL4 pathway (Wang et al., 2013). Furthermore, melatonin reduces the EBI by influencing NLRP3 inflammasome-associated apoptosis (Dong et al., 2016) and inhibiting NF-κB activation and attenuating HO-1, NQO-1, and c-GCLC expressions (Jumnongprakhon et al., 2015). The mechanism of these antiapoptosis effects was linked to the improvement of autophagy through a mitochondrial pathway (Chen et al., 2014b). Melatonin inhibits the disruption of tight junction proteins possibly linked to the adjustment of proinflammatory cytokines (Chen et al., 2014a). Taken together, these results demonstrate that regulation of melatonin attenuates symptomatic dysfunction (Chen et al., 2015).

Sirtuins

Sirtuins (SIRTs), including the seven SIRTs identified, are a family of deacetylases with homology. Lines of studies showed that SIRTs could modulate diverse biological functions, Sirtuin 1 (SIRT1) with antioxidative properties particularly. Demonstrating that sequential inhibition of forkhead transcription factors of the O class-, NF-κ B-, and p53-induced oxidative pathways, SIRT1 enhanced the neuroprotective role against EBI in rats (Zhang et al., 2016). A well-recognized antioxidant, astaxanthin, mitigates SAH-induced EBI by increasing SIRT1 and suppressing the TLR4 signaling pathway (Wu et al., 2014; Zhang et al., 2014; Zhang X. et al., 2019). Interestingly, derived from seaweeds, fucoxanthin (Fx) mitigates SAH-induced oxidative damage via the SIRT1-dependent pathway (Zhang X. S. et al., 2020). The activation of melanocortin 1 receptor with BMS-470539 immensely reduced EBI after SAH by restraining OS, apoptosis, and mitochondrial fission via the AMPK/SIRT1/PGC-1α signaling pathway (Xu W. et al., 2021). Modulated by SIRT1 activation, salvianolic acid B protects against SAH-triggered oxidative damage by upregulating the Nrf2 antioxidant signaling pathway (Zhang X. et al., 2018). Salvianolic acid homolog A also

presented antioxidative, antiapoptotic, and anti-inflammatory properties (Gu et al., 2017; Zhang X. et al., 2018).

Other members of the SIRT family are increasingly studied recently. SIRT3, a type of NAD-dependent deacetylase, remarkedly activated *in vivo* and *in vitro* following SAH, is involved in the PGC-1a/SIRT3 pathway attenuating OS (Zhang K. et al., 2020). Drawing on the successful experience of the SIRT6 protective role of the heart from I/R injury via upregulating antioxidants and suppressing OS, the activation of RXR ameliorated neurological deficits after SAH at least partially via adjusting the PPARγ/SIRT6/FoxO3a pathway (Zuo Y. et al., 2019).

Hydrogen Sulfide

Hydrogen sulfide (H_2S), a neuromodulator, which can be generated in the CNS from L-cysteine by cystathionine-β-synthase (CBS), may prove protective effects in experimental SAH (Xiong et al., 2020). The hypothesis that signaling through hydrogen sulfide may mediate protection from DCI clinically in patients with SAH was proposed in 2011 (Grobelny et al., 2011) and further demonstrated by Yu et al. (2014). Afterward, hydrogen sulfide attenuated brain edema formation and promoted the secretion of inflammatory cytokines (Cui et al., 2016). Soon after the proinflammation demonstrated in EBI after SAH, exogenous hydrogen sulfide functioning as an antioxidant and antiapoptotic mediator, donated by NaSH and L-cysteine, could significantly reduce EBI (Cui et al., 2016; Li et al., 2017; Xiong et al., 2020). Inspired by inhaled hydrogen gas markedly decreasing OS on ischemia/reperfusion injury and stroke in rats (Ohsawa et al., 2007), hydrogen gas therapy was conducted, and the rate of survival and neurological deficits were improved in a pilot study as expected (Camara et al., 2019). Mechanistically, the above advantageous effects might be linked to the suppression of the ROS/NLRP3 axis (Zhuang et al., 2019). Similarly, hydrogen-rich saline exhibited the satisfying outcome of alleviating EBI through alleviating OS following experimental SAH in both rabbit and rat models (Zhuang et al., 2012; Shao et al., 2016). Furthermore, sodium/hydrogen exchanger 1 participates in EBI activated by SAH via mediating OS (Song et al., 2019). As abovementioned earlier, a recent study shows that postconditioning with hydrogen gas ameliorated SAH-induced neuronal pyroptosis (Zhang C. S. et al., 2021). Produced endogenously through HO, carbon oxide (CO) minimizes neurobehavioral deficits, indicating that posttreatment with CO gas or CO-donors can be further tested as a potential therapy against SAH (Kamat et al., 2019).

Modifiable Factors

Peaking onset age between 50 and 60 years, many patients with aSAH have modifiable hypertension, dyslipidemia, diabetes mellitus, cardiovascular diseases, and so on (de Rooij et al., 2007; Zhang L. et al., 2017; Macdonald and Schweizer, 2017). To control the clinical status, they are recommended with antihypertensive drugs, statins, and so on, part of whom demonstrate the antioxidative effect in the laboratory, for example, telmisartan, ameliorates OS, and SAH-induced CVS (Erdi et al., 2016). One of the L-type calcium channel blockers, verapamil, can inhibit vasospasm, OS, and apoptosis following experimental SAH (Akkaya et al., 2019). Rosuvastatin, commonly used clinically, ameliorates EBI after SAH through restraining SOD formation and NF-κB activation in rats. Moreover, 3,4-dihydroxyphenylethanol may be a powerful agent in the treatment of EBI after SAH because of its free radical scavenging capacity and modulating the Akt and NF-κB signaling pathway (Zhong et al., 2016; Fu and Hu, 2016). In addition to the intervening abovementioned diseases, other drugs commonly used clinically, such as heparin (Hayman et al., 2017), albumin (Deng et al., 2021), and propofol (Zhang H. B. et al., 2019), all projected an antioxidative role. Some authors believe that preconditioning would provide the greatest chance of benefit but is obviously not effective (Mayor et al., 2013; Zolnourian et al., 2019; Ruan et al., 2020; Otsuka et al., 2021). Given the sophistication of brain damage after aSAH, therapeutic multimodality is promising. Supported by the evidence shown above, we suppose that the regular drug taken with high adherence may benefit favorable outcomes after aneurysm rupture than those who do not.

PERSPECTIVES AND LIMITATIONS

Shifted from phenotype research on OS in EBI to pathway-related research, the mechanisms become evident than at any time in the past (Zhang L. et al., 2017; Ye et al., 2018; Pan et al., 2021). However, since the term EBI was coined from an angle of preclinical mechanism insight, there is still a long way to apply clinically. Preclinical and clinical studies should proceed hand in hand, and none of the multi-omics and clinical trials should stop (Xu et al., 2017; Xu W. et al., 2018).

In addition to the traditional markers, such as malondialdehyde (MDA), SOD, reduced/oxidized glutathione (GSH/GSSG) ratio, and myeloperoxidase (MPO), new approaches that measure energetics and metabolomics of cells should be explored, such as the bioenergetic health index (BHI) (Chacko et al., 2016), to further guide the development of therapies. A lot of conducted studies showed that drugs introduced into the area of EBI after aSAH previously drew on the strength of the fields of ischemic stroke or traumatic brain injury. Furthermore, a close tracing of novel antioxidants is necessary, even in other disciplines with mutual adoption, promotion, and advancement, especially traditional Chinese medicine and nutrition (Wang et al., 2015; Zhang et al., 2015; Li Q. et al., 2016; Han et al., 2017b; Liu et al., 2017, 2020; Shao et al., 2019; Du et al., 2020; Wang T. et al., 2020). As the OS-related mechanisms and pathways have surfaced and matured, more modern technologies should emphasize their parts, such as designing a metabolite-derived protein alteration integrating glycolysis with Keap1-Nrf2 signaling directly (Bollong et al., 2018) or recombinant human drugs (Xie et al., 2018; Sun C. et al., 2019; Sun C. M. et al., 2019; Wang J. et al., 2020; Wu et al., 2020; Tu et al., 2021). Effective drugs validated in a laboratory should be carefully compared and put into clinical use properly. Typical drug pharmaceutical effects combined with evolving drug-loaded methods may be promising in future exploration. For example, the conventional antioxidant agent, curcumin, loaded into a nanosized PLGA-encapsulated

the therapeutic potential was enhanced for precision medicine in downregulating the NF-κB pathway and preventing OS in EBI (Li X. et al., 2016; Zhang et al., 2016b; Cai et al., 2017; Zhang Z. Y. et al., 2017).

There are several limitations in this study. First, at present, there remains a translational cleft between experimental SAH and clinical SAH, especially aSAH. Although injection and endovascular perforation models are well established and invaluable, no model, even the *in vivo* cerebral aneurysmal models, could perfectly replicate the actual rupture of an aneurysm in human beings. Second, the unequivocal definition of EBI could not be circumvented in animal models with the variation assessment points in 3, 12, 24, or 72 h. Clear evaluation time is still up for debate. Third, based on a multifactorial pathophysiology after EBI, OS plays a pivotal part but is still only one of the considerable phenotypes with promising therapeutic strategies covering as many pathways as possible.

CONCLUSION

Management of EBI after aSAH remains not only a challenge but also an opportunity. With in-depth understanding of oxidative pathophysiology of EBI, the way ahead becomes gradually clearer. Despite initial experimental studies demonstrating the effectiveness of the abovementioned antioxidants in EBI, these studies are comparatively rudimentary, with further translational medicine demanded to prove the utility of all of them clinically.

AUTHOR CONTRIBUTIONS

FL, RL, W-JT, KW, and YC contributed to the search and assessment of the available literature. FL and RL wrote the manuscript. XC and JZ helped to revise the manuscript to the final form. All authors contributed to the article and approved the submitted version.

FUNDING

This study was supported by the National Key Research and Development Program of China (Grant No. 2020YFC2004701).

REFERENCES

Akkaya, E., Evran, Ş, Çalış, F., Çevik, S., Hanımoğlu, H., Seyithanoğlu, M. H., et al. (2019). Effects of intrathecal verapamil on cerebral vasospasm in experimental rat study. *World Neurosurg.* 127, e1104–e1111. doi: 10.1016/j.wneu.2019.04.050

Asada, R., Nakatsuka, Y., Kanamaru, H., Kawakita, F., Fujimoto, M., Miura, Y., et al. (2021). Higher plasma osteopontin concentrations associated with subsequent development of chronic shunt-dependent hydrocephalus after aneurysmal subarachnoid hemorrhage. *Transl. Stroke Res.* 12, 808–816. doi: 10.1007/s12975-020-00886-x

Ayer, R. E., Sugawara, T., Chen, W., Tong, W., and Zhang, J. H. (2008a). Melatonin decreases mortality following severe subarachnoid hemorrhage. *J. Pineal Res.* 44, 197–204. doi: 10.1111/j.1600-079X.2007.00508.x

Ayer, R. E., Sugawara, T., and Zhang, J. H. (2008b). Effects of melatonin in early brain injury following subarachnoid hemorrhage. *Acta Neurochir. Suppl.* 102, 327–330. doi: 10.1007/978-3-211-85578-2_62

Bollong, M. J., Lee, G., Coukos, J. S., Yun, H., Zambaldo, C., Chang, J. W., et al. (2018). A metabolite-derived protein modification integrates glycolysis with KEAP1-NRF2 signalling. *Nature* 562, 600–604. doi:10.1038/s41586-018-0622-0

Bor, A., Rinkel, G., Adami, J., Koffijberg, H., Ekbom, A., Buskens, E., et al. (2008). Risk of subarachnoid haemorrhage according to number of affected relatives: a population based case-control study. *Brain* 131, 2662–2665. doi: 10.1093/brain/awn187

Brathwaite, S., and Macdonald, R. L. (2014). Current management of delayed cerebral ischemia: update from results of recent clinical trials. *Transl. Stroke Res.* 5, 207–226. doi: 10.1007/s12975-013-0316-8

Cahill, J., Calvert, J. W., and Zhang, J. H. (2006). Mechanisms of early brain injury after subarachnoid hemorrhage. *J. Cereb. Blood Flow Metab.* 26, 1341–1353. doi: 10.1038/sj.jcbfm.9600283

Cahill, J., and Zhang, J. H. (2009). Subarachnoid hemorrhage: is it time for a new direction? *Stroke* 40, S86–S87. doi: 10.1161/strokeaha.108.533315

Cai, J., Xu, D., Bai, X., Pan, R., Wang, B., Sun, S., et al. (2017). Curcumin mitigates cerebral vasospasm and early brain injury following subarachnoid hemorrhage via inhibiting cerebral inflammation. *Brain Behav.* 7:e00790. doi: 10.1002/brb3.790

Camara, R., Matei, N., Camara, J., Enkhjargal, B., Tang, J., and Zhang, J. H. (2019). Hydrogen gas therapy improves survival rate and neurological deficits in subarachnoid hemorrhage rats: a pilot study. *Med. Gas Res.* 9, 74–79. doi: 10.4103/2045-9912.260648

Caner, B., Hou, J., Altay, O., Fujii, M., and Zhang, J. H. (2012). Transition of research focus from vasospasm to early brain injury after subarachnoid hemorrhage. *J. Neurochem.* 123(Suppl. 2), 12–21. doi: 10.1111/j.1471-4159.2012.07939.x

Cao, Y., Li, Y., He, C., Yan, F., Li, J. R., Xu, H. Z., et al. (2021). Selective ferroptosis inhibitor liproxstatin-1 attenuates neurological deficits and neuroinflammation after subarachnoid hemorrhage. *Neurosci. Bull.* 37, 535–549. doi: 10.1007/s12264-020-00620-5

Chacko, B. K., Zhi, D., Darley-Usmar, V. M., and Mitchell, T. (2016). The bioenergetic health index is a sensitive measure of oxidative stress in human monocytes. *Redox Biol.* 8, 43–50. doi: 10.1016/j.redox.2015.12.008

Chao, B. H., Yan, F., Hua, Y., Liu, J. M., Yang, Y., Ji, X. M., et al. (2021). Stroke prevention and control system in China: CSPPC-stroke program. *Int. J. Stroke* 16, 265–272. doi: 10.1177/1747493020913557

Chen, F., Su, X., Lin, Z., Lin, Y., Yu, L., Cai, J., et al. (2017). Necrostatin-1 attenuates early brain injury after subarachnoid hemorrhage in rats by inhibiting necroptosis. *Neuropsychiatr. Dis. Treat.* 13, 1771–1782. doi: 10.2147/NDT.S140801

Chen, G., Fang, Q., Zhang, J., Zhou, D., and Wang, Z. (2011). Role of the Nrf2-ARE pathway in early brain injury after experimental subarachnoid hemorrhage. *J. Neurosci. Res.* 89, 515–523. doi: 10.1002/jnr.22577

Chen, J., Wang, L., Wu, C., Hu, Q., Gu, C., Yan, F., et al. (2014b). Melatonin-enhanced autophagy protects against neural apoptosis via a mitochondrial pathway in early brain injury following a subarachnoid hemorrhage. *J. Pineal Res.* 56, 12–19. doi: 10.1111/jpi.12086

Chen, J., Chen, G., Li, J., Qian, C., Mo, H., Gu, C., et al. (2014a). Melatonin attenuates inflammatory response-induced brain edema in early brain injury following a subarachnoid hemorrhage: a possible role for the regulation of pro-inflammatory cytokines. *J. Pineal Res.* 57, 340–347. doi: 10.1111/jpi.12173

Chen, J., Jin, H., Xu, H., Peng, Y., Jie, L., Xu, D., et al. (2019). The neuroprotective effects of necrostatin-1 on subarachnoid hemorrhage in rats are possibly mediated by preventing blood-brain barrier disruption and RIP3-mediated necroptosis. *Cell Transplant.* 28, 1358–1372. doi: 10.1177/0963689719867285

Chen, J., Qian, C., Duan, H., Cao, S., Yu, X., Li, J., et al. (2015). Melatonin attenuates neurogenic pulmonary edema via the regulation of inflammation

and apoptosis after subarachnoid hemorrhage in rats. *J. Pineal Res.* 59, 469–477. doi: 10.1111/jpi.12278

Chen, T., Pan, H., Li, J., Xu, H., Jin, H., Qian, C., et al. (2018). Inhibiting of RIPK3 attenuates early brain injury following subarachnoid hemorrhage: possibly through alleviating necroptosis. *Biomed. Pharmacother.* 107, 563–570. doi: 10.1016/j.biopha.2018.08.056

Connolly, E. S. Jr., Rabinstein, A. A., Carhuapoma, J. R., Derdeyn, C. P., Dion, J., Higashida, R. T., et al. (2012). Guidelines for the management of aneurysmal subarachnoid hemorrhage: a guideline for healthcare professionals from the American Heart Association/American Stroke Association. *Stroke* 43, 1711–1737. doi: 10.1161/STR.0b013e3182587839

Cui, Y., Duan, X., Li, H., Dang, B., Yin, J., Wang, Y., et al. (2016). Hydrogen sulfide ameliorates early brain injury following subarachnoid hemorrhage in rats. *Mol. Neurobiol.* 53, 3646–3657. doi: 10.1007/s12035-015-9304-1

de Rooij, N. K., Linn, F. H., van der Plas, J. A., Algra, A., and Rinkel, G. J. (2007). Incidence of subarachnoid haemorrhage: a systematic review with emphasis on region, age, gender and time trends. *J. Neurol. Neurosurg. Psychiatry* 78, 1365–1372. doi: 10.1136/jnnp.2007.117655

Deng, S., Liu, S., Jin, P., Feng, S., Tian, M., Wei, P., et al. (2021). Albumin reduces oxidative stress and neuronal apoptosis via the ERK/Nrf2/HO-1 pathway after intracerebral hemorrhage in rats. *Oxid. Med. Cell. Longev.* 2021:8891373. doi: 10.1155/2021/8891373

Deng, W., Kandhi, S., Zhang, B., Huang, A., Koller, A., and Sun, D. (2018). Extravascular blood augments myogenic constriction of cerebral arterioles: implications for hemorrhage-induced vasospasm. *J. Am. Heart Assoc.* 7:e008623. doi: 10.1161/jaha.118.008623

Ding, H., Wang, H., Zhu, L., and Wei, W. (2017). Ursolic acid ameliorates early brain injury after experimental traumatic brain injury in mice by activating the Nrf2 pathway. *Neurochem. Res.* 42, 337–346. doi: 10.1007/s11064-016-2077-8

Dong, Y., Fan, C., Hu, W., Jiang, S., Ma, Z., Yan, X., et al. (2016). Melatonin attenuated early brain injury induced by subarachnoid hemorrhage via regulating NLRP3 inflammasome and apoptosis signaling. *J. Pineal Res.* 60, 253–262. doi: 10.1111/jpi.12300

Dou, Y., Shen, H., Feng, D., Li, H., Tian, X., Zhang, J., et al. (2017). Tumor necrosis factor receptor-associated factor 6 participates in early brain injury after subarachnoid hemorrhage in rats through inhibiting autophagy and promoting oxidative stress. *J. Neurochem.* 142, 478–492. doi: 10.1111/jnc.14075

Du, C., Xi, C., Wu, C., Sha, J., Zhang, J., and Li, C. (2020). *Ginkgo biloba* extract protects early brain injury after subarachnoid hemorrhage via inhibiting thioredoxin interacting protein/NLRP3 signaling pathway. *Iran. J. Basic Med. Sci.* 23, 1340–1345. doi: 10.22038/ijbms.2020.42834.10090

Erdi, F., Keskin, F., Esen, H., Kaya, B., Feyzioglu, B., Kilinc, I., et al. (2016). Telmisartan ameliorates oxidative stress and subarachnoid haemorrhage-induced cerebral vasospasm. *Neurol. Res.* 38, 224–231. doi: 10.1080/01616412.2015.1105626

Eriksen, N., Rostrup, E., Fabricius, M., Scheel, M., Major, S., Winkler, M. K. L., et al. (2019). Early focal brain injury after subarachnoid hemorrhage correlates with spreading depolarizations. *Neurology* 92, e326–e341. doi: 10.1212/wnl.0000000000006814

Etminan, N., and Macdonald, R. L. (2017). Management of aneurysmal subarachnoid hemorrhage. *Handb. Clin. Neurol.* 140, 195–228. doi: 10.1016/B978-0-444-63600-3.00012-X

Fan, H., Ding, R., Liu, W., Zhang, X., Li, R., Wei, B., et al. (2021). Heat shock protein 22 modulates NRF1/TFAM-dependent mitochondrial biogenesis and DRP1-sparked mitochondrial apoptosis through AMPK-PGC1α signaling pathway to alleviate the early brain injury of subarachnoid hemorrhage in rats. *Redox Biol.* 40:101856. doi: 10.1016/j.redox.2021.101856

Fan, L. F., He, P. Y., Peng, Y. C., Du, Q. H., Ma, Y. J., Jin, J. X., et al. (2017). Mdivi-1 ameliorates early brain injury after subarachnoid hemorrhage via the suppression of inflammation-related blood-brain barrier disruption and endoplasmic reticulum stress-based apoptosis. *Free Radic. Biol. Med.* 112, 336–349. doi: 10.1016/j.freeradbiomed.2017.08.003

Fang, Q., Chen, G., Zhu, W., Dong, W., and Wang, Z. (2009). Influence of melatonin on cerebrovascular proinflammatory mediators expression and oxidative stress following subarachnoid hemorrhage in rabbits. *Mediators Inflamm.* 2009:426346. doi: 10.1155/2009/426346

Fang, Y., Gao, S., Wang, X., Cao, Y., Lu, J., Chen, S., et al. (2020). Programmed cell deaths and potential crosstalk with blood-brain barrier dysfunction after hemorrhagic stroke. *Front. Cell. Neurosci.* 14:68. doi: 10.3389/fncel.2020.00068

Fu, P., and Hu, Q. (2016). 3,4-Dihydroxyphenylethanol alleviates early brain injury by modulating oxidative stress and Akt and nuclear factor-κB pathways in a rat model of subarachnoid hemorrhage. *Exp. Ther. Med.* 11, 1999–2004. doi: 10.3892/etm.2016.3101

Fujii, S., Sawa, T., Ihara, H., Tong, K. I., Ida, T., Okamoto, T., et al. (2010). The critical role of nitric oxide signaling, via protein S-guanylation and nitrated cyclic GMP, in the antioxidant adaptive response. *J. Biol. Chem.* 285, 23970–23984. doi: 10.1074/jbc.M110.145441

Fumoto, T., Naraoka, M., Katagai, T., Li, Y., Shimamura, N., and Ohkuma, H. (2019). The role of oxidative stress in microvascular disturbances after experimental subarachnoid hemorrhage. *Transl. Stroke Res.* 10, 684–694. doi: 10.1007/s12975-018-0685-0

Galano, A., Tan, D. X., and Reiter, R. J. (2011). Melatonin as a natural ally against oxidative stress: a physicochemical examination. *J. Pineal Res.* 51, 1–16. doi: 10.1111/j.1600-079X.2011.00916.x

Go, Y. M., Chandler, J. D., and Jones, D. P. (2015). The cysteine proteome. *Free Radic. Biol. Med.* 84, 227–245. doi: 10.1016/j.freeradbiomed.2015.03.022

Gomis, P., Graftieaux, J. P., Sercombe, R., Hettler, D., Scherpereel, B., and Rousseaux, P. (2010). Randomized, double-blind, placebo-controlled, pilot trial of high-dose methylprednisolone in aneurysmal subarachnoid hemorrhage. *J. Neurosurg.* 112, 681–688. doi: 10.3171/2009.4.JNS081377

Grobelny, B. T., Ducruet, A. F., DeRosa, P. A., Kotchetkov, I. S., Zacharia, B. E., Hickman, Z. L., et al. (2011). Gain-of-function polymorphisms of cystathionine beta-synthase and delayed cerebral ischemia following aneurysmal subarachnoid hemorrhage. *J. Neurosurg.* 115, 101–107. doi: 10.3171/2011.2.JNS101414

Gu, X., Zheng, C., Zheng, Q., Chen, S., Li, W., Shang, Z., et al. (2017). Salvianolic acid A attenuates early brain injury after subarachnoid hemorrhage in rats by regulating ERK/P38/Nrf2 signaling. *Am. J. Transl. Res.* 9, 5643–5652.

Guo, Z., Hu, Q., Xu, L., Guo, Z. N., Ou, Y., He, Y., et al. (2016). Lipoxin A4 reduces inflammation through formyl peptide receptor 2/p38 MAPK signaling pathway in subarachnoid hemorrhage rats. *Stroke* 47, 490–497. doi: 10.1161/STROKEAHA.115.011223

Han, Y., Su, J., Liu, X., Zhao, Y., Wang, C., and Li, X. (2017a). Naringin alleviates early brain injury after experimental subarachnoid hemorrhage by reducing oxidative stress and inhibiting apoptosis. *Brain Res. Bull.* 133, 42–50. doi: 10.1016/j.brainresbull.2016.12.008

Han, Y., Zhang, T., Su, J., Zhao, Y., Chenchen, Wang, et al. (2017b). Apigenin attenuates oxidative stress and neuronal apoptosis in early brain injury following subarachnoid hemorrhage. *J. Clin. Neurosci.* 40, 157–162. doi: 10.1016/j.jocn.2017.03.003

Hänggi, D., Etminan, N., Macdonald, R., Steiger, H., Mayer, S., Aldrich, F., et al. (2015). NEWTON: nimodipine microparticles to enhance recovery while reducing toxicity after subarachnoid hemorrhage. *Neurocrit. Care* 23, 274–284. doi: 10.1007/s12028-015-0112-2

Hao, S., Song, C., Shang, L., Yu, J., Qiao, T., and Li, K. (2016). Phosphorylation of Akt by SC79 prevents iron accumulation and ameliorates early brain injury in a model of experimental subarachnoid hemorrhage. *Molecules* 21:325. doi: 10.3390/molecules21030325

Hartings, J. A., York, J., Carroll, C. P., Hinzman, J. M., Mahoney, E., Krueger, B., et al. (2017). Subarachnoid blood acutely induces spreading depolarizations and early cortical infarction. *Brain* 140, 2673–2690. doi: 10.1093/brain/awx214

Hayman, E. G., Patel, A. P., James, R. F., and Simard, J. M. (2017). Heparin and heparin-derivatives in post-subarachnoid hemorrhage brain injury: a multimodal therapy for a multimodal disease. *Molecules* 22:724. doi: 10.3390/molecules22050724

Hu, Q., Li, T., Wang, L., Xie, Y., Liu, S., Bai, X., et al. (2016). Neuroprotective effects of a smoothened receptor agonist against early brain injury after experimental subarachnoid hemorrhage in rats. *Front. Cell. Neurosci.* 10:306. doi: 10.3389/fncel.2016.00306

Huang, L., Hou, Y., Wang, L., Xu, X., Guan, Q., Li, X., et al. (2018). p38 inhibitor protects mitochondrial dysfunction by induction of DJ-1 mitochondrial translocation after subarachnoid hemorrhage. *J. Mol. Neurosci.* 66, 163–171. doi: 10.1007/s12031-018-1131-1

Huang, Y., Guo, Y., Huang, L., Fang, Y., Li, D., Liu, R., et al. (2021). Kisspeptin-54 attenuates oxidative stress and neuronal apoptosis in early brain injury after subarachnoid hemorrhage in rats via GPR54/ARRB2/AKT/GSK3β signaling pathway. *Free Radic. Biol. Med.* 171, 99–111. doi: 10.1016/j.freeradbiomed.2021.05.012

Jarocka-Karpowicz, I., Syta-Krzyżanowska, A., Kochanowicz, J., and Mariak, Z. D. (2020). Clinical prognosis for SAH Consistent with redox imbalance and lipid peroxidation. *Molecules* 25:1921. doi: 10.3390/molecules25081921

Jiang, W. C., Chen, C. M., Hamdin, C. D., Orekhov, A. N., Sobenin, I. A., Layne, M. D., et al. (2020). Therapeutic potential of heme oxygenase-1 in aneurysmal diseases. *Antioxidants (Basel)* 9:1150. doi: 10.3390/antiox9111150

Jing, C. H., Wang, L., Liu, P. P., Wu, C., Ruan, D., and Chen, G. (2012). Autophagy activation is associated with neuroprotection against apoptosis via a mitochondrial pathway in a rat model of subarachnoid hemorrhage. *Neuroscience* 213, 144–153. doi: 10.1016/j.neuroscience.2012.03.055

Jo, H., Mondal, S., Tan, D., Nagata, E., Takizawa, S., Sharma, A. K., et al. (2012). Small molecule-induced cytosolic activation of protein kinase Akt rescues ischemia-elicited neuronal death. *Proc. Natl. Acad. Sci. U.S.A.* 109, 10581–10586. doi: 10.1073/pnas.1202810109

Ju, Q., Li, X., Zhang, H., Yan, S., Li, Y., and Zhao, Y. (2020). NFE2L2 is a potential prognostic biomarker and is correlated with immune infiltration in brain lower grade glioma: a pan-cancer analysis. *Oxid. Med. Cell. Longev.* 2020:3580719. doi: 10.1155/2020/3580719

Jumnongprakhon, P., Govitrapong, P., Tocharus, C., Pinkaew, D., and Tocharus, J. (2015). Melatonin protects methamphetamine-induced neuroinflammation through NF-κB and Nrf2 pathways in glioma cell line. *Neurochem. Res.* 40, 1448–1456. doi: 10.1007/s11064-015-1613-2

Kamat, P. K., Ahmad, A. S., and Doré, S. (2019). Carbon monoxide attenuates vasospasm and improves neurobehavioral function after subarachnoid hemorrhage. *Arch Biochem. Biophys.* 676:108117. doi: 10.1016/j.abb.2019.108117

Kooijman, E., Nijboer, C. H., van Velthoven, C. T., Kavelaars, A., Kesecioglu, J., and Heijnen, C. J. (2014). The rodent endovascular puncture model of subarachnoid hemorrhage: mechanisms of brain damage and therapeutic strategies. *J. Neuroinflammation* 11:2. doi: 10.1186/1742-2094-11-2

Kusaka, G., Ishikawa, M., Nanda, A., Granger, D. N., and Zhang, J. H. (2004). Signaling pathways for early brain injury after subarachnoid hemorrhage. *J. Cereb. Blood Flow Metab.* 24, 916–925. doi: 10.1097/01.Wcb.0000125886.48838.7e

Lee, J. Y., Keep, R. F., He, Y., Sagher, O., Hua, Y., and Xi, G. (2010). Hemoglobin and iron handling in brain after subarachnoid hemorrhage and the effect of deferoxamine on early brain injury. *J. Cereb. Blood Flow Metab.* 30, 1793–1803. doi: 10.1038/jcbfm.2010.137

Li, Q., Chen, Y., Zhang, X., Zuo, S., Ge, H., Chen, Y., et al. (2016). Scutellarin attenuates vasospasm through the Erk5-KLF2-eNOS pathway after subarachnoid hemorrhage in rats. *J. Clin. Neurosci.* 34, 264–270. doi: 10.1016/j.jocn.2016.09.028

Li, T., Wang, L., Hu, Q., Liu, S., Bai, X., Xie, Y., et al. (2017). Neuroprotective roles of l-Cysteine in attenuating early brain injury and improving synaptic density via the CBS/H(2)S pathway following subarachnoid hemorrhage in rats. *Front. Neurol.* 8:176. doi: 10.3389/fneur.2017.00176

Li, X., Liu, W., Li, R., Guo, S., Fan, H., Wei, B., et al. (2020). TSG-6 attenuates oxidative stress-induced early brain injury in subarachnoid hemorrhage partly by the HO-1 and Nox2 Pathways. *J. Stroke Cerebrovasc. Dis.* 29:104986. doi: 10.1016/j.jstrokecerebrovasdis.2020.104986

Li, X., Zhao, L., Yue, L., Liu, H., Yang, X., Wang, X., et al. (2016). Evidence for the protective effects of curcumin against oxyhemoglobin-induced injury in rat cortical neurons. *Brain Res. Bull.* 120, 34–40. doi: 10.1016/j.brainresbull.2015.11.006

Li, Y., Liu, Y., Wu, P., Tian, Y., Liu, B., Wang, J., et al. (2021). Inhibition of ferroptosis alleviates early brain injury after subarachnoid hemorrhage in vitro and in vivo via reduction of lipid peroxidation. *Cell. Mol. Neurobiol.* 41, 263–278. doi: 10.1007/s10571-020-00850-1

Liu, F., Chen, Y., Hu, Q., Li, B., Tang, J., He, Y., et al. (2015). MFGE8/Integrin β3 pathway alleviates apoptosis and inflammation in early brain injury after subarachnoid hemorrhage in rats. *Exp. Neurol.* 272, 120–127. doi: 10.1016/j.expneurol.2015.04.016

Liu, F., Hu, Q., Li, B., Manaenko, A., Chen, Y., Tang, J., et al. (2014). Recombinant milk fat globule-EGF factor-8 reduces oxidative stress via integrin β3/nuclear factor erythroid 2-related factor 2/heme oxygenase pathway in subarachnoid hemorrhage rats. *Stroke* 45, 3691–3697. doi: 10.1161/strokeaha.114.006635

Liu, H., Guo, W., Guo, H., Zhao, L., Yue, L., Li, X., et al. (2020). Bakuchiol attenuates oxidative stress and neuron damage by regulating Trx1/TXNIP and the phosphorylation of AMPK after subarachnoid hemorrhage in mice. *Front. Pharmacol.* 11:712. doi: 10.3389/fphar.2020.00712

Liu, H., Zhao, L., Yue, L., Wang, B., Li, X., Guo, H., et al. (2017). Pterostilbene attenuates early brain injury following subarachnoid hemorrhage via inhibition of the NLRP3 inflammasome and Nox2-related oxidative stress. *Mol. Neurobiol.* 54, 5928–5940. doi: 10.1007/s12035-016-0108-8

Lu, Y., Zhang, X. S., Zhou, X. M., Gao, Y. Y., Chen, C. L., Liu, J. P., et al. (2019). Peroxiredoxin 1/2 protects brain against $H_{(2)}O_{(2)}$-induced apoptosis after subarachnoid hemorrhage. *FASEB J.* 33, 3051–3062. doi: 10.1096/fj.201801150R

Luo, C., Yang, Q., Liu, Y., Zhou, S., Jiang, J., Reiter, R. J., et al. (2019). The multiple protective roles and molecular mechanisms of melatonin and its precursor N-acetylserotonin in targeting brain injury and liver damage and in maintaining bone health. *Free Radic. Biol. Med.* 130, 215–233. doi: 10.1016/j.freeradbiomed.2018.10.402

Macdonald, R., Kassell, N., Mayer, S., Ruefenacht, D., Schmiedek, P., Weidauer, S., et al. (2008). Clazosentan to overcome neurological ischemia and infarction occurring after subarachnoid hemorrhage (CONSCIOUS-1): randomized, double-blind, placebo-controlled phase 2 dose-finding trial. *Stroke* 39, 3015–3021. doi: 10.1161/strokeaha.108.519942

Macdonald, R. L., Higashida, R. T., Keller, E., Mayer, S. A., Molyneux, A., Raabe, A., et al. (2011). Clazosentan, an endothelin receptor antagonist, in patients with aneurysmal subarachnoid haemorrhage undergoing surgical clipping: a randomised, double-blind, placebo-controlled phase 3 trial (CONSCIOUS-2). *Lancet Neurol.* 10, 618–625. doi: 10.1016/S1474-4422(11)70108-9

Macdonald, R. L., and Schweizer, T. A. (2017). Spontaneous subarachnoid haemorrhage. *Lancet* 389, 655–666. doi: 10.1016/s0140-6736(16)30668-7

Martinez-Cruz, F., Espinar, A., Pozo, D., Osuna, C., and Guerrero, J. M. (2002). Melatonin prevents focal rat cerebellum injury as assessed by induction of heat shock protein (HO-1) following subarachnoid injections of lysed blood. *Neurosci. Lett.* 331, 208–210. doi: 10.1016/s0304-3940(02)00884-4

Mayer, S., Aldrich, E., Bruder, N., Hmissi, A., Macdonald, R., Viarasilpa, T., et al. (2019). Thick and diffuse subarachnoid blood as a treatment effect modifier of clazosentan after subarachnoid hemorrhage. *Stroke* 50, 2738–2744. doi: 10.1161/strokeaha.119.025682

Mayor, F., Bilgin-Freiert, A., Connolly, M., Katsnelson, M., Dusick, J. R., Vespa, P., et al. (2013). Effects of remote ischemic preconditioning on the coagulation profile of patients with aneurysmal subarachnoid hemorrhage: a case-control study. *Neurosurgery* 73, 808–815; discussion 815. doi: 10.1227/NEU.0000000000000098

Mead, E. J., Maguire, J. J., Kuc, R. E., and Davenport, A. P. (2007). Kisspeptins: a multifunctional peptide system with a role in reproduction, cancer and the cardiovascular system. *Br. J. Pharmacol.* 151, 1143–1153. doi: 10.1038/sj.bjp.0707295

Mo, J., Enkhjargal, B., Travis, Z. D., Zhou, K., Wu, P., Zhang, G., et al. (2019). AVE 0991 attenuates oxidative stress and neuronal apoptosis via Mas/PKA/CREB/UCP-2 pathway after subarachnoid hemorrhage in rats. *Redox Biol.* 20, 75–86. doi: 10.1016/j.redox.2018.09.022

Moro, M. A., Almeida, A., Bolanos, J. P., and Lizasoain, I. (2005). Mitochondrial respiratory chain and free radical generation in stroke. *Free Radic. Biol. Med.* 39, 1291–1304. doi: 10.1016/j.freeradbiomed.2005.07.010

Murphy, A. N., Fiskum, G., and Beal, M. F. (1999). Mitochondria in neurodegeneration: bioenergetic function in cell life and death. *J. Cereb. Blood Flow Metab.* 19, 231–245. doi: 10.1097/00004647-199903000-00001

Murphy, M. P. (2009). How mitochondria produce reactive oxygen species. *Biochem. J.* 417, 1–13. doi: 10.1042/BJ20081386

Naraoka, M., Matsuda, N., Shimamura, N., Asano, K., Akasaka, K., Takemura, A., et al. (2018). Long-acting statin for aneurysmal subarachnoid hemorrhage: a randomized, double-blind, placebo-controlled trial. *J. Cereb. Blood Flow Metab.* 38, 1190–1198. doi: 10.1177/0271678X17724682

Ohsawa, I., Ishikawa, M., Takahashi, K., Watanabe, M., Nishimaki, K., Yamagata, K., et al. (2007). Hydrogen acts as a therapeutic antioxidant by selectively reducing cytotoxic oxygen radicals. *Nat. Med.* 13, 688–694. doi: 10.1038/nm1577

Otsuka, S., Setoyama, K., Takada, S., Nakanishi, K., Terashi, T., Norimatsu, K., et al. (2021). Preconditioning exercise in rats attenuates early brain injury resulting from subarachnoid hemorrhage by reducing oxidative stress, inflammation, and neuronal apoptosis. *Mol. Neurobiol.* 58, 5602–5617. doi: 10.1007/s12035-021-02506-7

Pan, J., Lao, L., Shen, J., Huang, S., Zhang, T., Fan, W., et al. (2021). Utility of serum NOX4 as a potential prognostic biomarker for aneurysmal subarachnoid hemorrhage. *Clin. Chim. Acta* 517, 9–14. doi: 10.1016/j.cca.2021.02.007

Pang, J., Peng, J., Matei, N., Yang, P., Kuai, L., Wu, Y., et al. (2018). Apolipoprotein E exerts a whole-brain protective property by promoting M1? Microglia quiescence after experimental subarachnoid hemorrhage in mice. *Transl. Stroke Res.* 9, 654–668. doi: 10.1007/s12975-018-0665-4

Pang, J., Peng, J., Yang, P., Kuai, L., Chen, L., Zhang, J. H., et al. (2019). White Matter injury in early brain injury after subarachnoid hemorrhage. *Cell Transplant.* 28, 26–35. doi: 10.1177/0963689718812054

Peng, J., Pang, J., Huang, L., Enkhjargal, B., Zhang, T., Mo, J., et al. (2019). LRP1 activation attenuates white matter injury by modulating microglial polarization through Shc1/PI3K/Akt pathway after subarachnoid hemorrhage in rats. *Redox Biol.* 21:101121. doi: 10.1016/j.redox.2019.101121

Petri, S., Kiaei, M., Damiano, M., Hiller, A., Wille, E., Manfredi, G., et al. (2006). Cell-permeable peptide antioxidants as a novel therapeutic approach in a mouse model of amyotrophic lateral sclerosis. *J. Neurochem.* 98, 1141–1148. doi: 10.1111/j.1471-4159.2006.04018.x

Post, R., Germans, M. R., Tjerkstra, M. A., Vergouwen, M. D. I., Jellema, K., Koot, R. W., et al. (2021). Ultra-early tranexamic acid after subarachnoid haemorrhage (ULTRA): a randomised controlled trial. *Lancet* 397, 112–118. doi: 10.1016/S0140-6736(20)32518-6

Prentice, H., Modi, J. P., and Wu, J. Y. (2015). Mechanisms of neuronal protection against excitotoxicity, endoplasmic reticulum stress, and mitochondrial dysfunction in stroke and neurodegenerative diseases. *Oxid. Med. Cell. Longev.* 2015:964518. doi: 10.1155/2015/964518

Qian, X., Li, X., Shi, Z., Bai, X., Xia, Y., Zheng, Y., et al. (2019). KDM3A senses oxygen availability to regulate PGC-1alpha-mediated mitochondrial biogenesis. *Mol. Cell* 76, 885–895.e7. doi: 10.1016/j.molcel.2019.09.019

Qu, X. F., Liang, T. Y., Wu, D. G., Lai, N. S., Deng, R. M., Ma, C., et al. (2021). Acyl-CoA synthetase long chain family member 4 plays detrimental role in early brain injury after subarachnoid hemorrhage in rats by inducing ferroptosis. *CNS Neurosci. Ther.* 27, 449–463. doi: 10.1111/cns.13548

Reisman, S. A., Lee, C. Y., Meyer, C. J., Proksch, J. W., Sonis, S. T., and Ward, K. W. (2014). Topical application of the synthetic triterpenoid RTA 408 protects mice from radiation-induced dermatitis. *Radiat. Res.* 181, 512–520. doi: 10.1667/RR13578.1

Rojo, A. I., Pajares, M., Garcia-Yague, A. J., Buendia, I., Van Leuven, F., Yamamoto, M., et al. (2018). Deficiency in the transcription factor NRF2 worsens inflammatory parameters in a mouse model with combined tauopathy and amyloidopathy. *Redox Biol.* 18, 173–180. doi: 10.1016/j.redox.2018.07.006

Rowland, M. J., Hadjipavlou, G., Kelly, M., Westbrook, J., and Pattinson, K. T. (2012). Delayed cerebral ischaemia after subarachnoid haemorrhage: looking beyond vasospasm. *Br. J. Anaesth.* 109, 315–329. doi: 10.1093/bja/aes264

Ru, X., Qu, J., Li, Q., Zhou, J., Huang, S., Li, W., et al. (2021). MiR-706 alleviates white matter injury via downregulating PKCα/MST1/NF-κB pathway after subarachnoid hemorrhage in mice. *Exp. Neurol.* 341:113688. doi: 10.1016/j.expneurol.2021.113688

Ruan, W., Hu, J., Zhou, H., Li, Y., Xu, C., Luo, Y., et al. (2020). Intranasal wnt-3a alleviates neuronal apoptosis in early brain injury post subarachnoid hemorrhage via the regulation of wnt target PPAN mediated by the moonlighting role of aldolase C. *Neurochem. Int.* 134:104656. doi: 10.1016/j.neuint.2019.104656

Rubio-Perez, C., Planas-Rigol, E., Trincado, J., Bonfill-Teixidor, E., Arias, A., Marchese, D., et al. (2021). Immune cell profiling of the cerebrospinal fluid enables the characterization of the brain metastasis microenvironment. *Nat. Commun.* 12:1503. doi: 10.1038/s41467-021-21789-x

Sasaki, T., Kasuya, H., Onda, H., Sasahara, A., Goto, S., Hori, T., et al. (2004). Role of p38 mitogen-activated protein kinase on cerebral vasospasm after subarachnoid hemorrhage. *Stroke* 35, 1466–1470. doi: 10.1161/01.STR.0000127425.47266.20

Schupper, A., Eagles, M., Neifert, S., Mocco, J., and Macdonald, R. (2020). Lessons from the CONSCIOUS-1 Study. *J. Clin. Med.* 9:2970. doi: 10.3390/jcm9092970

Sehba, F. A., Hou, J., Pluta, R. M., and Zhang, J. H. (2012). The importance of early brain injury after subarachnoid hemorrhage. *Prog. Neurobiol.* 97, 14–37. doi: 10.1016/j.pneurobio.2012.02.003

Shao, A., Lin, D., Wang, L., Tu, S., Lenahan, C., and Zhang, J. (2020). Oxidative stress at the crossroads of aging, stroke and depression. *Aging Dis.* 11, 1537–1566. doi: 10.14336/ad.2020.0225

Shao, A., Wu, H., Hong, Y., Tu, S., Sun, X., Wu, Q., et al. (2016). Hydrogen-rich saline attenuated subarachnoid hemorrhage-induced early brain injury in rats by suppressing inflammatory response: possible involvement of NF-κB pathway and NLRP3 inflammasome. *Mol. Neurobiol.* 53, 3462–3476. doi: 10.1007/s12035-015-9242-y

Shao, J., Wu, Q., Lv, S. Y., Zhou, X. M., Zhang, X. S., Wen, L. L., et al. (2019). Allicin attenuates early brain injury after experimental subarachnoid hemorrhage in rats. *J. Clin. Neurosci.* 63, 202–208. doi: 10.1016/j.jocn.2019.01.024

Shen, R., Zhou, J., Li, G., Chen, W., Zhong, W., and Chen, Z. (2020). SS31 attenuates oxidative stress and neuronal apoptosis in early brain injury following subarachnoid hemorrhage possibly by the mitochondrial pathway. *Neurosci. Lett.* 717:134654. doi: 10.1016/j.neulet.2019.134654

Shi, G., Cui, L., Chen, R., Liang, S., Wang, C., and Wu, P. (2020). TT01001 attenuates oxidative stress and neuronal apoptosis by preventing mitoNEET-mediated mitochondrial dysfunction after subarachnoid hemorrhage in rats. *Neuroreport* 31, 845–850. doi: 10.1097/wnr.0000000000001492

Sies, H., Berndt, C., and Jones, D. P. (2017). Oxidative stress. *Annu. Rev. Biochem.* 86, 715–748. doi: 10.1146/annurev-biochem-061516-045037

Sies, H., and Jones, D. P. (2020). Reactive oxygen species (ROS) as pleiotropic physiological signalling agents. *Nat. Rev. Mol. Cell Biol.* 21, 363–383. doi: 10.1038/s41580-020-0230-3

Song, H., Yuan, S., Zhang, Z., Zhang, J., Zhang, P., Cao, J., et al. (2019). Sodium/hydrogen exchanger 1 participates in early brain injury after subarachnoid hemorrhage both in vivo and in vitro via promoting neuronal apoptosis. *Cell Transplant.* 28, 985–1001. doi: 10.1177/0963689719834873

Song, S., Chen, Y., Han, F., Dong, M., Xiang, X., Sui, J., et al. (2018). Aloperine activates the Nrf2-ARE pathway when ameliorating early brain injury in a subarachnoid hemorrhage model. *Exp. Ther. Med.* 15, 3847–3855. doi: 10.3892/etm.2018.5896

Sq, G., Jq, L., Yl, H., Qz, D., Wd, Z., Hj, D., et al. (2020). Neuroprotective role of glutathione peroxidase 4 in experimental subarachnoid hemorrhage models. *Life Sci.* 257:118050. doi: 10.1016/j.lfs.2020.118050

Sun, B., Yang, S., Li, S., and Hang, C. (2018). Melatonin upregulates nuclear factor erythroid-2 related factor 2 (Nrf2) and mediates mitophagy to protect against early brain injury after subarachnoid hemorrhage. *Med. Sci. Monit.* 24, 6422–6430. doi: 10.12659/msm.909221

Sun, C., Enkhjargal, B., Reis, C., Zhang, T., Zhu, Q., Zhou, K., et al. (2019). Osteopontin-enhanced autophagy attenuates early brain injury via FAK-ERK pathway and improves long-term outcome after subarachnoid hemorrhage in rats. *Cells* 8:980. doi: 10.3390/cells8090980

Sun, C. M., Enkhjargal, B., Reis, C., Zhou, K. R., Xie, Z. Y., Wu, L. Y., et al. (2019). Osteopontin attenuates early brain injury through regulating autophagy-apoptosis interaction after subarachnoid hemorrhage in rats. *CNS Neurosci. Ther.* 25, 1162–1172. doi: 10.1111/cns.13199

Takeuchi, S., Kumagai, K., Toyooka, T., Otani, N., Wada, K., and Mori, K. (2021). Intravenous hydrogen therapy with intracisternal magnesium sulfate infusion in severe aneurysmal subarachnoid hemorrhage. *Stroke* 52, 20–27. doi: 10.1161/STROKEAHA.120.031260

Tanaka, N., Ikeda, Y., Ohta, Y., Deguchi, K., Tian, F., Shang, J., et al. (2011). Expression of Keap1-Nrf2 system and antioxidative proteins in mouse brain after transient middle cerebral artery occlusion. *Brain Res.* 1370, 246–253. doi: 10.1016/j.brainres.2010.11.010

Tomar, A., Vasisth, S., Khan, S. I., Malik, S., Nag, T. C., Arya, D. S., et al. (2017). Galangin ameliorates cisplatin induced nephrotoxicity in vivo by modulation of oxidative stress, apoptosis and inflammation through interplay of MAPK signaling cascade. *Phytomedicine* 34, 154–161. doi: 10.1016/j.phymed.2017.05.007

Toyota, Y., Shishido, H., Ye, F., Koch, L. G., Britton, S. L., Garton, H. J. L., et al. (2021). Hydrocephalus following experimental subarachnoid hemorrhage in rats with different aerobic capacity. *Int. J. Mol. Sci.* 22:4489. doi: 10.3390/ijms22094489

Tsai, T. H., Lin, S. H., Wu, C. H., Tsai, Y. C., Yang, S. F., and Lin, C. L. (2020). Mechanisms and therapeutic implications of RTA 408, an activator of Nrf2, in subarachnoid hemorrhage-induced delayed cerebral vasospasm and secondary brain injury. *PLoS One* 15:e0240122. doi: 10.1371/journal.pone.0240122

Tu, T., Yin, S., Pang, J., Zhang, X., Zhang, L., Zhang, Y., et al. (2021). Irisin contributes to neuroprotection by promoting mitochondrial biogenesis after experimental subarachnoid hemorrhage. *Front. Aging Neurosci.* 13:640215. doi: 10.3389/fnagi.2021.640215

Vecchione, C., Frati, A., Di Pardo, A., Cifelli, G., Carnevale, D., Gentile, M. T., et al. (2009). Tumor necrosis factor-alpha mediates hemolysis-induced vasoconstriction and the cerebral vasospasm evoked by subarachnoid hemorrhage. *Hypertension* 54, 150–156. doi: 10.1161/hypertensionaha.108.128124

Wang, J., and Doré, S. (2007). Heme oxygenase-1 exacerbates early brain injury after intracerebral haemorrhage. *Brain* 130, 1643–1652. doi: 10.1093/brain/awm095

Wang, J., Zuo, Y., Zhuang, K., Luo, K., Yan, X., Li, J., et al. (2020). Recombinant human milk fat globule-epidermal growth factor 8 attenuates microthrombosis after subarachnoid hemorrhage in rats. *J. Stroke Cerebrovasc. Dis.* 29:104536. doi: 10.1016/j.jstrokecerebrovasdis.2019.104536

Wang, T., Xu, L., Gao, L., Zhao, L., Liu, X. H., Chang, Y. Y., et al. (2020). Paeoniflorin attenuates early brain injury through reducing oxidative stress and neuronal apoptosis after subarachnoid hemorrhage in rats. *Metab. Brain Dis.* 35, 959–970. doi: 10.1007/s11011-020-00571-w

Wang, X., Li, S., Ma, J., Wang, C., Chen, A., Xin, Z., et al. (2019). Effect of gastrodin on early brain injury and neurological outcome after subarachnoid hemorrhage in rats. *Neurosci. Bull.* 35, 461–470. doi: 10.1007/s12264-018-00333-w

Wang, Y., Gao, A., Xu, X., Dang, B., You, W., Li, H., et al. (2015). The neuroprotection of lysosomotropic agents in experimental subarachnoid hemorrhage probably involving the apoptosis pathway triggering by cathepsins via chelating intralysosomal iron. *Mol. Neurobiol.* 52, 64–77. doi: 10.1007/s12035-014-8846-y

Wang, Z., Chen, G., Zhu, W. W., and Zhou, D. (2010). Activation of nuclear factor-erythroid 2-related factor 2 (Nrf2) in the basilar artery after subarachnoid hemorrhage in rats. *Ann. Clin. Lab. Sci.* 40, 233–239.

Wang, Z., Ji, C., Wu, L., Qiu, J., Li, Q., Shao, Z., et al. (2014). Tert-butylhydroquinone alleviates early brain injury and cognitive dysfunction after experimental subarachnoid hemorrhage: role of Keap1/Nrf2/ARE pathway. *PLoS One* 9:e97685. doi: 10.1371/journal.pone.0097685

Wang, Z., Ma, C., Meng, C. J., Zhu, G. Q., Sun, X. B., Huo, L., et al. (2012). Melatonin activates the Nrf2-ARE pathway when it protects against early brain injury in a subarachnoid hemorrhage model. *J. Pineal Res.* 53, 129–137. doi: 10.1111/j.1600-079X.2012.00978.x

Wang, Z., Wu, L., You, W., Ji, C., and Chen, G. (2013). Melatonin alleviates secondary brain damage and neurobehavioral dysfunction after experimental subarachnoid hemorrhage: possible involvement of TLR4-mediated inflammatory pathway. *J. Pineal Res.* 55, 399–408. doi: 10.1111/jpi.12087

Wu, H. J., Wu, C., Niu, H. J., Wang, K., Mo, L. J., Shao, A. W., et al. (2017). Neuroprotective mechanisms of melatonin in hemorrhagic stroke. *Cell. Mol. Neurobiol.* 37, 1173–1185. doi: 10.1007/s10571-017-0461-9

Wu, L., Su, Z., Zha, L., Zhu, Z., Liu, W., Sun, Y., et al. (2019). Tetramethylpyrazine nitrone reduces oxidative stress to alleviate cerebral vasospasm in experimental subarachnoid hemorrhage models. *Neuromolecular Med.* 21, 262–274. doi: 10.1007/s12017-019-08543-9

Wu, L. Y., Enkhjargal, B., Xie, Z. Y., Travis, Z. D., Sun, C. M., Zhou, K. R., et al. (2020). Recombinant OX40 attenuates neuronal apoptosis through OX40-OX40L/PI3K/AKT signaling pathway following subarachnoid hemorrhage in rats. *Exp. Neurol.* 326:113179. doi: 10.1016/j.expneurol.2020.113179

Wu, P., Li, Y., Zhu, S., Wang, C., Dai, J., Zhang, G., et al. (2017). Mdivi-1 alleviates early brain injury after experimental subarachnoid hemorrhage in rats, possibly via inhibition of Drp1-activated mitochondrial fission and oxidative stress. *Neurochem. Res.* 42, 1449–1458. doi: 10.1007/s11064-017-2201-4

Wu, Q., Zhang, X. S., Wang, H. D., Zhang, X., Yu, Q., Li, W., et al. (2014). Astaxanthin activates nuclear factor erythroid-related factor 2 and the antioxidant responsive element (Nrf2-ARE) pathway in the brain after subarachnoid hemorrhage in rats and attenuates early brain injury. *Mar. Drugs* 12, 6125–6141. doi: 10.3390/md12126125

Wu, Y., Peng, J., Pang, J., Sun, X., and Jiang, Y. (2017). Potential mechanisms of white matter injury in the acute phase of experimental subarachnoid haemorrhage. *Brain* 140:e36. doi: 10.1093/brain/awx084

Xie, Y., Guo, H., Wang, L., Xu, L., Zhang, X., Yu, L., et al. (2017). Human albumin attenuates excessive innate immunity via inhibition of microglial Mincle/Syk signaling in subarachnoid hemorrhage. *Brain Behav. Immun.* 60, 346–360. doi: 10.1016/j.bbi.2016.11.004

Xie, Y. K., Zhou, X., Yuan, H. T., Qiu, J., Xin, D. Q., Chu, X. L., et al. (2019). Resveratrol reduces brain injury after subarachnoid hemorrhage by inhibiting oxidative stress and endoplasmic reticulum stress. *Neural Regen. Res.* 14, 1734–1742. doi: 10.4103/1673-5374.257529

Xie, Z., Huang, L., Enkhjargal, B., Reis, C., Wan, W., Tang, J., et al. (2018). Recombinant Netrin-1 binding UNC5B receptor attenuates neuroinflammation and brain injury via PPARγ/NFκB signaling pathway after subarachnoid hemorrhage in rats. *Brain Behav. Immun.* 69, 190–202. doi: 10.1016/j.bbi.2017.11.012

Xiong, Y., Xin, D. Q., Hu, Q., Wang, L. X., Qiu, J., Yuan, H. T., et al. (2020). Neuroprotective mechanism of L-cysteine after subarachnoid hemorrhage. *Neural Regen. Res.* 15, 1920–1930. doi: 10.4103/1673-5374.280321

Xu, H., Cai, Y., Yu, M., Sun, J., Cai, J., Li, J., et al. (2021). Celastrol protects against early brain injury after subarachnoid hemorrhage in rats through alleviating blood-brain barrier disruption and blocking necroptosis. *Aging (Albany NY)* 13, 16816–16833. doi: 10.18632/aging.203221

Xu, P., Tao, C., Zhu, Y., Wang, G., Kong, L., Li, W., et al. (2021). TAK1 mediates neuronal pyroptosis in early brain injury after subarachnoid hemorrhage. *J. Neuroinflammation* 18:188. doi: 10.1186/s12974-021-02226-8

Xu, W., Gao, L., Zheng, J., Li, T., Shao, A., Reis, C., et al. (2018). The roles of MicroRNAs in stroke: possible therapeutic targets. *Cell Transplant.* 27, 1778–1788. doi: 10.1177/0963689718773361

Xu, W., Li, F., Liu, Z., Xu, Z., Sun, B., Cao, J., et al. (2017). MicroRNA-27b inhibition promotes Nrf2/ARE pathway activation and alleviates intracerebral hemorrhage-induced brain injury. *Oncotarget* 8, 70669–70684. doi: 10.18632/oncotarget.19974

Xu, W., Li, T., Gao, L., Zheng, J., Yan, J., Zhang, J., et al. (2019). Apelin-13/APJ system attenuates early brain injury via suppression of endoplasmic reticulum stress-associated TXNIP/NLRP3 inflammasome activation and oxidative stress in a AMPK-dependent manner after subarachnoid hemorrhage in rats. *J. Neuroinflammation* 16:247. doi: 10.1186/s12974-019-1620-3

Xu, W., Yan, J., Ocak, U., Lenahan, C., Shao, A., Tang, J., et al. (2021). Melanocortin 1 receptor attenuates early brain injury following subarachnoid hemorrhage by controlling mitochondrial metabolism via AMPK/SIRT1/PGC-1α pathway in rats. *Theranostics* 11, 522–539. doi: 10.7150/thno.49426

Xue, Y., Nie, D., Wang, L. J., Qiu, H. C., Ma, L., Dong, M. X., et al. (2021). Microglial polarization: novel therapeutic strategy against ischemic stroke. *Aging Dis.* 12, 466–479. doi: 10.14336/ad.2020.0701

Yan, H., Zhang, D., Hao, S., Li, K., and Hang, C. H. (2015). Role of mitochondrial calcium uniporter in early brain injury after experimental subarachnoid hemorrhage. *Mol. Neurobiol.* 52, 1637–1647. doi: 10.1007/s12035-014-8942-z

Yang, C., Li, T., Xue, H., Wang, L., Deng, L., Xie, Y., et al. (2018). Inhibition of necroptosis rescues SAH-induced synaptic impairments in hippocampus via CREB-BDNF pathway. *Front. Neurosci.* 12:990. doi: 10.3389/fnins.2018.00990

Yang, C., Zhang, X., Fan, H., and Liu, Y. (2009). Curcumin upregulates transcription factor Nrf2, HO-1 expression and protects rat brains against focal ischemia. *Brain Res.* 1282, 133–141. doi: 10.1016/j.brainres.2009.05.009

Yang, S., Chen, X., Li, S., Sun, B., and Hang, C. (2018). Melatonin treatment regulates SIRT3 expression in early brain injury (EBI) due to reactive oxygen species (ROS) in a mouse model of subarachnoid hemorrhage (SAH). *Med. Sci. Monit.* 24, 3804–3814. doi: 10.12659/msm.907734

Yang, Y., Chen, S., and Zhang, J. M. (2017). The updated role of oxidative stress in subarachnoid hemorrhage. *Curr. Drug Deliv.* 14, 832–842. doi: 10.2174/1567201813666161025115531

Yatsushige, H., Ostrowski, R. P., Tsubokawa, T., Colohan, A., and Zhang, J. H. (2007). Role of c-Jun N-terminal kinase in early brain injury after subarachnoid hemorrhage. *J. Neurosci. Res.* 85, 1436–1448. doi: 10.1002/jnr.21281

Ye, Z. N., Wu, L. Y., Liu, J. P., Chen, Q., Zhang, X. S., Lu, Y., et al. (2018). Inhibition of leukotriene B4 synthesis protects against early brain injury possibly via reducing the neutrophil-generated inflammatory response and oxidative stress after subarachnoid hemorrhage in rats. *Behav. Brain Res.* 339, 19–27. doi: 10.1016/j.bbr.2017.11.011

Yu, Y. P., Chi, X. L., and Liu, L. J. (2014). A hypothesis: hydrogen sulfide might be neuroprotective against subarachnoid hemorrhage induced brain injury. *ScientificWorldJournal* 2014:432318. doi: 10.1155/2014/432318

Yuan, B., Zhou, X. M., You, Z. Q., Xu, W. D., Fan, J. M., Chen, S. J., et al. (2020). Inhibition of AIM2 inflammasome activation alleviates GSDMD-induced

pyroptosis in early brain injury after subarachnoid haemorrhage. *Cell Death Dis.* 11:76. doi: 10.1038/s41419-020-2248-z

Yuan, S., Yu, Z., Zhang, Z., Zhang, J., Zhang, P., Li, X., et al. (2019). RIP3 participates in early brain injury after experimental subarachnoid hemorrhage in rats by inducing necroptosis. *Neurobiol. Dis.* 129, 144–158. doi: 10.1016/j.nbd.2019.05.004

Zeyu, Z., Yuanjian, F., Cameron, L., and Sheng, C. (2021). The role of immune inflammation in aneurysmal subarachnoid hemorrhage. *Exp. Neurol.* 336:113535. doi: 10.1016/j.expneurol.2020.113535

Zhan, C. P., Zhuge, C. J., Yan, X. J., Dai, W. M., and Yu, G. F. (2021). Measuring serum melatonin concentrations to predict clinical outcome after aneurysmal subarachnoid hemorrhage. *Clin. Chim. Acta* 513, 1–5. doi: 10.1016/j.cca.2020.12.006

Zhang, C. S., Han, Q., Song, Z. W., Jia, H. Y., Shao, T. P., and Chen, Y. P. (2021). Hydrogen gas post-conditioning attenuates early neuronal pyroptosis in a rat model of subarachnoid hemorrhage through the mitoKATP signaling pathway. *Exp. Ther. Med.* 22:836. doi: 10.3892/etm.2021.10268

Zhang, L., Wu, J., Duan, X., Tian, X., Shen, H., Sun, Q., et al. (2016c). Oxidase: a potential target for treatment of stroke. *Oxid. Med. Cell. Longev.* 2016:5026984. doi: 10.1155/2016/5026984

Zhang, D., Zhang, H., Hao, S., Yan, H., Zhang, Z., Hu, Y., et al. (2016a). Akt specific activator SC79 protects against early brain injury following subarachnoid hemorrhage. *ACS Chem. Neurosci.* 7, 710–718. doi: 10.1021/acschemneuro.5b00306

Zhang, L., Kong, X. J., Wang, Z. Q., Xu, F. S., and Zhu, Y. T. A. (2016b). Study on neuroprotective effects of curcumin on the diabetic rat brain. *J. Nutr. Health Aging* 20, 835–840. doi: 10.1007/s12603-016-0723-0

Zhang, H. B., Tu, X. K., Chen, Q., and Shi, S. S. (2019). Propofol reduces inflammatory brain injury after subarachnoid hemorrhage: involvement of PI3K/Akt pathway. *J. Stroke Cerebrovasc. Dis.* 28:104375. doi: 10.1016/j.jstrokecerebrovasdis.2019.104375

Zhang, K., Cheng, H., Song, L., and Wei, W. (2020). Inhibition of the peroxisome proliferator-activated receptor gamma coactivator 1-alpha (PGC-1α)/sirtuin 3 (SIRT3) pathway aggravates oxidative stress after experimental subarachnoid hemorrhage. *Med. Sci. Monit.* 26:e923688. doi: 10.12659/msm.923688

Zhang, L., Li, Z., Feng, D., Shen, H., Tian, X., Li, H., et al. (2017). Involvement of Nox2 and Nox4 NADPH oxidases in early brain injury after subarachnoid hemorrhage. *Free Radic. Res.* 51, 316–328. doi: 10.1080/10715762.2017.1311015

Zhang, T., Su, J., Guo, B., Zhu, T., Wang, K., and Li, X. (2014a). Ursolic acid alleviates early brain injury after experimental subarachnoid hemorrhage by suppressing TLR4-mediated inflammatory pathway. *Int. Immunopharmacol.* 23, 585–591. doi: 10.1016/j.intimp.2014.10.009

Zhang, T., Su, J., Wang, K., Zhu, T., and Li, X. (2014b). Ursolic acid reduces oxidative stress to alleviate early brain injury following experimental subarachnoid hemorrhage. *Neurosci. Lett.* 579, 12–17. doi: 10.1016/j.neulet.2014.07.005

Zhang, T., Wu, P., Budbazar, E., Zhu, Q., Sun, C., Mo, J., et al. (2019). Mitophagy reduces oxidative stress via Keap1 (kelch-like epichlorohydrin-associated protein 1)/Nrf2 (nuclear factor-E2-related factor 2)/PHB2 (prohibitin 2) pathway after subarachnoid hemorrhage in rats. *Stroke* 50, 978–988. doi: 10.1161/strokeaha.118.021590

Zhang, T., Wu, P., Zhang, J. H., Li, Y., Xu, S., Wang, C., et al. (2018). Docosahexaenoic acid alleviates oxidative stress-based apoptosis via improving mitochondrial dynamics in early brain injury after subarachnoid hemorrhage. *Cell. Mol. Neurobiol.* 38, 1413–1423. doi: 10.1007/s10571-018-0608-3

Zhang, T., Zuo, G., and Zhang, H. (2021). GPR18 agonist resolvin D2 reduces early brain injury in a rat model of subarachnoid hemorrhage by multiple protective mechanisms. *Cell. Mol. Neurobiol.* doi: 10.1007/s10571-021-01114-2 [Epub ahead of print].

Zhang, X., Lu, Y., Wu, Q., Dai, H., Li, W., Lv, S., et al. (2019). Astaxanthin mitigates subarachnoid hemorrhage injury primarily by increasing sirtuin 1 and inhibiting the Toll-like receptor 4 signaling pathway. *FASEB J.* 33, 722–737. doi: 10.1096/fj.201800642RR

Zhang, X., Wu, Q., Lu, Y., Wan, J., Dai, H., Zhou, X., et al. (2018). Cerebroprotection by salvianolic acid B after experimental subarachnoid hemorrhage occurs via Nrf2- and SIRT1-dependent pathways. *Free Radic. Biol. Med.* 124, 504–516. doi: 10.1016/j.freeradbiomed.2018.06.035

Zhang, X. S., Lu, Y., Tao, T., Wang, H., Liu, G. J., Liu, X. Z., et al. (2020). Fucoxanthin mitigates subarachnoid hemorrhage-induced oxidative damage via sirtuin 1-dependent pathway. *Mol. Neurobiol.* 57, 5286–5298. doi: 10.1007/s12035-020-02095-x

Zhang, X. S., Wu, Q., Wu, L. Y., Ye, Z. N., Jiang, T. W., Li, W., et al. (2016). Sirtuin 1 activation protects against early brain injury after experimental subarachnoid hemorrhage in rats. *Cell Death Dis.* 7:e2416. doi: 10.1038/cddis.2016.292

Zhang, X. S., Zhang, X., Zhou, M. L., Zhou, X. M., Li, N., Li, W., et al. (2014). Amelioration of oxidative stress and protection against early brain injury by astaxanthin after experimental subarachnoid hemorrhage. *J. Neurosurg.* 121, 42–54. doi: 10.3171/2014.2.Jns13730

Zhang, Z. Y., Jiang, M., Fang, J., Yang, M. F., Zhang, S., Yin, Y. X., et al. (2017). Enhanced therapeutic potential of nano-curcumin against subarachnoid hemorrhage-induced blood-brain barrier disruption through inhibition of inflammatory response and oxidative stress. *Mol. Neurobiol.* 54, 1–14. doi: 10.1007/s12035-015-9635-y

Zhang, Z. Y., Yang, M. F., Wang, T., Li, D. W., Liu, Y. L., Zhang, J. H., et al. (2015). Cysteamine alleviates early brain injury via reducing oxidative stress and apoptosis in a rat experimental subarachnoid hemorrhage model. *Cell. Mol. Neurobiol.* 35, 543–553. doi: 10.1007/s10571-014-0150-x

Zhao, H., Chen, Y., and Feng, H. (2018). P2X7 receptor-associated programmed cell death in the pathophysiology of hemorrhagic stroke. *Curr. Neuropharmacol.* 16, 1282–1295. doi: 10.2174/1570159X16666180516094500

Zhong, Y. W., Wu, J., Hu, H. L., Li, W. X., and Zhong, Y. (2016). Protective effect 3,4-dihydroxyphenylethanol in subarachnoid hemorrhage provoked oxidative neuropathy. *Exp. Ther. Med.* 12, 1908–1914. doi: 10.3892/etm.2016.3526

Zhu, Q., Enkhjargal, B., Huang, L., Zhang, T., Sun, C., Xie, Z., et al. (2018). Aggf1 attenuates neuroinflammation and BBB disruption via PI3K/Akt/NF-κB pathway after subarachnoid hemorrhage in rats. *J. Neuroinflammation* 15:178. doi: 10.1186/s12974-018-1211-8

Zhuang, K., Zuo, Y. C., Sherchan, P., Wang, J. K., Yan, X. X., and Liu, F. (2019). Hydrogen inhalation attenuates oxidative stress related endothelial cells injury after subarachnoid hemorrhage in rats. *Front. Neurosci.* 13:1441. doi: 10.3389/fnins.2019.01441

Zhuang, Z., Zhou, M. L., You, W. C., Zhu, L., Ma, C. Y., Sun, X. J., et al. (2012). Hydrogen-rich saline alleviates early brain injury via reducing oxidative stress and brain edema following experimental subarachnoid hemorrhage in rabbits. *BMC Neurosci.* 13:47. doi: 10.1186/1471-2202-13-47

Zolnourian, A., Galea, I., and Bulters, D. (2019). Neuroprotective role of the Nrf2 pathway in subarachnoid haemorrhage and its therapeutic potential. *Oxid. Med. Cell. Longev.* 2019:6218239. doi: 10.1155/2019/6218239

Zuo, G., Zhang, T., Huang, L., Araujo, C., Peng, J., Travis, Z., et al. (2019). Activation of TGR5 with INT-777 attenuates oxidative stress and neuronal apoptosis via cAMP/PKCε/ALDH2 pathway after subarachnoid hemorrhage in rats. *Free Radic. Biol. Med.* 143, 441–453. doi: 10.1016/j.freeradbiomed.2019.09.002

Zuo, Y., Huang, L., Enkhjargal, B., Xu, W., Umut, O., Travis, Z. D., et al. (2019). Activation of retinoid X receptor by bexarotene attenuates neuroinflammation via PPARγ/SIRT6/FoxO3a pathway after subarachnoid hemorrhage in rats. *J. Neuroinflammation* 16:47. doi: 10.1186/s12974-019-1432-5

Conflict of Interest: The authors declare that the research was conducted in the absence of any commercial or financial relationships that could be construed as a potential conflict of interest.

Publisher's Note: All claims expressed in this article are solely those of the authors and do not necessarily represent those of their affiliated organizations, or those of the publisher, the editors and the reviewers. Any product that may be evaluated in this article, or claim that may be made by its manufacturer, is not guaranteed or endorsed by the publisher.

frontiers in Aging Neuroscience

CASE REPORT
published: 14 December 2021
doi: 10.3389/fnagi.2021.765037

Intravenous Thrombolysis After Reversal of Dabigatran With Idarucizumab in Acute Ischemic Stroke: A Case Report

*Dan Xie[1], Xuefan Wang[1], Yao Li[1], Ruiling Chen[1], Yingying Zhao[1], Chunling Xu[1], Qian Zhang[2] and Yongbo Zhang[1]**

[1] Department of Neurology, Beijing Friendship Hospital, Capital Medical University, Beijing, China, [2] Department of Neurology, Beijing Tiantan Hospital, Capital Medical University, Beijing, China

OPEN ACCESS

Edited by:
Gaiqing Wang,
The Third People's Hospital of Hainan Province, China

Reviewed by:
Senta Frol,
University Medical Centre Ljubljana, Slovenia
Zhen-Ni Guo,
First Affiliated Hospital of Jilin University, China

***Correspondence:**
Yongbo Zhang
smart1226@sina.com;
yongbozhang@ccmu.edu.cn

Specialty section:
This article was submitted to Neuroinflammation and Neuropathy, a section of the journal Frontiers in Aging Neuroscience

Received: 26 August 2021
Accepted: 28 October 2021
Published: 14 December 2021

Citation:
Xie D, Wang X, Li Y, Chen R, Zhao Y, Xu C, Zhang Q and Zhang Y (2021) Intravenous Thrombolysis After Reversal of Dabigatran With Idarucizumab in Acute Ischemic Stroke: A Case Report. Front. Aging Neurosci. 13:765037. doi: 10.3389/fnagi.2021.765037

Background: As there is a growing concern about the cerebral embolism events secondary to non-valvular atrial fibrillation (NVAF), novel oral anticoagulant (NOAC) has been more and more widely used as an anticoagulation treatment for the prevention of stroke. However, in the face of life-threatening bleeding or emergency surgery/treatment, NOAC-related antagonists such as idarucizumab need to be urgently used to reverse the NOAC. Using recombinant tissue plasminogen activator (rt-PA) intravenous thrombolysis for acute ischemic stroke requires a time window of 4.5 h. This case reports rt-PA intravenous thrombolysis after reversal of dabigatran anticoagulation with idarucizumab in patients with acute ischemic stroke.

Case Presentation: We report the case of 62-year-old Chinese female with NVAF treated with dabigatran 110 mg twice daily, and missed a dose on the eve of the stroke. The patient presented with acute ischemic stroke causing the angle of mouth deviated to right side and left limb weakness in the early morning of the next day. However, the last dosing time of dabigatran was between 24 and 48 h, the patients were given rt-PA intravenous thrombolysis after reversal of dabigatran anticoagulation with idarucizumab, while any potential relative contraindication had been excluded by means of laboratory test and CT scan in the hospitalization services. National Institute of Health stroke scale (NIHSS) score was reduced from 4 to 1, and the patient was discharged after 2 weeks.

Conclusion: Our case report adds to the evidence that idarucizumab administration is safe and effective in the setting of patients with atrial fibrillation treated with dabigatran who develop acute ischemic stroke requiring rt-PA intravenous thrombolysis.

Keywords: acute ischemic stroke, dabigatran, anticoagulation, intravenous thrombolysis, idarucizumab

BACKGROUND

Acute ischemic stroke is a serious threat to the health of Chinese residents and increased yearly. It is the leading cause of death for urban residents in China and characterized by high morbidity and lethality, high rate of recurrence and disability, and high treatment cost. Cardiac embolism secondary to non-valvular atrial fibrillation (NVAF) accounts for 13–26% of ischemic stroke patients for whom long-term and stable anticoagulant therapy is very important (Ist-3 collaborative group, 2015; Seiffge et al., 2019). Compared with warfarin, novel oral anticoagulant (NOAC) significantly reduced the incidence of stroke by 19%, among which dabigatran significantly reduced the incidence of stroke by 34%. There was no significant difference in the overall incidence of major bleeding between the two (Ruff et al., 2014). Thus, clinical application of NOAC has been both recommend by "2019 AHA/ACC/HRS Guideline for the Management of Patients with Atrial Fibrillation" and the "Guideline of stroke prevention in Chinese patients with atrial fibrillation (2017)" (Zhang et al., 2017; January et al., 2019). In order to save the patients' lives and improve the prognosis, it is particularly critical to treat the patients with corresponding antagonists when life-threatening bleeding or emergency surgery/treatment occurs in the users of NOAC as their widespread clinical application in China. Idarucizumab, an antagonist of dabigatran, was approved in China in February 2019. However, there is still very limited data on the efficacy and safety on idarucizumab's use in China. Here, we report the first case of acute stroke using the recombinant tissue plasminogen activator (rt-PA) intravenous thrombolysis after the reversal of dabigatran anticoagulation with idarucizumab within the time window of thrombolysis in China.

CASE REVIEW

The 62-year-old female patient was admitted to a neurology emergency at 8:50 a.m. on November 1, 2019, due to "sudden verbal slant accompanied by left limb weakness for 1.5 h." She was suddenly appeared the left side of the mouth aslant, conscious of numbness and weakness of the limb on the same side, when she was having breakfast in the morning (7:20 a.m.), and could still walk by herself without headache, dizziness, unclear vision, speech deficit, or any other manifestations. Her family drove her to the hospital immediately. She had a history of hypertension for more than 30 years without regularly monitoring. The highest blood pressure was 150/100 mmHg, taking valsartan 80 mg Qd. She also had a hyperlipidemia history for 6 years, with long-term administration rosuvastatin 5 mg Qn. She was hospitalized in our Department of Cardiology 6 months ago due to "atrial flutter" and received metoprolol 12.5 mg twice daily. One month ago, she had been hospitalized again in another hospital and diagnosed as "pathological sinus syndrome and paroxysmal atrial fibrillation" due to "atrial fibrillation," and was treated with dabigatran 110 mg twice daily but without a good compliance. She had no special family history or history of migraine. Physical examination: BP: 131/81 mmHg (right) and 130/84 mmHg (left). There was no uplift or depression in the anterior cardiac area, and the strongest apex pulsation point was 0.5–1.0 cm within the midline of the fifth intercostal left clavicle. There was no lifting pulsation, no tremor or pericardial friction. The relative voiced boundary of the heart is normal. Heart rate: 76 beats/min, regular rhythm, normal cardiac sounds, A2 > P2, no extracardiac sounds, no cardiac murmurs, and no pericardial fricative sounds in the auscultation area of each valve.

The patient had clear mind and fluent speech, equal circle of bilateral pupils, direct/indirect response to light exists, and the eyeball moves fully in each direction, without diplopia and nystagmus. The left frontal line, nasolabial groove shallow, show the mouth angle to the right, extending tongue in the center. Double soft palate lift normal, uvula in the middle, pharyngeal reflex normal. Muscle strength of left limb grade V, bilateral finger nose test and heel-knee-tibia test accurate, bilateral Babinski's sigh negative. There were hypoesthesia of the left limb, negative response upon meningeal stimulation, and a normal water swallow test result. In the carotid auscultation area, bilateral carotid artery vascular murmur was not heard. The calculated National Institute of Health stroke scale (NIHSS) score was a total of 4 points (2 points for facial paralysis, left weakness 1 point and left numbness 1 point).

The patient mentioned that she did not usually take any medication in the morning but she missed one dose of dabigatran (110 mg) the last evening after she took dabigatran at around 8 a.m. the same day. Accordingly, the last NOAC dose taking was between 24 and 48 h. Upon her emergency fast track for stroke, completed head CT, ECG, blood routine, biochemical, and coagulation function test were followed. Her head CT was normal, blood glucose was 5.5 mmol/L, and the ECG showed sinus rhythm of 72 beats/min. Coagulation function results showed activated partial thromboplastin time (APTT) 32.7 s, prothrombin time (PT) 12.3 s, International standard ratio (INR) 1.06, and creatinine clearance (Ccr) 68.62 ml/min. As ecarin coagulation time (ECT) and direct prothrombin activity were tested, idarucizumab was given at 11 a.m. with a dose of 2.5 g, followed by another 2.5 g at an interval of 5 min, and coagulation function was tested again after the administration (**Table 1**). The rt-PA thrombolysis therapy was initiated at 11:35 a.m. after the completion of the administration of idarucizumab, with a dose of 0.9 mg/kg. During the thrombolysis process, vital signs such as heart rate and blood pressure were monitored, and the NIHSS score was evaluated every 15 min (**Figure 1**). The symptoms of facial paralysis and limb numbness and weakness of the patient were significantly improved after thrombolysis. The NIHSS score was 1 (facial paralysis 1), and the patient was admitted to the stroke ward for further treatment.

Vital signs were monitored within 24 h after admission; the patient got external auditory canal bleeding 3 h after thrombolysis. The further investigation and inquiry on her medical history showed a history of ear trauma 1 week before. Bleeding was stopped *via* external auditory canal tamponage. The cranial MRI and systemic vascular examination were arranged to find the cause of stroke, no abnormal signal was found in T1-weighted imaging, T1WI (T1), T2-weighted imaging, T2WI (T2), and diffusion-weighted imaging (DWI), and

TABLE 1 | Hemostasis testing before (1), in course of (2), and after (3, 4) idarucizumab administration.

	Blood sample 1 9:20 a.m. 1/11	Blood sample 2 11:09 a.m. 1/11	Blood sample 3 11:18 a.m. 1/11	Blood sample 4 11:20 a.m. 2/11	Reference value of units
Activated partial thromboplastin time (APTT)	32.7	29.4	30.2	31.90	28.00–42.50 s
Prothrombin time (PT)	12.3	12.2	11.7	12.0	11.00–15.00 s
Normalized ratio (INR)	1.06	1.05	1.01	1.04	0.80–1.20
Fibrinogen degradation product (FDP)	0.60	0.80	2.90	1.60	0.00–5.00 μg/ml
D-dimers	0.40	0.33	0.70	0.40	0.000–1.000 μg/ml
Fibrinogen (Fbg)	2.64	2.50	2.20	2.08	2.00–4.00 g/L
Prothrombin activity [PT(A)]	88.1	89.2	94.2	91.4	70.00–120.00%
Antithrombin III	98.9	76.1	90.8	78.8	70.00–120.00%

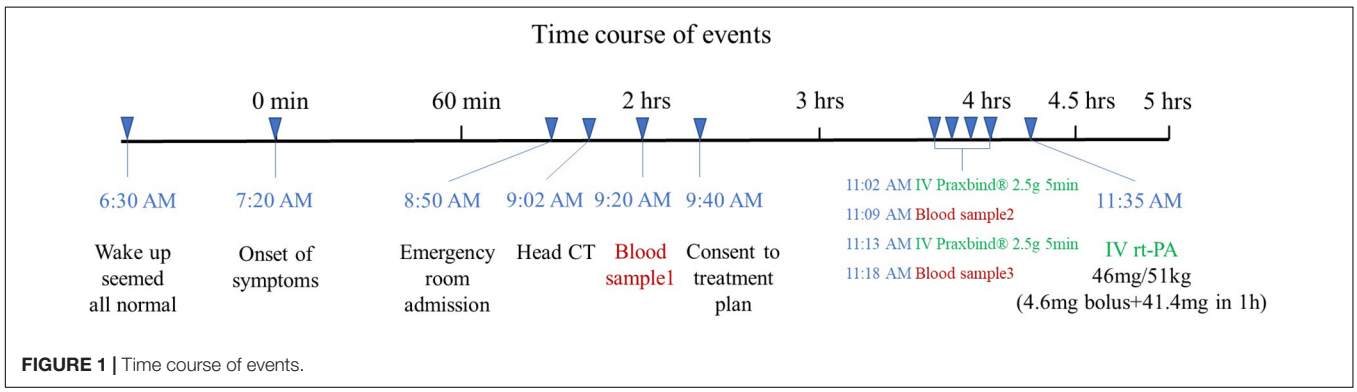

FIGURE 1 | Time course of events.

there was no microhemorrhage-related signal in susceptibility weighted imaging (SWI) (**Figure 2**). In the magnetic resonance angiography (MRA) measurement, intracranial vessels were indicated normal and bilateral embryonic posterior cerebral arteries were observed. Carotid ultrasound showed bilateral carotid intima thickening with plaque formation and plaque was found in the right subclavian artery. Arteriovenous ultrasound of lower extremity showed normal. Transcranial Doppler showed a rapid increase in the flow rate of the left middle cerebral artery, and 5–6 microembolic could be found in foaming experiment, supporting a direct pathway from pulmonary circulation to the systemic circulation (RLS). Cardiac systemic examination was completed: 24-h Holter showed sinus bradycardia, short atrial tachycardia, and atrial premature beats (some of which were not transmitted). Widening ascending aorta was shown on echocardiography. Thrombus was not found in bilateral atrium and left auricle in transesophageal echocardiography, also no septal shunt beam was observed in the atrial septal fossa ovale. From the data that were collected from the other hospital, left atrium was slightly larger and the middle branch of the right pulmonary vein was mutated on the CT angiography (CTA) of the left atria and pulmonary veins on 26th September (**Figure 3**). Diagnosis of transient ischemic attack, cardiogenic cerebral embolism, paroxysmal atrial fibrillation, pulmonary arteriovenous fistula, hypertension with Grade 2, and hyperlipidemia were observed after admission. She was suggested to restart the anticoagulant treatment deal to the CHA_2DS_2-VAS score was 4 and HAS-BLED score was 2. The pulmonary artery digital subtraction angiography (DSA) was also suggested after patients were discharged.

DISCUSSION

In China, the anticoagulation compliance rate (INR 2.0–3.0) among the atrial fibrillation patients who are taking the warfarin was only 36% and most of their INR ware remained at <2.0 (Zhao and Huang, 2018). In recent years, the anticoagulant treatment has been effectively simplified with the marketing of direct oral anticoagulants. NOAC has been selected by more and more patients with atrial fibrillation in clinical since its efficacy and safety have been confirmed in multiple international clinical trials such as RE-LY (Poller et al., 2009; Davis et al., 2017). In our case, an embolic stroke still occurred while the patient took dabigatran 110 mg twice daily. There were two causes to be considered: (1) The dose of dabigatran was insufficient, it should be adjusted to 150 mg twice daily after stroke. (2) Although the patient was prescribed with dabigatran, she failed to follow medical advice and took the medicine regularly, which may be the incentive cause for an embolic stroke. Therefore, the dosage of dabigatran should be adjusted according to the happening of the embolization stroke and the compliance of patients should be considered in the selection of anticoagulation. In the process of NOAC, doctors and patients are also concerned about the possible life-threatening bleeding such as acute intracranial hemorrhage and massive gastrointestinal bleeding, or the emergency cases such as acute abdominal disease and fracture requiring **emergency surgery/treatment**. As a specific antagonist of dabigatran, idarucizumab, which has just been approved in China in February 2019, can bind to dabigatran irreversibly and effectively as it has an affinity for dabigatran 350 times than dabigatran for thrombin, was recommended by

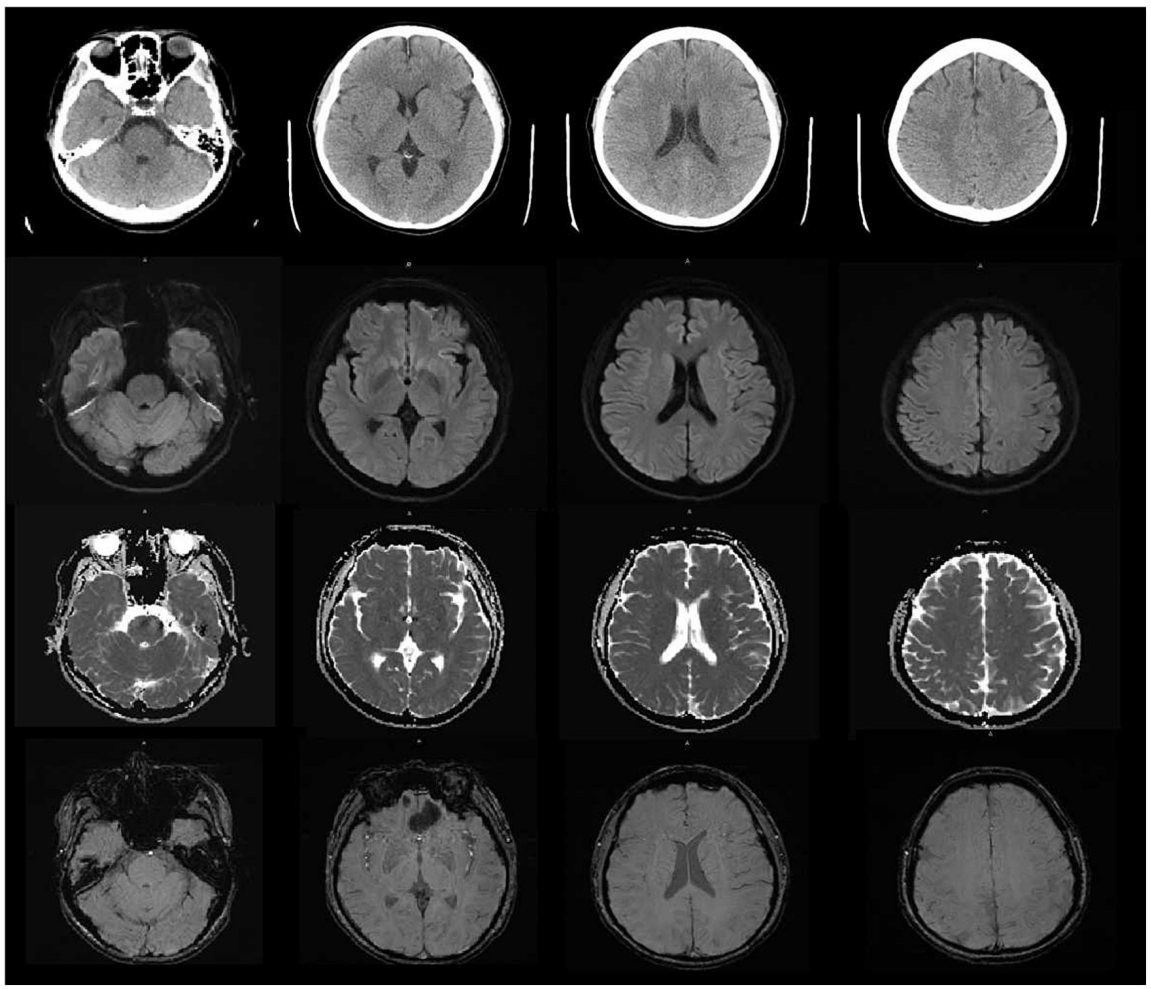

FIGURE 2 | The cranial MRI showed no abnormal signal was found in T1-weighted imaging,T1WI (TI), T2-weighted imaging,T2WI (T2), diffusion-weighted imaging (DWI) and susceptibility weighted imaging (SWI).

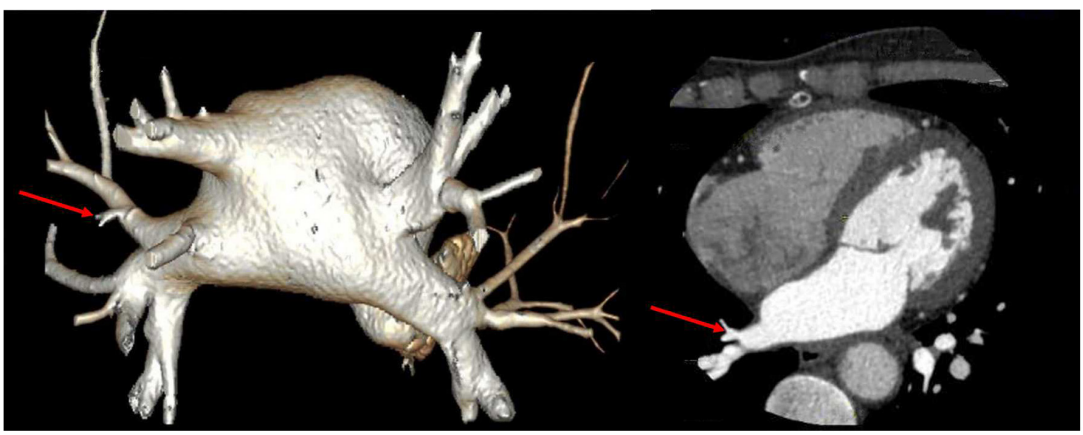

FIGURE 3 | CT angiography (CTA) of left atria-pulmonary vein showed the middle branch of the right pulmonary vein was variable.

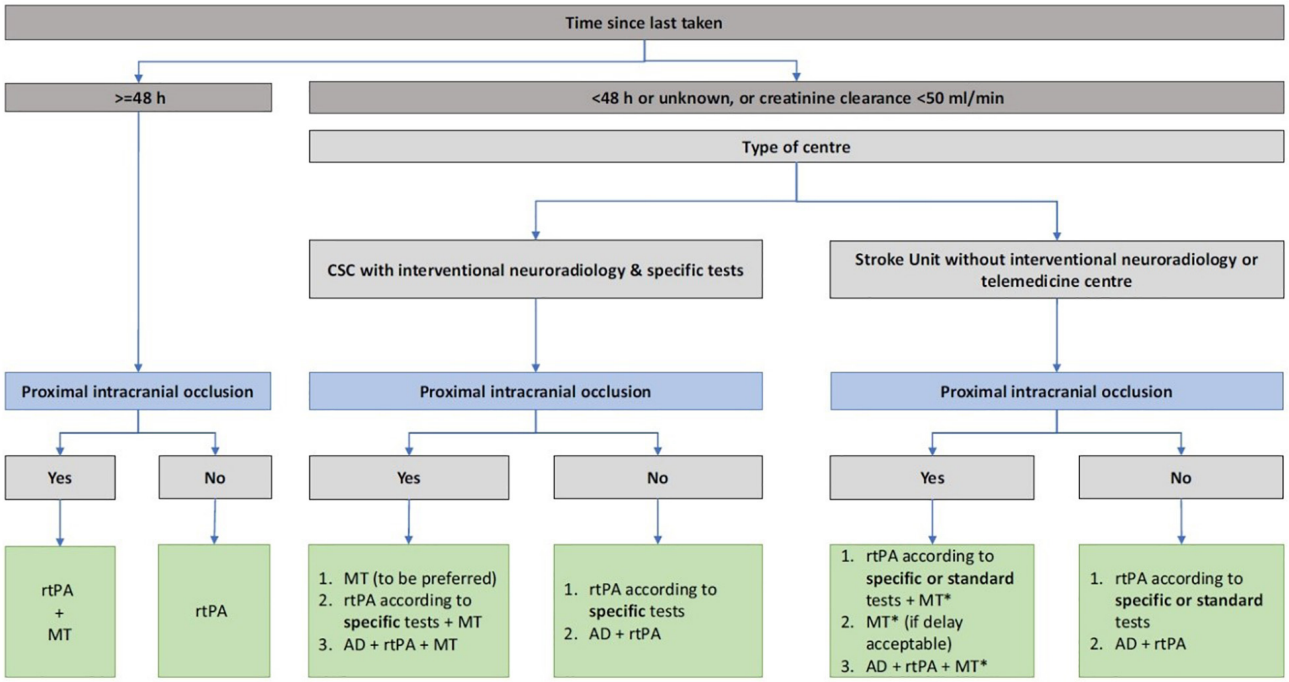

FIGURE 4 | The different treatment of acute ischemic stroke in patients according to the last dosing time of novel oral anticoagulant, renal function, stroke center qualification.

the European Heart Rhythm Association for the treatment of patients with bleeding and emergency surgery under oral NOAC (Steffel et al., 2018). As an exogenous humanized monoclonal antigen–antibody binding fragment (Fab), idarucizumab can quickly intravenous administration and irreversibly bind to dabigatran immediately. Idarucizumab can specifically bind to free dabigatran, dabigatran that has been bound to thrombin, and the active metabolites of dabigatran to form a complex, resulting in the inability of dabigatran to bind to thrombin, reversal the anticoagulant effect of dabigatran. Moreover, idarucizumab has no endogenous target, and no reversal effect on heparin or other anticoagulant drugs, so it does not interfere with the coagulation cascade and has no procoagulant effect (Schiele et al., 2013; Eikelboom et al., 2015; Frontera et al., 2016). In our case, intravenous infusion of idarucizumab lasted for 16 min, and rt-PA treatment could be initiated immediately 10–15 min later. The European Stroke Organization guidelines provide evidence-based recommendations to assist physicians in their clinical decisions with regard to intravenous thrombolysis for acute ischemic stroke, and recommend intravenous thrombolysis with alteplase to improve functional outcome in patients with acute ischemic stroke within 4.5 h after symptom onset (Berge et al., 2021). Idarucizumab could affect immediately that is more suitable for stroke patients within 4.5 h for intravenous thrombolysis or within 6 h for arterial thrombectomy in emergency. However, this case also has the following limitations: (1) the patient failed to initiate thrombolytic therapy within 3 h after the onset as it took a certain amount of time for her to obtain idarucizumab due to the unavailability at emergency department. (2) The time of last dose of dabigatran was between 24 and 48 h. Although coagulation indexes, such as APTT and PT and INR index, had been monitored before and after use, no obvious changes were found. The more important coagulation indexes like ECT, TT, and direct prothrombin activity were unavailable in emergency laboratory. At that point, it was difficult to decide whether rt-PA could be used without reversal of idarucizumab. It shouldbe expected to get improving in similar cases. With the application of idarucizumab, we also needed to be alerted to the occurrence of adverse events. The REVERSE-AD study showed that 0.6% of patients who used idarucizumab had hypersensitivity reactions within 5 days of administration, such as fever and bronchospasm, hyperventilation, skin rash, and itching. And other adverse reactions such as hereditary fructose intolerance, transient proteinuria also had been reported (U.S.Food and Drug Adminstration, 2015). In a French retrospective research, patients with an acute ischemic stroke treated with dabigatran within 48 h were given intravenous thrombolysis after the reversal of idarucizumab without direct prothrombin activity monitoring (Touzé et al., 2018). According to the relationship between the onset time of stroke and her last dose for dabigatran, a different treatment plan was thereby recommended, combining with different medical conditions (**Figure 4**). Caponi reviewed 55 thrombolytic cases after idarucizumab reversal of dabigatran showed that 81.9% (45 cases) of patients had improved NIHSS score (median 5 points), together with follow-up mRS <2 in 56% of patients, suggest that effectiveness for intravenous thrombolysis (IVT) has been preserved. In a retrospective study of 120 patients

with acute ischemic/hemorrhagic stroke in Germany, the efficacy and safety of idarucizumab reversal of dabigatran in intravenous thrombolysis with an acute ischemic stroke had been confirmed (Caponi et al., 2018). There is a new data analysis which has performed a comprehensive review of 251 cases of patients with acute ischemic stroke (AIS) performed IVT after idarucizumab reversal. Regardless of stroke severity and age, there was a significant NIHSS reduction of 6 points post-stroke and linear regression revealed a correlation of admission NIHSS to NIHSS reduction ($p < 0.001$). Reassuring evidence about the safety and efficacy of this therapeutic strategy was provided (Frol et al., 2021). However, in patients with hemorrhagic stroke, the application of idarucizumab can prevent the expansion of hematoma and improve the prognosis of patients as the bleeding may be caused by dabigatran (Kermer et al., 2020). These suggest the safety and usability of reversal of dabigatran in IVT.

CONCLUSION

As the first case of ischemic stroke treated with intravenous thrombolysis after idarucizumab reversal of dabigatran in China, this case was considered a mild stroke (NIHSS $\leq$5 points). After treatment, the NIHSS score of patient was significantly improved indicating a good prognosis. In this case, the efficacy of idarucizumab in the treatment of acute ischemic stroke patients using dabigatran was confirmed, and no directly related side-effects was found, suggesting that idarucizumab could be used as an emergency medication for patients with an acute stroke. As the only approved NOAC antagonist in China, the efficacy and safety of idarucizumab need to be confirmed in more clinical cases. Especially in the clinical application of acute stroke patients, the stratification screening in emergency situations, selection of medication, and laboratory tests still need to be improved.

DATA AVAILABILITY STATEMENT

The original contributions presented in the study are included in the article/supplementary material, further inquiries can be directed to the corresponding author.

ETHICS STATEMENT

Written informed consent was obtained from the individual(s) for the publication of any potentially identifiable images or data included in this article.

AUTHOR CONTRIBUTIONS

All authors listed have made a substantial, direct, and intellectual contribution to the work, and approved it for publication.

FUNDING

This study was supported by the National Natural Science Foundation of China, No. 81671191 to YOZ and Inner Mongolia Natural Science Foundation, No. 2020MS03017 to DX.

ACKNOWLEDGMENTS

We are particularly grateful to the Radiology Department of Tiantan Hospital for providing the imaging data.

REFERENCES

Berge, E., Whiteley, W., Audebert, H., De Marchis, G. M., Fonseca, A. C., Padiglioni, C., et al. (2021). European Stroke Organisation (ESO) guidelines on intravenous thrombolysis for acute ischaemic stroke. *Eur. Stroke J.* 6, I–LXII. doi: 10.1177/2396987321989865

Caponi, C., Mengoni, A., Romoli, M., Marando, C., Gallina, A., Marsili, E., et al. (2018). Intravenous thrombolysis in stroke after dabigarran reversal with idarucizumab:case series and systemic review. *J. Neurol. Neurosurg. Psychiatry* 90, 619–623. doi: 10.1136/jnnp-2018-318658

Davis, S., Butcher, K., Diener, H. C., Bernstein, R., Campbell, B., Cloud, G., et al. (2017). Thrombolysis and thrombectomy in patients treated with dabigatran with acute ischemic stroke: expert opinion. *Int. J. Stroke* 12, 9–12. doi: 10.1177/1747493016669849

Eikelboom, J. W., Quinlan, D. J., van Ryn, J., and Weitz, J. I. (2015). Idarucizumab: theantidote for reversal of dabigatran. *Circulation* 132, 2412–2422.

Frol, S., Sagris, D., Oblak, J. P., Šabovič, M., and Ntaios, G. (2021). Intravenous thrombolysis after dabigatran reversal by idarucizumab: a systematic review of the literature. *Front. Neurol.* 12:666086. doi: 10.3389/fneur.2021.666086

Frontera, J. A., Lewin, J. J. III, Rabinstein, A. A., Aisiku, I. P., Alexandrov, A. W., Cook, A. M., et al. (2016). Guideline for reversal of antithrombotics in intracranial hemorrhage: a statement for healthcare professionals from the neurocritical care society and society of critical care medicine. *Neurocrit. Care* 24, 6–46.

Ist-3 collaborative group (2015). Association between brain imaging signs, early and late outcomes, and response to intravenous alteplase after acute ischaemic stroke in the third International Stroke Trial (IST-3): secondary analysis of a randomised controlled trial. *Lancet Neurol.* 14, 485–496. doi: 10.1016/S1474-4422(15)00012-5

January, C. T., Wann, L. S., Calkins, H., Chen, L. Y., Cigarroa, J. E., Cleveland, J. C. Jr., et al. (2019). AHA/ACC/HRS focused update of the 2014 AHA/ACC/HRS guideline for the management of patients with atrial fibrillation. *J. Am. Coll. Cardiol.* 74, 104–132. doi: 10.1016/j.jacc.2019.01.011

Kermer, P., Eschenfelder, C. C., Diener, H. C., Grond, M., Abdalla, Y., Abraham, A., et al. (2020). Antagonizing dabigatran by idarucizumab in cases of ischemic stroke or intracranial hemorrhage in Germany—updated series of 120 cases. *Int. J. Stroke* 15, 609–618.

Poller, L., Jespersen, J., and Ibrahim, S. (2009). Dabigatran versus warfarin in patients with atrial fibrillation. *N. Engl. J. Med.* 361, 1139–1151.

Ruff, C. T., Giugliano, R. P., Braunwald, E., Hoffman, E. B., Deenadayalu, N., Ezekowitz, M. D., et al. (2014). Comparison of the efficacy and safety of new oral anticoagulants with warfarin in patients with atrial fibrillation: a meta-analysis of randomised trials. *Lancet* 383, 955–962.

Schiele, F., Van Ryn, J., Canada, K., Newsome, C., Sepulveda, E., Park, J., et al. (2013). A specific antidote for dabigatran: functional and structural characterization. *Blood* 121, 3554–3562. doi: 10.1182/blood-2012-11-468207

Seiffge, D. J., Werring, D. J., Paciaroni, M., Dawson, J., Warach, S., Milling, T. J., et al. (2019). Timing of anticoagulation after recent ischaemic stroke in patients with atrial fibrillation. *Lancet Neurol.* 18, 117–126.

Steffel, J., Verhamme, P., Potpara, T. S., Albaladejo, P., Antz, M., Desteghe, L., et al. (2018). ESC scientific document group. The 2018 European Heart Rhythm Association Practical Guide on the use of non-vitamin K antagonist oral anticoagulants in patients with atrial fibrillation. *Eur. Heart J.* 39, 1330–1393. doi: 10.1093/eurheartj/ehy136

Touzé, E., Gruel, Y., Gouin, T., De Maistre, E., Susen, S., Sie, P., et al. (2018). Intravenous thrombolysis for acute ischaemic stroke in patients on direct oral anticoagulants. *Eur. J. Neurol.* 25, 747–e52.

U.S.Food and Drug Adminstration (2015). *Highlight of PRAXBIND(idarucizumab) Injection Prescribing Information [EB/OL]*. Available online at: https://www.fda.gov/drugsatfda_docs/label/2018/761025s002lbl.pdf (accessed February 06, 2020).

Zhang, S., Yan-min, Y., Cong-Xin, H., Dejia, H., Kejiang, C., Jun, Z., et al. (2017). Guideline of stroke prevention in Chinese patients with atrial fibrillation. *Chin. J .Cardiac. Arrhythm.* 2018, 17–30.

Zhao, X. X., and Huang, S. Q. (2018). Early secondary prevention of cardiogenic stroke caused by atrial fibrillation. *Acad. J. Second Mil. Med. Univ.* 39, 35–39. doi: 10.1016/b978-0-323-55429-9.00003-0

Conflict of Interest: The authors declare that the research was conducted in the absence of any commercial or financial relationships that could be construed as a potential conflict of interest.

Publisher's Note: All claims expressed in this article are solely those of the authors and do not necessarily represent those of their affiliated organizations, or those of the publisher, the editors and the reviewers. Any product that may be evaluated in this article, or claim that may be made by its manufacturer, is not guaranteed or endorsed by the publisher.

frontiers in Aging Neuroscience

MINI REVIEW
published: 01 February 2022
doi: 10.3389/fnagi.2022.813756

Microstructure and Genetic Polymorphisms: Role in Motor Rehabilitation After Subcortical Stroke

Jingchun Liu[1] *and Caihong Wang*[2]*

[1]Department of Radiology and Tianjin Key Laboratory of Functional Imaging, Tianjin Medical University General Hospital, Tianjin, China, [2]Department of MRI, Key Laboratory for Functional Magnetic Resonance Imaging and Molecular Imaging of Henan Province, The First Affiliated Hospital of Zhengzhou University, Zhengzhou, China

Background and Purpose: Motor deficits are the most common disability after stroke, and early prediction of motor outcomes is critical for guiding the choice of early interventions. Two main factors that may impact the response to rehabilitation are variations in the microstructure of the affected corticospinal tract (CST) and genetic polymorphisms in brain-derived neurotrophic factor (BDNF). The purpose of this article was to review the role of these factors in stroke recovery, which will be useful for constructing a predictive model of rehabilitation outcomes.

Summary of Review: We review the microstructure of the CST, including its origins in the primary motor area (M1), primary sensory area (S1), premotor cortex (PMC), and supplementary motor area (SMA). Damage to these fibers is disease-causing and can directly affect rehabilitation after subcortical stroke. BDNF polymorphisms are not disease-causing but can indirectly affect neuroplasticity and thus motor recovery. Both factors are known to be correlated with motor recovery. Further work is needed using large longitudinal patient samples and animal experiments to better establish the role of these two factors in stroke rehabilitation.

Conclusions: Microstructure and genetic polymorphisms should be considered possible predictors or covariates in studies investigating motor recovery after subcortical stroke. Future predictive models of stroke recovery will likely include a combination of structural and genetic factors to allow precise individualization of stroke rehabilitation strategies.

Keywords: cerebral infarction, corticospinal tract (CST), genetic polymorphisms, motor, rehabilitation

OPEN ACCESS

Edited by:
Yujie Chen,
Army Medical University, China

Reviewed by:
Yutaka Oouchida,
Osaka Kyoiku University, Japan
Jia-Ching Shieh,
Chung Shan Medical University, Taiwan

***Correspondence:**
Caihong Wang
fccwangch@zzu.edu.cn

Received: *12 November 2021*
Accepted: *07 January 2022*
Published: *01 February 2022*

Citation:
Liu J and Wang C (2022) Microstructure and Genetic Polymorphisms: Role in Motor Rehabilitation After Subcortical Stroke. Front. Aging Neurosci. 14:813756. doi: 10.3389/fnagi.2022.813756

INTRODUCTION

Most stroke patients experience motor deficits (Johnson and Westlake, 2021) that adversely affect clinical outcomes and impair activities of daily living (Patel et al., 2020). The early prediction of motor outcomes is of great significance for improving prognosis and designing interventions. Many factors impact motor rehabilitation, including individual factors (e.g., age and sex) and disease severity (e.g., lesion location, lesion size, and white-matter tract integrity; Sterr et al., 2014). However, these traditional factors have many limitations in predicting rehabilitation outcomes

following subcortical stroke. The white-matter tract integrity of motor pathway in traditional factors is an important factor in directly assessing the prognosis of patient motor function (Liu et al., 2020). However, there are still some challenges in using a single white-matter tract integrity indicator to predict the recovery of motor function in clinical applications. Increasing evidence suggests that genetic polymorphisms may partially explain the frequently reported variability in individual responses to interventions for rehabilitation (Shiner et al., 2016). However, the relationship between genetic polymorphisms and the degree of motor rehabilitation is complex, therefore the single genetic factor also cannot comprehensively predict rehabilitation outcomes after subcortical stroke. Currently, several studies have found that a predictive model combining the microstructural integrity of the motor pathway in traditional factors and gene polymorphisms is significantly better than for models with only one factor for stroke patients (Chang et al., 2017).

The integrity of motor pathways (e.g., the corticospinal and cortico-rubro-spinal tracts) plays an important role in motor dysfunction and recovery after stroke (Kim et al., 2018; Guo et al., 2019; Zolkefley et al., 2021). The corticospinal tract (CST) is the most important motor output pathway and has been deemed the most common locus of motor deficits in subcortical stroke. CST fibers arise from the primary motor area (M1), the premotor cortex (PMC), the supplementary motor area (SMA), and the primary somatosensory area (S1; Schieber, 2007; Welniarz et al., 2017). Differential involvement of the CST plays an important role in determining the outcomes of motor rehabilitation following subcortical stroke.

Genetic polymorphisms that can affect neuroplasticity include those of brain-derived neurotrophic factor (BDNF), the dopamine neurotransmitter system, and apolipoprotein E (Stewart and Cramer, 2017). Since BDNF is the most important neurotrophin, BDNF polymorphisms play a key role in neuroprotection and motor recovery after subcortical stroke (Berretta et al., 2014; Balkaya and Cho, 2019).

The purpose of this article was to review the role of CST microstructure and BDNF polymorphisms in motor recovery after subcortical stroke, which will be useful for constructing predictive models of rehabilitation outcomes and thus for precise individualization of rehabilitation strategies.

MICROSTRUCTURE OF THE CST AFFECTS MOTOR RECOVERY

The CST is the most important motor output tract, and studies have found that its impairment affects motor rehabilitation (Schaechter et al., 2009; Radlinska et al., 2010). The CST can be reconstructed using diffusion tensor tractography (Mori and van Zijl, 2002), which can visualize the spatial relationship between the CST and infarct sites and the extent of CST damage. Studies have shown that if the CST is mostly or completely impaired by the infarct, nerve fiber tract damage is more serious, usually with partial or complete interruption, which correlates with poor recovery of motor function after treatment. In patients with infarcts near the CST, nerve fiber tract compression and deformation but no obvious damage is observed, and good motor function recovery is achieved after treatment. With no obvious relationship between the CST and the lesion, motor function involvement is not observed (Liu et al., 2020). Changes in diffusion tensor imaging (DTI) parameters can be used to observe the spatial relationship between the CST and infarct lesions, and the degree of CST damage observed predicts the prognosis of patients with subcortical stroke. DTI responds to the pathophysiological changes in the infarcted tissue, evaluates the degree of lesion tissue damage, and predicts clinical prognosis. One of the parameters accessed by DTI is fractional anisotropy (FA), a measure of microstructural integrity. A longitudinal study showed that the FA value in the affected CST changes dynamically, decreasing rapidly within 1 month after stroke, slowly decreasing from 1 to 3 months after stroke, and showing little change after three months (Yu et al., 2009). A significant correlation has been reported between FA in the CST and motor outcomes in patients with stroke (Stinear et al., 2007; Xue et al., 2021). Although M1 is thought to be the main origin of CST fibers, CST fibers also arise from the PMC, SMA, and S1 (Schieber, 2007; Welniarz et al., 2017). Considering the functional differences between these brain regions, CST fibers originating from these cortical regions may be responsible for different functions, and impairments of these fibers may result in distinct functional deficits. Therefore, some DTI studies have attempted to reconstruct the trajectories of CST fibers with different origins (Newton et al., 2006; Seo and Jang, 2013).

Considering the CST as a whole tract, cross-sectional studies have shown that decreases in the FA value of the CST (Liu et al., 2015) are related to motor recovery in subcortical stroke (Schaechter et al., 2009). In addition, the CST injury was also evaluated by other methods, involving the percentage of damage of CST fibers (Riley et al., 2011; Liu et al., 2020), raw- and weighted-CST lesion loads (Zhu et al., 2010). Liu et al. further found that the isotropy of M1 fibers was correlated with walking endurance and that of SMA fibers with motor dexterity in healthy adults. They also found that the early damage of CST originating from the M1 and SMA is closely associated with motor outcomes and brain structural changes in chronic stroke patients (Liu et al., 2020). These results suggest that the microstructures of the CST affect motor rehabilitation. Therefore, CST microstructure could be used to predict long-term motor outcomes, which is clinically important because the early prediction of motor outcomes is critical for designing suitable interventions for patients with subcortical stroke. Kim et al. (2021) indicated that CST microstructure was a significant predictor of improvement in chronic stroke survivors with mild-to-moderate motor impairment. Lin et al. (2019) compared the prediction performance of four different CST injury methods and showed that CST injury explained ∼20% of the variance in the magnitude of upper extremity recovery even after controlling for the severity of the initial impairment. Moreover, Burke Quinlan et al. evaluated CST injury by probing FA and the percentage of damage of CST fibers. They found that the best prediction in multivariate modeling was achieved using CST injury, and Lasso regression confirmed this result (Burke Quinlan et al., 2015).

However, at present, DTI research in cerebral infarction disease is still in the initial stage, mostly limited to small sample sizes and short- or medium-term research, thus lacking large sample sizes and long-term studies. Moreover, the data from related animal trials and clinical trials are still very limited. Therefore, some challenges remain in using a single CST indicator to predict the recovery of motor function in clinical applications.

BDNF POLYMORPHISMS AFFECT MOTOR RECOVERY

Cerebral infarction is a class of diseases in which brain-tissue ischemia and hypoxia cause cellular metabolic disorders, ultimately leading to neuronal degeneration and death. It has been shown that endogenous BDNF and its receptor, tyrosine kinase (Trk) B, are increased under conditions of pathological change after stroke (Endres et al., 2000). BDNF is a member of the neurotrophin family and the most abundant neurotrophin in the body. It is synthesized in the central and peripheral nervous systems and is important in neuronal survival, differentiation, metabolism, damage repair, and regeneration (McTigue et al., 1998). BDNF promotes the repair and regeneration of neurons, accelerates the release of synaptic transmitters, strengthens synaptic transduction, promotes axonal growth, and promotes sensory neuron development, all of great value in the play of nerve-cell function (Lu et al., 2003; Fletcher et al., 2018). Therefore, BDNF plays a key role in neuroplasticity and motor recovery after subcortical stroke. It has been reported that local cerebral ischemia and hypoxia in acute stroke increase the expression of BDNF-specific receptors to protect nerve cells from damage (Tejeda et al., 2019). These studies demonstrate that BDNF levels can be used as an important indicator of treatment effect and prognosis after subcortical stroke.

Furthermore, it has been shown that BDNF can cross the blood-brain barrier; BDNF levels in the serum can thus reflect the level of BDNF in the brain. Testing the serum BDNF levels of patients can objectively and effectively reveal the severity of acute stroke. Early studies reported that an increase in serum BDNF levels correlated with motor recovery (Luo et al., 2019). Salinas et al. (2017) found that lower serum BDNF levels were associated with an increased risk of incident stroke. Some studies have also found that reduced BDNF levels are associated with severe functional impairment during the acute phase of ischemic stroke (Lasek-Bal et al., 2015; Stanne et al., 2016). Further studies also showed a reverse relationship between brain tissue damage and BDNF levels in the serum. For example, Qiao et al. (2017) found that BDNF levels decreased with increased infarct volumes; that is, the lower the level of BDNF, the higher the degree of damage to brain tissue. This showed that BDNF was protective against cerebral infarction and involved in the occurrence and development of cerebral infarction. In addition, greater levels of BDNF are associated with lesser white matter hyperintensity and better visual memory (Pikula et al., 2013). Serum BDNF has also been associated with post-stroke depression, and low serum BDNF levels may indicate the development of depression in patients with acute ischemic stroke (Yang et al., 2011).

BDNF is widely expressed in the central nervous system (CNS) and plays an important role in neural differentiation and synaptic plasticity (Binder and Scharfman, 2004). Moreover, BDNF polymorphisms affect the process of neuroplasticity by affecting the expression levels of neurotrophic factors in the brain (Stewart and Cramer, 2017). Several studies have shown that the single-nucleotide polymorphism (SNP) val^{66}met (G189A or rs6265) of BDNF (Akbarian et al., 2018) is associated with stroke recovery (Shiner et al., 2016). Compared with stroke patients with the Val/Val gene, those with the Met gene had lower motor scores in the acute phase (7 days after stroke). However, the difference was not statistically significant 1 month after stroke (Mirowska-Guzel et al., 2012). Kim et al. (2012) found that stroke patients with the Met gene had lower motor scores than did those with the Val/Val gene in the subacute phase (4 months after stroke) but did not find similar results at 2 months after stroke. Some current findings have found that val^{66}met SNPs do not predict long-term functional outcomes in stroke patients (French et al., 2018). Liepert et al. (2015) observed 67 patients with ischemic stroke, and their results indicated that polymorphic BDNF was closely related to the recovery of function after ischemic stroke. These findings indicate that BDNF contributes to the recovery and maintenance of brain function following stroke.

Animal experiments can provide a deeper understanding of complex physiological and pathological phenomena. Animal studies have shown that BDNF levels dynamically change, gradually increasing after birth, reaching a stable level in adulthood (Silhol et al., 2005), and gradually decreasing with advancing age (Wang et al., 2019). In a rat cerebral infarction model, BDNF and TrkB were permanently reduced at the center of cerebral infarcts, while the immune response in the ischemic penumbra was increased (Ferrer et al., 2001). Some researchers have found that the neuronal survival rate decreases significantly when BDNF activity is inhibited by the TrkB-Fc fusion protein (Larsson et al., 1999). These studies suggest that endogenous BDNF may protect neurons from ischemic damage and function as an endogenous neuroprotective agent. The neuroprotective role of BDNF in stroke has been demonstrated in subsequent intervention studies using exogenous BDNF. Zhang and Pardridge (2001) treated a mouse model of cerebral infarction with exogenous BDNF and observed reduced infarct volume at both 24 h and 7 days after treatment vs. control groups. Kiprianova et al. (1999) showed that intravenous infusion of BDNF in a continuous mouse model of stroke prevented the death of hippocampal CA1 neurons. Jiang et al. (2011) found no significant reduction in infarct volume in a mouse model of stroke after nasal BDNF administration but did find improvement in neurological recovery compared with control groups. These findings confirm that exogenous BDNF is meaningful in the treatment of cerebral infarction and revealed that BDNF also plays an active role in the treatment of stroke. In addition, rat models with knockout of the BDNF val^{66}met single-nucleotide homolog (*BDNF$^{met/met}$*) showed

phenotypic characteristics similar o hose of humans (Chen et al., 2006). Compared with wild-type mice, *BDNF*$^{met/met}$ mice exhibited severe motor impairment only at 7 days after stroke, but not at 2 weeks or 1 month (Qin et al., 2011). Additionally, *BDNF*$^{met/met}$ mice showed reduced angiogenesis and elevated expression of thrombospondin-1 (TSP-1) and its receptor CD36, which are antiangiogenic factors. It has been suggested that the *Met* allele is associated with angiogenic deficits after stroke (Qin et al., 2011). These findings indicate that the relationship between BDNF polymorphisms and the degree of motor rehabilitation is complex and dependent on post-stroke stage. Therefore, combining brain microstructure findings with those from genetics can predict motor rehabilitation in stroke patients better than using a single index.

RELATIONSHIP AMONG CST INTEGRITY, GENETICS, AND PREDICTION MODELS OF MOTOR RECOVERY

From what has been discussed above, both CST integrity and BDNF genotype were shown to significantly influence to motor recovery of patients with stroke. Exploring the main factors that affect the efficacy of high-frequency repetitive transcranial magnetic stimulation to improve motor function in subacute stroke patients with moderate to severe upper extremity motor involvement, Chang et al. (2016) also found that the functional integrity of CST and BDNF genotype had the greatest impact on the improvement of upper extremity motor recovery. As well as, BDNF levels play a key role in white-matter microstructural plasticity (Lu et al., 2005; Jickling and Sharp, 2015). Luo et al. (2019) found that serum BDNF was positively correlated with FA in the CST in stroke patients with good motor recovery, whereas no such results were found in stroke patients with poor motor recovery. Park et al. found that in patients with stroke, FA in the ipsilesional CST was positively correlated with the motor outcome at 3 months in the presence of the Met genotype. These researchers concluded that the microstructural integrity of the intra-hemispheric tracts might be related to different processes of motor recovery dependent on the BDNF genotype (Park et al., 2020). Kim et al. (2016) also showed that poorer motor function was associated with higher radial diffusivity values in the CST for the *Val/Met* and *Met/Met* genotype groups in the early chronic stroke phase, which demonstrated that motor recovery in stroke patients might be affected by the BDNF val^{66}met polymorphism, possibly through its effects on the distinct pathological processes underlying CST degeneration. In general, direct and/or indirect relationships between microstructure and genes are suggested by these findings, but causal relationships of these two factors have not been established. Exploring the microstructure of the CST as a potential mediator between gene expression and motor recovery is an urgent priority for understanding the rehabilitation mechanisms operating after subcortical stroke.

Few studies have combined data on CST microstructure with data on BDNF polymorphisms for the prediction of motor rehabilitation after stroke. Chang et al. predicted motor outcomes at 3 months using patient characteristics, integrity of the CST, and BDNF genotype. They found that in all stroke patients, the independent predictors of motor outcome at 3 months were baseline upper-extremity motor impairment, age, stroke type, and CST integrity. Further, in the group with severe motor impairment at baseline, the number of *Met* alleles in the BDNF genotype was an independent predictor of stroke (Chang et al., 2017). These results indicate that in patients with subacute stroke, the prediction of post-stroke motor recovery using CST integrity could be improved by the addition of the BDNF genotype factor. Therefore, prediction models combining CST with BDNF genotype are better than models with only one factor for stroke patients with severe motor impairment. Although using this combination strategy in patients at different stroke stages requires further validation in clinical applications, this idea provides new perspectives on how to establish a prediction model of post-stroke motor rehabilitation in the future.

CONCLUSIONS

The microstructure of the CST and BDNF polymorphism status plays a key role in motor recovery after subcortical stroke. Future predictive models of stroke recovery are likely to include a combination of structural and genetic factors to determine patient-specific interventions for rehabilitation. These two factors are dynamic changes across different stages of stroke rehabilitation and may change depending on the amount of rehabilitation in patients with subcortical stroke. Moreover, their relationships and their predictive effect on stroke rehabilitation remain unclear. Linear mixed-effects model could be used to investigate the evolution of these two factors in a longitudinal dataset. Therefore, future studies should focus on verifying the roles of microstructure and genetic polymorphisms in motor rehabilitation in longitudinal designs with large samples, as well as on gene-knockout effects in mouse models of stroke to explore the relevant neurological mechanisms. These approaches will help to realize personalized rehabilitation strategies for stroke patients.

AUTHOR CONTRIBUTIONS

JL and CW contributed to conception and design of the study. JL wrote the first draft. All authors contributed to the article and approved the submitted version.

FUNDING

This study was supported by the Natural Science Foundation of China (81871327 and 82030053), the Tianjin Key Technology R&D Program (17ZXMFSY00090), and the Young Talents Promotion Program of Henan Province (2021HYTP012).

REFERENCES

Akbarian, S. A., Salehi-Abargouei, A., Pourmasoumi, M., Kelishadi, R., Nikpour, P., and Heidari-Beni, M. (2018). Association of Brain-derived neurotrophic factor gene polymorphisms with body mass index: a systematic review and meta-analysis. *Adv. Med. Sci.* 63, 43–56. doi: 10.1016/j.advms.2017.07.002

Balkaya, M., and Cho, S. (2019). Genetics of stroke recovery: BDNF val66met polymorphism in stroke recovery and its interaction with aging. *Neurobiol. Dis.* 126, 36–46. doi: 10.1016/j.nbd.2018.08.009

Berretta, A., Tzeng, Y. C., and Clarkson, A. N. (2014). Post-stroke recovery: the role of activity-dependent release of brain-derived neurotrophic factor. *Expert Rev. Neurother.* 14, 1335–1344. doi: 10.1586/14737175.2014.969242

Binder, D. K., and Scharfman, H. E. (2004). Brain-derived neurotrophic factor. *Growth Factors* 22, 123–131. doi: 10.1080/08977190410001723308

Burke Quinlan, E., Dodakian, L., See, J., McKenzie, A., Le, V., Wojnowicz, M., et al. (2015). Neural function, injury and stroke subtype predict treatment gains after stroke. *Ann. Neurol.* 77, 132–145. doi: 10.1002/ana.24309

Chang, W. H., Park, E., Lee, J., Lee, A., and Kim, Y. H. (2017). Association between brain-derived neurotrophic factor genotype and upper extremity motor outcome after stroke. *Stroke* 48, 1457–1462. doi: 10.1161/STROKEAHA.116.015264

Chang, W. H., Uhm, K. E., Shin, Y. I., Pascual-Leone, A., and Kim, Y. H. (2016). Factors influencing the response to high-frequency repetitive transcranial magnetic stimulation in patients with subacute stroke. *Restor. Neurol. Neurosci.* 34, 747–755. doi: 10.3233/RNN-150634

Chen, Z. Y., Jing, D., Bath, K. G., Ieraci, A., Khan, T., Siao, C. J., et al. (2006). Genetic variant BDNF (Val66Met) polymorphism alters anxiety-related behavior. *Science* 314, 140–143. doi: 10.1126/science.1129663

Endres, M., Fan, G., Hirt, L., Fujii, M., Matsushita, K., Liu, X., et al. (2000). Ischemic brain damage in mice after selectively modifying BDNF or NT4 gene expression. *J. Cereb. Blood Flow Metab.* 20, 139–144. doi: 10.1097/00004647-200001000-00018

Ferrer, I., Krupinski, J., Goutan, E., Marti, E., Ambrosio, S., and Arenas, E. (2001). Brain-derived neurotrophic factor reduces cortical cell death by ischemia after middle cerebral artery occlusion in the rat. *Acta Neuropathol.* 101, 229–238. doi: 10.1007/s004010000268

Fletcher, J. L., Murray, S. S., and Xiao, J. (2018). Brain-derived neurotrophic factor in central nervous system myelination: a new mechanism to promote myelin plasticity and repair. *Int. J. Mol. Sci.* 19:4131. doi: 10.3390/ijms19124131

French, M. A., Morton, S. M., Pohlig, R. T., and Reisman, D. S. (2018). The relationship between BDNF Val66Met polymorphism and functional mobility in chronic stroke survivors. *Top. Stroke Rehabil.* 25, 276–280. doi: 10.1080/10749357.2018.1437938

Guo, J., Liu, J., Wang, C., Cao, C., Fu, L., Han, T., et al. (2019). Differential involvement of rubral branches in chronic capsular and pontine stroke. *Neuroimage Clin.* 24:102090. doi: 10.1016/j.nicl.2019.102090

Jiang, Y., Wei, N., Lu, T., Zhu, J., Xu, G., and Liu, X. (2011). Intranasal brain-derived neurotrophic factor protects brain from ischemic insult *via* modulating local inflammation in rats. *Neuroscience* 172, 398–405. doi: 10.1016/j.neuroscience.2010.10.054

Jickling, G. C., and Sharp, F. R. (2015). Biomarker panels in ischemic stroke. *Stroke* 46, 915–920. doi: 10.1161/STROKEAHA.114.005604

Johnson, B. P., and Westlake, K. P. (2021). Chronic poststroke deficits in gross and fine motor control of the ipsilesional upper limb. *Am. J. Phys. Med. Rehabil.* 100, 345–348. doi: 10.1097/PHM.0000000000001569

Kim, H., Lee, H., Jung, K. I., Ohn, S. H., and Yoo, W. K. (2018). Changes in diffusion metrics of the red nucleus in chronic stroke patients with severe corticospinal tract injury: a preliminary study. *Ann. Rehabil. Med.* 42, 396–405. doi: 10.5535/arm.2018.42.3.396

Kim, E. J., Park, C. H., Chang, W. H., Lee, A., Kim, S. T., Shin, Y. I., et al. (2016). The brain-derived neurotrophic factor Val66Met polymorphism and degeneration of the corticospinal tract after stroke: a diffusion tensor imaging study. *Eur. J. Neurol.* 23, 76–84. doi: 10.1111/ene.12791

Kim, B., Schweighofer, N., Haldar, J. P., Leahy, R. M., and Winstein, C. J. (2021). Corticospinal tract microstructure predicts distal arm motor improvements in chronic stroke. *J. Neurol. Phys. Ther.* 45, 273–281. doi: 10.1097/NPT.0000000000000363

Kim, J. M., Stewart, R., Park, M. S., Kang, H. J., Kim, S. W., Shin, I. S., et al. (2012). Associations of BDNF genotype and promoter methylation with acute and long-term stroke outcomes in an East Asian cohort. *PLoS One* 7:e51280. doi: 10.1371/journal.pone.0051280

Kiprianova, I., Freiman, T. M., Desiderato, S., Schwab, S., Galmbacher, R., Gillardon, F., et al. (1999). Brain-derived neurotrophic factor prevents neuronal death and glial activation after global ischemia in the rat. *J. Neurosci. Res.* 56, 21–27. doi: 10.1002/(SICI)1097-4547(19990401)56:1<21::AID-JNR3>3.0.CO;2-Q

Larsson, E., Nanobashvili, A., Kokaia, Z., and Lindvall, O. (1999). Evidence for neuroprotective effects of endogenous brain-derived neurotrophic factor after global forebrain ischemia in rats. *J. Cereb. Blood Flow Metab.* 19, 1220–1228. doi: 10.1097/00004647-199911000-00006

Lasek-Bal, A., Jedrzejowska-Szypulka, H., Rozycka, J., Bal, W., Holecki, M., Dulawa, J., et al. (2015). Low concentration of BDNF in the acute phase of ischemic stroke as a factor in poor prognosis in terms of functional status of patients. *Med. Sci. Monit.* 21, 3900–3905. doi: 10.12659/msm.895358

Liepert, J., Heller, A., Behnisch, G., and Schoenfeld, A. (2015). [Polymorphism of brain derived neurotrophic factor and recovery of functions after ischemic stroke]. *Nervenarzt* 86, 1255–1260. doi: 10.1007/s00115-015-4325-6

Lin, D. J., Cloutier, A. M., Erler, K. S., Cassidy, J. M., Snider, S. B., Ranford, J., et al. (2019). Corticospinal tract injury estimated from acute stroke imaging predicts upper extremity motor recovery after stroke. *Stroke* 50, 3569–3577. doi: 10.1161/STROKEAHA.119.025898

Liu, J., Qin, W., Zhang, J., Zhang, X., and Yu, C. (2015). Enhanced interhemispheric functional connectivity compensates for anatomical connection damages in subcortical stroke. *Stroke* 46, 1045–1051. doi: 10.1161/STROKEAHA.114.007044

Liu, J., Wang, C., Qin, W., Ding, H., Guo, J., Han, T., et al. (2020). Corticospinal fibers with different origins impact motor outcome and brain after subcortical stroke. *Stroke* 51, 2170–2178. doi: 10.1161/STROKEAHA.120.029508

Lu, D., Mahmood, A., and Chopp, M. (2003). Biologic transplantation and neurotrophin-induced neuroplasticity after traumatic brain injury. *J. Head Trauma Rehabil.* 18, 357–376. doi: 10.1097/00001199-200307000-00006

Lu, B., Pang, P. T., and Woo, N. H. (2005). The yin and yang of neurotrophin action. *Nat. Rev. Neurosci.* 6, 603–614. doi: 10.1038/nrn1726

Luo, W., Liu, T., Li, S., Wen, H., Zhou, F., Zafonte, R., et al. (2019). The serum BDNF level offers minimum predictive value for motor function recovery after stroke. *Transl. Stroke Res.* 10, 342–351. doi: 10.1007/s12975-018-0648-5

McTigue, D. M., Horner, P. J., Stokes, B. T., and Gage, F. H. (1998). Neurotrophin-3 and brain-derived neurotrophic factor induce oligodendrocyte proliferation and myelination of regenerating axons in the contused adult rat spinal cord. *J. Neurosci.* 18, 5354–5365. doi: 10.1523/JNEUROSCI.18-14-05354.1998

Mirowska-Guzel, D., Gromadzka, G., Czlonkowski, A., and Czlonkowska, A. (2012). BDNF -270 C>T polymorphisms might be associated with stroke type and BDNF -196 G>A corresponds to early neurological deficit in hemorrhagic stroke. *J. Neuroimmunol.* 249, 71–75. doi: 10.1016/j.jneuroim.2012.04.011

Mori, S., and van Zijl, P. C. (2002). Fiber tracking: principles and strategies - a technical review. *NMR Biomed.* 15, 468–480. doi: 10.1002/nbm.781

Newton, J. M., Ward, N. S., Parker, G. J., Deichmann, R., Alexander, D. C., Friston, K. J., et al. (2006). Non-invasive mapping of corticofugal fibres from multiple motor areas—relevance to stroke recovery. *Brain* 129, 1844–1858. doi: 10.1093/brain/awl106

Park, E., Lee, J., Chang, W. H., Lee, A., Hummel, F. C., and Kim, Y. H. (2020). Differential relationship between microstructural integrity in white matter tracts and motor recovery following stroke based on brain-derived neurotrophic factor genotype. *Neural Plast.* 2020:5742421. doi: 10.1155/2020/5742421

Patel, P., Kaingade, S. R., Wilcox, A., and Lodha, N. (2020). Force control predicts fine motor dexterity in high-functioning stroke survivors. *Neurosci. Lett.* 729:135015. doi: 10.1016/j.neulet.2020.135015

Pikula, A., Beiser, A. S., Chen, T. C., Preis, S. R., Vorgias, D., DeCarli, C., et al. (2013). Serum brain-derived neurotrophic factor and vascular endothelial growth factor levels are associated with risk of stroke and vascular brain injury: framingham study. *Stroke* 44, 2768–2775. doi: 10.1161/STROKEAHA.113.001447

Qiao, H. J., Li, Z. Z., Wang, L. M., Sun, W., Yu, J. C., and Wang, B. (2017). Association of lower serum Brain-derived neurotrophic factor levels with

larger infarct volumes in acute ischemic stroke. *J. Neuroimmunol.* 307, 69–73. doi: 10.1016/j.jneuroim.2017.04.002

Qin, L., Kim, E., Ratan, R., Lee, F. S., and Cho, S. (2011). Genetic variant of BDNF (Val66Met) polymorphism attenuates stroke-induced angiogenic responses by enhancing anti-angiogenic mediator CD36 expression. *J. Neurosci.* 31, 775–783. doi: 10.1523/JNEUROSCI.4547-10.2011

Radlinska, B., Ghinani, S., Leppert, I. R., Minuk, J., Pike, G. B., and Thiel, A. (2010). Diffusion tensor imaging, permanent pyramidal tract damage and outcome in subcortical stroke. *Neurology* 75, 1048–1054. doi: 10.1212/WNL.0b013e3181f39aa0

Riley, J. D., Le, V., Der-Yeghiaian, L., See, J., Newton, J. M., Ward, N. S., et al. (2011). Anatomy of stroke injury predicts gains from therapy. *Stroke* 42, 421–426. doi: 10.1161/STROKEAHA.110.599340

Salinas, J., Beiser, A., Himali, J. J., Satizabal, C. L., Aparicio, H. J., Weinstein, G., et al. (2017). Associations between social relationship measures, serum brain-derived neurotrophic factor and risk of stroke and dementia. *Alzheimers Dement. (N Y)* 3, 229–237. doi: 10.1016/j.trci.2017.03.001

Schaechter, J. D., Fricker, Z. P., Perdue, K. L., Helmer, K. G., Vangel, M. G., Greve, D. N., et al. (2009). Microstructural status of ipsilesional and contralesional corticospinal tract correlates with motor skill in chronic stroke patients. *Hum. Brain Mapp.* 30, 3461–3474. doi: 10.1002/hbm.20770

Schieber, M. H. (2007). Chapter 2 Comparative anatomy and physiology of the corticospinal system. *Handb. Clin. Neurol.* 82, 15–37. doi: 10.1016/S0072-9752(07)80005-4

Seo, J. P., and Jang, S. H. (2013). Different characteristics of the corticospinal tract according to the cerebral origin: DTI study. *Am. J. Neuroradiol.* 34, 1359–1363. doi: 10.3174/ajnr.A3389

Shiner, C. T., Pierce, K. D., Thompson-Butel, A. G., Trinh, T., Schofield, P. R., and McNulty, P. A. (2016). BDNF genotype interacts with motor function to influence rehabilitation responsiveness poststroke. *Front. Neurol.* 7:69. doi: 10.3389/fneur.2016.00069

Silhol, M., Bonnichon, V., Rage, F., and Tapia-Arancibia, L. (2005). Age-related changes in brain-derived neurotrophic factor and tyrosine kinase receptor isoforms in the hippocampus and hypothalamus in male rats. *Neuroscience* 132, 613–624. doi: 10.1016/j.neuroscience.2005.01.008

Stanne, T. M., Aberg, N. D., Nilsson, S., Jood, K., Blomstrand, C., Andreasson, U., et al. (2016). Low circulating acute brain-derived neurotrophic factor levels are associated with poor long-term functional outcome after ischemic stroke. *Stroke* 47, 1943–1945. doi: 10.1161/STROKEAHA.115.012383

Sterr, A., Dean, P. J., Szameitat, A. J., Conforto, A. B., and Shen, S. (2014). Corticospinal tract integrity and lesion volume play different roles in chronic hemiparesis and its improvement through motor practice. *Neurorehabil. Neural Repair* 28, 335–343. doi: 10.1177/1545968313510972

Stewart, J. C., and Cramer, S. C. (2017). Genetic variation and neuroplasticity: role in rehabilitation after stroke. *J. Neurol. Phys. Ther.* 41, S17–S23. doi: 10.1097/NPT.0000000000000180

Stinear, C. M., Barber, P. A., Smale, P. R., Coxon, J. P., Fleming, M. K., and Byblow, W. D. (2007). Functional potential in chronic stroke patients depends on corticospinal tract integrity. *Brain* 130, 170–180. doi: 10.1093/brain/awl333

Tejeda, G. S., Esteban-Ortega, G. M., San Antonio, E., Vidaurre, O. G., and Diaz-Guerra, M. (2019). Prevention of excitotoxicity-induced processing of BDNF receptor TrkB-FL leads to stroke neuroprotection. *EMBO Mol. Med.* 11:e9950. doi: 10.15252/emmm.201809950

Wang, G., Zhou, Y., Wang, Y., Li, D., Liu, J., and Zhang, F. (2019). Age-associated dopaminergic neuron loss and midbrain glia cell phenotypic polarization. *Neuroscience* 415, 89–96. doi: 10.1016/j.neuroscience.2019.07.021

Welniarz, Q., Dusart, I., and Roze, E. (2017). The corticospinal tract: evolution, development and human disorders. *Dev. Neurobiol.* 77, 810–829. doi: 10.1002/dneu.22455

Xue, Q., Yang, X. H., Teng, G. J., and Hu, S. D. (2021). Chronic pontine strokes: diffusion tensor imaging of corticospinal tract indicates the prognosis in terms of motor outcome. *J. Xray Sci. Technol.* 29, 477–489. doi: 10.3233/XST-200817

Yang, L., Zhang, Z., Sun, D., Xu, Z., Yuan, Y., Zhang, X., et al. (2011). Low serum BDNF may indicate the development of PSD in patients with acute ischemic stroke. *Int. J. Geriatr. Psychiatry* 26, 495–502. doi: 10.1002/gps.2552

Yu, C., Zhu, C., Zhang, Y., Chen, H., Qin, W., Wang, M., et al. (2009). A longitudinal diffusion tensor imaging study on Wallerian degeneration of corticospinal tract after motor pathway stroke. *Neuroimage* 47, 451–458. doi: 10.1016/j.neuroimage.2009.04.066

Zhang, Y., and Pardridge, W. M. (2001). Neuroprotection in transient focal brain ischemia after delayed intravenous administration of brain-derived neurotrophic factor conjugated to a blood-brain barrier drug targeting system. *Stroke* 32, 1378–1384. doi: 10.1161/01.str.32.6.1378

Zhu, L. L., Lindenberg, R., Alexander, M. P., and Schlaug, G. (2010). Lesion load of the corticospinal tract predicts motor impairment in chronic stroke. *Stroke* 41, 910–915. doi: 10.1161/STROKEAHA.109.577023

Zolkefley, M. K. I., Firwana, Y. M. S., Hatta, H. Z. M., Rowbin, C., Nassir, C., Hanafi, M. H., et al. (2021). An overview of fractional anisotropy as a reliable quantitative measurement for the corticospinal tract (CST) integrity in correlation with a Fugl-Meyer assessment in stroke rehabilitation. *J. Phys. Ther. Sci.* 33, 75–83. doi: 10.1589/jpts.33.75

Conflict of Interest: The authors declare that the research was conducted in the absence of any commercial or financial relationships that could be construed as a potential conflict of interest.

Publisher's Note: All claims expressed in this article are solely those of the authors and do not necessarily represent those of their affiliated organizations, or those of the publisher, the editors and the reviewers. Any product that may be evaluated in this article, or claim that may be made by its manufacturer, is not guaranteed or endorsed by the publisher.

frontiers in Aging Neuroscience

ORIGINAL RESEARCH
published: 16 February 2022
doi: 10.3389/fnagi.2022.803780

Altered Global Signal Topography in Alcohol Use Disorders

Ranran Duan[1†], Lijun Jing[1†], Yanfei Li[1], Zhe Gong[1], Yaobing Yao[1], Weijian Wang[2,3,4,5], Yong Zhang[2,3,4,5], Jingliang Cheng[2,3,4,5], Ying Peng[6], Li Li[7] and Yanjie Jia[1]**

[1]Department of Neurology, The First Affiliated Hospital of Zhengzhou University, Zhengzhou, China, [2]Department of Magnetic Resonance Imaging, The First Affiliated Hospital of Zhengzhou University, Zhengzhou, China, [3]Engineering Technology Research Center for Detection and Application of Brain Function of Henan Province, The First Affiliated Hospital of Zhengzhou University, Zhengzhou, China, [4]Key Laboratory of Magnetic Resonance and Brain Function of Henan Province, The First Affiliated Hospital of Zhengzhou University, Zhengzhou, China, [5]Key Laboratory of Brain Function and Cognitive Magnetic Resonance Imaging of Zhengzhou, The First Affiliated Hospital of Zhengzhou University, Zhengzhou, China, [6]Department of Neurology, Sun Yat-sen Memorial Hospital, Sun Yat-sen University, Guangzhou, China, [7]Department of Anesthesiology, Beijing Friendship Hospital, Capital Medical University, Beijing, China

The most common symptom of patients with alcohol use disorders (AUD) is cognitive impairment that negatively affects abstinence. Presently, there is a lack of indicators for early diagnosis of alcohol-related cognitive impairment (ARCI). We aimed to assess the cognitive deficits in AUD patients with the help of a specific imaging marker for ARCI. Data-driven dynamic and static global signal topography (GST) methods were applied to explore the cross-talks between local and global neuronal activities in the AUD brain. Twenty-six ARCI, 54 AUD without cognitive impairment (AUD-NCI), and gender/age-matched 40 healthy control (HC) subjects were recruited for this study. We found that there was no significant difference with respect to voxel-based morphometry (VBM) and static GST between AUD-NCI and ARCI groups. And in dynamic GST measurements, the AUD-NCI patients had the highest coefficient of variation (CV) at the right insula, followed by ARCI and the HC subjects. In precuneus, the order was reversed. There was no significant correlation between the dynamic GST and behavioral scores or alcohol consumption. These results suggested that dynamic GST might have potential implications in understanding AUD pathogenesis and disease management.

Keywords: alcohol-related cognitive impairment (ARCI), functional MRI, global signal topography, static GST, dynamic GST

OPEN ACCESS

Edited by:
Nicola Canessa, University Institute of Higher Studies in Pavia, Italy

Reviewed by:
Xiaoli Wang, Weifang Medical University, China
Liming Hsu, University of North Carolina at Chapel Hill, United States

****Correspondence:***
Li Li
li_anethesia@163.com
Yanjie Jia
jiayanjie1971@zzu.edu.cn

†These authors have contributed equally to this work and share first authorship

Specialty section:
This article was submitted to Neurocognitive Aging and Behavior, a section of the journal Frontiers in Aging Neuroscience

Received: *28 October 2021*
Accepted: *24 January 2022*
Published: *16 February 2022*

Citation:
Duan R, Jing L, Li Y, Gong Z, Yao Y, Wang W, Zhang Y, Cheng J, Peng Y, Li L and Jia Y (2022) Altered Global Signal Topography in Alcohol Use Disorders. Front. Aging Neurosci. 14:803780. doi: 10.3389/fnagi.2022.803780

Abbreviations: AUD, alcohol-use disorders; ARBD, alcohol-related brain damage; ARCI, alcohol-related cognitive impairment; GST, global signal topography; HC, healthy control; VBM, voxel-based morphometry; MRI, magnetic resonance imaging; fMRI, functional magnetic resonance imaging; ESMN, executive and salience mode network; DMN, default mode network; DSM-5, diagnostic and statistical manual of mental disorders; CIWA-Ar, clinical institute withdrawal assessment-alcohol scale revised; MMSE, mini-mental state examination; ADS, alcohol dependence scale; OCDS, obsessive compulsive drinking scale; VAS, visual analog scale; PSQI, Pittsburgh Sleep Quality Index; PHQ-9, patient health questionnaire-9; MPRAGE, magnetization-prepared rapid gradient echo; WM, white matter; GM, gray matter; FWHM, full width at half maximum; DPARSF, the data processing assistant for resting-state fMRI analysis toolkit; CSF, cerebrospinal fluid; SD, standard deviation.

INTRODUCTION

Uncontrolled and persistent alcohol consumption can exert a multitude of adverse health effects, such as chronic liver and kidney damages, and is considered a global public health concern. Alcohol use disorder (AUD) or alcoholism is a widespread health burden worldwide, affecting individuals at any level of socio-economic status. Studies have shown that AUD is considerably more prevalent in men than women in developing countries, resulting in an increased psychological and economic burden (Carvalho et al., 2019; Rehm and Shield, 2019). Like dose-dependent toxicity in most fatal health problems, heavy consumption of alcohol is directly related to an increased risk of developing AUD-linked multi-organ disorders (Schuckit, 2009). AUD is characterized by the emotional and/or psychological inability to resist oneself binge or heavy drinking habits, despite the known serious side-effects of excessive or persistent alcohol drinking (Wilcox et al., 2015). Interestingly, cognitive impairment has been frequently observed (∼30–80%) in individuals undergoing AUD treatment (Bruijnen et al., 2019, 2021). It has been found that chronic alcohol abuse-induced thiamine deficiency serves as the major pathological contributor to AUDs, including alcohol-related brain damage (ARBD), with the symptomatic manifestation of cognitive deficits, apathy, severe memory deficits, vision impairment, and confabulations (Toledo Nunes et al., 2019; Kim et al., 2020; Oey et al., 2021). However, patients suffering from alcohol-related cognitive impairment (ARCI; Heirene et al., 2018) themselves do not lodge subjective complaints, possibly due to the lack of judgment ability under the influence of addiction (Walvoort et al., 2016). On the other hand, it has been shown in the clinical literature that cognitive deficits indulge addictive behaviors (Melugin et al., 2021). Moreover, cognitive impairment can also contribute to the lack of self-control in maintaining abstinence from longstanding alcohol abuse. Above all, many of the deficits associated with heavy alcohol consumption are potentially curable by abstinence (Ridley et al., 2013). However, the pattern and rate of cognitive recovery are not yet fully understood (Bates et al., 2002). Early identification of ARCI would be of major interest and potentially useful in daily clinical practice. There is an urgent need to explore the underlying pathophysiological processes and identify biomarkers.

Recently functional MRI (fMRI) studies have revealed that substance use (such as heroin, cigarette, and alcohol) can modulate spontaneous neuronal activity in the brain (Myrick et al., 2008; Franklin et al., 2011; Langleben et al., 2014; Cabrera et al., 2016). Furthermore, resting-state fMRI (rs-fMRI) has been evolved as an efficient diagnostic tool to examine AUD-induced neural pathogenesis. Aberrant brain functional connectivity patterns in the executive and salience mode network (ESMN) as well as default mode network (DMN) have been found across different categories of AUD and are associated with cognition and behavior-related disorders (Zhang and Volkow, 2019). Heavy alcohol drinking, a characteristic hallmark of AUD, can induce neurodegeneration, leading to long-term cognitive and behavioral dysfunctions that may transform one's social drinking habit to addiction (Marshall et al., 2020). Alcohol addiction causes severe damage to the motivational circuit in three successive steps—exaggerated compulsive habit formation, overwhelming stress with lack of rewards, and compromised physical executive functions (Koob and Volkow, 2016). It has been delineated that chronic AUD can induce communication malfunction across large-scale brain networks (Zilverstand et al., 2018). Therefore, we exploited global signal topography (GST) to explore the cross-talks between local and global neuronal activities (Yang et al., 2017; Han et al., 2019; Zhang et al., 2019).

Although the rs-fMRI global signal data is contaminated by physiological noise and artifacts, however, recent studies have suggested that these data provide information about widespread neuronal activities (Power et al., 2014; Liu et al., 2017; Li et al., 2019). Furthermore, a direct relationship between GS and neural activity modulation has been established by the correlation of GS with local field potential readout at any certain position in the cerebral cortex (Schölvinck et al., 2010; Han et al., 2019). Hence, significant research studies were carried out to develop GST to analyze the correlation between local and global signals in the rs-fMRI study. It has been observed that the lower GST correlates with different cortical locations, such as the higher-order cortices and sensory cortex (Ao et al., 2021). Moreover, GST can be modulated by individual factors, like conscious state and attention-demanding tasks (Ao et al., 2021). In addition, abnormal GST has been detected in patients with bipolar disorder, schizophrenia, epilepsy, and major depressive disorder (Li et al., 2019, 2021; Wang et al., 2021). Together, these findings suggest a mechanistic insight into how GST and local neural activity coordinate to organize layers of information in the brain. Therefore, investigating the altered GST dynamics in AUD patients may provide potential insight into neural pathogenesis.

Here, we tested the hypothesis that the altered dynamic and static GST might play roles in the AUD neuro-pathogenesis and progression on three experimental groups. The dynamic GST measured the variations of dynamic coordination processes during scanning, while static GST indicated the coordination between global and local neuronal activities.

MATERIALS AND METHODS

Participants

The Medical Ethics Committee of the Zhengzhou University's First Affiliated Hospital approved the study protocol in compliance with the Helsinki Declaration, as revised in 2008. All participants were required to provide their signed written informed consent prior to completing the survey.

Individuals with AUD were recruited from a variety of sources, including the inpatient ward, internet posting, and advertisements. The control participants were volunteers from the local communities.

Inclusion criteria for recruitment of the participants were: (1) meeting the fifth edition of the Diagnostic and Statistical Manual of Mental Disorders (DSM-5) for moderate to severe AUD, as clinically assessed by the principal investigator; (2) on average, drinking more than 14 units of alcohol every

week, according to the U.K. Chief Medical Officers (Health, 2017; Hawkins and McCambridge, 2021); (3) having Clinical Institute Withdrawal Assessment-Alcohol scale Revised (CIWA-Ar) score <9; and (4) able to understand and give written consent to study procedures.

Exclusion criteria for both healthy control (HC) and AUD patients were: (1) having a history of addiction, psychiatric disorder, and neurological and/or physical disorders that could influence brain morphology; (2) having contraindications in MRI; and (3) reportedly receiving interfering medications.

Cognitive dysfunctions were assessed on the Mini-Mental State Examination (MMSE) and Montreal Cognitive Assessment (MoCA) scales. Participants' age ranged between 18 and 65 years. The Structured Clinical Interview (SCID)-non-patient edition was applied to screen the control subjects (Shabani et al., 2021) to confirm that they had no existing or previous mental disorders. On the other hand, AUD subjects were selected based on the Alcohol Dependence Scale (ADS) assessment, CIWA-Ar, Obsessive Compulsive Drinking Scale (OCDS), Visual Analog Scale (VAS), Pittsburgh Sleep Quality Index (PSQI), and Patient Health Questionnaire -9 (PHQ-9).

Neuroimaging Data Acquisition

SIEMENS 3.0T scanner (MAGNETOM Prisma, Siemens, Germany) with a 16-channel head coil was used to obtain the fMRI data at the First Affiliated Hospital of Zhengzhou University. All participants were instructed to keep their eyes closed. Earplugs and foam padding were used to control head movements. At the end of scanning, subjects were reviewed whether they fell asleep anytime during the scanning. First, 3D anatomical T1-weighted magnetization-prepared rapid gradient echo (MPRAGE) MRI data with pulse sequence (TR 2,000 ms, TE 2.06 ms, T1 = 900 ms, the field of view 256*256 mm^2, flip angle 9°, slice thickness 1.0 mm, matrix 256*256, 176 single-shot interleaved slices with no gap with isotropic voxel size 1*1*1 mm^3) were obtained for all participants. Then, the rs-fMRI data were obtained using the parameters like TR 1,000 ms, TE 30 ms, the field of view 220*220 mm^2, slice thickness 2.2 mm, slice gap 0.4 mm, flip angle 70°, and voxel size 2.0*2.0*2.2 mm^3, with 52 slices and 400 dynamics. The slices aligned along the anterior and posterior commissure lines (AC-PC) were acquired with a total scan time of 360 s.

Pre-processing

The CAT12 toolbox[1] was used to pre-process all T1-weighted images using standard pipeline steps. After checking the image artifacts, the image origin was adjusted to the AC line. Image normalization was carried out as per the Montreal Neurologic Institute's space and segmentation models into white matter (WM), gray matter (GM), and cerebrospinal regions. Then, images were reassigned to a volume-image resolution of $1.5 \times 1.5 \times 1.5$ mm^3. At the final step, the GM maps were relapsed using 6 mm full width at half maximum (FWHM) Gaussian kernel.

The Data Processing Assistant for Resting-State fMRI analysis toolkit (DPARSF) was used to pre-process rs-fMRI data. The first ten volumes were discarded, and the slice-timing was adjusted accordingly, along with realignment. Then image normalization was performed with respect to the standard EPI template (resampled into 3*3*3 mm^3). Participants were excluded if the head motion was >3 mm in maximum displacement or >3° rotation in angular motion. No participant was excluded in this step. Then images were smoothed using a 6*6*6 mm^3 FWHM Gaussian kernel and readjusted to minimize the low-frequency drift. Finally, the band-pass filter (0.01–0.1Hz) removed the high-frequency physiological noises. Friston 24-motion parameter model was applied to obtain signals from the cerebrospinal fluid (CSF) and WM areas, which were relapsed as noise covariates. The outliners were despiked using the 3rd order spline fit to clean the respective segments of the time course. Outliners were identified using AFNI 3dDespike[2].

Voxel-Based Morphometry (VBM)

Spatial segmentation and normalization were applied into three voxel classes: GM, WM, and CSF, using volume segmentation and adaptive maximum a posterior (MAP) filtering approach. Regional GM volume differences were tested using normalized GM maps. Then the obtained GM maps were flattened using a 6 mm FWHM Gaussian kernel for further analysis. The 0.1 absolute masking threshold was applied to the VBM data.

Statistical Analysis

Analysis of the Static GST

The static GST was measured by pairwise time course correlation between the GS and each voxel segment. The GS time series was calculated as the mean pre-processed BOLD signal, averaged over all GM voxels for each of the time points, excluding WM and ventricle signals. Fisher's r-to-z transformation was applied to convert correlation coefficients into *z* scores. Here, the correlation map was constructed by the FC.

Analysis of the Dynamic GST

The dynamic GST correlation was calculated using a sliding window-based method, as described elsewhere (Allen et al., 2014). The length of the rectangular window was set to 22 TRs (44 s) with a step size of 1 TR. Pearson correlation coefficient was first computed for each sliding window between the time series and GST for each voxel in the GM, and then the coefficient was transformed into Fisher's *z*-score. The standard deviation (SD) of the dynamic GST correlation of each voxel was then calculated. To eliminate the influences of parameter selection, the window length of 30 TRs with a step size of 1 TR was applied.

RESULTS

Participants

The study cohort consisted of 40 HCs, and 80 patients with AUD. The recruited AUD patients were divided based on their MMSE and MoCA scores into the cognitive impairment

[1]http://dbm.neuro.uni-jena.de/cat12/

[2]https://afni.nimh.nih.gov/

TABLE 1 | Patient demographics and clinical characteristics.

	Control group (n = 40)	AUD group (n = 80)	p
General character			
Age (y)	48.63 ± 7.56	48.12 ± 6.64	0.084
Sex (F%)	1 (2.5%)	1 (1.25%)	0.396
Years of schooling (y)	9.4 ± 3.3	9.01 ± 2.9	0.693
Height (cm)	174.50 ± 5.26	172.91 ± 3.47	0.350
Weight (Kg)	70.50 ± 4.38	76.05 ± 3.47	0.095
Time of alcohol drinking	0.24 ± 0.74	20.51 ± 2.78	**0.000***
Pure alcohol (g, total)	629.99 ± 192.17	325,262.37 ± 30,806.74	**0.001***
Characteristics of performance in multidimensional neuropsychological battery			
MMSE	29.6	27.4	0.061
MoCA	26.3	24.4	0.058
ADS	1.50 ± 0.74	26.06 ± 3.55	**0.001***
CIWA-Ar	0.51 ± 0.12	8.15 ± 2.74	**0.009***
OCDs	2.23 ± 1.67	12.67 ± 2.57	**0.000***
VAS	1.63 ± 0.74	2.12 ± 0.89	0.053
PHQ-9	5.32 ± 0.1.74	6.79 ± 1.52	0.065
Characteristics of various MRI-defined lesions in CSVD participants			
High voiceover signal in the lateral ventricle (score)	1.7	1.9	0.071
Encephalatrophy (GCA)	1.2	1.4	0.34

*$p < 0.05$.

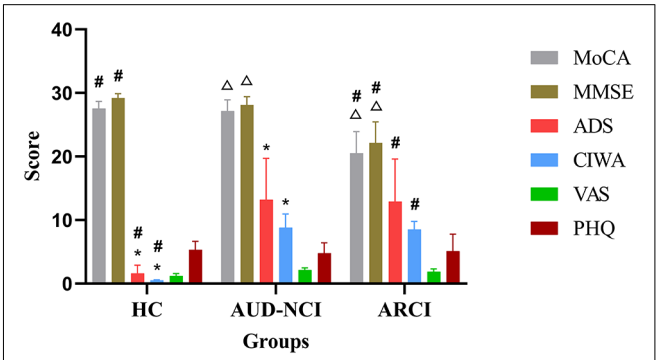

FIGURE 1 | Cognitive assessment scales compared in these three groups. *$p < 0.05$ HC group vs. AUD-NCI group. #$p < 0.05$ HC group vs. ARCI group. △$p < 0.05$ AUD-NCI group vs. ARCI group. AUD, alcohol use disorder; NCI, non-cognitive impairment; HCs, healthy controls; ARCI, alcohol-related cognitive impairment.

group (ARCI; MMSE<24 and MoCA<26) and non-cognitive impairment group (AUD-NCI; MMSE≥24 and MoCA≥26). Among the AUD subjects, 26 patients exhibited cognitive impairment. The years of alcohol consumption of the AUD group participants ranged from 17 to 23 years. The mean drinking frequency was 4.8 times per week. The median total quantity of pure alcohol consumption was 325.262 kg. The ADS score of the AUD group was 26.06 ± 3.55 ($p < 0.05$).

The MoCA and MMSE scores were lower in the AUD group than in the HC group ($p > 0.05$), and the ADS, CIWA-Ar, and OCDs scores were higher in the AUD group than in the HC group ($p < 0.05$). The high voiceover signal in the lateral ventricle score and encephalatrophy (GCA) in the AUD group were higher than in the HC group ($p > 0.05$). The detailed demographic information and clinical characteristics are presented in **Table 1**.

We could not detect any significant differences across the groups with respect to age, sex, height, weight, education, and handedness in the demographic data. However, the AUD patients presented significantly higher ADS scores as well as the items of DSM-5 AUD Criteria ($p < 0.05$, **Figure 1**). The analysis of variance (ANOVA) method was used for the statistical analysis of the results.

VBM Analysis of the AUD-NCI and ARCI Groups

There were no significant differences in total GM, WM, and CSF values between AUD-NCI and ARCI groups. VBM analysis between AUD-NCI and ARCI patients showed no significant differences using a whole-brain threshold of $p < 0.05$.

Static GST in the HCs, and Patients With AUD-NCI and ARCI

There were no differences in the static GST values between HC, AUD-NCI, and ARCI groups as measured by ANOVA.

Dynamic GST in AUD Patients

In dynamic GST measurements, control subjects had the lowest coefficient of variation (CV: SD/mean) at the right insula, followed by ARCI, and then the AUD-NCI patients. Notably, the CV order was found reversed in the precuneus region (**Figures 2**, **3**, **Table 2**).

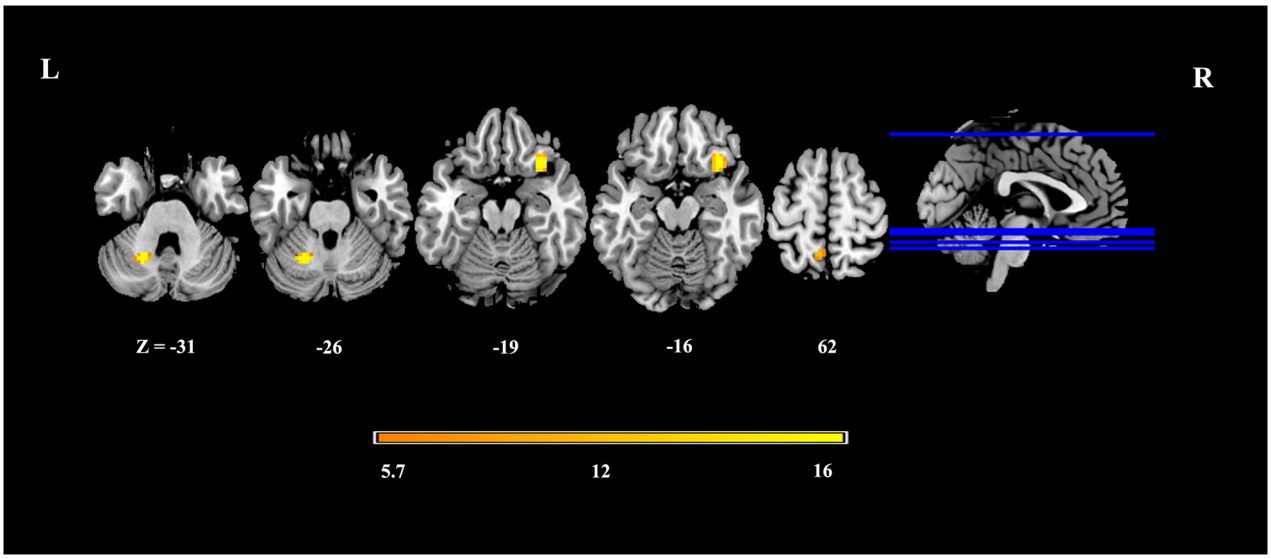

FIGURE 2 | Altered dynamic GS topography in AUD patients.

Correlation Analyses

The correlation analyses showed no significant correlations between the dynamic GST and total quantity of pure alcohol, MMSE, MOCA, ADS, OCDS, VAS, or PHQ-9.

DISCUSSION

AUD is one of the most prevalent and devastating neurological and addictive disorders (Leclercq et al., 2020). Alcohol addiction can potentially increase the risks of suicidal tendency due to impaired judgment capacity, increased impulsivity related to mood disorders, psychotic disorders, anxiety, and cognitive deficits (Kudva et al., 2021). Cognitive dysfunction in AUD patients can affect their psycho-social behavior and therapeutic outcomes. However, the cognition assessment scales and the commonly used MRI sequences are not efficient enough to detect early-stage alcohol-induced damage. Hence, we aimed to assess the cognitive deficits in AUD patients through the development of a specific imaging marker for AUD-linked cognitive deficits.

Here, we aimed to explore the correlations between altered dynamic and static GST and cognitive deficits in AUD patients. This study investigated the modified large-scale brain functional organization in AUD using a data-driven image analysis method. Using a threshold of FWE-corrected $p < 0.05$, VBM analyses could not show any differences between the HC, AUD-NCI, and ARCI groups. There were also no significant differences in the static GST values between the HC, AUD-NCI, and ARCI groups as measured by ANOVA. Interestingly, for the dynamic GST measurements, we observed that HC group subjects had the lowest CV values at the right insula, followed by ARCI, and AUD-NCI subjects in the ascending order. Whereas in the case of the precuneus region, this order was reversed. According to the previous studies, there is a significant correlation between global signal amplitude and functional connectivity with the level of consciousness, irrespective of physiologic, pathologic, and pharmacologic etiologies. These two regions are known to be involved in the memory uptake and storage processes (Tanabe et al., 2020), which were changed in the dynamic GST analysis earlier than the cognitive scale assessment and fMRI examination. Collectively, these findings suggest that the GST is not static, rather dynamic, thus providing useful information about the pathophysiological mechanisms of AUD.

In line with previous findings, AUD patients exhibited impairments in the insula and precuneus regions (Fukushima et al., 2020; Bordier et al., 2021). Recent fMRI studies have demonstrated that AUD can enhance activation in the insula, inferior frontal gyrus, and precuneus (Noori et al., 2016; Quaglieri et al., 2020). The precuneus has been functionally linked to resting-state cognitive activities, including the evaluation and collection of information, extraction of episodic memory, emotion, and anxiety, and self-referred mental activity (Krienke et al., 2014). Furthermore, our study indicated that in AUD patients, functional alterations in the precuneus might affect the episodic memory-related circuits. A study has shown that insula as part of the salience network mediates external stimuli-induced attention and arousal responses (Bordier et al., 2021). The insula, as the central hub of the salience network, regulates attention shifting between the exogenous and endogenous states.

VBM studies have revealed AUD-induced atrophic patterns in the anterior and posterior cingulate cortices, lateral prefrontal cortex, hippocampus, insular-opercular cortex, striatum, and thalamus (Xiao et al., 2015; Yang et al., 2016; Galandra et al., 2018). However, in our cohort, we could not find any significant morphometric differences between the groups in the

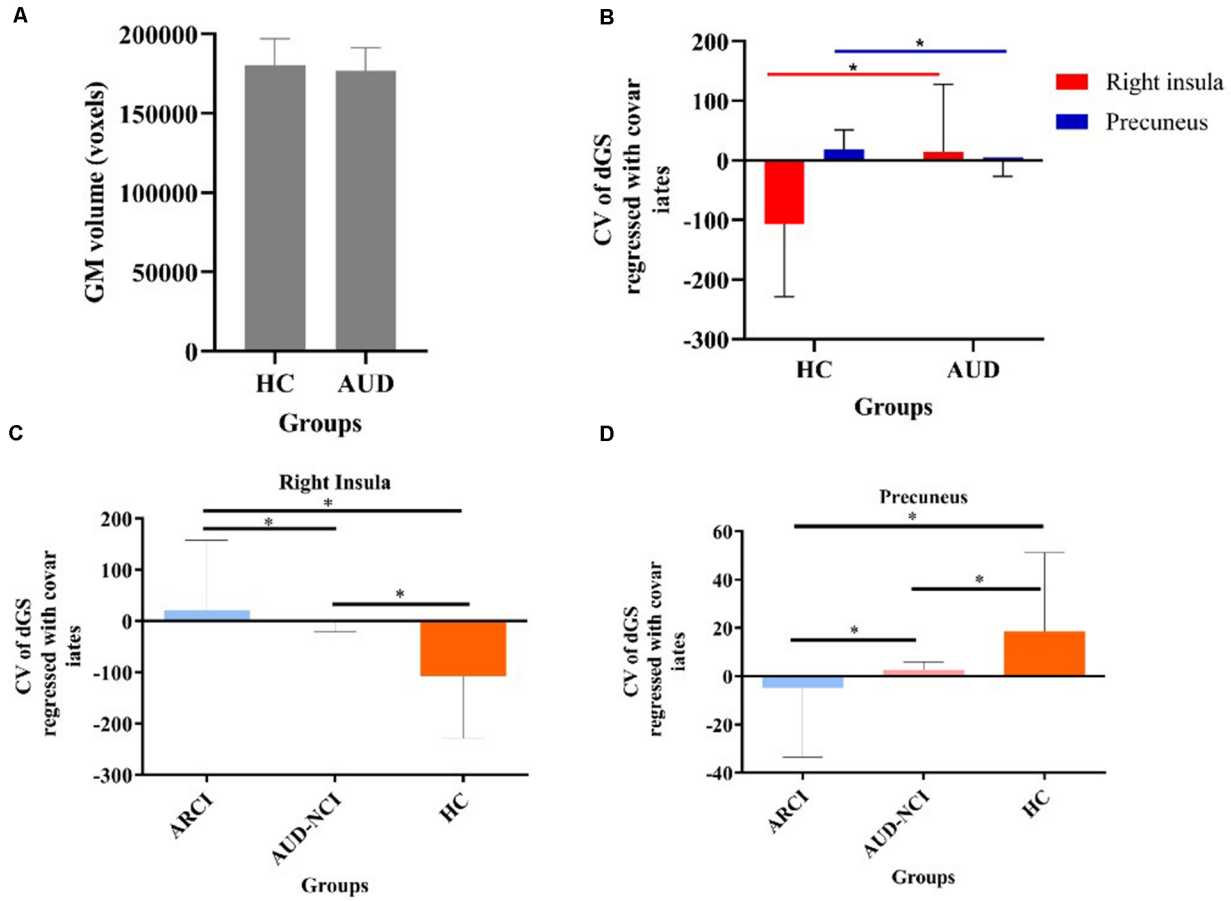

FIGURE 3 | The static and temporal dynamic changes of intrinsic brain activity in control and AUD groups. **(A)** Gray matter (GM) volume in voxels between HC and AUD group ($p > 0.05$). **(B)** Dynamic global signal topography (GST; right insula and precuneus) in HC and AUD groups ($p < 0.05$). **(C)** Dynamic GST in the right insula in different groups ($p < 0.05$). **(D)** Dynamic GST in precuneus in different groups. *$p < 0.05$.

TABLE 2 | Altered dynamic GS topography in AUD patients compared with HCs.

Clusters	Number of voxels	Regions	MNI	F
1	39	Cerebellum Anterior Lobe	−21, −57, −30	25.92
2	48	Right insula Inferior frontal gyrus	33, 18, −18	25.68
3	15	Parietal lobe Left Precuneus Postcentral gyrus	−6, −54, 66	22.60

GS, global signal; AUD, alcohol use disorder; HCs, healthy controls.

corresponding brain regions. However, there were significant differences in dynamic GST values across the groups, suggesting that dynamic GST could detect AUD-mediated changes before the manifestation of cortical atrophy.

According to the data, we found that the two indexes were different among the three groups. However, there was no obvious linear correlation between the amount of consumed alcohol and behavioral scores in AUD patients. The possible reasons were speculated as follows: (1) the sample size we included was not large enough. More participants are needed to find the correlation; (2) all the included patients were able to cooperate with the examination, but the cognitive function decline was not severe enough; (3) there are individual differences with respect to brain damage caused by regular alcohol consumption due to altered metabolic enzyme activity and other unknown mechanisms; and (4) the dynamic GST abnormality might have happened prior to behavioral scale changes in alcohol dependence.

There were several limitations in this study. First and most importantly, this study involved a very small sample size which limited our ability to detect effects on the statistical scale. In the future, we will plan to carry out studies involving a larger

sample size with higher statistical significance, primarily focusing on the dynamic GST. Secondly, as the cohort consisted of only severe-to-moderate AUD patients, sampling bias should be taken into account. To confirm whether the BOLD activity was a state-dependent endophenotype, mild AUD patients should be examined using the same method. Thirdly, ADS score and alcohol consumption rate was evaluated based on the self-administered questionnaires that might increase the risk of possible recall bias and false positives. However, despite these limitations, this study is likely to broaden our understanding of alcohol addiction and its impact on neural network modulation to facilitate pathology detection and treatment strategy.

DATA AVAILABILITY STATEMENT

The raw data supporting the conclusions of this article will be made available by the authors, without undue reservation.

ETHICS STATEMENT

The studies involving human participants were reviewed and approved by the Ethics Committee of First Affiliated Hospital of Zhengzhou University (2018-KY-91) and abided by the Declaration of Helsinki. The patients/participants provided their written informed consent to participate in this study. Written informed consent was obtained from the individual(s) for the publication of any potentially identifiable images or data included in this article.

AUTHOR CONTRIBUTIONS

YJ was the project holder. YJ and LL contributed to conception and study design. RD and LJ were responsible for study follow-up and contributed to this article. YL, ZG, and YY were responsible for patients' recruitment, diagnosis, and treatment. WW was responsible for fcMRI acquisition. YZ, JC, and YP analyzed the data. All authors contributed to the article and approved the submitted version.

FUNDING

This research was supported by the National Key R&D Program of China (2018YFC1314400, 2018YFC1314403) and the National Natural Science Foundation of China (Grant nos. 81371385, U1604170, and 81870926).

ACKNOWLEDGMENTS

We thank the devoted researchers in participant enrollment, data collection, and project maintenance: Yang Gao, Tingting Luan, Chaopeng Zhang, Jinwei Zhang, Yi Zhao, Haojie Xie, Yongyan Zhou, Yingzhe Shao, Kaixin Wang, Juan Du, and Chunyang Pan.

REFERENCES

Allen, E. A., Damaraju, E., Plis, S. M., Erhardt, E. B., Eichele, T., and Calhoun, V. D. (2014). Tracking whole-brain connectivity dynamics in the resting state. *Cereb. Cortex* 24, 663–676. doi: 10.1093/cercor/bhs352

Ao, Y., Ouyang, Y., Yang, C., and Wang, Y. (2021). Global signal topography of the human brain: a novel framework of functional connectivity for psychological and pathological investigations. *Front. Hum. Neurosci.* 15:644892. doi: 10.3389/fnhum.2021.644892

Bates, M. E., Bowden, S. C., and Barry, D. (2002). Neurocognitive impairment associated with alcohol use disorders: implications for treatment. *Exp. Clin. Psychopharmacol.* 10, 193–212. doi: 10.1037//1064-1297.10.3.193

Bordier, C., Weil, G., Bach, P., Scuppa, G., Nicolini, C., Forcellini, G., et al. (2021). Increased network centrality of the anterior insula in early abstinence from alcohol. *Addict. Biol.* 27:e13096. doi: 10.1111/adb.13096

Bruijnen, C., Dijkstra, B. A. G., Walvoort, S. J. W., Markus, W., VanDerNagel, J. E. L., Kessels, R. P. C., et al. (2019). Prevalence of cognitive impairment in patients with substance use disorder. *Drug Alcohol Rev.* 38, 435–442. doi: 10.1111/dar.12922

Bruijnen, C., Walvoort, S. J. W., Dijkstra, B. A. G., de Jong, C. A. J., and Kessels, R. P. C. (2021). The course of cognitive performance during inpatient treatment in patients with alcohol use disorder with, n. o., mild or major neurocognitive disorders. *Alcohol Alcohol.* 56, 89–100. doi: 10.1093/alcalc/agaa100

Cabrera, E. A., Wiers, C. E., Lindgren, E., Miller, G., Volkow, N. D., and Wang, G. J. (2016). Neuroimaging the effectiveness of substance use disorder treatments. *J. Neuroimmune Pharmacol.* 11, 408–433. doi: 10.1007/s11481-016-9680-y

Carvalho, A. F., Heilig, M., Perez, A., Probst, C., and Rehm, J. (2019). Alcohol use disorders. *Lancet* 394, 781–792. doi: 10.1016/S0140-6736(19)31775-1

Franklin, T., Wang, Z., Suh, J. J., Hazan, R., Cruz, J., Li, Y., et al. (2011). Effects of varenicline on smoking cue-triggered neural and craving responses. *Arch. Gen. Psychiatry* 68, 516–526. doi: 10.1001/archgenpsychiatry.2010.190

Fukushima, S., Kuga, H., Oribe, N., Mutou, T., and Ueno, T. (2020). Behavioural cue reactivity to alcohol-related and non-alcohol-related stimuli among individuals with alcohol use disorder: an fMRI study with a visual task. *PLoS One* 15:e0229187. doi: 10.1371/journal.pone.0229187

Galandra, C., Basso, G., Manera, M., Crespi, C., Giorgi, I., Vittadini, G., et al. (2018). Salience network structural integrity predicts executive impairment in alcohol use disorders. *Sci. Rep.* 8:14481. doi: 10.1038/s41598-018-32828-x

Han, S., Wang, X., He, Z., Sheng, W., Zou, Q., Li, L., et al. (2019). Decreased static and increased dynamic global signal topography in major depressive disorder. *Prog. Neuropsychopharmacol. Biol. Psychiatry* 94:109665. doi: 10.1016/j.pnpbp.2019.109665

Hawkins, B. R., and McCambridge, J. (2021). Partners or opponents? alcohol industry strategy and the 2016 revision of the U.K. low-risk drinking guidelines. *J. Stud. Alcohol Drugs* 82, 84–92. doi: 10.15288/jsad.2021.82.84

Health, D. O. (2017). Communicating the UK chief medical officers' alcohol guidelines. Available online at: https://assets.publishing.service.gov.uk/government/uploads/system/uploads/attachment_data/file/602132/Communicating_2016_CMO_guidelines_Mar_17.pdf

Heirene, R., John, B., and Roderique-Davies, G. (2018). Identification and evaluation of neuropsychological tools used in the assessment of alcohol-related cognitive impairment: a systematic review. *Front. Psychol.* 9:2618. doi: 10.3389/fpsyg.2018.02618

Kim, J. W., Byun, M. S., Yi, D., Lee, J. H., Ko, K., Jeon, S. Y., et al. (2020). Association of moderate alcohol intake with in vivo amyloid-beta deposition in human brain: a cross-sectional study. *PLoS Med.* 17:e1003022. doi: 10.1371/journal.pmed.1003022

Koob, G. F., and Volkow, N. D. (2016). Neurobiology of addiction: a neurocircuitry analysis. *Lancet Psychiatry* 3, 760–773. doi: 10.1016/S2215-0366(16)00104-8

Krienke, U. J., Nikesch, F., Spiegelhalder, K., Hennig, J., Olbrich, H. M., and Langosch, J. M. (2014). Impact of alcohol-related video sequences on functional MRI in abstinent alcoholics. *Eur. Addict. Res.* 20, 33–40. doi: 10.1159/000349909

Kudva, K. G., Abdin, E., Vaingankar, J. A., Chua, B. Y., and Subramaniam, M. (2021). The relationship between suicidality and socio-demographic variables, physical disorders and psychiatric disorders: results from the singapore mental health study 2016. *Int. J. Environ. Res. Public Health* 18:4365. doi: 10.3390/ijerph18084365

Langleben, D. D., Ruparel, K., Elman, I., Loughead, J. W., Busch, E. L., Cornish, J., et al. (2014). Extended-release naltrexone modulates brain response to drug cues in abstinent heroin-dependent patients. *Addict. Biol.* 19, 262–271. doi: 10.1111/j.1369-1600.2012.00462.x

Leclercq, S., Le Roy, T., Furgiuele, S., Coste, V., Bindels, L. B., Leyrolle, Q., et al. (2020). Gut microbiota-induced changes in β-hydroxybutyrate metabolism are linked to altered sociability and depression in alcohol use disorder. *Cell Rep.* 33:108238. doi: 10.1016/j.celrep.2020.108238

Li, J., Bolt, T., Bzdok, D., Nomi, J. S., and Uddin, L. Q. (2019). Topography and behavioral relevance of the global signal in the human brain. *Sci. Rep.* 9:14268. doi: 10.1038/s41598-019-50750-8

Li, R., Wang, H., Wang, L., Zhang, L., Zou, T., Wang, X., et al. (2021). Shared and distinct global signal topography disturbances in subcortical and cortical networks in human epilepsy. *Hum. Brain Mapp.* 42, 412–426. doi: 10.1002/hbm.25231

Liu, T. T., Nalci, A., and Falahpour, M. (2017). The global signal in fMRI: nuisance or information. *Neuroimage* 150, 213–229. doi: 10.1016/j.neuroimage.2017.02.036

Marshall, S. A., McClain, J. A., Wooden, J. I., and Nixon, K. (2020). Microglia dystrophy following binge-like alcohol exposure in adolescent and adult male rats. *Front. Neuroanat.* 14:52. doi: 10.3389/fnana.2020.00052

Melugin, P. R., Nolan, S. O., and Siciliano, C. A. (2021). Bidirectional causality between addiction and cognitive deficits. *Int. Rev. Neurobiol.* 157, 371–407. doi: 10.1016/bs.irn.2020.11.001

Myrick, H., Anton, R. F., Li, X., Henderson, S., Randall, P. K., and Voronin, K. (2008). Effect of naltrexone and ondansetron on alcohol cue-induced activation of the ventral striatum in alcohol-dependent people. *Arch. Gen. Psychiatry* 65, 466–475. doi: 10.1001/archpsyc.65.4.466

Noori, H. R., Cosa Linan, A., and Spanagel, R. (2016). Largely overlapping neuronal substrates of reactivity to drug, gambling, food and sexual cues: a comprehensive meta-analysis. *Eur. Neuropsychopharmacol.* 26, 1419–1430. doi: 10.1016/j.euroneuro.2016.06.013

Oey, M. J., Postma, A., Hoes, S., and Oudman, E. (2021). Behavioural effects of light intervention in people with korsakoff syndrome: a pilot study. *Neuropsychol. Rehabil.* 31, 1–16. doi: 10.1080/09602011.2021.1890623

Power, J. D., Mitra, A., Laumann, T. O., Snyder, A. Z., Schlaggar, B. L., and Petersen, S. E. (2014). Methods to detect, characterize and remove motion artifact in resting state fMRI. *Neuroimage* 84, 320–341. doi: 10.1016/j.neuroimage.2013.08.048

Quaglieri, A., Mari, E., Boccia, M., Piccardi, L., and Giannini, A. M. (2020). Brain network underlying executive functions in gambling and alcohol use disorders: an activation likelihood estimation meta-analysis of fMRI studies. *Brain Sci.* 10:353. doi: 10.3390/brainsci10060353

Rehm, J., and Shield, K. D. (2019). Global burden of disease and the impact of mental and addictive disorders. *Curr. Psychiatry Rep.* 21:10. doi: 10.1007/s11920-019-0997-0

Ridley, N. J., Draper, B., and Withall, A. (2013). Alcohol-related dementia: an update of the evidence. *Alzheimers Res. Ther.* 5:3. doi: 10.1186/alzrt157

Schölvinck, M. L., Maier, A., Ye, F. Q., Duyn, J. H., and Leopold, D. A. (2010). Neural basis of global resting-state fMRI activity. *Proc. Natl. Acad. Sci. U S A* 107, 10238–10243. doi: 10.1044/2021_LSHSS-21-00075

Schuckit, M. A. (2009). Alcohol-use disorders. *Lancet* 373, 492–501. doi: 10.1016/S0140-6736(09)60009-X

Shabani, A., Masoumian, S., Zamirinejad, S., Hejri, M., Pirmorad, T., and Yaghmaeezadeh, H. (2021). Psychometric properties of structured clinical interview for DSM-5 disorders-clinician version (SCID-5-CV). *Brain Behav.* 11:e01894. doi: 10.1002/brb3.1894

Tanabe, S., Huang, Z., Zhang, J., Chen, Y., Fogel, S., Doyon, J., et al. (2020). Altered global brain signal during physiologic, pharmacologic and pathologic states of unconsciousness in humans and rats. *Anesthesiology* 132, 1392–1406. doi: 10.1097/ALN.0000000000003197

Toledo Nunes, P., Vedder, L. C., Deak, T., and Savage, L. M. (2019). A pivotal role for thiamine deficiency in the expression of neuroinflammation markers in models of alcohol-related brain damage. *Alcohol. Clin. Exp. Res.* 43, 425–438. doi: 10.1111/acer.13946

Walvoort, S. J., van der Heijden, P. T., Kessels, R. P., and Egger, J. I. (2016). Measuring illness insight in patients with alcohol-related cognitive dysfunction using the Q8 questionnaire: a validation study. *Neuropsychiatr. Dis. Treat.* 12, 1609–1615. doi: 10.2147/NDT.S104442

Wang, X., Liao, W., Han, S., Li, J., Wang, Y., Zhang, Y., et al. (2021). Frequency-specific altered global signal topography in drug-naïve first-episode patients with adolescent-onset schizophrenia. *Brain Imaging Behav.* 15, 1876–1885. doi: 10.1007/s11682-020-00381-9

Wilcox, C. E., Mayer, A. R., Bogenschutz, M. P., Ling, J., Dekonenko, C., and Cumbo, H. (2015). Cognitive control network function in alcohol use disorder before and during treatment with lorazepam. *Subst. Use Misuse* 50, 40–52. doi: 10.3109/10826084.2014.957771

Xiao, P., Dai, Z., Zhong, J., Zhu, Y., Shi, H., and Pan, P. (2015). Regional gray matter deficits in alcohol dependence: a meta-analysis of voxel-based morphometry studies. *Drug Alcohol Depend.* 153, 22–28. doi: 10.1016/j.drugalcdep.2015.05.030

Yang, G. J., Murray, J. D., Glasser, M., Pearlson, G. D., Krystal, J. H., Schleifer, C., et al. (2017). Altered global signal topography in schizophrenia. *Cereb. Cortex* 27, 5156–5169. doi: 10.1093/cercor/bhw297

Yang, X., Tian, F., Zhang, H., Zeng, J., Chen, T., Wang, S., et al. (2016). Cortical and subcortical gray matter shrinkage in alcohol-use disorders: a voxel-based meta-analysis. *Neurosci. Biobehav. Rev.* 66, 92–103. doi: 10.1016/j.neubiorev.2016.03.034

Zhang, J., Magioncalda, P., Huang, Z., Tan, Z., Hu, X., Hu, Z., et al. (2019). Altered global signal topography and its different regional localization in motor cortex and hippocampus in mania and depression. *Schizophr. Bull.* 45, 902–910. doi: 10.1093/schbul/sby138

Zhang, R., and Volkow, N. D. (2019). Brain default-mode network dysfunction in addiction. *Neuroimage* 200, 313–331. doi: 10.1016/j.neuroimage.2019.06.036

Zilverstand, A., Huang, A. S., Alia-Klein, N., and Goldstein, R. Z. (2018). Neuroimaging impaired response inhibition and salience attribution in human drug addiction: a systematic review. *Neuron* 98, 886–903. doi: 10.1016/j.neuron.2018.03.048

Conflict of Interest: The authors declare that the research was conducted in the absence of any commercial or financial relationships that could be construed as a potential conflict of interest.

frontiers in Aging Neuroscience

ORIGINAL RESEARCH
published: 18 February 2022
doi: 10.3389/fnagi.2022.835373

Morphological and Hemodynamic Risk Factors for the Rupture of Proximal Anterior Cerebral Artery Aneurysms (A1 Segment)

Mingwei Xu[1], Nan Lv[2], Kai Sun[1], Rujun Hong[1], Hao Wang[1], Xuhui Wang[1], Lunshan Xu[1], Lizhao Chen[1] and Minhui Xu[1]**

[1] Department of Neurosurgery, Daping Hospital, Army Medical University, Chongqing, China, [2] Department of Neurosurgery, Changhai Hospital, Naval Medical University, Shanghai, China

OPEN ACCESS

Edited by:
Yang Zhang,
Chongqing University, China

Reviewed by:
Yue He,
Huazhong University of Science and Technology, China
Zongduo Guo,
First Affiliated Hospital of Chongqing Medical University, China

***Correspondence:**
Lizhao Chen
chenlizhao1971@163.com
Minhui Xu
minhuixu66@aliyun.com

Specialty section:
This article was submitted to Neurocognitive Aging and Behavior, a section of the journal Frontiers in Aging Neuroscience

Received: *14 December 2021*
Accepted: *24 January 2022*
Published: *18 February 2022*

Citation:
Xu M, Lv N, Sun K, Hong R, Wang H, Wang X, Xu L, Chen L and Xu M (2022) Morphological and Hemodynamic Risk Factors for the Rupture of Proximal Anterior Cerebral Artery Aneurysms (A1 Segment). Front. Aging Neurosci. 14:835373. doi: 10.3389/fnagi.2022.835373

Objective: The treatment of unruptured small intracranial aneurysms remains controversial. A distinguishing characteristic of A1 segment aneurysms is that they tend to rupture when they are small, which may be related to their distinctive morphology and hemodynamics. Our study sought to investigate the rupture risk factors of A1 segment aneurysms by analyzing the clinical risk factors, morphology, and hemodynamic characteristics of A1 segment aneurysms.

Methods: We retrospectively enrolled 49 (23 ruptured, 26 unruptured) consecutive patients presenting to our institute with A1 segment aneurysms between January 2010 and March 2020. Independent risk factors associated with the rupture of A1 segment aneurysms were analyzed by multivariate regression analysis in the ruptured group and unruptured group.

Results: Clinical risk factors, including age, sex, hypertension, smoking history, and SAH family history revealed no difference between the ruptured and unruptured groups. The ruptured group presented a significantly larger size (Size, $P = 0.007$), aspect ratio (AR, $P = 0.002$), size ratio (SR, $P = 0.001$), bottleneck index (BN, $P = 0.016$), dome-to-neck ratio (DN, $P = 0.001$), and oscillatory shear index (OSI) ($P = 0.001$) than the unruptured group. The normalized wall shear stress (NWSS) of the ruptured aneurysms was lower than the unruptured group ($P = 0.001$). In the multivariate regression analysis, only SR (OR = 3.672, $P = 0.003$) and NWSS (OR = 0.474, $P = 0.01$) were independent risk factors in the A1 segment aneurysm rupture.

Conclusion: A higher SR and lower NWSS revealed a close connection with the rupture of A1 segment aneurysms in our study, thus providing a reference for clinical decision-making in treating A1 segment unruptured aneurysms.

Keywords: intracranial aneurysms, proximal anterior cerebral artery (A1 segment), morphology, hemodynamics, computational fluid dynamics

INTRODUCTION

The incidence of the aneurysms arising from a proximal anterior cerebral artery (A1 segment) is relatively low, with an incidence of 0.59–4%, as reported in the literature (Wakabayashi et al., 1985; Suzuki et al., 1992; Wanibuchi et al., 2001; Dashti et al., 2007; Lee et al., 2010; Park et al., 2013; Bhaisora et al., 2014; Maiti et al., 2016; Ding et al., 2017; Kim and Lim, 2019). A1 segment aneurysms are characterized by small size at rupture, multiplicity, associated vascular anomaly, and many incorporating perforators (Suzuki et al., 1992; Dashti et al., 2007; Lee et al., 2010; Park et al., 2013). Clinically, most ruptured A1 segment aneurysms are small, with a maximum size of < 5 mm, which stands in contrast with previous studies suggesting that small intracranial aneurysms (<5 mm) should be managed conservatively (Wiebers et al., 2003; Juvela et al., 2008; Investigators et al., 2012). Furthermore, A1 segment aneurysms are closely related to the perforating arteries around them, which may affect the perforating arteries and result in serious neurological dysfunction. Therefore, A1 segment aneurysms are dangerous, and it is significant to assess the risk factors of A1 segment aneurysm rupture. Aneurysm ruptures are reported to be related to morphological and hemodynamic parameters; however, results remain highly controversial (Dhar et al., 2008; Kashiwazaki and Kuroda, 2013; Duan et al., 2016; Lv et al., 2016b). This may be because most of these studies are not location-specific, and aneurysms at different locations may have distinctive morphological and hemodynamic characteristics. Due to their extremely rare occurrence, there are few published studies on the morphological and hemodynamic characteristics of A1 segment aneurysms. Our study focused on A1 segment aneurysms and investigated the potential risk factors for aneurysm rupture, including morphology and hemodynamics.

MATERIALS AND METHODS

Patient Selection and Clinical Characteristics

We reviewed the clinical data of 2,247 aneurysms in 1,987 patients admitted to our institute between January 2010 and September 2020. The patient selection criteria were as follows:

Inclusion criteria: (1) Patients with A1 saccular aneurysms, (2) Complete clinical medical records; (3) Clinical or imaging evidence for the presence or absence of subarachnoid hemorrhage; (4) CTA image data meet the need for morphological and hemodynamic analysis.

Exclusion criteria: (1) Patients with A1 or fusiform aneurysms; (2) Patients with multiple aneurysms and the distance between aneurysms were too close to each other for CFD simulation, such as an anterior communicating aneurysm; (3) Patients with other cerebrovascular diseases, including arteriovenous malformation and arteriovenous fistula, etc.; (4) CTA data could not meet the needs of morphological and hemodynamic analysis.

Of the 1,987 patients, 52 had A1 segment aneurysms. Of the 52 A1 segment aneurysms, 1 case of blood blister aneurysms and 2 cases of fusiform aneurysms were excluded from the comparative analysis because it was difficult to study their morphological and hemodynamic indicators. Among the 49 A1 segment aneurysms, 23 were identified as ruptured aneurysms and 26 as unruptured aneurysms based on the evidence of subarachnoid hemorrhage (SAH) on a CT scan. This study assessed the currently recognized clinical risk factors for the rupture of aneurysms, including age, sex, hypertension, diabetes, smoking history, and family history of familial SAH. The definitions of hypertension, diabetes, and smoking history were by those laid forth by the previous articles of our research group (Lv et al., 2016a).

Measurement and Calculation of Morphological Characteristics

There are six morphological parameters used in the study, including size, AR, SR, DN, height-to-width ratio (HW), bottleneck factor (BN), which were defined as previously reported (Hoh et al., 2007; Dhar et al., 2008). The size, height, width, and diameter of the artery of the aneurysm were measured, as shown in **Figure 1**. The maximum distance and the vertical distance from the aneurysm dome to the neck plane are defined as the size and the height of the aneurysm, respectively. And the width is the maximum diameter of the body perpendicular to the height. The DICOM data of patients' CTA were analyzed by Mimics 17.0 (Mimics 17.0, Materialize, Belgium) to reconstruct 3D models of A1 segment aneurysms. Calculation of morphological parameters was performed using MATLAB 9.2 (MathWorks, Natick, Massachusetts, United States).

Other radiologic findings, including irregular shape, hypoplasia/aplasia of A1, fenestration of A1, and multiplicity, were also included in this study to investigate their relationship with the rupture of the A1 segment aneurysm. An irregular shape of an aneurysm was defined as a lobulated aneurysm or small bleb protruding from the aneurysm sac. Hypoplasia of A1 was defined as the diameter of the ipsilateral A1, which was less than

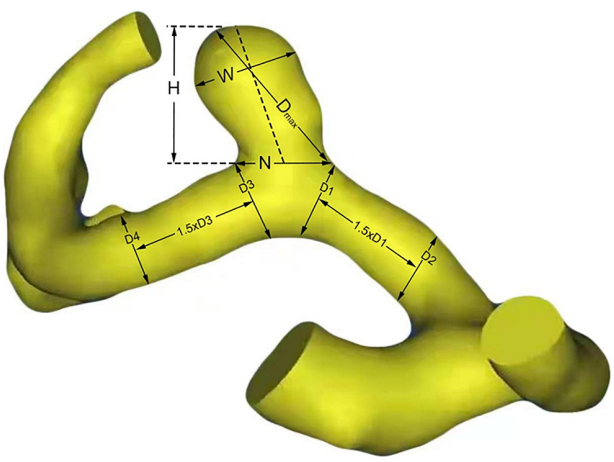

FIGURE 1 | Definitions of morphological parameters. H, W, and N represent the height, width and neck size of aneurysm, respectively. Size = Dmax; Aspect ratio (AR) = H/N; Size ratio (SR) = 4Dmax/(D1 + D2 + D3 + D4); Dome-to-neck ratio (DN) = Dmax/N; height-to-width ratio (HW) = H/W; Bottleneck factor = Width/Neck.

50% of the contralateral side. The irregular shape and vascular anomalies were assessed using a high-resolution CTA.

Computational Fluid Dynamic Simulating and Hemodynamic Parameter Calculations

Geomagic Studio 9.0 (3D Systems, Inc.) and ICEM CFD 11.0 (ANSYS, Inc.) were used for the 3D models building of A1 aneurysms. As previously described, each vessel model was divided into the aneurysm, parent artery, and other vessels (Xu et al., 2013). The number of volume element grids for each 3D model was approximately between 1000,000 and 1400,000. Computational Fluid Dynamic (CFD) simulations were performed by CFX 11.0 (ANSYS, Inc.), assuming that the blood flow is laminar and incompressible and the vessel is rigid (Valencia et al., 2006). The density of the blood flow was 1,050 kg/m^3 and the dynamic viscosity was 0.00345 Pa·s. According to a transcranial Doppler from a healthy subject, the flow inlet boundary conditions were set as typical pulsatile velocity profile (He and Ku, 1996) and the outlet boundary conditions were set as opening with zero static pressure (Lv et al., 2020). The total cardiac cycle was set to 0.8 s with a time step of 0.001 s, and the numeric simulation was performed by two consecutive cardiac cycles. The output was set as the result from the last cycle.

Quantitative hemodynamic parameters involved in this study include normalized wall shear stress (NWSS), the oscillatory shear index (OSI), the ratio of low WSS area (LSAR, below 10% of the mean WSS), normalized pressure (NP), and relative residence time (RRT) (Xiang et al., 2011).

Statistical Analysis

SPSS version 23.0 (IBM Corp, Armonk, NY, United States) and Microsoft Excel 2013 were used for statistical analyses. The parameters were expressed as the number of patients (%) or median (interquartile range). The chi-square test and the Mann-Whitney *U*-test were performed for categorical variables and quantitative data, respectively. To assess independent risk factors for the rupture of A1 segment aneurysms, multivariate logistic regression analysis was performed for all relevant parameters. Statistical significance considered significant if $P < 0.05$.

RESULTS

Clinical Characteristics

In this study, 49 patients with A1 segment aneurysms were included (16 men and 33 women) with a mean age of 60 years (range, 37–75 years). A total of 49 cases of A1 segment aneurysms were divided into the ruptured group (23 cases) and the unruptured group (26 cases) according to the evidence of SAH in the CT scan. The clinical characteristics of the 49 A1 segment aneurysms are listed in **Table 1**. No significant differences were detected in baseline characteristics (including age, sex, hypertension, diabetes, smoking history, and family history of SAH) between the two groups, thereby indicating that the morphological and hemodynamic characteristics were comparable.

Morphological and Hemodynamic Parameters

The characteristics of morphology and hemodynamics of the 49 A1 segment aneurysms are represented in **Table 2**. In terms of morphological indices, significant differences were defined between the ruptured and unruptured groups. A larger size ($p = 0.007$), SR ($p = 0.001$), AR ($p = 0.002$), DN ($P = 0.001$), and BN ($P = 0.016$) and a significantly higher proportion of aneurysms with irregular shapes ($P = 0.008$) were found in the ruptured group. There were no significant differences in other morphological characteristics of vascular anomalies, including hypoplasia/aplasia of A1 ($P = 0.5252$), fenestration of A1 ($P = 0.873$), and multiplicity ($P = 0.566$) between the ruptured and unruptured groups.

In the comparative analyses of hemodynamic parameters, the ruptured A1 segment aneurysms were proven to have a significantly lower normalized WSS ($P = 0.001$) and higher OSI ($P = 0.001$) than the unruptured group. Other hemodynamic characteristics, including the percentage of low WSS area (LSA) ($P = 0.088$), pressure ($P = 0.869$), and RRT ($P = 0.175$), revealed no significant differences. Hemodynamic patterns of six representative cases are shown in **Figure 2**.

Multivariate Analysis

To identify independent risk factors of A1 segment aneurysm rupture, all differential morphological and hemodynamic indicators were included in a further multivariate regression analysis. Finally, our study revealed that independent variables of the rupture status of A1 segment aneurysms were SR (odds ratio = 3.672; $p = 0.003$) and normalized WSS (odds ratio = 0.474; $p = 0.01$) in **Table 3**.

DISCUSSION

The incidence of A1 segment aneurysms is relatively low, accounting for about 0.59–4% of all intracranial aneurysms (Wakabayashi et al., 1985; Suzuki et al., 1992; Wanibuchi et al., 2001; Dashti et al., 2007; Maiti et al., 2016; Ding et al., 2017). In this study, A1 segment aneurysms accounted for 2.61% of all aneurysms and 2.31% of all aneurysms diagnosed during the study period. However, owing to the extremely rare occurrence, little attention has been paid to A1 aneurysms, especially to their risk factors for rupture. To our knowledge, it is the first study to identify possible risk factors for A1 segment aneurysm rupture by combining morphological and hemodynamic analyses.

The majority of small unruptured intracranial aneurysms (IAs) are increasingly being detected due to advanced imaging techniques. The International Study of Unruptured Intracranial Aneurysms (ISUIA) report elucidates that the annual rupture risk of UIAs $\leq$ 6 mm is very low (0.069%), while the rupture risk of UIAs $>$ 7 mm increases to 2.6% (Wiebers et al., 2003). Previous studies have suggested that a high rupture rate of A1 segment aneurysms, which are prone to rupture at smaller sizes

TABLE 1 | Clinical characteristics of A1 aneurysms.

	A1 segment aneurysms			
Variables	**Total (*n* = 49)**	**Ruptured (*n* = 23)**	**Unruptured (*n* = 26)**	***P*-value**
Clinical characteristics				
Age (Years)	60 (51, 67)	57 (47, 64)	62 (57, 68)	0.078
Male, n (%)	16 (32.65%)	8 (34.78%)	8 (30.77%)	0.765
Hypertension, n (%)	26 (53.06%)	10 (43.48%)	16 (61.854%)	0.206
Diabetes, n (%)	5 (10.2%)	2 (8.69%)	3 (11.56%)	0.743
Smoking, n (%)	8 (16.33%)	4 (17.39%)	4 (15.38%)	0.85
Earlier SAH, n (%)	3 (6.12%)	1 (4.35%)	2 (7.69%)	0.929

TABLE 2 | Morphological and hemodynamic characteristics of A1 aneurysms.

	A1 segment aneurysms			
Variables	**Total (*n* = 49)**	**Ruptured (*n* = 23)**	**Unruptured (*n* = 26)**	***P*-value**
Morphological characteristics				
Size (mm)	3.07 (2.47, 3.85)	3.51 (2.78, 4.45)	2.69 (2.12, 3.45)	0.007
Aspect ratio (AR)	1.06 (0.83, 1.24)	1.21 (1.07, 1.35)	0.9 (0.72, 1.08)	0.002
Size ratio (SR)	1.41 (1.07, 1.81)	1.60 (1.38, 2.21)	1.12 (0.92, 1.53)	0.001
Dome-to-neck ratio (DN)	1.17 (0.83, 1.24)	1.36 (1.19, 1.64)	1.04 (0.84, 1.18)	0.001
Bottleneck index (BN)	1.10 (1.00, 1.25)	1.18 (1.05, 1.42)	1.04 (0.89, 1.17)	0.016
Height-width ratio (HW)	0.93 (0.80, 1.07)	0.98 (0.85, 1.13)	0.88 (0.84, 0.94)	0.161
Irregular shape	11 (22.45%)	9 (39.13%)	2 (7.69%)	0.008
Hypoplasia/aplasia of A1	17 (34.69%)	10 (43.48%)	9 (34.62%)	0.525
Fenestration of A1	6 (12.24)	3 (13.04%)	3 (11.54%)	0.873
Multiplicity	9 (18.37%)	5 (21.74%)	4 (13.79%)	0.566
Hemodynamic characteristics				
Normalized WSS	0.68 (0.44, 0.84)	0.57 (0.53, 0.66)	0.73 (0.64, 0.89)	0.001
Percentage of low WSS area (LSA)	0 (0.00, 0.004)	0.0001 (0.00, 0.046)	0 (0.00, 0.0016)	0.088
Oscillatory shear index	0.0116 (0.0073, 0.0198)	0.0192 (0.0112, 0.0269)	0.0084 (0.0058, 0.0136)	0.001
Pressure	1.18 (1.06, 1.30)	1.21 (1.06, 1.31)	1.16 (1.06, 1.31)	0.869
Relative residence time	0.20 (0.13, 0.42)	0.27 (0.15, 0.50)	0.18 (0.11, 0.23)	0.175

Variables are expressed as median (interquartile range), or number of patients (%).

(Suzuki et al., 1992; Dashti et al., 2007; Lee et al., 2010; Park et al., 2013). In the study by Kim and Lim (2019), the average size of 30 A1 aneurysms was 4.1 mm; however, the rupture rate was as high as 40%. In Maiti et al. (2016) reported a series of 16 consecutive A1 segment aneurysms with a rupture rate as high as 50%, but the average rupture size of the rupture group was only 4.38 mm. In this series here, the greatest size of a ruptured A1 aneurysm was 6.59 mm, while the median size was 3.51 mm, and the rupture rate was as high as 46.94%. Moreover, A1 aneurysms are usually involved or even attached to many small perforators, which can incur serious neurologic deficits once they rupture. These findings indicate that A1 segment aneurysms are dangerous even if they are small; however, clinical treatment of unruptured small A1 aneurysms remains controversial for physicians, and reliable predictors are required to assess rupture risk.

Many studies have been carried out on the relationship between the risk of IAs rupture and morphology and hemodynamics, but the conclusions remain controversial, which may be related to the fact that the risk of IAs rupture varies across different locations (Forget et al., 2001). As a result, prior rupture risk factors may not necessarily apply to A1 segment aneurysms. Moreover, due to their rare incidence, previous studies on the rupture risk factors of A1 segment aneurysms have been limited. Kim and Lim (2019) pointed out that A1 segment aneurysms with irregular shapes, high aspect, or height-width ratio value showed a high risk of rupture by studying 32 cases of A1 aneurysms; however, hemodynamic variables were not included in this study. Xiang et al. (2011) found that the combination of morphological model (SR) and hemodynamics (WSS and OSI) could discriminate IA rupture status with high AUC values in a study of 119 IAs. Therefore, in this study, we only considered A1 aneurysms. Clinical risk factors, morphological indices, and hemodynamic indices of A1 aneurysms were studied together.

Previous studies have confirmed that clinical characteristics are closely related to the risk of IAs rupture (Bor et al., 2015). Our study demonstrated that clinical characteristics of age, sex, and hypertension showed no significant difference between the two groups, suggesting that the morphological and hemodynamic results were comparable. Another anatomical characteristic of

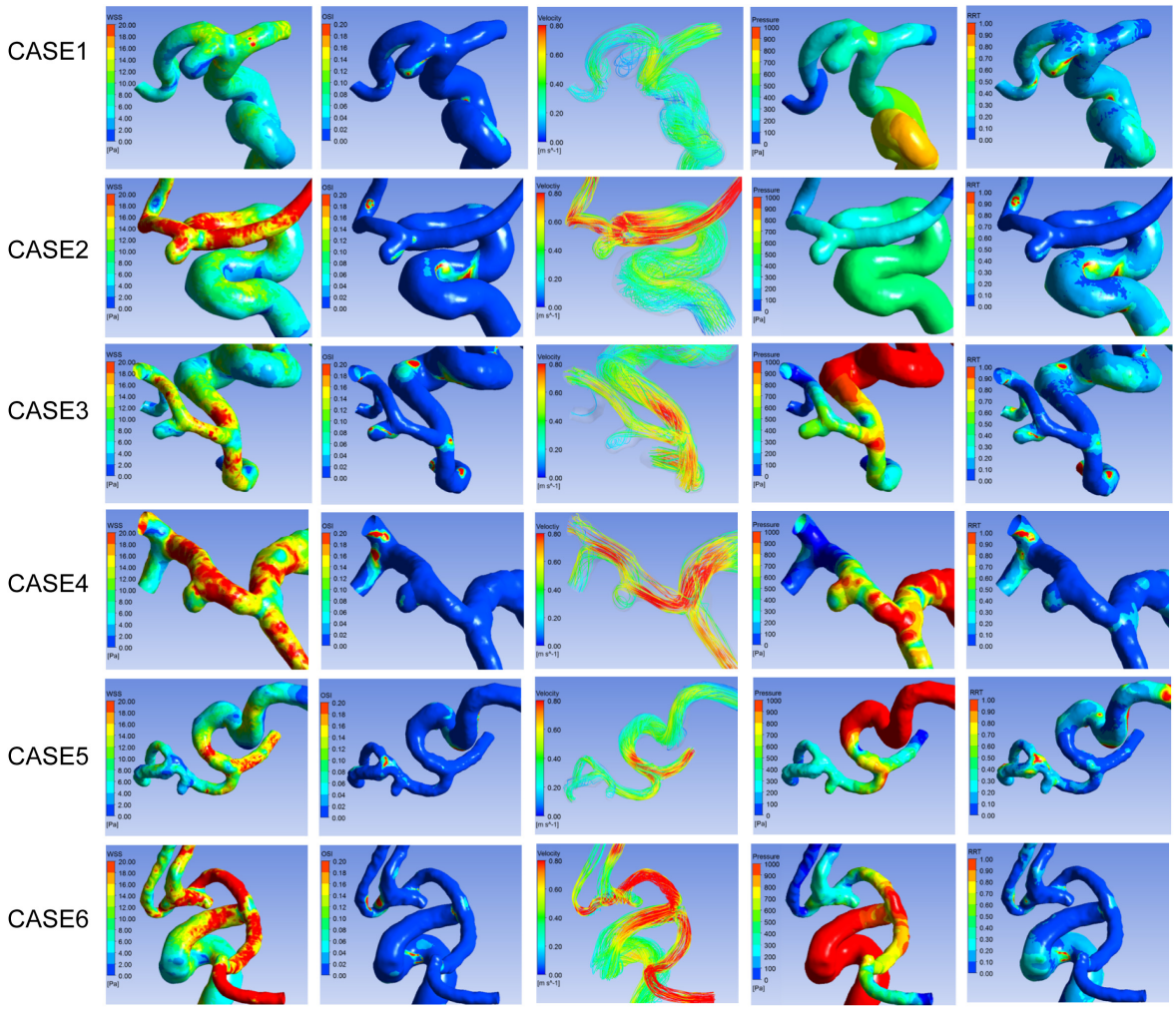

FIGURE 2 | Hemodynamic patterns of six representative A1 segment aneurysms. Cases1, 3, and 5 were ruptured aneurysms, and 2, 4, and 6 were unruptured aneurysms. Cases 1 and 2, 3 and 4, 5 and 6 located in proximal, middle, and distal segment of A1, respectively. From left to right shows distribution of WSS, OSI, Pressure, RRT, and flow pattern at the systolic peak of each aneurysm respectively.

A1 segment aneurysms is associated with vascular anatomical variations, including hypoplasia, aplasia, or fenestration of the A1 segment of the ACA, which may contribute to higher rupture rate of A1 aneurysms than arising from other location. Variant anatomies were reported in 21, 31.3, and 42.9% of patients with A1 segment aneurysms, in the studies by Suzuki et al. (1992); Bhaisora et al. (2014), and Maiti et al. (2016), respectively. In this study, 34.69% of the patients with A1 segment aneurysms had contralateral A1 hypoplasia or aplasia, and 12.24% of the patients were associated with fenestration of the A1 trunk, which is consistent with previous reports. However, the proportion of association of variant anatomy was not significantly different in this study. These results suggest that the variant anatomy of the A1 trunk may be related to the formation, but not the rupture of A1 segment aneurysms.

Previous studies have demonstrated that some morphological parameters are related to the rupture of intracranial aneurysms, among which aneurysm size is the most commonly used parameter in the clinical decision-making of aneurysm treatment. In our series of cases, the size of aneurysms was not statistically significant in the regression analysis, although it was larger in the ruptured group. Although AR, SR, DN, BN, and irregular morphology were statistically different in the univariate analysis, only SR was statistically different in the multivariate regression analysis, suggesting that a higher SR value is an independent risk factor for the A1 segment aneurysm rupture. This conclusion is consistent with previous results. In 2008, Dhar et al. (2008) proposed SR as a new indicator for predicting the rupture of intracranial aneurysms. Due to the inclusion of the

TABLE 3 | Independent risk factors for rupture of A1 aneurysms.

Variables	*P*-value	Odds ratio	95% confidence interval
Size ratio (SR)	0.003	3.672	1.578–8.540
Normalized WSS	0.010	0.0474	0.268–0.837

morphology of aneurysmal parent arteries, rupture of intracranial aneurysms can be more accurately predicted than aneurysm size. Kashiwazaki and Kuroda (2013) also pointed out that for small aneurysms (<5 mm), SR values, rather than aneurysm size, are a better predictor of rupture risk. Rahman et al. (2010) also demonstrated in a prospective study that SR was associated with aneurysm rupture. Only A1 segment aneurysms were included in this study, most of which were small aneurysms. Our results also confirmed SR as an independent risk factor for rupture of A1 aneurysms.

Hemodynamics is thought to be closely related to the occurrence, growth, and rupture of intracranial aneurysms (Duan et al., 2016). Previous studies have shown that low WSS and high OSI can promote endothelial surface adhesion molecules upregulation, inflammatory cell infiltration, and lead to tumor wall degradation and eventual rupture (Malek et al., 1999). Can and Du (2016) reported that high OSI was associated with the growth of the aneurysm. In this study, accepted hemodynamic indicators related to aneurysm rupture were also included, including NWSS, LSA, OSI, NP, and RRT. And our study demonstrated lower NWSS and higher OSI in the ruptured group. However, in the multi-factor regression analysis, only NWSS remained an independent risk factor for A1 segment aneurysm rupture. Previous studies on the relationship between hemodynamics and intracranial aneurysm rupture have been controversial, which may be due to the fact that these studies were not site-specific. At the same time, it has been pointed out that hemodynamic parameters combined with morphological parameters could predict the IAs rupture more accurately. Tremmel et al. (2009) reported that aneurysm hemodynamics with a higher SR are characterized by multiple vortices, more complex flow patterns, and lower NWSS in the apex area, which may be associated with aneurysm rupture. In this study, only A1 segment aneurysms were included, and morphological and hemodynamic indicators were also included. The results confirmed that higher SR and lower NWSS were related to the A1 segment aneurysm rupture, which was consistent with the conclusion of Tremmel et al. (2009) and may provide a reference for clinical treatment of A1 segment unruptured aneurysms. This study demonstrated higher SR and lower NWSS values as independent risk factors for the A1 segment aneurysm rupture. However, several limitations existed in this study. Firstly, due to the extremely rare occurrence of A1 segment aneurysms, the relatively small sample size might have affected analyses. Morphological and hemodynamic parameters were used together for the reliability of the multivariate regression analysis. Secondly, as a retrospective study, the boundary conditions in hemodynamics analysis were not patient-specific, whereas the CFD simulation models were patient-specific.

CONCLUSION

In this study, the characteristics of unruptured A1 segment aneurysms with ruptured A1 segment aneurysms were compared and higher SR and lower NWSS values were identified as discriminators of the rupture status of A1 aneurysms. This may provide a reference for clinical treatment of A1 segment unruptured aneurysms.

DATA AVAILABILITY STATEMENT

The original contributions presented in the study are included in the article/supplementary material, further inquiries can be directed to the corresponding author/s.

ETHICS STATEMENT

The studies involving human participants were reviewed and approved by the Ethics Committee of Army Specialty Medical Center, Army Medical University. The patients/participants provided their written informed consent to participate in this study. Written informed consent was obtained from the individual(s) for the publication of any potentially identifiable images or data included in this article.

AUTHOR CONTRIBUTIONS

MingX, KS, and RH collected the patients' clinical data. MingX and NL performed morphological analysis and computational fluid dynamics simulation. XW and HW completed the data statistics. MingX and RH drafted the manuscript. LC and LX designed the research project and revised the manuscript with MinhX. MinhX and HW participated in the case diagnosis. All authors read and approved the final manuscript.

FUNDING

This work was supported by the Joint Medical Research Project of Chongqing Science and Technology Bureau and Chongqing Health Commission (Project No. 2018ZDXM032).

ACKNOWLEDGMENTS

We would like to thank the Department of Neurosurgery, Changhai Hospital, Second Military Medical University for their support and collaboration in this study.

REFERENCES

Bhaisora, K. S., Behari, S., Prasadh, G., Srivastava, A. K., Mehrotra, A., Sahu, R. N., et al. (2014). A I-segment aneurysms: management protocol based on a new classification. *Neurol. India* 62, 410–416. doi: 10.4103/0028-3886.141284

Bor, A. S., Tiel Groenestege, A. T., TerBrugge, K. G., Agid, R., Velthuis, B. K., Rinkel, G. J., et al. (2015). Clinical, radiological, and flow-related risk factors for growth of untreated, unruptured intracranial aneurysms. *Stroke* 46, 42–48. doi: 10.1161/STROKEAHA.114.005963

Can, A., and Du, R. (2016). Association of Hemodynamic Factors With Intracranial Aneurysm Formation and Rupture: systematic Review and Meta-analysis. *Neurosurgery* 78, 510–520. doi: 10.1227/NEU.0000000000001083

Dashti, R., Hernesniemi, J., Lehto, H., Niemelä, M., Lehecka, M., Rinne, J., et al. (2007). Microneurosurgical management of proximal anterior cerebral artery aneurysms. *Surg. Neurol.* 68, 366–377. doi: 10.1016/j.surneu.2007.07.084

Dhar, S., Tremmel, M., Mocco, J., Kim, M., Yamamoto, J., Meng, H., et al. (2008). Morphology parameters for intracranial aneurysm rupture risk assessment. *Neurosurgery* 63, 185–196. doi: 10.1227/01.NEU.0000316847.64140.81

Ding, X., Nisson, P. L., James, W. S., Lawton, M. T., Ren, S., Jia, L., et al. (2017). Aneurysms of the Proximal Segment of the Anterior Cerebral Artery: a new Classification System with Corresponding Therapeutic Options. *World Neurosurg.* 104, 291–302. doi: 10.1016/j.wneu.2017.04.106

Duan, G., Lv, N., Yin, J., Xu, J., Hong, B., Xu, Y., et al. (2016). Morphological and hemodynamic analysis of posterior communicating artery aneurysms prone to rupture: a matched case-control study. *J. Neurointerv. Surg.* 8, 47–51. doi: 10.1136/neurintsurg-2014-011450

Forget, T. R. Jr., Benitez, R., Veznedaroglu, E., Sharan, A., Mitchell, W., Silva, M., et al. (2001). A review of size and location of ruptured intracranial aneurysms. *Neurosurgery* 49, 1322–1325. doi: 10.1097/00006123-200112000-00006 discussion 1325-1326,

He, X., and Ku, D. N. (1996). Pulsatile flow in the human left coronary artery bifurcation: average conditions. *J. Biomech. Eng.* 118, 74–82. doi: 10.1115/1.2795948

Hoh, B. L., Sistrom, C. L., Firment, C. S., Fautheree, G. L., Velat, G. J., Whiting, J. H., et al. (2007). Bottleneck factor and height-width ratio: association with ruptured aneurysms in patients with multiple cerebral aneurysms. *Neurosurgery* 61, 716–722. doi: 10.1227/01.NEU.0000298899.77097.BF

Investigators, U. J., Morita, A., Kirino, T., Hashi, K., Aoki, N., Fukuhara, S., et al. (2012). ., et al. The natural course of unruptured cerebral aneurysms in a Japanese cohort. *New Engl. J. Med.* 366, 2474–2482. doi: 10.1056/NEJMoa1113260

Juvela, S., Porras, M., and Poussa, K. (2008). Natural history of unruptured intracranial aneurysms: probability of and risk factors for aneurysm rupture. *J. Neurosurg.* 108, 1052–1060. doi: 10.3171/JNS/2008/108/5/1052

Kashiwazaki, D., and Kuroda, S. (2013). Size ratio can highly predict rupture risk in intracranial small (<5 mm) aneurysms. *Stroke* 44, 2169–2173. doi: 10.1161/strokeaha.113.001138

Kim, M. K., and Lim, Y. C. (2019). Aneurysms of the Proximal (A1) Segment of the Anterior Cerebral Artery:A Clinical Analysis of 31 Cases. *World Neurosurg.* 127, e488–e496. doi: 10.1016/j.wneu.2019.03.178

Lee, J. M., Joo, S. P., Kim, T. S., Go, E. J., Choi, H. Y., and Seo, B. R. (2010). Surgical management of anterior cerebral artery aneurysms of the proximal (A1) segment. *World Neurosurg.* 74, 478–482. doi: 10.1016/j.wneu.2010.06.040

Lv, N., Feng, Z., Wang, C., Cao, W., Fang, Y., Karmonik, C., et al. (2016a). Morphological Risk Factors for Rupture of Small (<7 mm) Posterior Communicating Artery Aneurysms. *World Neurosurg.* 87, 311–315. doi: 10.1016/j.wneu.2015.12.055

Lv, N., Wang, C., Karmonik, C., Fang, Y., Xu, J., Yu, Y., et al. (2016b). Morphological and Hemodynamic Discriminators for Rupture Status in Posterior Communicating Artery Aneurysms. *PLoS One* 11:e0149906. doi: 10.1371/journal.pone.0149906

Lv, N., Karmonik, C., Chen, S., Wang, X., Fang, Y., Huang, Q., et al. (2020). Wall Enhancement, Hemodynamics, and Morphology in Unruptured Intracranial Aneurysms with High Rupture Risk. *Transl. Stroke Res.* 11, 882–889. doi: 10.1007/s12975-020-00782-4

Maiti, T. K., Bir, S., Konar, S., Bollam, P., Cuellar-Saenz, H. H., and Nanda, A. (2016). Management of Proximal Anterior Cerebral Artery Aneurysms: anatomical Variations and Technical Nuances. *World Neurosurg.* 85, 85–95. doi: 10.1016/j.wneu.2015.07.022

Malek, A. M., Alper, S. L., and Izumo, S. (1999). Hemodynamic shear stress and its role in atherosclerosis. *JAMA* 282, 2035–2042. doi: 10.1001/jama.282.21.2035

Park, H. S., Choi, J. H., Kang, M., and Huh, J. T. (2013). Management of aneurysms of the proximal (A1) segment of the anterior cerebral artery. *J. Cerebrovasc. Endovasc. Neurosurg.* 15, 13–19. doi: 10.7461/jcen.2013.15.1.13

Rahman, M., Smietana, J., Hauck, E., Oh, B., Hopkins, N., Siddiqui, A., et al. (2010). . Size ratio correlates with intracranial aneurysm rupture status: a prospective study. *Stroke* 41, 916–920. doi: 10.1161/STROKEAHA.109.574244

Suzuki, M., Onuma, T., Sakurai, Y., Mizoi, K., Ogawa, A., and Yoshimoto, T. (1992). Aneurysms arising from the proximal (A1) segment of the anterior cerebral artery. A study of 38 cases. *J. Neurosurg.* 76, 455–458. doi: 10.3171/jns.1992.76.3.0455

Tremmel, M., Dhar, S., Levy, E. I., Mocco, J., and Meng, H. (2009). Influence of intracranial aneurysm-to-parent vessel size ratio on hemodynamics and implication for rupture: results from a virtual experimental study. *Neurosurgery* 64, 622–630. doi: 10.1227/01.NEU.0000341529 discussion 630-621.

Valencia, A. A., Guzman, A. M., Finol, E. A., and Amon, C. H. (2006). Blood flow dynamics in saccular aneurysm models of the basilar artery. *J. Biomech. Eng.* 128, 516–526. doi: 10.1115/1.2205377

Wakabayashi, T., Tamaki, N., Yamashita, H., Saya, H., Suyama, T., and Matsumoto, S. (1985). Angiographic classification of aneurysms of the horizontal segment of the anterior cerebral artery. *Surg. Neurol.* 24, 31–34. doi: 10.1016/0090-3019(85)90059-x

Wanibuchi, M., Kurokawa, Y., Ishiguro, M., Fujishige, M., and Inaba, K. (2001). Characteristics of aneurysms arising from the horizontal portion of the anterior cerebral artery. *Surg. Neurol.* 55, 148–154. doi: 10.1016/s0090-3019(01)00396-2

Wiebers, D. O., Whisnant, J. P., Huston, J. III, Meissner, I., Brown, R. D. Jr., and Piepgras, D. G. (2003). Unruptured intracranial aneurysms: natural history, clinical outcome, and risks of surgical and endovascular treatment. *Lancet* 362, 103–110. doi: 10.1016/s0140-6736(03)13860-3

Xiang, J., Natarajan, S. K., Tremmel, M., Ma, D., Mocco, J., Hopkins, L. N., et al. (2011). Hemodynamic-morphologic discriminants for intracranial aneurysm rupture. *Stroke* 42, 144–152. doi: 10.1161/STROKEAHA.110.592923

Xu, J., Yu, Y., Wu, X., Wu, Y., Jiang, C., Wang, S., et al. (2013). Morphological and hemodynamic analysis of mirror posterior communicating artery aneurysms. *PLoS One* 8:e55413. doi: 10.1371/journal.pone.0055413

Conflict of Interest: The authors declare that the research was conducted in the absence of any commercial or financial relationships that could be construed as a potential conflict of interest.

Publisher's Note: All claims expressed in this article are solely those of the authors and do not necessarily represent those of their affiliated organizations, or those of the publisher, the editors and the reviewers. Any product that may be evaluated in this article, or claim that may be made by its manufacturer, is not guaranteed or endorsed by the publisher.

frontiers in Aging Neuroscience

SYSTEMATIC REVIEW
published: 16 March 2022
doi: 10.3389/fnagi.2022.831910

TNF-α (G-308A) Polymorphism, Circulating Levels of TNF-α and IGF-1: Risk Factors for Ischemic Stroke—An Updated Meta-Analysis

Ranran Duan[1†], Na Wang[2†], Yanan Shang[3†], Hengfen Li[3], Qian Liu[3], Li Li[4] and Xiaofeng Zhao[3*]*

[1] Department of Neurology, First Affiliated Hospital of Zhengzhou University, Zhengzhou, China, [2] Department of Neurorehabilitation, Second Affiliated Hospital of Zhengzhou University, Zhengzhou, China, [3] Department of Psychiatry, First Affiliated Hospital of Zhengzhou University, Zhengzhou, China, [4] Department of Anesthesiology, Beijing Friendship Hospital, Capital Medical University, Beijing, China

Objective: Accumulated studies have explored gene polymorphisms and circulating levels of tumor necrosis factor (TNF)-α and insulin-like growth factor (IGF)-1 in the etiology of ischemic stroke (IS). Of the numerous etiopathological factors for IS, a single-nucleotide polymorphism (SNP) rs1800629 located in the *TNF*-α gene promoter region and increased levels of TNF-α were found to be associated with IS in different ethnic backgrounds. However, the published results are inconsistent and inconclusive. The primary objective of this meta-analysis was to investigate the concordance between rs1800629 polymorphism and IS. A secondary aim was to explore circulating levels of TNF-α and IGF-1 with IS in different ethnic backgrounds and different sourced specimens.

Methods: In this study, we examined whether rs1800629 genetic variant and levels of TNF-α and IGF-1 were related to the etiology of IS by performing a meta-analysis. Relevant case-control studies were retrieved by database searching and systematically selected according to established inclusion criteria.

Results: A total of 47 articles were identified that explored the relationship between the rs1800629 polymorphism and levels of TNF-α and IGF-1 with IS risk susceptibility. Statistical analyses revealed a significant association between the rs1800629 polymorphism and levels of TNF-α and IGF-1 with IS pathogenesis.

Conclusion: Our findings demonstrated that the TNF-α rs1800629 polymorphism, the increased levels of TNF-α, and decreased levels of IGF-1 were involved in the etiology of IS.

Keywords: TNF-α, IGF-1, ischemic stroke, meta-analysis, gene polymorphism

OPEN ACCESS

Edited by:
Yu-Min Kuo,
National Cheng Kung University, Taiwan

Reviewed by:
Wei Wu,
Nanjing Medical University, China
Antonino Tuttolomondo,
University of Palermo, Italy

***Correspondence:**
Li Li
li_anethesia@163.com
Xiaofeng Zhao
zxf0605004@163.com

† These authors have contributed equally to this work

Specialty section:
This article was submitted to Neuroinflammation and Neuropathy, a section of the journal Frontiers in Aging Neuroscience

Received: *09 December 2021*
Accepted: *27 January 2022*
Published: *16 March 2022*

Citation:
Duan R, Wang N, Shang Y, Li H, Liu Q, Li L and Zhao X (2022) TNF-α (G-308A) Polymorphism, Circulating Levels of TNF-α and IGF-1: Risk Factors for Ischemic Stroke—An Updated Meta-Analysis. Front. Aging Neurosci. 14:831910. doi: 10.3389/fnagi.2022.831910

INTRODUCTION

Ischemic stroke (IS) is the second leading cause of mortality and physical disability following the onset of neuropathological complications worldwide (Strong et al., 2007; Navis et al., 2019). Presently, it is crucial to identify the potential risk factors of IS that are associated with challenges in the early detection of stroke symptoms as well as poor survival outcomes.

Pro-inflammatory cytokines play a major role in the process of activation of various cellular mechanisms, including differentiation and proliferation processes. If the pro-inflammatory cytokine storm occurs in the cerebral tissue (King et al., 2013; Clausen et al., 2014; Arango-Dávila et al., 2015; Wu et al., 2016), it will contribute to additional brain injuries, such as IS (Jiang et al., 2020). Among the identified cytokines, the pathogenic roles of tumor necrosis factor α (TNF-α) have been extensively investigated. It has been demonstrated that an increased level of TNF-α is associated with greater neurological deficits and poorer treatment outcomes in IS patients (Pasarica et al., 2005; Cui et al., 2012; Bokhari et al., 2014; Boehme et al., 2016; Lasek-Bal et al., 2019). In preclinical studies, the application of TNF-α agonists or reduced expression of TNF-α has exhibited potential neuroprotective effects in the cerebral cortex of IS patients. Notably, Clausen et al. (2020) have demonstrated significantly increased risks of stroke in patients with elevated concentrations of TNFR1 and TNFR2 factors in plasma, suggesting that TNF-α level might serve as a risk factor for IS as well as the biomarker for the patient survival rate. Similarly, insulin-like growth factor-1 (IGF-1) that demonstrates cell proliferation, an inhibitor of cell apoptosis, exerts neuroprotective effects in both white and gray matter under different detrimental conditions. It is a key regulator of cell proliferation and an inhibitor of cell apoptosis and necrosis a key regulator in the development, cell differentiation, plasticity and survival of the nervous system (Juul, 2003; Benarroch, 2012; Shaheen et al., 2018). Based on this evidence, it can be speculated that IGF-1 might be involved in the etiology of IS.

Previous studies have also explored the association between the *TNF*-α gene polymorphism and peripheral blood levels of TNF-α and IGF-1 with IS onset in different ethnic-specific backgrounds. However, the findings from such studies have been inconsistent or inconclusive due to their highly diverse patients' populations, differentially sourced specimens, small sample sizes, and most importantly, little influence of single-nucleotide polymorphisms (SNPs) on IS pathobiology. To overcome these roadblocks, an updated meta-analysis was performed to further testify whether (1) the *TNF*-α genetic SNPs could increase the susceptibility of different populations to IS and (2) the peripheral blood TNF-α and IGF-1 levels could be used as the biomarker for assessing the risks for IS in ethnic-specific background.

METHODS

Inclusion Criteria

For this meta-analysis, full-length relevant articles and case studies were selected based on the following inclusion criteria: (1) The diagnosis of IS patients was based on the CT or MRI examinations; (2) selected studies were all case-control studies; (3) data on SNP frequency of circulating TNF-α and IGF-1 levels were clearly obtained; and (4) the frequency of each allele and genotype met the criteria for Hardy-Weinberg disequilibrium in both the case and control groups. In contrast, some studies were excluded based on the criteria that they were either case-only studies based on a family design or abstract-only reviews without the full case report.

Search Strategy

We used the keywords "tumor necrosis factor-alpha," human recombinant tumor necrosis factor-alpha, "cachectin/tumor necrosis factor," tumor necrosis factor ligand superfamily member 2, "TNF alpha," "TNF-alpha insulin-like somatomedin peptide I," "insulin-like somatomedin peptide I," "IGF-I-SmC," "IGF-1 insulin-like growth factor I," "ischemic stroke," "cryptogenic stroke," and "cryptogenic embolism stroke" to search for the full-length case studies in the PubMed, Web of Science, Embase, Elsevier, Cochrane, Medline, and APA databases published until September 9, 2021. We thoroughly reviewed the retrieved literature and the corresponding reference lists. To avoid including duplicate articles, we selected studies from the larger sample size in the analysis.

Data Extraction

Three of the authors independently extracted the following data from each publication: Author, country of origin, racial descent of the study population, the number of eligible cases with proper controls, circulating levels of TNF-α, IGF-1 (mean and standard deviation), rs1800629 (G-308A) genotype, and allele frequencies.

Data Analysis and Statistical Methods

The data analysis using statistical methods was carried out according to the methods described in our previous study (Zhao et al., 2013).

RESULTS

Strictly following the inclusion criteria, 47 properly controlled full-length studies, including 23 rs1800629 genotype-related studies (Um et al., 2003; Balding et al., 2004; Lee et al., 2004; Um and Kim, 2004; Karahan et al., 2005; Rubattu et al., 2005; Harcos et al., 2006; Lalouschek et al., 2006; Llamas Sillero et al., 2007; Banerjee et al., 2008; Shi et al., 2009; Kim et al., 2010; Tong et al., 2010; Sultana et al., 2011; Cui et al., 2012; Tuttolomondo et al., 2012; Zhao et al., 2012; Djordjevic et al., 2013; Wawrzynek et al., 2014; Gu et al., 2015; Kumar et al., 2016; Palm et al., 2020; Kamdee et al., 2021) and 13 case reports (Zaremba and Losy, 2001a,b; Intiso et al., 2004; Domac et al., 2007; Jefferis et al., 2009; Cure et al., 2013; Bokhari et al., 2014; de Sousa Parreira et al., 2015; Wytrykowska et al., 2016; Billinger et al., 2017; Shishkova et al., 2018; Zhang Y. Y. et al., 2018; Ma et al., 2020) on the circulating level of TNF-α were finally selected for the meta-analysis (**Figure 1**). Genotype-related literature included a total of 9,120 patients and 9,249 healthy controls (Caucasian, n = 10; Asian, n = 15). PCR screening was used to detect genotypes, and all genotypes met Hardy-Weinberg disequilibrium criteria. Similarly, the TNF-α circulation levels were measured in 1,497 cases and 1,444 control subjects. The distribution of articles based on the ethnic specificity was Caucasian (n = 6), Asian (n = 6), and American (n = 2) and that based on the laboratory findings was plasma data (n = 3), serum data (n = 9), cerebrospinal fluid (CSF)

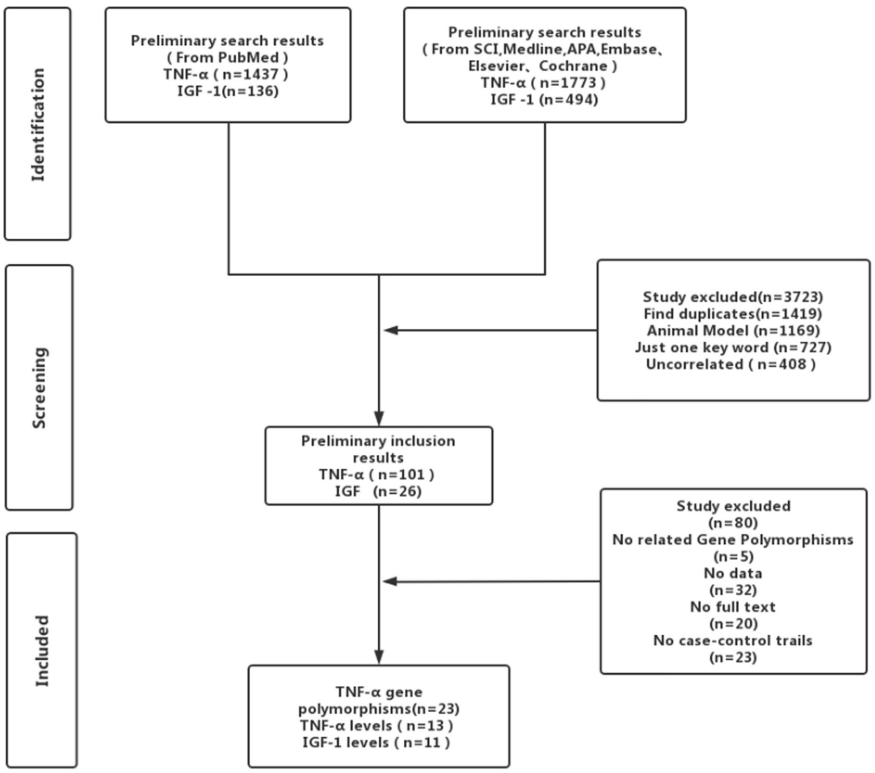

FIGURE 1 | Flowchart of the included articles.

data (n = 1), and gingival fluid data (n = 1). We identified 11 articles concerning the relationship between TNF-α circulation levels and IS, three articles for plasma data (Schwab et al., 1997; Kaplan et al., 2007; Wang Y. et al., 2014), eight articles for serum data (Denti et al., 2004; Johnsen et al., 2005; Aberg et al., 2011; Iso et al., 2012; Dong et al., 2014; Wang T. et al., 2014; Shaheen et al., 2018; Zhang W. et al., 2018); 2,075 patients in case group; and 2,174 in the control group (**Tables 1–3**). All the selected articles were analyzed using the STATA15.0 software.

We selected the nucleotide G to A modification as the risk factor among genotypes and established 2 models (GG vs. GA + AA and G vs. A). The heterogeneity test in each group indicated the presence of high heterogeneity among the samples. Heterogeneity models I–V were randomly selected for testing, which showed results for each model, namely, GG vs. GA + AA model [odds ratio (OR) = 1.22, 95% confidence interval (CI) = 1.05–1.42, **Figure 2**] and G vs. A model (OR = 1.19, 95% CI = 1.03–1.38, **Figure 3**). We found positive correlations for the GG vs. GA + AA and G vs. A models, suggesting that G-A mutation might be a risk factor for IS.

To further study the source of heterogeneity and whether there were differences among races, we conducted a racial stratification analysis on the same dataset. Among them, positive results were found in the Asian race with the models such as GG vs. GA + AA (OR = 1.33, 95% CI = 1.09–1.62, **Figure 4**) and G vs. A (OR = 1.30, 95% CI = 1.07–1.57, **Figure 5**), while no positive results were found in case of the Caucasian population. Together, these results indicate that the intensity of G modification-associated risk factors can be linked to racial differences, especially as a potential risk factor for the Asian population.

In the TNF-α level detection, the data of Q25–Q75 in the original text were transformed into mean and SD. We conducted continuous variable analysis by recording mean, SD, and total number.

We distributed the cases into the particular group to establish the model based on the sample source. We found that the serum model had a positive result with the SMD value of 0.54 (95% CI = 0.21–0.87, **Figure 6**) and also had heterogeneity in sample quality. We need to conduct further studies to identify if the advent of heterogeneity can be caused by racial differences. Furthermore, non-positive results were found in the South American population, and positive results were found in the Asian (SMD = 0.75, 95% CI = 0.31–1.20, **Figure 7**) and Caucasian populations (SMD = 0.18, 95% CI = −0.07–0.42, **Figure 7**). To further explore the interactions between serological indicators and races, serum results were grouped according to ethnic specificity, which yielded positive results for the Asian population (SMD = 0.75, 95% CI = 0.31–1.20, **Figure 7**). Therefore, elevated serum TNF-α levels were considered to be a risk factor for IS in the Asian population. The same method was conducted to explore the connection of IGF-1 concentration with IS in different ethnic backgrounds. The decreased serum IGF-1 levels were considered to be a risk factor for IS in the Asian population not in the Caucasian population (SMD = −0.61, 95% CI = −1.16 to −0.50, **Figures 8–10**).

TABLE 1 | Summary of studies exploring the relationship between rs1800629 of TNF-α gene polymorphism and IS.

References	Race	Case			Control			Case		Control	
		GG	GA	AA	GG	GA	AA	G	A	G	A
Um et al. (2003)	Asian	261	32	1	484	82	15	554	34	1,050	112
Balding et al. (2004)	Caucasian	59	40	6	233	140	16	158	52	606	172
Lee et al. (2004)	Asian	139	13	0	138	25	2	291	13	3.1	29
Um and Kim (2004)	Asian	325	40	1	509	86	15	690	42	1,104	116
Karahan et al. (2005)	Caucasian	70	16	0	15	8	0	156	16	158	8
Rubattu et al. (2005)	Caucasian	84	29	2	152	27	1	197	33	331	29
Harcos et al. (2006)	Caucasian	262	71	3	229	97	7	595	77	555	111
Lalouschek et al. (2006)	Caucasian	282	116	6	310	97	8	680	128	717	113
Sillero et al. (2007)	Caucasian	248	42	2	245	51	6	538	46	541	63
Banerjee et al. (2008)	Asian	150	25	1	181	31	0	325	27	393	31
Shi et al. (2009)	Asian	63	4	0	64	6	0	130	4	134	6
Kim et al. (2010)	Asian	220	17	0	190	25	1	457	17	405	27
Tong et al. (2010)	Asian	597	51	0	552	96	0	1,245	51	1,200	96
Tong et al. (2010)	Asian	92	8	0	70	30	0	192	8	170	30
Sultana et al. (2011)	Asian	17	211	10	12	207	7	245	231	221	224
Cui et al. (2012)	Asian	1,237	148	3	886	136	5	2,622	154	1,908	146
Cui et al. (2012)	Asian	868	90	3	710	107	4	1,826	96	1,527	115
Tuttolomondo et al. (2012)	Caucasian	83	12	1	35	11	2	178	14	81	15
Zhao et al. (2012)	Asian	993	127	4	1,028	131	4	2,113	135	2,187	139
Djordjevic et al. (2013)	Caucasian	21	5	0	69	28	3	47	5	166	34
Wawrzynek et al. (2014)	Caucasian	87	9	5	84	15	1	181	19	183	17
Gu et al. (2015)	Asian	508	100	8	501	99	7	1,116	116	1,101	113
Kumar et al. (2016)	Asian	218	29	3	225	23	2	465	35	473	27
Palm et al. (2020)	Caucasian	567	209	17	322	124	11	1,343	243	758	148
Kamdee et al. (2021)	Asian	166	31	3	181	19	0	363	37	381	19

TABLE 2 | Summary of studies exploring the relationship between the levels of TNF-α and IS.

References	Case		Control		Sample size		Origin
	Mean	*SD*	Mean	*SD*	Case	Control	
Bokhari et al. (2014)	64.00	68.80	1.00	2.10	131	47	Plasma
de Sousa Parreira et al. (2015)	7.70	6.44	9.20	9.00	93	134	Plasma
Billinger et al. (2017)	2.30	7.00	2.00	6.50	12	14	Plasma
Intiso et al. (2004)	30.10	12.50	29.00	13.90	41	40	Serum
Zaremba and Losy (2001b)	14.00	10.20	9.10	1.60	23	15	Serum
Domac et al. (2007)	44.32	16.92	16.70	5.50	70	22	Serum
Jefferis et al. (2009)	1.83	0.79	1.81	0.77	299	587	Serum
Cure et al. (2013)	75.60	25.00	65.90	9.10	54	50	Serum
Wytrykowska et al. (2016)	12.86	7.33	10.26	4.38	42	34	Serum
Shishkova et al. (2018)	1.29	1.00	1.14	1.57	196	119	Serum
Zhang W. et al. (2018)	3.88	2.30	2.53	1.55	182	40	Serum
Ma et al. (2020)	118.50	27.20	96.20	23.60	288	300	Serum
Zaremba and Losy (2001a)	9.10	5.80	6.60	0.50	23	15	Cerebrospinal fluid
Wytrykowska et al. (2016)	74.78	108.89	30.31	51.37	43	27	Gingival crevicular fluid

Sensitivity Analysis

Sensitivity analysis of the data showed that it did not affect the results of meta-analysis (OR = 1.17, 95% CI = 1.09–1.26 for rs1800629; OR = 0.54, 95% CI = 0.21–0.87 for TNF-α; OR = –0.61, 95% CI = –1.16 to –0.05 for IGF-1).

Publication Bias

Begg's test was used to verify publication bias, which showed that publication bias was negligible (z = 1.24, p = 0.22 for rs1800629; z = 0.73, p = 0.47 for TNF-α; z = 0.96, p = 0.34 for IGF-1).

TABLE 3 | Summary of studies exploring the relationship between the levels of IGF-1 and IS.

References	Race	Case		Control		Sample size		Origin
		Mean	*SD*	Mean	*SD*	Case	Control	
Schwab et al. (1997)	No mentioned	105.00	23.00	161.00	10.00	20	8	Plasma
Kaplan et al. (2007)	African-American	150.30	58.30	152.20	58.30	370	1,122	Plasma
Wang Y. et al. (2014)	China	122.32	86.60	77.60	53.15	79	75	Plasma
Denti et al. (2004)	Italy	69.00	45.00	102.00	67.00	85	88	Serum
Johnsen et al. (2005)	Danish	107.10	33.30	112.90	33.20	254	254	Serum
Aberg et al. (2011)	Western Sweden	171.00	3.30	145.40	9.40	407	40	Serum
Iso et al. (2012)	Japan	113.00	52.00	106.00	48.00	71	71	Serum
Dong et al. (2014)	China	130.40	32.80	141.40	25.40	240	200	Serum
Wang T. et al. (2014)	China	107.16	18.03	122.79	15.55	124	96	Serum
Shaheen et al. (2018)	Arab	143.40	12.60	156.00	11.20	200	100	Serum
Zhang W. et al. (2018)	China	115.50	37.30	158.50	27.80	225	120	Serum

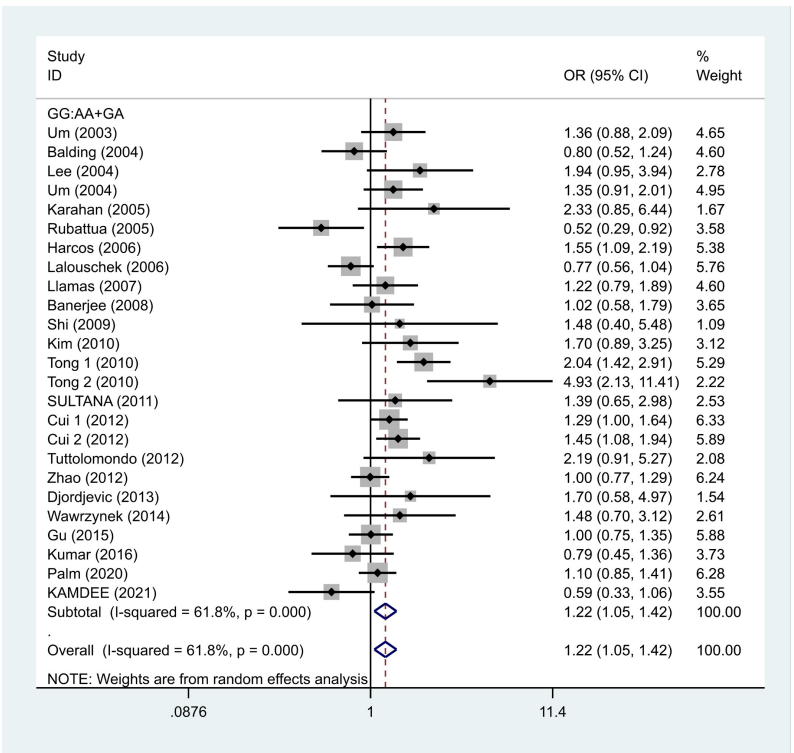

FIGURE 2 | Results of the random-effects meta-analysis for the TNF-α G308A genotype (GG vs. AA + GA) in IS and control groups.

DISCUSSION

This updated meta-analysis study provided evidence that the rs1800629 SNP was associated with IS susceptibility. In addition, the level of TNF-α cytokine was elevated in IS patients compared with that in controls. Of particular interest, we first explored the relationship between levels of IGF-1 in the etiology of IS by performing a meta-analysis method. Especially, in the subgroup analysis, increased levels of TNF-α cytokine were found among the Asian and Caucasian populations, respectively. In contrast, no significant differences were found between IS patients and controls regarding the concentrations of IGF-1. Notably, we also first explored the interactions between differentially sourced specimens and specific ethnic backgrounds. Based on the stratification of the specimen and specific ethnic background, elevated concentrations of TNF-α and decreased levels of IGF-1 were noted in the serum samples of IS patients in the Asian population but not in the Caucasian population. These findings help us understand the role of gene polymorphisms and abnormal levels of cytokines such as TNF-α and IGF-1 in the pathogenesis of IS. In line with previous findings, our results also demonstrated that the rs1800629 polymorphisms were associated with the IS pathogenesis (Wu et al., 2019). The level of TNF-α was increased in IS patients as compared with that of the control subjects. Importantly, our updated meta-analysis, including 44 studies with 11,480 patents related to genetic SNPs and serum

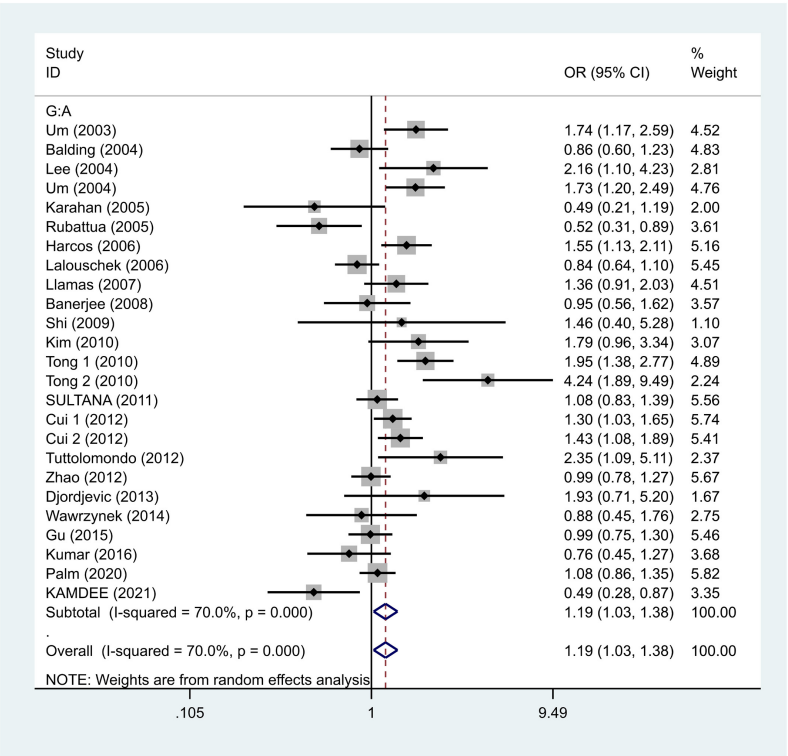

FIGURE 3 | Results of the random-effects meta-analysis for the TNF-α G308A allele (G vs. A) in IS and control groups.

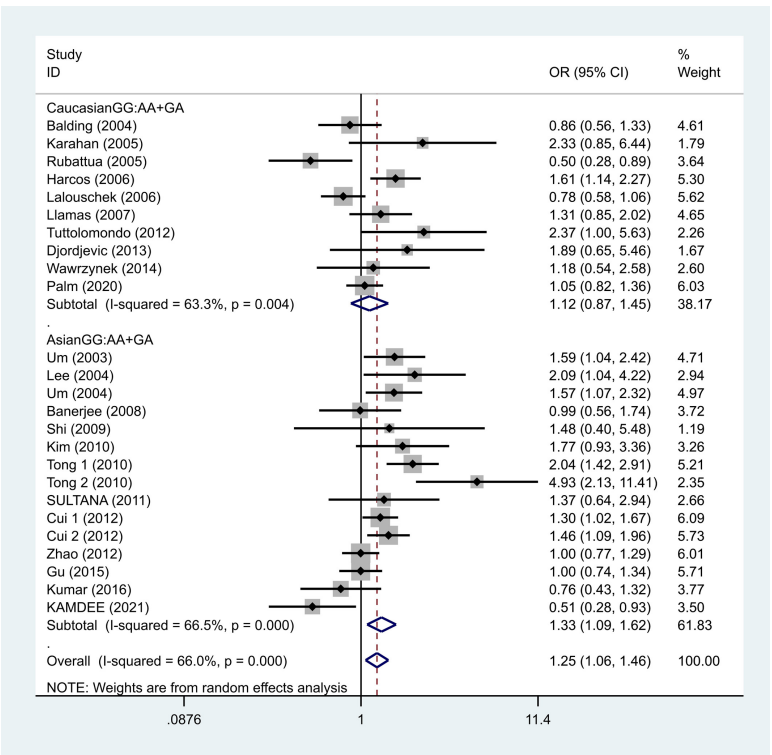

FIGURE 4 | Results of the random-effects meta-analysis for the TNF-α G308A genotype (GG vs. AA + GA) in Caucasian, Asian, IS, and control groups, respectively.

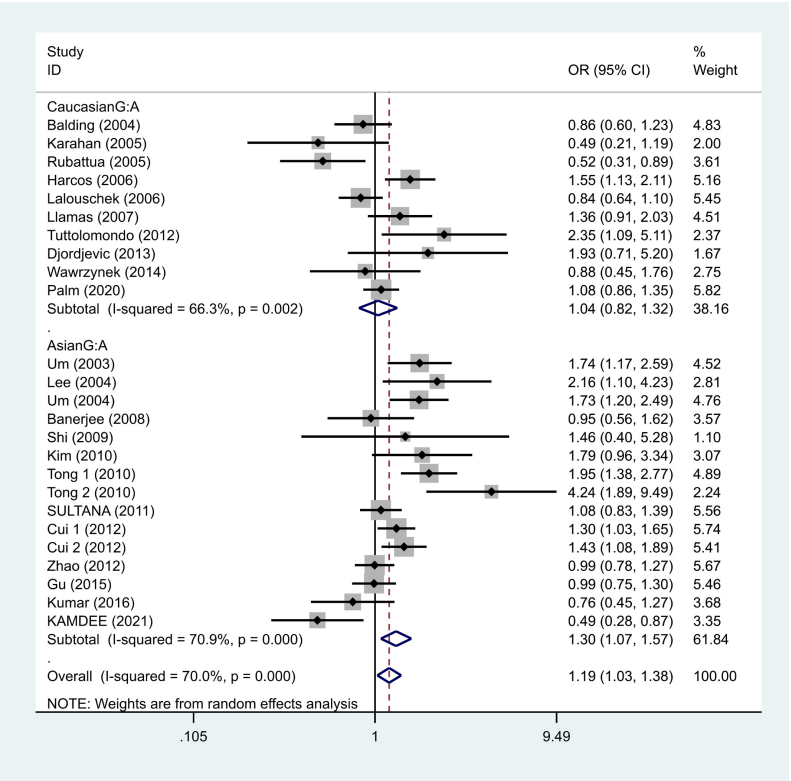

FIGURE 5 | Results of the random-effects meta-analysis for the TNF-α G308A allele (G vs. A) in Caucasian, Asian, IS, and control groups, respectively.

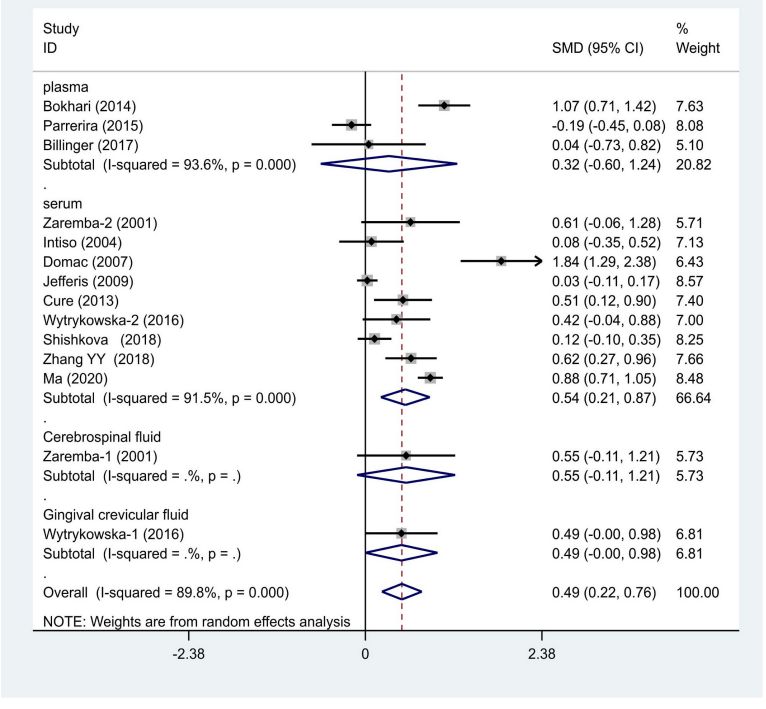

FIGURE 6 | Results of meta-analysis for the level of TNF-α and IS.

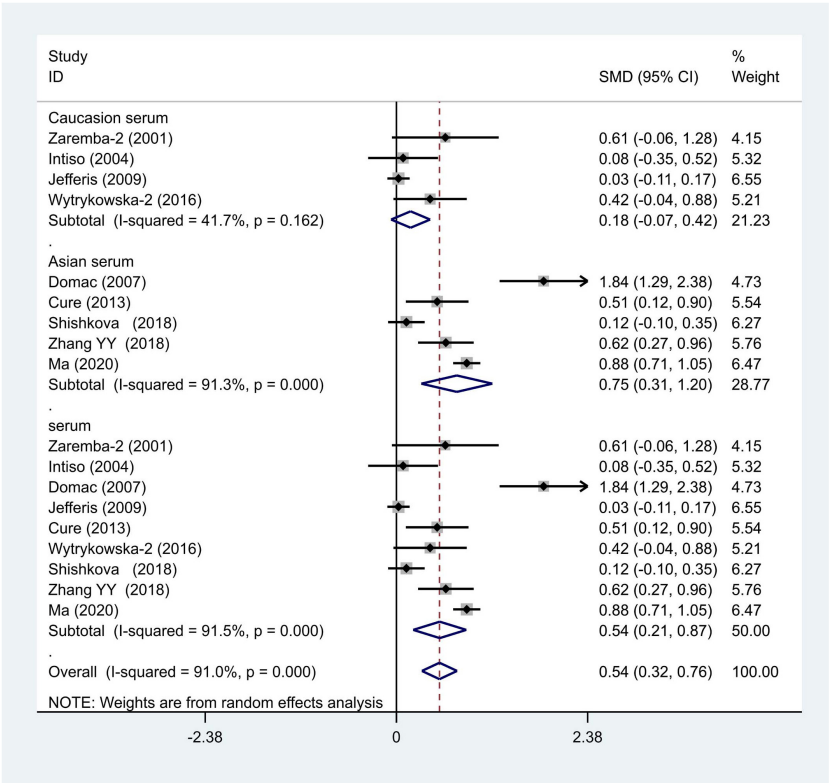

FIGURE 7 | Results of meta-analysis for the level of TNF-α in the Asian and Caucasian populations, respectively.

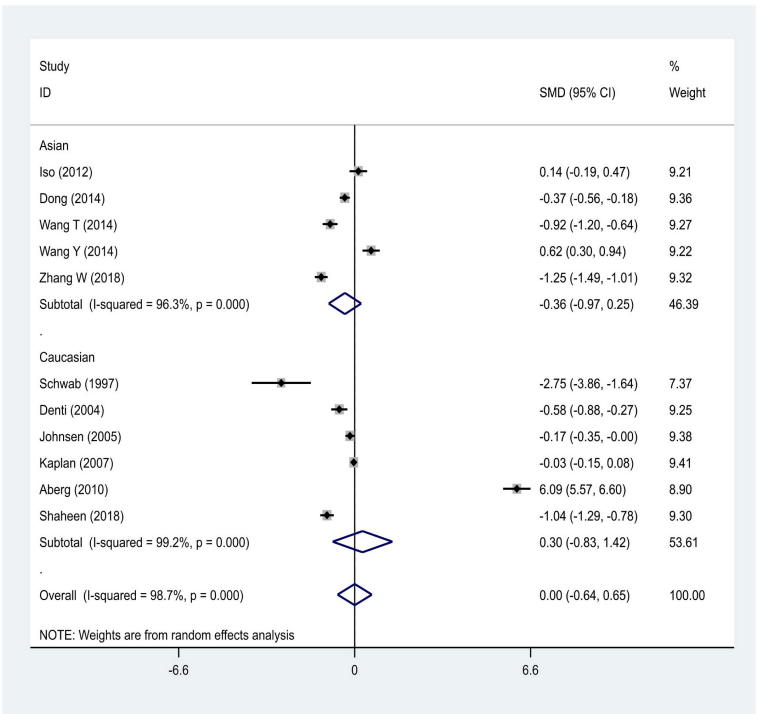

FIGURE 8 | Results of meta-analysis for the level of IGF-1 in the Asian and Caucasian populations, respectively.

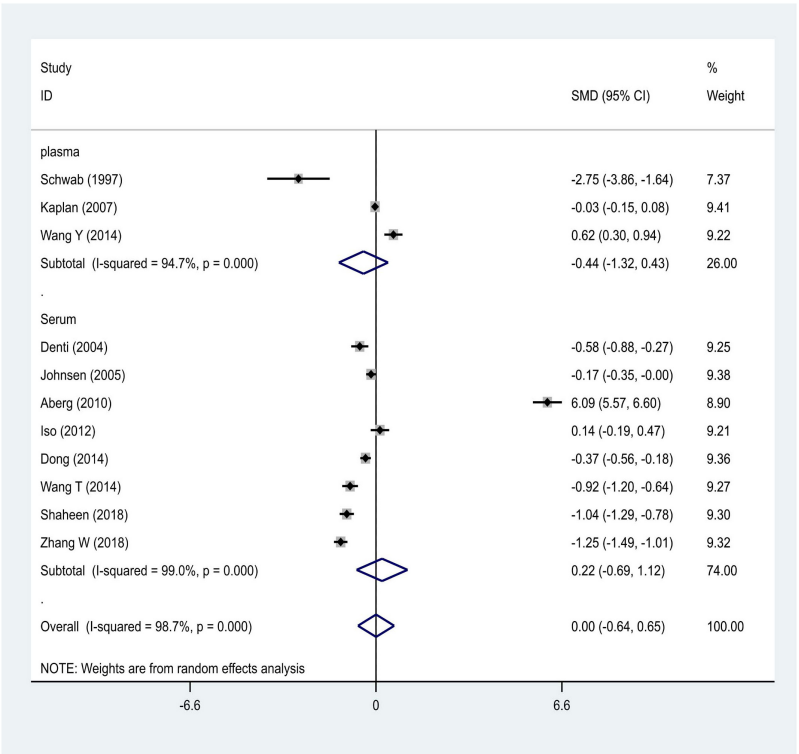

FIGURE 9 | Results of meta-analysis for the IGF-1 level in plasma and serum, respectively.

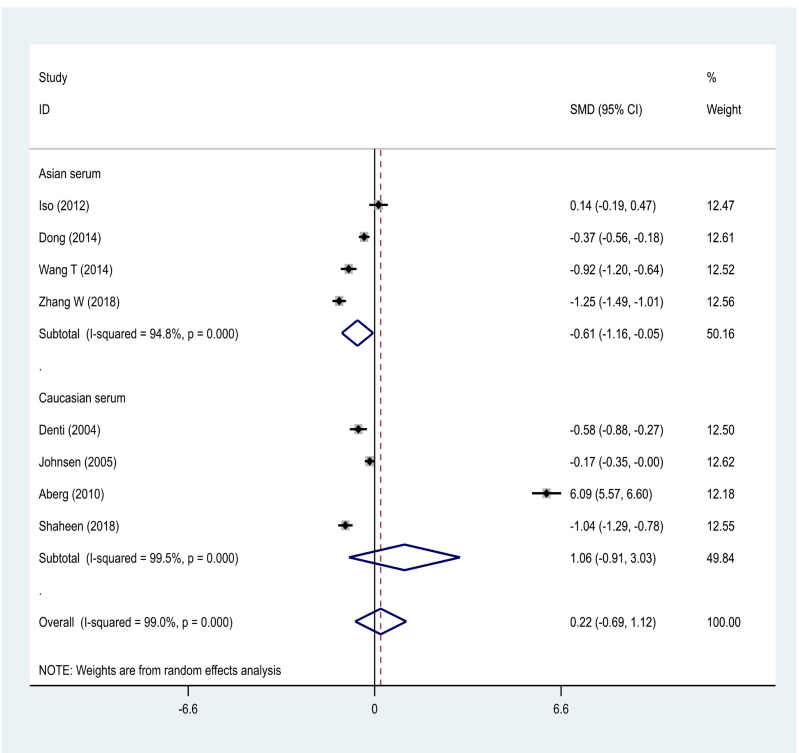

FIGURE 10 | Results of meta-analysis for the IGF-1 serum levels in Caucasian, Asian, IS, and control groups, respectively.

levels of cytokines in IS patients, was larger than the previous study (Wu et al., 2019). We speculated that the greater number of studies and larger sample sizes might obtain precise and valuable results.

The human *TNF*-α gene is located on chromosome 6p21.1–21.3 within the highly polymorphic region of the major histocompatibility complex (MHC). Among the several known *TNF*-α gene polymorphisms, studies have extensively focused on the G-308A (rs1800629) mutation in the etiology of IS. The polymorphisms are reportedly located in the *TNF*-α gene promoter region, which contains a number of regulatory elements that can influence the transcriptional activity of the gene (Wilson et al., 1997), and may also influence the DNA binding affinity of transcription factors leading to differential expressions of the *TNF*-α gene and the disease susceptibility (Wilson et al., 1997). Hence, it has been suggested that a more common regulatory variant may be a more likely risk factor for common disorders than rare variants within the gene coding region (Zill et al., 2002). Notably, the G308A (rs1800629) variant involved SNP mutation in the promoter region, which could upregulate the *TNF*-α gene's transcriptional activity, resulting in the increased plasma concentrations of TNF-α in IS pathogenesis, and this finding was verified using genetic association analysis.

In IS, the activated microglia and astrocytes release high levels of TNF-α, which is considered toxic for negatively influencing synaptic transmission and plasticity in the learning and memory processes (Beattie et al., 2002), which is the core symptom of IS patients. In contrast, TNF-α combines with its receptors, leading to NF-κB activation that may play dual roles in inducing neurotoxicity as well as neuroprotective responses in brain cells depending on the stage of neuronal development, target cell type, and receptor subtypes (Shohami et al., 1999; Vila et al., 2000; Wang et al., 2000; Castillo and Leira, 2001; Cárdenas et al., 2002; Hallenbeck, 2002; Hurtado et al., 2002). Moreover, in clinical studies, patients with high TNF-α levels (Vila et al., 2000; Wang et al., 2000) have been shown to develop greater neurological deficits and poorer outcomes. In contrast, blocking TNF-α improves clinical outcomes (Tobinick et al., 2012). Similar phenomena have also been observed in several preclinical studies (King et al., 2013; Clausen et al., 2014; Arango-Dávila et al., 2015; Wu et al., 2016; Lin et al., 2020). Importantly, posttreatment with TNF-α neutralizing antibodies or TNF-α agonists alleviates poststroke brain injury in rodents (Vakili et al., 2011). Furthermore, at the molecular level, R-7050 acts as an anti-TNF-α receptor inhibitor demonstrating protection against stroke-induced brain injury (King et al., 2013; Clausen et al., 2014; Arango-Dávila et al., 2015; Wu et al., 2016) as well as enhancing the brain TNFRI and NF-κB signaling cascades along with increased levels of the Nrf2 protein in stroke rats, suggesting that R-7050 may enhance Nrf2 signaling, thus representing the involvement of another signal transduction to alleviate inflammatory responses in IS (Lin et al., 2021). Regarding the role of inflammation in stroke pathogenesis, Della Corte (Della Corte et al., 2016) has reviewed the role of immune-inflammatory variables in patients with IS, assessing the therapeutic perspectives that it offers. Patients with the cardioembolic (CEI) subtype of IS was reported to show significantly higher median plasma levels of TNF-α, compared with that of other subtypes. Multiple linear regression showed a significant association between the Scandinavian Stroke Scale (SSS) score at admission and diagnostic subtype infarct volume of cardioembolic strokes and some inflammatory variable. Tuttolomondo suggested that cardioembolic strokes have a worse clinical presentation and produce larger and more disabling strokes than other IS subtypes reporting a possible explanation of higher immuno-inflammatory activation of the acute phase (Albanese et al., 2005; Tuttolomondo et al., 2008).

Therefore, in stroke, the TNF-α signal transduction is activated during ischemic injuries, and this fact has been further verified in subsequent clinical studies. In our study, the presence of the TNF-α-308 GG genotype and a higher serum concentration of TNF-α increases the likelihood of a stroke pathology. Thus, the TNF-α signal transduction response may explain our results. The molecular mechanism of the association between IGF-1 and IS has not yet been fully elucidated. Previous studies have demonstrated that the IGF-1 couples with protein-3 primarily *via* the PI3-kinase pathway, which, on the one hand, mediates cell survival of neurons under oxidative stress (Gustafsson et al., 2004), and, on the other hand, is preceded by improvement in the blood-brain barrier and suppression of local inflammatory mediators, indicating a unique anti-inflammatory role for IGF-1 in the blood–brain barrier as a novel target for IGF-1-mediated neuroprotection response (Bake et al., 2014; De Geyter et al., 2016). This was verified in both preclinical and clinical studies and our results (Bake et al., 2014; De Geyter et al., 2016; Mehrpour et al., 2016; Lee et al., 2021). This meta-analysis results demonstrated the association between serum IGF-1 levels and ischemic stroke in the Asian population not in the Caucasian population. These differences can be explained by different genetic backgrounds.

One major limitation for this study is that except for different genetic backgrounds, we did not address the relationship between proinflammatory gene polymorphisms and stroke subtypes, because a more common, regulatory variant may be more likely to be involved in the etiology of IS (Hahn and Blakely, 2002). It has been suggested that etiologic factors for the development of the particular subtype may be different in stroke subtypes. As it has been mentioned except for other risk factors, age and sex may also involve in the etiology of different stroke subtypes (Moond et al., 2020; Tang et al., 2020). Thus, in future studies, we will consider stroke severity, subtype, hypertension, dyslipidemia, diabetes, and psychosocial stress in the etiology of IS (Sarfo et al., 2022).

CONCLUSION

This updated meta-analysis study demonstrated that the GG genotype might be considered as a risk factor for IS (especially in Asians), and the circulating levels of TNF-α were elevated in the Caucasian and Asian patients as compared with controls. At the same time, a positive association was found between serum IGF-1 levels and IS in the Asian population but not in the Caucasian population. Therefore, based on previous meta-analysis results and those combined with ours, we proposed that therapeutic strategies to decrease the circulating levels of TNF-α

and increased levels of IGF-1 might be considered as a promising therapeutic target with potential neuroprotective effects for the treatment of IS.

DATA AVAILABILITY STATEMENT

The original contributions presented in the study are included in the article/**Supplementary Material**, further inquiries can be directed to the corresponding author/s.

AUTHOR CONTRIBUTIONS

XZ and LL equally contributed to the study design of this review. RD, NW, and YS equally performed the literature search, interpreted the data, and wrote the manuscript. QL and HL profoundly enriched the manuscript by adding important intellectual content. All authors contributed to the article and approved the submitted version.

SUPPLEMENTARY MATERIAL

The Supplementary Material for this article can be found online at: https://www.frontiersin.org/articles/10.3389/fnagi.2022.831910/full#supplementary-material

Supplementary Figure 1 | The result of publication bias between the allele of TNF-α (G:A) and IS.

Supplementary Figure 2 | The result of publication bias between IGF-1, TNF-α, and IS. **(A)** The result of publication bias between IGF-1 and IS and **(B)** the result of publication bias between TNF-α and IS.

REFERENCES

Aberg, D., Jood, K., Blomstrand, C., Jern, C., Nilsson, M., Isgaard, J., et al. (2011). Serum IGF-I levels correlate to improvement of functional outcome after ischemic stroke. *J. Clin. Endocrinol. Metab.* 96, E1055–E1064. doi: 10.1210/jc.2010-2802

Albanese, A., Tuttolomondo, A., Anile, C., Sabatino, G., Pompucci, A., Pinto, A., et al. (2005). Spontaneous chronic subdural hematomas in young adults with a deficiency in coagulation factor XIII. Report of three cases. *J. Neurosurg.* 102, 1130–1132. doi: 10.3171/jns.2005.102.6.1130

Arango-Dávila, C. A., Vera, A., Londoño, A. C., Echeverri, A. F., Cañas, F., Cardozo, C. F., et al. (2015). Soluble or soluble/membrane TNF-α inhibitors protect the brain from focal ischemic injury in rats. *Int. J. Neurosci.* 125, 936–940. doi: 10.3109/00207454.2014.980906

Bake, S., Selvamani, A., Cherry, J., and Sohrabji, F. (2014). Blood brain barrier and neuroinflammation are critical targets of IGF-1-mediated neuroprotection in s troke for middle-aged female rats. *PLoS One* 9:e91427. doi: 10.1371/journal.pone.0091427

Balding, J., Livingstone, W. J., Pittock, S. J., Mynett-Johnson, L., Ahern, T., Hodgson, A., et al. (2004). The IL-6 G-174C polymorphism may be associated with ischaemic stroke in patients without a history of hypertension. *Ir. J. Med. Sci.* 173, 200–203. doi: 10.1007/bf02914551

Banerjee, I., Gupta, V., Ahmed, T., Faizaan, M., Agarwal, P., and Ganesh, S. (2008). Inflammatory system gene polymorphism and the risk of stroke: a case-control study in an Indian population. *Brain Res. Bull.* 75, 158–165. doi: 10.1016/j.brainresbull.2007.08.007

Beattie, E. C., Stellwagen, D., Morishita, W., Bresnahan, J. C., Ha, B. K., Von Zastrow, M., et al. (2002). Control of synaptic strength by glial TNFalpha. *Science* 295, 2282–2285. doi: 10.1126/science.1067859

Benarroch, E. E. (2012). Insulin-like growth factors in the brain and their potential clinical implications. *Neurology* 79, 2148–2153. doi: 10.1212/WNL.0b013e3182752eef

Billinger, S. A., Sisante, J. V., Mattlage, A. E., Alqahtani, A. S., Abraham, M. G., Rymer, M. M., et al. (2017). The relationship of pro-inflammatory markers to vascular endothelial function after acute stroke. *Int. J. Neurosci.* 127, 486–492. doi: 10.1080/00207454.2016.1198344

Boehme, A. K., Mcclure, L. A., Zhang, Y., Luna, J. M., Del Brutto, O. H., Benavente, O. R., et al. (2016). Inflammatory markers and outcomes after lacunar stroke: levels of inflammatory markers in treatment of stroke study. *Stroke* 47, 659–667. doi: 10.1161/STROKEAHA.115.012166

Bokhari, F. A., Shakoori, T. A., Butt, A., and Ghafoor, F. (2014). TNF-alpha: a risk factor for ischemic stroke. *J. Ayub Med. Coll. Abbottabad* 26, 111–114.

Cárdenas, A., Moro, M. A., Leza, J. C., O'shea, E., Dávalos, A., Castillo, J., et al. (2002). Upregulation of TACE/ADAM17 after ischemic preconditioning is involved in brain tolerance. *J. Cereb. Blood Flow Metab.* 22, 1297–1302. doi: 10.1097/01.WCB.0000033968.83623.D0

Castillo, J., and Leira, R. (2001). Predictors of deteriorating cerebral infarct: role of inflammatory mechanisms. Would its early treatm ent be useful? *Cerebrovasc. Dis.* 11(Suppl. 1), 40–48. doi: 10.1159/000049124

Clausen, B. H., Degn, M., Martin, N. A., Couch, Y., Karimi, L., Ormhøj, M., et al. (2014). Systemically administered anti-TNF therapy ameliorates functional outcomes after focal cerebral ische mia. *J. Neuroinflammation* 11:203. doi: 10.1186/s12974-014-0203-6

Clausen, B. H., Wirenfeldt, M., Høgedal, S. S., Frich, L. H., Nielsen, H. H., Schrøder, H. D., et al. (2020). Characterization of the TNF and IL-1 systems in human brain and blood after ischemic stroke. *Acta Neuropathol. Commun.* 8:81. doi: 10.1186/s40478-020-00957-y

Cui, G., Wang, H., Li, R., Zhang, L., Li, Z., Wang, Y., et al. (2012). Polymorphism of tumor necrosis factor alpha (TNF-alpha) gene promoter, circulating TNF-alpha level, a nd cardiovascular risk factor for ischemic stroke. *J. Neuroinflammation* 9:235. doi: 10.1186/1742-2094-9-235

Cure, M. C., Tufekci, A., Cure, E., Kirbas, S., Ogullar, S., Kirbas, A., et al. (2013). Low-density lipoprotein subfraction, carotid artery intima-media thickness, nitric oxide, and tumor n ecrosis factor alpha are associated with newly diagnosed ischemic stroke. *Ann. Indian Acad. Neurol.* 16, 498–503. doi: 10.4103/0972-2327.120438

De Geyter, D., De Smedt, A., Stoop, W., De Keyser, J., and Kooijman, R. (2016). Central IGF-I Receptors in the Brain are Instrumental to Neuroprotection by Systemically Injected IGF -I in a Rat Model for Ischemic Stroke. *CNS Neurosci. Ther.* 22, 611–616. doi: 10.1111/cns.12550

de Sousa Parreira, J., Kallaur, A. P., Lehmann, M. F., Oliveira, S. R., Frizon, D. A., Delongui, F., et al. (2015). Tumor necrosis factor beta NcoI polymorphism (rs909253) is associated with inflammatory and metabolic markers in acute ischemic stroke. *Metab. Brain Dis.* 30, 159–167. doi: 10.1007/s11011-014-9584-6

Della Corte, V., Tuttolomondo, A., Pecoraro, R., Di Raimondo, D., Vassallo, V., and Pinto, A. (2016). Inflammation, endothelial dysfunction and arterial stiffness as therapeutic targets in cardiovascular medicine. *Curr. Pharm. Des.* 22, 4658–4668. doi: 10.2174/1381612822666160510124801

Denti, L., Annoni, V., Cattadori, E., Salvagnini, M. A., Visioli, S., Merli, M. F., et al. (2004). Insulin-like growth factor 1 as a predictor of ischemic stroke outcome in the elderly. *Am. J. Med.* 117, 312–317. doi: 10.1016/j.amjmed.2004.02.049

Djordjevic, V., Divac-Rankov, A., Stankovic, M., Brankovic-Sreckovic, V., and Radojkovic, D. (2013). Tumor necrosis factor alpha and alpha-1 antitrypsin gene variants in Serbian pediatric arterial ischemic stroke patients. *Genetika* 45, 621–628. doi: 10.2298/GENSR1303621D

Domac, F. M., Somay, G., Misirli, H., and Erenoglu, N. Y. (2007). Tumor necrosis factor alpha serum levels and inflammatory response in acute ischemic stroke. *Neurosciences* 12:25. doi: 10.1177/1545968306290225

Dong, X., Chang, G., Ji, X. F., Tao, D. B., and Wang, Y. X. (2014). The relationship between serum insulin-like growth factor I levels and ischemic stroke risk. *PLoS One* 9:e94845. doi: 10.1371/journal.pone.0094845

Gu, L., Wu, G., Su, L., Yan, Y., and Wei, A. (2015). TNF-a (-238G/A and -308G/A) gene polymorphisms may not contribute to the risk of ischemic stroke. *Int. J. Neurosci.* 126, 219–226. doi: 10.3109/00207454.2015.1010200

Gustafsson, H., Tamm, C., and Forsby, A. (2004). Signalling pathways for insulin-like growth factor type 1-mediated expression of uncoupling protein 3. *J. Neurochem.* 88, 462–468. doi: 10.1046/j.1471-4159.2003.02162.x

Hahn, M. K., and Blakely, R. D. (2002). Monoamine transporter gene structure and polymorphisms in relation to psychiatric and other complex d isorders. *Pharmacogenomics J.* 2, 217–235. doi: 10.1038/sj.tpj.6500106

Hallenbeck, J. M. (2002). The many faces of tumor necrosis factor in stroke. *Nat. Med.* 8, 1363–1368. doi: 10.1038/nm1202-1363

Harcos, P., Laki, J., Kiszel, P., Széplaki, Z., Szolnoki, Z., Kovács, M., et al. (2006). Decreased frequency of the TNF2 allele of TNF-alpha -308 promoter polymorphism is associated with lac unar infarction. *Cytokine* 33, 100–105. doi: 10.1016/j.cyto.2005.12.006

Hurtado, O., Lizasoain, I., Fernández-Tomé, P., Alvarez-Barrientos, A., Leza, J. C., Lorenzo, P., et al. (2002). TACE/ADAM17-TNF-alpha pathway in rat cortical cultures after exposure to oxygen-glucose deprivation or glutamate. *J. Cereb. Blood Flow Metab.* 22, 576–585. doi: 10.1097/00004647-200205000-00009

Intiso, D., Zarrelli, M. M., Lagioia, G., Rienzo, F. D., and Dagger, R. J. (2004). Tumor necrosis factor alpha serum levels and inflammatory response in acute ischemic stroke patients. *Neurol. Sci.* 24, 390–396. doi: 10.1007/s10072-003-0194-z

Iso, H., Maruyama, K., Ikehara, S., Yamagishi, K., and Tamakoshi, A. (2012). Cellular growth factors in relation to mortality from cardiovascular disease in middle-aged Japanese: the JACC study. *Atherosclerosis* 224, 154–160. doi: 10.1016/j.atherosclerosis.2012.05.026

Jefferis, B. J., Whincup, P. H., Welsh, P., Wannamethee, S. G., Rumley, A., Lennon, L. T., et al. (2009). Circulating TNFα levels in older men and women do not show independent prospective relations with MI or stroke. *Atherosclerosis* 205, 302–308. doi: 10.1016/j.atherosclerosis.2008.12.001

Jiang, C. T., Wu, W. F., Deng, Y. H., and Ge, J. W. (2020). Modulators of microglia activation and polarization in ischemic stroke (Review). *Mol. Med. Rep.* 21, 2006–2018. doi: 10.3892/mmr.2020.11003

Johnsen, S. P., Hundborg, H. H., Sørensen, H. T., Orskov, H., Tjønneland, A., and Overvad, K. (2005). Insulin-like growth factor (IGF) I, -II, and IGF binding protein-3 and risk of ischemic stroke. *J. Clin. Endocrinol. Metab.* 90, 5937–5941. doi: 10.1210/jc.2004-2088

Juul, A. (2003). Serum levels of insulin-like growth factor I and its binding proteins in health and disease. *Growth Horm. IGF Res.* 13, 113–170. doi: 10.1016/s1096-6374(03)00038-8

Kamdee, K., Panadsako, N., Mueangson, O., Nuinoon, M., and Chunglok, W. (2021). Promoter polymorphism of TNFα (rs1800629) is associated with ischemic stroke susceptibility in a southern Thai population. *Biomed. Rep.* 15:78. doi: 10.3892/br.2021.1454

Kaplan, R. C., Mcginn, A. P., Pollak, M. N., Kuller, L. H., Strickler, H. D., Rohan, T. E., et al. (2007). Association of total insulin-like growth factor-I, insulin-like growth factor binding protein-1 (IGFB P-1), and IGFBP-3 levels with incident coronary events and ischemic stroke. *J. Clin. Endocrinol. Metab.* 92, 1319–1325. doi: 10.1210/jc.2006-1631

Karahan, Z. C., Deda, G., Sipahi, T., Elhan, A. H., and Akar, N. (2005). TNF-alpha -308G/A and IL-6 -174 G/C polymorphisms in the Turkish pediatric stroke patients. *Thromb. Res.* 115, 393–398. doi: 10.1016/j.thromres.2004.09.008

Kim, O. J., Lee, J. H., Choi, J. K., Oh, S. H., Hong, S. H., Oh, D., et al. (2010). Association between tumor necrosis factor-alpha (-308G-A and -238G-A) polymorphisms and homocysteine levels in patients with ischemic strokes and silent brain infarctions. *Cerebrovasc. Dis.* 30, 483–490. doi: 10.1159/000319023

King, M. D., Alleyne, C. H., and Dhandapani, K. M. (2013). TNF-alpha receptor antagonist, R-7050, improves neurological outcomes following intracerebral hemorrh age in mice. *Neurosci. Lett.* 542, 92–96. doi: 10.1016/j.neulet.2013.02.051

Kumar, P., Kumar, A., Misra, S., Sagar, R., Faruq, M., Suroliya, V., et al. (2016). Tumor necrosis factor-alpha (308G/A, +488G/A, 857C/T and -1031T/C) gene polymorphisms and risk of ischemic stroke in north Indian population: a hospital based case–control study. *Meta Gene* 7, 34–39. doi: 10.1016/j.mgene.2015.11.003

Lalouschek, W., Schillinger, M., Hsieh, K., Endler, G., Greisenegger, S., Marculescu, R., et al. (2006). Polymorphisms of the inflammatory system and risk of ischemic cerebrovascular events. *Clin. Chem. Lab. Med.* 44, 918–923. doi: 10.1515/CCLM.2006.165

Lasek-Bal, A., Jedrzejowska-Szypulka, H., Student, S., Warsz-Wianecka, A., Zareba, K., Puz, P., et al. (2019). The importance of selected markers of inflammation and blood-brain barrier damage for short-term isch emic stroke prognosis. *J. Physiol. Pharmacol.* 70, 209–217. doi: 10.26402/jpp.2019.2.04

Lee, B. C., Ahn, S. Y., Doo, H. K., Yim, S. V., Lee, H. J., Jin, S. Y., et al. (2004). Susceptibility for ischemic stroke in Korean population is associated with polymorphisms of the inter leukin-1 receptor antagonist and tumor necrosis factor-alpha genes, but not the interleukin-1beta gene. *Neurosci. Lett.* 357, 33–36. doi: 10.1016/j.neulet.2003.12.041

Lee, J., Lee, J., Lee, M., Lim, J. S., Kim, J. H., Yu, K. H., et al. (2021). Association between Serum Insulin-Like Growth Factor-1 and Neurological Severity in Acute Ischemic St roke. *J. Clin. Neurol.* 17, 206–212. doi: 10.3988/jcn.2021.17.2.206

Lin, S. Y., Wang, Y. Y., Chang, C. Y., Wu, C. C., Chen, W. Y., Kuan, Y. H., et al. (2020). Effects of β-adrenergic blockade on metabolic and inflammatory responses in a rat model of ischemic stroke. *Cells* 9:1373. doi: 10.3390/cells9061373

Lin, S. Y., Wang, Y. Y., Chang, C. Y., Wu, C. C., Chen, W. Y., Liao, S. L., et al. (2021). TNF-α receptor inhibitor alleviates metabolic and inflammatory changes in a rat model of ischemic stroke. *Antioxidants* 10:851. doi: 10.3390/antiox10060851

Ma, Z., Yue, Y., Luo, Y., Wang, W., Cao, Y., and Fang, Q. (2020). Clinical utility of the inflammatory factors combined with lipid markers in the diagnostic and progno stic assessment of ischemic stroke: based on logistic regression models. *J. Stroke Cerebrovasc. Dis.* 29:104653. doi: 10.1016/j.jstrokecerebrovasdis.2020.104653

Mehrpour, M., Rahatlou, H., Hamzehpur, N., Kia, S., and Safdarian, M. (2016). Association of insulin-like growth factor-I with the severity and outcomes of acute ischemic stroke. *Iran. J. Neurol.* 15, 214–218.

Moond, V., Bansal, K., and Jain, R. (2020). Risk factors and subtyping of ischemic stroke in young adults in the indian population. *Cureus* 12:e11388. doi: 10.7759/cureus.11388

Navis, A., Garcia-Santibanez, R., and Skliut, M. (2019). Epidemiology and outcomes of ischemic stroke and transient ischemic attack in the adult and geriatric population. *J. Stroke Cerebrovasc. Dis.* 28, 84–89. doi: 10.1016/j.jstrokecerebrovasdis.2018.09.013

Palm, F., Aigner, A., Pussinen, P. J., Urbanek, C., Buggle, F., Safer, A., et al. (2020). Association of a multigenetic pro-inflammatory profile with ischaemic stroke. *Cerebrovasc. Dis.* 49, 170–176. doi: 10.1159/000507042

Pasarica, D., Gheorghiu, M., Topârceanu, F., Bleotu, C., Ichim, L., and Trandafir, T. (2005). Neurotrophin-3, TNF-alpha and IL-6 relations in serum and cerebrospinal fluid of ischemic stroke patients. *Roum. Arch. Microbiol. Immunol.* 64, 27–33.

Rubattu, S., Speranza, R., Ferrari, M., Evangelista, A., Beccia, M., Stanzione, R., et al. (2005). A role of TNF-alpha gene variant on juvenile ischemic stroke: a case-control study. *Eur. J. Neurol.* 12, 989–993. doi: 10.1111/j.1468-1331.2005.01136.x

Sarfo, F. S., Ovbiagele, B., Akpa, O., Akpalu, A., Wahab, K., Obiako, R., et al. (2022). Risk factor characterization of ischemic stroke subtypes among West Africans. *Stroke* 53, 134–144. doi: 10.1161/STROKEAHA.120.032072

Schwab, S., Spranger, M., Krempien, S., Hacke, W., and Bettendorf, M. (1997). Plasma insulin-like growth factor I and IGF binding protein 3 levels in patients with acute cerebral ischemic injury. *Stroke* 28, 1744–1748. doi: 10.1161/01.str.28.9.1744

Shaheen, H., Sobhy, S., El Mously, S., Niazi, M., and Gomaa, M. (2018). Insulin-like growth factor-1 in acute ischemic stroke. *Egypt. J. Neurol. Psychiatr. Neurosurg.* 54:42. doi: 10.1186/s41983-018-0042-y

Shi, K. L., He, B., Wang, J. J., and Zou, L. P. (2009). Role of TNF-alpha gene variation in idiopathic childhood ischemic stroke: a case-control study. *J. Child Neurol.* 24, 25–29. doi: 10.1177/0883073808321046

Shishkova, V. N., Adasheva, T. V., Remenik, A. Y., Valyaeva, V. N., and Shklovsky, V. M. (2018). Prognostic significance of clinical-anthropometric, biochemical, metabolic, vascular-inflammatory an d molecular-genetic markers in the development of the first ischemic stroke. *Zh. Nevrol. Psikhiatr. Im. S S Korsakova* 118, 4–11. doi: 10.17116/jnevro2018118214-11

Shohami, E., Ginis, I., and Hallenbeck, J. M. (1999). Dual role of tumor necrosis factor alpha in brain injury. *Cytokine Growth Factor Rev.* 10, 119–130. doi: 10.1016/s1359-6101(99)00008-8

Sillero, L. P., Fernández de Velasco Casarrubios, J., García-Raso, A., Meseguer Gancedo, E., Santos Montero, A. B., and Tomás Martínez, J. F. (2007). Polymorphism -238 G/A of tumor necrosis factor alpha gene promoter is a genetic risk factor for ischemic cerebrovascular disease. *J. Mol. Neurosci.* 32, 108–110. doi: 10.1007/s12031-007-0021-8

Strong, K., Mathers, C., and Bonita, R. (2007). Preventing stroke: saving lives around the world. *Lancet Neurol.* 6, 182–187. doi: 10.1016/S1474-4422(07)70031-5

Sultana, S., Kolla, V. K., Jeedigunta, Y., Penagaluru, P. K., Joshi, S., Rani, P. U., et al. (2011). Tumour necrosis factor alpha and interleukin 10 gene polymorphisms and the risk of ischemic stroke in south Indian population. *J. Genet.* 90, 361–364. doi: 10.1007/s12041-011-0079-5

Tang, M., Yao, M., Zhu, Y., Peng, B., Zhou, L., and Ni, J. (2020). Sex differences of ischemic stroke in young adults-A single-center Chinese cohort study. *J. Stroke Cerebrovasc. Dis.* 29:105087. doi: 10.1016/j.jstrokecerebrovasdis.2020.105087

Tobinick, E., Kim, N. M., Reyzin, G., Rodriguez-Romanacce, H., and Depuy, V. (2012). Selective TNF inhibition for chronic stroke and traumatic brain injury: an observational study involving 629 consecutive patients treated with perispinal etanercept. *CNS Drugs* 26, 1051–1070. doi: 10.1007/s40263-012-0013-2

Tong, Y., Geng, Y., Xu, J., Wang, Z., Zhang, Y., Lin, L., et al. (2010). The role of functional polymorphisms of the TNF-α gene promoter in the risk of ischemic stroke in Chinese Han and Uyghur populations: two case–control studies. *Clin. Chim. Acta* 411, 1291–1295. doi: 10.1016/j.cca.2010.05.007

Tuttolomondo, A., Pedone, C., Pinto, A., Di Raimondo, D., Fernandez, P., Di Sciacca, R., et al. (2008). Predictors of outcome in acute ischemic cerebrovascular syndromes: the GIFA study. *Int. J. Cardiol.* 125, 391–396. doi: 10.1016/j.ijcard.2007.03.109

Tuttolomondo, A., Raimondo, D. D., Forte, G. I., Casuccio, A., Vaccarino, L., Scola, L., et al. (2012). Single nucleotide polymorphisms (SNPs) of pro-inflammatory/anti-inflammatory and thrombotic/fibrinolytic genes in patients with acute ischemic stroke in relation to TOAST subtype. *Cytokine* 58, 398–405. doi: 10.1016/j.cyto.2012.02.012

Um, J. Y., An, N. H., and Kim, H. M. (2003). TNF-alpha and TNF-beta gene polymorphisms in cerebral infarction. *J. Mol. Neurosci.* 21, 167–171. doi: 10.1385/JMN:21:2:167

Um, J. Y., and Kim, H. M. (2004). Tumor necrosis factor alpha gene polymorphism is associated with cerebral infarction. *Brain Res. Mol. Brain Res.* 122, 99–102. doi: 10.1016/j.molbrainres.2003.11.019

Vakili, A., Mojarrad, S., Akhavan, M. M., and Rashidy-Pour, A. (2011). Pentoxifylline attenuates TNF-α protein levels and brain edema following temporary focal cerebral isc hemia in rats. *Brain Res.* 1377, 119–125. doi: 10.1016/j.brainres.2011.01.001

Vila, N., Castillo, J., Dávalos, A., and Chamorro, A. (2000). Proinflammatory cytokines and early neurological worsening in ischemic stroke. *Stroke* 31, 2325–2329. doi: 10.1161/01.str.31.10.2325

Wang, Y., Zhang, Y., Huang, J., Chen, X., Gu, X., Wang, Y., et al. (2014). Increase of circulating miR-223 and insulin-like growth factor-1 is associated with the pathogenesis of acute ischemic stroke in patients. *BMC Neurol.* 14:77. doi: 10.1186/1471-2377-14-77

Wang, T., Bin, L. I., and Zhong P. A. (2014). The relationship between the serum VILIP-1,IGF-1 concentration and cognitive impairment in patients with cerebral infarction. *J. Apoplexy Nerv. Dis.* 31, 121–124.

Wang, X., Li, X., Erhardt, J. A., Barone, F. C., and Feuerstein, G. Z. (2000). Detection of tumor necrosis factor-alpha mRNA induction in ischemic brain tolerance by means of real- time polymerase chain reaction. *J. Cereb. Blood Flow Metab.* 20, 15–20. doi: 10.1097/00004647-200001000-00004

Wawrzynek, A., Dobiała, J., Wender, M., Kozubski, W., and Michałowska-Wender, G. (2014). TNF-α gene G-308A polymorphism and the risk of ischemic stroke. *Neurol. Neurochir. Pol.* 48, 387–390. doi: 10.1016/j.pjnns.2014.09.007

Wilson, A. G., Symons, J. A., Mcdowell, T. L., Mcdevitt, H. O., and Duff, G. W. (1997). Effects of a polymorphism in the human tumor necrosis factor alpha promoter on transcriptional activa tion. *Proc. Natl. Acad. Sci. U.S.A.* 94, 3195–3199. doi: 10.1073/pnas.94.7.3195

Wu, J. C., Zhang, X., Wang, J. H., Liu, Q. W., Wang, X. Q., Wu, Z. Q., et al. (2019). Gene polymorphisms and circulating levels of the TNF-alpha are associated with ischemic stroke: a met a-analysis based on 19,873 individuals. *Int. Immunopharmacol.* 75:105827. doi: 10.1016/j.intimp.2019.105827

Wu, M. H., Huang, C. C., Chio, C. C., Tsai, K. J., Chang, C. P., Lin, N. K., et al. (2016). Inhibition of peripheral TNF-α and downregulation of microglial activation by Alpha-lipoic acid and e tanercept protect rat brain against ischemic stroke. *Mol. Neurobiol.* 53, 4961–4971. doi: 10.1007/s12035-015-9418-5

Wytrykowska, A., Prosba-Mackiewicz, M., and Nyka, W. M. (2016). IL-1β, TNF-α, and IL-6 levels in gingival fluid and serum of patients with ischemic stroke. *J. Oral Sci.* 58, 509–513. doi: 10.2334/josnusd.16-0278

Zaremba, J., and Losy, J. (2001a). Early TNF-alpha levels correlate with ischaemic stroke severity. *Acta Neurol. Scand.* 104, 288–295. doi: 10.1034/j.1600-0404.2001.00053.x

Zaremba, J., and Losy, J. (2001b). The levels of TNF-alpha in cerebrospinal fluid and serum do not correlate with the counts of the white blood cells in acute phase of ischaemic stroke. *Folia Morphol.* 60, 91–97.

Zhang, Y. Y., Huang, N. N., Zhao, Y. X., Li, Y. S., Wang, D., Fan, Y. C., et al. (2018). Elevated tumor necrosis factor-a-induced protein 8-like 2 mRNA from peripheral blood mononuclear cell s in patients with acute ischemic stroke. *Int. J. Med. Sci.* 15, 1713–1722. doi: 10.7150/ijms.27817

Zhang, W., Wang, W., and Kuang, L. (2018). The relation between insulin-like growth factor 1 levels and risk of depression in ischemic stroke. *Int. J. Geriatr. Psychiatry* 33, e228–e233. doi: 10.1002/gps.4774

Zhao, N., Liu, X., Wang, Y., Liu, X., Li, J., Yu, L., et al. (2012). Association of inflammatory gene polymorphisms with ischemic stroke in a Chinese Han population. *J. Neuroinflammation* 9:162. doi: 10.1186/1742-2094-9-162

Zhao, X., Huang, Y., Ma, H., Jin, Q., Wang, Y., and Zhu, G. (2013). Association between major depressive disorder and the norepinephrine transporter polymorphisms T-182C and G1287A: a meta-analysis. *J. Affect. Disord.* 150, 23–28. doi: 10.1016/j.jad.2013.03.016

Zill, P., Engel, R., Baghai, T. C., Juckel, G., Frodl, T., Muller-Siecheneder, F., et al. (2002). Identification of a naturally occurring polymorphism in the promoter region of the norepinephrine tra nsporter and analysis in major depression. *Neuropsychopharmacology* 26, 489–493. doi: 10.1016/S0893-133X(01)00386-4

Conflict of Interest: The authors declare that the research was conducted in the absence of any commercial or financial relationships that could be construed as a potential conflict of interest.

Publisher's Note: All claims expressed in this article are solely those of the authors and do not necessarily represent those of their affiliated organizations, or those of the publisher, the editors and the reviewers. Any product that may be evaluated in this article, or claim that may be made by its manufacturer, is not guaranteed or endorsed by the publisher.

frontiers in Aging Neuroscience

MINI REVIEW
published: 23 March 2022
doi: 10.3389/fnagi.2022.863379

Emerging Limb Rehabilitation Therapy After Post-stroke Motor Recovery

*Fei Xiong[1], Xin Liao[2], Jie Xiao[2], Xin Bai[2], Jiaqi Huang[2], Bi Zhang[2], Fang Li[2] and Pengfei Li[2]**

[1] Department of Operation Room, The First People's Hospital of Jiande, Hangzhou, China, [2] Department of Orthopedics, The First People's Hospital of Jiande, Hangzhou, China

Stroke, including hemorrhagic and ischemic stroke, refers to the blood supply disorder in the local brain tissue for various reasons (aneurysm, occlusion, etc.). It leads to regional brain circulation imbalance, neurological complications, limb motor dysfunction, aphasia, and depression. As the second-leading cause of death worldwide, stroke poses a significant threat to human life characterized by high mortality, disability, and recurrence. Therefore, the clinician has to care about the symptoms of stroke patients in the acute stage and formulate an effective postoperative rehabilitation plan to facilitate the recovery in patients. We summarize a novel application and update of the rehabilitation therapy in limb motor rehabilitation of stroke patients to provide a potential future stroke rehabilitation strategy.

Keywords: stroke, rehabilitation, limb motor function, mirror therapy, robot-assist therapy, motor imagery, music therapy, visual reality

OPEN ACCESS

Edited by:
Anwen Shao,
Zhejiang University, China

Reviewed by:
Liang Wu,
Wenzhou Medical University, China
Jianwei Lei,
The Second Affiliated Hospital of Nanchang University, China

****Correspondence:***
Pengfei Li
lipf303433629@yeah.net

Specialty section:
This article was submitted to Neurocognitive Aging and Behavior, a section of the journal Frontiers in Aging Neuroscience

Received: *27 January 2022*
Accepted: *24 February 2022*
Published: *23 March 2022*

Citation:
Xiong F, Liao X, Xiao J, Bai X, Huang J, Zhang B, Li F and Li P (2022) Emerging Limb Rehabilitation Therapy After Post-stroke Motor Recovery. Front. Aging Neurosci. 14:863379. doi: 10.3389/fnagi.2022.863379

INTRODUCTION

Stroke is an acute cerebrovascular disease with high morbidity, mortality, and disability. It is the second leading cause of death worldwide, accounting for 11.6% of deaths. According to the Global Burden of Disease report, an estimated 12.2 million strokes are there worldwide, resulting in 143 million disability-adjusted life years (DALYs) and 6.55 million deaths (GBD 2019 Stroke Collaborators, 2021). China has the highest number of stroke cases globally. The number of patients belonging to the low-income and youth groups is rapidly increasing, with significant gender and regional differences. According to the WHO, in 2019, stroke was the leading cause of death and DALYs in China (World Health Organization [WHO], 2020). Stroke results in lasting sensory, cognitive and visual impairment, impaired limb motor function, and eventually reduce various bodily functions (Katzan et al., 2018a,b). Motor dysfunction is the most common complication of stroke, followed by hemiplegia in about 80% of patients. Half of these symptoms will accompany patients for life and seriously affect their day-to-day activities (Kim et al., 2020). Studies have shown that hemiplegia is the leading cause of long-term disability in stroke patients from the United States, Japan, and France [(Leys et al., 2008; Ovbiagele and Nguyen-Huynh, 2011; Iso, 2021)]. The fatality rate is significantly lower than before with the progress and development of stroke treatment. However, 80% of the survivors have severe sequelae, and the disability rate is about 75% (Langhorne et al., 2018). Effective rehabilitation training can alleviate functional disability, restore the motor function in hemiplegic limbs, and accelerate the rehabilitation process in post-stroke patients (Laver et al., 2020). At present, patient rehabilitation with limb movement

disorders after stroke primarily emphasizes early intervention, somehow ignoring the intervention received during the recovery and the sequelae period. There is a decline in the quality-of-life of patients and aggravation of disease conditions. Therefore, improving limb motor function of stroke patients through rehabilitation is essential. Traditional rehabilitation therapy, including massage, acupuncture, physiotherapy, and electrical stimulation, has been widely employed in the clinical practice (McCrimmon et al., 2015; Yang et al., 2016; Cabanas-Valdés et al., 2021). With the progress of science and technology, several potential neurological rehabilitations are being developed using new technologies to restore movement in the stroke patients. In this review, we summarize the novel methods and applications to restore limb motor dysfunction in stroke rehabilitation, which could provide a potential therapeutic strategy against stroke in the future.

ROBOT-ASSISTED THERAPY

Robotic rehabilitation opens up a new way in stroke rehabilitation (Hesse et al., 2003; Lambercy et al., 2011; Rodgers et al., 2020). RAT uses robot equipment to treat neurological injury and assist in post-stroke rehabilitation. Therefore, it has become a research hotspot in the rehabilitation field. Based on the neuroplasticity principle and the functional remodeling mechanism, multidisciplinary therapeutics such as mechanics, rehabilitation medicine, sensing technology, and control engineering are fully integrated with providing rehabilitation training to the patients through an automated rehabilitation treatment process (Masiero et al., 2014; Morone et al., 2017, 2020). As a result, the RAT can provide high-intensity task-oriented training to stroke patients, reduce the burden on clinical staff, save medical care costs, and improve rehabilitation efficiency. For motor function recovery, robotic devices are mainly divided into exoskeleton robots and end-effector robots. The skeletal robot consists of an external electromechanical system associated with the segments and joints of stroke patients. Therefore, it can move parallel to the bones of patients and directly control individual joints, thereby reducing the abnormal posture (Chang and Kim, 2013; Calabrò et al., 2021; Moggio et al., 2021). On the other hand, end-effector robots apply mechanical forces to the distal extremities for providing force support. However, it could result in abnormal motion patterns because of the limited control over the proximal extremities.

Lamberti et al. (2021) conducted a clinical study consisting of 236 stroke patients (145 males, 91 females) admitted to a rehabilitation program with robot-assisted gait training. After accomplishing a rehabilitation program, the results have shown that the patients exhibited significant improvements in Functional Independence Measure and Functional Ambulatory Category, with a substantial recovery in women, indicating that using robotics for female stroke patients may favor a selective selection functional effect of recovery. A randomized clinical trial with 51 participants compared the effect of RAT and constraint-induced movement therapy to investigate motor recovery in stroke. Wolf Motor Function Test and Fugl-Meyer Assessment Upper Limb were designated as the primary outcome. Upper limb function and motor recovery improved in both the groups, indicating the significant potential of these new methods during stroke rehabilitation (Terranova et al., 2021). Furthermore, previous studies have observed RAT-reduced muscle tone in patients with upper limb spasms after stroke. It suggests that RAT can attenuate limb spasms caused by upper motor neuron disease, associated with repetitive motion and drafting (Veerbeek et al., 2017; Cho et al., 2018; Cho and Song, 2019). In addition, Song et al. (2021) confirmed that RAT could improve motor function and stimulate cortical activation, revealing the other mechanism involved in RAT. A multicentric, randomized controlled trial conducted in Britain compared RAT effectiveness, enhanced upper limb therapy, and usual care. A total of 770 subjects included were randomly assigned to each group. The primary outcome of successful upper limb function (Action Research Arm Test) at three months post rehabilitation did not show any advantages of RAT compared with the standard care of patients having moderate or severe upper limb dysfunction. The results indicated that RAT was not ready for routine clinical practice at the current stage (Rodgers et al., 2019).

At present, RAT has some limitations for further application. Because of the different designs and groups, there are deviations in the results of published reports. The clinical studies have significant heterogeneity in choosing different types of robotic equipment, enrolled patients, intervention time, and intervention intensity. In addition, it raises the issue of compliance among patients actively participating in the training and ensuring rehabilitation post-stroke efficiency (Yoxon et al., 2022).

MOTOR IMAGERY TRAINING

Motor imagery (MI), also called mental imagery, executes a particular movement or task without the actual signal output (Hanakawa, 2016; Savaki and Raos, 2019). Although the limb motor function in stroke patients is damaged, the exercise program flowchart stored in the brain is still partially preserved. Therefore, regions within the primary motor cortex, cerebellum, and basal ganglia circuits can be activated during MI (Kraft et al., 2015; Tong et al., 2017). In addition, MI can also induce the functional redistribution and regulation of neural circuits, remodeling the brain neural networks, and improving motor function relearning ability (de Vries and Mulder, 2007; Gowda et al., 2021). Furthermore, repeated training can form a normal motor reflex arc, thus, promoting limb function recovery in the stroke patients (Grabherr et al., 2015; López et al., 2019; Ladda et al., 2021). In the recent years, MIT has gradually been applied in rehabilitation as an active, low-cost, relatively simple, and efficient implementing method, attracting attention in active motor rehabilitation of stroke patients.

Motor imagery training could improve the precision and accuracy of upper limb movements and elevate the movement of hemiplegic limbs (Grabherr et al., 2015). Recently, the application of brain imaging has established the efficacy of MIT in rehabilitating stroke patients (Lioi et al., 2020; Mehler et al., 2020; Colamarino et al., 2022). Early application of MIT in post-stroke

hemiplegic patients can enhance sensory information input, promote dormant synapse activation, accelerate the ischemic penumbra reperfusion, and improve cerebral blood supply, thus, enhancing the rehabilitation effect of stroke (Tavazzi et al., 2022). A recently published meta-analysis of ten randomized controlled trials showed that MIT effectively improved upper and lower limb function in stroke patients to complement traditional rehabilitation techniques (Monteiro et al., 2021). The ability to perform motor imagery involves the experience of a particular movement or task and depends on working memory, internally influencing motor representation. Therefore, MIT can improve motor performance by activating neuroplasticity in parietal lobes and related areas (Yoxon and Welsh, 2019, Yoxon and Welsh, 2020). A study applied functional task-oriented MIT in nine individuals and found that MIT could improve upper limbs and motor function of hemiplegic patients and increase visual-motor imagination ability. Page et al. conducted a series of clinical trials on MIT. They observed that compared with the control group, the MIT group (30 min of MIT twice a week for six weeks) developed the ability to perform new activities. It suggested that MI could improve the upper limb motor function and strengthen the learning ability of new skills (Page et al., 2001, 2007, 2009).

Although the efficacy of MIT in improving motor function is evident in stroke patients, many issues require clarification in future studies. First, most studies found that MIT can improve the neurological functions of stroke patients in the short term, but there are a few studies on its long-term effects in rehabilitation. In addition, published reports depicted a variable intervention time of MIT. However, the too long or too short intervention time can lead to unsatisfactory effects or make patients tired, and the choice of proper time duration and intervals are essential. At last, there is no clear standard for undergoing MIT, which may be why MIT has not been recognized and accepted by the patients. A systematic review of 32 articles observed high heterogeneity in the methodological quality and conflicting outcomes from these studies (Guerra et al., 2017). More large-scale randomized controlled trials are needed to determine the most appropriate intervention, density, duration, long-term effects of MIT, the value of MI in stroke rehabilitation, and promoting home-based rehabilitation of stroke patients.

VIRTUAL REALITY-ASSISTED THERAPY

Virtual reality (VR) technology uses computer synthesis of 3D environment models to create and experience virtual world technology. It is a multisource information fusion interactive 3D dynamic view. It also provides the physical behavior of the system simulation with scene display, force/tactile sensing device, position tracker, and other equipment. Immersive real feelings can be obtained through visual, auditory, or tactile real-time perception and operation of various objects inside the virtual world (Chang et al., 2020; Xiong et al., 2021). Due to high safety, high interest, timely evaluation, and feedback, VR has been gradually applied in rehabilitation treatment after stroke (Gao et al., 2021; Hao et al., 2021; Xiong et al., 2021).

A randomized controlled trial of 43 participants with stroke showed that the conventional rehabilitative approach combined with VR improves the perceived health-related quality-of-life in stroke patients (Rodríguez-Hernández et al., 2021), confirmed by other clinical studies (Erhardsson et al., 2020; Thielbar et al., 2020; Gueye et al., 2021). A systematic review of 87 studies with 3,540 participants suggested that VR interventions could effectively improve upper- and lower-limb motor function, balance, gait, and daily function of stroke patients without any cognitive benefits (Zhang et al., 2021). Moreover, the underlying mechanism may be associated with the regulation of inflammation, oxidative stress, and neuroplasticity (Huang et al., 2022). VR games have also become popular in the recent years. For example, Nintendo's VR game comprises a wireless controller, infrared sensor, and a display screen. The sensor in the controller can alter the movement of characters in the game based on the mobility of patients to carry out various virtual games, thereby improving the upper limb movement function in the stroke patients (Hsu et al., 2011; Şimşek and Çekok, 2016; Carregosa et al., 2018; Marques-Sule et al., 2021). Some literature demonstrated no significant difference between VR and traditional training effects (Caglio et al., 2012; Crosbie et al., 2012; Laver et al., 2017). Although VR is not necessarily superior to traditional rehabilitation technology, it can be an effective alternative to rehabilitate stroke patients.

Numerous studies have identified that VR can play a beneficial role in improving limb motor function post-stroke. However, other studies with negative results suggest that more large-scale, multicentric, scientifically designed, and well-conducted clinical randomized controlled trials are needed to clarify VR effects. In addition, some VR rehabilitation equipment can only perform simple human-computer interaction. The patients need to wear complex sensing equipment, and certain virtual scenes do not provide enough immersion. Therefore, a more intelligent VR system should be designed in the future, which could better integrate motor function assessment. It should be a portable and straightforward hardware system with vivid 3D animated characters so that VR technology can improve motor dysfunction after stroke.

MIRROR THERAPY

Mirror therapy also called mirror visual feedback therapy, is based on visual stimulation and flat mirror imaging. It observes the movement of healthy limbs to create the illusion of normal movement of paralyzed limbs through visual feedback, simulation of reality, and optical illusion. As a cheap, convenient, and straightforward treatment, mirror therapy cannot only for the clinical use but also for training patients at home. Mirror therapy was first proposed in 1996 and effectively reduced pain in patients with amputated arms (Ramachandran and Rogers-Ramachandran, 1996). Subsequently, studies conducted in stroke patients with hemiplegia after ictus showed that mirror therapy could significantly rehabilitate patients with upper limb motor dysfunction (Yavuzer et al., 2008; Nogueira et al., 2021; Zhuang et al., 2021). In addition, the role and impact of

mirror therapy have also been explored in lower limb motor rehabilitation (Sütbeyaz et al., 2007; Li et al., 2018; Louie et al., 2019). Compared with the control group, the lower limb motor function and the daily living activities in the mirror group were significantly improved (Gandhi et al., 2020). Furthermore, a randomized controlled trial with 30 patients applied mirror therapy combined with transferable electrical stimulation to treat chronic stroke. The results depicted a significant improvement of muscle strength, Modified Ashworth Scale, Berg Balance Scale, velocity, cadence, step length, and the stride length of gait in the group treated with afferent electrical stimulation through mirror therapy (Lee and Lee, 2019).

Although the neurophysiological mechanism of mirror therapy is not fully elucidated, recent studies have revealed some possible mechanisms. Mirror therapy can reduce asymmetrical activation between the hemispheres, stimulate the ipsilateral, and the contralateral primary motor cortex, extensively activate the mirror neuron system, and induce partial motor neuron pathways on the affected side, facilitating brain function remodeling (Deconinck et al., 2015; Shih et al., 2017; Ding et al., 2019; Jaafar et al., 2021). Furthermore, the mirror neuron system can contribute to the recovery of limb motor function (Rizzolatti et al., 2009; Garrison et al., 2010). In addition, mirror therapy elevates the excitability of the cortical regions through visual feedback and promotes the remodeling of brain function, leading to motor function recovery (Calmels et al., 2006; Nojima et al., 2012).

Mirror therapy is a safe and widely used operable adjunctive therapy with a positive impact. However, the optimal intervention stage and the most effective intensity of mirror therapy have not been determined because of the varying protocols and the small sample size of the current studies. Therefore, it is suggested to standardize the implementation of mirror therapy, refine the efficacy standard, and conduct multicentric, randomized controlled trials with large sample sizes in the future. In addition, the development of more portable devices could provide updated rehabilitation services in stroke patients.

MUSIC THERAPY

Music-based interventions have emerged as a promising tool for motor rehabilitation after stroke because they integrate motor training with multimodal stimulation (Altenmüller and Schlaug, 2015). Music therapy is currently divided into passive and active treatment based on patient participation. Passive music therapy means "listening to music," the melody, rhythm, and other factors that act on the nervous system of the patient during listening to music. Active music therapy is the ability of a patient to imitate percussion rhythms or play musical instruments under the guidance of a music therapist (Sihvonen et al., 2017; Grau-Sánchez et al., 2020; Daniel et al., 2021). The therapeutic effect promotes the recovery of limb motor function through continuous stimulation of the motor cortex within the brain (Rojo et al., 2011; Grau-Sánchez et al., 2013; Ripollés et al., 2016). The impact of music therapy in stroke is primarily manifested through improving the exercise completion quality, strengthening the cognitive function recovery, and reducing depression and other related negative emotions after stroke (Kim et al., 2011; Le Danseur et al., 2019; Haire et al., 2021; Palumbo et al., 2021).

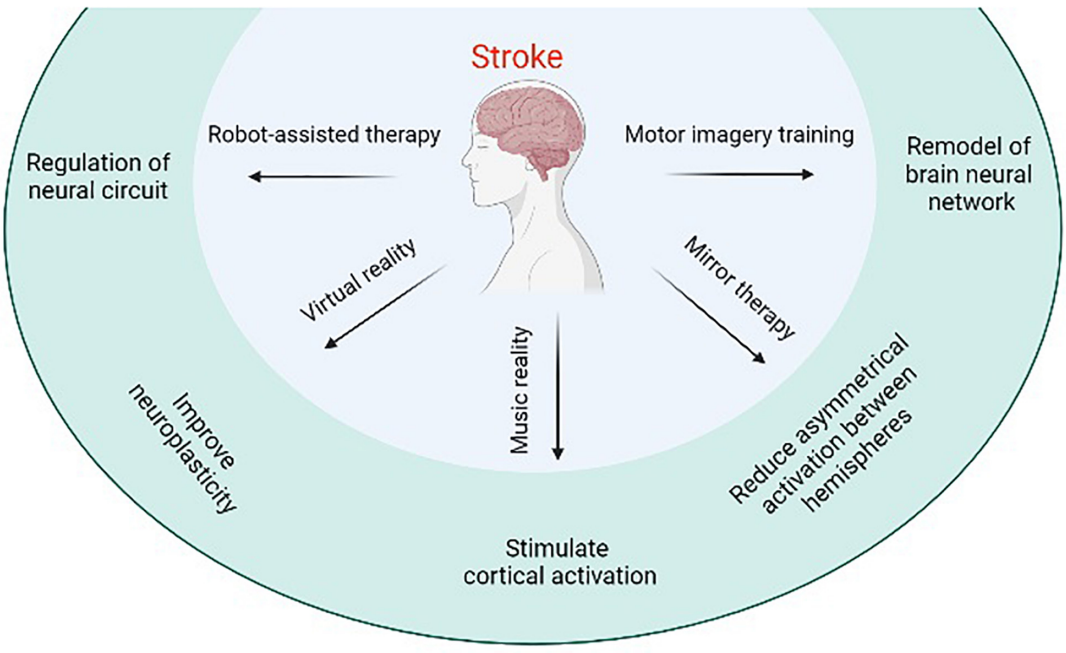

FIGURE 1 | Schematic illustration of emerging the modern rehabilitation methods.

Music therapy can affect the brain structure and function of stroke patients and has a significant effect in treating neurological defects (Särkämö et al., 2008; Huang et al., 2021). Segura et al. (2021) designed a home-based enriched music-supported therapy program for patients recovering from chronic stroke for self-rehabilitation at home. After a ten-week intervention of three sessions per week, the patients improved the upper limb motor function by achieving most motor tests of the Minimal Detectable Change or Minimal Clinically Important Difference. Fujioka et al. (2018) investigated the effects of music-supported therapy in chronic stroke patients on motor, cognitive, and psychosocial functions compared with conventional physical training. The results revealed the beneficial effect of music therapy in all the measured aspects. Moreover, Tong et al. (2015) applied music support therapy to 30 patients with stroke. After four weeks of treatment, it was observed that the time and motion quality completing the Wolf Motor Function Test of patients are significantly better in the music group than those in the mute group. Furthermore, most patients within the music group could independently finish the playing task (Tong et al., 2015). In addition, music could act on the network structure of the brain stem, awaken the cerebral cortex, regulate the peripheral nerves, improve muscle function, and enhance the physical vitality of stroke patients (Fujioka et al., 2012b; Särkämö and Soto, 2012; Barclay et al., 2020). Music can also transmit impulses to the reticular structure of the brain stem and cerebral cortex through auditory pathways, inducing the release of brain-derived neurotrophic factors (Chen et al., 2021). Moreover, music therapy can affect the endocrine function of the hypothalamic-pituitary region through acoustic vibration. It promotes the secretion of pituitary hormones, enzymes, and active substances beneficial to nerve recovery. As a result, blood flow is regulated, and nerve cells are excited, promoting the recovery of limb motor function and improving daily living activities (Yamasaki et al., 2012).

Does the type of music affect the impact of rehabilitation? Stroke patients mainly improve their upper limb and finger function utilizing active music therapy by playing a musical instrument. However, the beneficial effects do not relate to what kind of music is being played. For passive music therapy, most studies used nostalgic music and classical music or chose the favorite music of patients (Fujioka et al., 2012a; Palumbo et al., 2021), which helped relax the patients and made them more willing to participate in the rehabilitation training. Rhythmic auditory stimulation is a neuromusic therapy technique utilizing rhythm to improve motor function. Its primary mechanism could be the synchronous effect between the auditory and motor centers, causing resonance. Fujioka et al. showed that β oscillation was related to prosodic stimulation in the auditory area, motor area, inferior frontal gyrus, and cerebellum (Fujioka et al., 2012a, 2015). Therefore, music can cause the generation of β oscillation, which may be the better choice in rehabilitating stroke patients.

Many randomized controlled trials have established that music-based therapy can treat post-stroke motor dysfunction. However, the therapeutic effect of music therapy is still controversial (Schauer and Mauritz, 2003; Särkämö et al., 2008; Tong et al., 2015; Fotakopoulos and Kotlia, 2018). Therefore, more large randomized controlled trials and high-quality meta-analyses are needed to guide clinical practice better.

CONCLUSION

Stroke-induced neurological injury significantly reduces limb motor function in patients and leads to a decline in the quality of life. RAI, MIT, music therapy, and other emerging modern rehabilitation methods have a particular effect on improving limb motor function of stroke patients, making up for the deficiency of traditional rehabilitation measures, saving human and material resources, and becoming the hot spots of rehabilitation research (**Figure 1**). Several high-quality, large-sample, multicentric randomized controlled studies are needed in the future to promote positive development in stroke rehabilitation research. The current research results are neutral, and the intervention and control groups have a similar effect on movement recovery. To improve the design and implementation method of stroke rehabilitation research, we expanded the inclusion criteria to improve the inclusion rate and the universality of results, ensure the implementation of allocation hiding, and characterize the leading indicators of follow-up measures on time. The focus of future research may include but is not limited to the molecular level of the mechanism underlying rehabilitation, artificial intelligence in rehabilitation technology, and medical big data analysis, trying to achieve the best rehabilitation effect on stroke patients.

AUTHOR CONTRIBUTIONS

PL and FX designed and wrote the manuscript. XL provided constructive advice on the structure of this manuscript. JX, XB, JH, BZ, and FL gave constructive advice and participated in proofreading of this article. All the authors contributed to the article and approved the submitted version.

FUNDING

This work was supported by the Hangzhou Medical and Health Science and Technology Project (Grant No. B20210533) to FX and the Hangzhou Medical and Health Science and Technology Project (Grant No. B20200395) to PL.

REFERENCES

Altenmüller, E., and Schlaug, G. (2015). Apollo's gift: new aspects of neurologic music therapy. *Prog. Brain Res.* 217, 237–252. doi: 10.1016/bs.pbr.2014.11.029

Barclay, R. E., Stevenson, T. J., Poluha, W., Semenko, B., and Schubert, J. (2020). Mental practice for treating upper extremity deficits in individuals with hemiparesis after stroke. *Cochrane Database Syst. Rev.* 5:Cd005950.

Cabanas-Valdés, R., Calvo-Sanz, J., Serra-Llobet, P., Alcoba-Kait, J., González-Rueda, V., and Rodríguez-Rubio, P. R. (2021). The Effectiveness of Massage Therapy for Improving Sequelae in Post-Stroke Survivors. A Systematic Review and Meta-Analysis. *Int. J. Environ. Res. Public Health* 18:4424. doi: 10.3390/ijerph18094424

Caglio, M., Latini-Corazzini, L., D'Agata, F., Cauda, F., Sacco, K., Monteverdi, S., et al. (2012). Virtual navigation for memory rehabilitation in a traumatic brain injured patient. *Neurocase* 18, 123–131. doi: 10.1080/13554794.2011.568499

Calabrò, R. S., Morone, G., Naro, A., Gandolfi, M., Liotti, V., D'Aurizio, C., et al. (2021). Robot-Assisted Training for Upper Limb in Stroke (ROBOTAS): An Observational, Multicenter Study to Identify Determinants of Efficacy. .*J Clin. Med.* 10:5245. doi: 10.3390/jcm10225245

Calmels, C., Holmes, P., Jarry, G., Hars, M., Lopez, E., Paillard, A., et al. (2006). Variability of EEG synchronization prior to and during observation and execution of a sequential finger movement. *Hum. Brain Mapp.* 27, 251–266. doi: 10.1002/hbm.20181

Carregosa, A. A., Aguiar Dos Santos, L. R., Masruha, M. R., Coêlho, M., Machado, T. C., Souza, D. C. B., et al. (2018). Virtual Rehabilitation through Nintendo Wii in Poststroke Patients: Follow-Up. *J. Stroke Cerebrovasc. Dis.* 27, 494–498. doi: 10.1016/j.jstrokecerebrovasdis.2017.09.029

Chang, C., Bang, K., Wetzstein, G., Lee, B., and Gao, L. (2020). Toward the next-generation VR/AR optics: a review of holographic near-eye displays from a human-centric perspective. *Optica* 7, 1563–1578. doi: 10.1364/OPTICA.406004

Chang, W. H., and Kim, Y. H. (2013). Robot-assisted Therapy in Stroke Rehabilitation. *J. Stroke* 15, 174–181. doi: 10.5853/jos.2013.15.3.174

Chen, W., Zheng, J., Shen, G., Ji, X., Sun, L., Li, X., et al. (2021). Music Therapy Alleviates Motor Dysfunction in Rats With Focal Cerebral Ischemia-Reperfusion Injury by Regulating BDNF Expression. *Front. Neurol.* 12:666311. doi: 10.3389/fneur.2021.666311

Cho, K. H., and Song, W. K. (2019). Robot-Assisted Reach Training With an Active Assistant Protocol for Long-Term Upper Extremity Impairment Poststroke: A Randomized Controlled Trial. *Arch. Phys. Med. Rehabil.* 100, 213–219. doi: 10.1016/j.apmr.2018.10.002

Cho, K. H., Hong, M. R., and Song, W. K. (2018). Upper limb robotic rehabilitation for chronic stroke survivors: a single-group preliminary study. *J. Phys. Ther. Sci.* 30, 580–583. doi: 10.1589/jpts.30.580

Colamarino, E., Pichiorri, F., Toppi, J., Mattia, D., and Cincotti, F. (2022). Automatic Selection of Control Features for Electroencephalography-Based Brain-Computer Interface Assisted Motor Rehabilitation: The GUIDER Algorithm. *Brain Topogr.* 35, 182–190. doi: 10.1007/s10548-021-00883-9

Crosbie, J. H., Lennon, S., McGoldrick, M. C., McNeill, M. D., and McDonough, S. M. (2012). Virtual reality in the rehabilitation of the arm after hemiplegic stroke: a randomized controlled pilot study. *Clin. Rehabil.* 26, 798–806. doi: 10.1177/0269215511434575

Daniel, A., Koumans, H., and Ganti, L. (2021). Impact of Music Therapy on Gait After Stroke. *Cureus* 13:e18441. doi: 10.7759/cureus.18441

de Vries, S., and Mulder, T. (2007). Motor imagery and stroke rehabilitation: a critical discussion. *J. Rehabil. Med.* 39, 5–13. doi: 10.2340/16501977-0020

Deconinck, F. J., Smorenburg, A. R., Benham, A., Ledebt, A., Feltham, M. G., and Savelsbergh, G. J. (2015). Reflections on mirror therapy: a systematic review of the effect of mirror visual feedback on the brain. *Neurorehabil. Neural. Repair* 29, 349–361. doi: 10.1177/1545968314546134

Ding, L., Wang, X., Guo, X., Chen, S., Wang, H., Cui, X., et al. (2019). Effects of camera-based mirror visual feedback therapy for patients who had a stroke and the neural mechanisms involved: protocol of a multicentre randomised control study. *BMJ Open* 9:e022828. doi: 10.1136/bmjopen-2018-022828

Erhardsson, M., Alt Murphy, M., and Sunnerhagen, K. S. (2020). Commercial head-mounted display virtual reality for upper extremity rehabilitation in chronic stroke: a single-case design study. *J. Neuroeng. Rehabil.* 17:154. doi: 10.1186/s12984-020-00788-x

Fotakopoulos, G., and Kotlia, P. (2018). The Value of Exercise Rehabilitation Program Accompanied by Experiential Music for Recovery of Cognitive and Motor Skills in Stroke Patients. *J. Stroke Cerebrovasc. Dis.* 27, 2932–2939. doi: 10.1016/j.jstrokecerebrovasdis.2018.06.025

Fujioka, T., Dawson, D. R., Wright, R., Honjo, K., Chen, J. L., Chen, J. J., et al. (2018). The effects of music-supported therapy on motor, cognitive, and psychosocial functions in chronic stroke. *Ann. N. Y. Acad. Sci.* Epub online ahead of print. doi: 10.1111/nyas.13706

Fujioka, T., Ross, B., and Trainor, L. J. (2015). Beta-Band Oscillations Represent Auditory Beat and Its Metrical Hierarchy in Perception and Imagery. *J. Neurosci.* 35, 15187–15198. doi: 10.1523/jneurosci.2397-15.2015

Fujioka, T., Trainor, L. J., Large, E. W., and Ross, B. (2012a). Internalized timing of isochronous sounds is represented in neuromagnetic β oscillations. *J. Neurosci.* 32, 1791–1802. doi: 10.1523/JNEUROSCI.4107-11.2012

Fujioka, T., Ween, J. E., Jamali, S., Stuss, D. T., and Ross, B. (2012b). Changes in neuromagnetic beta-band oscillation after music-supported stroke rehabilitation. *Ann. N. Y. Acad. Sci.* 1252, 294–304. doi: 10.1111/j.1749-6632.2011.06436.x

Gandhi, D. B., Sterba, A., Khatter, H., and Pandian, J. D. (2020). Mirror Therapy in Stroke Rehabilitation: Current Perspectives. *Ther. Clin. Risk Manag.* 16, 75–85. doi: 10.2147/TCRM.S206883

Gao, Y., Ma, L., Lin, C., Zhu, S., Yao, L., Fan, H., et al. (2021). Effects of Virtual Reality-Based Intervention on Cognition, Motor Function, Mood, and Activities of Daily Living in Patients With Chronic Stroke: A Systematic Review and Meta-Analysis of Randomized Controlled Trials. *Front. Aging Neurosci.* 13:766525. doi: 10.3389/fnagi.2021.766525

Garrison, K. A., Winstein, C. J., and Aziz-Zadeh, L. (2010). The mirror neuron system: a neural substrate for methods in stroke rehabilitation. *Neurorehabil. Neural. Repair* 24, 404–412. doi: 10.1177/1545968309354536

GBD 2019 Stroke Collaborators (2021). Global, regional, and national burden of stroke and its risk factors, 1990-2019: a systematic analysis for the Global Burden of Disease Study 2019. *Lancet Neurol.* 20, 795–820. doi: 10.1016/S1474-4422(21)00252-0

Gowda, A. S., Memon, A. N., Bidika, E., Salib, M., Rallabhandi, B., and Fayyaz, H. (2021). Investigating the Viability of Motor Imagery as a Physical Rehabilitation Treatment for Patients With Stroke-Induced Motor Cortical Damage. *Cureus* 13:e14001. doi: 10.7759/cureus.14001

Grabherr, L., Jola, C., Berra, G., Theiler, R., and Mast, F. W. (2015). Motor imagery training improves precision of an upper limb movement in patients with hemiparesis. *NeuroRehabilitation* 36, 157–166. doi: 10.3233/NRE-151203

Grau-Sánchez, J., Amengual, J. L., Rojo, N., Veciana de Las Heras, M., Montero, J., Rubio, F., et al. (2013). Plasticity in the sensorimotor cortex induced by Music-supported therapy in stroke patients: a TMS study. *Front. Hum. Neurosci.* 7:494. doi: 10.3389/fnhum.2013.00494

Grau-Sánchez, J., Münte, T. F., Altenmüller, E., Duarte, E., and Rodríguez-Fornells, A. (2020). Potential benefits of music playing in stroke upper limb motor rehabilitation. *Neurosci. Biobehav. Rev.* 112, 585–599. doi: 10.1016/j.neubiorev.2020.02.027

Guerra, Z. F., Lucchetti, A. L. G., and Lucchetti, G. (2017). Motor Imagery Training After Stroke: A Systematic Review and Meta-analysis of Randomized Controlled Trials. *J. Neurol. Phys. Ther.* 41, 205–214. doi: 10.1097/NPT.0000000000000200

Gueye, T., Dedkova, M., Rogalewicz, V., Grunerova-Lippertova, M., and Angerova, Y. (2021). Early post-stroke rehabilitation for upper limb motor function using virtual reality and exoskeleton: equally efficient in older patients. *Neurol. Neurochir. Pol.* 55, 91–96. doi: 10.5603/PJNNS.a2020.0096

Haire, C. M., Vuong, V., Tremblay, L., Patterson, K. K., Chen, J. L., and Thaut, M. H. (2021). Effects of therapeutic instrumental music performance and motor imagery on chronic post-stroke cognition and affect: A randomized controlled trial. *NeuroRehabilitation* 48, 195–208. doi: 10.3233/NRE-208014

Hanakawa, T. (2016). Organizing motor imageries. *Neurosci. Res.* 104, 56–63. doi: 10.1016/j.neures.2015.11.003

Hao, J., Xie, H., Harp, K., Chen, Z., and Siu, K. C. (2021). Effects of Virtual Reality Intervention on Neural Plasticity in Stroke Rehabilitation: A Systematic Review. *Arch. Phys. Med. Rehabil.* S0003–9993, 01305–8. doi: 10.1016/j.apmr.2021.06.024

Hesse, S., Schulte-Tigges, G., Konrad, M., Bardeleben, A., and Werner, C. (2003). Robot-assisted arm trainer for the passive and active practice of bilateral forearm and wrist movements in hemiparetic subjects. *Arch. Phys. Med. Rehabil.* 84, 915–920. doi: 10.1016/s0003-9993(02)04954-7

Hsu, J. K., Thibodeau, R., Wong, S. J., Zukiwsky, D., Cecile, S., and Walton, D. M. (2011). A "Wii" bit of fun: the effects of adding Nintendo Wii(®) Bowling to a standard exercise regimen for residents of long-term care with upper extremity dysfunction. *Physiother. Theory Pract.* 27, 185–193. doi: 10.3109/09593985.2010.483267

Huang, C. Y., Chiang, W. C., Yeh, Y. C., Fan, S. C., Yang, W. H., Kuo, H. C., et al. (2022). Effects of virtual reality-based motor control training on inflammation, oxidative stress, neuroplasticity and upper limb motor function in patients with chronic stroke: a randomized controlled trial. *BMC Neurol.* 22:21. doi: 10.1186/s12883-021-02547-4

Huang, W. H., Dou, Z. L., Jin, H. M., Cui, Y., Li, X., and Zeng, Q. (2021). The Effectiveness of Music Therapy on Hand Function in Patients With Stroke: A Systematic Review of Randomized Controlled Trials. *Front. Neurol.* 12:641023. doi: 10.3389/fneur.2021.641023

Iso, H. (2021). Cardiovascular disease, a major global burden: Epidemiology of stroke and ischemic heart disease in Japan. *Glob. Health Med.* 3, 358–364. doi: 10.35772/ghm.2020.01113

Jaafar, N., Che Daud, A. Z., Ahmad Roslan, N. F., and Mansor, W. (2021). Mirror Therapy Rehabilitation in Stroke: A Scoping Review of Upper Limb Recovery and Brain Activities. *Rehabil. Res. Pract.* 2021:9487319. doi: 10.1155/2021/9487319

Katzan, I. L., Schuster, A., Newey, C., Uchino, K., and Lapin, B. (2018a). Patient-reported outcomes across cerebrovascular event types: More similar than different. *Neurology* 91, e2182–e2191.

Katzan, I. L., Thompson, N. R., Uchino, K., and Lapin, B. (2018b). The most affected health domains after ischemic stroke. *Neurology* 90, e1364–e1371. doi: 10.1212/WNL.0000000000005327

Kim, D. S., Park, Y. G., Choi, J. H., Im, S. H., Jung, K. J., Cha, Y. A., et al. (2011). Effects of music therapy on mood in stroke patients. *Yonsei Med. J.* 52, 977–981. doi: 10.3349/ymj.2011.52.6.977

Kim, J., Thayabaranathan, T., Donnan, G. A., Howard, G., Howard, V. J., Rothwell, P. M., et al. (2020). Global Stroke Statistics 2019. *Int. J. Stroke* 15, 819–838. doi: 10.1177/1747493020909545

Kraft, E., Schaal, M. C., Lule, D., König, E., and Scheidtmann, K. (2015). The functional anatomy of motor imagery after sub-acute stroke. *NeuroRehabilitation* 36, 329–337. doi: 10.3233/NRE-151221

Ladda, A. M., Lebon, F., and Lotze, M. (2021). Using motor imagery practice for improving motor performance - A review. *Brain Cogn.* 150:105705. doi: 10.1016/j.bandc.2021.105705

Lambercy, O., Dovat, L., Yun, H., Wee, S. K., Kuah, C. W., Chua, K. S., et al. (2011). Effects of a robot-assisted training of grasp and pronation/supination in chronic stroke: a pilot study. *J. Neuroeng. Rehabil.* 8:63. doi: 10.1186/1743-0003-8-63

Lamberti, N., Manfredini, F., Lissom, L. O., Lavezzi, S., Basaglia, N., and Straudi, S. (2021). Beneficial Effects of Robot-Assisted Gait Training on Functional Recovery in Women after Stroke: A Cohort Study. *Medicina* 57:1200. doi: 10.3390/medicina57111200

Langhorne, P., Collier, J. M., Bate, P. J., Thuy, M. N., and Bernhardt, J. (2018). Very early versus delayed mobilisation after stroke. *Cochrane Database Syst. Rev.* 10:Cd006187.

Laver, K. E., dey-Wakeling, Z. A., Crotty, M., Lannin, N. A., George, S., and Sherrington, C. (2020). Telerehabilitation services for stroke. *Cochrane Database Syst. Rev.* 1:Cd010255.

Laver, K. E., Lange, B., George, S., Deutsch, J. E., Saposnik, G., and Crotty, M. (2017). Virtual reality for stroke rehabilitation. *Cochrane Database Syst. Rev.* 11:Cd008349.

Le Danseur, M., Crow, A. D., Stutzman, S. E., Villarreal, M. D., and Olson, D. M. (2019). Music as a Therapy to Alleviate Anxiety During Inpatient Rehabilitation for Stroke. *Rehabil. Nurs.* 44, 29–34. doi: 10.1097/rnj.0000000000000102

Lee, D., and Lee, G. (2019). Effect of afferent electrical stimulation with mirror therapy on motor function, balance, and gait in chronic stroke survivors: a randomized controlled trial. *Eur. J. Phys. Rehabil. Med.* 55, 442–449. doi: 10.23736/S1973-9087.19.05334-6

Leys, D., Béjot, Y., Debette, S., and Giroud, M. (2008). Burden of stroke in France. *Int. J. Stroke* 3, 117–119. doi: 10.1111/j.1747-4949.2008.00188.x

Li, Y., Wei, Q., Gou, W., and He, C. (2018). Effects of mirror therapy on walking ability, balance and lower limb motor recovery after stroke: a systematic review and meta-analysis of randomized controlled trials. *Clin. Rehabil.* 32, 1007–1021. doi: 10.1177/0269215518766642

Lioi, G., Butet, S., Fleury, M., Bannier, E., Lécuyer, A., Bonan, I., et al. (2020). A Multi-Target Motor Imagery Training Using Bimodal EEG-fMRI Neurofeedback: A Pilot Study in Chronic Stroke Patients. *Front. Hum. Neurosci.* 14:37. doi: 10.3389/fnhum.2020.00037

López, N. D., Monge Pereira, E., Centeno, E. J., and Miangolarra Page, J. C. (2019). Motor imagery as a complementary technique for functional recovery after stroke: a systematic review. *Top. Stroke Rehabil.* 26, 576–587. doi: 10.1080/10749357.2019.1640000

Louie, D. R., Lim, S. B., and Eng, J. J. (2019). The Efficacy of Lower Extremity Mirror Therapy for Improving Balance, Gait, and Motor Function Poststroke: A Systematic Review and Meta-Analysis. *J. Stroke Cerebrovasc. Dis.* 28, 107–120. doi: 10.1016/j.jstrokecerebrovasdis.2018.09.017

Marques-Sule, E., Arnal-Gómez, A., Buitrago-Jiménez, G., Suso-Martí, L., Cuenca-Martínez, F., and Espí-López, G. V. (2021). Effectiveness of Nintendo Wii and Physical Therapy in Functionality, Balance, and Daily Activities in Chronic Stroke Patients. *J. Am. Med. Dir. Assoc.* 22, 1073–1080. doi: 10.1016/j.jamda.2021.01.076

Masiero, S., Poli, P., Rosati, G., Zanotto, D., Iosa, M., Paolucci, S., et al. (2014). The value of robotic systems in stroke rehabilitation. *Expert Rev. Med. Devices* 11, 187–198. doi: 10.1586/17434440.2014.882766

McCrimmon, C. M., King, C. E., Wang, P. T., Cramer, S. C., Nenadic, Z., and Do, A. H. (2015). Brain-controlled functional electrical stimulation therapy for gait rehabilitation after stroke: a safety study. *J. Neuroeng. Rehabil.* 12:57. doi: 10.1186/s12984-015-0050-4

Mehler, D. M. A., Williams, A. N., Whittaker, J. R., Krause, F., Lührs, M., Kunas, S., et al. (2020). Graded fMRI Neurofeedback Training of Motor Imagery in Middle Cerebral Artery Stroke Patients: A Preregistered Proof-of-Concept Study. *Front. Hum. Neurosci.* 14:226. doi: 10.3389/fnhum.2020.00226

Moggio, L., de Sire, A., Marotta, N., Demeco, A., and Ammendolia, A. (2021). Exoskeleton versus end-effector robot-assisted therapy for finger-hand motor recovery in stroke survivors: systematic review and meta-analysis. *Top. Stroke Rehabil.* 1–12. Epub online ahead of print. doi: 10.1080/10749357.2021.1967657

Monteiro, K. B., Cardoso, M. D. S., Cabral, V., Santos, A., Silva, P. S. D., Castro, J. B. P., et al. (2021). Effects of Motor Imagery as a Complementary Resource on the Rehabilitation of Stroke Patients: A Meta-Analysis of Randomized Trials. *J. Stroke Cerebrovasc Dis.* 30:105876. doi: 10.1016/j.jstrokecerebrovasdis.2021.105876

Morone, G., Cocchi, I., Paolucci, S., and Iosa, M. (2020). Robot-assisted therapy for arm recovery for stroke patients: state of the art and clinical implication. *Expert Rev. Med. Devices* 17, 223–233. doi: 10.1080/17434440.2020.1733408

Morone, G., Paolucci, S., Cherubini, A., De Angelis, D., Venturiero, V., Coiro, P., et al. (2017). Robot-assisted gait training for stroke patients: current state of the art and perspectives of robotics. *Neuropsychiatr. Dis. Treat* 13, 1303–1311. doi: 10.2147/NDT.S114102

Nogueira, N., Parma, J. O., Leão, S., Sales, I. S., Macedo, L. C., Galvão, A., et al. (2021). Mirror therapy in upper limb motor recovery and activities of daily living, and its neural correlates in stroke individuals: A systematic review and meta-analysis. *Brain Res. Bull.* 177, 217–238. doi: 10.1016/j.brainresbull.2021.10.003

Nojima, I., Mima, T., Koganemaru, S., Thabit, M. N., Fukuyama, H., and Kawamata, T. (2012). Human motor plasticity induced by mirror visual feedback. *J. Neurosci.* 32, 1293–1300. doi: 10.1523/JNEUROSCI.5364-11.2012

Ovbiagele, B., and Nguyen-Huynh, M. N. (2011). Stroke epidemiology: advancing our understanding of disease mechanism and therapy. *Neurotherapeutics* 8, 319–329. doi: 10.1007/s13311-011-0053-1

Page, S. J., Levine, P., and Leonard, A. (2007). Mental practice in chronic stroke: results of a randomized, placebo-controlled trial. *Stroke* 38, 1293–1297. doi: 10.1161/01.STR.0000260205.67348.2b

Page, S. J., Levine, P., Sisto, S. A., and Johnston, M. V. (2001). Mental practice combined with physical practice for upper-limb motor deficit in subacute stroke. *Phys. Ther.* 81, 1455–1462. doi: 10.1093/ptj/81.8.1455

Page, S. J., Szaflarski, J. P., Eliassen, J. C., Pan, H., and Cramer, S. C. (2009). Cortical plasticity following motor skill learning during mental practice in stroke. *Neurorehabil. Neural. Repair* 23, 382–388. doi: 10.1177/1545968308326427

Palumbo, A., Aluru, V., Battaglia, J., Geller, D., Turry, A., Ross, M., et al. (2021). Music Upper Limb Therapy-Integrated (MULT-I) Provides a Feasible Enriched Environment and Reduces Post Stroke Depression: A Pilot Randomized Controlled Trial. *Am. J. Phys. Med. Rehabil.* Epub online ahead of print. doi: 10.1097/PHM.0000000000001938

Ramachandran, V. S., and Rogers-Ramachandran, D. (1996). Synaesthesia in phantom limbs induced with mirrors. *Proc. Biol. Sci.* 263, 377–386. doi: 10.1098/rspb.1996.0058

Ripollés, P., Rojo, N., Grau-Sánchez, J., Amengual, J. L., Càmara, E., Marco-Pallarés, J., et al. (2016). Music supported therapy promotes motor plasticity in individuals with chronic stroke. *Brain Imaging Behav.* 10, 1289–1307. doi: 10.1007/s11682-015-9498-x

Rizzolatti, G., Fabbri-Destro, M., and Cattaneo, L. (2009). Mirror neurons and their clinical relevance. *Nat. Clin. Pract. Neurol.* 5, 24–34. doi: 10.1038/ncpneuro0990

Rodgers, H., Bosomworth, H., Krebs, H. I., van Wijck, F., Howel, D., Wilson, N., et al. (2020). Robot-assisted training compared with an enhanced upper limb therapy programme and with usual care for upper limb functional limitation after stroke: the RATULS three-group RCT. *Health Technol. Assess.* 24, 1–232. doi: 10.3310/hta24540

Rodgers, H., Bosomworth, H., Krebs, H. I., van Wijck, F., Howel, D., Wilson, N., et al. (2019). Robot assisted training for the upper limb after stroke (RATULS): a multicentre randomised controlled trial. *Lancet* 394, 51–62. doi: 10.1016/S0140-6736(19)31055-4

Rodríguez-Hernández, M., Criado-Álvarez, J. J., Corregidor-Sánchez, A. I., Martín-Conty, J. L., Mohedano-Moriano, A., and Polonio-López, B. (2021). Effects of Virtual Reality-Based Therapy on Quality of Life of Patients with Subacute Stroke: A Three-Month Follow-Up Randomized Controlled Trial. *Int. J. Environ. Res. Public Health* 18:2810. doi: 10.3390/ijerph18062810

Rojo, N., Amengual, J., Juncadella, M., Rubio, F., Camara, E., Marco-Pallares, J., et al. (2011). Music-supported therapy induces plasticity in the sensorimotor cortex in chronic stroke: a single-case study using multimodal imaging (fMRI-TMS). *Brain INJ* 25, 787–793. doi: 10.3109/02699052.2011.576305

Särkämö, T., and Soto, D. (2012). Music listening after stroke: beneficial effects and potential neural mechanisms. *Ann. N. Y. Acad. Sci.* 1252, 266–281. doi: 10.1111/j.1749-6632.2011.06405.x

Särkämö, T., Tervaniemi, M., Laitinen, S., Forsblom, A., Soinila, S., Mikkonen, M., et al. (2008). Music listening enhances cognitive recovery and mood after middle cerebral artery stroke. *Brain* 131, 866–876. doi: 10.1093/brain/awn013

Savaki, H. E., and Raos, V. (2019). Action perception and motor imagery: Mental practice of action. *Prog. Neurobiol.* 175, 107–125. doi: 10.1016/j.pneurobio.2019.01.007

Schauer, M., and Mauritz, K. H. (2003). Musical motor feedback (MMF) in walking hemiparetic stroke patients: randomized trials of gait improvement. *Clin. Rehabil.* 17, 713–722. doi: 10.1191/0269215503cr668oa

Segura, E., Grau-Sánchez, J., Sanchez-Pinsach, D., De la Cruz, M., Duarte, E., Arcos, J. L., et al. (2021). Designing an app for home-based enriched Music-supported Therapy in the rehabilitation of patients with chronic stroke: a pilot feasibility study. *Brain INJ* 35, 1585–1597. doi: 10.1080/02699052.2021.1975819

Shih, T. Y., Wu, C. Y., Lin, K. C., Cheng, C. H., Hsieh, Y. W., Chen, C. L., et al. (2017). Effects of action observation therapy and mirror therapy after stroke on rehabilitation outcomes and neural mechanisms by MEG: study protocol for a randomized controlled trial. *Trials* 18:459. doi: 10.1186/s13063-017-2205-z

Sihvonen, A. J., Särkämö, T., Leo, V., Tervaniemi, M., Altenmüller, E., and Soinila, S. (2017). Music-based interventions in neurological rehabilitation. *Lancet Neurol.* 16, 648–660. doi: 10.1016/S1474-4422(17)30168-0

Şimşek, T. T., and Çekok, K. (2016). The effects of Nintendo Wii(TM)-based balance and upper extremity training on activities of daily living and quality of life in patients with sub-acute stroke: a randomized controlled study. *Int. J. Neurosci.* 126, 1061–1070. doi: 10.3109/00207454.2015.1115993

Song, K. J., Chun, M. H., Lee, J., and Lee, C. (2021). The effect of robot-assisted gait training on cortical activation in stroke patients: A functional near-infrared spectroscopy study. *NeuroRehabilitation* 49, 65–73. doi: 10.3233/NRE-210034

Sütbeyaz, S., Yavuzer, G., Sezer, N., and Koseoglu, B. F. (2007). Mirror therapy enhances lower-extremity motor recovery and motor functioning after stroke: a randomized controlled trial. *Arch. Phys. Med. Rehabil.* 88, 555–559. doi: 10.1016/j.apmr.2007.02.034

Tavazzi, E., Bergsland, N., Pirastru, A., Cazzoli, M., Blasi, V., and Baglio, F. (2022). MRI markers of functional connectivity and tissue microstructure in stroke-related motor rehabilitation: A systematic review. *Neuroimage Clin.* 33:102931. doi: 10.1016/j.nicl.2021.102931

Terranova, T. T., Simis, M., Santos, A. C. A., Alfieri, F. M., Imamura, M., Fregni, F., et al. (2021). Robot-Assisted Therapy and Constraint-Induced Movement Therapy for Motor Recovery in Stroke: Results From a Randomized Clinical Trial. *Front. Neurorobot.* 15:684019. doi: 10.3389/fnbot.2021.684019

Thielbar, K. O., Triandafilou, K. M., Barry, A. J., Yuan, N., Nishimoto, A., Johnson, J., et al. (2020). Home-based Upper Extremity Stroke Therapy Using a Multiuser Virtual Reality Environment: A Randomized Trial. *Arch. Phys. Med. Rehabil.* 101, 196–203. doi: 10.1016/j.apmr.2019.10.182

Tong, Y., Forreider, B., Sun, X., Geng, X., Zhang, W., Du, H., et al. (2015). Music-supported therapy (MST) in improving post-stroke patients' upper-limb motor function: a randomised controlled pilot study. *Neurol. Res.* 37, 434–440. doi: 10.1179/1743132815Y.0000000034

Tong, Y., Pendy, J. T. Jr., Li, W. A., Du, H., Zhang, T., Geng, X., et al. (2017). Motor Imagery-Based Rehabilitation: Potential Neural Correlates and Clinical Application for Functional Recovery of Motor Deficits after Stroke. *Aging Dis.* 8, 364–371. doi: 10.14336/AD.2016.1012

Veerbeek, J. M., Langbroek-Amersfoort, A. C., van Wegen, E. E., Meskers, C. G., and Kwakkel, G. (2017). Effects of Robot-Assisted Therapy for the Upper Limb After Stroke. *Neurorehabil. Neural. Repair.* 31, 107–121.

World Health Organization [WHO] (2020). *Global Health Estimates 2020: Deaths by Cause, Age, Sex, by Country and by Region, 2000-2019*. Geneva: WHO.

Xiong, J., Hsiang, E. L., He, Z., Zhan, T., and Wu, S. T. (2021). Augmented reality and virtual reality displays: emerging technologies and future perspectives. *Light Sci. Appl.* 10:216. doi: 10.1038/s41377-021-00658-8

Yamasaki, A., Booker, A., Kapur, V., Tilt, A., Niess, H., Lillemoe, K. D., et al. (2012). The impact of music on metabolism. *Nutrition* 28, 1075–1080. doi: 10.1016/j.nut.2012.01.020

Yang, A., Wu, H. M., Tang, J. L., Xu, L., Yang, M., and Liu, G. J. (2016). Acupuncture for stroke rehabilitation. *Cochrane Database Syst. Rev.* 2016:Cd004131.

Yavuzer, G., Selles, R., Sezer, N., Sütbeyaz, S., Bussmann, J. B., Köseoğlu, F., et al. (2008). Mirror therapy improves hand function in subacute stroke: a randomized controlled trial. *Arch. Phys. Med. Rehabil.* 89, 393–398. doi: 10.1016/j.apmr.2007.08.162

Yoxon, E., and Welsh, T. N. (2019). Rapid motor cortical plasticity can be induced by motor imagery training. *Neuropsychologia* 134:107206.

Yoxon, E., and Welsh, T. N. (2020). Motor system activation during motor imagery is positively related to the magnitude of cortical plastic changes following motor imagery training. *Behav. Brain Res.* 390:112685.

Yoxon, E., Brillinger, M., and Welsh, T. N. (2022). Behavioural indexes of movement imagery ability are associated with the magnitude of corticospinal adaptation following movement imagery training. *Brain Res.* 1777:147764.

Zhang, B., Li, D., Liu, Y., Wang, J., and Xiao, Q. (2021). Virtual reality for limb motor function, balance, gait, cognition and daily function of stroke patients: A systematic review and meta-analysis. *J. Adv. Nurs.* 77, 3255–3273. doi: 10.1111/jan.14800

Zhuang, J. Y., Ding, L., Shu, B. B., Chen, D., and Jia, J. (2021). Associated Mirror Therapy Enhances Motor Recovery of the Upper Extremity and Daily Function after Stroke: A Randomized Control Study. *Neural Plast.* 2021:7266263. doi: 10.1155/2021/7266263

Conflict of Interest: The authors declare that the research was conducted in the absence of any commercial or financial relationships that could be construed as a potential conflict of interest.

frontiers | Frontiers in Aging Neuroscience

ORIGINAL RESEARCH
published: 01 April 2022
doi: 10.3389/fnagi.2022.865244

Systemic-Immune-Inflammation Index as a Promising Biomarker for Predicting Perioperative Ischemic Stroke in Older Patients Who Underwent Non-cardiac Surgery

Faqiang Zhang[1†], Mu Niu[2†], Long Wang[3†], Yanhong Liu[1], Likai Shi[1], Jiangbei Cao[1], Weidong Mi[1], Yulong Ma[1] and Jing Liu[1*]*

[1] Anesthesia and Operation Center, The First Medical Center, Chinese PLA General Hospital, Beijing, China, [2] Department of Neurology, The Affiliated Hospital of Xuzhou Medical University, Xuzhou Medical University, Xuzhou, China, [3] Department of Pain Medicine, The First Medical Center, Chinese PLA General Hospital, Beijing, China

OPEN ACCESS

Edited by:
Yujie Chen,
Army Medical University, China

Reviewed by:
Xiaobin Gu,
First Affiliated Hospital of Zhengzhou University, China
Kaifu Ke,
Affiliated Hospital of Nantong University, China
Yanan Wang,
West China Hospital of Sichuan University, China

***Correspondence:**
Yulong Ma
yulongma123@163.com
Jing Liu
liuj301@163.com

† These authors have contributed equally to this work

Specialty section:
This article was submitted to Neuroinflammation and Neuropathy, a section of the journal Frontiers in Aging Neuroscience

Received: 29 January 2022
Accepted: 07 March 2022
Published: 01 April 2022

Citation:
Zhang F, Niu M, Wang L, Liu Y, Shi L, Cao J, Mi W, Ma Y and Liu J (2022) Systemic-Immune-Inflammation Index as a Promising Biomarker for Predicting Perioperative Ischemic Stroke in Older Patients Who Underwent Non-cardiac Surgery. Front. Aging Neurosci. 14:865244. doi: 10.3389/fnagi.2022.865244

Objective: This study aimed to investigate the clinical prognostic values of the preoperative systemic-immune-inflammation index (SII) in older patients undergoing non-cardiac surgery, using perioperative ischemic stroke as the primary outcome.

Methods: This retrospective cohort study included older patients who underwent non-cardiac surgery between January 2008 and August 2019. The patients were divided into SII $<$ 583 and SII $\geq$ 583 group according to the optimal SII cut-off value. The outcome of interest was ischemic stroke within 30 days after surgery. Primary, sensitivity, and subgroup analyses were performed to confirm that preoperative SII qualifies as a promising, independent prognostic indicator. Propensity score matching (PSM) analysis was further applied to address the potential residual confounding effect of covariates to examine the robustness of our results.

Results: Among the 40,670 included patients with a median age of 70 years (interquartile range: 67, 74), 237 (0.58%) experienced an ischemic stroke within 30 days after surgery. SII $\geq$ 583 was associated with an increased risk of perioperative ischemic stroke in multivariate regression analysis [odds ratio (OR), 1.843; 95% confidence interval (CI), 1.369–2.480; $P < 0.001$]. After PSM adjustment, all covariates were well balanced between the two groups. The correlation between the SII and perioperative ischemic stroke remained significantly robust (OR: 2.195; 95% CI: 1.574–3.106; $P < 0.001$) in the PSM analysis.

Conclusion: Preoperative SII, which includes neutrophil, platelet, and lymphocyte counts obtained from routine blood analysis, was a potential prognostic biomarker for predicting perioperative ischemic stroke after non-cardiac surgery in older patients. An elevated SII, based on an optimal cut-off value of 583, was an independent risk factor for perioperative ischemic stroke.

Keywords: systemic-immune-inflammation index (SII), perioperative stroke, postoperative complication, inflammation, older patients, biomarker

INTRODUCTION

With the rapidly aging population worldwide, the number of older patients undergoing surgery and general anesthesia has increased substantially. Given the advanced age or broad range of comorbidities, older adults are more vulnerable to postoperative complications (Handforth et al., 2015; Marcantonio, 2017). Perioperative ischemic stroke is an uncommon but lethal procedure-related complication, in which nearly half of all patients die within 10 years (Zhang et al., 2022). Due to the initially "silent" signs or symptoms and the delay to diagnostic imaging, perioperative ischemic stroke is not only difficult to identify, but, when finally diagnosed, it is also more likely for patients to have missed the narrow time window for safe treatment with tissue-type plasminogen activator thrombolysis (Mao et al., 2017). Therefore, the search for preoperative biomarkers is an urgent and challenging task in clinical practice. These biomarkers would allow for better population stratification and optimal allocation of healthcare resources.

Inflammation is intimately associated with the occurrence, progression, and prognosis of ischemic stroke (Macrez et al., 2011). In animal models of brain ischemia, brain-infiltrating innate and adaptive immune cells contribute to ischemic cerebral damage and exacerbate neurological deficits (Mracsko et al., 2014). In addition, the inflammatory response results in activation of coagulation, in turn, coagulation factors potentiate inflammatory reactions (Redecha et al., 2007). Furthermore, preoperative chronic inflammation, characterized by the aberrant accumulation of inflammatory cells and inflammatory factors, increases postoperative cardiovascular complications and all-cause mortality (Ettinger et al., 2015; Fragiadakis et al., 2015). Systemic inflammation levels can be evaluated and quantified using a variety of hematological markers routinely measured in the clinical settings or the indices calculated from these measurements (Nøst et al., 2021). Neutrophil-to-lymphocyte ratio (NLR), platelet-to-lymphocyte ratio (PLR), C-reactive protein (CRP), and Glasgow prognostic score (GPS) are closely associated with postoperative outcomes in patients who undergo tumor resection (Jomrich et al., 2021). Systemic-immune-inflammation index (SII) (Hu et al., 2014), derived from neutrophil, lymphocyte, and platelet counts, has not been assessed or applied to predict perioperative ischemic stroke in older patients undergoing non-cardiac surgery.

In this study, we examined the prognostic value of the preoperative SII in older patients undergoing non-cardiac surgery. We hypothesized that an elevated SII could indicate an increased risk of perioperative ischemic stroke. Herein, we performed a large retrospective cohort study of older patients undergoing non-cardiac surgery to investigate the association between preoperative SII and perioperative ischemic stroke.

MATERIALS AND METHODS

The study protocol was reviewed and approved by the institutional ethics committee of Chinese PLA General Hospital (No. S2021-135-01), and the need for informed content was exempted. This manuscript adhered to the applicable guidelines as presented in the Strengthening the Reporting of Observational Studies in Epidemiology statement.

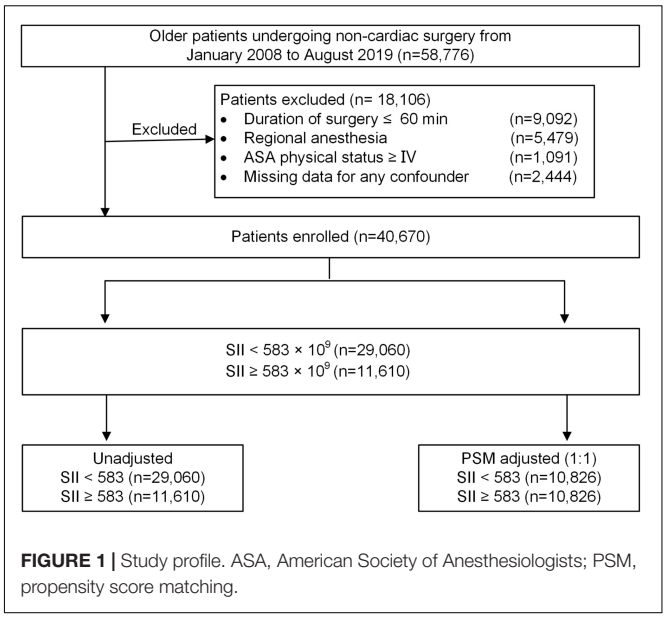

FIGURE 1 | Study profile. ASA, American Society of Anesthesiologists; PSM, propensity score matching.

Inclusion and Exclusion Criteria

Patients who underwent non-cardiac surgery between January 2008 and August 2019 at Chinese PLA General Hospital were initially screened from a perioperative retrospective database. The inclusion criteria were as follows: (1) aged 65 yr or older; (2) underwent non-cardiac surgery; (3) received general anesthesia; and (4) were with duration of surgery >60 min. Patients who presented with an American Society of Anesthesiologists (ASA) classification of ≥IV, were performed under regional anesthesia, or had missing clinical data were excluded. Among patients who underwent multiple surgeries during the study period, only the first eligible surgery was considered. A flow diagram of the patient selection process is displayed in **Figure 1**.

Clinical Outcome

The primary outcome of interest was perioperative ischemic stroke, defined as an episode of neurological dysfunction, such as motor, sensory, or cognitive dysfunction, caused by focal cerebral, spinal, or retinal infarction within 30 postoperative days (Sacco et al., 2013). Diagnoses of stroke are confirmed by a combination of neuroimaging and clinical evidence of cerebrovascular ischemia during hospital stay. In our study, perioperative ischemic stroke patients were identified if discharge records included at least 1 ICD-9-CM/ICD-10-CM diagnosis code for stroke (**Supplementary Table 1**).

Definition of Variables and Data Collection

Serum concentrations of preoperative peripheral platelet, neutrophil, and lymphocyte were the most recent blood counts measured within 3 days prior to surgery. The SII, NLR, and PLR were calculated as follows:

SII = platelet × neutrophil/lymphocyte, NLR = neutrophil/lymphocyte, PLR = platelet/lymphocyte. In order to visualize perioperative ischemic stroke in relation to SII, NLR, and PLR, parameters were grouped into high and low by the optimal cut-off points using the receiver operating characteristic curve (ROC).

The exposure of interest was preoperative SII. Result from the ROC analysis indicated that the optimal cut-off value for the SII was set at 583×10^9 for predicting perioperative ischemic stroke. Consequently, the SII was stratified into low ($< 583 \times 10^9$) and high ($\geq 583 \times 10^9$) for subsequent analyses.

Preoperative covariates of interest, such as age, sex, body mass index (BMI), ASA classification, hypertension, diabetes mellitus, prior ischemic stroke, coronary heart disease, arterial fibrillation, peripheral vascular disease, renal dysfunction, and preoperative use of β-blockers or aspirin, were noted. The indices derived from the preoperative laboratory data, including hemoglobin, albumin, total bilirubin, prothrombin time, were defined as the most recent blood counts measured within 3 days prior to surgery. In addition, we collected surgical and anesthetic information, such as preoperative mean arterial pressure (MAP), surgical procedures, duration of procedures, estimated blood loss, intraoperative hypotension (MAP $\leq$ 65 mmHg), crystalloid or colloid infusion, blood product transfusion, non-steroid anti-inflammatory drugs (NSAIDs) use, glucocorticoid medication, cumulative opioid consumption, and volatile anesthetic use.

Propensity Score-Matched Analysis and Adjustment

Propensity score matching (PSM) was applied to address the potential residual confounding effect of the covariates such as demographic variables and clinical parameters, which would result in a biased outcome. The propensity score, a composite score, was computed based on the probability of patients having different levels of SII and derived from synthesized baseline parameters using the multivariate logistic regression model (Williamson and Forbes, 2014). After the propensity score generation, patients with SII $<$ 583 and SII $\geq$ 583 were randomly matched at a 1:1 ratio using the greedy nearest-neighbor matching approach (maximum caliper width, 0.1). Kernel density plots of the propensity scores were applied to examine the equivalence between the matched patients. The standardized mean difference (SMD) was reported and performed to evaluate the baseline differences between the two groups, where a value $<$ 0.1 indicated minor differences (Cheung et al., 2019).

Statistical Analysis

Data were statistically analyzed using IBM SPSS Statistics for Windows, version 26.0 (IBM, Corp.) and R statistical software (R version 4.0.5, R Foundation for Statistical Computing). Continuous variables were summarized as mean [standard deviation (SD)], or median [interquartile range (IQR)]. Categorical data were displayed as numbers and percentages. The NLR or PLR score was converted into a two-level categorical variable based on the ROC analysis. The SII was also evaluated as continuous variable. We applied an extended multivariate logistic regression model approach to evaluate the clinical effect of the SII on perioperative ischemic stroke. Based on the type of surgical procedure, we conducted sensitivity analysis by only including non-neurosurgical patients to test the robustness of our findings. Subsequently, we further analyzed subgroups to appraise the primary correlation between the SII and perioperative ischemic stroke according to age, sex, intraoperative hypotension, diabetes mellitus, and prior ischemic stroke (Selim, 2007). The comparison group in this study referred to patients with SII $<$ 583, unless stated otherwise. For all tests, statistical significance was inferred at a two-sided P-value $<$ 0.05.

RESULTS

Study Population

A total of 58,776 older patients who underwent non-cardiac surgery from January 2008 to August 2019 were enrolled in the study. **Figure 1** illustrates the flow diagram of patient selection. After applying the inclusion and exclusion criteria, 40,670 eligible patients remained in the analysis, with a median age of 70 years (IQR: 67, 74), of whom 18,334 (45.1%) were women. Among the patients, 14,811 (36.4%) underwent intra-abdominal surgery, 1,903 (4.7%) underwent neurosurgery; and 6,224 (15.3%) received blood product transfusion. The prevalence of intraoperative hypotension (MAP $\leq$ 65 mmHg) in the cohort was 45.1% (n = 18,349). Of the entire patient cohort, 237 (0.58%) experienced an ischemic stroke within 30 days after surgery. The stroke incidence was consistent with previously reported rates of 0.1–0.7% in patients who underwent non-cardiac surgery (Vasivej et al., 2016; Woo et al., 2021).

The median NLR, PLR, and SII values were 2.00 (IQR:1.49, 2.83), 120.5 (IQR:93.1, 159.0), and 413.0 (IQR:287.0, 626.5), respectively. Using the ROC analysis, NLR, PLR, and SII accurately predicted perioperative ischemic stroke, with area under curve of 0.599 (95% CI: 0.534–0.632), 0.560 (95% CI: 0.505–0.616), and 0.721 (95% CI: 0.673–0.758), respectively. The Youden index of NLR, PLR, and SII were 0.165, 0.129, and 0.184, respectively. The optimal cut-off points derived for NLR, PLR, and SII to predict perioperative ischemic stroke were 3, 119, and 583×10^9, respectively. The ROC curve of NLR, PLR, and SII for stroke risk classifier are shown in **Supplementary Figures 1–3**.

The patients were then grouped into low ($<$ 583, n = 29,060, 71.5%) and high ($\geq$ 583, n = 11,610, 28.5%) SII groups. The differences in baseline characteristics between the groups are presented in **Table 1**. Some baseline clinical characteristics in the study were relatively similar between the SII $<$ 583 and SII $\geq$ 583 groups. However, other characteristics, such as sex, ASA classification, preoperative hemoglobin level, surgical procedures, duration of procedures, estimated blood loss, intraoperative hypotension, colloid infusion, blood transfusion, and opioid analgesic medication, differed between the two groups. Patients with SII $\geq$ 583 had more cardiovascular and cerebrovascular comorbidities (hypertension, diabetes mellitus, prior ischemic stroke, coronary heart disease, and peripheral vascular disease) and higher long-term administration of β-blockers and aspirin, than did those with SII $<$ 583. Compared

TABLE 1 | Baseline characteristics of unadjusted sample and propensity score-matched sample (patients from 2008–2019).

Characteristic	Unadjusted sample (n = 40,670)				PSM adjusted (1:1) (n = 21,652)			
	SII < 583 (n = 29,060)	SII ≥ 583 (n = 11,610)	P-value	SMD	SII < 583 (n = 10,826)	SII ≥ 583 (n = 10,826)	P-value	SMD
Demographics								
Age, y†	70.0 (67.0,73.0)	70.0 (67.0,75.0)	0.126	0.152	70.0 (67.0,74.0)	70.0 (67.0,74.0)	0.556	0.004
Female (%) †	13651 (47.0)	4683 (40.3)	<0.001	0.134	4458 (41.2)	4427 (40.9)	0.679	0.006
BMI, kg/m^2†	24.5 (22.3,26.9)	23.7 (21.5,26.0)	0.089	0.233	24.0 (21.6,26.4)	23.8 (21.5,26.0)	0.136	0.097
ASA classification (%) †								
Class I	741 (2.5)	234 (2.0)	<0.001	0.197	261 (2.4)	230 (2.1)	0.356	0.022
Class II	22885 (78.8)	8255 (71.1)			7826 (72.3)	7793 (72.0)		
Class III	5434 (18.7)	3121 (26.9)			2739 (25.3)	2803 (25.9)		
Previous medical history								
Hypertension (%) †	10874 (37.4)	4685 (40.4)	<0.001	0.060	4211 (38.9)	4360 (40.3)	0.257	0.021
Diabetes mellitus (%) †	6096 (21.0)	2756 (23.7)	<0.001	0.066	2436 (22.5)	2554 (23.6)	0.178	0.076
Prior ischemic stroke (%) †	1552 (5.3)	847 (7.3)	<0.001	0.080	682 (6.3)	765 (7.1)	0.228	0.068
Coronary heart disease (%) †	2879 (9.9)	1231 (10.6)	0.037	0.023	1070 (9.9)	1146 (10.6)	0.093	0.023
Atrial fibrillation or VHD (%) †	454 (1.6)	202 (1.7)	0.215	0.014	165 (1.5)	180 (1.7)	0.447	0.011
Peripheral vascular disease (%) †	1996 (6.9)	892 (7.7)	0.004	0.031	811 (7.5)	802 (7.4)	0.836	0.003
Renal dysfunction (%) †*	338 (1.2)	234 (2.0)	<0.001	0.068	191 (1.8)	205 (1.9)	0.456	0.047
β-blockers medication (%) †	2051 (7.1)	999 (8.6)	<0.001	0.058	869 (8.2)	931 (8.6)	0.167	0.065
Aspirin medication (%) †	2553 (8.8)	1174 (10.1)	<0.001	0.045	1024 (9.5)	1086 (10.0)	0.293	0.043
Preoperative laboratory data								
Hemoglobin, g/L†	132.0 (122.0,142.0)	125.0 (111.0,138.0)	<0.001	0.437	128.0 (114.0,140.0)	127.0 (113.0,139.0)	0.156	0.083
Albumin, g/L†	40.3 (38.1,42.5)	40.5 (38.2,43.0)	0.223	0.481	38.9 (36.2,41.4)	38.8 (36.0,41.7)	0.837	0.005
Total bilirubin, μmol/L†	10.9 (8.4,14.2)	10.6 (7.8,15.6)	<0.001	0.291	10.7 (8.3,14.6)	10.6 (7.7,14.9)	0.202	0.093
Prothrombin time, s†	13.1 (12.6,13.6)	13.2 (12.7,13.9)	0.123	0.176	13.2 (12.7,13.8)	13.2 (12.7,13.8)	0.600	0.028
Surgical and anesthetic factors								
Preoperative MAP, mmHg	95.7 (88.7,103.0)	95.0 (87.3,102.3)	0.098	0.070	95.0 (87.3,102.3)	95.0 (88.0,102.7)	0.169	0.024
Surgical procedures (%)								
Trauma surgery	433 (1.5)	602 (5.2)	<0.001	0.352	404 (3.7)	353 (3.3)		
Spine	2751 (9.5)	715 (6.2)			758 (7.0)	711 (6.6)	0.258	0.041
Intra-abdominal surgery	9652 (33.2)	5159 (44.4)			4688 (43.3)	4690 (43.3)		
Joint arthroplasty	3726 (12.8)	1031 (8.9)			987 (9.1)	1027 (9.5)		
Urologic or gynecologic	3972 (13.7)	1219 (10.5)			1138 (10.6)	1209 (11.1)		
Neurosurgery	1380 (4.7)	523 (4.5)			516 (4.8)	515 (4.8)		
Thoracic or vascular	3362 (11.6)	1225 (10.5)			1172 (10.8)	1199 (11.1)		
Other (plastic surgery, etc.)	3784 (13.0)	1136 (9.8)			1163 (10.7)	1122 (10.3)		
Duration of procedures, min	155.0 (110.0,215.0)	170.0 (120.0.0,235.0)	<0.001	0.162	168.0 (118.0,231.0)	170.0 (120.0,235.0)	0.356	0.076
Estimated blood loss, mL	100.0 (50.0,200.0)	150.0 (50.0,300.0)	<0.001	0.083	140.0 (90.0,280.0)	145.7 (100.0,300.0)	0.167	0.096
MAP ≤ 65 mmHg (%)	12600 (43.4)	5749 (49.5)	<0.001	0.070	5125 (47.3)	5285 (48.8)	0.234	0.072
Crystalloid infusion, ml/kg/h	8.6 (6.5,11.4)	8.9 (6.6,11.8)	0.167	0.073	8.8 (6.6,11.7)	8.8 (6.5,11.7)	0.845	0.006
Colloid infusion, ml/kg/h	2.9 (1.3,4.3)	3.1 (1.8,4.5)	<0.001	0.123	3.0 (1.6,4.4)	3.0 (1.8,4.5)	0.111	0.066
Blood transfusion (%)	3902 (13.4)	2322 (20.0)	<0.001	0.177	1998 (18.5)	2082 (19.2)	0.189	0.052
NSAIDs (%)	20502 (70.6)	8366 (72.1)	0.003	0.033	7667 (70.8)	7709 (71.2)	0.539	0.009
Glucocorticoid (%)	23749 (81.7)	9557 (82.3)	0.165	0.015	8905 (82.3)	8932 (82.5)	0.643	0.007
Opioid dose, mg‡	120.0 (9.0,150.0)	135.0 (105.0,165.0)	<0.001	0.081	135.0 (100.0,150.0)	135.0 (105.0,165.0)	0.256	0.047
Volatile anesthetic (%)	27098 (93.2)	10819 (93.2)	0.840	0.002	10097 (93.3)	10110 (93.4)	0.744	0.005
Preoperative NLR								
<3	27796 (95.7)	4098 (35.3)	<0.001	1.643	10215 (94.4)	3951 (36.5)	<0.001	1.583
≥3	1264 (4.3)	7512 (64.7)			611 (5.6)	6875 (63.5)		
Preoperative PLR								
<119	18897 (65.0)	959 (8.3)	<0.001	1.458	6821 (63.0)	914 (8.4)	<0.001	1.385
≥119	10163 (35.0)	10651 (91.7)			4005 (37.0)	9912 (91.6)		
Perioperative ischemic stroke (%)	126 (0.434)	111 (0.956)	<0.001	0.856	49 (0.453)	107 (0.988)	<0.001	0.939

The data are presented as the median (inter-quartile range), mean (standard deviation) or n (%).

**Creatinine > 177 μm/l.*

†*Variables included in the propensity score.*

‡*Including those prescribed intraoperatively and postoperatively (until 7 days after surgery).*

SII, systemic-immune-inflammation index; PSM, propensity score matching; SMD, standardized mean difference; BMI, body mass index; ASA, American Society of Anesthesiologists; VHD, valvular heart disease; MAP, mean arterial pressure; NSAIDs, non-steroid anti-inflammatory drugs; NLR, neutrophil-lymphocyte ratio; PLR, platelet-to-lymphocyte ratio.

to patients with SII < 583, those with SII ≥ 583 had higher preoperative NLR and PLR scores.

Primary Analysis: Correlation Between SII and Perioperative Ischemic Stroke

We initially evaluated the association between the SII as continuous variable and perioperative ischemic stroke using univariate and multivariate logistic analyses. The univariate analysis showed that the SII was associated with perioperative ischemic stroke [odds ratio (OR): 1.285; 95% confidence interval (CI): 1.174–1.542; $P < 0.001$]. In the multivariate logistic regression model, the adjusted OR of SII was 1.213 (95% CI: 1.169–1.468; $P < 0.001$). The SII as continuous variable was an independent predictor of perioperative ischemic stroke (**Supplementary Table 2**).

When investigating the prognostic values of SII as categorical variable, the results of our univariate analysis revealed that age, hypertension, diabetes mellitus, prior ischemic stroke, coronary heart disease, arterial fibrillation, peripheral vascular disease, β-blockers use, aspirin medication, preoperative MAP, surgical procedures, duration of procedures, estimated blood loss, intraoperative hypotension (MAP ≤ 65 mmHg), crystalloid infusion, NSAIDs use, NLR, PLR, and SII were prognostic factors for perioperative ischemic stroke, whereas sex, BMI, ASA classification, renal dysfunction, preoperative laboratory data (hemoglobin, albumin, total bilirubin, and prothrombin time), colloid infusion, blood product transfusion, glucocorticoid use, opioid analgesic medication, and volatile anesthetic use had no prognostic significance (**Supplementary Table 3**). An elevated SII was strongly associated with an increased risk of perioperative ischemic stroke in the unadjusted analysis [OR: 2.217; 95% (CI): 1.714–2.863; $P < 0.001$] (**Table 2**).

Based on the extended multivariate logistic regression models (**Table 2**), patients with SII ≥ 583 showed a significantly higher OR of perioperative ischemic stroke in all three models consistently (OR range: 1.843–2.301, $P < 0.001$ for all) (**Table 2**). The NLR, but not PLR, was also an independent predictor of perioperative ischemic stroke in the adjusted analysis (OR: 1.036; 95% CI: 1.007–1.062; $P = 0.007$) (**Supplementary Table 3**). The other independent risk factors for predicting perioperative ischemic stroke are shown in **Supplementary Table 3**.

Propensity Score-Matched Analysis and Adjustment

Then, we performed PSM analysis to assess the prognostic value of the SII further. Prior to matching, the median propensity score in older patients with SII ≥ 583 was 0.266 (IQR: 0.203–0.377) vs. 0.231 (IQR: 0.194–0.346) in those without SII < 583. PSM resulted in 10,826 patients in the SII ≥ 583 group matched to 10,826 patients in the SII < 583 group. The distribution of propensity scores in the high and low SII groups is graphically illustrated before and after matching (**Figure 2**). After matching, the mean (SD) propensity score was similar between those with high [0.314 (0.127)] and low [0.318 (0.121)] SII. The baseline demographic and clinical characteristics of the variables were generally well balanced between the two groups, with SMD less than 0.10 for all covariates (**Table 1**). Following multivariate logistic regression adjustment after PSM (n = 10,826), the correlation between SII and perioperative ischemic stroke remained significantly robust (OR: 2.195; 95% CI: 1.574–3.106; $P < 0.001$) (**Table 2** and **Supplementary Table 4**).

TABLE 2 | Association between SII and perioperative ischemic stroke using the logistic regression model and propensity score analysis.

Analysis method	OR	95% CI	*P*-value
Logistic regression analysis (*n* = 40,670)			
Model 1 (univariate model)*	2.217	1.714–2.863	<0.001
Model 2 (preoperative patient-related covariates adjusted)†	1.887	1.404–2.534	<0.001
Model 3 (Surgical and anesthetic covariates adjusted) ‡	2.301	1.768–2.989	<0.001
Model 4 (fully adjusted)‖	1.843	1.369–2.480	<0.001
Propensity score analysis (multivariate)			
Model PSM (*n* = 10,826)¶	2.195	1.574–3.106	<0.001

SII, systemic-immune-inflammation index; OR, odds ratio; CI, confidence interval; PSM, propensity score matching.

**Model 1 was a univariate regression model.*

†Model 2 included preoperative SII, age, female sex, BMI, ASA classification, hypertension, diabetes mellitus; prior ischemic stroke, coronary heart disease, arterial fibrillation, peripheral vascular disease, renal dysfunction, βblockers medication, aspirin medication, preoperative laboratory data (hemoglobin, albumin, total bilirubin, prothrombin time), preoperative NLR, preoperative PLR.

‡Model 3 included preoperative SII, preoperative MAP, surgical procedures, duration of procedures, estimated blood loss, MAP ≤ 65 mmHg, crystalloids infusion, colloids infusion, blood transfusion, NSAIDs, glucocorticoid, opioid dose, volatile anesthetic.

*‖Model 4 included all the variables. Univariate and multivariate results are showed in **Supplementary Table 3**.*

*¶10,826 pairs were matched using propensity score method. Univariate and multivariate results are showed in **Supplementary Table 4**.*

Sensitivity Analysis

The incidence of perioperative ischemic stroke is closely associated with the type and complexity of surgical procedures (Selim, 2007). The surgical procedures with the incidence of perioperative ischemic stroke at Chinese PLA General Hospital are shown in **Figure 3**. The surgical categories with highest overall incidence of perioperative ischemic stroke were neurosurgery (3.153%), followed by spine surgery (0.837%) and joint arthroplasty (0.631%). To further test the robustness of our results, we performed a sensitivity analysis excluding neurosurgeries. The adjusted OR of perioperative ischemic stroke in neurosurgical patients with the SII was 2.297 (95% CI: 1.192–4.429; $P = 0.013$). The association between preoperative SII and perioperative ischemic stroke remained stable in those non-neurosurgical patients (OR: 1.691; 95% CI: 1.202–2.376; $P < 0.002$) (**Table 3**).

Subgroup Analyses

Among 11,610 older patients with SII ≥ 583, 925 (8.0%) were aged ≥ 80 years, 4,683 (40.3%) were female, 5,749 (49.5%) had a duration of intraoperative hypotension (MAP ≤ 65 mmHg) ≥ 10 min, 8,854 (23.7%) presented with diabetes mellitus, and 847 (7.3%) had prior ischemic stroke. The subgroup analyses for the prediction of a poor neurological outcome were summarized according to age, sex,

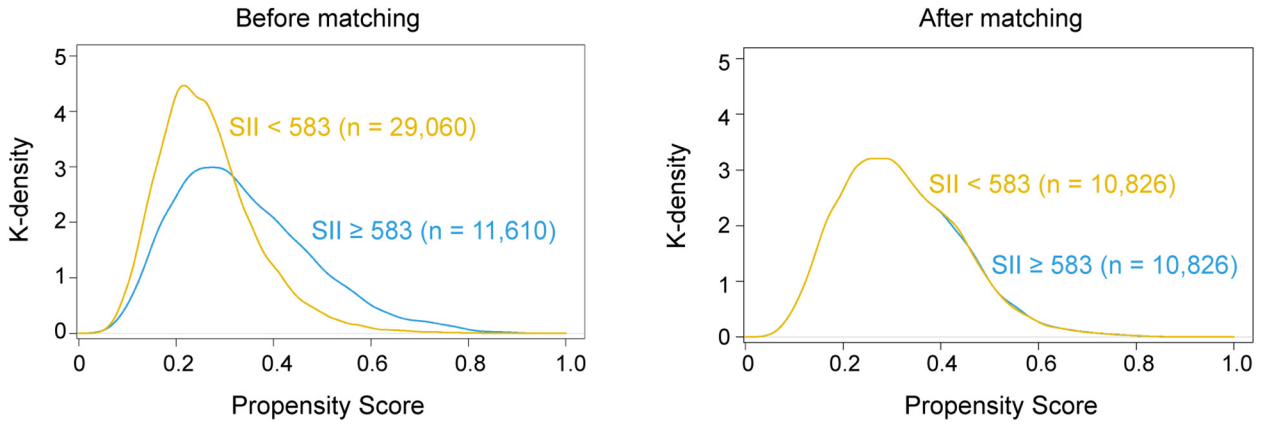

FIGURE 2 | Distribution of propensity scores before and after matching.

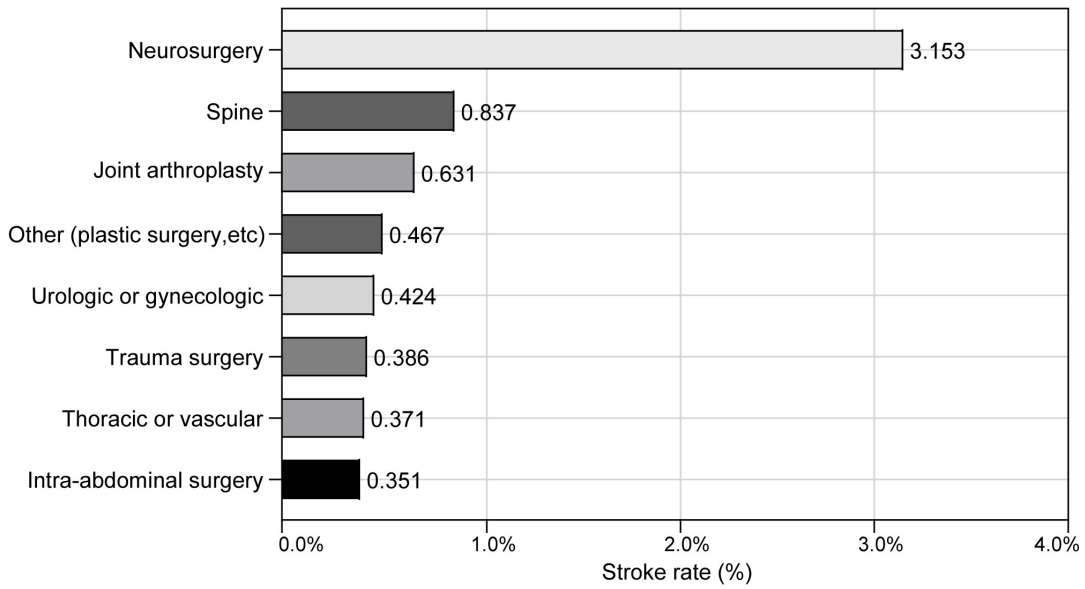

FIGURE 3 | Incidence of perioperative ischemic stroke among the different surgical procedures.

intraoperative hypotension, diabetes mellitus, and prior ischemic stroke (**Figure 4**). The OR of the SII was significant for age subgroups [≥ 80 years: OR (95% CI): 4.368 (1.127–6.508), $P = 0.036$; < 80 years: OR (95% CI): 1.766 (1.298–2.401), $P < 0.001$]. Additionally, an increased risk of perioperative ischemic stroke was observed in both male (OR: 1.900; 95% CI: 1.262–2.883; $P = 0.002$) and female (OR: 1.724; 95% CI: 1.109–2.655; $P = 0.014$). In patients with suboptimal intraoperative hypotension (duration of MAP ≤ 65 mmHg ≥ 10 min), the SII was significantly correlated with perioperative ischemic stroke (OR: 2.104; 95% CI: 1.382–2.184; $P < 0.001$). This increased risk was also significant in those with intraoperative hypotension (MAP duration ≤ 65 mmHg < 10 min). The correlation between preoperative SII and perioperative ischemic stroke was significant in individuals with (OR: 3.074; 95% CI: 1.765–5.404; $P < 0.001$) and without (OR: 1.520; 95% CI: 1.053–2.184; $P = 0.024$) diabetes. Additionally, an elevated SII was only significantly associated with an increased risk of perioperative ischemic stroke in the prior ischemic stroke group (OR: 2.678; 95% CI: 1.534–4.733; $P < 0.001$), whereas it was not significant in the no prior ischemic stroke group (OR: 1.440; 95% CI: 0.997–2.069; $P = 0.055$).

DISCUSSION

Using this cohort of 40,670 older elderly patients who had undergone non-cardiac surgery, we evaluated the prognostic value of inflammatory biomarkers or indices in predicting perioperative ischemic stroke. Our analysis indicated that preoperative elevated SII was substantially correlated with an increased risk of perioperative ischemic stroke. In addition, after adjustment, NLR, but not PLR, was an independent prognostic factor for perioperative ischemic stroke.

TABLE 3 | Sensitivity analysis of the association between SII and perioperative ischemic stroke (adjustment through multivariate logistic regression).

	SII < 583 and perioperative ischemic stroke cases, n	SII ≥ 583 and perioperative ischemic stroke cases, n	OR	95% CI	*P*-value
Entire cohort (*n* = 40,670; PIS = 237)	29,060 (126)	11,610 (111)	1.842	1.369–2.480	<0.001
Type of surgery					
Neurosurgery (*n* = 1,903; PIS = 60)	1,380 (28)	523 (32)	2.297	1.192–4.429	0.013
Non-neurosurgery (*n* = 38,767; PIS = 177)	27,680 (98)	11,087 (79)	1.691	1.202–2.376	0.002

SII, systemic-immune-inflammation index; OR, odds ratio; CI, confidence interval; PIS, perioperative ischemic stroke.

Extensive evidence has shown that the disruption of immune state homeostasis and inflammation are closely interrelated with the occurrence and progression of various diseases. In particular, immune checkpoint inhibitors have been approved to treat several cancers (Johansson et al., 2016). As such, the potential predictive values of inflammation-related biomarkers or inflammation-based scores have been exploited to improve diagnostic precision and predict disease progression. Given their easy accessibility, appropriate cost-effectiveness, and universal applicability, the NLR, PLR, and SII deserve more attention. Previous studies have indicated that the NLR is a significant independent risk factor for tumorigenesis, tumor invasion, and metastasis (Mantovani et al., 2008; Gukovsky et al., 2013). In addition, PLR was significantly correlated with adverse postoperative outcomes, including death, and cardiovascular and cerebrovascular events in cardiac or non-cardiac surgeries (De Giorgi et al., 2019; Dey et al., 2021). The SII was developed based on a combination of inflammatory cells (neutrophils and lymphocytes) and thrombotic factor (platelets). A high SII independently predicted recurrence and mortality in patients with pancreatic cancer or gastroesophageal adenocarcinoma (Aziz et al., 2019; Jomrich et al., 2021). Additionally, the association of elevated SII ($> 694.3 \times 10^9$) with postoperative major adverse cardiovascular events was elucidated in individuals with coronary heart disease (Yang et al., 2020). An increased SII ($\geq 455.6 \times 10^9$) also showed significant prognostic value for predicting all-cause mortality and major postoperative complications in patients undergoing isolated tricuspid valve surgery (Yoon et al., 2021).

Utilizing biomarkers to stratify high-risk patients and predict perioperative ischemic stroke remains an elusive and major challenge in clinical decision-making. For instance, in this

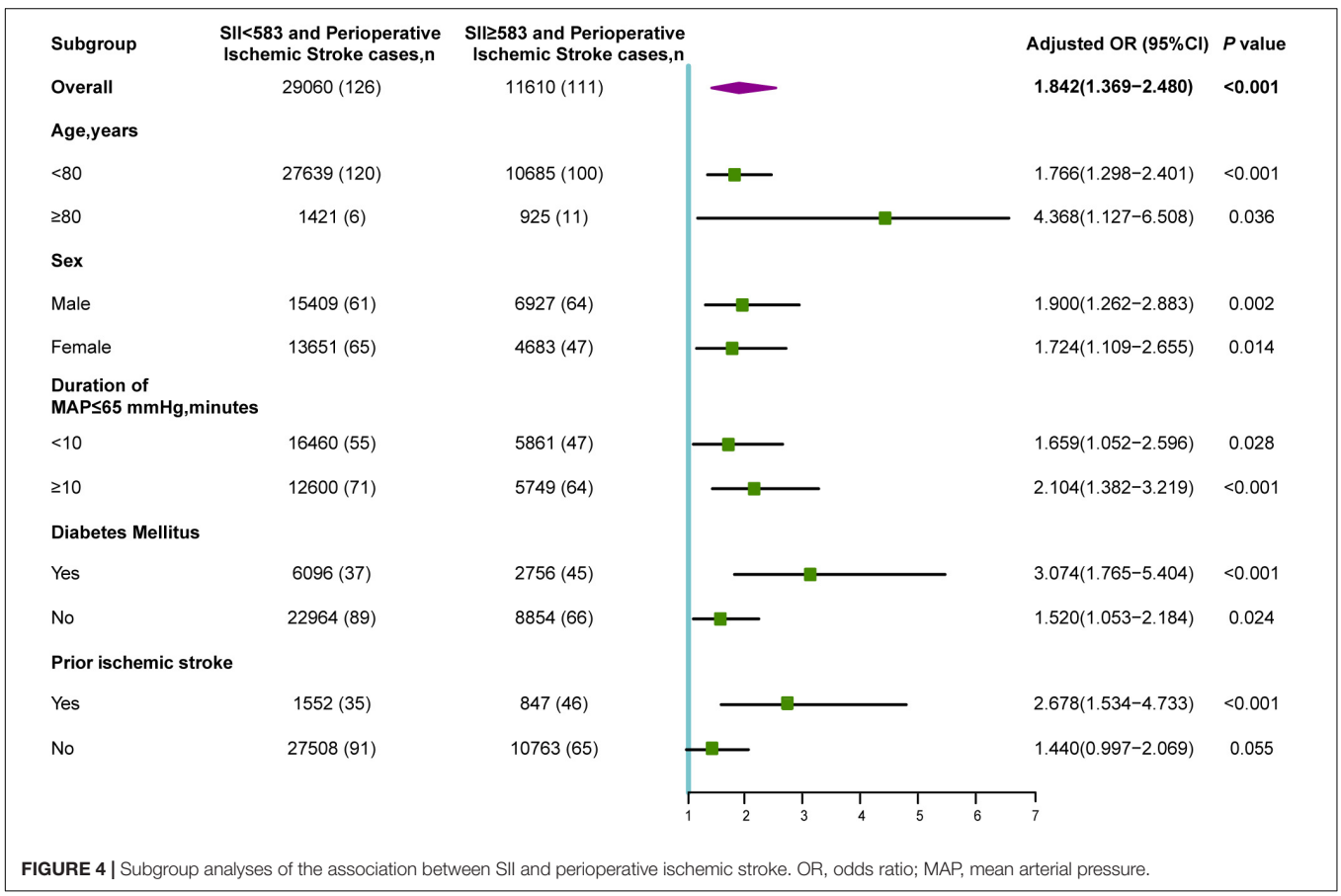

FIGURE 4 | Subgroup analyses of the association between SII and perioperative ischemic stroke. OR, odds ratio; MAP, mean arterial pressure.

study, PLR did not exhibit significant predictive values in older patients undergoing non-cardiac surgery, whereas NLR appeared to be a relatively weak risk factor. Consistent with prior studies, the predictive values of NLR and PLR remained inconsistent and controversial (Li et al., 2020; Yoon et al., 2021). However, we demonstrated that the preoperative elevated SII exhibited a favorable prognostic value for perioperative ischemic stroke in the univariate and extended multivariate logistic regression models. The SII maintained a good prognostic value in neurosurgical and non-neurosurgical patients, indicating the reliability of the prognostic ability in different surgical populations. Going further, we revealed that preoperative increased SII was a potential risk indicator for increased risk of perioperative ischemic stroke in non-cardiac surgery patients, particularly in patients $\geq$ 80 years of age, male, with intraoperative hypotension, with diabetes, and with prior ischemic stroke. These results implied that the preoperative SII might potentially emerge as a simple, promising, and useful prognostic biomarker for perioperative ischemic stroke prediction in older patients who underwent non-cardiac surgery. In particular, preoperative SII showed broader applicability as a useful prognostic indicator due to the easy accessibility and appropriate cost-effectiveness.

Several possible explanations may account for the association between preoperative SII and perioperative ischemic stroke. Elevated SII was most often observed in patients with neutrophilia, lymphopenia and thrombocythemia, indicating an integration of compromised innate responses and aberrant adaptive immune responses. Moreover, immune-mediated brain damage has gained increasing attention and recognition. Accumulating evidence indicates a critical role of neuroinflammation in the pathogenesis of perioperative ischemic stroke and secondary brain injury.

The aggregation and migration of neutrophils are closely involved in ischemic brain damage, disruption of blood-brain barrier integrity, and functional recovery after stroke (Shi et al., 2020). Activated neutrophils can also damage vascular endothelial cells and brain tissues by releasing toxic reactive oxygen species and proteases such as matrix metalloproteinase-9, resulting in acute neuroinflammation (Prasad et al., 2011). Thrombocytosis is correlated with inflammatory conditions in patients with thromboembolism (Boyle et al., 2013). Initial platelet plug formation, agglutination and platelet thromboinflammatory responses are important for blood clotting, systemic inflammatory reactions, and endothelial reorganization (Sprague et al., 2008; Chan et al., 2015; Telen, 2016). In contrast, lymphopenia may lead to the temporary suspension of some mechanisms, which normally maintain the balance between host tolerance and host defense (Baker et al., 2017). In addition, neutrophil-platelet interactions play a role in modulating the function of these cells and precipitating vascular inflammation (von Brühl et al., 2012; Kim et al., 2015). Furthermore, perioperative factors, including surgery and general anesthesia, may amplify the risk of preoperative aberrant innate and adaptive immune states, particularly in older surgical patients. In this context, in our study, the preoperative SII may be even more promising as a predictive biomarker than NLR and PLR, due to the combined effect of neutrophil, lymphocyte, and platelet counts.

This cohort study has several strengths. First, to our knowledge, no previous studies have assessed the prognostic value of preoperative SII in older patients undergoing non-cardiac surgery. Second, considering the low incidence of perioperative ischemic stroke, we attempted to incorporate as many patients as possible and finally included 40,670 eligible patients in our study. Third, we used the PSM analysis adjusted for several potentially confounding variables, including patient demographics, preoperative medical history, and preoperative laboratory data. Fourth, multiple statistical approaches, such as sensitivity and subgroup analyses, were successfully performed to confirm that the preoperative SII qualifies as a promising, independent prognostic indicator of perioperative ischemic stroke in older patients undergoing non-cardiac surgery.

This study has several inevitable limitations that warrant acknowledgement. First, owing to its observational nature, we could only demonstrate associations but not causality. Thus, prospective and properly designed studies are urgently needed to confirm and validate the cause-and-effect relationship between preoperative SII and perioperative ischemic stroke in older patients. Second, our study is a single-center design, which limits its generalizability. Thus, our findings are hypothesis-generating, and further external validation of our results is important before generalizing the SII in clinical use. Third, since high-sensitivity CRP and procalcitonin are not routinely tested in clinical settings, we did not include these two inflammatory biomarkers, which may have introduced bias. Fourth, although we carefully adjusted for a multitude of potential confounders, residual confounding and unmeasured factors cannot be entirely ruled out.

CONCLUSION

In conclusion, the preoperative SII was an independent prognostic factor in older patients undergoing non-cardiac surgery. The SII components are routinely collected in the clinical settings, thus the SII qualifies as a novel, promising prognostic index after corroboration by subsequent larger studies. Our findings highlight the clinical importance of inflammation-based markers and the essential role of the immune system in perioperative ischemic stroke. Nevertheless, the SII requires more properly designed studies to validate its prognostic value in older patients undergoing non-cardiac surgery.

DATA AVAILABILITY STATEMENT

The original contributions presented in the study are included in the article/**Supplementary Material**, further inquiries can be directed to the corresponding author/s.

ETHICS STATEMENT

The studies involving human participants were reviewed and approved by the Medical Ethics Committee of Chinese PLA

General Hospital. The ethics committee waived the requirement of written informed consent for participation.

AUTHOR CONTRIBUTIONS

JL and YM: conception and design. FZ, MN, and LW: development of methodology. FZ and JC: acquisition of data. MN and LS: analysis and interpretation of data. WM and YL: supervise the study. FZ, MN, LW, JL, and YM: drafting, review, and revision of the manuscript. All authors approved the final manuscript.

FUNDING

This work was supported by the National Key Research and Development Program of China (2018YFC2001901), the Capital Health Research and Development of Special (2022-4-5025), and the National Natural Science Foundation of China (82171464).

ACKNOWLEDGMENTS

We would like to thank Lan Sun and Wei Wei of Hangzhou Le9 Healthcare Technology Co., Ltd., for help in the clinical data collection of this study.

SUPPLEMENTARY MATERIAL

The Supplementary Material for this article can be found online at: https://www.frontiersin.org/articles/10.3389/fnagi.2022.865244/full#supplementary-material

REFERENCES

Aziz, M. H., Sideras, K., Aziz, N. A., Mauff, K., Haen, R., Roos, D., et al. (2019). The Systemic-immune-inflammation Index Independently Predicts Survival and Recurrence in Resectable Pancreatic Cancer and its Prognostic Value Depends on Bilirubin Levels: A Retrospective Multicenter Cohort Study. *Annal. Surgery* 270, 139–146. doi: 10.1097/SLA.0000000000002660

Baker, D., Herrod, S. S., Alvarez-Gonzalez, C., Giovannoni, G., and Schmierer, K. (2017). Interpreting Lymphocyte Reconstitution Data From the Pivotal Phase 3 Trials of Alemtuzumab. *JAMA Neurol* 74, 961–969. doi: 10.1001/jamaneurol.2017.0676

Boyle, S., White, R. H., Brunson, A., and Wun, T. (2013). Splenectomy and the incidence of venous thromboembolism and sepsis in patients with immune thrombocytopenia. *Blood* 121, 4782–4790. doi: 10.1182/blood-2012-12-467068

Chan, L. W., Wang, X., Wei, H., Pozzo, L. D., White, N. J., and Pun, S. H. (2015). A synthetic fibrin cross-linking polymer for modulating clot properties and inducing hemostasis. *Sci. Transl. Med.* 7:277ra29. doi: 10.1126/scitranslmed.3010383

Cheung, K. S., Chan, E. W., Chen, L., Seto, W. K., Wong, I. C. K., and Leung, W. K. (2019). Diabetes Increases Risk of Gastric Cancer After Eradication: A Territory-Wide Study With Propensity Score Analysis. *Diabetes Care* 42, 1769–1775. doi: 10.2337/dc19-0437

De Giorgi, U., Procopio, G., Giannarelli, D., Sabbatini, R., Bearz, A., Buti, S., et al. (2019). Association of Systemic Inflammation Index and Body Mass Index with Survival in Patients with Renal Cell Cancer Treated with Nivolumab. *Clin. Cancer Res.* 25, 3839–3846. doi: 10.1158/1078-0432.CCR-18-3661

Dey, S., Kashav, R., Kohli, J. K., Magoon, R., ItiShri, Walian, A., et al. (2021). Systemic Immune-Inflammation Index Predicts Poor Outcome After Elective Off-Pump CABG: A Retrospective, Single-Center Study. *J. Cardiothor. Vascular Anesthes.* 35, 2397–2404. doi: 10.1053/j.jvca.2020.09.092

Ettinger, M., Calliess, T., Kielstein, J. T., Sibai, J., Brückner, T., Lichtinghagen, R., et al. (2015). Circulating biomarkers for discrimination between aseptic joint failure, low-grade infection, and high-grade septic failure. *Clin. Infect Dis.* 61, 332–341. doi: 10.1093/cid/civ286

Fragiadakis, G. K., Gaudillière, B., Ganio, E. A., Aghaeepour, N., Tingle, M., Nolan, G. P., et al. (2015). Patient-specific Immune States before Surgery Are Strong Correlates of Surgical Recovery. *Anesthesiology* 123, 1241–1255. doi: 10.1097/aln.0000000000000887

Gukovsky, I., Li, N., Todoric, J., Gukovskaya, A., and Karin, M. (2013). Inflammation, autophagy, and obesity: common features in the pathogenesis of pancreatitis and pancreatic cancer. *Gastroenterology* 144, 1199–209.e4. doi: 10.1053/j.gastro.2013.02.007

Handforth, C., Clegg, A., Young, C., Simpkins, S., Seymour, M. T., Selby, P. J., et al. (2015). The prevalence and outcomes of frailty in older cancer patients: a systematic review. *Ann. Oncol.* 26, 1091–1101. doi: 10.1093/annonc/mdu540

Hu, B., Yang, X. R., Xu, Y., Sun, Y. F., Sun, C., Guo, W., et al. (2014). Systemic immune-inflammation index predicts prognosis of patients after curative resection for hepatocellular carcinoma. *Clin. Cancer Res.* 20, 6212–6222. doi: 10.1158/1078-0432.Ccr-14-0442

Johansson, H., Andersson, R., Bauden, M., Hammes, S., Holdenrieder, S., and Ansari, D. (2016). Immune checkpoint therapy for pancreatic cancer. *World J. Gastroenterol.* 22, 9457–9476. doi: 10.3748/wjg.v22.i43.9457

Jomrich, G., Paireder, M., Kristo, I., Baierl, A., Ilhan-Mutlu, A., Preusser, M., et al. (2021). High Systemic Immune-Inflammation Index is an Adverse Prognostic Factor for Patients With Gastroesophageal Adenocarcinoma. *Ann. Surgery* 273, 532–541. doi: 10.1097/SLA.0000000000003370

Kim, K., Li, J., Tseng, A., Andrews, R. K., and Cho, J. (2015). NOX2 is critical for heterotypic neutrophil-platelet interactions during vascular inflammation. *Blood* 126, 1952–1964. doi: 10.1182/blood-2014-10-605261

Li, Z., Li, S., Ying, X., Zhang, L., Shan, F., Jia, Y., et al. (2020). The clinical value and usage of inflammatory and nutritional markers in survival prediction for gastric cancer patients with neoadjuvant chemotherapy and D2 lymphadenectomy. *Gastric Cancer* 23, 540–549. doi: 10.1007/s10120-019-01027-6

Macrez, R., Ali, C., Toutirais, O., Le Mauff, B., Defer, G., Dirnagl, U., et al. (2011). Stroke and the immune system: from pathophysiology to new therapeutic strategies. *Lancet Neurol* 10, 471–480. doi: 10.1016/s1474-4422(11)70066-7

Mantovani, A., Allavena, P., Sica, A., and Balkwill, F. (2008). Cancer-related inflammation. *Nature* 454, 436–444. doi: 10.1038/nature07205

Mao, L., Li, P., Zhu, W., Cai, W., Liu, Z., Wang, Y., et al. (2017). Regulatory T cells ameliorate tissue plasminogen activator-induced brain haemorrhage after stroke. *Brain* 140, 1914–1931. doi: 10.1093/brain/awx111

Marcantonio, E. R. (2017). Delirium in Hospitalized Older Adults. *N. Engl. J. Med.* 377, 1456–1466. doi: 10.1056/NEJMcp1605501

Mracsko, E., Liesz, A., Stojanovic, A., Lou, W. P.-K., Osswald, M., Zhou, W., et al. (2014). Antigen dependently activated cluster of differentiation 8-positive T cells cause perforin-mediated neurotoxicity in experimental stroke. *J. Neurosci.* 34, 16784–16795. doi: 10.1523/JNEUROSCI.1867-14.2014

Nøst, T. H., Alcala, K., Urbarova, I., Byrne, K. S., Guida, F., Sandanger, T. M., et al. (2021). Systemic inflammation markers and cancer incidence in the UK Biobank. *Eur. J. Epidemiol.* 36, 841–848. doi: 10.1007/s10654-021-00752-6

Prasad, A., Jia, Y., Chakraborty, A., Li, Y., Jain, S. K., Zhong, J., et al. (2011). Inositol hexakisphosphate kinase 1 regulates neutrophil function in innate immunity by inhibiting phosphatidylinositol-(3,4,5)-trisphosphate signaling. *Nat. Immunol.* 12, 752–760. doi: 10.1038/ni.2052

Redecha, P., Tilley, R., Tencati, M., Salmon, J. E., Kirchhofer, D., Mackman, N., et al. (2007). Tissue factor: a link between C5a and neutrophil activation in antiphospholipid antibody induced fetal injury. *Blood* 110, 2423–2431. doi: 10.1182/blood-2007-01-070631

Sacco, R. L., Kasner, S. E., Broderick, J. P., Caplan, L. R., Connors, J. J., Culebras, A., et al. (2013). An updated definition of stroke for the 21st century: a statement

for healthcare professionals from the American Heart Association/American Stroke Association. *Stroke* 44, 2064–2089. doi: 10.1161/STR.0b013e318296aeca

Selim, M. (2007). Perioperative stroke. *N. Engl. J. Med.* 356, 706–713. doi: 10.1056/NEJMra062668

Shi, K., Zou, M., Jia, D., Shi, S., Yang, X., Liu, Q., et al. (2020). tPA Mobilizes Immune Cells that Exacerbate Hemorrhagic Transformation in Stroke. *Circ. Res.* 128, 62–75. doi: 10.1161/circresaha.120.317596

Sprague, D. L., Elzey, B. D., Crist, S. A., Waldschmidt, T. J., Jensen, R. J., and Ratliff, T. L. (2008). Platelet-mediated modulation of adaptive immunity: unique delivery of CD154 signal by platelet-derived membrane vesicles. *Blood* 111, 5028–5036. doi: 10.1182/blood-2007-06-097410

Telen, M. J. (2016). Beyond hydroxyurea: new and old drugs in the pipeline for sickle cell disease. *Blood* 127, 810–819. doi: 10.1182/blood-2015-09-618553

Vasivej, T., Sathirapanya, P., and Kongkamol, C. (2016). Incidence and Risk Factors of Perioperative Stroke in Noncardiac, and Nonaortic and Its Major Branches Surgery. *J. Stroke Cerebrovas. Dis.* 25, 1172–1176. doi: 10.1016/j.jstrokecerebrovasdis.2016.01.051

von Brühl, M. L., Stark, K., Steinhart, A., Chandraratne, S., Konrad, I., Lorenz, M., et al. (2012). Monocytes, neutrophils, and platelets cooperate to initiate and propagate venous thrombosis in mice in vivo. *J. Exp. Med.* 209, 819–835. doi: 10.1084/jem.20112322

Williamson, E. J., and Forbes, A. (2014). Introduction to propensity scores. *Respirology* 19, 625–635. doi: 10.1111/resp.12312

Woo, S. H., Marhefka, G. D., Cowan, S. W., and Ackermann, L. (2021). Development and Validation of a Prediction Model for Stroke, Cardiac, and Mortality Risk After Non-Cardiac Surgery. *J. Am. Heart Assoc.* 10:e018013. doi: 10.1161/jaha.120.018013

Yang, Y. L., Wu, C. H., Hsu, P. F., Chen, S. C., Huang, S. S., Chan, W. L., et al. (2020). Systemic immune-inflammation index (SII) predicted clinical outcome in patients with coronary artery disease. *Eur. J. Clin. Invest* 50:e13230. doi: 10.1111/eci.13230

Yoon, J., Jung, J., Ahn, Y., and Oh, J. (2021). Systemic Immune-Inflammation Index Predicted Short-Term Outcomes in Patients Undergoing Isolated Tricuspid Valve Surgery. *J. Clin. Med.* 10:4147. doi: 10.3390/jcm10184147

Zhang, F., Ma, Y., Yu, Y., Sun, M., Li, H., Lou, J., et al. (2022). Type 2 Diabetes Increases Risk of Unfavorable Survival Outcome for Postoperative Ischemic Stroke in Patients Who Underwent Non-cardiac Surgery: A Retrospective Cohort Study. *Front. Aging Neurosci.* 13:810050. doi: 10.3389/fnagi.2021.810050

Conflict of Interest: The authors declare that the research was conducted in the absence of any commercial or financial relationships that could be construed as a potential conflict of interest.

Publisher's Note: All claims expressed in this article are solely those of the authors and do not necessarily represent those of their affiliated organizations, or those of the publisher, the editors and the reviewers. Any product that may be evaluated in this article, or claim that may be made by its manufacturer, is not guaranteed or endorsed by the publisher.

frontiers | Frontiers in Aging Neuroscience

TYPE Correction
PUBLISHED 08 December 2022
DOI 10.3389/fnagi.2022.1101574

OPEN ACCESS

EDITED AND REVIEWED BY
Yujie Chen,
Army Medical University, China

*CORRESPONDENCE
Yulong Ma
yulongma123@163.com
Jing Liu
liuj301@163.com

†These authors have contributed equally to this work

SPECIALTY SECTION
This article was submitted to Neuroinflammation and Neuropathy, a section of the journal Frontiers in Aging Neuroscience

RECEIVED 18 November 2022
ACCEPTED 28 November 2022
PUBLISHED 08 December 2022

CITATION
Zhang F, Niu M, Wang L, Liu Y, Shi L, Cao J, Mi W, Ma Y and Liu J (2022) Corrigendum: Systemic-immune-inflammation index as a promising biomarker for predicting perioperative ischemic stroke in older patients who underwent non-cardiac surgery. *Front. Aging Neurosci.* 14:1101574. doi: 10.3389/fnagi.2022.1101574

Corrigendum: Systemic-immune-inflammation index as a promising biomarker for predicting perioperative ischemic stroke in older patients who underwent non-cardiac surgery

Faqiang Zhang[1†], Mu Niu[2†], Long Wang[3†], Yanhong Liu[1], Likai Shi[1], Jiangbei Cao[1], Weidong Mi[1], Yulong Ma[1*] and Jing Liu[1*]

[1]Anesthesia and Operation Center, The First Medical Center, Chinese PLA General Hospital, Beijing, China, [2]Department of Neurology, The Affiliated Hospital of Xuzhou Medical University, Xuzhou Medical University, Xuzhou, China, [3]Department of Pain Medicine, The First Medical Center, Chinese PLA General Hospital, Beijing, China

KEYWORDS

systemic-immune-inflammation index (SII), perioperative stroke, postoperative complication, inflammation, older patients, biomarker

A corrigendum on
Systemic-immune-inflammation index as a promising biomarker for predicting perioperative ischemic stroke in older patients who underwent non-cardiac surgery

by Zhang, F., Niu, M., Wang, L., Liu, Y., Shi, L., Cao, J., Mi, W., Ma, Y., and Liu, J. (2022). *Front. Aging Neurosci.* 14:865244. doi: 10.3389/fnagi.2022.865244

In the original article, there was a mistake in Figure 1 as published. "ASA physical status V" should be "ASA physical status ≥ IV." In addition the corresponding *n* number was give as 391, but should be 1,091. In addition, the corresponding n number for "Missing data for any confounder" was 3,144 but should be 2,444. The revised Figure 1 appears below.

There was also an error in **Materials and methods**, "*Inclusion and exclusion criteria*," Paragraph 1. "Patients who presented with an American Society of Anesthesiologists (ASA) classification of V" should be "Patients who presented with an American Society of Anesthesiologists (ASA) classification of ≥IV." The corrected paragraph appears below:

"Patients who underwent non-cardiac surgery between January 2008 and August 2019 at Chinese PLA General Hospital were initially screened from a perioperative retrospective database. The inclusion criteria were as follows: (1) aged 65 yr or older; (2) underwent non-cardiac surgery; (3) received general anesthesia; and (4) were with duration of surgery > 60 min. Patients who presented with an American Society of Anesthesiologists (ASA) classification of ≥IV, were performed under regional anesthesia, or had missing clinical data were excluded. Among patients who underwent multiple surgeries during the study period, only the first eligible surgery was considered. A flow diagram of the patient selection process is displayed in Figure 1." In the original article, there was also a mistake in the **Abstract**, "*Conclusion*" as published. The Abstract conclusion stated, "after non-cardiac surgery in elderly older patients." This should be "after non-cardiac surgery in older patients." The corrected paragraph appears below:

"**Conclusion:** Preoperative SII, which includes neutrophil, platelet, and lymphocyte counts obtained from routine blood analysis, was a potential prognostic biomarker for predicting perioperative ischemic stroke after non-cardiac surgery in older patients. An elevated SII, based on an optimal cut-off value of 583, was an independent risk factor for perioperative ischemic stroke."

In the original article, there was also an error in Table 1 and Supplementary Tables 2–4. The covariates previously stated "Class III and IV" and "Arterial fibrillation." The corrected covariates are "Class III" and "Atrial fibrillation or VHD." The corrected Table 1 appears below. The corrected Supplementary Tables 2–4 appear in the Supplementary Material of the original article.

In the original article there was also an error in **Materials and methods**, "*Clinical outcome*." The definition of perioperative ischemic stroke was incomplete. The following information was not provided: "Diagnoses of stroke are confirmed by a combination of neuroimaging and clinical evidence of cerebrovascular ischemia during hospital stay." The corrected paragraph appears below:

"The primary outcome of interest was perioperative ischemic stroke, defined as an episode of neurological dysfunction, such as motor, sensory, or cognitive dysfunction, caused by focal cerebral, spinal, or retinal infarction within 30 postoperative days (Sacco et al., 2013). Diagnoses of stroke are confirmed by a combination of neuroimaging and clinical evidence of cerebrovascular ischemia during hospital stay. In our study, perioperative ischemic stroke patients were identified if discharge records included at least 1 ICD-9-CM/ICD-10-CM diagnosis code for stroke (Supplementary Table 1)."

We apologize for these errors and state that this does not change the scientific conclusions of the article in any way. The original article has been updated.

Publisher's note

References

Sacco, R. L., Kasner, S. E., Broderick, J. P., Caplan, L. R., Connors, J. J., Culebras, A., et al. (2013). An updated definition of stroke for the 21st century: a statement for healthcare professionals from the American Heart Association/American Stroke Association. *Stroke* 44, 2064–2089. doi: 10.1161/STR.0b013e318296aeca

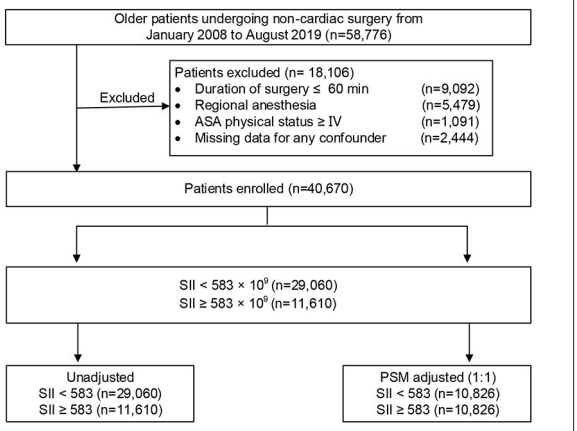

FIGURE 1
Study profile. ASA, American Society of Anesthesiologists; PSM, propensity score matching.

TABLE 1 Baseline characteristics of unadjusted sample and propensity score-matched sample (patients from 2008–2019).

Characteristic	Unadjusted sample ($n = 40,670$)				PSM adjusted (1:1) ($n = 21,652$)			
	SII < 583 ($n = 29,060$)	SII ≥ 583 ($n = 11,610$)	*P*-value	SMD	SII < 583 ($n = 10,826$)	SII ≥ 583 ($n = 10,826$)	*P*-value	SMD
Demographics								
Age, y†	70.0 (67.0,73.0)	70.0 (67.0,75.0)	0.126	0.152	70.0 (67.0,74.0)	70.0 (67.0,74.0)	0.556	0.004
Female (%)†	13651 (47.0)	4683 (40.3)	<0.001	0.134	4458 (41.2)	4427 (40.9)	0.679	0.006
BMI, kg/m^2†	24.5 (22.3,26.9)	23.7 (21.5,26.0)	0.089	0.233	24.0 (21.6,26.4)	23.8 (21.5,26.0)	0.136	0.097
ASA classification (%)†								
Class I	741 (2.5)	234 (2.0)	<0.001	0.197	261 (2.4)	230 (2.1)	0.356	0.022
Class II	22885 (78.8)	8255 (71.1)			7826 (72.3)	7793 (72.0)		
Class III	5434 (18.7)	3121 (26.9)			2739 (25.3)	2803 (25.9)		
Previous medical history								
Hypertension (%)†	10874 (37.4)	4685 (40.4)	<0.001	0.060	4211 (38.9)	4360 (40.3)	0.257	0.021
Diabetes mellitus (%)†	6096 (21.0)	2756 (23.7)	<0.001	0.066	2436 (22.5)	2554 (23.6)	0.178	0.076
Prior ischemic stroke (%)†	1552 (5.3)	847 (7.3)	<0.001	0.080	682 (6.3)	765 (7.1)	0.228	0.068
Coronary heart disease (%)†	2879 (9.9)	1231 (10.6)	0.037	0.023	1070 (9.9)	1146(10.6)	0.093	0.023
Atrial fibrillation or VHD (%)†	454 (1.6)	202 (1.7)	0.215	0.014	165 (1.5)	180 (1.7)	0.447	0.011
Peripheral vascular disease (%)†	1996 (6.9)	892 (7.7)	0.004	0.031	811 (7.5)	802 (7.4)	0.836	0.003
Renal dysfunction (%)†*	338 (1.2)	234 (2.0)	<0.001	0.068	191 (1.8)	205 (1.9)	0.456	0.047
β-blockers medication (%)†	2051 (7.1)	999 (8.6)	<0.001	0.058	869 (8.2)	931 (8.6)	0.167	0.065
Aspirin medication (%)†	2553 (8.8)	1174 (10.1)	<0.001	0.045	1024 (9.5)	1086 (10.0)	0.293	0.043
Preoperative laboratory data								
Hemoglobin, g/L†	132.0 (122.0,142.0)	125.0 (111.0,138.0)	<0.001	0.437	128.0 (114.0,140.0)	127.0 (113.0,139.0)	0.156	0.083
Albumin, g/L†	40.3 (38.1,42.5)	40.5 (38.2,43.0)	0.223	0.481	38.9 (36.2,41.4)	38.8 (36.0,41.7)	0.837	0.005
Total bilirubin, μmol/L†	10.9 (8.4,14.2)	10.6 (7.8,15.6)	<0.001	0.291	10.7 (8.3,14.6)	10.6 (7.7,14.9)	0.202	0.093
Prothrombin time, s†	13.1 (12.6,13.6)	13.2 (12.7,13.9)	0.123	0.176	13.2 (12.7,13.8)	13.2 (12.7,13.8)	0.600	0.028
Surgical and anesthetic factors								
Preoperative MAP, mmHg	95.7 (88.7,103.0)	95.0 (87.3,102.3)	0.098	0.070	95.0 (87.3,102.3)	95.0 (88.0,102.7)	0.169	0.024
Surgical procedures (%)								
Trauma surgery	433 (1.5)	602 (5.2)	<0.001	0.352	404 (3.7)	353 (3.3)		
Spine	2751 (9.5)	715 (6.2)			758 (7.0)	711 (6.6)	0.258	0.041

(Continued)

TABLE 1 (Continued)

Characteristic	Unadjusted sample ($n = 40,670$)				PSM adjusted (1:1) ($n = 21,652$)			
	SII < 583 ($n = 29,060$)	SII ≥ 583 ($n = 11,610$)	*P*-value	SMD	SII < 583 ($n = 10,826$)	SII ≥ 583 ($n = 10,826$)	*P*-value	SMD
Intra-abdominal surgery	9652 (33.2)	5159 (44.4)			4688 (43.3)	4690 (43.3)		
Joint arthroplasty	3726 (12.8)	1031 (8.9)			987 (9.1)	1027 (9.5)		
Urologic or gynecologic	3972 (13.7)	1219 (10.5)			1138 (10.6)	1209 (11.1)		
Neurosurgery	1380 (4.7)	523 (4.5)			516 (4.8)	515 (4.8)		
Thoracic or vascular	3362 (11.6)	1225 (10.5)			1172 (10.8)	1199 (11.1)		
Other (plastic surgery, etc.)	3784 (13.0)	1136 (9.8)			1163 (10.7)	1122 (10.3)		
Duration of procedures, min	155.0 (110.0,215.0)	170.0 (120.0.0,235.0)	<0.001	0.162	168.0 (118.0,231.0)	170.0 (120.0,235.0)	0.356	0.076
Estimated blood loss, mL	100.0 (50.0,200.0)	150.0 (50.0,300.0)	<0.001	0.083	140.0 (90.0,280.0)	145.7 (100.0,300.0)	0.167	0.096
MAP ≤ 65 mmHg (%)	12600 (43.4)	5749 (49.5)	<0.001	0.070	5125 (47.3)	5285 (48.8)	0.234	0.072
Crystalloid infusion, ml/kg/h	8.6 (6.5,11.4)	8.9 (6.6,11.8)	0.167	0.073	8.8 (6.6,11.7)	8.8 (6.5,11.7)	0.845	0.006
Colloid infusion, ml/kg/h	2.9 (1.3,4.3)	3.1 (1.8,4.5)	<0.001	0.123	3.0 (1.6,4.4)	3.0 (1.8,4.5)	0.111	0.066
Blood transfusion (%)	3902 (13.4)	2322 (20.0)	<0.001	0.177	1998 (18.5)	2082 (19.2)	0.189	0.052
NSAIDs (%)	20502 (70.6)	8366 (72.1)	0.003	0.033	7667 (70.8)	7709 (71.2)	0.539	0.009
Glucocorticoid (%)	23749 (81.7)	9557 (82.3)	0.165	0.015	8905 (82.3)	8932 (82.5)	0.643	0.007
Opioid dose, mg‡	120.0 (9.0,150.0)	135.0 (105.0,165.0)	<0.001	0.081	135.0 (100.0,150.0)	135.0 (105.0,165.0)	0.256	0.047
Volatile anesthetic (%)	27098 (93.2)	10819 (93.2)	0.840	0.002	10097 (93.3)	10110 (93.4)	0.744	0.005
Preoperative NLR								
<3	27796 (95.7)	4098 (35.3)	<0.001	1.643	10215 (94.4)	3951 (36.5)	<0.001	1.583
≥3	1264 (4.3)	7512 (64.7)			611 (5.6)	6875 (63.5)		
Preoperative PLR								
<119	18897 (65.0)	959 (8.3)	<0.001	1.458	6821 (63.0)	914 (8.4)	<0.001	1.385
≥119	10163 (35.0)	10651 (91.7)			4005 (37.0)	9912 (91.6)		
Perioperative ischemic stroke (%)	126 (0.434)	111 (0.956)	<0.001	0.856	49 (0.453)	107 (0.988)	<0.001	0.939

The data are presented as the median (inter-quartile range), mean (standard deviation) or n (%).

* Creatinine > 177 μm/l.

† Variables included in the propensity score.

‡ Including those prescribed intraoperatively and postoperatively (until 7 days after surgery).

SII, systemic-immune-inflammation index; PSM, propensity score matching; SMD, standardized mean difference; BMI, body mass index; ASA, American Society of Anesthesiologists; VHD, valvular heart disease; MAP, mean arterial pressure; NSAIDs, non-steroid anti-inflammatory drugs; NLR, neutrophil-lymphocyte ratio; PLR, platelet-to-lymphocyte ratio.

frontiers | Frontiers in Aging Neuroscience

ORIGINAL RESEARCH
published: 26 April 2022
doi: 10.3389/fnagi.2022.878484

A Novel Blood Inflammatory Indicator for Predicting Deterioration Risk of Mild Traumatic Brain Injury

Xintong Ge[1,2†], Luoyun Zhu[3,4†], Meimei Li[1,2†], Wenzhu Li[1,2], Fanglian Chen[5], Yongmei Li[4], Jianning Zhang[5,6] and Ping Lei[1,2]*

[1] Department of Geriatrics, Tianjin Medical University General Hospital, Tianjin, China, [2] Tianjin Geriatrics Institute, Tianjin, China, [3] Department of Medical Examination, Tianjin Medical University General Hospital, Tianjin, China, [4] Key Laboratory of Immune Microenvironment and Disease, Department of Pathogen Biology, School of Basic Medical Sciences, Tianjin Medical University, Tianjin, China, [5] Key Laboratory of Injuries, Variations and Regeneration of Nervous System, Key Laboratory of Post-trauma Neuro-repair and Regeneration in Central Nervous System, Tianjin Neurological Institute, Tianjin, China, [6] Department of Neurosurgery, Tianjin Medical University General Hospital, Tianjin, China

OPEN ACCESS

Edited by:
Anwen Shao,
Zhejiang University, China

Reviewed by:
Yujie Chen,
Army Medical University, China
Simona Lattanzi,
Marche Polytechnic University, Italy

***Correspondence:**
Ping Lei
leiping1974@163.com

† These authors have contributed equally to this work and share first authorship

Specialty section:
This article was submitted to Neuroinflammation and Neuropathy, a section of the journal Frontiers in Aging Neuroscience

Received: *18 February 2022*
Accepted: *18 March 2022*
Published: *26 April 2022*

Citation:
Ge X, Zhu L, Li M, Li W, Chen F, Li Y, Zhang J and Lei P (2022) A Novel Blood Inflammatory Indicator for Predicting Deterioration Risk of Mild Traumatic Brain Injury. Front. Aging Neurosci. 14:878484. doi: 10.3389/fnagi.2022.878484

Mild traumatic brain injury (mTBI) has a relatively higher incidence in aging people due to walking problems. Cranial computed tomography and magnetic resonance imaging provide the standard diagnostic tool to identify intracranial complications in patients with mTBI. However, it is still necessary to further explore blood biomarkers for evaluating the deterioration risk at the early stage of mTBI to improve medical decision-making in the emergency department. The activation of the inflammatory response is one of the main pathological mechanisms leading to unfavorable outcomes of mTBI. As complete blood count (CBC) analysis is the most extensively used laboratory test in practice, we extracted clinical data of 994 patients with mTBI from two large clinical cohorts (MIMIC-IV and eICU-CRD) and selected inflammation-related indicators from CBC analysis to investigate their relationship with the deterioration after mTBI. The combinatorial indices neutrophil-to-lymphocyte ratio (NLR), red cell distribution width-to-platelet ratio (RPR), and NLR times RPR (NLTRP) were supposed to be potential risk predictors, and the data from the above cohorts were integratively analyzed using our previously reported method named MeDICS. We found that NLR, RPR, and NLTRP levels were higher among deteriorated patients than non-deteriorated patients with mTBI. Besides, high NLTRP was associated with increased deterioration risk, with the odds ratio increasing from NLTRP of 1–2 (2.69, 1.48–4.89) to > 2 (4.44, 1.51–13.08), using NLTRP of 0–1 as the reference. NLTRP had a moderately good prognostic performance with an area under the ROC curve of 0.7554 and a higher prediction value than both NLR and RPR, indicated by the integrated discrimination improvement index. The decision curve analysis also showed greater clinical benefits of NLTRP than NLR and RPR in a large range of threshold probabilities. Subgroup analysis further suggested that NLTRP is an independent risk factor for the deterioration after mTBI. In addition, *in vivo* experiments confirmed the association between NLTRP and neural/systemic

inflammatory response after mTBI, which emphasized the importance of controlling inflammation in clinical treatment. Consequently, NLTRP is a promising biomarker for the deterioration risk of mTBI. It can be used in resource-limited settings, thus being proposed as a routinely available tool at all levels of the medical system.

Keywords: mild traumatic brain injury, risk factor, inflammation, neutrophil, lymphocyte, red cell distribution width, platelet

INTRODUCTION

Traumatic brain injury (TBI) ranges in severity, including the amount of brain damage and transient symptoms. Mild TBI (mTBI), the slightest neurotrauma, accounts for 80–90% of reported TBI cases and results in approximately 42 million emergency department visits worldwide each year (Gardner and Yaffe, 2015; Capizzi et al., 2020). Because of walking problems, mTBI has a relatively higher incidence in aging people. Most patients are characterized by a brief neurological impairment with no or only slight structural damage and a Glasgow Coma Scale (GCS) of 13–15 (Maas et al., 2017).

Cranial computed tomography (CT) is a standard diagnostic tool to identify intracranial complications of TBI. With its widespread application in the emergency department, doctors can quickly learn whether the individual has intracranial lesions, such as brain contusion, intracranial hemorrhage, subdural hematoma, and epidural hematoma, to propose the next-step medical suggestion for the patient—admit to the inpatient department, continue to stay in the emergency department for further diagnosis and treatment, or back home for rest and observation. Under normal circumstances, CT-negative patients or CT-positive patients with minor brain/cranial damage will choose to go home for observation or receive short-term treatments in the emergency and outpatient department. However, 11.7% of patients with mTBI may suffer from clinical deterioration with decreased GCS caused by secondary brain injury. Approximately 3.5% of patients with mTBI even need neurosurgical interventions (Marincowitz et al., 2018). Consequently, it is still necessary to further develop methods for evaluating the deterioration risk at the early stage of mTBI so that low-risk patients can be safely treated in the emergency department.

The use of blood biomarkers is an important supplementary tool for identifying patients with mTBI at deterioration risk. Recently, researchers have focused on several chemicals released from neural cells that may serve as biomarkers for neurological complications. S100B, a low-molecular-weight (21 kDa) protein that is mainly synthesized by astrocytes, could be rapidly released from damaged cells into circulation. Due to its excellent negative predictive value for mTBI, it has been regarded as an alternative choice for cranial CT scanning with appropriate evidence-based medicine (Undén et al., 2013). However, the determination of serum S100B needs a special measurement platform that ensures standardized and reproductive testing, and only three analyzers (Elecsys-Cobas, Roche; Liaison XL, Diasorin; and Vidas 3, bioMerieux) are in clinical use till date (Bouvier et al., 2016; Oris et al., 2019). Unfortunately, in most regions of the world, even in some high-level neurosurgical centers, the laboratory equipment are not supplied. For other potential biomarkers, including GFAP, UCH-L1, NFL, Tau, and some miRNAs, they have not been used in clinical work due to the lack of sufficient evidence from large-scale clinical trials and the compatible measurement platform in routine clinical practice. Taken together, there is an urgent need to find other blood biomarkers that are easily accessible and highly reliable to assist medical decision-making for patients with mTBI.

The activation of inflammation is one of the main pathological mechanisms leading to secondary brain injury and unfavorable outcomes in patients with mTBI (Le Bail et al., 2021). As complete blood count (CBC) analysis is the most extensively applied clinical laboratory test, we employed one of the largest reported mTBI cohorts in this study and screened the inflammation-related indicators from CBC analysis to investigate their relationship with the deterioration after mTBI. Specifically, the combinatorial indices neutrophil-to-lymphocyte ratio (NLR), RDW-to-platelet ratio (RPR), and NLR times RPR (NLTRP) were supposed to be potential risk predictors. The research findings are expected to provide solid evidence for the novel blood indicator as a routinely available biomarker at all levels of the medical system in predicting the outcome of mTBI.

MATERIALS AND METHODS

Database Introduction

All data were extracted from the online international databases—Multiparameter Intelligent Monitoring in Intensive Care IV (MIMIC-IV, version 1.0) database and eICU Collaborative Research Database (eICU-CRD, version 2.0)—that are maintained by the Laboratory for Computational Physiology at the Massachusetts Institute of Technology (Cambridge, MA, United States). MIMIC-IV database was approved by the institutional review boards of the Massachusetts Institute of Technology and Beth Israel Deaconess Medical Center

Abbreviations: ASHD, arteriosclerotic heart disease; AUC, area under ROC curve; CBC, complete blood count; CCI, controlled cortical impact; CI, confidence interval; COPD, chronic obstructive pulmonary disease; CT, computed tomography; DCA, decision curve analysis; eICU-CRD, eICU collaborative research database; GCS, glasgow coma scale; HBP, high blood pressure; IDI, integrated discrimination improvement; MeDICS, MIMIC-III and eICU database integration cases study; MIMIC-III, multiparameter intelligent monitoring in intensive Care III; mTBI, mild traumatic brain injury; NLR, neutrophil-to-lymphocyte ratio; NLTRP, neutrophil-to-lymphocyte ratio times RDW-to-platelet ratio; OR, odds ratio; RDW, red cell distribution width; ROC, receiver-operating characteristic; RPR, RDW-to-platelet ratio.

(Boston, MA, United States). It contains 523, 740 admissions at this medical center from 2008 to 2019, including a new ED module (not existing in MIMIC-III, the older version of the database) that contains data for patients while they are in the emergency department. EICU-CRD was released under the Health Insurance Portability and Accountability Act safe harbor provision, and the reidentification risk was certified as meeting safe harbor standards by Privacert (Cambridge, MA; Certification no. 1031219-2). It covers 200, 859 admissions in 2014 and 2015 from 208 hospitals across the United States. Besides, the source hospital of MIMIC-IV does not participate in the eICU-CRD program.

The data from the MIMIC-IV database and eICU-CRD are openly available. Data extraction was performed using Navicat Premium Version 12.1.11 (Preimumsoft^{TM} CyberTech Ltd., Hongkong SAR, China).

Study Population

Patients with a diagnosis of concussion in the MIMIC-IV database and intracranial injury in eICU-CRD were potentially eligible for inclusion in the mTBI cohort. If they had more than one hospitalization record, only those of the first hospital admission were kept. Patients were excluded if they met the following criteria: had no records of GCS within 24 h after hospital admission, had a record of GCS less than 13 during hospitalization, were younger than 18 years of age, had no binary gender, and/or had no records of whole blood RDW and platelet count within 24 h after hospital admission.

It should be mentioned that the lowest GCS of enrolled patients during hospitalization was not less than 13, so that the patients with moderate or severe TBI exacerbated by mTBI were excluded. Although these patients do not show severe symptoms in the acute stage of TBI, most of them can be observed with serious intracranial injuries by cranial CT and obvious changes in consciousness when the condition gets worse. Doctors can use the existing conventional examination methods to fully judge the condition and risks, thus making medical decisions on hospital admission and even neurosurgery. Therefore, these patients were not included in this study.

Data Extraction

Structure Query Language was used to extract data from the two databases. The following information was extracted: age, gender, important past history and comorbidities, GCS records, neutrophil count, lymphocyte count, RDW, and platelet count within 24 h after hospital admission. The past history and comorbidities include arteriosclerotic heart disease (ASHD), chronic obstructive pulmonary disease (COPD), high blood pressure (HBP), liver failure or cirrhosis, renal failure or uremia, stroke, malignancy, and use of antiplatelet/anticoagulant/antithrombotic drugs. For patients with more than one record of the neutrophil count, lymphocyte count, RDW, or platelet count within 24 h after hospital admission, the average value was calculated, respectively, and NLR, RPR, and NLTRP were then figured out using these values. In addition, the outcome of the study was designed to be a deterioration in GCS, which was defined as a decline from a 14 or 15 scale at admission to a 13 scale (the lowest scale of mTBI) within 24 h after hospital admission.

To integrate the data from the MIMIC-IV database and eICU-CRD, we used our self-developed MeDICS (MIMIC-IV and eICU Database Integrated Cohort Study) method as previously reported (Ge et al., 2021). This method could be applied to establish diagnostic and prognostic models for various diseases, and its value in exploring the biomarker for acute TBI has been verified by a retrospective clinical study with the same research objective using an external cohort (Wang et al., 2021). Briefly, ICU-stay-ID or patient-unit-stay-ID was regarded as the unique ID for each patient in the cohort. Incompatible data, such as patient-health system-stay-ID, were excluded. Besides, as the two databases may have different definitions of the same diseases, the disease codes were unified by manual review. Furthermore, the same variables with inconsistent data types in the two databases, such as numbers and strings, were also unified.

Management of Missing Data and Outliers

Variables with missing data are common in the MIMIC-IV database and eICU-CRD. As described in the "Study population" section, patients with missing records of GCS, neutrophil count, lymphocyte count, RDW, or platelet count within 24 h after hospital admission were excluded from the analysis. Variables with more than 20% missing values, such as patients' height and weight, were also excluded. In addition, the NLTRP outliers with more than 3.00, the upper quartile plus 1.5-fold of interquartile range, were excluded as non-normally distributed outliers, along with their related data, including NLR and RPR.

Animals and Grouping Methods

Adult male C57BL/6 mice (n = 72, aged 12 weeks, weighing 20–25 g) were purchased from the Chinese Academy of Military Science (Beijing, China). All experimental procedures were conducted in accordance with the EC Directive 86/609/EEC for animal experiments and were approved by Tianjin Medical University Animal Care and Use Committee (Grant No. IRB2021-DWFL-359). The mice were quarantined and housed for 2 weeks before being randomly divided into 4 groups (n = 6/group, 3 independent experiments): sham, TBI, TBI + SC75741, and TBI + MCC950. The treatment was administered at 1 h post-injury. Briefly, SC75741 (Selleckchem, Houston, TX, United States), the NF-κB selective inhibitor, was dosed in the mice at 15 mg/ml intraperitoneally. MCC950 (Selleckchem), the specific inhibitor of pyroptosis initiating receptor NLRP3, was applied to the mice at 10 mg/kg intraperitoneally.

Mild Closed Head Injury Mouse Model

The mice were anesthetized with 4.6% isoflurane. A molded acrylic cast was designed to fix the head and provide a 3.0-mm space below for acceleration and deceleration beneath the point of impact, and the surgical tape was used to secure the mouse in

a prone position. After shaving the head, a self-designed standard manufacturing concave metal disk was adhered to the skull immediately caudal to the bregma as a helmet. The impounder tip of the injury device (eCCI model 6.3, American Instruments, Richmond, VA, United States) was then extended to its full impact distance, positioned on the center of the disk surface, and reset to induce a closed head injury. The impact parameters were set as follows: 5.0 m/s velocity, 2.5 mm depth, and 200 ms dwell time. After the impact procedure, the mice were placed in a well-ventilated cage at 37°C until they regained consciousness. The sham-operated mice underwent the same procedures except for the impact (Ge et al., 2018).

Complete Blood Count Analysis

The mice were anesthetized with 4.6% isoflurane by intraperitoneal injection at 6 h post-injury. Whole blood samples were then collected *via* cardiac puncture and were anticoagulated with heparin. To determine neutrophil count, lymphocyte count, RDW, and platelet count, the blood sample was sent for CBC analysis using Sysmex XN-2000 Automated Hematology Analyzer (Kobe, Hyogo, Japan).

Enzyme Linked Immunosorbent Assay

Peripheral blood was drawn by cardiac puncture at 6 h post-injury for serum inflammatory indicator measurement. After that, the mice were sacrificed by transcardiac perfusion with PBS. The injured cerebral cortex was then dissected to collect brain extracts. The ELISA assay of the inflammatory mediators, including TNF-α, IL-1β, and IL-10, was determined by referring to the manufacturer's instructions (Cat# MTA00B, MLB00C, M1000B; R&D, Minneapolis, MN, United States).

Statistical Analysis

For the data collected from the MIMIC-IV database and eICU-CRD, continuous variables were expressed as mean ± *SD* and compared using Student's *t*-test, the Wilcoxon rank-sum test, or the Kruskal–Wallis rank-sum test, as appropriate. Categorical data were expressed as numbers (percentages) and compared using the chi-square test.

The association between NLTRP and the deterioration risk was determined using the logistic regression model and presented as an odds ratio (OR) with a 95% confidence interval (CI). NLTRP values were divided into three groups of tertiles, with the first tertile (0–1) selected as the reference group. The Lowess Smoothing technique was used to explore the crude relationship between NLTRP and the deterioration risk. Multivariable logistic regression analyses were used to control confounders. Model 1 was adjusted for the confounders, namely, age and gender. Model 2 was adjusted for the confounders, namely, age, gender, history, and comorbidities, including ASHD, COPD, HBP, liver failure or cirrhosis, renal failure, or uremia, stroke, malignancy, and use of antiplatelet/anticoagulant/antithrombotic drugs. These confounders were selected based on their potential influences on NLTRP or the clinical course. Potential multicollinearity was tested using the variance inflation factor, with a value of ≥ 5 indicating the presence of multicollinearity. The receiver-operating characteristic (ROC) curve was depicted to show the outcome prediction performance and confirm the best cutoff value, and the integrated discrimination improvement (IDI) index was calculated to compare the predictive values of different indicators. Decision curve analysis (DCA) was further performed to evaluate the clinical benefits of various indicators. In addition, stratification in subgroup analysis was performed according to age, gender, history, and comorbidities to explore their possible interaction with NLTRP to determine the deterioration risk.

The data from the *in vivo* study were expressed as mean ± standard deviation, and the statistical comparisons were made using Student's *t*-test or one-way ANOVA followed by the Tukey HSD *post-hoc* test, as appropriate.

All statistical analyses were performed using Stata/MP Version 14.0 (Stata Corp., College Station, TX, United States) and PASW Statistics Version 18.0 (IBM, Armonk, NY, United States). A two-tailed *p*-value of less than 0.05 was considered to be statistically significant.

RESULTS

Study Population and Baseline Characteristics

In total, 994 patients who met the selection criteria were enrolled in the cohort, which included 889 non-deteriorated subjects and 105 deteriorated subjects, establishing a deterioration rate of 10.6%. The detailed procedure for population selection is shown in **Figure 1**. Demographic characteristics of the cohort are presented in **Table 1**. The patients with mTBI in the cohort had an average age of 53.27 years, which was consistent with the recent report on the incidence of TBI in America (Peterson and Thomas, 2021). No difference in the deterioration risk was observed based on age and gender. Besides, important history and comorbidities during hospitalization, including ASHD, COPD, HBP, liver failure or cirrhosis, renal failure or uremia, stroke, malignancy, or use of antiplatelet/anticoagulant/antithrombotic drugs, also did not affect the deterioration after mTBI. For the indicators of the CBC analysis, neutrophil count, lymphocyte count, RDW, and platelet count did not show independent differences between non-deteriorated and deteriorated subjects. However, it was worth noting that the combinatorial indices NLR ($p = 0.0017$), RPR ($p = 0.0011$), and NLTRP ($p < 0.001$) were all lower for non-deteriorated subjects than deteriorated subjects.

High NLTRP Is Related to Increased Deterioration Risk of mTBI

The relationship between NLTRP and deterioration risk for patients with mTBI is shown in **Figure 2A** using the Lowess Smoothing technique, which yielded an approximately linear correlation. NLTRP values were divided into three groups of tertiles (NLTRP 1–2, $n = 74$; NLTRP > 2, $n = 16$), with the first tertile (NLTRP 0–1, $n = 904$) being selected

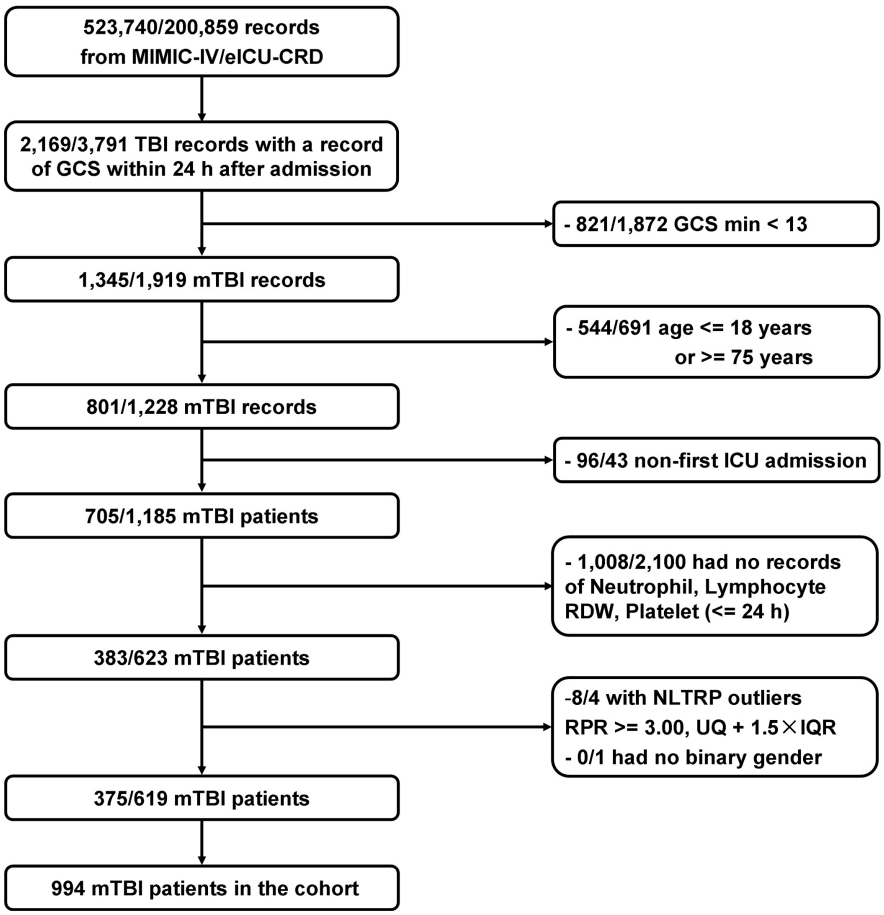

FIGURE 1 | Flowchart of the study population. In total, 994 patients who met the selection criteria were enrolled. GCS, Glasgow Coma Scale; IQR, interquartile range; mTBI, mild traumatic brain injury; NLTRP, neutrophil-to-lymphocyte ratio times red cell distribution width-to-platelet ratio; RDW, red cell distribution width; UQ, upper tertile.

as the reference for all comparisons in multivariable logistic regression models. As shown in **Table 2**, the ORs with 95% CI for the second, (1–2) and third (> 2) tertiles in the crude model were 2.69 (1.48–4.89) and 4.44 (1.51–13.08), respectively. Therefore, high NLTRP was associated with an increased deterioration risk of mTBI. Besides, a similar trend could be observed in Model 1 and Model 2, in which the confounders, including age, gender, history, and comorbidities, were adjusted. It also suggested that the second and third tertiles had successively higher ORs (95% CI) than the first tertile in all models. In addition, the mean-variance inflation factor was 1.33 and 1.26 for Model 1 and Model 2, indicating that no multicollinearity was existed.

The outcome prediction value of NLTRP was examined using the ROC curve. As shown in **Figure 2B**, its performance was moderately good for the deterioration risk (AUC = 0.7554) with a cutoff value (Youden's index) of 0.0729, corresponding to a sensitivity of 81.90% and specificity of 56.13%. It is much higher than that of NLR (AUC = 0.6486) and RPR (AUC = 0.6102). IDI index also indicated NLTRP had a higher outcome prediction value than NLR (0.0879 ± 0.0196, $p < 0.0001$) and RPR (0.0546 ± 0.0150, $p = 0.0003$). In addition, the results of DCA for NLTRP, NLR, and RPR are shown in **Figure 2C**. It further suggests that the clinical benefits of NLTRP are greater than both NLR and RPR across a large range of threshold probabilities.

Subgroup Analysis Confirms the Association Between NLTRP and Deterioration Risk of mTBI

As shown in **Table 3**, a subgroup analysis revealed the associations between NLTRP and the deterioration risk of patients with mTBI of different ages, gender, past history, and comorbidities, including ASHD, HBP, renal failure, or uremia, and use of antiplatelet/anticoagulant/antithrombotic drugs. As the number of patients with COPD, liver failure or cirrhosis, stroke, and malignancy was too small in the cohort (especially for the deteriorated subjects), their subgroup analysis could not be performed. After adjusting for covariates, the interactive effects could not be observed in all subgroups, suggesting that NLTRP is an independent risk factor for the deterioration after mTBI.

TABLE 1 | Baseline characteristics of the patients with mTBI.

Variables	Total (*n* = 994)	Non-deteriorated (*n* = 889)	Deteriorated (*n* = 105)	*p*-value
Age, Years	53.27 ± 16.27	53.06 ± 16.35	55.08 ± 15.53	0.115
Male, *n* (%)	665 (66.9)	592 (66.6)	73 (69.5)	0.541
Past history and comorbidities, *n* (%)				
ASHD				0.807
Yes	70 (7.0)	62 (7.0)	8 (7.6)	
No	924 (93.0)	827 (93.0)	97 (92.4)	
COPD				0.799
Yes	16 (1.6)	14 (1.6)	2 (2.0)	
No	978 (98.4)	875 (98.4)	103 (98.0)	
HBP				0.265
Yes	196 (19.7)	171 (19.2)	25 (23.8)	
No	798 (80.3)	718 (80.8)	80 (76.2)	
Liver failure or cirrhosis				0.635
Yes	22 (2.2)	19 (2.1)	3 (2.9)	
No	972 (97.8)	102 (97.9)	870 (97.1)	
Renal failure or uremia				0.695
Yes	49 (4.9)	43 (4.8)	6 (5.7)	
No	945 (95.1)	846 (95.2)	99 (94.3)	
Stroke				0.719
Yes	24 (2.4)	22 (2.2)	2 (1.9)	
No	970 (97.6)	867 (97.8)	103 (98.1)	
Malignancy				0.871
Yes	17 (1.7)	15 (1.7)	2 (1.9)	
No	977 (98.3)	874 (98.3)	103 (98.1)	
Antiplatelets/-coagulants/-thrombotics				0.749
Yes	64 (6.4)	58 (6.5)	6 (5.7)	
No	930 (93.6)	831 (93.5)	99 (94.3)	
CBC analysis				
Neutrophil, K/μL	245.37 ± 433.29	245.38 ± 436.14	245.26 ± 410.35	0.501
Lymphocyte, K/μL	43.92 ± 79.18	43.85 ± 76.57	44.45 ± 98.94	0.471
RDW,%	91.21 ± 84.00	91.46 ± 115.44	89.14 ± 120.58	0.577
Platelet, K/μL	220.55 ± 85.62	222.30 ± 82.44	205.71 ± 108.22	0.970
NLR	6.50 ± 5.48	6.33 ± 5.36	7.98 ± 6.21	0.0017**
RPR	0.076 ± 0.055	0.074 ± 0.047	0.096 ± 0.086	0.0011**
NLTRP	0.463 ± 0.421	0.438 ± 0.389	0.673 ± 0.485	<0.001***

*The data were expressed as mean ± SD or n (%). ***p < 0.001, **p < 0.01. ASHD, arteriosclerotic heart disease; CBC, complete blood count; COPD, chronic obstructive pulmonary disease; HBP, high blood pressure; NLR, neutrophil-to-lymphocyte ratio; RDW, red cell distribution width; RPR, red cell distribution width-to-platelet ratio; NLTRP, neutrophil-to-lymphocyte ratio times red cell distribution width-to-platelet ratio.*

Anti-inflammatory Treatments Decrease NLTRP After mTBI on the Mouse Model

In vivo experiments on the mTBI mice were designed to further explain the clinical findings. Briefly, the whole blood neutrophil count, lymphocyte count, RDW, and platelet count were all determined at 6 h post-injury, which has been widely reported to be the first time-point of the inflammation peak in mTBI mice (Zhang et al., 2014; Hubbard et al., 2021). We found that the combinatorial indices NLTRP, NLR, and RPR were all increased significantly after mTBI, while no statistical differences in neutrophil count, lymphocyte count, RDW, and platelet count could be observed (**Figures 3A–D**). In addition, the anti-inflammatory agents SC75741 and MCC950 that inhibited the expression levels of inflammatory mediators (TNF-α, IL-1β, and IL-10) in the brain and serum (**Figures 3E–J**) could reverse the level change in NLTRP post-injury (**Figure 3B**). These results suggest that NLTRP is a powerful indicator for inflammation after mTBI, thus a good biomarker for the deterioration risk.

DISCUSSION

Aging patients with mTBI have a small but clinically important risk of deterioration, giving rise to a wide variety of hospital admission practices in different regions and medical centers. Overutilization of the inpatient ward and intensive care unit for these patients leads to increased healthcare costs, decreased hospitalization resource availability, delays in admitting other critically ill patients, and subsequent emergency department

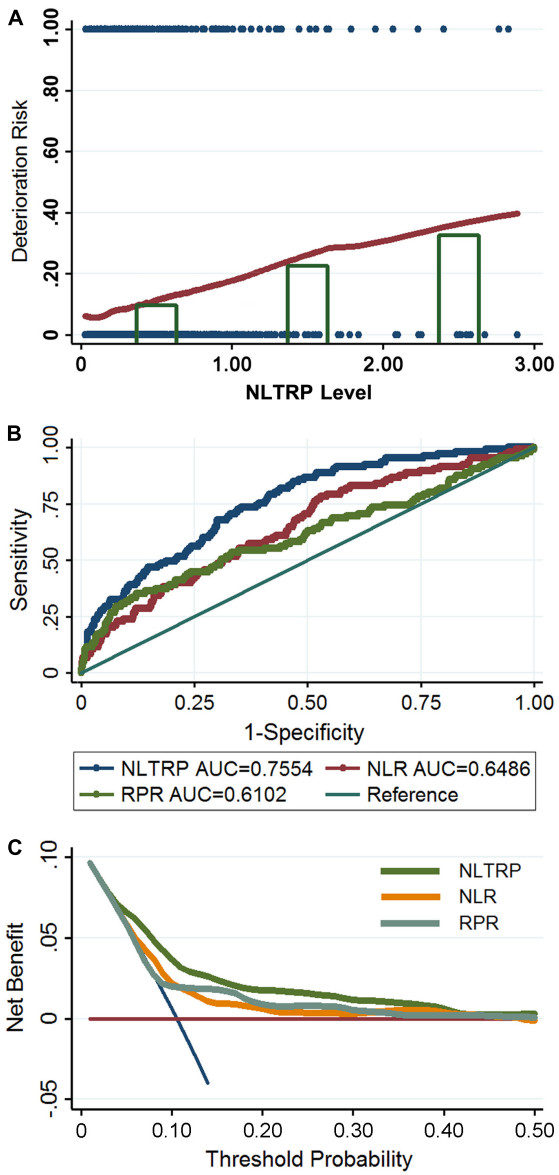

FIGURE 2 | Association between NLTRP and the deterioration risk of patients with mTBI. **(A)** The Lowess Smoothing revealed an approximately linear relationship between NLTRP and the deterioration risk. The NLTRP values were divided into tertiles, and the third (>2) and the second tertiles (1–2) were associated with high deterioration risk, compared to the first (0–1) tertile. The blue dot represents each patient enrolled in the cohort. Individuals with a deterioration outcome were presented with the risk of 1, and those with a non-deterioration outcome were presented with a risk of 0. **(B)** The ROC curve for NLTRP, NLR, and RPR. **(C)** The DCA for NLTRP, NLR, and RPR. AUC, area under curve; DCA, decision curve analysis; ROC, receiver-operating characteristic; mTBI, mild traumatic brain injury; NLR, neutrophil-to-lymphocyte ratio; RPR, red cell distribution width-to-platelet ratio; NLTRP, neutrophil-to-lymphocyte ratio times red cell distribution width-to-platelet ratio.

TABLE 2 | The ORs for all-cause deterioration of mTBI across groups of NLTRP.

NLTRP levels	OR	95% CI	*p*-value
Crude			
0–1	1		
1–2	2.69	1.48–4.89	0.001**
>2	4.44	1.51–13.08	0.007**
Model 1			
0–1	1		
1–2	2.60	1.43–4.74	0.002**
>2	4.27	1.45–12.64	0.009**
Model 2			
0–1	1		
1–2	2.59	1.42–4.73	0.002**
>2	4.43	1.48–13.25	0.008**

*Multivariable logistic regression models were used to calculate ORs with 95% CI. Model 1 was adjusted for the confounders, namely, age and gender. Model 2 was adjusted for the confounders, namely, age, gender, past history, and comorbidities, including ASHD, COPD, HBP, liver failure or cirrhosis, renal failure or uremia, stroke, malignancy, and use of antiplatelet/anticoagulant/antithrombotic drugs. The mean-variance inflation factor was 1.33 and 1.26 for Model 1 and Model 2. **p < 0.01. ASHD, arteriosclerotic heart disease; CI, confidence interval; COPD, chronic obstructive pulmonary disease; HBP, high blood pressure; NLTRP, neutrophil-to-lymphocyte ratio times red cell distribution width-to-platelet ratio; OR, odds ratio.*

crowding. But underuse of the inpatient ward may lead to poor outcomes due to the delayed recognition of clinical deterioration (Lewis et al., 2020). To solve the problem, cranial CT and MRI have been more and more widely applied in the emergency department in recent years. In addition, many researchers have focused on the early prediction of prognosis in patients with TBI. At present, two highly influential prognostic models, CRASH (Perel et al., 2008) and IMPACT (Steyerberg et al., 2008) have been established. However, both of them were not generated specifically for mTBI. The development populations for both models were weighted toward severe TBI, and patients with mild and moderate TBI were underrepresented (Maas et al., 2017). Therefore, their accuracy in predicting the prognosis of mTBI needs to be further evaluated. From this, we designed this study to explore a routinely available and reliable biomarker to predict the deterioration risk of mTBI and found a novel indicator from CBC analysis, NLTRP. The research findings do not mean NLTRP can replace cranial CT or MRI for making important medical decisions by the emergency doctor, such as whether to admit a patient to the inpatient department. Instead, we recommend using NLTRP as an auxiliary tool combined with clinical and imaging manifestations to evaluate the deterioration risk for patients with mTBI, especially in primary medical institutions without CT or MRI equipment.

There is sufficient laboratory evidence for neuroinflammation and systemic inflammation following mTBI, characterized by level changes of inflammatory markers in the acute phase after brain injury (Visser et al., 2021). However, patients with mTBI are not likely to accept invasive techniques, such as lumbar puncture, to take a cerebrospinal fluid examination. In clinical practice, the inflammatory indicator change that is most likely to draw attention from doctors is the abnormal increase in white blood cell count in circulation, but it does not have any clinical guiding significance for the lack of specificity. Recent studies have suggested that several systemic

TABLE 3 | Subgroup analysis of the associations between NLTRP and deterioration of mTBI.

Subgroups	ORs (95% CI)			*p* for interaction
	NLTRP 0–1	NLTRP 1–2	NLTRP > 2	
Age				0.055
18–45	1	3.54 (0.68–18.48)	U.C.	
45–60	1	2.60 (0.87–7.73)	8.15 (1.27–52.43)	
60–75	1	2.13 (0.90–5.07)	3.07 (0.55–17.11)	
Gender				0.152
Male	1	1.95 (0.78–4.87)	3.50 (1.47–8.30)	
Female	1	0.77 (0.42–1.42)	1.33 (0.76–2.33)	
ASHD				0.499
Yes	1	1.89 (0.06–24.82)	5.26 (1.26–48.46)	
No	1	2.71 (1.44–5.09)	3.91 (1.17–13.03)	
HBP				0.885
Yes	1	2.03 (0.59–7.05)	3.72 (0.30–45.91)	
No	1	2.93 (1.44–5.92)	4.27 (1.23–14.79)	
Renal failure or uremia				0.495
Yes	1	1.17 (0.43–9.16)	3.51 (0.04–33.8)	
No	1	2.36 (1.25–4.47)	4.21 (1.25–14.12)	
Antiplatelets/-coagulants/-thrombotics				0.299
Yes	1	2.77 (0.19–40.10)	U.C.	
No	1	2.62 (1.40–4.89)	5.50 (1.76–17.23)	

Confounders adjustment was performed as in Model 2. Multivariable logistic regression models were used to calculate ORs with a 95% CI. As the number of patients with COPD, liver failure or cirrhosis, stroke, and malignancy is too small in the cohort (especially for the deteriorated subjects), their subgroup analysis could not be performed. ASHD, arteriosclerotic heart disease; CI, confidence interval; HBP, high blood pressure; NLTRP, neutrophil-to-lymphocyte ratio times red cell distribution width-to-platelet ratio; OR, odds ratio; U.C., unable to calculate.

inflammatory indicators may correlate with the development and outcome of mTBI (Visser et al., 2021). Specifically, NLR has been widely investigated as an available prognostic biomarker and inflammatory indicator for TBI (Sabouri et al., 2020). It represents the degree of secondary brain damage led by neutrophils and their products. Neutrophils are among the first leukocytes whose number increases dramatically in the peripheral blood and enter the central nervous system through the damaged blood–brain barrier soon after TBI. They exacerbate oxidative stress, neurovascular unit damage, and neuronal cell death. However, lymphocytes are important for the repair of damaged brain tissue by releasing growth factors and regulating microglial function (Sabouri et al., 2020). Although higher NLR is correlated with positive CT findings in patients with mTBI (Alexiou et al., 2020), it has a relatively low discriminative value to predict secondary neurological impairment (Le Bail et al., 2021). Additionally, in two independent clinical cohorts of mild, moderate, and severe TBI, RPR is a desirable prognostic biomarker and an indicator for the development of inflammatory response (Ge et al., 2021; Wang et al., 2021). In this regard, RDW characterizes the heterogeneity in the size of erythrocytes and is widely utilized as an indicator to differentiate types of anemia. Under inflammation status, the pro-inflammatory cytokines could inhibit erythrocyte maturation and accelerate the release of larger reticulocytes into blood circulation, thus increasing RDW (Sun et al., 2016). Besides, along with the well-known roles in hemostasis, platelets are also crucial regulators in local and systemic inflammation. Increased platelet destruction and consumption could be caused by infectious and inflammatory damage to megakaryocytes (Levi, 2016). Nevertheless, in the pre-analysis for the mTBI cohort of this study, RPR was found to have a poor relationship with the deterioration risk of mTBI. Therefore, we selected NLTRP to be the potential biomarker for further research. As it is the product of NLR and RPR, it could amplify the prediction value of NLR and RPR in theory.

Our findings from the clinical cohort provided solid evidence for recognizing the deterioration risk of mTBI using NLTRP. Although the exact mechanism underlying the deterioration after mTBI with elevated NLTRP remains unclear, it may be partially attributed to the development of neural and systemic inflammatory responses following brain injury. Consequently, we further conducted *in vivo* experiments to explain possible mechanisms. As an upstream switch of inflammation, NF-κB signaling exerts critical effects on regulating the development of neuroinflammation in mTBI (Ghadiri et al., 2020). Besides, the NLRP3 inflammasome could trigger the inflammatory cascade (pyroptosis) in the injured brain after mTBI (O'Brien et al., 2020). In this study, we used specific NF-κB and NLRP3 inhibitors to observe the level changes in NLTRP, NLR, and RPR under the condition of inflammatory suppression. NLTRP, NLR, and RPR were all observed to be increased after mTBI, and NLTRP was also decreased, notably after the above treatments. These results confirmed the conserved response to TBI between species and proved the hypothesis that increased NLTRP was a manifestation of the inflammatory response after mTBI.

A

Groups	Neutrophil, K/μL		Lymphocyte, K/μL		RDW, %		Plt count, K/μL	
	Mean ± SD	p value	Mean ± SD	p value	Mean ± SD	p value	Mean ± SD	p value
Sham	2.81±0.69		7.15±1.48		17.97±3.04		735.88±117.35	
mTBI	3.64±0.96	p1=0.114	5.62±1.11	p1=0.069	19.59±3.14	p1=0.386	619.08±107.26	p1=0.102
TBI+SC75741	3.15±0.66	p2=0.327	6.60±1.30	p2=0.186	18.50±3.39	p2=0.576	692.78±110.37	p2=0.268
TBI+MCC950	3.23±0.61	p3=0.396	6.58±1.39	p3=0.213	18.69±3.55	p3=0.655	682.36±103.86	p3=0.324

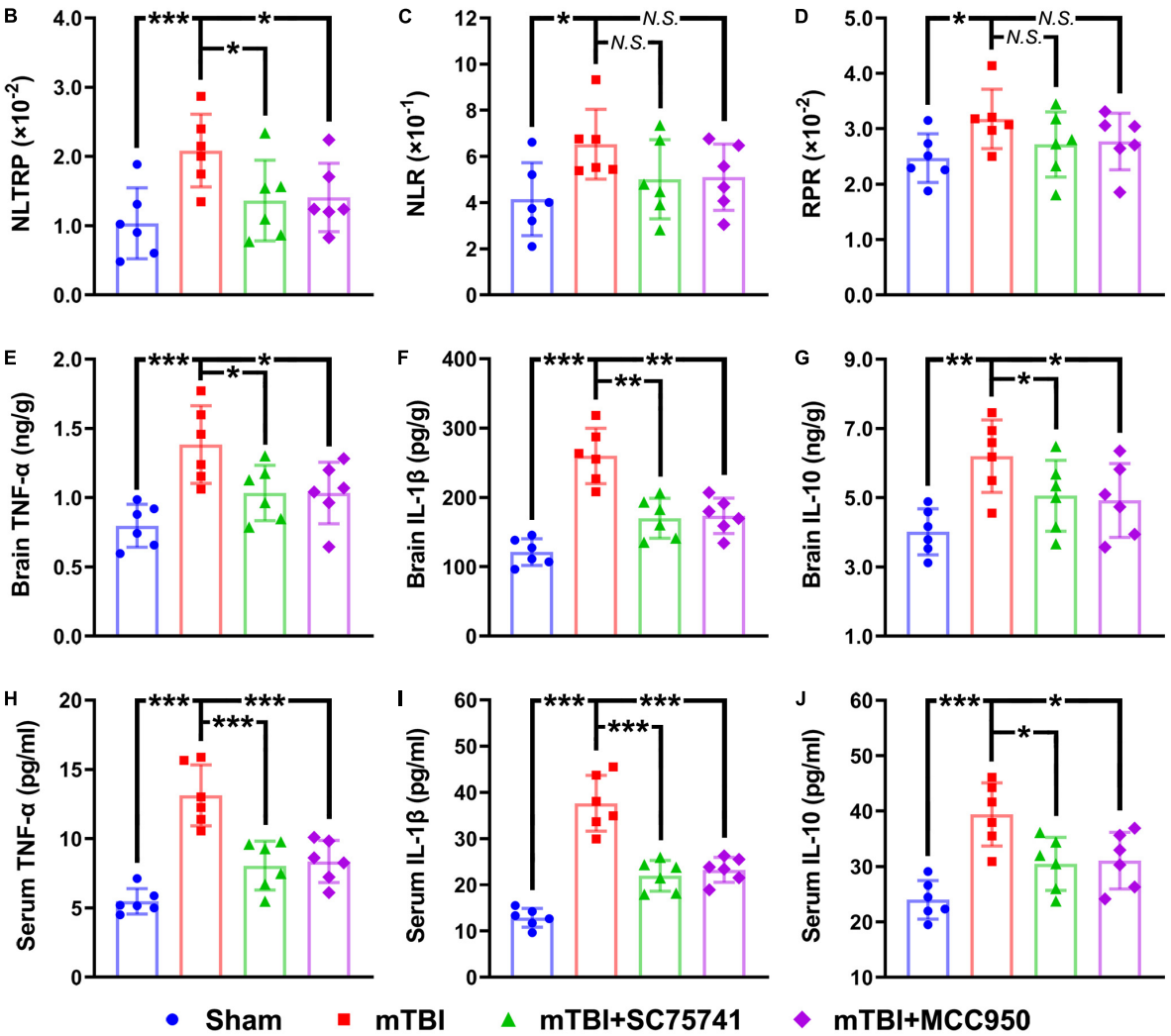

FIGURE 3 | NLTRP changes after mTBI and anti-inflammatory treatments in the mice model. **(A)** Blood neutrophil count, lymphocyte count, RDW, and platelet count of the mTBI mice. **(B–D)** NLTRP, NLR, and RPR levels of the mTBI mice. **(E–G)** The expression levels of inflammatory mediators TNF-α, IL-1β, and IL-10 in the mice brain. **(H–J)** Blood TNF-α, IL-1β, and IL-10 levels of the mTBI mice (n = 6/group). Data are presented as mean ± SD. p1, control vs. mTBI group; p2, mTBI vs. mTBI + SC75741 group; p3, mTBI vs. mTBI + MCC950 group. ***$p < 0.001$, **$p < 0.01$, *$p < 0.05$. mTBI, mild traumatic brain injury; NLR, neutrophil-to-lymphocyte ratio; NS, no significance; RDW, red cell distribution width; RPR, red cell distribution width-to-platelet ratio; NLTRP, neutrophil-to-lymphocyte ratio times red cell distribution width-to-platelet ratio.

Notably, inflammation is one of the main pathological mechanisms leading to secondary injury after an acute insult to the brain, not only for neurotrauma but also for ischemic and hemorrhagic injury. Inflammatory biomarkers, including NLR and the systemic inflammatory response index, have been proved to be independently associated with the deterioration of stroke patients, thus have great potential to be available for clinical practice due to their easy accessibility and cost-effectiveness

(Lattanzi et al., 2017, 2021; Świtońska et al., 2020). It further suggests the wide availability of inflammatory indicators, such as NLTRP, in the prognosis evaluation for various neurological diseases.

Several limitations, especially the retrospective nature of the design, should be considered when interpreting the results of this study. On the one hand, patients' information for cranial CT scanning, Abbreviated Injury Scale—Injury Severity Score at admission, and Glasgow Outcome Scale—Extended were not collected in MIMIC-IV and eICU-CRD, which led to the absence of these data in the cohort. Although similar research using the GCS sub-score from the databases has reported a better machine-learning prognosis model, it may be difficult for clinical application as the model includes up to 20 features (Palepu et al., 2021). On the other hand, an external validation dataset needs to be built in the future to further verify the research findings. From this, a multicenter prospective study is being organized by our research group aiming at promoting the clinical application of NLTRP for patients with mTBI.

CONCLUSION

NLTRP is a promising indicator for the deterioration risk of patients with mTBI. Its level change after brain injury is attributed to the development of neural and systemic inflammatory responses, which further emphasizes the importance of controlling inflammation in clinical treatment. Due to its low cost, easy availability, and high reproducibility, NLTRP can be regarded as a reliable clinical tool at all levels of the medical system.

DATA AVAILABILITY STATEMENT

The original contributions presented in the study are included in the article, further inquiries can be directed to the corresponding author.

ETHICS STATEMENT

XG completed the National Institutes of Health's web-based course Protecting Human Research Participants (certification no: 36320014) to access the databases. Written informed consent for participation was not required for this study in accordance with the national legislation and the institutional requirements. The animal study was reviewed and approved by Tianjin Medical University Animal Care and Use Committee.

AUTHOR CONTRIBUTIONS

XG and PL contributed to the conception and design of the study. XG and LZ developed the method and performed data extraction and statistical analysis. LZ conducted laboratory examinations. ML conducted *in vivo* experiments. FC, YL, and JZ provided methodological and technical support. XG wrote the manuscript. PL reviewed the manuscript. All authors contributed to manuscript revision, read, and approved the submitted version.

FUNDING

This study was supported by grants from the National Natural Science Foundation of China (Nos. 82071394 and 82072166) and the Science and Technology Project of Tianjin Municipal Health Commission (No. TJWJ2021QN005).

ACKNOWLEDGMENTS

We express gratitude to Dongdong Jia from Sheweisi Biotechnology Co., Ltd. for the technical support.

REFERENCES

Alexiou, G., Lianos, G., Tzima, A., Sotiropoulos, A., Nasios, A., Metaxas, D., et al. (2020). Neutrophil to lymphocyte ratio as a predictive biomarker for computed tomography scan use in mild traumatic brain injury. *Biomark. med.* 14, 1085–1090. doi: 10.2217/bmm-2020-0150

Bouvier, D., Duret, T., Rouzaire, P., Jabaudon, M., Rouzaire, M., Nourrisson, C., et al. (2016). Preanalytical, analytical, gestational and pediatric aspects of the S100B immuno-assays. *Clin. chem. Lab. Med.* 54, 833–842. doi: 10.1515/cclm-2015-0771

Capizzi, A., Woo, J., and Verduzco-Gutierrez, M. (2020). Traumatic brain injury: an overview of epidemiology, pathophysiology, and medical management. *Med. Clin. North Am.* 104, 213–238. doi: 10.1016/j.mcna.2019.11.001

Gardner, R. C., and Yaffe, K. (2015). Epidemiology of mild traumatic brain injury and neurodegenerative disease. *Mol. Cell. Neurosci.* 66, 75–80. doi: 10.1016/j.mcn.2015.03.001

Ge, X., Yu, J., Huang, S., Yin, Z., Han, Z., Chen, F., et al. (2018). A novel repetitive mild traumatic brain injury mouse model for chronic traumatic encephalopathy research. *J. Neurosci. Methods* 308, 162–172. doi: 10.1016/j.jneumeth.2018.07.021

Ge, X., Zhu, L., Li, W., Sun, J., Chen, F., Li, Y., et al. (2021). Red cell distribution width to platelet count ratio: a promising routinely available indicator of mortality for acute traumatic brain injury. *J. Neurotrauma* 39, 159–171. doi: 10.1089/neu.2020.7481

Ghadiri, T., Gorji, A., Vakilzadeh, G., Hajali, V., Khodagholi, F., and Sharifzadeh, M. (2020). Neuronal injury and death following focal mild brain injury: The role of network excitability and seizure. *Iran. J. Basic Med. Sci.* 23, 63–70. doi: 10.22038/ijbms.2019.37558.8932

Hubbard, W. B., Banerjee, M., Vekaria, H., Prakhya, K. S., Joshi, S., Wang, Q. J., et al. (2021). Differential leukocyte and platelet profiles in distinct models of traumatic brain injury. *Cells* 10:500. doi: 10.3390/cells10030500

Lattanzi, S., Cagnetti, C., Provinciali, L., and Silvestrini, M. (2017). Neutrophil-to-lymphocyte ratio and neurological deterioration following acute cerebral hemorrhage. *Oncotarget* 8, 57489–57494. doi: 10.18632/oncotarget.15423

Lattanzi, S., Norata, D., Divani, A., Di Napoli, M., Broggi, S., Rocchi, C., et al. (2021). Systemic inflammatory response index and futile recanalization in patients with ischemic stroke undergoing endovascular treatment. *Brain sci.* 11:1164. doi: 10.3390/brainsci11091164

Le Bail, A., Jardine, C. G., Cottenceau, V., Petit, L., Matthieu, B., and Carrie, C. (2021). Ability of neutrophil-to-lymphocyte ratio to predict secondary neurological impairment in patients with mild to moderate head injury. a

retrospective study. *Am. J. Emerg. Med.* 50, 46–50. doi: 10.1016/j.ajem.2021.06.030

Levi, M. (2016). Platelets in critical Illness. *Semin. Thromb. Hemost.* 42, 252–257. doi: 10.1055/s-0035-1570080

Lewis, L., Papa, L., Bazarian, J., Weber, A., Howard, R., and Welch, R. (2020). Biomarkers may predict unfavorable neurological outcome after mild traumatic brain injury. *J. Neurotrauma* 37, 2624–2631. doi: 10.1089/neu.2020.7071

Maas, A., Menon, D., Adelson, P., Andelic, N., Bell, M., Belli, A., et al. (2017). Traumatic brain injury: integrated approaches to improve prevention, clinical care, and research. *Lancet. Neurol.* 16, 987–1048. doi: 10.1016/s1474-4422(17)30371-x

Marincowitz, C., Lecky, F., Townend, W., Borakati, A., Fabbri, A., and Sheldon, T. (2018). The risk of deterioration in GCS13-15 patients with traumatic brain injury identified by computed tomography imaging: a systematic review and meta-analysis. *J. Neurotrauma* 35, 703–718. doi: 10.1089/neu.2017.5259

O'Brien, W., Pham, L., Symons, G., Monif, M., Shultz, S., and McDonald, S. (2020). The NLRP3 inflammasome in traumatic brain injury: potential as a biomarker and therapeutic target. *J. Neuroinflammation* 17:104. doi: 10.1186/s12974-020-01778-5

Oris, C., Chabanne, R., Durif, J., Kahouadji, S., Brailova, M., and Sapin, V. (2019). Measurement of S100B protein: evaluation of a new prototype on a bioMérieux Vidas® 3 analyzer. *Clin. Chem. Lab. Med.* 57, 1177–1184. doi: 10.1515/cclm-2018-1217

Palepu, A., Murali, A., Ballard, J., Li, R., Ramesh, S., Nguyen, H., et al. (2021). Digital signatures for early traumatic brain injury outcome prediction in the intensive care unit. *Sci. Rep.* 11:19989. doi: 10.1038/s41598-021-99397-4

Perel, P., Arango, M., Clayton, T., Edwards, P., Komolafe, E., Poccock, S., et al. (2008). Predicting outcome after traumatic brain injury: practical prognostic models based on large cohort of international patients. *BMJ* 336, 425–429. doi: 10.1136/bmj.39461.643438.25

Peterson, A. B., and Thomas, K. E. (2021). Incidence of nonfatal traumatic brain injury-related hospitalizations - united states, 2018. *MMWR Morb. Mortal. Wkly. Rep.* 70, 1664–1668. doi: 10.15585/mmwr.mm7048a3

Sabouri, E., Majdi, A., Jangjui, P., Rahigh Aghsan, S., and Naseri Alavi, S. (2020). Neutrophil-to-lymphocyte ratio and traumatic brain injury: a review study. *World Neurosurgery* 140, 142–147. doi: 10.1016/j.wneu.2020.04.185

Steyerberg, E., Mushkudiani, N., Perel, P., Butcher, I., Lu, J., McHugh, G., et al. (2008). Predicting outcome after traumatic brain injury: development and international validation of prognostic scores based on admission characteristics. *PLoS Med.* 5:e165. doi: 10.1371/journal.pmed.0050165

Sun, P., Zhang, F., Chen, C., Bi, X., Yang, H., An, X., et al. (2016). The ratio of hemoglobin to red cell distribution width as a novel prognostic parameter in esophageal squamous cell carcinoma: a retrospective study from southern China. *Oncotarget* 7, 42650–42660. doi: 10.18632/oncotarget.9516

Świtońska, M., Piekuś-Słomka, N., Słomka, A., Sokal, P., Żekanowska, E., and Lattanzi, S. (2020). Neutrophil-to-lymphocyte ratio and symptomatic hemorrhagic transformation in ischemic stroke patients undergoing revascularization. *Brain Sci.* 10:771. doi: 10.3390/brainsci10110771

Undén, J., Ingebrigtsen, T., and Romner, B. (2013). Scandinavian guidelines for initial management of minimal, mild and moderate head injuries in adults: an evidence and consensus-based update. *BMC Med.* 11:50. doi: 10.1186/1741-7015-11-50

Visser, K., Koggel, M., Blaauw, J., van der Horn, H., Jacobs, B., and van der Naalt, J. (2021). Blood-based biomarkers of inflammation in mild traumatic brain injury: a systematic review. *Neurosci. Biobehav. Rev.* 132, 154–168. doi: 10.1016/j.neubiorev.2021.11.036

Wang, R., He, M., Zhang, J., Wang, S., and Xu, J. (2021). A prognostic model incorporating red cell distribution width to platelet ratio for patients with traumatic brain injury. *Ther. Clin. Risk Manag.* 17, 1239–1248. doi: 10.2147/tcrm.s337040

Zhang, Q., Zhou, C., Hamblin, M., and Wu, M. (2014). Low-level laser therapy effectively prevents secondary brain injury induced by immediate early responsive gene X-1 deficiency. *J. Cereb. Blood Flow Metab.* 34, 1391–1401. doi: 10.1038/jcbfm.2014.95

Conflict of Interest: The authors declare that the research was conducted in the absence of any commercial or financial relationships that could be construed as a potential conflict of interest.

Publisher's Note: All claims expressed in this article are solely those of the authors and do not necessarily represent those of their affiliated organizations, or those of the publisher, the editors and the reviewers. Any product that may be evaluated in this article, or claim that may be made by its manufacturer, is not guaranteed or endorsed by the publisher.

frontiers | Frontiers in Aging Neuroscience

MINI REVIEW
published: 29 April 2022
doi: 10.3389/fnagi.2022.899678

Melatonin as a Potential Neuroprotectant: Mechanisms in Subarachnoid Hemorrhage-Induced Early Brain Injury

Chengyan Xu[1†], Zixia He[2†] and Jiabin Li[3]*

[1] Department of Neurosurgery, The Children's Hospital Zhejiang University School of Medicine, National Clinical Research Center for Child Health, Hangzhou, China, [2] Department of Outpatient, The Children's Hospital Zhejiang University School of Medicine, National Clinical Research Center for Child Health, Hangzhou, China, [3] Department of Pharmacy, The Children's Hospital Zhejiang University School of Medicine, National Clinical Research Center for Child Health, Hangzhou, China

OPEN ACCESS

Edited by:
Anwen Shao,
Zhejiang University, China

Reviewed by:
Gongchang Yu,
Shandong First Medical University, China
Yuanhan Zhu,
Jiaxing University Medical College, China

***Correspondence:**
Jiabin Li
6513077@zju.edu.cn

[†] These authors have contributed equally to this work

Specialty section:
This article was submitted to Neuroinflammation and Neuropathy, a section of the journal Frontiers in Aging Neuroscience

Received: *19 March 2022*
Accepted: *12 April 2022*
Published: *29 April 2022*

Citation:
Xu C, He Z and Li J (2022) Melatonin as a Potential Neuroprotectant: Mechanisms in Subarachnoid Hemorrhage-Induced Early Brain Injury. Front. Aging Neurosci. 14:899678. doi: 10.3389/fnagi.2022.899678

Subarachnoid hemorrhage (SAH) is a common cerebrovascular disease with high mortality and disability rates. Despite progressive advances in drugs and surgical techniques, neurological dysfunction in surviving SAH patients have not improved significantly. Traditionally, vasospasm has been considered the main cause of death and disability following SAH, but anti-vasospasm therapy has not benefited clinical prognosis. Many studies have proposed that early brain injury (EBI) may be the primary factor influencing the prognosis of SAH. Melatonin is an indole hormone and is the main hormone secreted by the pineal gland, with low daytime secretion levels and high nighttime secretion levels. Melatonin produces a wide range of biological effects through the neuroimmune endocrine network, and participates in various physiological activities in the central nervous system, reproductive system, immune system, and digestive system. Numerous studies have reported that melatonin has extensive physiological and pharmacological effects such as anti-oxidative stress, anti-inflammation, maintaining circadian rhythm, and regulating cellular and humoral immunity. In recent years, more and more studies have been conducted to explore the molecular mechanism underlying melatonin-induced neuroprotection. The studies suggest beneficial effects in the recovery of intracerebral hemorrhage, cerebral ischemia-reperfusion injury, spinal cord injury, Alzheimer's disease, Parkinson's disease and meningitis through anti-inflammatory, antioxidant and anti-apoptotic mechanisms. This review summarizes the recent studies on the application and mechanism of melatonin in SAH.

Keywords: subarachnoid hemorrhage, early brain injury, melatonin, mechanism, apoptosis, inflammation, vasospasm, oxidative stress

INTRODUCTION

Subarachnoid hemorrhage (SAH) is one of the common cerebrovascular diseases, and its incidence varies in different countries and regions; the overall incidence is about 6/100,000 people per year (Etminan et al., 2019). The incidence of SAH gradually increases with age. Due to the advances in medical and surgical techniques, the mortality rate of SAH has decreased over the past few

decades but still remains prevalent (Macdonald and Schweizer, 2017). In addition, 33% of SAH survivors experienced a high disability rate and required long-term care (Al-Khindi et al., 2010). Vasospasm has traditionally been considered a major cause of death and disability post-SAH as it can induce delayed cerebral ischemia. Therefore, most of the studies in the past decades have focused on reducing vasospasm with the aim of improving outcomes of SAH patients (Kassell et al., 1985; Macdonald and Weir, 1991; Cook, 1995; Crowley et al., 2008; Macdonald, 2016; Etminan and Macdonald, 2021). However, delayed cerebral ischemia still occurs in a considerable proportion of SAH patients, even if the cerebral vasospasm is reversed in the early stage. In addition, not all cerebral infarction after SAH is caused by cerebral vasospasm in clinical practice. Cerebral infarction may occur immediately after the occurrence of SAH in some patients, without any cerebral angiography findings (Naidech et al., 2006). Several recent large clinical trials have suggested that treating vasospasm does not significantly improve patient outcomes (Macdonald et al., 2008, 2011; Shen et al., 2013). It is suggested that there may be other mechanisms of injury affecting the prognosis of SAH patients. Recently, the concept of early brain injury (EBI) was proposed, which refers to brain injury occurring within 72 h after the occurrence of SAH (Cahill and Zhang, 2009). EBI is an event with complex pathophysiological changes, including increased intracranial pressure, decreased cerebral blood flow, and direct hematoma toxicity to the brain tissue. These subsequently lead to the destruction of the blood-brain barrier (BBB), oxidative stress injury, cellular death, inflammatory response, microcirculation dysfunction and mitochondrial disorder, causing neurologic injury and poor outcome after SAH (Cahill et al., 2006; Ostrowski et al., 2006; Sehba et al., 2012; Fujii et al., 2013; Ji and Chen, 2016). Therefore, exploring efficient therapeutic methods targeting EBI is essential in treating SAH.

Melatonin is a type of neuroendocrine hormone produced by the pineal gland, with low daytime levels and high nighttime levels (Tordjman et al., 2017; Cardinali, 2021). It participates in regulating the immune, reproductive, endocrine and central nervous systems, and has attracted widespread attention due to its strong anti-inflammatory and antioxidant properties (Majidinia et al., 2018; He et al., 2021; Kvetnoy et al., 2022). Recent studies have shown that melatonin exerts a neuroprotective role in many neurological diseases such as stroke (Lee et al., 2007; Tai et al., 2010), trauma injury (Samantaray et al., 2009; Osier et al., 2018), neurodegenerative diseases (Alamdari et al., 2021; Roy et al., 2022), and spinal cord injury (Hong et al., 2010; Zhang et al., 2018). The mechanisms involved include anti-inflammation, anti-apoptosis, anti-oxidative stress, and BBB protection. In addition, numerous studies have been carried out on the role and mechanism of melatonin in SAH, and the results established that melatonin can improve brain injury after SAH through a variety of mechanisms, thus alleviating neurological impairment and improving prognosis (Martinez-Cruz et al., 2002). This study summarizes the current literature on melatonin treatment in EBI after SAH (**Table 1**). It explores the relevant mechanism of melatonin-induced neuroprotection, providing a theoretical basis for the experimental study and clinical application of melatonin treatment for SAH.

THE EFFECT AND MECHANISM OF MELATONIN IN SUBARACHNOID HEMORRHAGE

Melatonin and Vasospasm

Cerebral vasospasm is a common complication of SAH, which usually appears around 3 days after SAH, and reaches its peak within 10 days after SAH (Etminan et al., 2011; Gaspard, 2020). Delayed cerebral ischemia caused by cerebral vasospasm leads to cerebral infarction, cerebral hernia and other malignant complications (Kumar et al., 2016; Ikram et al., 2021). In the acute stage following SAH, the nitric oxide (NO)/NO synthase (NOS) system and vasoconstrictor factors may be involved in the occurrence of cerebral vasospasm. The NO/NOS system plays an important role regulating hemodynamics. NO regulates cerebral blood flow and blood pressure by dilating blood vessels, inhibiting platelet aggregation, and diminishing leukocyte adhesion to the intima (Toda et al., 2009; Attia et al., 2015; Vanhoutte, 2018). After SAH onset, decreased NO levels are observed, leading to CBF reduction, cerebral vasoconstriction, and platelet aggregation. In addition, as a form of free radical, NO enters the intima cells, causing damage to mitochondria and blood vessels (Sehba and Bederson, 2011; Crobeddu et al., 2016; Ehlert et al., 2016; Guo et al., 2016). Endothelin-1 (ET-1) is a potential vasoconstrictor mainly released by astrocytes and leukocytes during the early inflammatory response stage after SAH (Cosentino and Katusić, 1994; La and Reid, 1995; Vergouwen et al., 2012). Previous studies found that ET-1 levels in serum and plasma increased within a few minutes after SAH, and the expression of its receptor increased within 48 h (Lin et al., 2004, 2006). The declined levels of NO increases the expression of ET-1, causing continuous vasocontraction and degenerative morphological changes of the vessels. Notably, previous studies mainly focus on the spasms of large blood vessels, while ignoring the microvascular changes. The cerebral microvasculature has been recently identified as an important intervention target after SAH. Changes in the anatomical structure of cerebral microvessels, sufficient to cause functional deficits, are found in the early post-SAH period. After SAH occurrence, constriction of microvessels contributes to intima remodeling, basal lamina degradation, increased vascular permeability, and eventually leads to microcirculation disorders and brain injury (Nagai et al., 1976; Sehba and Friedrich, 2011).

To explore whether melatonin treatment reverses vasospasm in a SAH model, light microscopic measurements of the basilar arteries were performed to illustrate the arterial wall changes (Fang et al., 2009). Melatonin injection simultaneously with SAH or 2 h after SAH both were found to attenuate the constriction of vessels (Aydin et al., 2005). Additionally, melatonin-induced improvement of cerebral vasospasm is associated with increased serum NO levels, decreased arginase levels, and oxidative stress in the brain (Aladag et al., 2009). Furthermore, the potential

TABLE 1 | Neuroprotection of melatonin treatment in SAH.

Therapeutic paradigm	Main findings	References
5 mg or 10 mg/kg, injected into the cisterna magna at 1 h before SAH.	Melatonin prevents focal cerebellum injury by induction of HO-1. The antioxidant capability of melatonin is higher than vitamin E.	Martinez-Cruz et al., 2002
5 mg/kg, intraperitoneally injection every 12 h for 48 h, start at 2 h after SAH.	Melatonin prevents SAH-induced vasospasm and apoptosis of endothelial cells of vessels.	Aydin et al., 2005
15 mg or 150 mg/kg, intraperitoneally injection at 2 h after SAH.	High doses of melatonin (150 mg/kg) reduce brain edema and mortality after SAH.	Ayer et al., 2008b
15 mg or 150 mg/kg, intraperitoneally injection at 2 h after SAH.	High doses of melatonin (150 mg/kg) reduce brain edema and mortality after SAH, which is unrelated to oxidative stress inhibition.	Ayer et al., 2008a
10 mg/kg, intraperitoneally injection immediately after SAH, then daily for 2 days.	Melatonin alleviates oxidative stress, restores BBB permeability and reduces brain edema after SAH.	Ersahin et al., 2009
20 mg/kg, intraperitoneally injection at 6 h after SAH, twice daily for 5 days.	Melatonin alleviates cerebral vasospasm by elevating NO levels in serum and downregulating the levels of arginase and oxidative stress in the brain.	Aladag et al., 2009
5 mg/kg, intraperitoneally injection every 12 h for 120 h, start immediately after SAH.	Melatonin attenuates inflammatory response and oxidative stress in the spasmodic artery and alleviates cerebral vasospasm post-SAH.	Fang et al., 2009
150 mg/kg, intraperitoneally injection at 2 h and 24 h after SAH	Melatonin attenuates EBI *via* activating the Nrf2-ARE pathway and regulating oxidative stress by inducing antioxidant and detoxifying enzymes.	Wang et al., 2012
150 mg/kg, intraperitoneally injection at 2 and 24 h after SAH	Melatonin exerts neuroprotection through anti-oxidative and anti-inflammatory signaling pathways following SAH.	Wang et al., 2013
150 mg/kg, intraperitoneally injection at 2 h after SAH.	Melatonin improves the neurological outcome by reducing neuronal apoptosis and enhancing autophagy *via* a mitochondrial pathway.	Chen et al., 2014b
150 mg/kg, intraperitoneally injection at 2 h after SAH.	Melatonin inhibits the degradation of tight junction proteins, attenuates cerebral edema, improves BBB dysfunctions by inhibiting the inflammatory response.	Chen et al., 2014a
150 mg/kg, intraperitoneally injection at 2 h after SAH.	Melatonin attenuates neurogenic pulmonary edema by preventing alveolar-capillary barrier dysfunctions *via* repressing the inflammatory response and reducing apoptosis after SAH.	Chen et al., 2015
150 mg/kg, intraperitoneally injection at 2 h after SAH.	Melatonin attenuates the EBI post-SAH by inhibiting NLRP3 inflammasome-associated apoptosis.	Dong et al., 2016
150 mg/kg, intraperitoneally injection at 2 and 12 h after SAH.	Melatonin attenuates EBI following SAH *via* the MR/Sirt1/NF-κB signaling pathway.	Zhao et al., 2017
150 mg/kg, intraperitoneally injection at 2 h after SAH.	Melatonin exerts a neuroprotective effect after SAHA by inhibiting mitophagy-associated NLRP3 inflammasome.	Cao et al., 2017
150 mg/kg, intraperitoneally injection at 2 and 12 h after SAH.	Melatonin attenuates EBI after SAH by regulating the H19-miR-675-P53 and H19-let-7a-NGF signaling pathways.	Yang et al., 2018b
15 mg or 150 mg/kg, intraperitoneally injection at 2 h after SAH.	Melatonin attenuates SAH-induced EBI by diminishing neuronal apoptosis and autophagy, partially involving the ROS-MST1 pathway.	Shi et al., 2018
150 mg/kg, intraperitoneally injection at 2 and 12 h after SAH.	Melatonin attenuates EBI after SAH by regulating the protein expression of SIRT3.	Yang et al., 2018a
150 mg/kg, intraperitoneally injection at 2 and 12 h after SAH.	Melatonin provides protection against EBI post-SAH by inducing mitophagy and increasing the expression of NRF2.	Sun et al., 2018
Intraperitoneally injection at 2 h after SAH.	Melatonin treatment attenuates EBI following SAH *via* the JAK1/STAT3 signaling pathway.	Li et al., 2019
150 mg/kg, intraperitoneally injection at 2 and 12 h after SAH.	Melatonin ameliorates cerebral vasospasm by regulating the H19/miR-138/eNOS and H19/miR-675/HIF1α signaling pathways.	Hou et al., 2020
50 mg/kg, 150 mg/kg, or 300 mg/kg, intraperitoneally injection at 15 min after SAH.	Melatonin exerts a white matter-protective effect in SAH pathophysiology, possibly by attenuating apoptosis in oligodendrocytes.	Liu et al., 2020
150 mg/kg, intraperitoneally injection at 12 h after SAH.	Melatonin ameliorates delayed brain injury following SAH *via* H19/miR-675/HIF1A/TLR4 signaling pathway.	Xu et al., 2022

underlying mechanism of melatonin treatment after SAH was studied. Hou et al. (2020) reported that melatonin ameliorates post-SAH vasospasm by regulating the expression of endothelial nitric oxide synthase (eNOS) and hypoxia-inducible factor-1 (HIF-1α) *via* the H19/miR-138/eNOS/NO and H19/miR-675/HIF-1α signaling pathways. However, the crosstalk of the pathway network is complex, and the exact mechanism behind the anti-vasospasm effect of melatonin needs further research. Recently, a clinical trial provided evidence for the delayed elevation of circulatory daytime melatonin after SAH and described the role of aneurysm location, resulting in high levels during the critical phase (Neumaier et al., 2021). However, the relationship between endogenous melatonin level changes and vasospasm were not discussed. Further clinical trials focusing on the role of endogenous changes and administration of melatonin in vasospasm after SAH may provide more clinical evidence for the clinical application of melatonin in SAH.

Melatonin and Inflammation

Previous studies have found that in the early SAH stage, erythrocyte degradation products accumulated in the subarachnoid space, activating an inflammatory response and

participating in the acceleration of brain injury (Schallner et al., 2015; Zhang et al., 2016). Both experimental studies and clinical trials have demonstrated that the aseptic inflammatory response after SAH can aggravate tissue damage and is an independent predictor of mortality in SAH patients (Pradilla et al., 2010; Muroi et al., 2011; Luo et al., 2021; Devlin et al., 2022). Microglia are innate immune cells of the central nervous system and can be activated rapidly under inflammatory conditions, trauma, or other stimulating factors. Previous studies have confirmed that microglia can be activated within minutes of the occurrence of SAH and contribute to the process of inflammation (Coulibaly and Provencio, 2020; Heinz et al., 2021; Chen et al., 2022). When microglia are activated in a normal physiological state, they can remove harmful substances by phagocytosis. However, when microglia are overactivated, they exacerbate brain injury by releasing pro-inflammatory factors and oxidative metabolites, promoting the activation of neutrophils and macrophages, thus resulting in the destruction of BBB, inflammatory response and neuronal damage (Lucke-Wold et al., 2016; van Dijk et al., 2016; Schneider et al., 2018). Similar to microglia, astrocytes can also synthesize and secrete inflammatory factors (such as cytokines and chemokines) and participate in the inflammatory response of SAH (Gris et al., 2019; Zhang et al., 2021). In addition to inflammatory cells, inflammatory-related proteins such as C-reactive protein, intercellular adhesion molecule (ICAM)-1, high mobility group box 1 (HMGB1), and galectin-3 also play key roles in the inflammatory reaction following SAH (Lin et al., 2007; Sun et al., 2014; Nishikawa and Suzuki, 2018; Mota Telles et al., 2021). Damage-associated molecular patterns (DAMPs) are released by neurons, astrocytes, microglia and endothelial cells in the early stage of SAH, activating local and peripheral immune cells and releasing cytokines to promote an inflammatory response. This process leads to early brain injury (Chaudhry et al., 2018; Lu et al., 2018; Ahmed et al., 2021; Balança et al., 2021). Furthermore, pro-inflammatory cytokines, such as interleukin-1 β (IL-1β), interleukin-6 (IL-6) and tumor necrosis factor -α (TNF-α), can trigger an inflammatory cascade that ultimately leads to the destruction of the BBB, and cause secondary injury post-SAH (Duris et al., 2018; Savarraj et al., 2018; Okada and Suzuki, 2020). Therefore, therapies inhibiting the inflammatory response may alleviate the EBI after SAH, thereby improving the prognosis of patients.

Melatonin has shown anti-inflammatory properties in SAH. It can reduce neuroinflammation and improve axonal hypomyelination by modulating M1/M2 microglia polarization *via* the JAK2-STAT3-telomerase pathway (Zhou et al., 2021). Moreover, melatonin reduces the release of pro-inflammatory mediators (IL-1β, IL-6, and TNF-α, etc.), alleviates the inflammatory response, thus improving secondary brain damage and neurobehavioral dysfunction after SAH (Fang et al., 2009). In addition, inhibition of inflammation by melatonin effectively protects the integrity of the BBB structure and function, and reduces the degree of brain edema (Chen et al., 2014a, 2015). Wang et al. (2013) found that melatonin markedly decreased the expressions of TLR4 pathway-related agents, such as HMGB1, toll-like receptor 4 (TLR4), myeloid differentiation factor 88 (MyD88), indicating the involvement of the TLR4 pathway in melatonin-induced neuroprotection. Among the inflammatory responses after SAH, NLRP3 inflammasome activation has recently been investigated. NLRP3 inflammasome activation promotes the maturation and secretion of pro-inflammatory cytokines and participates in cell death processes such as pyroptosis. Various studies have revealed that reduction of NLRP3 inflammasome activation exerts strong neuroprotective effects in the acute phase following SAH, which was associated with the downregulation of pro-inflammatory cytokines. Cao et al. (2017) proposed that melatonin is neuroprotective against EBI post-SAH *via* inhibiting mitophagy-associated NLRP3 inflammasome. In addition, Dong et al. (2016) demonstrated that melatonin treatment attenuates brain injury by inhibiting NLRP3 inflammasome-associated apoptosis following SAH. Notably, NLRP3 signal activation is performed by microglia, and reduced NLRP3 is related to decreased white matter injury after melatonin treatment in SAH (Liu et al., 2020).

Melatonin and Apoptosis

Apoptosis is one of the main pathophysiological processes of EBI, and its degree is closely related to the neurological function recovery after SAH (He et al., 2012; Hong et al., 2014). Previous experiments have shown that apoptosis of neurons begins within 10 min after the occurrence of SAH (Friedrich et al., 2012). The increased intracranial pressure, cerebral edema and oxidative stress induced by SAH can all lead to extensive cell apoptosis, including neurons, glial cells and vascular endothelial cells (Ostrowski et al., 2006; Hasegawa et al., 2011; Shao et al., 2020). Apoptosis after SAH involves many pathways, including the death receptor pathway, mitochondrial pathway, and dependent or independent caspase pathway (Cahill et al., 2006). The mitochondrial pathway is mediated by the Bcl-2 family and manifests as increased permeability of the mitochondrial membrane. Cytochrome c transfers from mitochondria to the cytoplasmic septum and participates in apoptosome assembly with apoptosis protease-activator factor 1 (Apaf-1), thus leading to the activation of caspase-9. Subsequently, caspase-3 is further activated to induce apoptosis (Ceccatelli et al., 2004; Bornstein et al., 2020). The caspase-independent pathway is mainly mediated by the mitochondrial release of apoptosis-inducing factor (AIF). AIF exists in the mitochondrial membrane gap in its normal state, and can be transferred to the nucleus after SAH to induce DNA destruction and cell apoptosis without caspase activation (Lorenzo et al., 1999; Lorenzo and Susin, 2007; Norberg et al., 2010). Death receptors participate in external apoptosis pathways. The expression of Fas and TNF ligands of death receptors are upregulated after SAH, binding to death receptors and activating the caspase cascade (Gorojod et al., 2017; Cha et al., 2019). These pathways interact with each other and participate in the occurrence and regulation of apoptosis after SAH. By intervening on the above pathways, apoptosis may be effectively alleviated, thus improving the neurological injury and promoting the recovery of neurologic function after SAH.

The neuroprotective role of melatonin by diminishing cellular apoptosis in EBI after SAH was investigated. A study published in 2005 first reported the anti-apoptosis effect of melatonin in a SAH rabbit model by reducing the apoptosis of endothelial cells

(Aydin et al., 2005). Subsequently, many studies confirmed the role of melatonin in alleviating neuronal apoptosis after SAH, contributing to the amelioration of spatial learning and memory deficits and improvement of therapeutic outcomes (Wang et al., 2012, 2013; Dong et al., 2016; Sun et al., 2018). Moreover, melatonin can reduce oligodendrocyte apoptosis associated with the attenuation of white matter injury. The mechanism of the above anti-apoptosis effects is related to enhancing autophagy, which improves cell apoptosis *via* a mitochondrial pathway (Chen et al., 2014b). In addition, melatonin reduces cellular apoptosis partially *via* the regulation of the melatonin receptor/Sirt1/NF-κB signaling pathway (Zhao et al., 2017), ROS/mammalian sterile 20-like kinase 1 (MST1) pathway (Shi et al., 2018), ROS/SIRT3 pathway (Yang et al., 2018a), and JAK/STAT pathway (Li et al., 2019). Recently, many studies have shown that melatonin abolished apoptosis by regulating microRNAs. Xu et al. (2022) established that melatonin affects HIF-1α and ameliorates delayed brain injury following SAH *via* the H19/miR-675/HIF1A/TLR4 pathway. In contrast, Yang et al. (2018b) demonstrated that long non-coding RNA and microRNA-675/let-7a mediate the protective effect of melatonin against EBI after SAH *via* targeting TP53 and neural growth factor. Notably, melatonin not only reduces cell apoptosis in the brain but also prevents alveolar-capillary barrier dysfunctions *via* repressing cell apoptosis in the lung, thus attenuating neurogenic pulmonary edema after SAH (Chen et al., 2015).

Melatonin and Blood-Brain Barrier Disruption

BBB is mainly composed of capillary endothelial cells, pericytes, astrocytes, and vascular basilemma. Due to the tight connection between capillary endothelial cells, the cell gap is small. In the physiological state, most substances (such as plasma components, red blood cells, etc.) cannot pass the BBB except for a few lipid-soluble small molecules (Daneman and Barres, 2005; Zhao et al., 2015). In SAH, the expression of type IV collagen is significantly increased, which degrades the BBB basement membrane and is accompanied by the elevation of vascular endothelial growth factor, activation of endothelial cell apoptosis, resulting in the enhanced permeability of BBB (Yang and Rosenberg, 2011; Kanamaru and Suzuki, 2019; Li et al., 2020). Cerebral edema directly results from BBB dysfunction, which includes vasogenic and cytotoxic edema (Rosenberg, 1999; Sandoval and Witt, 2008). Vasogenic edema refers to blood flow from the vessels to brain tissue due to the apoptosis of endothelial cells and glial cells around blood vessels. The increase of intracranial pressure after SAH induces the decrease of CBF, which causes global cerebral ischemia, leading to the failure of the Na^+ /K^+ pump, and resulting in cytotoxic edema (Okada et al., 2020; Chen et al., 2021). Clinical studies have shown that about 8% of patients were found to have global cerebral edema after head CT examination upon admission, and another 12% of patients developed prominent cerebral edema within 6 days following SAH (Cahill et al., 2006). Severe cerebral edema often leads to increased intracranial pressure, acute cerebral ischemia, cerebral hernia, and death. Therefore, it is of great significance to protect the integrity of BBB and reduce the development of cerebral edema, aiming to improve the prognosis of patients (Michinaga and Koyama, 2015).

Pragmatic therapeutic strategies for brain edema such as acupuncture, osmotherapy, non-peptide vasopressin receptor antagonist, and calcium channel blockers are used in clinical practice (Rowland et al., 2019; Corry et al., 2020; Hinson et al., 2020; Guo et al., 2022). Although the above-mentioned treatment approaches have been well-studied and display partial protective effects in attenuating cerebral edema, a single therapy capable of inhibiting cerebral edema is yet to be found due to the complex mechanisms involved. Recently, experimental studies have shown that melatonin not only reduces cerebral edema but also protects the BBB by preventing the disruption of tight junction protein expression (ZO-1, occludin, and claudin-5), indicating that melatonin may be an effective alternative for alleviating brain edema after SAH (Ayer et al., 2008a,b; Chen et al., 2014a; Li et al., 2019; Liu et al., 2020). Additionally, melatonin can easily cross the BBB, while preserving BBB permeability and reducing brain edema (Ersahin et al., 2009).

Melatonin and Oxidative Stress

Superoxide dismutase (SOD), glutathione peroxidase, catalase and other important antioxidant enzymes in brain tissue are down-regulated after SAH, leading to a decrease in antioxidant capacity. Meanwhile, vasospasm and cerebral edema caused by SAH lead to cerebral ischemia, resulting in the production of a large number of oxygen ions (O^{2-}) and hydrogen peroxide (H_2O_2) (Yang et al., 2017; Shao et al., 2020). The high concentration of Fe^{2+} and Fe^{3+} produced by erythrocyte degradation can combine with H_2O_2 and O^{2-} by Fenton reaction to form hydroxyl radicals. Hydroxyl radicals are among the most toxic reactive oxygen species (ROS), which can directly damage neurovascular units and cause neurologic injury. In addition, free radicals-induced oxidative stress cause brain damage by promoting lipid peroxidation, protein degradation, and DNA destruction, resulting in neuronal apoptosis, endothelial cell damage, and BBB destruction. These changes result in severe brain injury and neurological deterioration after SAH (Lu et al., 2019; Wu et al., 2021). Therefore, the intervention of oxidative stress can inhibit the secondary cascade reaction of pathological changes and reduce subsequent brain damage (Zhang et al., 2014; Lin et al., 2021a).

Melatonin is a powerful antioxidant. Its antioxidant effects include direct scavenging of free radicals, stimulation of antioxidant enzyme activity and gene expression, stimulation of glutathione synthesis, reduction of electron leakage of mitochondrial electron transport chain, and reduction of cytokine production (Reiter et al., 2016; Galano and Reiter, 2018). Previous research has shown that lipopolysaccharides-induced hyperreactivity of vascular smooth muscle is mediated through enhanced release of ROS and prostanoids, and melatonin inhibits the vascular hyperreactivity *via* selective scavenging of ROS (Müller-Schweinitzer et al., 2004). Melatonin can cause a significant increase in brain glutathione (GSH) and superoxidase dismutase (SOD) content, as well as Na^+-K^+-ATPase activity and GSH/GSSG ratio, which is accompanied by significant decreases

in ROS, malondialdehyde (MDA) levels, and myeloperoxidase (MPO) activity, thereby providing neuroprotection from EBI following SAH (Ersahin et al., 2009; Fang et al., 2009; Yang et al., 2018a). Besides, melatonin alleviates SAH-induced EBI by inhibiting the ROS-stimulated activation of the MST1 pathway (Shi et al., 2018), NLRP3 inflammasome (Cao et al., 2017), and SIRT3 pathway (Yang et al., 2018a). An *in vivo* and *in vitro* study demonstrated that H_2O_2 markedly upregulated the expression of H19, miR-675, and NGF, and downregulated let-7a and TP53 levels. These findings were reversed by melatonin treatment, revealing the potential antioxidant mechanisms of melatonin (Yang et al., 2018b). It is worth noting that Nrf2 is a global promoter of antioxidant response and has potential protective effects against post-SAH EBI. It has been shown that Nrf2-knockout animals have poorer outcomes in SAH. Melatonin can increase the effects of the antioxidant system by upregulating the expression of Nrf2 (Wang et al., 2012; Sun et al., 2018).

CONCLUSION AND PROSPECTS

Melatonin is a neuroendocrine hormone that protects the central nervous system mainly through anti-vasospasm, anti-oxidative stress, anti-inflammatory response, anti-apoptosis and BBB protection. At present, the study of melatonin in SAH is mostly limited to animal and cell models, and lack of clinical evidence. So far, four clinical studies with small cohort of patients have explored the association between melatonin and SAH patients. Melatonin could decrease fatigue, but has no significant impact on depression and apathy post-stroke (Gilard et al., 2016). In addition, melatonin administration has no effect on delayed cerebral ischemia, but may reduce mortality of SAH (Lin et al., 2021b). Another prospective and observational study enrolls 169 aneurysmal SAH patients, to ascertain the relationship between endogenous melatonin level and neurological outcome post-SAH. The results indicate that higher level of serum melatonin is associated with poor outcome after SAH (Zhan et al., 2021). As many factors can affects the concentrations of serum melatonin such as the severity of brain injury, and rhythm of melatonin secretion, the accurate influence and changes of melatonin after SAH need to be studied. Neumaier et al. (2021) reports that there is a delayed upregulation of circulatory daytime melatonin levels after SAH, and higher concentration of melatonin is related with patients with anterior communicating artery aneurysms or poor clinical outcome, indicating the potential role of hypothalamic dysfunction. Further large-scale clinical trials are needed to verify its neuroprotective effect in SAH patients. Additionally, the effects of melatonin in patients with different degrees of injury and ages should be explored. Moreover, the secretion of melatonin in the body follows the circadian rhythm. The time of administration likely plays an essential role in achieving the optimal therapeutic effect, and needs further study. Furthermore, the drug dosage and administration interval of melatonin used in current studies vary greatly. The optimal dose and administration frequency should be determined to effectively improve the therapeutic effect. Finally, melatonin regulates biological rhythms, and a large proportion of SAH patients have sleep disorders. Determining the therapeutic strategy of melatonin for this population is worth exploring.

AUTHOR CONTRIBUTIONS

CX and ZH conceived the perspective of the work and searched the literature and drafted the manuscript. JL critically revised the article. All authors contributed to and approved to the final manuscript.

REFERENCES

Ahmed, H., Khan, M. A., Kahlert, U. D., Niemelä, M., Hänggi, D., Chaudhry, S. R., et al. (2021). Role of adaptor protein myeloid differentiation 88 (MyD88) in post-subarachnoid hemorrhage inflammation: a systematic review. *Int. J. Mol. Sci.* 22:4185. doi: 10.3390/ijms22084185

Aladag, M. A., Turkoz, Y., Parlakpinar, H., Ozen, H., Egri, M., and Unal, S. C. (2009). Melatonin ameliorates cerebral vasospasm after experimental subarachnoidal haemorrhage correcting imbalance of nitric oxide levels in rats. *Neurochem. Res.* 34, 1935–1944. doi: 10.1007/s11064-009-9979-7

Alamdari, A. F., Rahnemayan, S., Rajabi, H., Vahed, N., Kashani, H. R. K., Rezabakhsh, A., et al. (2021). Melatonin as a promising modulator of aging related neurodegenerative disorders: role of microRNAs. *Pharmacol. Res.* 173:105839. doi: 10.1016/j.phrs.2021.105839

Al-Khindi, T., Macdonald, R. L., and Schweizer, T. A. (2010). Cognitive and functional outcome after aneurysmal subarachnoid hemorrhage. *Stroke* 41, e519–e536.

Attia, M. S., Lass, E., and Loch Macdonald, R. (2015). Nitric oxide synthases: three pieces to the puzzle? *Acta Neurochir. Suppl.* 120, 131–135. doi: 10.1007/978-3-319-04981-6_22

Aydin, M. V., Caner, H., Sen, O., Ozen, O., Atalay, B., Cekinmez, M., et al. (2005). Effect of melatonin on cerebral vasospasm following experimental subarachnoid hemorrhage. *Neurol. Res.* 27, 77–82. doi: 10.1179/016164105X18331

Ayer, R. E., Sugawara, T., Chen, W., Tong, W., and Zhang, J. H. (2008a). Melatonin decreases mortality following severe subarachnoid hemorrhage. *J. Pineal Res.* 44, 197–204. doi: 10.1111/j.1600-079X.2007.00508.x

Ayer, R. E., Sugawara, T., and Zhang, J. H. (2008b). Effects of melatonin in early brain injury following subarachnoid hemorrhage. *Acta Neurochir. Suppl.* 102, 327–330. doi: 10.1007/978-3-211-85578-2_62

Balança, B., Desmurs, L., Grelier, J., Perret-Liaudet, A., and Lukaszewicz, A. C. (2021). DAMPs and RAGE pathophysiology at the acute phase of brain injury: an overview. *Int. J. Mol. Sci.* 22:2439. doi: 10.3390/ijms22052439

Bornstein, R., Gonzalez, B., and Johnson, S. C. (2020). Mitochondrial pathways in human health and aging. *Mitochondrion* 54, 72–84. doi: 10.1016/j.mito.2020.07.007

Cahill, J., Calvert, J. W., and Zhang, J. H. (2006). Mechanisms of early brain injury after subarachnoid hemorrhage. *J. Cereb. Blood Flow Metab.* 26, 1341–1353.

Cahill, J., and Zhang, J. H. (2009). Subarachnoid hemorrhage: is it time for a new direction? *Stroke* 40, S86–S87. doi: 10.1161/STROKEAHA.108.533315

Cao, S., Shrestha, S., Li, J., Yu, X., Chen, J., Yan, F., et al. (2017). Melatonin-mediated mitophagy protects against early brain injury after subarachnoid hemorrhage through inhibition of NLRP3 inflammasome activation. *Sci. Rep.* 7:2417. doi: 10.1038/s41598-017-02679-z

Cardinali, D. P. (2021). Melatonin and healthy aging. *Vitam. Horm.* 115, 67–88. doi: 10.1016/bs.vh.2020.12.004

Ceccatelli, S., Tamm, C., Sleeper, E., and Orrenius, S. (2004). Neural stem cells and cell death. *Toxicol. Lett.* 149, 59–66. doi: 10.1016/j.toxlet.2003.12.060

Cha, Z., Cheng, J., Xiang, H., Qin, J., He, Y., Peng, Z., et al. (2019). Celastrol enhances TRAIL-induced apoptosis in human glioblastoma *via* the death receptor pathway. *Cancer Chemother. Pharmacol.* 84, 719–728. doi: 10.1007/s00280-019-03900-8

Chaudhry, S. R., Hafez, A., Rezai Jahromi, B., Kinfe, T. M., Lamprecht, A., Niemelä, M., et al. (2018). Role of damage associated molecular pattern molecules (DAMPs) in aneurysmal subarachnoid hemorrhage (aSAH). *Int. J. Mol. Sci.* 19:2035. doi: 10.3390/ijms19072035

Chen, J., Chen, G., Li, J., Qian, C., Mo, H., Gu, C., et al. (2014a). Melatonin attenuates inflammatory response-induced brain edema in early brain injury following a subarachnoid hemorrhage: a possible role for the regulation of pro-inflammatory cytokines. *J. Pineal Res.* 57, 340–347. doi: 10.1111/jpi.12173

Chen, J., Wang, L., Wu, C., Hu, Q., Gu, C., Yan, F., et al. (2014b). Melatonin-enhanced autophagy protects against neural apoptosis *via* a mitochondrial pathway in early brain injury following a subarachnoid hemorrhage. *J. Pineal Res.* 56, 12–19. doi: 10.1111/jpi.12086

Chen, J., Qian, C., Duan, H., Cao, S., Yu, X., Li, J., et al. (2015). Melatonin attenuates neurogenic pulmonary edema *via* the regulation of inflammation and apoptosis after subarachnoid hemorrhage in rats. *J. Pineal Res.* 59, 469–477. doi: 10.1111/jpi.12278

Chen, J., Zheng, Z. V., Lu, G., Chan, W. Y., Zhang, Y., and Wong, G. K. C. (2022). Microglia activation, classification and microglia-mediated neuroinflammatory modulators in subarachnoid hemorrhage. *Neural Regen. Res.* 17, 1404–1411. doi: 10.4103/1673-5374.330589

Chen, S., Shao, L., and Ma, L. (2021). Cerebral edema formation after stroke: emphasis on blood-brain barrier and the lymphatic drainage system of the brain. *Front. Cell Neurosci.* 15:716825. doi: 10.3389/fncel.2021.716825

Cook, D. A. (1995). Mechanisms of cerebral vasospasm in subarachnoid haemorrhage. *Pharmacol. Ther.* 66, 259–284. doi: 10.1016/0163-7258(94)00080-m

Corry, J. J., Asaithambi, G., Shaik, A. M., Lassig, J. P., Marino, E. H., Ho, B. M., et al. (2020). Conivaptan for the reduction of cerebral edema in intracerebral hemorrhage: a safety and tolerability study. *Clin. Drug Investig.* 40, 503–509. doi: 10.1007/s40261-020-00911-9

Cosentino, F., and Katusić, Z. S. (1994). Does endothelin-1 play a role in the pathogenesis of cerebral vasospasm? *Stroke* 25, 904–908. doi: 10.1161/01.str.25.4.904

Coulibaly, A. P., and Provencio, J. J. (2020). Aneurysmal subarachnoid hemorrhage: an overview of inflammation-induced cellular changes. *Neurotherapeutics* 17, 436–445. doi: 10.1007/s13311-019-00829-x

Crobeddu, E., Pilloni, G., Tardivo, V., Fontanella, M. M., Panciani, P. P., Spena, G., et al. (2016). Role of nitric oxide and mechanisms involved in cerebral injury after subarachnoid hemorrhage: is nitric oxide a possible answer to cerebral vasospasm? *J. Neurosurg. Sci.* 60, 385–391.

Crowley, R. W., Medel, R., Kassell, N. F., and Dumont, A. S. (2008). New insights into the causes and therapy of cerebral vasospasm following subarachnoid hemorrhage. *Drug Discov. Today* 13, 254–260. doi: 10.1016/j.drudis.2007.11.010

Daneman, R., and Barres, B. A. (2005). The blood-brain barrier–lessons from moody flies. *Cell* 123, 9–12. doi: 10.1016/j.cell.2005.09.017

Devlin, P., Ishrat, T., and Stanfill, A. G. (2022). A systematic review of inflammatory cytokine changes following aneurysmal subarachnoid hemorrhage in animal models and humans. *Transl. Stroke Res.* doi: 10.1007/s12975-022-01001-y

Dong, Y., Fan, C., Hu, W., Jiang, S., Ma, Z., Yan, X., et al. (2016). Melatonin attenuated early brain injury induced by subarachnoid hemorrhage *via* regulating NLRP3 inflammasome and apoptosis signaling. *J. Pineal Res.* 60, 253–262. doi: 10.1111/jpi.12300

Duris, K., Lipkova, J., Splichal, Z., Madaraszova, T., and Jurajda, M. (2018). Early inflammatory response in the brain and anesthesia recovery time evaluation after experimental subarachnoid hemorrhage. *Transl. Stroke Res.* doi: 10.1007/s12975-018-0641-z

Ehlert, A., Manthei, G., Hesselmann, V., Mathias, K., Bein, B., and Pluta, R. (2016). A case of hyperacute onset of vasospasm after aneurysmal subarachnoid hemorrhage and refractory vasospasm treated with intravenous and intraventricular nitric oxide: a mini review. *World Neurosurg.* 91, .e611–.e618. doi: 10.1016/j.wneu.2016.04.047

Ersahin, M., Toklu, H. Z., Cetinel, S., Yüksel, M., Yeğen, B. C., and Sener, G. (2009). Melatonin reduces experimental subarachnoid hemorrhage-induced oxidative brain damage and neurological symptoms. *J. Pineal Res.* 46, 324–332. doi: 10.1111/j.1600-079X.2009.00664.x

Etminan, N., Chang, H. S., Hackenberg, K., De Rooij, N. K., Vergouwen, M. D. I., Rinkel, G. J. E., et al. (2019). Worldwide incidence of aneurysmal subarachnoid hemorrhage according to region, time period, blood pressure, and smoking prevalence in the population: a systematic review and meta-analysis. *JAMA Neurol.* 76, 588–597. doi: 10.1001/jamaneurol.2019.0006

Etminan, N., and Macdonald, R. L. (2021). Neurovascular disease, diagnosis, and therapy: subarachnoid hemorrhage and cerebral vasospasm. *Handb. Clin. Neurol.* 176, 135–169. doi: 10.1016/B978-0-444-64034-5.00009-2

Etminan, N., Vergouwen, M. D., Ilodigwe, D., and Macdonald, R. L. (2011). Effect of pharmaceutical treatment on vasospasm, delayed cerebral ischemia, and clinical outcome in patients with aneurysmal subarachnoid hemorrhage: a systematic review and meta-analysis. *J. Cereb. Blood Flow Metab.* 31, 1443–1451. doi: 10.1038/jcbfm.2011.7

Fang, Q., Chen, G., Zhu, W., Dong, W., and Wang, Z. (2009). Influence of melatonin on cerebrovascular proinflammatory mediators expression and oxidative stress following subarachnoid hemorrhage in rabbits. *Mediators Inflamm.* 2009:426346. doi: 10.1155/2009/426346

Friedrich, V., Flores, R., and Sehba, F. A. (2012). Cell death starts early after subarachnoid hemorrhage. *Neurosci. Lett.* 512, 6–11. doi: 10.1016/j.neulet.2012.01.036

Fujii, M., Yan, J., Rolland, W. B., Soejima, Y., Caner, B., and Zhang, J. H. (2013). Early brain injury, an evolving frontier in subarachnoid hemorrhage research. *Transl. Stroke Res.* 4, 432–446. doi: 10.1007/s12975-013-0257-2

Galano, A., and Reiter, R. J. (2018). Melatonin and its metabolites vs oxidative stress: from individual actions to collective protection. *J. Pineal Res.* 65, e12514. doi: 10.1111/jpi.12514

Gaspard, N. (2020). How do i manage cerebral vasospasm and delayed cerebral ischemia? *Minerva Anestesiol.* 86, 1331–1339. doi: 10.23736/S0375-9393.20.14507-3

Gilard, V., Ferracci, F. X., Langlois, O., Derrey, S., Proust, F., and Curey, S. (2016). Effects of melatonin in the treatment of asthenia in aneurysmal subarachnoid hemorrhage. *Neurochirurgie* 62, 295–299. doi: 10.1016/j.neuchi.2016.06.010

Gorojod, R. M., Alaimo, A., Porte Alcon, S., Saravia, F., and Kotler, M. L. (2017). Interplay between lysosomal, mitochondrial and death receptor pathways during manganese-induced apoptosis in glial cells. *Arch. Toxicol.* 91, 3065–3078. doi: 10.1007/s00204-017-1936-7

Gris, T., Laplante, P., Thebault, P., Cayrol, R., Najjar, A., Joannette-Pilon, B., et al. (2019). Innate immunity activation in the early brain injury period following subarachnoid hemorrhage. *J. Neuroinflammation* 16:253. doi: 10.1186/s12974-019-1629-7

Guo, Z. N., Shao, A., Tong, L. S., Sun, W., Liu, J., and Yang, Y. (2016). The role of nitric oxide and sympathetic control in cerebral autoregulation in the setting of subarachnoid hemorrhage and traumatic brain injury. *Mol. Neurobiol.* 53, 3606–3615. doi: 10.1007/s12035-015-9308-x

Guo, Z. Q., Jiang, H., Huang, Y., Gu, H. M., Wang, W. B., and Chen, T. D. (2022). Early complementary acupuncture improves the clinical prognosis of traumatic brain edema: a randomized controlled trial. *Medicine (Baltimore)* 101:e28959. doi: 10.1097/MD.0000000000028959

Hasegawa, Y., Suzuki, H., Sozen, T., Altay, O., and Zhang, J. H. (2011). Apoptotic mechanisms for neuronal cells in early brain injury after subarachnoid hemorrhage. *Acta Neurochir. Suppl.* 110, 43–48. doi: 10.1007/978-3-7091-0353-1_8

He, F., Wu, X., Zhang, Q., Li, Y., Ye, Y., Li, P., et al. (2021). Bacteriostatic potential of melatonin: therapeutic standing and mechanistic insights. *Front. Immunol.* 12:683879. doi: 10.3389/fimmu.2021.683879

He, Z., Ostrowski, R. P., Sun, X., Ma, Q., Huang, B., Zhan, Y., et al. (2012). CHOP silencing reduces acute brain injury in the rat model of subarachnoid hemorrhage. *Stroke* 43, 484–490. doi: 10.1161/STROKEAHA.111.626432

Heinz, R., Brandenburg, S., Nieminen-Kelhä, M., Kremenetskaia, I., Boehm-Sturm, P., Vajkoczy, P., et al. (2021). Microglia as target for anti-inflammatory approaches to prevent secondary brain injury after subarachnoid hemorrhage (SAH). *J. Neuroinflammation* 18:36. doi: 10.1186/s12974-021-02085-3

Hinson, H. E., Sun, E., Molyneaux, B. J., Von Kummer, R., Demchuk, A., Romero, J., et al. (2020). Osmotherapy for malignant cerebral edema in a phase 2 prospective, double blind, randomized, placebo-controlled study

of IV glibenclamide. *J. Stroke Cerebrovasc. Dis.* 29:104916. doi: 10.1016/j.jstrokecerebrovasdis.2020.104916

Hong, Y., Palaksha, K. J., Park, K., Park, S., Kim, H. D., Reiter, R. J., et al. (2010). Melatonin plus exercise-based neurorehabilitative therapy for spinal cord injury. *J. Pineal Res.* 49, 201–209. doi: 10.1111/j.1600-079X.2010.00786.x

Hong, Y., Shao, A., Wang, J., Chen, S., Wu, H., Mcbride, D. W., et al. (2014). Neuroprotective effect of hydrogen-rich saline against neurologic damage and apoptosis in early brain injury following subarachnoid hemorrhage: possible role of the Akt/GSK3β signaling pathway. *PLoS One* 9:e96212. doi: 10.1371/journal.pone.0096212

Hou, G., Chen, H., Yin, Y., Pan, Y., Zhang, X., and Jia, F. (2020). MEL ameliorates post-SAH cerebral vasospasm by affecting the expression of eNOS and HIF1α *via* H19/miR-138/eNOS/NO and H19/miR-675/HIF1α. *Mol. Ther.Nucleic Acids* 19, 523–532. doi: 10.1016/j.omtn.2019.12.002

Ikram, A., Javaid, M. A., Ortega-Gutierrez, S., Selim, M., Kelangi, S., Anwar, S. M. H., et al. (2021). Delayed cerebral ischemia after subarachnoid hemorrhage. *J. Stroke Cerebrovasc. Dis.* 30:106064.

Ji, C., and Chen, G. (2016). Signaling pathway in early brain injury after subarachnoid hemorrhage: news update. *Acta Neurochir. Suppl.* 121, 123–126. doi: 10.1007/978-3-319-18497-5_21

Kanamaru, H., and Suzuki, H. (2019). Potential therapeutic molecular targets for blood-brain barrier disruption after subarachnoid hemorrhage. *Neural Regen. Res.* 14, 1138–1143. doi: 10.4103/1673-5374.251190

Kassell, N. F., Sasaki, T., Colohan, A. R., and Nazar, G. (1985). Cerebral vasospasm following aneurysmal subarachnoid hemorrhage. *Stroke* 16, 562–572. doi: 10.1161/01.str.16.4.562

Kumar, G., Shahripour, R. B., and Harrigan, M. R. (2016). Vasospasm on transcranial doppler is predictive of delayed cerebral ischemia in aneurysmal subarachnoid hemorrhage: a systematic review and meta-analysis. *J. Neurosurg.* 124, 1257–1264. doi: 10.3171/2015.4.JNS15428

Kvetnoy, I., Ivanov, D., Mironova, E., Evsyukova, I., Nasyrov, R., Kvetnaia, T., et al. (2022). Melatonin as the cornerstone of neuroimmunoendocrinology. *Int. J. Mol. Sci.* 23:1835. doi: 10.3390/ijms23031835

La, M., and Reid, J. J. (1995). Endothelin-1 and the regulation of vascular tone. *Clin. Exp. Pharmacol. Physiol.* 22, 315–323. doi: 10.1111/j.1440-1681.1995.tb02008.x

Lee, M. Y., Kuan, Y. H., Chen, H. Y., Chen, T. Y., Chen, S. T., Huang, C. C., et al. (2007). Intravenous administration of melatonin reduces the intracerebral cellular inflammatory response following transient focal cerebral ischemia in rats. *J. Pineal Res.* 42, 297–309. doi: 10.1111/j.1600-079X.2007.00420.x

Li, S., Yang, S., Sun, B., and Hang, C. (2019). Melatonin attenuates early brain injury after subarachnoid hemorrhage by the JAK-STAT signaling pathway. *Int. J. Clin. Exp. Pathol.* 12, 909–915.

Li, Y., Wu, P., Bihl, J. C., and Shi, H. (2020). Underlying mechanisms and potential therapeutic molecular targets in blood-brain barrier disruption after subarachnoid hemorrhage. *Curr. Neuropharmacol.* 18, 1168–1179. doi: 10.2174/1570159X18666200106154203

Lin, C. L., Jeng, A. Y., Howng, S. L., and Kwan, A. L. (2004). Endothelin and subarachnoid hemorrhage-induced cerebral vasospasm: pathogenesis and treatment. *Curr. Med. Chem.* 11, 1779–1791. doi: 10.2174/0929867043364919

Lin, C. L., Kwan, A. L., Dumont, A. S., Su, Y. F., Kassell, N. F., Wang, C. J., et al. (2007). Attenuation of experimental subarachnoid hemorrhage-induced increases in circulating intercellular adhesion molecule-1 and cerebral vasospasm by the endothelin-converting enzyme inhibitor CGS 26303. *J. Neurosurg.* 106, 442–448. doi: 10.3171/jns.2007.106.3.442

Lin, C. L., Winardi, W., Jeng, A. Y., and Kwan, A. L. (2006). Endothelin-converting enzyme inhibitors for the treatment of subarachnoid hemorrhage-induced vasospasm. *Neurol. Res.* 28, 721–729. doi: 10.1179/016164106x152007

Lin, F., Li, R., Tu, W. J., Chen, Y., Wang, K., Chen, X., et al. (2021a). An update on antioxidative stress therapy research for early brain injury after subarachnoid hemorrhage. *Front. Aging Neurosci.* 13:772036. doi: 10.3389/fnagi.2021.772036

Lin, S. H., Galet, C., Zanaty, M., Bayman, E., Rogers, W. K., Hasan, D., et al. (2021b). Melatonin and risk of mortality in subjects with aneurysmal subarachnoid hemorrhage. *Clin. Neurol. Neurosurg.* 210:106990. doi: 10.1016/j.clineuro.2021.106990

Liu, D., Dong, Y., Li, G., Zou, Z., Hao, G., Feng, H., et al. (2020). Melatonin attenuates white matter injury *via* reducing oligodendrocyte apoptosis after subarachnoid hemorrhage in mice. *Turk. Neurosurg.* 30, 685–692. doi: 10.5137/1019-5149.JTN.27986-19.3

Lorenzo, H. K., and Susin, S. A. (2007). Therapeutic potential of AIF-mediated caspase-independent programmed cell death. *Drug Resist. Updat.* 10, 235–255. doi: 10.1016/j.drup.2007.11.001

Lorenzo, H. K., Susin, S. A., Penninger, J., and Kroemer, G. (1999). Apoptosis inducing factor (AIF): a phylogenetically old, caspase-independent effector of cell death. *Cell Death Differ.* 6, 516–524. doi: 10.1038/sj.cdd.4400527

Lu, Y., Zhang, X. S., Zhang, Z. H., Zhou, X. M., Gao, Y. Y., Liu, G. J., et al. (2018). Peroxiredoxin 2 activates microglia by interacting with toll-like receptor 4 after subarachnoid hemorrhage. *J. Neuroinflammation* 15:87. doi: 10.1186/s12974-018-1118-4

Lu, Y., Zhang, X. S., Zhou, X. M., Gao, Y. Y., Chen, C. L., Liu, J. P., et al. (2019). Peroxiredoxin 1/2 protects brain against H(2)O(2)-induced apoptosis after subarachnoid hemorrhage. *FASEB J.* 33, 3051–3062. doi: 10.1096/fj.201801150R

Lucke-Wold, B. P., Logsdon, A. F., Manoranjan, B., Turner, R. C., Mcconnell, E., Vates, G. E., et al. (2016). Aneurysmal subarachnoid hemorrhage and neuroinflammation: a comprehensive review. *Int. J. Mol. Sci.* 17:497. doi: 10.3390/ijms17040497

Luo, F., Li, Y., Zhao, Y., Sun, M., He, Q., Wen, R., et al. (2021). Systemic immune-inflammation index predicts the outcome after aneurysmal subarachnoid hemorrhage. *Neurosurg. Rev.* 45, 1607–1615. doi: 10.1007/s10143-021-01681-4

Macdonald, R. L. (2016). Origins of the concept of vasospasm. *Stroke* 47, e11–15. doi: 10.1161/STROKEAHA.114.006498

Macdonald, R. L., Higashida, R. T., Keller, E., Mayer, S. A., Molyneux, A., Raabe, A., et al. (2011). Clazosentan, an endothelin receptor antagonist, in patients with aneurysmal subarachnoid haemorrhage undergoing surgical clipping: a randomised, double-blind, placebo-controlled phase 3 trial (CONSCIOUS-2). *Lancet Neurol.* 10, 618–625. doi: 10.1016/S1474-4422(11)70108-9

Macdonald, R. L., Kassell, N. F., Mayer, S., Ruefenacht, D., Schmiedek, P., Weidauer, S., et al. (2008). Clazosentan to overcome neurological ischemia and infarction occurring after subarachnoid hemorrhage (CONSCIOUS-1): randomized, double-blind, placebo-controlled phase 2 dose-finding trial. *Stroke* 39, 3015–3021. doi: 10.1161/STROKEAHA.108.519942

Macdonald, R. L., and Schweizer, T. A. (2017). Spontaneous subarachnoid haemorrhage. *Lancet* 389, 655–666.

Macdonald, R. L., and Weir, B. K. (1991). A review of hemoglobin and the pathogenesis of cerebral vasospasm. *Stroke* 22, 971–982. doi: 10.1161/01.str.22.8.971

Majidinia, M., Reiter, R. J., Shakouri, S. K., Mohebbi, I., Rastegar, M., Kaviani, M., et al. (2018). The multiple functions of melatonin in regenerative medicine. *Ageing Res. Rev.* 45, 33–52. doi: 10.1016/j.arr.2018.04.003

Martinez-Cruz, F., Espinar, A., Pozo, D., Osuna, C., and Guerrero, J. M. (2002). Melatonin prevents focal rat cerebellum injury as assessed by induction of heat shock protein (HO-1) following subarachnoid injections of lysed blood. *Neurosci. Lett.* 331, 208–210. doi: 10.1016/s0304-3940(02)00884-4

Michinaga, S., and Koyama, Y. (2015). Pathogenesis of brain edema and investigation into anti-edema drugs. *Int. J. Mol. Sci.* 16, 9949–9975. doi: 10.3390/ijms16059949

Mota Telles, J. P., Rabelo, N. N., Junior, J. R., Teixeira, M. J., and Figueiredo, E. G. (2021). C-Reactive protein levels are higher in patients with fusiform intracranial aneurysms: a case-control study. *World Neurosurg.* 146, e896–e901. doi: 10.1016/j.wneu.2020.11.042

Müller-Schweinitzer, E., Gilles, H., Grapow, M., Kern, T., Reineke, D., and Zerkowski, H. R. (2004). Attenuation of lipopolysaccharide-induced hyperreactivity of human internal mammary arteries by melatonin. *J. Pineal Res.* 37, 92–97. doi: 10.1111/j.1600-079X.2004.00139.x

Muroi, C., Mink, S., Seule, M., Bellut, D., Fandino, J., and Keller, E. (2011). Monitoring of the inflammatory response after aneurysmal subarachnoid haemorrhage in the clinical setting: review of literature and report of preliminary clinical experience. *Acta Neurochir. Suppl.* 110, 191–196. doi: 10.1007/978-3-7091-0353-1_33

Nagai, H., Katsumata, T., Ohya, M., and Kageyama, N. (1976). Effect of subarachnoid haemorrhage on micro-circulation in hypothalamus and brain stem of dogs. *Neurochirurgia (Stuttg)* 19, 135–144. doi: 10.1055/s-0028-1090403

Naidech, A. M., Drescher, J., Tamul, P., Shaibani, A., Batjer, H. H., and Alberts, M. J. (2006). Acute physiological derangement is associated with early radiographic

cerebral infarction after subarachnoid haemorrhage. *J. Neurol. Neurosurg. Psychiatry* 77, 1340–1344. doi: 10.1136/jnnp.2006.089748

Neumaier, F., Weiss, M., Veldeman, M., Kotliar, K., Wiesmann, M., Schulze-Steinen, H., et al. (2021). Changes in endogenous daytime melatonin levels after aneurysmal subarachnoid hemorrhage - preliminary findings from an observational cohort study. *Clin. Neurol. Neurosurg.* 208:106870. doi: 10.1016/j.clineuro.2021.106870

Nishikawa, H., and Suzuki, H. (2018). Possible role of inflammation and galectin-3 in brain injury after subarachnoid hemorrhage. *Brain Sci.* 8:30. doi: 10.3390/brainsci8020030

Norberg, E., Orrenius, S., and Zhivotovsky, B. (2010). Mitochondrial regulation of cell death: processing of apoptosis-inducing factor (AIF). *Biochem. Biophys. Res. Commun.* 396, 95–100. doi: 10.1016/j.bbrc.2010.02.163

Okada, T., and Suzuki, H. (2020). Mechanisms of neuroinflammation and inflammatory mediators involved in brain injury following subarachnoid hemorrhage. *Histol. Histopathol.* 35, 623–636. doi: 10.14670/HH-18-208

Okada, T., Suzuki, H., Travis, Z. D., and Zhang, J. H. (2020). The stroke-induced blood-brain barrier disruption: current progress of inspection technique, mechanism, and therapeutic target. *Curr. Neuropharmacol.* 18, 1187–1212. doi: 10.2174/1570159X18666200528143301

Osier, N., Mcgreevy, E., Pham, L., Puccio, A., Ren, D., Conley, Y. P., et al. (2018). Melatonin as a therapy for traumatic brain injury: a review of published evidence. *Int. J. Mol. Sci.* 19:1539. doi: 10.3390/ijms19051539

Ostrowski, R. P., Colohan, A. R., and Zhang, J. H. (2006). Molecular mechanisms of early brain injury after subarachnoid hemorrhage. *Neurol. Res.* 28, 399–414. doi: 10.1179/016164106X115008

Pradilla, G., Chaichana, K. L., Hoang, S., Huang, J., and Tamargo, R. J. (2010). Inflammation and cerebral vasospasm after subarachnoid hemorrhage. *Neurosurg. Clin. N. Am.* 21, 365–379.

Reiter, R. J., Mayo, J. C., Tan, D. X., Sainz, R. M., Alatorre-Jimenez, M., and Qin, L. (2016). Melatonin as an antioxidant: under promises but over delivers. *J. Pineal Res.* 61, 253–278. doi: 10.1111/jpi.12360

Rosenberg, G. A. (1999). Ischemic brain edema. *Prog. Cardiovasc. Dis.* 42, 209–216.

Rowland, M. J., Ezra, M., Winkler, A., Garry, P., Lamb, C., Kelly, M., et al. (2019). Calcium channel blockade with nimodipine reverses MRI evidence of cerebral oedema following acute hypoxia. *J. Cereb. Blood Flow Metab.* 39, 285–301. doi: 10.1177/0271678X17726624

Roy, J., Wong, K. Y., Aquili, L., Uddin, M. S., Heng, B. C., Tipoe, G. L., et al. (2022). Role of melatonin in Alzheimer's disease: from preclinical studies to novel melatonin-based therapies. *Front. Neuroendocrinol.* 65:100986. doi: 10.1016/j.yfrne.2022.100986

Samantaray, S., Das, A., Thakore, N. P., Matzelle, D. D., Reiter, R. J., Ray, S. K., et al. (2009). Therapeutic potential of melatonin in traumatic central nervous system injury. *J. Pineal Res.* 47, 134–142. doi: 10.1111/j.1600-079X.2009.00703.x

Sandoval, K. E., and Witt, K. A. (2008). Blood-brain barrier tight junction permeability and ischemic stroke. *Neurobiol. Dis.* 32, 200–219. doi: 10.1016/j.nbd.2008.08.005

Savarraj, J. P., Mcguire, M. F., Parsha, K., Hergenroeder, G., Bajgur, S., Ahn, S., et al. (2018). Disruption of thrombo-inflammatory response and activation of a distinct cytokine cluster after subarachnoid hemorrhage. *Cytokine* 111, 334–341. doi: 10.1016/j.cyto.2018.09.003

Schallner, N., Pandit, R., Leblanc, R. III, Thomas, A. J., Ogilvy, C. S., Zuckerbraun, B. S., et al. (2015). Microglia regulate blood clearance in subarachnoid hemorrhage by heme oxygenase-1. *J. Clin. Invest.* 125, 2609–2625. doi: 10.1172/JCI78443

Schneider, U. C., Xu, R., and Vajkoczy, P. (2018). Inflammatory events following subarachnoid hemorrhage (SAH). *Curr. Neuropharmacol.* 16, 1385–1395. doi: 10.2174/1570159X16666180412110919

Sehba, F. A., and Bederson, J. B. (2011). Nitric oxide in early brain injury after subarachnoid hemorrhage. *Acta Neurochir. Suppl.* 110, 99–103. doi: 10.1007/978-3-7091-0353-1_18

Sehba, F. A., and Friedrich, V. (2011). Early micro vascular changes after subarachnoid hemorrhage. *Acta Neurochir. Suppl.* 110, 49–55. doi: 10.1007/978-3-7091-0353-1_9

Sehba, F. A., Hou, J., Pluta, R. M., and Zhang, J. H. (2012). The importance of early brain injury after subarachnoid hemorrhage. *Prog. Neurobiol.* 97, 14–37. doi: 10.1016/j.pneurobio.2012.02.003

Shao, A., Lin, D., Wang, L., Tu, S., Lenahan, C., and Zhang, J. (2020). Oxidative stress at the crossroads of aging, stroke and depression. *Aging Dis.* 11, 1537–1566. doi: 10.14336/AD.2020.0225

Shen, J., Pan, J. W., Fan, Z. X., Xiong, X. X., and Zhan, R. Y. (2013). Dissociation of vasospasm-related morbidity and outcomes in patients with aneurysmal subarachnoid hemorrhage treated with clazosentan: a meta-analysis of randomized controlled trials. *J. Neurosurg.* 119, 180–189. doi: 10.3171/2013.3.JNS121436

Shi, L., Liang, F., Zheng, J., Zhou, K., Chen, S., Yu, J., et al. (2018). Melatonin regulates apoptosis and autophagy *Via* ROS-MST1 pathway in subarachnoid hemorrhage. *Front. Mol. Neurosci.* 11:93. doi: 10.3389/fnmol.2018.00093

Sun, B., Yang, S., Li, S., and Hang, C. (2018). Melatonin upregulates nuclear factor erythroid-2 related factor 2 (Nrf2) and mediates mitophagy to protect against early brain injury after subarachnoid hemorrhage. *Med. Sci. Monit.* 24, 6422–6430. doi: 10.12659/MSM.909221

Sun, Q., Wu, W., Hu, Y. C., Li, H., Zhang, D., Li, S., et al. (2014). Early release of high-mobility group box 1 (HMGB1) from neurons in experimental subarachnoid hemorrhage *in vivo* and *in vitro*. *J. Neuroinflammation* 11:106. doi: 10.1186/1742-2094-11-106

Tai, S. H., Chen, H. Y., Lee, E. J., Chen, T. Y., Lin, H. W., Hung, Y. C., et al. (2010). Melatonin inhibits postischemic matrix metalloproteinase-9 (MMP-9) activation *via* dual modulation of plasminogen/plasmin system and endogenous MMP inhibitor in mice subjected to transient focal cerebral ischemia. *J. Pineal Res.* 49, 332–341. doi: 10.1111/j.1600-079X.2010.00797.x

Toda, N., Ayajiki, K., and Okamura, T. (2009). Cerebral blood flow regulation by nitric oxide: recent advances. *Pharmacol. Rev.* 61, 62–97. doi: 10.1124/pr.108.000547

Tordjman, S., Chokron, S., Delorme, R., Charrier, A., Bellissant, E., Jaafari, N., et al. (2017). Melatonin: pharmacology, functions and therapeutic benefits. *Curr. Neuropharmacol.* 15, 434–443. doi: 10.2174/1570159X14666161228122115

van Dijk, B. J., Vergouwen, M. D., Kelfkens, M. M., Rinkel, G. J., and Hol, E. M. (2016). Glial cell response after aneurysmal subarachnoid hemorrhage - functional consequences and clinical implications. *Biochim. Biophys. Acta* 1862, 492–505. doi: 10.1016/j.bbadis.2015.10.013

Vanhoutte, P. M. (2018). Nitric oxide: from good to bad. *Ann. Vasc. Dis.* 11, 41–51. doi: 10.3400/avd.ra.17-00134

Vergouwen, M. D., Algra, A., and Rinkel, G. J. (2012). Endothelin receptor antagonists for aneurysmal subarachnoid hemorrhage: a systematic review and meta-analysis update. *Stroke* 43, 2671–2676. doi: 10.1161/STROKEAHA.112.666693

Wang, Z., Ma, C., Meng, C. J., Zhu, G. Q., Sun, X. B., Huo, L., et al. (2012). Melatonin activates the Nrf2-ARE pathway when it protects against early brain injury in a subarachnoid hemorrhage model. *J. Pineal Res.* 53, 129–137. doi: 10.1111/j.1600-079X.2012.00978.x

Wang, Z., Wu, L., You, W., Ji, C., and Chen, G. (2013). Melatonin alleviates secondary brain damage and neurobehavioral dysfunction after experimental subarachnoid hemorrhage: possible involvement of TLR4-mediated inflammatory pathway. *J. Pineal Res.* 55, 399–408. doi: 10.1111/jpi.12087

Wu, F., Liu, Z., Li, G., Zhou, L., Huang, K., Wu, Z., et al. (2021). Inflammation and oxidative stress: potential targets for improving prognosis after subarachnoid hemorrhage. *Front. Cell Neurosci.* 15:739506. doi: 10.3389/fncel.2021.739506

Xu, Z., Zhang, F., Xu, H., Yang, F., Zhou, G., Tong, M., et al. (2022). Melatonin affects hypoxia-inducible factor 1α and ameliorates delayed brain injury following subarachnoid hemorrhage *via* H19/miR-675/HIF1A/TLR4. *Bioengineered* 13, 4235–4247. doi: 10.1080/21655979.2022.2027175

Yang, S., Chen, X., Li, S., Sun, B., and Hang, C. (2018a). Melatonin treatment regulates SIRT3 expression in early brain injury (EBI) due to reactive oxygen species (ROS) in a mouse model of subarachnoid hemorrhage (SAH). *Med. Sci. Monit.* 24, 3804–3814. doi: 10.12659/MSM.907734

Yang, S., Tang, W., He, Y., Wen, L., Sun, B., and Li, S. (2018b). Long non-coding RNA and microRNA-675/let-7a mediates the protective effect of melatonin against early brain injury after subarachnoid hemorrhage *via* targeting TP53 and neural growth factor. *Cell Death Dis.* 9:99. doi: 10.1038/s41419-017-0155-8

Yang, Y., Chen, S., and Zhang, J. M. (2017). The updated role of oxidative stress in subarachnoid hemorrhage. *Curr. Drug Deliv.* 14, 832–842. doi: 10.2174/1567201813666161025115531

Yang, Y., and Rosenberg, G. A. (2011). Blood-brain barrier breakdown in acute and chronic cerebrovascular disease. *Stroke* 42, 3323–3328. doi: 10.1161/STROKEAHA.110.608257

Zhan, C. P., Zhuge, C. J., Yan, X. J., Dai, W. M., and Yu, G. F. (2021). Measuring serum melatonin concentrations to predict clinical outcome after aneurysmal subarachnoid hemorrhage. *Clin. Chim. Acta* 513, 1–5. doi: 10.1016/j.cca.2020.12.006

Zhang, L., Guo, K., Zhou, J., Zhang, X., Yin, S., Peng, J., et al. (2021). Ponesimod protects against neuronal death by suppressing the activation of A1 astrocytes in early brain injury after experimental subarachnoid hemorrhage. *J. Neurochem.* 158, 880–897. doi: 10.1111/jnc.15457

Zhang, X. S., Zhang, X., Zhou, M. L., Zhou, X. M., Li, N., Li, W., et al. (2014). Amelioration of oxidative stress and protection against early brain injury by astaxanthin after experimental subarachnoid hemorrhage. *J. Neurosurg.* 121, 42–54. doi: 10.3171/2014.2.JNS13730

Zhang, Y., Zhang, W. X., Zhang, Y. J., Liu, Y. D., Liu, Z. J., Wu, Q. C., et al. (2018). Melatonin for the treatment of spinal cord injury. *Neural Regen. Res.* 13, 1685–1692.

Zhang, Z. H., Han, Y. L., Wang, C. X., Zhou, C. H., Wu, L. Y., Zhang, H. S., et al. (2016). The effect of subarachnoid erythrocyte lysate on brain injury: a preliminary study. *Biosci. Rep.* 36:e00359. doi: 10.1042/BSR20160100

Zhao, L., Liu, H., Yue, L., Zhang, J., Li, X., Wang, B., et al. (2017). Melatonin attenuates early brain injury *via* the melatonin receptor/Sirt1/NF-κB signaling pathway following subarachnoid hemorrhage in mice. *Mol. Neurobiol.* 54, 1612–1621. doi: 10.1007/s12035-016-9776-7

Zhao, Z., Nelson, A. R., Betsholtz, C., and Zlokovic, B. V. (2015). Establishment and dysfunction of the blood-brain barrier. *Cell* 163, 1064–1078. doi: 10.1016/j.cell.2015.10.067

Zhou, Q., Lin, L., Li, H., Wang, H., Jiang, S., Huang, P., et al. (2021). Melatonin reduces neuroinflammation and improves axonal hypomyelination by modulating M1/M2 microglia polarization *via* JAK2-STAT3-telomerase pathway in postnatal rats exposed to lipopolysaccharide. *Mol. Neurobiol.* 58, 6552–6576. doi: 10.1007/s12035-021-02568-7

Conflict of Interest: The authors declare that the research was conducted in the absence of any commercial or financial relationships that could be construed as a potential conflict of interest.

Publisher's Note: All claims expressed in this article are solely those of the authors and do not necessarily represent those of their affiliated organizations, or those of the publisher, the editors and the reviewers. Any product that may be evaluated in this article, or claim that may be made by its manufacturer, is not guaranteed or endorsed by the publisher.

frontiers | Frontiers in Aging Neuroscience

ORIGINAL RESEARCH
published: 06 May 2022
doi: 10.3389/fnagi.2022.870718

Dynamic Relationship Between Interhemispheric Functional Connectivity and Corticospinal Tract Changing Pattern After Subcortical Stroke

Jingchun Liu[1†], Caihong Wang[2*†], Jingliang Cheng[2], Peifang Miao[2] and Zhen Li[3]*

[1] Department of Radiology and Tianjin Key Laboratory of Functional Imaging, Tianjin Medical University General Hospital, Tianjin, China, [2] Department of MRI, Key Laboratory for Functional Magnetic Resonance Imaging and Molecular Imaging of Henan Province, The First Affiliated Hospital of Zhengzhou University, Zhengzhou, China, [3] Department of Interventional Radiology, The First Affiliated Hospital of Zhengzhou University, Zhengzhou, China

OPEN ACCESS

Edited by:
Gaiqing Wang,
The Third People's Hospital of Hainan Province, China

Reviewed by:
Xujun Duan,
University of Electronic Science and Technology of China, China
Jiajia Zhu,
First Affiliated Hospital of Anhui Medical University, China
Zhifeng Kou,
Wayne State University, United States

***Correspondence:**
Caihong Wang
fccwangch@zzu.edu.cn
Jingchun Liu
jingchunliutjmu@126.com

[†]These authors have contributed equally to this work and share first authorship

Specialty section:
This article was submitted to Neurocognitive Aging and Behavior, a section of the journal Frontiers in Aging Neuroscience

Received: 07 February 2022
Accepted: 05 April 2022
Published: 06 May 2022

Citation:
Liu J, Wang C, Cheng J, Miao P and Li Z (2022) Dynamic Relationship Between Interhemispheric Functional Connectivity and Corticospinal Tract Changing Pattern After Subcortical Stroke.
Front. Aging Neurosci. 14:870718.
doi: 10.3389/fnagi.2022.870718

Background and Purpose: Increased interhemispheric resting-state functional connectivity (rsFC) between the bilateral primary motor cortex (M1) compensates for corticospinal tract (CST) impairment, which facilitates motor recovery in chronic subcortical stroke. However, there is a lack of data on the evolution patterns and correlations between M1–M1 rsFC and diffusion indices of CSTs with different origins after subcortical stroke and their relations with long-term motor outcomes.

Methods: A total of 44 patients with subcortical stroke underwent longitudinal structural and functional magnetic resonance imaging (MRI) examinations and clinical assessments at four time points. Diffusion tensor imaging was used to extract fractional anisotropy (FA) values of the affected CSTs with different origins. Resting-state functional MRI was used to calculate the M1–M1 rsFC. Longitudinal patterns of functional and anatomic changes in connections were explored using a linear mixed-effects model. Dynamic relationships between M1–M1 rsFC and FA values of the affected specific CSTs and the impact of these variations on the long-term motor outcomes were analyzed in patients with subcortical stroke.

Results: Stroke patients showed a significantly decreased FA in the affected specific CSTs and a gradually increasing M1–M1 rsFC from the acute to the chronic stage. The FA of the affected M1 fiber was negatively correlated with the M1–M1 rsFC from the subacute to the chronic stage, FA of the affected supplementary motor area fiber was negatively correlated with the M1–M1 rsFC in the subacute stage, and FA of the affected M1 fiber in the acute stage was correlated with the long-term motor recovery after subcortical stroke.

Conclusion: Our findings show that the FA of the affected M1 fiber in the acute stage had the most significant correlation with long-term motor recovery and may be used as an imaging biomarker for predicting motor outcomes after stroke. The compensatory role of the M1–M1 rsFC enhancement may start from the subacute stage in stroke patients with CST impairment.

Keywords: cerebral infarction, corticospinal tract, diffusion tensor imaging, functional neuroimaging, motor, neuronal plasticity

INTRODUCTION

Stroke is the leading cause of significant lifelong motor deficits (Johnson and Westlake, 2021), which adversely affect the clinical outcomes and impair the activities of daily living (Patel et al., 2020). The integrity of motor pathways plays an important role in motor recovery in stroke patients with motor deficits (Guo et al., 2019; Zolkefley et al., 2021). The corticospinal tract (CST) is the principal tract for controlling primary motor activity and has been deemed as the most common locus of motor impairment after subcortical stroke (Schaechter et al., 2009; DeVetten et al., 2010). Diffusion tensor imaging (DTI) is a widely used method for providing information about cellular integrity and pathology (Le Bihan, 2003), analyzing the integrity of white matter fiber tracts (Mori and van Zijl, 2002), and observing the relationship between white matter tracts and infarcts (Kunimatsu et al., 2003; Lee et al., 2005). One of the diffusion indices accessed by DTI is fractional anisotropy (FA), a measure of the white matter tracts' integrity. Considering the CST as a whole tract, a previous longitudinal study showed that the FA values of the affected CST changed dynamically (Yu et al., 2009), and the baseline FA values of the CST can be used to predict the degree of motor recovery (Shaheen et al., 2022). CST fibers arise from the primary motor cortex (M1), premotor cortex (PMC), primary somatosensory area (S1), and supplementary motor area (SMA) (Schieber, 2007; Welniarz et al., 2017). Liu et al. (2020) reconstructed a fine map of the CST fibers with different cortical origins and found that the integrity of M1 and SMA fibers was closely associated with the motor outcomes and structural brain changes. These results suggest that the preserved microstructural integrity of CST affects motor recovery. However, the differences in the evolution patterns of specific CST changes and their correlations with long-term motor recovery in patients with subcortical stroke remain largely unknown. M1 is thought to be the main origin of CST fibers (Seo and Jang, 2013). Therefore, we hypothesize that the FA values of the affected M1 fibers decrease rapidly, impacting the response to motor rehabilitation, and are helpful for understanding the mechanisms of neurological rehabilitation after subcortical stroke.

The resting-state functional connectivity (rsFC) is defined as the statistical dependency among spatially remote neurophysiological events (Friston, 2011), which has been widely used to investigate functional alterations and motor recovery after stroke (Yin et al., 2012). Some cross-sectional studies have suggested a beneficial effect of the restoration or enhancement of the rsFC on the motor function in patients with subcortical stroke (Peng et al., 2019; Chen et al., 2020). The interhemispheric rsFC of M1 has been shown to exhibit different evolution patterns across patients with subcortical stroke. For example, enhanced rsFC between the bilateral M1 areas appears in the first week post-stroke in some patients (Golestani et al., 2013) and starts at a later time (1–12 weeks post-stroke) in some patients (Xu et al., 2014), while it does not show any increase within 1 year after stroke in some patients (Xu et al., 2014). However, the inflection points of M1–M1 rsFC dynamic changes in patients with subcortical stroke remain largely unknown. The first several weeks post-stroke are critical for motor rehabilitation (Verheyden et al., 2008). Therefore, we hypothesize that interhemispheric rsFC reorganization starts in the acute or subacute stage and is critical for selecting the individual time window of intervention in patients with subcortical stroke.

Both integrity of the affected CST and enhanced interhemispheric rsFC are important factors for motor recovery after stroke (Xia et al., 2021). Another critical element is the relationship between these two factors. Previous studies have shown that a decreased M1–M1 rsFC was negatively correlated with the percentage of CST damage within 4 weeks after subcortical stroke (Carter et al., 2012). Liu and coauthors further found that an enhanced interhemispheric rsFC was negatively correlated with the FA values of CST impairment in chronic patients (>6 months) with subcortical stroke (Liu et al., 2015). These cross-sectional studies indicated that the correlations between the two factors were completely opposite in the subacute and chronic stages post-stroke. However, the dynamic relationship between CST impairment and rsFC reorganization in different stages after subcortical stroke remains largely unknown. Moreover, previous studies failed to determine whether the compensatory relationship between enhanced interhemispheric FC and CST damage starts from the inflection point of M1–M1 rsFC changes in subcortical stroke.

In this study, we aimed (a) to explore the evolution patterns of the diffusion indices of specific CSTs in a longitudinal dataset of

Abbreviations: CST, corticospinal tract; DTI, diffusion tensor imaging; DWI, diffusion-weighted imaging; EPI, echo-planar imaging; FA, fractional anisotropy; FOV, field of view; M1, primary motor cortex; MNI, Montreal Neurological Institute; MRI, magnetic resonance imaging; NIHSS, National Institutes of Health Stroke Scale; PMC, premotor cortex; ROI, region of interest; rsFC, resting-state functional connectivity; S1, primary somatosensory area; SMA, supplementary motor area; TE, echo time; TR, repetition time; WE_FM, Fugl–Meyer Assessment of the whole extremity.

44 patients with subcortical stroke; (b) to identify the trajectories of M1–M1 rsFC changes in these patients; (c) to uncover the dynamic relationships between M1–M1 rsFC and diffusion indices of specific CSTs in different stages after stroke and their relationships with long-term motor recovery; and (d) to identify the period of M1–M1 rsFC changes in which the compensatory relationship between enhanced interhemispheric rsFC and CST damage begins in patients with subcortical stroke.

MATERIALS AND METHODS

Subjects

The experimental protocol was approved by the local medical research ethics committee, and written informed consent was obtained from each participant. The study followed a longitudinal design (four time points: ≤7 days, 1 month, 3 months, and >6 months), and the dataset (44 patients and 10 healthy controls) was used to explore the differences in the evolution patterns of specific CSTs and M1–M1 rsFC changes in patients with subcortical stroke.

The inclusion criteria for patients with stroke were as follows: (a) first-onset acute ischemic stroke; (b) a single lesion in the basal ganglia and neighboring regions; and (c) right-handedness before stroke onset (Oldfield, 1971). The exclusion criteria were as follows: (a) recurrent stroke defined by clinical history and magnetic resonance imaging (MRI) evaluation; (b) any other brain abnormalities on MR images; (c) modified Fazekas scale for white matter hyperintensities greater than 1 (Fazekas et al., 1987); and (d) history of any other neurological and psychiatric disorders. During the collection of the dataset, 58 patients with subcortical stroke were initially recruited for this study. Fourteen patients were excluded due to loss of follow-up after inclusion ($n = 9$), recurrent stroke ($n = 3$), and other brain abnormalities ($n = 2$). Finally, 44 patients with data on the four time points were included in this study. All patients with subcortical ischemic stroke were recruited from the Tianjin Medical University General Hospital ($n = 7$) and the First Affiliated Hospital of Zhengzhou University ($n = 37$).

MR Data Acquisition

Multimodal MRI data were obtained using two 3.0-Tesla Discovery MR750 MR scanners (General Electric, Milwaukee, WI) from two hospitals. Tight but comfortable foam padding was used to minimize head movement, and earplugs were used to reduce the scanner noise. Diffusion-weighted imaging (DWI), sagittal 3D T1- and T2-weighted images, and T2 fluid-attenuated inversion recovery images were acquired to identify the stroke lesion, recurrent stroke, white matter hyperintensity, and other brain abnormalities. DTI was used to extract the FA values of affected CSTs with different origins. The rs-fMRI was used to calculate the M1–M1 rsFC.

Diffusion tensor imaging data were acquired using a spin-echo single-shot echo-planar imaging (EPI) sequence. Diffusion-sensitized gradients were applied along 64 non-collinear directions with a b-value of 1000 s/mm^2. In addition, three sets of b = 0 images were obtained. Using an integrated parallel acquisition technique (iPAT) with an acceleration factor of 2 allowed us to obtain images with less distortion from susceptibility artifacts. We collected 50 slices from each participant. The scan parameters were repetition time (TR)/echo time (TE) = 11000/77.6 ms; field of view (FOV) = 256 × 256 mm; matrix = 128 × 128; flip angle (FA) = 90°; and slice thickness = 3 mm without gap. Resting-state fMRI data were obtained using a gradient-echo single-shot EPI sequence with the following imaging parameters: TR/TE = 2000/30 ms; FOV = 240 × 240 mm; matrix = 64 × 64; FA = 90°; slice thickness = 3 mm; gap = 1 mm; 38 interleaved transversal slices; and 180 volumes. During the resting-state fMRI scans, all subjects were instructed to keep their eyes closed, stay as still as possible, think of nothing, and not fall asleep. Sagittal 3D T1WI was acquired by brain volume with the following imaging parameters: TR/TE = 8.2/3.2 ms; inversion time = 450 ms; FA = 11°; FOV = 256 mm × 256 mm; matrix = 256 × 256; slice thickness = 1 mm, no gap; and 188 slices. DWI parameters: TR/TE, matrix, FOV, slices, and slice thickness were 3,000 ms/61 ms, 160 × 160, 240 × 240 mm, 20, and 6 mm, respectively, with b-value = 1,000 s/mm^2. T2-FLAIR parameters: TR/TE, matrix, slices, and slice thickness were 8,500 ms/158 ms, 256 × 256, 20, and 5 mm, respectively. T2WI was acquired from clinically used sequences.

Behavioral Assessments

For longitudinal analysis of patients with stroke (four time points: ≤7 days, 1 month, 3 months, and >6 months), global functional deficits were assessed using the National Institutes of Health Stroke Scale (NIHSS), and motor outcomes were evaluated by the Fugl–Meyer Assessment of the whole extremity (WE_FM) at four time points.

Preprocessing of DTI Data

The DTI data were preprocessed using the FMRIB's Diffusion Toolbox (FSL 5.0; http://www.fmrib.ox.ac.uk/fsl). All diffusion-weighted images were visually inspected by two radiologists for apparent artifacts due to subject motion and instrument malfunction. For each subject, the diffusion-weighted images were registered to the corresponding b = 0 images with an affine transformation to correct for eddy-current distortion and motion displacement. Then, skulls in the images were removed using the brain extract toolbox. The diffusion tensor was reconstructed using the linear least-square fitting algorithm, which was used for calculating the diffusion indices. Then, we coregistered the individual diffusion indices into the Montreal Neurological Institute (MNI) space using a two-step method. First, we coregistered the brain-extracted b = 0 images of each subject with his/her T1-weighted images using an affine method (12 parameters), and then, the T1-weighted images were affinely coregistered into the T1 template of the MNI space. Finally, the diffusion indices were written into the MNI space using the affine parameters generated from the above steps and were resliced to 2 × 2 × 2 mm^3.

The integrity of each CST fiber was assessed by the FA and the percentage of impairment. Based on the fine map of the CST (Liu et al., 2020), the FA values of each CST fiber were extracted from each patient at four time points. Moreover, we only extracted FA values from the cerebral peduncle, where the

CST fibers have a relatively coherent arrangement. FA values can accurately estimate the white matter integrity only in the white matter regions with coherent fiber arrangement. We used the mean FA value of all voxels within each CST to represent the FA of the CST. Acute stroke lesions and the fine map (Liu et al., 2020) of the CST fibers were used to calculate the percentage of the impairment of each CST fiber for each patient in the acute stage. First, acute stroke lesions were acquired based on the DWI data. The individual's DWI data were spatially normalized to the EPI template in the MNI space and resampled into a 1 mm^3 voxel. Stroke lesions were independently outlined on the normalized DWI using the MRIcron tool (https://www.nitrc.org/projects/mricron) by three radiologists with more than 9 years of experience. The intra-class correlation coefficient for the lesion volume was 0.98, and the result from the most senior radiologist was selected as the final lesion contour. Second, for each axial slice with an overlap between the stroke lesion and a given CST fiber, the impairment percentage of the CST fiber at this slice was defined as the ratio of the area of the overlap region to the area of the CST fiber. Finally, the largest percentage in these slices was defined as the impairment percentage of the CST fiber in this patient.

Seed Masks

The left and right M1s were separately extracted from the Human Brainnetome Atlas (Fan et al., 2016). Subsequently, we separately extracted the overlapping regions of the left and right M1 with the 50% probability fine map (Liu et al., 2020) of the CST to define the left and right seed masks for the rsFC analysis (left: MNI coordinates: −12, −21, 66; cluster size: 61 voxels; right: MNI coordinates: 12, −21, 66; cluster size: 62 voxels).

Preprocessing of the Resting-State fMRI Data

The resting-state fMRI data were preprocessed using the Statistical Parametric Mapping software (SPM12, http://www.fil.ion.ucl.ac.uk/spm). The first 10 volumes from each subject were discarded to allow the signal to reach equilibrium and to let the participants adapt to the scanning noise. The remaining 170 volumes were corrected for the acquisition time delay between slices. None of the 44 subjects had a maximum displacement of >2 mm or a maximum rotation of >2.0°. The fMRI dataset was spatially normalized to the MNI EPI template and resampled into $3 \times 3 \times 3$ mm^3 voxels. Thereafter, several nuisance variables were regressed out from the fMRI data, including the averaged signals of the ventricles, white matter, and the whole brain, and the Friston 24 regressors (including six head motion parameters, six head motion parameters one time point before, and the 12 corresponding squared items) (Friston et al., 1996). Then, a band-pass frequency filter (0.01–0.08 Hz) was applied to reduce the low-frequency drift and high-frequency noise (Greicius et al., 2003). Finally, the filtered BOLD images were spatially smoothed using an isotropic Gaussian kernel of 8 mm full width at half maximum (FWHM).

Using the defined seed masks as the regions of interest (ROI), ROI-based rsFC analysis was performed. For each individual dataset, the Pearson correlation coefficient between the mean time series of the left and right ROIs was computed and converted into the z value using Fisher's r-to-z transformation to improve the normality.

Evolution of CST and rsFC Changes After Stroke

We used a linear mixed-effects model to investigate the evolution patterns of specific CST and M1–M1 rsFC changes in patients with stroke and healthy controls in the longitudinal dataset (44 patients and 10 healthy controls). The random intercept term accounts for the correlation due to repeated measurements within a single patient (Gibbons et al., 1988). All patients were assumed to have a common slope (fixed effect) where only the intercepts were allowed to vary (random effect). The model parameters were estimated by the restricted maximum likelihood method and considered significant if the P values were less than 0.05. In healthy controls, we characterized the trajectories of these specific CSTs and M1–M1 rsFC changes to establish references to identify the stroke-induced changes. In both the patient and control groups, we identified significant longitudinal specific CSTs (four fibers from M1, PMC, S1, and SMA) and M1–M1 rsFC changes by assessing the significance of the slopes (five comparisons for the patient group and five comparisons for the control group). For each specific CST and M1–M1 rsFC change, we investigated the differences in the evolution pattern by comparing the slopes between stroke and control groups (five comparisons between the two groups). In the above-mentioned analyses, we performed the comparisons 15 times. To reduce the possible false-positive findings, we used the Bonferroni method ($P < 0.05/15 = 3.33 \times 10^{-3}$) to correct for multiple comparisons.

Correlation Analysis

We assessed the relationships between the FA values of the affected specific CSTs and M1–M1 rsFC at four time points. Then, we examined the correlations between the FA values and impairment percentage of each CST fiber in the acute stage and the WE_FM scores in the chronic stage. For all correlation analyses, we used partial correlations to factor out the age, sex, and FA values of the CST fibers with other origins. In the above-mentioned analyses, we performed the correlations 24 times (16 correlations between the FA of the affected CST and M1–M1 rsFC at four time points, and eight correlations between the integrity of the affected CST and long-term motor outcomes). To reduce the possible false-positive findings, we used the Bonferroni method ($P < 0.05/24 = 2.08 \times 10^{-3}$) to correct for multiple comparisons.

RESULTS

Demographic and Clinical Information

The clinical and demographic data of the stroke patients and controls are listed in **Table 1**. The longitudinal dataset (44 patients with subcortical stroke and 10 healthy controls) included rs-fMRI, DTI, and WE_FM data from the acute to chronic stages. The stroke lesions involved the internal capsule and surrounding structures, including the internal capsule, thalamus, basal ganglia, and corona radiata (**Figure 1**). A total of 24 out of 44 patients had infarct lesions in the right hemisphere and 20

TABLE 1 | Demographic and clinical information of the participants.

Variables	Patients with subcortical stroke ($n = 44$)	Healthy controls ($n = 10$)
Age, y	53.8 ± 8.8 (30–72)	55.9 ± 5.2 (48–66)
Sex (M/F)	33/11	3/7
Time points		
1, d	6 (2–7)	0 (0–0)
2, d	35 (31–40.8)	44.5 (33.3–59)
3, mo	3.3 (3.1–3.5)	4.9 (4.3–6.6)
4, mo	6.5 (6.1–7.2)	8.5 (7.1–11.6)
Lesion location		
Left hemisphere	20 (45.5%)	
Right hemisphere	24 (54.5%)	
NIHSS		
1	2 (2–3)	
2	1 (1–2)	
3	1 (0–2)	
4	0 (0–1)	
WE_FM		
1	89.4 ± 19.3 (15–100)	
2	93.5 ± 16.7 (20–100)	
3	96.1 ± 11.9 (39–100)	
4	96.2 ± 9.9 (52–100)	

Data are presented as means ± SD (range) for continuous data, medians (Q1-Q3) for time points and NIHSS, and n (%) for categorical data. NIHSS, National Institutes of Health Stroke Scale; WE_FM, Fugl–Meyer Assessment of the whole extremity.

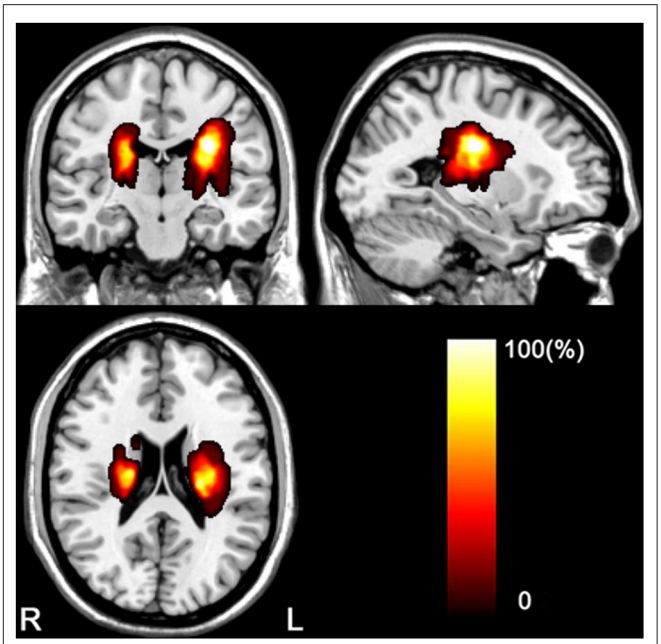

FIGURE 1 | Lesion incidence map of patients with stroke. L, left; R, right.

in the left hemisphere. The motor function of the patients was partially or completely recovered with an FMA > 52/100 for the whole extremities.

Evolution of CST Changes After Stroke

In 44 subcortical stroke patients with longitudinal DTI data, we observed longitudinal changes in the CSTs from different origins. The trajectories of the specific CST changes are shown in **Figure 2**. The statistical significance of the longitudinal specific CST changes in the stroke and control groups and the slope differences in the specific CST changes between the two groups are provided in **Table 2**. For the M1 fiber (**Figure 2A**), the stroke group showed a significant longitudinal change (decline over time; $P = 2.83 \times 10^{-7}$, Bonferroni's correction) and had a steeper slope ($P = 4.00 \times 10^{-17}$, Bonferroni's correction) than the control group. For the PMC fiber (**Figure 2B**), the stroke group demonstrated a steeper slope ($P = 7.08 \times 10^{-8}$, Bonferroni's correction), but the longitudinal change (decline over time; $P = 5.76 \times 10^{-3} > 0.05/15 = 3.33 \times 10^{-3}$, Bonferroni's correction) did not differ between the groups. For the S1 fiber (**Figure 2C**), the stroke group showed a significant longitudinal change (decline over time; $P = 3.32 \times 10^{-4}$, Bonferroni's correction) and had a steeper slope ($P = 2.43 \times 10^{-11}$, Bonferroni's correction) than the control group. For the SMA fiber (**Figure 2D**), the stroke group showed a longitudinal change (decline over time; $P = 3.27 \times 10^{-3}$, Bonferroni's correction) and had a steeper slope ($P = 8.33 \times 10^{-9}$, Bonferroni's correction) than the control group.

Evolution of M1–M1 rsFC Changes After Stroke

In 44 subcortical stroke patients with longitudinal resting-state fMRI data, we observed longitudinal M1–M1 rsFC changes. The trajectories of the M1–M1 rsFC changes are shown in **Figure 2**. The statistical significance of the longitudinal M1–M1 rsFC changes in the stroke and control groups and the slope differences in the M1–M1 rsFC changes between the two groups are provided in **Table 2**. With respect to M1–M1 rsFC (**Figure 2E**), the stroke group exhibited a longitudinal change (an increase over time; $P = 1.55 \times 10^{-6}$, Bonferroni's correction) and had a steeper slope ($P = 1.11 \times 10^{-16}$, Bonferroni's correction) than the control group.

Correlation Analyses

The FA values of the M1 fiber were significantly negatively correlated with the M1–M1 rsFC in the subacute stage (3 months post-stroke) (partial correlation coefficient [pr] = −0.548, $P = 3.06 \times 10^{-4}$) (**Figure 3A**) and chronic stage (> 6 months post-stroke) ($pr = -0.473$, $P = 2.07 \times 10^{-3}$) (**Figure 3B**) after subcortical stroke. Similarly, a negative correlation was observed between the FA values of the SMA fiber and M1–M1 rsFC in the subacute stage (3 months post-stroke) ($pr = -0.508$, $P = 9.63 \times 10^{-4}$) (**Figure 3C**) after subcortical stroke. However, none of the FA values of the affected PMC and S1 fibers were correlated with the M1–M1 rsFC at the four time points after subcortical stroke ($P > 0.05/24 = 2.08 \times 10^{-3}$, Bonferroni's correction).

In the 44 patients with subcortical stroke, the FA values of the affected M1 fiber in the acute stage were positively correlated with

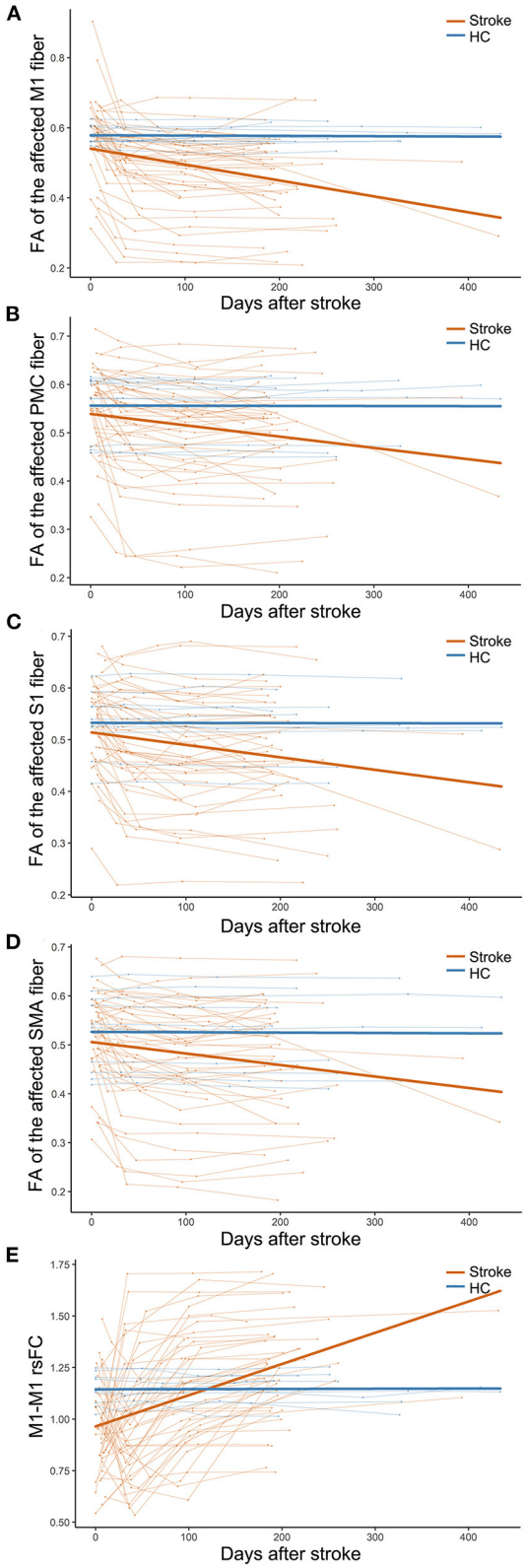

FIGURE 2 | Trajectories of CST and M1–M1 rsFC changes in patients with subcortical stroke. **(A–D)** Show the longitudinal evolutionary trajectories of the *(Continued)*

FIGURE 2 | CSTs with different origins. **(E)** Shows the longitudinal evolutionary trajectories of M1–M1 rsFC. The thin red (stroke) and blue (HC) lines represent the individual changes over time and the thick red and blue lines indicate the estimated average changes in the two groups. CST, corticospinal tract; FA, fractional anisotropy; HC, healthy controls; M1, primary motor cortex; PMC, premotor cortex; rsFC, resting-state functional connectivity; S1, primary sensory area; and SMA, supplementary motor area.

TABLE 2 | Longitudinal evolution patterns of CST and M1–M1 rsFC changes after subcortical stroke.

Variables	Stroke	HC	Stroke vs. HC
FA value of CST			
M1 fiber	**$4.00 \times 10^{-17*}$**	0.90	**$2.83 \times 10^{-7*}$**
PMC fiber	**$7.08 \times 10^{-8*}$**	0.97	5.76×10^{-3}
S1fiber	**$2.43 \times 10^{-11*}$**	0.96	**$3.32 \times 10^{-4*}$**
SMA fiber	**$8.33 \times 10^{-9*}$**	0.91	**$3.27 \times 10^{-3*}$**
M1–M1 rsFC	**$1.11 \times 10^{-16*}$**	0.97	**$1.55 \times 10^{-6*}$**

*Data are presented as the uncorrected or corrected P values. Bold values and * indicates that the result remained valid after Bonferroni's correction (*$P < 0.05/15 = 3.33 \times 10^{-3}$). CST, corticospinal tract; FA, fractional anisotropy; HC, healthy controls; M1, primary motor cortex; PMC, premotor cortex; rsFC, resting-state functional connectivity; S1, primary sensory area; SMA, supplementary motor area; vs, versus.*

the WE_FM scores in the chronic stage ($pr = 0.495$, $P = 8.55 \times 10^{-4}$, Bonferroni's correction; **Figure 4A**). However, none of the FA values of the affected PMC ($pr = 0.362$, $P = 1.84 \times 10^{-2}$, Bonferroni's correction; **Figure 4B**), S1 ($pr = 0.429$, $P = 4.64 \times 10^{-3}$, Bonferroni's correction; **Figure 4C**), and SMA ($pr = 0.399$, $P = 8.78 \times 10^{-3}$, Bonferroni's correction; **Figure 4D**) fibers was correlated with the WE_FM scores in the chronic stage ($P > 0.05/24 = 2.08 \times 10^{-3}$, Bonferroni's correction). None of the early impairments of the affected M1, PMC, S1, and SMA fibers were correlated with the WE_FM scores in the chronic stage ($P > 0.05/24 = 2.08 \times 10^{-3}$, Bonferroni's correction).

DISCUSSION

In this study, we found significantly reduced FA values of the affected specific CST fibers and increased M1–M1 rsFC. The enhanced M1–M1 rsFC values were negatively correlated with the FA values of the affected M1 fiber from the subacute to the chronic stage and negatively with the FA values of the affected SMA fiber in the subacute stage. These findings suggest that early interhemispheric functional reorganization may play a beneficial role in motor rehabilitation. We also found that the FA values of the affected M1 fiber in the acute stage were significantly correlated with the motor recovery in the chronic stage, indicating that the affected M1 fiber was critical to predicting the long-term motor outcomes after subcortical stroke.

Regarding CST as a whole tract, a previous study found that the ratios of the FA values decreased continuously during the first 3 months and then stabilized in patients with subcortical stroke (Yu et al., 2009). However, the CST fibers arise from M1, PMC, SMA, and S1 areas (Schieber, 2007; Welniarz et al., 2017). Considering the functional differences among these CST fibers

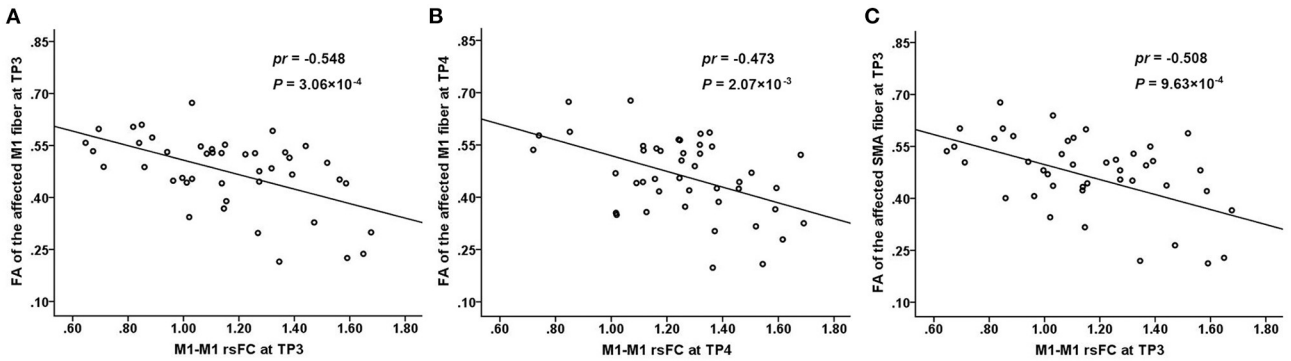

FIGURE 3 | Correlations between the connectivity measures. There is a significantly negative correlation between the FA values of the affected M1 fiber and M1–M1 rsFC at TP3 (3 months post-stroke) **(A)** and TP4 (>6 months post-stroke) **(B)** after subcortical stroke. There is a significantly negative correlation between the FA values of the affected SMA fiber and M1–M1 rsFC at TP3 (3 months post-stroke) **(C)** after subcortical stroke. FA, fractional anisotropy; M1, primary motor cortex; rsFC, resting-state functional connectivity; SMA, supplementary motor area; TP, time point.

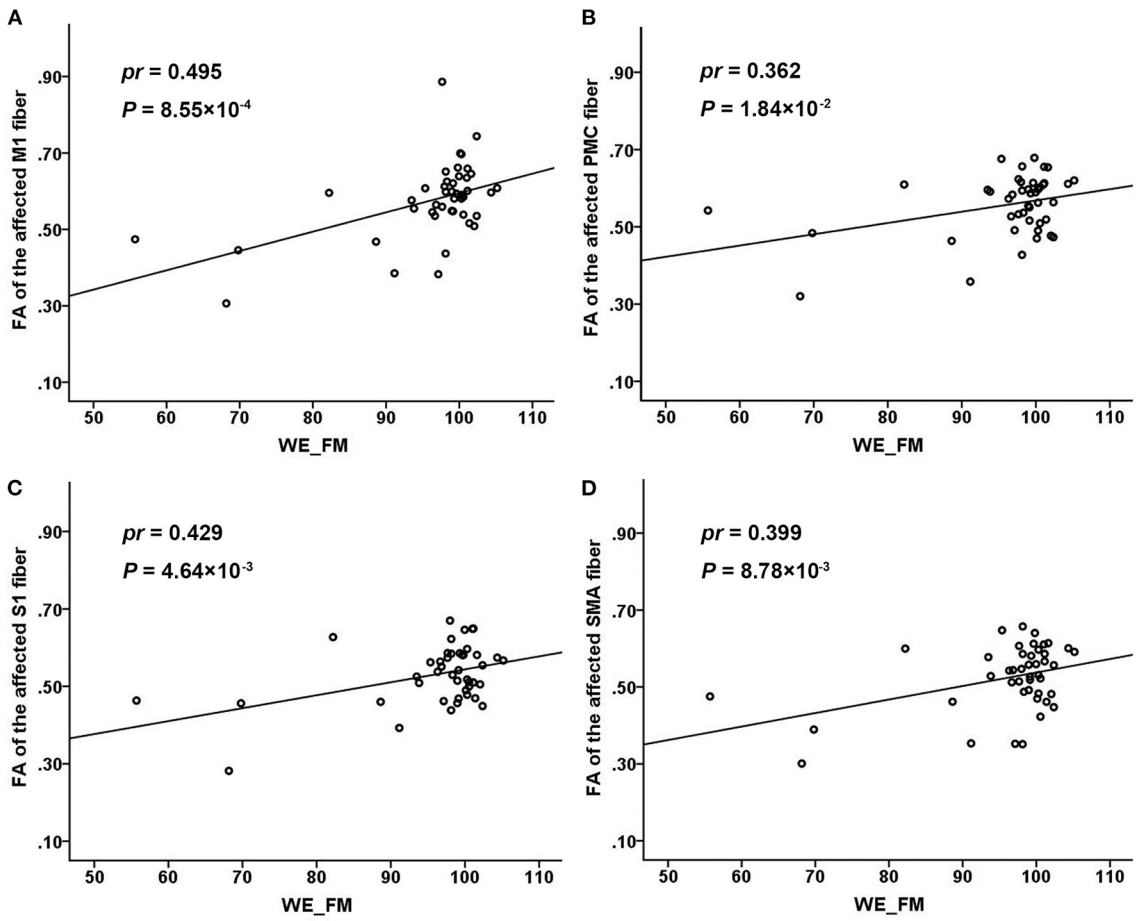

FIGURE 4 | Associations of the FA values of different CST fibers with chronic WE_FM scores in subcortical stroke. The FA values of the affected M1 **(A)**, PMC **(B)**, S1 **(C)**, and SMA **(D)** fibers in the acute stage were positively correlated with the WE_FM scores in the chronic stage. CST, corticospinal tract; FA, fractional anisotropy; M1, primary motor cortex; PMC, premotor cortex; S1, primary sensory area; SMA, supplementary motor area; WE_FM, Fugl–Meyer Assessment of the whole extremity.

with different origins, the differential involvement of the CST branches may result in distinct functional deficits. We further analyzed the dynamic evolution of the diffusion indicators of the affected specific CST fibers. According to the average changes in the affected specific CSTs, we found that the FA values of M1, S1, and SMA fibers decreased significantly and rapidly after subcortical stroke, which might reflect the pathological process of Wallerian degeneration (Yu et al., 2009). For each individual change, the FA values of the CST fibers decreased rapidly within 1 month after stroke, then slowly reduced from 1 month to 3 months, followed by stabilization after 3 months in patients with subcortical stroke. Furthermore, the FA values of the affected M1 fiber decreased more rapidly than those of other fibers. The M1 has been considered the main origin of the CST, and the affected M1 fiber seems to be more vulnerable to direct damage by stroke lesions after subcortical stroke than the other CST fibers.

In subcortical stroke patients, the evolution patterns of M1–M1 rsFC changes were complex in different individuals. Previous studies have shown that some patients exhibit a decrease in the rsFC of bilateral M1 within 24 h after stroke (Golestani et al., 2013), while it may be at a later time (1–2 weeks) in other patients (Xu et al., 2014). Consistent with these findings, we also found that most of the patients with subcortical stroke exhibited a decrease in the interhemispheric rsFC of M1 at an initial stage. According to the existing literature (Feeney and Baron, 1986; Andrews, 1991), the initial decrease in the M1–M1 rsFC may be caused by an imbalance in the interhemispheric activity changes, which has been found in the first week after stroke in rats (Jablonka et al., 2010). However, few patients showed an increase in the rsFC at the first time point. This might be explained by the later first time point (7 days post-stroke) of MRI acquisition in a few patients. In order to observe the changes rapidly, it is necessary to add time points in the acute stage in a future study. In the final stable stage (nearly 1 year post-stroke), some studies have suggested that the interhemispheric rsFC of M1 returns to a normal level in some patients (Wang et al., 2010; Urbin et al., 2014), reaches a greater than normal level in some others, and remains at a lower level in some patients (Xu et al., 2014). Similarly, we also found different changes in the M1–M1 rsFC in the chronic stage (>6 months) after subcortical stroke. The restoration of the M1–M1 rsFC may be related to the disappearance of the temporary transhemispheric diaschisis (Andrews, 1991), sprouting of axons to establish new connections and novel projection patterns (Carmichael, 2006, 2008), and/or functional reorganization within the motor network (Wang et al., 2010).

For CST as a whole tract, a previous study found that the percentage of CST damage was negatively correlated with the interhemispheric rsFC reduction in subacute stroke patients (<4 weeks post-stroke) with subcortical lesions (Carter et al., 2012). However, we did not find any significant correlations between the FA values of CST impairment and M1–M1 rsFC in early subacute patients with subcortical stroke. This discrepancy may be explained by the difference in the time points of MRI acquisition between the two studies. Our patients were scanned at <7 days, 1 month, 3 months, and >6 months post-stroke. Liu et al. (2015) found that the M1–M1 rsFC increase was negatively correlated with the CST damage in patients with chronic subcortical stroke (>6 mouths post-stroke). The result of this cross-sectional study is consistent with our finding of a negative correction between these two measures in chronic patients with subcortical stroke. This finding indicates that the CST impairment from a focal stroke lesion could be compensated by the enhanced interhemispheric rsFC of M1, which may reflect a form of reactive functional reorganization. We further found that an increased M1–M1 rsFC is negatively correlated with impairment of the affected M1 and SMA fibers starting from the subacute stage (3 months post-stroke) after stroke, indicating that the rehabilitation of enhanced interhemispheric rsFC possibly occurs in the subacute stage after subcortical stroke. This finding suggests that the rehabilitation of M1–M1 rsFC enhancement may be beneficial for the motor recovery of stroke patients with CST injury, which has important clinical implications, as this kind of rehabilitation may be more efficacious if patients can strengthen rehabilitation training or physical stimulation (e.g., transcranial magnetic stimulation, transcranial direct current stimulation) in these regions in the subacute stage. This will also be our goal in our future studies.

The microstructure integrity of the CSTs is correlated with motor recovery in patients with subcortical stroke (Liu and Wang, 2022). The M1 is the main site of origin of the CST, and the M1 fiber seems to be more important for motor function than the other CST fibers (Schieber, 2007; Welniarz et al., 2017; Liu et al., 2020). Liu et al. (2020) found that the early impairments of M1 and SMA fibers were significantly associated with motor deficits in chronic stroke patients. In our study, we also provided sufficient evidence on the importance of the M1 fibers for motor function. For example, the FA values of the affected M1 fiber were correlated with the long-term motor outcomes. However, we did not find any significant correlations for CST fibers originating from the SMA, S1, and PMC, indicating that these fibers make a limited contribution to motor deficits assessed by clinical motor scales. In general, these findings indicate that the M1 fiber is a reliable predictive indicator of the long-term motor outcome in patients with subcortical stroke. In addition, we also assessed the integrity of the M1 fibers in the acute stage, which may help to predict the clinical benefits of different rehabilitative strategies. For example, if the M1 fibers are completely interrupted in patients with subcortical stroke, a little clinical benefit can be obtained from physical stimulation targeting the M1 areas. In this situation, alternative rehabilitative strategies which can enhance an alternative motor pathway (Ruber et al., 2012; Schulz et al., 2017) or establish new motor fibers (Carmichael et al., 2017) may be preferable.

In this study, the evolution patterns of affected CST fibers with different cortical origins and M1–M1 rsFC and their dynamic relationships were studied in patients with subcortical stroke. The enhanced interhemispheric rsFC of M1 may reflect a compensatory mechanism for motor deficits caused by the impairment of the affected M1 and SMA fibers from the subacute to chronic stages. FA values of the affected M1 fiber in the acute stage were significantly correlated with the long-term motor recovery, which may be used to screen imaging biomarkers for predicting motor outcomes. These findings may be helpful in the design of individualized rehabilitative plans.

DATA AVAILABILITY STATEMENT

The raw data supporting the conclusions of this article will be made available by the authors, without undue reservation.

ETHICS STATEMENT

The studies involving human participants were reviewed and approved by Tianjin Medical University General Hospital medical research Ethics Committee. The patients/participants provided their written informed consent to participate in this study.

AUTHOR CONTRIBUTIONS

JL and CW contributed to the conception and design of the study. JL and JC performed the experiments and analyzed the data. ZL and PM were involved in the clinical assessment. JL wrote the first draft. All authors contributed to the manuscript revision and approved the submitted version.

FUNDING

This study was supported by the Natural Science Foundation of China (81871327 and 82030053), the Tianjin Key Technology R&D Program (17ZXMFSY00090), the Tianjin Key Medical Discipline (Specialty) Construction Project, and the Young Talents Promotion Program of Henan Province (2021HYTP012).

ACKNOWLEDGMENTS

We thank Yujing Li, Jing Pan, and the neurology team at the General Hospital for patients recruitment and collection of clinical data. We thank all the volunteers and patients for their participation in the study.

REFERENCES

Andrews, R. J. (1991). Transhemispheric diaschisis. A review and comment. *Stroke* 22, 943–949. doi: 10.1161/01.STR.22.7.943

Carmichael, S. T. (2006). Cellular and molecular mechanisms of neural repair after stroke: making waves. *Ann. Neurol.* 59, 735–742. doi: 10.1002/ana.20845

Carmichael, S. T. (2008). Themes and strategies for studying the biology of stroke recovery in the poststroke epoch. *Stroke* 39, 1380–1388. doi: 10.1161/STROKEAHA.107.499962

Carmichael, S. T., Kathirvelu, B., Schweppe, C. A., and Nie, E. H. (2017). Molecular, cellular and functional events in axonal sprouting after stroke. *Exp. Neurol.* 287, 384–394. doi: 10.1016/j.expneurol.2016.02.007

Carter, A. R., Patel, K. R., Astafiev, S. V., Snyder, A. Z., Rengachary, J., Strube, M. J., et al. (2012). Upstream dysfunction of somatomotor functional connectivity after corticospinal damage in stroke. *Neurorehabil. Neural. Repair.* 26, 7–19. doi: 10.1177/1545968311411054

Chen, J., Sun, D., Zhang, S., Shi, Y., Qiao, F., Zhou, Y., et al. (2020). Effects of home-based telerehabilitation in patients with stroke: a randomized controlled trial. *Neurology* 95, e2318–e2330. doi: 10.1212/WNL.0000000000010821

DeVetten, G., Coutts, S. B., Hill, M. D., Goyal, M., Eesa, M., O'Brien, B., et al. (2010). Acute corticospinal tract Wallerian degeneration is associated with stroke outcome. *Stroke* 41, 751–756. doi: 10.1161/STROKEAHA.109.573287

Fan, L., Li, H., Zhuo, J., Zhang, Y., Wang, J., Chen, L., et al. (2016). The Human Brainnetome Atlas: A New Brain Atlas Based on Connectional Architecture. *Cereb. Cortex.* 26, 3508–3526. doi: 10.1093/cercor/bhw157

Fazekas, F., Chawluk, J. B., Alavi, A., Hurtig, H. I., and Zimmerman, R. A. (1987). MR signal abnormalities at 1.5 T in Alzheimer's dementia and normal aging. *AJR Am. J. Roentgenol.* 149, 351–356. doi: 10.2214/ajr.149.2.351

Feeney, D. M., and Baron, J. C. (1986). Diaschisis. *Stroke* 17, 817–830. doi: 10.1161/01.STR.17.5.817

Friston, K. J. (2011). Functional and effective connectivity: a review. *Brain Connect.* 1, 13–36. doi: 10.1089/brain.2011.0008

Friston, K. J., Williams, S., Howard, R., Frackowiak, R. S., and Turner, R. (1996). Movement-related effects in fMRI time-series. *Magn. Reson. Med.*35, 346–355. doi: 10.1002/mrm.1910350312

Gibbons, R. D., Hedeker, D., Waternaux, C., and Davis, J. M. (1988). Random regression models: a comprehensive approach to the analysis of longitudinal psychiatric data. *Psychopharmacol. Bull.* 24, 438–443.

Golestani, A. M., Tymchuk, S., Demchuk, A., and Goodyear, B. G. (2013). Longitudinal evaluation of resting-state FMRI after acute stroke with hemiparesis. *Neurorehabil. Neural. Rep.* 27, 153–163. doi: 10.1177/1545968312457827

Greicius, M. D., Krasnow, B., Reiss, A. L., and Menon, V. (2003). Functional connectivity in the resting brain: A network analysis of the default mode hypothesis. *Proc. Nat. Acad. Sci. U. S. A.* 100, 253–258. doi: 10.1073/pnas.0135058100

Guo, J., Liu, J., Wang, C., Cao, C., Fu, L., Han, T., et al. (2019). Differential involvement of rubral branches in chronic capsular and pontine stroke. *Neuroimage Clin.* 24, 102090. doi: 10.1016/j.nicl.2019.102090

Jablonka, J. A., Burnat, K., Witte, O. W., and Kossut, M. (2010). Remapping of the somatosensory cortex after a photothrombotic stroke: dynamics of the compensatory reorganization. *Neuroscience* 165, 90–100. doi: 10.1016/j.neuroscience.2009.09.074

Johnson, B. P., and Westlake, K. P. (2021). Chronic poststroke deficits in gross and fine motor control of the ipsilesional upper limb. *Am. J. Phys. Med. Rehabil.* 100, 345–348. doi: 10.1097/PHM.0000000000001569

Kunimatsu, A., Aoki, S., Masutani, Y., Abe, O., Mori, H., and Ohtomo, K. (2003). Three-dimensional white matter tractography by diffusion tensor imaging in ischaemic stroke involving the corticospinal tract. *Neuroradiology* 45, 532–535. doi: 10.1007/s00234-003-0974-4

Le Bihan, D. (2003). Looking into the functional architecture of the brain with diffusion MRI. *Nat. Rev. Neurosci.* 4, 469–480. doi: 10.1038/nrn1119

Lee, J. S., Han, M. K., Kim, S. H., Kwon, O. K., and Kim, J. H. (2005). Fiber tracking by diffusion tensor imaging in corticospinal tract stroke: topographical correlation with clinical symptoms. *Neuroimage* 26, 771–776. doi: 10.1016/j.neuroimage.2005.02.036

Liu, J., Qin, W., Zhang, J., Zhang, X., and Yu, C. (2015). Enhanced interhemispheric functional connectivity compensates for anatomical connection damages in subcortical stroke. *Stroke* 46, 1045–1051. doi: 10.1161/STROKEAHA.114.007044

Liu, J., and Wang, C. (2022). Microstructure and genetic polymorphisms: role in motor rehabilitation after subcortical stroke. *Front. Aging Neurosci.* 14, 813756. doi: 10.3389/fnagi.2022.813756

Liu, J., Wang, C., Qin, W., Ding, H., Guo, J., Han, T., et al. (2020). Corticospinal fibers with different origins impact motor outcome and brain after subcortical stroke. *Stroke* 51, 2170–2178. doi: 10.1161/STROKEAHA.120.029508

Mori, S., and van Zijl, P. C. (2002). Fiber tracking: principles and strategies - a technical review. *NMR Biomed.* 15, 468–480. doi: 10.1002/nbm.781

Oldfield, R. C. (1971). The assessment and analysis of handedness: the Edinburgh inventory. *Neuropsychologia* 9, 97–113. doi: 10.1016/0028-3932(71)90067-4

Patel, P., Kaingade, S. R., Wilcox, A., and Lodha, N. (2020). Force control predicts fine motor dexterity in high-functioning stroke survivors. *Neurosci. Lett.* 729, 135015. doi: 10.1016/j.neulet.2020.135015

Peng, Y., Liu, J., Hua, M., Liang, M., and Yu, C. (2019). Enhanced effective connectivity from ipsilesional to contralesional M1 in well-recovered subcortical stroke patients. *Front. Neurol.* 10, 909. doi: 10.3389/fneur.2019.00909

Ruber, T., Lindenberg, R., and Schlaug, G. (2012). Compensatory role of the cortico-rubro-spinal tract in motor recovery after stroke. *Neurology* 78. doi: 10.1212/WNL.0b013e31826356e8

Schaechter, J. D., Fricker, Z. P., Perdue, K. L., Helmer, K. G., Vangel, M. G., Greve, D. N., et al. (2009). Microstructural status of ipsilesional and contralesional corticospinal tract correlates with motor skill in chronic stroke patients. *Hum. Brain Mapp.* 30, 3461–3474. doi: 10.1002/hbm.20770

Schieber, M. H. (2007). Chapter 2 Comparative anatomy and physiology of the corticospinal system. *Handb. Clin. Neurol.* 82, 15–37. doi: 10.1016/S0072-9752(07)80005-4

Schulz, R., Park, E., Lee, J., Chang, W. H., Lee, A., Kim, Y. H., et al. (2017). Synergistic but independent: The role of corticospinal and alternate motor fibers for residual motor output after stroke. *Neuroimage. Clin.* 15, 118–124. doi: 10.1016/j.nicl.2017.04.016

Seo, J. P., and Jang, S. H. (2013). Different characteristics of the corticospinal tract according to the cerebral origin: DTI study. *AJNR Am. J. Neuroradiol.* 34, 1359–1363. doi: 10.3174/ajnr.A3389

Shaheen, H. A., Sayed, S. S., Magdy, M. M., Saad, M. A., Magdy, A. M., and Daker, L. I. (2022). Prediction of motor recovery after ischemic stroke: Clinical and diffusion tensor imaging study. *J. Clin. Neurosci.* 96, 68–73. doi: 10.1016/j.jocn.2021.12.029

Urbin, M. A., Hong, X., Lang, C. E., and Carter, A. R. (2014). Resting-state functional connectivity and its association with multiple domains of upper-extremity function in chronic stroke. *Neurorehabil. Neural. Rep.* 28, 761–769. doi: 10.1177/1545968314522349

Verheyden, G., Nieuwboer, A., De Wit, L., Thijs, V., Dobbelaere, J., Devos, H., et al. (2008). Time course of trunk, arm, leg, and functional recovery after ischemic stroke. *Neurorehabil. Neural Rep.* 22, 173–179. doi: 10.1177/1545968307305456

Wang, L., Yu, C., Chen, H., Qin, W., He, Y., Fan, F., et al. (2010). Dynamic functional reorganization of the motor execution network after stroke. *Brain* 133, 1224–1238. doi: 10.1093/brain/awq043

Welniarz, Q., Dusart, I., and Roze, E. (2017). The corticospinal tract: evolution, development, and human disorders. *Dev. Neurobiol.* 77, 810–829. doi: 10.1002/dneu.22455

Xia, Y., Huang, G., Quan, X., Qin, Q., Li, H., Xu, C., et al. (2021). Dynamic structural and functional reorganizations following motor stroke. *Med. Sci. Monit.* 27, e929092. doi: 10.12659/MSM.929092

Xu, H., Qin, W., Chen, H., Jiang, L., Li, K., and Yu, C. (2014). Contribution of the resting-state functional connectivity of the contralesional primary sensorimotor cortex to motor recovery after subcortical stroke. *PLoS ONE.* 9, e84729. doi: 10.1371/journal.pone.0084729

Yin, D., Song, F., Xu, D., Peterson, B. S., Sun, L., Men, W., et al. (2012). Patterns in cortical connectivity for determining outcomes in hand function after subcortical stroke. *PLoS ONE.* 7, e52727. doi: 10.1371/journal.pone.0052727

Yu, C., Zhu, C., Zhang, Y., Chen, H., Qin, W., Wang, M., et al. (2009). A longitudinal diffusion tensor imaging study on Wallerian degeneration of corticospinal tract after motor pathway stroke. *Neuroimage* 47, 451–458. doi: 10.1016/j.neuroimage.2009.04.066

Zolkefley, M. K. I., Firwana, Y. M. S., Hatta, H. Z. M., Rowbin, C., Nassir, C., Hanafi, M. H., et al. (2021). An overview of fractional anisotropy as a reliable quantitative measurement for the corticospinal tract (CST) integrity in correlation with a Fugl-Meyer assessment in stroke rehabilitation. *J. Phys. Ther. Sci.* 33, 75–83. doi: 10.1589/jpts.33.75

Conflict of Interest: The authors declare that the research was conducted in the absence of any commercial or financial relationships that could be construed as a potential conflict of interest.

Publisher's Note: All claims expressed in this article are solely those of the authors and do not necessarily represent those of their affiliated organizations, or those of the publisher, the editors and the reviewers. Any product that may be evaluated in this article, or claim that may be made by its manufacturer, is not guaranteed or endorsed by the publisher.

frontiers | Frontiers in Aging Neuroscience

ORIGINAL RESEARCH
published: 09 May 2022
doi: 10.3389/fnagi.2022.863489

Analyzing Corin–BNP–NEP Protein Pathway Revealing Differential Mechanisms in AF-Related Ischemic Stroke and No AF-Related Ischemic Stroke

Xiaozhu Shen[1,2†], Nan Dong[1,3†], Yiwen Xu[4], Lin Han[1], Rui Yang[1], Juan Liao[1], Xianxian Zhang[1], Tao Xie[1], Yugang Wang[1], Chen Chen[1], Mengqian Liu[4], Yi Jiang[5], Liqiang Yu[1] and Qi Fang[1]**

[1] Department of Neurology, The First Affiliated Hospital of Soochow University, Suzhou, China, [2] Department of Geriatrics, Lianyungang Second People's Hospital, Lianyungang, China, [3] Department of Neurology, Suzhou Industrial Park Xinghai Hospital, Suzhou, China, [4] Department of General Medicine, Lianyungang Hospital, Affiliated to Jiangsu University (Lianyungang Second People's Hospital), Lianyungang, China, [5] Bengbu Medical College, Bengbu, China

OPEN ACCESS

Edited by:
Yujie Chen,
Army Medical University, China

Reviewed by:
Zhenhua Zhou,
The Third Military Medical University, China
Dorin Dragoş,
Carol Davila University of Medicine and Pharmacy, Romania

***Correspondence:**
Yiwen Xu
1076405885@qq.com
Qi Fang
fangqi_008@126.com

† These authors have contributed equally to this work

Specialty section:
This article was submitted to Cellular and Molecular Mechanisms of Brain-aging, a section of the journal Frontiers in Aging Neuroscience

Received: 27 January 2022
Accepted: 14 March 2022
Published: 09 May 2022

Citation:
Shen X, Dong N, Xu Y, Han L, Yang R, Liao J, Zhang X, Xie T, Wang Y, Chen C, Liu M, Jiang Y, Yu L and Fang Q (2022) Analyzing Corin–BNP–NEP Protein Pathway Revealing Differential Mechanisms in AF-Related Ischemic Stroke and No AF-Related Ischemic Stroke. Front. Aging Neurosci. 14:863489. doi: 10.3389/fnagi.2022.863489

Background: The incidence of atrial fibrillation (AF)-related stroke increases with aging. Natriuretic peptides (NPs) family, including Corin-B type natriuretic peptide (BNP)-neprilysin (NEP) protein levels increased with age and are risk markers of cardiovascular and cerebrovascular diseases, such as AF and cardioembolic stroke. Aging is also linked to epigenetics, specifically DNA methylation. However, only a few studies have investigated the effect of DNA methylation on the NP system. Thus, the present study aimed to investigate whether the Corin-BNP-NEP protein pathway is involved in the pathogenesis of AF-stroke and CpG methylation in the promoter region of the Corin protein gene has an effect on AF-related ischemic stroke.

Methods: A total of 82 patients hospitalized with acute ischemic strokes were enrolled in this study. The differences in clinical information were compared between the AF-stroke (n = 37) and no AF-stroke groups (n = 45). Plasma-soluble Corin and NEP were detected using an ELISA kit. CpG methylation in the promoter region of the gene was assessed by a next-generation sequencing-based bisulfite sequencing polymerase chain reaction (BSP).

Results: (1) Patients in AF-stroke were older, had higher initial NIHSS score, 90-day mRs, higher D2-dimer, INR, and APTT, and low TG, TC, and HbA1c (all $p < 0.05$). (2) Serum levels of Corin and BNP in the AF-stroke group were significantly higher than that in the no AF-stroke group ($p < 0.05$). No significant difference was detected in the serum levels of NEP between the two groups. (3) The levels of CpG methylation in the promoter region of the Corin protein gene in the AF-stroke group was

significantly lower than that in the no AF-stroke group ($p < 0.05$). The CpG sites with maximal methylation differences between the two groups were CORIN:678, CORIN:682, CORIN:694, and CORIN:700.

Conclusion: The current findings raise the possibility that the Corin–BNP–NEP protein pathway may be involved in the pathogenesis of AF-related ischemic stroke. Deficient CpG methylation in the promoter region of the Corin protein gene is associated with AF-related ischemic stroke.

Keywords: atrial fibrillation, cardioembolism, B-type natriuretic peptide, Corin peptide, neprilysin, DNA methylation

INTRODUCTION

In recent years, the aging of the global population has led to an increased burden of disease and disability. A large-scale population-based national stroke survey shows that the burden of stroke in China has been increasing over the past 30 years, and ischemic stroke constituted 69.677.8% incidence and prevalence of strokes (Wang et al., 2017). Hitherto, several classification methods are available for ischemic stroke. Using the Trial of Org 10172 in acute stroke treatment (TOAST) criteria, ischemic stroke can be divided into large artery atherosclerosis (LAA), cardioembolism (CE), small artery occlusion (SAO), stroke of other determined etiology (OC), and stroke of undetermined etiology (SUD) (Liu et al., 2020). CE stroke accounts for 14–30% of all cerebral infarctions (Maida et al., 2020). AF is one of the main causes of CE stroke. It is age-related, and AF-associated ischemic strokes have a high rate of disability and mortality (Zhou et al., 2016; GBD 2016 Causes of Death Collaborators, 2017). The prevention and treatment of AF-associated ischemic stroke are crucial for healthy aging.

For a prolonged period, the circulating levels of natriuretic peptides (NPs) have been widely used as clinical biomarkers of cardiovascular function. B-type natriuretic peptide (BNP) is a hormone belonging to the natriuretic peptide family that retains a common ring structure and conserved amino acid sequence. BNP is cleaved from the proBNP precursor by enzymatic processing between amino acid residues 76 and 77, similar to the amino-terminal portion of proBNP (i.e., NT-proBNP), and this enzymatic reaction was undertaken by the enzyme Corin (Yandle and Richards, 2015). Several enzymes are involved in NP degradation, among which Neprilysin (NEP) plays a dominant role. It cleaves BNP at two main positions, of which the cleavage between Met-4 and Val-5 is the primary site within the ring structure between Arg-17 and Ile-18 (Yandle and Richards, 2015; Chen and Burnett, 2017). Corin-BNP-NEP constitutes a protein pathway from generation to decomposition. The plasma levels of BNP (Everett et al., 2015; Yoshida et al., 2019) and the risk markers of cardiovascular and cerebrovascular diseases, such as AF and CE stroke, are increased with age (Berntsson et al., 2014; Goetze et al., 2020). Whether the Corin-BNP-NEP protein pathway is involved in the occurrence of AF-associated stroke is yet to be elaborated.

Epigenetics, specifically DNA methylation (DNAm), is linked to aging (Day et al., 2013; Horvath, 2013; Tharakan et al., 2020). DNAm is the most abundant epigenetic marker in the human genome for controlling gene expression (Belsky et al., 2022). It usually occurs in CpG islands and is mostly in the proximal promoter region of the human genome, which modifies an individual's biological function by regulating gene expression or genome sequence stability (Deng et al., 2019). DNAm modifications are heterogeneous in terms of organ and tissue components. Abnormal DNAm has been associated with many cardiovascular, cerebrovascular, and other diseases, including Alzheimer's disease (AD), Parkinson's disease (PD), ischemic stroke, coronary artery disease (CAD), myocardial infarction, and cancer (Deng et al., 2019; Miao et al., 2019; Martínez-Iglesias et al., 2020; Sharma et al., 2020; Wang et al., 2021).

Previous studies have shown that epigenetics is closely related to aging, which in turn is related to NP. Strikingly, only a few studies have evaluated the effect of DNAm in the NP system. Thus, the present study aimed to investigate whether the Corin–BNP–NEP protein pathway is involved in the pathogenesis of AF-stroke and CpG methylation in the promoter region of the Corin protein gene has an effect on AF-related ischemic stroke.

MATERIALS AND METHODS

Patients and Samples

Subjects were enrolled after obtaining written informed consent and approval from the Ethics Committee of Soochow University. This study recruited patients with first-ever ischemic or hemorrhagic stroke onset within 48 h confirmed by brain computed tomography (CT) or magnetic resonance imaging (MRI) from three hospitals between September 2019 and December 2020. This study was approved by Soochow University (No. 2019-057). The inclusion criteria were as follows: (1) Age $\geq$ 18 years; (2) Within 24 h of onset, CTA + CTP suggested the presence of infarct core or within 1 week from onset to the time of cranial MRI examination, and acute cerebral infarction lesions were visible on MR DWI sequences; (3) Patients with the first onset of previous cerebral infarction with no significant sequelae left and re-acute onset; (4) Patients who completed ECG or Holter and ECG monitoring during their stay in the hospital. Patients who fulfilled one of the following conditions were excluded: (1) Patients with cerebral hemorrhage and occupancy (emergency head CT excludes cerebral hemorrhage, while post-infarction hemorrhage is not excluded if the patient

was hospitalized); (2) Patients with transient ischemic attack; (3) Severe infection or septic shock; (4) History of severe trauma with surgical treatment; (5) significant hepatic and renal insufficiency; (6) Endocrine, immune, and oncological diseases; (7) Pregnancy; (8) other causes of cardiogenic stroke, including patent foramen ovale, left atrial mucinous tumor, rheumatic heart disease, dilated cardiomyopathy, and hypertrophic cardiomyopathy; (9) Other causes that can cause acute multiple foci of infarction, such as vasculitis, coagulation system diseases, and tumor embolism.

Finally, 82 patients were enrolled in this study. Two groups were divided based on whether AF was detected during the course of the disease: the AF-stroke group (n = 37) and the no AF-stroke group (n = 45). In the no AF-stroke group, large artery atherosclerosis accounted for 100% of the cases, according to TOAST typing.

About 5 ml venous blood was collected from subjects within 4.5 h of onset and before revascularization treatment and stored in EDTA anticoagulation tubes. Of this, 3 ml was frozen at –80°C until sequencing, and the remaining 2 ml was subjected to centrifugation at 5°C, and about 600 ml plasma was obtained and stored at –80°C.

Basic Data Collection

During enrollment, the medical history was taken, and the routine physical examination of the participants was performed by experienced physicians. Medical history included age, sex, systolic blood pressure (SBP), initial NIHSS score, treatment options (i.e., thrombolysis, embolectomy, bridging therapy, and conservative treatment), and 90-day mRs. Laboratory tests included D2-dimer, INR, PLT, Fib, APTT, Cr, TC, TG, LDL-C, Hcy, Glucose, HbA1c, and TnI.

Plasma Soluble Corin, B Type Natriuretic Peptide, and Neprilysin Level Tests

Plasma-soluble Corin level was measured using a human CRN ELISA kit (Catalog: IC-CRN-Hu, IC ImmunoClone Inc., Shanghai, China); plasma-soluble NEP was measured using a human NEP ELISA kit (Catalog: JL15469, Jianglai Inc., Shanghai, China); plasma soluble BNP level was collected from clinical data.

Next-Generation Sequencing-Based Bisulfite Sequencing Polymerase Chain Reaction

Gene-specific DNAm was assessed by BSP, according to a previously published method (Pan et al., 2018). Briefly, BSP primers were designed using the online MethPrimer software, and the sequences of primers were as follows: *CORIN*: Forward 5′-GAAGGAAATTTTGTTTATGATTTTGGGAGGGT-3′ and Reverse 5′-ATAACCTCTTAATCCCRATAAATTCAAAATCAACC-3′; *CORIN*: Forward 5′-GATTTTTAGGTATTAATTGGGGGTYGGGGAATT-3′ and Reverse 5′- CCTCCAAACATCTAATAAACTTAACTACACAC-3′. An equivalent of 1 μg of genomic DNA was converted using the ZYMO EZ DNA Methylation-Gold Kit (Zymo Research, Irvine, CA, United States) and 0.05% of the elution products were used as templates for PCR amplification with 35 cycles using KAPA 2G Robust HotStart PCR Kit (Kapa Biosystems, Wilmington, MA, United States). For each sample, the BSP products of multiple genes were pooled equally, and 5′-phosphorylated and 3′-dA-tailed products were ligated to the barcoded adapter using T4 DNA ligase (NEB). The barcoded libraries from all samples were sequenced on the Illumina platform.

For the bisulfite sequencing reads of each sample, firstly, adapters and low-quality reads were removed using Trimmomatic-0.36 software. After removing the adapter sequences and filtering out the low-quality reads, the clean sequencing reads were aligned to the target sequences using Bsmap (v2.73) software with the default parameters, which combines genome hashing and bitwise masking to achieve fast and accurate bisulfite mapping. Methylation levels were defined as the fraction of read counts of "C" in the total read counts of both "C" and "T" for each covered C site. Based on such read fraction, methylated cytosine was called using a binomial distribution to compute the probabilistic mass function for each methylation context (CpG). Two-tailed Fisher's exact test was used to identify the cytosines that are differentially methylated between two samples or groups. Only those CpGs covered by a minimum of 200 reads in at least one sample were considered for testing.

Statistical Analysis

Data were analyzed using the SPSS software (IBM SPSS Statistics for Windows, version 25.0; IBM Corp., Armonk, NY, United States), GraphPad Software (GraphPad Prism for Windows, version 9.0.0; San Diego, CA, United States), and R software package version 4.1.2.[1] $p < 0.05$ in a two-tailed test indicated statistical significance. Baseline information included in the analysis included age, sex, SBP, initial NIHSS score, treatment options (i.e., thrombolysis, embolectomy, bridging therapy, and conservative treatment), 90-day mRs, D2-dimer, INR, PLT, Fib, APTT, Cr, TC, TG, LDL-C, Hcy, glucose, HbA1c, and TnI. The Kolmogorov–Smirnov test was used to assess the normality of numerical variables. Mann–Whitney U-tests were used for analysis in the case of non-normal distribution, described by median and quartile range (IQR). The continuous variables of normal distribution were analyzed by independent sample t-test and expressed as mean ± standard deviation (SD), and chi-squared test or Fisher exact test for categorical variables. Mann–Whitney U-test was used to assess the difference in the plasma levels of Corin, BNP, and NEP between the two groups. Based on the absolute coordinates of the detected gene region, the map shows the average methylation level of each site in each sample and is labeled with different colors according to the biological groups, using the formula model function in R language to simulate the combined trend line. Cluster analysis was performed to assess the methylation levels of CpG sites in all samples and display the categorical correlation of methylation levels between samples and sites in the form of heat maps. The color changes from blue to red indicated a gradually increasing methylation level. Then, the average methylation level

[1] http://www.R-project.org

of each CpG site in each sample was evaluated using box plot + bee colony plot to show the methylation distribution of each region between the AF-stroke and no AF-stroke groups and analyze the difference between the two groups by the Wilcox test.

RESULTS

Clinical Characteristics of the Participants

The clinical parameters of all participants are summarized in **Table 1**. Compared to the no AF-stroke group, patients in the AF-stroke were older, had higher initial NIHSS score and 90-day mRs, higher D2-dimer, INR, APTT, and lower TG, TC, and HbA1c (all $p < 0.05$). In addition, no statistical difference was observed in gender, SBP, PLT, Fib, Cr, LDL-C, Hcy, glucose, and TnI between the two groups (all $p > 0.05$).

Schematic of the Methylation Level Distribution of Each CpG Site

The schematic of the methylation level distribution of each CpG site of the AF-stroke and no AF-stroke groups in the promoter region of the Corin protein gene as shown in **Figure 1A**. Based on the absolute coordinates of the detected gene region, the map shows the average methylation level of each site in each sample and is labeled with different colors according to biological groupings, using the formula model function in R language to simulate the combined trend line. The CpG sites with the maximal methylation differences between the two groups are CORIN:678, CORIN:682, CORIN:694, and CORIN:700, respectively.

Methylation Level Clustering Heatmap of All Samples

The methylation level clustering heatmap of all samples in the AF-stroke and no AF-stroke groups is shown in **Figure 1B**. Cluster analysis was performed on the methylation levels of CpG sites in all samples, which displayed the categorical correlation of methylation levels between samples and sites in the form of heatmaps. The color changes from blue to red indicated that the methylation level increases gradually.

Plasma Levels of Corin, B Type Natriuretic Peptide, Neprilysin

The plasma level of Corin in the AF-stroke group [8.17 (4.68–30.62) ng/ml] was significantly higher than that in the no AF-stroke group [4.93 (2.12–9.01) ng/ml] ($p < 0.05$). The plasma levels of BNP were significantly higher in the AF-stroke group [269.85 (64.54–633.90) pg/ml] than in the no AF-stroke group [13.27 (0–72.12) pg/mL] ($p < 0.001$). No significant difference was observed in the plasma levels of NEP between the AF-stroke group [130.5 (8.63–274.88) pg/ml] and the no AF-stroke group [131.12 (3.57–253.94) pg/ml] ($p > 0.05$; **Table 1** and **Figure 2**).

Comparison of CpG Methylation Levels

The comparison of CpG methylation levels in the promoter region of the Corin protein gene between the AF-stroke and no AF-stroke groups is shown in **Figure 1C**. The average methylation level of each CpG site in each sample was estimated using the box plot + bee colony plot to show the methylation distribution of each region between the AF-stroke and no AF-stroke groups, and the difference between these two groups was analyzed by the Wilcox test. The levels of CpG methylation in the promoter region of the Corin protein gene were significantly lower in the AF-stroke group than that in the no AF-stroke group ($p < 0.05$).

DISCUSSION

Increasing age has been widely recognized as a major risk factor for ischemic stroke in patients with AF, which is about 1.4- to 3.3-fold (Liao et al., 2019). This phenomenon was confirmed in the baseline clinical characteristics of the participants. The average age of the AF-stroke group [73 (64.5–82.5) years] was significantly higher than that of the no AF-stroke group [65 (56.5–74) years]. AF-related stroke is associated with a higher mortality rate, more disability, longer hospitalization, and worse function recovery compared to the no-AF-related stroke (Liao et al., 2019), which is also confirmed in the baseline treatment in this study. The patients in the AF-stroke group were older, had a higher initial NIHSS score, and 90-day mRs than those in the no AF-stroke group.

Biological aging is the gradual, progressive decline in system integrity that causes morbidity and disability (Field et al., 2018; Belsky et al., 2022). Field et al. (2018) and Belsky et al. (2020, 2022) quantitated the pace of biological aging from a DNAm blood test. The vascular stiffness of the elderly population increases with aging. Vascular aging is a pivotal risk factor for dysfunction and related diseases. DNAm is involved in vascular aging and plays a central role in regulating age-related vascular diseases. Moreover, arterial stiffness and vascular aging trigger cerebrovascular dysfunction and constriction of the blood-brain barrier, leading to cerebrovascular diseases (Thorin-Trescases et al., 2018; Xu et al., 2021). The evaluation of vascular aging might aid in stroke risk assessment in a community-based Chinese cohort conducted with 11,474 participants (Yang et al., 2019). As described above, DNAm is a dynamically reversible process involving altered gene transcription without modifying the DNA sequence. It changes with age (Acton et al., 2021) and plays a critical role in vascular aging. Age-related CpG sites from blood samples based on DNAm can be used to construct the modeling tools to predict biological aging (Li et al., 2018).

Several studies demonstrated that DNAm regulates several cardiovascular and cerebrovascular diseases, such as cardiac remodeling, heart failure, atherosclerosis, stroke, dementia, and AD (Chen et al., 2021; Xu et al., 2021). Recent studies have highlighted the critical role of mechanosensory-related epigenetics in local endothelial dysfunction and regional susceptibility to vascular disease. DNA de/methylation promotes

TABLE 1 | Clinical characteristics of the participants.

Characteristics	AF-stroke (*n* = 37)	noAF-stroke (*n* = 45)	T/U/X^2	*Z*	*p*-value
Median Age (IQR)—year	73(64.5, 82.5)	65(56.5, 74)	573	-2.42	0.016
Sex—no. (%)			2.821		0.093
Male	20(54.1)	16(35.6)			
Female	17(45.9)	29(64.4)			
Median SBP(IQR)—mmHg	144(130.5, 162.5)	154(137.5, 172.5)	657.5	-1.631	0.103
Initial NIHSS score—no. (%)			19.326		<0.001
0–5	4(10.8)	24(53.3)			
6–14	18(48.6)	15(10.8)			
≥15	15(40.5)	6(13.3)			
Treatment options—no. (%)			14.375		0.002
Thrombolysis	17(45.9)	36(80)			
Embolectomy	8(21.6)	1(2.2)			
Bridging therapy	4(10.8)	1(2.2)			
conservative treatment	8(21.6)	7(15.6)			
90-day-mRS—no. (%)			15.62		0.016
0	5(13.5)	16(35.6)			
1	4(10.8)	6(13.3)			
2	1(2.7)	5(11.1)			
3	4(10.8)	5(11.1)			
4	12(32.4)	11(24.4)			
5	6(16.2)	1(2.2)			
6	5(13.5)	1(2.2)			
Median D2-dimer (IQR)—mg/L	1.06(0.60, 1.93)	0.39(0.25, 0.85)	443.5	-3.629	<0.001
Median INR(IQR)	1.10(1.05, 1.16)	1.04(1.02, 1.07)	432.5	-3.735	<0.001
Mean PLT(SD)—$\hat{}10^9$/L	190.89 ± 98.23	218.49 ± 45.91	1.573		0.122
Median Fib (IQR)—g/L	3.20(2.60, 4.15)	3.28(2.59, 3.96)	798	-0.322	0.748
Median APTT(IQR)—S	34.4(31.5, 37.9)	32.3(28.05, 36.3)	610.5	-2.069	0.039
Median Cr (IQR)—mmol/L	66.20(54.10, 85.95)	66.20(53.20, 77.40)	745	-0.815	0.415
Median TC(IQR)—mmol/L	3.84(3.20, 4.40)	4.31(3.58, 5.27)	611	-2.064	0.039
Median TG(IQR)—mmol/L	0.99(0.73, 1.31)	1.17(0.93, 1.60)	617.5	-2.004	0.045
Mean LDL-C(IQR)—mmol/L	2.37(1.73, 2.91)	2.61(1.93, 3.27)	699	-1.524	0.128
Median Hcy(IQR)—mmol/L	12.10(9.25, 17.00)	9.40(8.75, 12.50)	637	-1.823	0.068
Median Glucose (IQR)—mmol/L	6.38(5.50, 7.67)	7.00(5.50, 9.55)	697	-1.263	0.207
Median HbA1c(IQR)—%	5.60(5.30, 6.35)	6.30(5.75, 7.95)	521	-2.905	0.004
Median TnI(IQR)—μg/L	14.70(9.75, 30.37)	11.26(7.29, 18.67)	628.5	-1.901	0.057
Median Corin (IQR)—ng/ml	8.17(4.68, 30.62)	4.93(2.12, 9.01)	612	-2.055	0.040
Median BNP(IQR)—pg/ml	269.85(64.54, 633.90)	13.27(0, 72.12)	342.5	-4.624	<0.001
Median NEP(IQR)—pg/ml	130.5(8.63, 274.88)	131.1(3.57, 253.94)	789	-0.407	0.684

SBP, systolic pressure; DBP, diastolic pressure; NIHSS, National Institutes of Health Stroke Scale; BMI, body mass index; 90-day-mRs, 90-day -Modified Rank in Scale.

endothelial dysfunction in major arterial and venous diseases, leading to altered hemodynamics, which can be used as a biomarker in the early stages of vascular disease (Karthika et al., 2021). Based on these theories, we investigated whether DNAm enhances the understanding of vascular aging and related diseases. The current results showed that the characteristics of the AF-stroke group included older age, high severity, and poor prognosis, indicating that AF-related stroke may be associated with aging, while the no AF-stroke group was associated with factors associated with vascular aging, especially atherosclerosis risk factors (for example, hypertension, hypercholesterolemia, and smoking; Lakatta, 2008; Gomez-Marcos et al., 2016; **Table 1** and **Figure 2**). This phenomenon may be attributed to the fact that the no AF-stroke group selected in our study exhibited the LAA-type stroke. The study showed that risk factors associated with vascular aging are associated with no AF-stroke and, therefore, may play a role in the pathogenesis of stroke in the no AF-stroke group. Next, we selected the four methylation sites with maximal differences between the groups: CORIN:678, CORIN:682, CORIN:694, and CORIN:700 (**Figures 1A–C**). The hypomethylation levels at these CpG sites serve as peripheral blood biomarkers for predicting AF-related stroke.

The concentration levels of each component of the NP family are critical to ensure proper control of systemic and local cardiovascular function. In order to achieve the ultimate optimal levels of NPs, a fine balance is required between gene

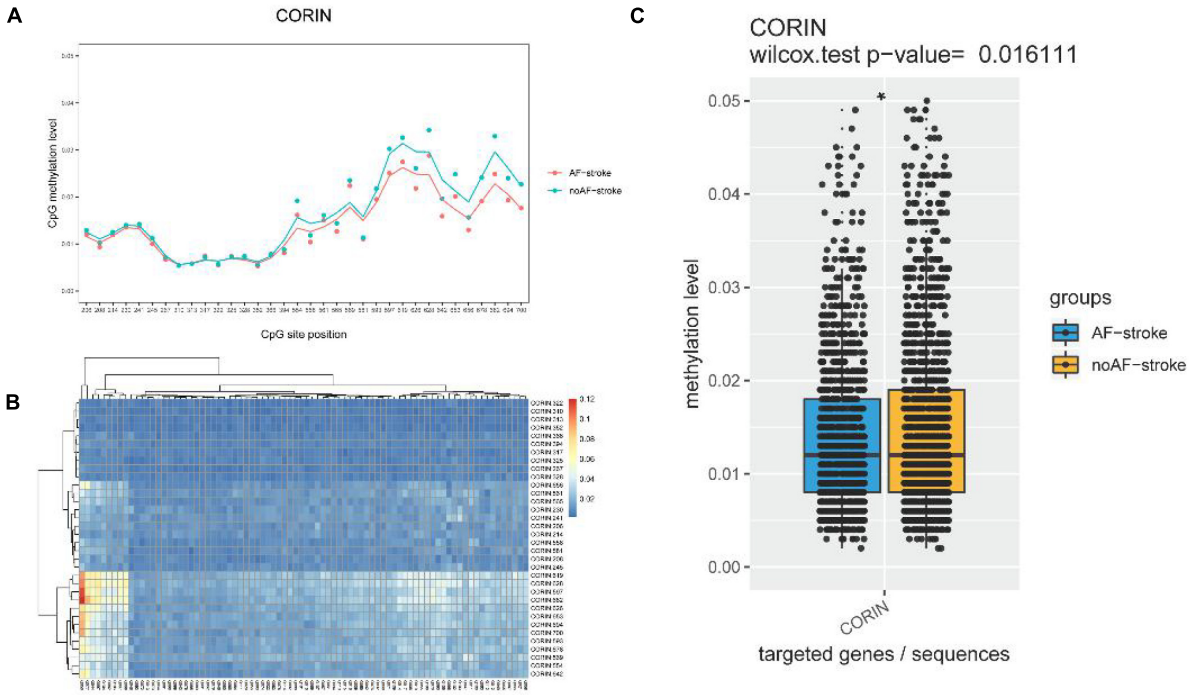

FIGURE 1 | (A) Schematic diagram of the methylation level distribution of each CpG site of group AF-stroke and group noAF-stroke in the target area. Based on the absolute coordinates of the detected gene region, the map shows the average methylation level of each site in each sample and is labeled with different colors according to biological groupings, using the formula model function in R language to simulate the combined trend line. The sites with the greatest methylation differences between the two groups are CORIN:678, CORIN:682, CORIN:694, and CORIN:700. **(B)** Methylation level clustering heat map of all samples in group AF-stroke and group noAF-stroke. Perform cluster analysis on the methylation levels of CpG sites in all samples, and display the categorical relationship of methylation levels between samples and sites in the form of heat maps. The color changes from blue to red, indicating that the methylation level is gradually increasing. **(C)** Comparison of CpG methylation levels in target areas between group AF-stroke and group noAF-stroke. Count the average methylation level of each CpG site in each sample, use box plot + bee colony plot to show the methylation distribution of each region between group AF-stroke and group noAF-stroke, and analyze the difference between these two groups by the Wilcox test. And there was a significant difference between these two groups, $*p < 0.05$.

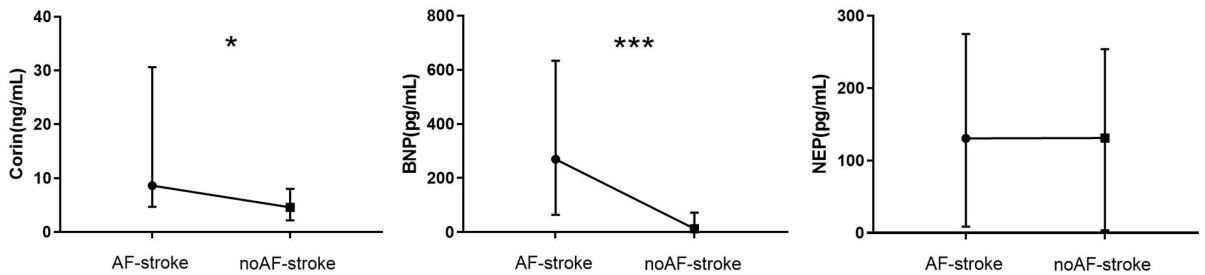

FIGURE 2 | Plasma levels of Corin–BNP–NEP in groups AF-stroke and noAF-stroke. Plasma levels of Corin in AF-stroke group [8.17 (4.68, 30.62) ng/ml] were significantly higher than in noAF-stroke group [4.93 (2.12, 9.01) ng/ml], $*p < 0.05$. Plasma levels of BNP in AF-stroke group [269.85 (64.54, 633.90) pg/ml] were significantly higher than in noAF-stroke group [13.27 (0, 72.12) pg/ml], $***p < 0.001$. There was no significant difference in the levels of NEP between groups AF-stroke.

expression, protein secretion, and clearance, with a key role of gene expression regulation and translation (Rubattu et al., 2020). The heterogeneous group of molecular biomarkers of AF encompasses the products of the neurohormonal cascade, including Corin–BNP–NEP. These biomarkers could be used for AF diagnosis and prediction of the transition from paroxysmal to persistent AF (Tsioufis et al., 2019). Hijazi et al. (2016) developed a novel biomarker-based risk score for predicting stroke in AF, termed the age, biomarkers, and clinical history (ABC) stroke risk score based on the independent association between NT-proBNP and the occurrence of AF-associated stroke. This finding suggested a strong association between the NP system and stroke associated with AF. Our prospective study showed that the plasma levels of Corin and BNP in the AF-stroke group were significantly higher than those in the no AF-stroke group (**Table 1** and **Figure 2**). A previous meta-analysis suggested that

elevated blood levels of natriuretic peptides (BNP/NT-proBNP) are repeatedly associated with cardioembolic stroke (Llombart et al., 2015). Fukuhara et al. (2020). demonstrated that BNP is inversely correlated with a favorable outcome of stroke if the estimation is within 24 h of stroke onset. These findings were also verified in the current study.

Corin is one of the major enzymes in the splicing of proBNP into BNP. Peng et al. (2015) found that the serum-soluble Corin level was lower in patients with stroke than in healthy controls, which further deemed a pathogenic role of serum-soluble Corin in stroke. Strikingly, the study did not measure NP levels, which could affect the activity of Corin. The follow-up study showed that serum-soluble Corin deficiency predicted major disability or death within 3 months after stroke onset, suggesting a probable role of serum-soluble Corin deficiency in stroke prognosis (Hu et al., 2016). A study by Chen demonstrated that plasma concentrations of Corin and NT-proBNP were significantly higher in patients with AF than in healthy controls (Chen et al., 2015), which could explain why the plasma concentrations of Corin and BNP were higher in the AF-stroke group than in the no AF-stroke group in our study.

Neprilysin is a ubiquitous membrane protease that is inactivated via the degradation of 40 peptides, including BNP (Bayes-Genis et al., 2016; Campbell, 2017). The current results did not show any significant difference in serum NEP levels between the AF-stroke and no AF-stroke groups (**Table 1** and **Figure 2**), which has not been explained previously. It has been hypothesized that only the active form of NEP affects the BNP levels (Feygina et al., 2019). In a clinical trial, sacubitril/valsartan was used to intervene in the NEP activity of patients with heart failure. Consequently, increased concentrations of NEP substrates, such as atrial natriuretic peptide (ANP), substance P, and glucagon-like peptide 1 were observed, but no changes were detected in plasma BNP. On the other hand, the concentration of NT-proBNP decreased slightly (Nougué et al., 2019). This correlation between NEP and BNP might explain the above findings.

Nevertheless, the present study has some limitations. This was a single-center retrospective study, which might have selection bias. Due to the small sample size, the subsequent analysis may be limited. Since the current study population was of Asian descent, the results may not be applicable to other ethnic groups. Herein, we could not distinguish between paroxysmal, persistent, long-standing persistent, and permanent AF as Holter monitoring was not performed in this study. Also, the secondary outcomes, including mortality and hemorrhage, needed in future large-scale studies were not evaluated.

CONCLUSION

In summary, the plasma-soluble Corin and BNP level was significantly higher in patients with the AF-stroke group than in the no AF-stroke group, while NEP was negative. The current findings raised the possibility that the Corin–BNP–NEP protein pathway is involved in the pathogenesis of AF-stroke. In addition, we also found that deficient CpG methylation in the promoter region of the Corin protein gene is associated with AF-related ischemic stroke.

DATA AVAILABILITY STATEMENT

The original contributions presented in the study are included in the article/supplementary material, further inquiries can be directed to the corresponding author/s.

ETHICS STATEMENT

The studies involving human participants were reviewed and approved by the Ethics Committee of the First Hospital Affiliated to Soochow University. The patients/participants provided their written informed consent to participate in this study.

AUTHOR CONTRIBUTIONS

QF and XS conceived and designed the research. XS, ND, and YX analyzed the data and drafted the manuscript. LH, RY, JL, XZ, TX, YW, CC, ML, YJ, and LY collected the data and performed the research. All authors reviewed, edited the manuscript, and approved the final version of the manuscript.

FUNDING

This study was supported by the National Natural Science Foundation of China (82071300), the Suzhou Gusu Health Talent Program Training Project (GSWS2020002), the Suzhou Introduction of Clinical Medicine Team Project (SZYJTD201802), the Science and Technology Project of Lianyungang Health Commission (202024), the Jiangsu Province "Six One Project" Top Talent to be funded project (LGY2019062), the Scientific Research Project of Bengbu Medical College (2020byzd341), the Jiangsu Provincial Geriatric Health Research Grant Project (LD2021034 and LR2021049), and the Jiangsu Province Postgraduate Practice Innovation Program (SJCX21_1726).

REFERENCES

Acton, R., Yuan, W., Gao, F., Xia, Y., Bourne, E., Wozniak, E., et al. (2021). The genomic loci of specific human tRNA genes exhibit ageing-related DNA hypermethylation. *Nat. Commun.* 12:2655. doi: 10.1038/s41467-021-22639-6

Bayes-Genis, A., Barallat, J., and Richards, A. M. (2016). A test in context: neprilysin: function, inhibition, and biomarker. *J. Am. Coll. Cardiol.* 68, 639–653. doi: 10.1016/j.jacc.2016.04.060

Belsky, D., Caspi, A., Arseneault, L., Baccarelli, A., Corcoran, D., Gao, X., et al. (2020). Quantification of the pace of biological aging in humans through a

blood test, the DunedinPoAm DNA methylation algorithm. *Elife* 9:e54870. doi: 10.7554/eLife.54870

Belsky, D., Caspi, A., Corcoran, D., Sugden, K., Poulton, R., Arseneault, L., et al. (2022). DunedinPACE, a DNA methylation biomarker of the pace of aging. *Elife* 11:e73420. doi: 10.7554/eLife.73420

Berntsson, J., Zia, E., Borné, Y., Melander, O., Hedblad, B., and Engström, G. (2014). Plasma natriuretic peptides and incidence of subtypes of ischemic stroke. *Cerebrovasc. Dis.* 37, 444–450.

Campbell, D. J. (2017). Long-term neprilysin inhibition - implications for ARNIs. *Nat. Rev. Cardiol.* 14, 171–186. doi: 10.1038/nrcardio.2016.200

Chen, F., Xia, Y., Liu, Y., Zhang, Y., Song, W., Zhong, Y., et al. (2015). Increased plasma corin levels in patients with atrial fibrillation. *Clin. Chim. Acta* 447, 79–85. doi: 10.1016/j.cca.2015.05.017

Chen, Y. S., Ouyang, X. P., Yu, X. H., Novák, P., Zhou, L., He, P. P., et al. (2021). N6-adenosine methylation (m^6A) RNA modification: an emerging role in cardiovascular diseases. *J. Cardiovasc. Transl. Res.* 14, 857–872. doi: 10.1007/s12265-021-10108-w

Chen, Y., and Burnett, J. C. (2017). Biochemistry, therapeutics, and biomarker implications of neprilysin in cardiorenal disease. *Clin. Chem.* 63, 108–115. doi: 10.1373/clinchem.2016.262907

Day, K., Waite, L., Thalacker-Mercer, A., West, A., Bamman, M., Brooks, J., et al. (2013). Differential DNA methylation with age displays both common and dynamic features across human tissues that are influenced by CpG landscape. *Genome Biol.* 14:R102. doi: 10.1186/gb-2013-14-9-r102

Deng, G., Xu, N., Huang, Q., Tan, J., Zhang, Z., Li, X., et al. (2019). Association between promoter DNA methylation and gene expression in the pathogenesis of ischemic stroke. *Aging (Albany NY)* 11, 7663–7677. doi: 10.18632/aging.102278

Everett, B., Zeller, T., Glynn, R., Ridker, P., and Blankenberg, S. (2015). High-sensitivity cardiac troponin I and B-type natriuretic peptide as predictors of vascular events in primary prevention: impact of statin therapy. *Circulation* 131, 1851–1860. doi: 10.1161/CIRCULATIONAHA.114.014522

Feygina, E. E., Artemieva, M. M., Postnikov, A. B., Tamm, N. N., Bloshchitsyna, M. N., Medvedeva, N. A., et al. (2019). Detection of neprilysin-derived BNP fragments in the circulation: possible insights for targeted neprilysin inhibition therapy for heart failure. *Clin. Chem.* 65, 1239–1247. doi: 10.1373/clinchem.2019.303438

Field, A. E., Robertson, N. A., Wang, T., Havas, A., Ideker, T., and Adams, P. D. (2018). DNA methylation clocks in aging: categories, causes, and consequences. *Mol. Cell* 71, 882–895. doi: 10.1016/j.molcel.2018.08.008

Fukuhara, K., Ogata, T., Takeshita, S., and Tsuboi, Y. (2020). Serum B-type natriuretic peptide level and timing of its measurement as a predictor of acute ischemic stroke outcome. *eNeurologicalSci* 18:100217. doi: 10.1016/j.ensci.2019.100217

GBD 2016 Causes of Death Collaborators (2017). Global, regional, and national age-sex specific mortality for 264 causes of death, 1980-2016: a systematic analysis for the global burden of disease study 2016. *Lancet* 390, 1151–1210. doi: 10.1016/S0140-6736(17)32152-9

Goetze, J., Bruneau, B., Ramos, H., Ogawa, T., de Bold, M., and de Bold, A. (2020). Cardiac natriuretic peptides. *Nat. Rev. Cardiol.* 17, 698–717.

Gomez-Marcos, M. A., Martinez-Salgado, C., Gonzalez-Sarmiento, R., Hernandez-Rivas, J. M., Sanchez-Fernandez, P. L., Recio-Rodriguez, J. I., et al. (2016). Association between different risk factors and vascular accelerated ageing (EVA study): study protocol for a cross-sectional, descriptive observational study. *BMJ Open* 6:e011031. doi: 10.1136/bmjopen-2016-011031

Hijazi, Z., Lindbäck, J., Alexander, J. H., Hanna, M., Held, C., Hylek, E. M., et al. (2016). The ABC (age, biomarkers, clinical history) stroke risk score: a biomarker-based risk score for predicting stroke in atrial fibrillation. *Eur. Heart J.* 37, 1582–1590. doi: 10.1093/eurheartj/ehw054

Horvath, S. (2013). DNA methylation age of human tissues and cell types. *Genome Biol.* 14:R115.

Hu, W. D., Chen, S., Song, Y. L., Zhu, F. F., Shi, J. J., Han, X. J., et al. (2016). Serum soluble corin deficiency predicts major disability within 3 months after acute stroke. *PLoS One* 11:e0163731. doi: 10.1371/journal.pone.0163731

Karthika, C. L., Ahalya, S., Radhakrishnan, N., Kartha, C. C., and Sumi, S. (2021). Hemodynamics mediated epigenetic regulators in the pathogenesis of vascular diseases. *Mol. Cell. Biochem.* 476, 125–143. doi: 10.1007/s11010-020-03890-9

Lakatta, E. G. (2008). Arterial aging is risky. *J. Appl. Physiol.* 105, 1321–1322. doi: 10.1152/japplphysiol.91145.2008

Li, X., Li, W., and Xu, Y. (2018). Human age prediction based on DNA methylation using a gradient boosting regressor. *Genes* 9:424. doi: 10.3390/genes9090424

Liao, J., Chao, T., and Chen, S. (2019). How do aging and comorbidities impact risk of ischemic stroke in patients with atrial fibrillation. *Trends Cardiovasc. Med.* 29, 386–391. doi: 10.1016/j.tcm.2018.11.003

Liu, L. P., Chen, W. Q., Zhou, H. Y., Duan, W. Y., Li, S. J., Huo, X. C., et al. (2020). Chinese stroke association guidelines for clinical management of cerebrovascular disorders: executive summary and 2019 update of clinical management of ischaemic cerebrovascular diseases. *Stroke Vasc. Neurol.* 5, 159–176. doi: 10.1136/svn-2020-000378

Llombart, V., Antolin-Fontes, A., Bustamante, A., Giralt, D., Rost, N. S., Furie, K., et al. (2015). B-type natriuretic peptides help in cardioembolic stroke diagnosis: pooled data meta-analysis. *Stroke* 46, 1187–1195. doi: 10.1161/STROKEAHA.114.008311

Maida, C., Norrito, R., Daidone, M., Tuttolomondo, A., and Pinto, A. (2020). Neuroinflammatory mechanisms in ischemic stroke: focus on cardioembolic stroke, background, and therapeutic approaches. *Int. J. Mol. Sci.* 21:6454. doi: 10.3390/ijms21186454

Martínez-Iglesias, O., Carrera, I., Carril, J., Fernández-Novoa, L., Cacabelos, N., and Cacabelos, R. (2020). DNA Methylation in neurodegenerative and cerebrovascular disorders. *Int. J. Mol. Sci.* 21:2220. doi: 10.3390/ijms21062220

Miao, L., Yin, R., Zhang, Q., Hu, X., Huang, F., Chen, W., et al. (2019). Integrated DNA methylation and gene expression analysis in the pathogenesis of coronary artery disease. *Aging (Albany NY)* 11, 1486–1500. doi: 10.18632/aging.101847

Nougué, H., Pezel, T., Picard, F., Sadoune, M., Arrigo, M., Beauvais, F., et al. (2019). Effects of sacubitril/valsartan on neprilysin targets and the metabolism of natriuretic peptides in chronic heart failure: a mechanistic clinical study. *Eur. J. Heart Fail.* 21, 598–605. doi: 10.1002/ejhf.1342

Pan, X., Gong, D., Nguyen, D. N., Zhang, X., Hu, Q., Lu, H., et al. (2018). Early microbial colonization affects DNA methylation of genes related to intestinal immunity and metabolism in preterm pigs. *DNA Res.* 25, 287–296. doi: 10.1093/dnares/dsy001

Peng, H., Zhu, F. F., Shi, J. J., Han, X. J., Zhou, D., Liu, Y., et al. (2015). Serum soluble corin is decreased in stroke. *Stroke* 46, 1758–1763. doi: 10.1161/STROKEAHA.114.008368

Rubattu, S., Stanzione, R., Cotugno, M., Bianchi, F., Marchitti, S., and Forte, M. (2020). Epigenetic control of natriuretic peptides: implications for health and disease. *Cell. Mol. Life Sci.* 77, 5121–5130. doi: 10.1007/s00018-020-03573-0

Sharma, A., Shashikiran, U., Uk, A., Shetty, R., Satyamoorthy, K., and Rai, P. (2020). Aberrant DNA methylation and miRNAs in coronary artery diseases and stroke: a systematic review. *Brief. Funct. Genomics* 19, 259–285. doi: 10.1093/bfgp/elz043

Tharakan, R., Ubaida-Mohien, C., Moore, A., Hernandez, D., Tanaka, T., and Ferrucci, L. (2020). Blood DNA methylation and aging: a cross-sectional analysis and longitudinal validation in the InCHIANTI study. *J. Gerontol. A Biol. Sci. Med. Sci.* 75, 2051–2055. doi: 10.1093/gerona/glaa052

Thorin-Trescases, N., de Montgolfier, O., Pinçon, A., Raignault, A., Caland, L., Labbé, P., et al. (2018). Impact of pulse pressure on cerebrovascular events leading to age-related cognitive decline. *Am. J. Physiol. Heart Circ. Physiol.* 314, H1214–H1224. doi: 10.1152/ajpheart.00637.2017

Tsioufis, C., Konstantinidis, D., Nikolakopoulos, I., Vemmou, E., Kalos, T., Georgiopoulos, G., et al. (2019). Biomarkers of atrial fibrillation in hypertension. *Curr. Med. Chem.* 26, 888–897.

Wang, C., Ni, W., Yao, Y., Just, A., Heiss, J., Wei, Y., et al. (2021). DNA methylation-based biomarkers of age acceleration and all-cause death, myocardial infarction, stroke, and cancer in two cohorts: the NAS, and KORA F4. *EBioMedicine* 63:103151. doi: 10.1016/j.ebiom.2020.103151

Wang, W., Jiang, B., Sun, H., Ru, X., Sun, D., Wang, L., et al. (2017). Prevalence, incidence, and mortality of stroke in china: results from a nationwide population-based survey of 480 687 adults. *Circulation* 135, 759–771. doi: 10.1161/CIRCULATIONAHA.116.025250

Xu, H., Li, S., and Liu, Y. S. (2021). Roles and mechanisms of DNA methylation in vascular aging and related diseases. *Front. Cell Dev. Biol.* 9:699374. doi: 10.3389/fcell.2021.699374

Yandle, T. G., and Richards, A. M. (2015). B-type natriuretic peptide circulating forms: analytical and bioactivity issues. *Clin. Chim. Acta* 448, 195–205. doi: 10.1016/j.cca.2015.07.004

Yang, Y., Wang, A., Yuan, X., Zhao, Q., Liu, X., Chen, S., et al. (2019). Association between healthy vascular aging and the risk of the first stroke in a community-based Chinese cohort. *Aging (Albany NY)* 11, 5807–5816. doi: 10.18632/aging.102170

Yoshida, Y., Nakanishi, K., Daimon, M., Ishiwata, J., Sawada, N., Hirokawa, M., et al. (2019). Alteration of cardiac performance and serum B-type natriuretic peptide level in healthy aging. *J. Am. Coll. Cardiol.* 74, 1789–1800. doi: 10.1016/j.jacc.2019.07.080

Zhou, M., Wang, H., Zhu, J., Chen, W., Wang, L., Liu, S., et al. (2016). Cause-specific mortality for 240 causes in China during 1990-2013: a systematic subnational analysis for the global burden of disease study 2013. *Lancet* 387, 251–272. doi: 10.1016/S0140-6736(15)00551-6

Conflict of Interest: The authors declare that the research was conducted in the absence of any commercial or financial relationships that could be construed as a potential conflict of interest.

Publisher's Note: All claims expressed in this article are solely those of the authors and do not necessarily represent those of their affiliated organizations, or those of the publisher, the editors and the reviewers. Any product that may be evaluated in this article, or claim that may be made by its manufacturer, is not guaranteed or endorsed by the publisher.

frontiers | Frontiers in Aging Neuroscience

ORIGINAL RESEARCH
published: 13 June 2022
doi: 10.3389/fnagi.2022.905224

Multiple Pipeline Embolization Devices for the Treatment of Complex Intracranial Aneurysm: A Multi-Center Study

*Feng Fan[1], Yu Fu[1], Jianmin Liu[2], Xinjian Yang[3], Hongqi Zhang[4], Tianxiao Li[5], Huaizhang Shi[6], Jieqing Wan[7], Yuanli Zhao[8], Yunyan Wang[9], Wenfeng Feng[10], Donglei Song[11], Yang Wang[12], Guohua Mao[13], Aisha Maimaitili[14] and Sheng Guan[1]**

[1] Department of Neurointervention Radiology, The First Affiliated Hospital of Zhengzhou University, Zhengzhou, China, [2] Changhai Hospital Affiliated to Naval Medical University, Shanghai, China, [3] Department of Interventional Neuroradiology, Beijing Neurosurgical Institute, Beijing Tiantan Hospital, Capital Medical University, Beijing, China, [4] Department of Neurosurgery, Xuanwu Hospital, Capital Medical University, Beijing, China, [5] Zhengzhou University People's Hospital, Zhengzhou, China, [6] First Affiliated Hospital of Harbin Medical University, Harbin, China, [7] Renji Hospital, School of Medical, Shanghai Jiao Tong University, Shanghai, China, [8] Peking University International Hospital, Beijing, China, [9] Qilu Hospital of Shandong University, Jinan, China, [10] Nanfang Hospital, Southern Medical University, Guangzhou, China, [11] Shanghai Donglei Brain Hospital, Shanghai, China, [12] First Affiliated Hospital of Nanchang University, Nanchang, China, [13] Second Affiliated Hospital of Nanchang University, Nanchang, China, [14] First Affiliated Hospital of Xinjiang Medical University, Ürümqi, China

OPEN ACCESS

Edited by:
Anwen Shao,
Zhejiang University, China

Reviewed by:
Chaohua Wang,
Sichuan University, China
Xifeng Li,
Southern Medical University, China

***Correspondence:**
Sheng Guan
gsradio@126.com

Specialty section:
This article was submitted to Neurocognitive Aging and Behavior, a section of the journal Frontiers in Aging Neuroscience

Received: *26 March 2022*
Accepted: *06 May 2022*
Published: *13 June 2022*

Citation:
Fan F, Fu Y, Liu J, Yang X, Zhang H, Li T, Shi H, Wan J, Zhao Y, Wang Y, Feng W, Song D, Wang Y, Mao G, Maimaitili A and Guan S (2022) Multiple Pipeline Embolization Devices for the Treatment of Complex Intracranial Aneurysm: A Multi-Center Study. Front. Aging Neurosci. 14:905224. doi: 10.3389/fnagi.2022.905224

Background: The Pipeline for Uncoilable or Failed Aneurysms (PUFS) trial primarily demonstrated the safety and efficacy of the implantation of multiple pipeline embolization devices (multi-PEDs) for large/giant intracranial aneurysms. However, no study has focused on when, why, or how to apply multi-PEDs.

Objective: The purpose of this study was to investigate the indications and strategies of using multi-PEDs for complex intracranial aneurysms.

Methods: Patients who had been treated with two or more PEDs were included in the post-market multicenter registry study from 2014 to 2019, across 14 centers in China. Indications, strategies, perioperative safety, and clinical outcomes were retrospectively analyzed. The modified Rankin scale (mRS) score was used to evaluate clinical outcomes comprehensively, and the O'Kelly–Marotta (OKM) grading scale was used to evaluate aneurysm healing results.

Results: A total of 55 intracranial aneurysms were treated with multi-PEDs. There were 20 fusiform aneurysms with a large range, 25 large/giant saccular aneurysms, six aneurysms with failed treatment, and four aneurysms with greatly varied diameters of the parent artery. The strategies included telescope techniques in 40 patients and overlap techniques in 15 patients. In total, 120 stents were deployed in 55 patients. The operation styles included 25 patients (55.6%) with two PEDs, 21 patients (38.2%) with two PEDs combined with coiling, four patients (7.3%) with three PEDs, four patients (7.3%) with three PEDs combined with coiling, and one patient (1.8%) with four PEDs. Angiography revealed OKM D in two, OKM C in seven, and OKM A and B in 46 cases after surgery. During the perioperative period, eight patients developed neurological

dysfunction, three of whom died. A total of thirty-four patients were followed up with digital subtraction angiography for 2–45 (8.2 ± 8.0) months. Angiography revealed OKM D in 26, OKM C in five, and OKM B in three. At the last follow-up, the mRS score was 0–1 in 52 patients.

Conclusion: The treatment of anterior circulation aneurysms with multi-PEDs is safe and effective. The implantation of multi-PEDs could be considered for large-scale fusiform aneurysms, large/giant saccular aneurysms with a jet-sign, salvage of failed PED treatments, and in cases where the diameter of the parent artery varies greatly.

Keywords: anterior circulation, giant intracranial aneurysm, pipeline embolization device, posterior circulation, salvage therapy

INTRODUCTION

The pipeline embolization device (PED) was approved by the Food and Drug Administration (FDA) in 2011 for the treatment of large and giant wide-neck intracranial aneurysms in the internal carotid artery. The PED for the intracranial treatment of aneurysms trial demonstrated significant advancements in aneurysm treatments (Nelson et al., 2011). Recently, an increasing number of cerebrovascular centers have considered PED as the preferred choice for unruptured complex aneurysms (Crobeddu et al., 2013). However, whether two or more PEDs are better for particular aneurysms remains controversial (Mona et al., 2013). This problem has potential effects on treatment strategies, safety, efficacy, and cost (El-Chalouhi et al., 2014). Thus, we here performed a retrospective analysis to explore the indications and strategies for the application of multiple pipeline embolization devices (multi-PEDs) for intracranial aneurysms.

MATERIALS AND METHODS

Study Design and Patient Population

This was a multicenter, retrospective study performed in China. All patients in this study were selected from the PLUS registry study (ClinicalTrials.gov identifier: NCT03831672), which included those treated with PEDs for ruptured and unruptured intracranial aneurysms from November 2014 to October 2019. We enrolled 1,171 patients with 1,322 aneurysms from 14 medical centers. Our subgroup study aimed to investigate the indications and strategies for using multi-PEDs for complex intracranial aneurysms.

The inclusion criteria were as follows: (1) intracranial aneurysms treated with two or more PEDs or (2) salvage for failed PED treatment. Exclusion criteria comprised of (1) two or more PEDs used to treat aneurysms in different arteries and (2) subarachnoid hemorrhage (SAH).

Antiplatelet Procedure

Patients were treated with aspirin (100 mg daily) and clopidogrel (75 mg daily) for 5–7 days before the operation. The aspirin and clopidogrel doses were adjusted preoperatively after platelet function testing. Platelet function tests were performed on all patients using thromboelastography. The platelet inhibition rates induced by arachidonic acid (AA) and adenosine diphosphate (ADP) were measured. Aspirin was considered effective if the inhibition rate of AA was $\geq$ 50%, and aspirin insensitivity was defined if it is $<$ 50%. Patients insensitive to aspirin insisted or increased the dose appropriately. Clopidogrel was considered effective if the inhibition rate of ADP was $\geq$ 30%, and clopidogrel resistance was defined if it was $<$ 30%. Patients insensitive to clopidogrel were administered ticagrelor (90 mg, two times daily). Dual antiplatelet therapy was continued for 3–6 months postoperatively. Individualized implementation was adjusted according to both the clinical syndromes and follow-up images.

Procedural Technique

All patients were treated under general anesthesia *via* a transfemoral arterial approach. After standard angiographic projection, intra-arterial 3D rotational angiography was performed in all patients to determine the size and optimal working position, through 3D reconstruction and PED simulation procedures. A 7-F sheath (Shuttle Sheath, Cook Medical, Bloomington, IN, United States) was used to guide the multifunctional 5-F catheter (Medtronic, Minneapolis, MN, United States) and 0.035-inch super-slippery microguidewire (CHIKAI, Asahi Intecc, Nagoya, Japan) to the initial segment of the internal carotid artery or the first segment of the vertebral artery. Under the working position, a 5-F distal support catheter (Navien, 115 or 125 cm, Covidien, Medtronic) was inserted near the aneurysm neck. Assisted by the microcatheter, the microguidewire, and the 5-F distal support catheter, the stent catheter (Marksman, Covidien) was passed through the aneurysm neck and was placed at the distal segment of the parent artery. If the coil was indispensable, the embolization microcatheter was positioned through the 7-F guiding sheath, in parallel to the 5-F distal support catheter, and the head part of the microcatheter was introduced into the sac with the assistance of a 0.014-inch microguidewire. Subsequently, a multi-PED system was implanted. These strategies included telescope and overlap techniques.

Angiography in the working position was performed to clarify the retention of contrast and patency of the parent artery and distal branches. Flat-panel intra-arterial rotational angiography (VasoCT, Philips Healthcare, Best, Netherlands) or dynamic computed tomography angiography (DynaCT, Siemens

Healthcare, Forchheim, Germany) was performed to assess device deployment. If necessary, post-operative adjustment could be applied to correct poor opening or wall attachment. X per-CT scan was performed to evaluate cerebral hemorrhage or SAH.

Study Endpoints

Procedural success was defined as follows: (1) PED deployment with complete coverage of the aneurysm neck and good wall attachment, and (2) patency of the parent artery and distal branches. Angiographic and clinical follow-ups were performed at 3, 6, and 12 months and annually thereafter. The primary angiographic endpoint was complete aneurysm occlusion with no stenosis of the parent artery. The O'Kelly–Marotta (OKM) grading scale was used to evaluate aneurysm embolization (O'kelly et al., 2010). The stenosis of the parent artery was defined as a stenosis rate of > 50% on imaging (Kwolek et al., 2015). Clinical outcomes were assessed using the modified Rankin scale (mRS) (Wang et al., 2020). Major adverse cerebrovascular complications included transient ischemic attack, embolization in the new territory, and SAH.

RESULTS

Baseline Patient and Aneurysm Characteristics

Among the 55 patients, 31 were men and 24 were women. Their ages ranged from 8 to 76 (46.7 ± 15.9) years. Among them, 49 patients presented with headache, visual disturbance, ischemia-related symptoms, or other symptoms, and six cases presented with accidental findings. All patients underwent digital subtraction angiography (DSA) before endovascular treatment. A total of thirty-nine aneurysms were located in the internal carotid arteries, 13 in the vertebrobasilar arteries, two in the middle cerebral arteries, and one in the posterior cerebral artery. The maximum diameter was 4.1–51.1 (24.2 ± 14.1) mm, and the morphological aneurysm classifications included 30 sacs, 21 fusiform, and four irregular sacs (**Table 1**).

TABLE 1 | Baseline patient and aneurysm characteristics.

	Study population
Age, year	46.7 ± 15.9
Male sex	31 (56.4%)
Morphology	
Saccular	30 (54.5%)
Fusiform*	21 (38.2%)
Irregularity	4 (7.3%)
Location	
ICA	39 (70.9%)
MCA	2 (3.6%)
VA	8 (14.5%)
VB	3 (5.5%)
BA	2 (3.6%)
PCA	1 (1.8%)
Size (Maximum diameter)	
< 10 mm	6 (10.9%)
10 mm–25 mm	28 (50.9%)
> 25 mm	21 (38.2%)

Data are showm as n (%) or the mean ± SD. Fusiform includes fusiform aneurysms, snakelike aneurysms and dissection aneurysms involving a large range. ICA, Internal carotid artery; MCA, Middle cerebral artery; VA, Intracranial segment of vertebral artery; VB, Both vertebral and basilar arteries were involved; BA, Basilar artery; PCA, Posterior cerebral artery.

Operative Results

Multiple pipeline embolization devices were successfully implanted in 55 patients. These cases included 20 fusiform aneurysms with a large range, 25 large/giant saccular aneurysms, six aneurysms with failed treatment, and four aneurysms in which the diameters of the parent artery varied greatly. The strategies included telescope techniques in 40 patients and overlap techniques in 15 patients. In total, 120 PEDs were deployed in 55 patients. The operation styles included 25 patients (55.6%) with two PEDs, 21 patients (38.2%) with two PEDs combined with coiling, four patients (7.3%) with three PEDs, four patients (7.3%) with three PEDs combined with coiling, and one patient (1.8%) with four PEDs. The PEDs were successfully opened in 53 patients and required adjustment in two patients. Angiography revealed OKM A and B in 46 patients, OKM C in seven patients, and OKM D in two patients (**Table 2**).

During the perioperative period, eight patients developed neurological dysfunction (**Table 3**). A total of three patients died, one patient developed SAH and received conservative treatment (mRS 2), one patient developed post-operative hypoperfusion (mRS 4), one patient developed thrombogenesis during the operation (mRS 0), and two patients developed transient ischemic attacks (mRS 0-1). Among the three died patients, two were with brainstem compression and ischemic stroke of posterior circulation and one suffered with SAH of anterior circulation in the early post-operative period.

Radiographic and Clinical Results

A total of thirty-four patients were followed up with DSA for 2–45 (8.2 ± 8.0) months. Angiography revealed complete occlusion in 26 patients (OKM D), near occlusion in five patients (OKM C), and the lack of occlusion in three patients (OKM B). During follow-up, one patient had internal carotid artery occlusion on the operation side (mRS 0), one patient had asymptomatic occlusion of the ophthalmic artery on the operation side (mRS 0), and one patient had transitory blindness (mRS 0). The remaining patients had no stenosis of the parent arteries and no new neurological complications. At the last follow-up, the mRS score was 0–1 in 52 patients (**Table 4**).

DISCUSSION

There is an increasing number of reports on the treatment of intracranial aneurysms with PED. However, few studies have focused on the application of multi-PEDs. This study included 55 complex aneurysms, which accounted for approximately 4.2% of all aneurysms (55/1322) at our institutions. A retrospective analysis was conducted to explore the safety, efficacy, indications,

TABLE 2 | Treatment details and results.

	Frequency
PED type	
PED Classic	31 (56.4%)
PED Flex	24 (43.6%)
Reasons of Multi-PEDs	
Fusiform with a large range	20 (36.4%)
Large/giant saccular aneurysms	25 (45.6%)
Salvage for failed treatment	6 (10.9%)
Diameters vary greatly	4 (7.3%)
Operation Styles	
PED + PED	25 (55.6%)
PED + PED + Coil	21 (38.2%)
PED + PED + PED	4 (7.3%)
PED + PED + PED + Coil	4 (7.3%)
PED + PED + PED + PED	1 (1.8%)
Device deployment	
Successful	53 (96.4%)
Successful after adjustment	2 (3.6%)
Unsuccessful	0
Radiographic Result (perioperative period)	
OKM A and B	46 (83.6%)
OKM C	7 (12.7%)
OKM D	2 (3.6%)
Clinical Results (perioperative period)	
mRS $\leq$ 2	51 (92.7%)
mRS > 2	4 (7.3%)
Perioperative complications	8 (14.5%)
TIA	3 (5.5%)
ENT	3 (5.5%)
SAH	2 (3.6%)

Data are presented as n (%) or n (%). TIA, transient ischemic attack; ENT, embolization in the new territory; SAH, subarachnoid hemorrhage; OKM, O'Kelly–Marotta grading scale.

and strategies of multi-PED implantation. These aneurysms had the following characteristics: (1) fusiform aneurysms with a large range; (2) large/giant aneurysms with jet-sign after a PED implantation; (3) aneurysms with failed PED treatment, requiring salvage; and (4) aneurysms where the diameter of the parent artery varied greatly between the inflow and outflow vessels (> 2 mm). Our study demonstrated that multi-PED implantation is safe and effective for the treatment of complex intracranial aneurysms, yielding high occlusion and low complication rates.

Indications for Multiple Pipeline Embolization Devices

For fusiform aneurysms with a large range, it is difficult for a PED to cover the entire lesion, or even if it can cover the neck of the aneurysm, anchoring of the PED in the parent artery is unstable, and stent displacement may occur during or after the procedure. Griffin retrospectively reviewed consecutive patients treated with PEDs for fusiform aneurysms. On DSA follow-up, only 15 aneurysms (60%) were completely occluded, which was a relatively lower rate than that for saccular aneurysms (Griffin et al., 2021). Conversely, our study showed satisfactory outcomes, with 85.7% (12/14) of fusiform aneurysms shown to be occluded using multi-PEDs. Furthermore, this can be achieved within 3 months if the coil fills the neck and if multi-PEDs are telescoped for reconstruction (**Figure 1**). Unfortunately, such aneurysms are more common in the posterior circulation. A total of two of the 14 patients in our study experienced severe ischemic complications, leading to post-operative death. This was in line with Griessenauer who reported that the complication rate of PED use in the basilar artery was significantly higher than that for PED use in the anterior circulation, particularly in the incidence of multiple stent ischemia complications, which is in the range of 50–70% (Griessenauer et al., 2018). Given the above, the application of multi-PEDs is not suitable for large-scale basilar artery or aneurysm-like lesions. For such lesions, if PED implantation is the only choice, it is better to cover the entire lesion with one PED or a long low profile self-expandable (LEO) stent, followed by one PED to cover the lesion within the LEO stent; otherwise, the strategy should be changed.

The PUFS trial first demonstrated the safety and effectiveness of multi-PEDs in the treatment of large or giant intracranial aneurysms. The mean size in this study was 18.2 mm and the majority of patients (98.1%) were treated with more than one PED (average of 3.15 PEDs). At 1 year, angiography showed complete occlusion in 76 of the 96 patients (86.8%)

TABLE 3 | Perioperative complications.

Case	Location	Operation styles	Complications	Treatment	mRS	
					Pre-operation	3∼10 days after operation
Case 1	ICA	PED + PED + Coil	SAH	Conservative treatment	1	2
Case 2	VB	PED + PED	ENT	Conservative treatment	0	6
Case 3	MCA	PED + PED	TIA	Conservative treatment	1	1
Case 4	ICA	PED + PED	SAH	Surgery	1	6
Case 5	ICA	PED + PED + Coil	TIA	Tirofiban	0	0
Case 6	VB	PED + PED + Coil	TIA	Conservative treatment	1	1
Case 7	ICA	PED + PED + PED	ENT	Conservative treatment	0	4
Case 8	VB	PED + PED	ENT	Conservative treatment	1	6

TIA, transient ischemic attacks; ENT, embolization in new territory; SAH, subarachnoid hemorrhage.

TABLE 4 | Radiographic and clinical results.

	Frequency
Clinical results	
mRS ≤ 2	52/52 (100%)
mRS > 2	0
Radiographic results	
OKM A and B	3/34 (8.8%)
OKM C	5/34 (14.7%)
OKM D	26/34 (76.5%)
Parent artery status	
Patent	33/34 (97.1%)
Stenosis	0
Occluded	1/34 (2.9%)

Data are shown as n (%), n/N (%).

(Becske et al., 2013). In Japan, Oishi used PED to treat 100 large/giant aneurysms of the internal carotid artery, and each patient used 1.42 PEDs on average. Follow-up angiography showed an occlusion rate of 69.2% at 1 year (Oishi et al., 2018). These two studies showed quite different occlusion rates, which may be caused by the large number of PEDs used in PUFS. This finding was consistent with the results of our study. In our study, 49 aneurysms (≥ 10 mm) were implanted with 108 PEDs in total. For each patient in the study, 2.2 PEDs were used on average and the occlusion rate was 83.3% (25/30). Furthermore, these large/giant arteries were more common in the outer curve of the parent artery. Niimi applied Doppler technology to measure the blood flow velocity of an extracorporeal aneurysm model and proposed that the velocity and rupture risk of the aneurysm in outer curved vessels were higher than those in inner curved vessels (Niimi et al., 1984). Meng conducted a comparative study on low-curvature and high-curvature aneurysms with stent implantation, using dog and rabbit aneurysm models, and found that, with the increase in the parent artery curvature, the influence of stents on aneurysm hemodynamics decreased (Meng et al., 2014). Therefore, the usual solution strategy was to compact or overlap the stents. Damiano conducted a computational study and reported that the effect of a compact PED was less than that of two overlapping PEDs in saccular aneurysms (Damiano et al., 2017). However, Chalouhi stated that the use of multiple stents increased the incidence of ischemia-related symptoms (Chalouhi et al., 2014). In our study, only one patient with anterior circulation developed severe nerve defects (mRS 4), but recovered rapidly. Another patient had a large aneurysm with a jet sign at the neck. We attempted to use multi-PEDs to enhance the diversion effect and achieved positive results as seen at the 3-month DSA follow-up examination (**Figure 2**). In addition, a patient received two telescoped PEDs, without coil embolization, because of the large difference in diameter between the outflow and inflow vessels. However, the aneurysm was found to be unoccluded, and the sac enlarged, after 36 months. The aneurysm was eventually occluded by 10 months, after the application of another two overlapped PEDs in retreatment (**Figure 3**). It can be concluded that overlapping PEDs are suitable for use in large/giant aneurysms, particularly when there is a jet-sign after PED implantation. As described, the use of multi-PEDs has a certain safety and efficacy in the anterior circulation. For the posterior circulation lesions, due to the large number of perforating arteries, strict evaluation and further study remain indispensable.

Poor wall attachment plays a significant role in the treatment of complex lesions, including immediate and delayed stent displacement or retraction (Brinjikji et al., 2016; Heit et al., 2017). When this occurs, salvage of failed PED treatment is necessary. In our study, there were five patients with proximal retraction into the sac and poor adhesion during implantation. In these cases, we chose to deploy a second PED. Follow-up demonstrated that the aneurysms were completely occluded, patency of the parent arteries was satisfactory, and there were no related complications. Thus, for aneurysms with very tortuous parent arteries, acute

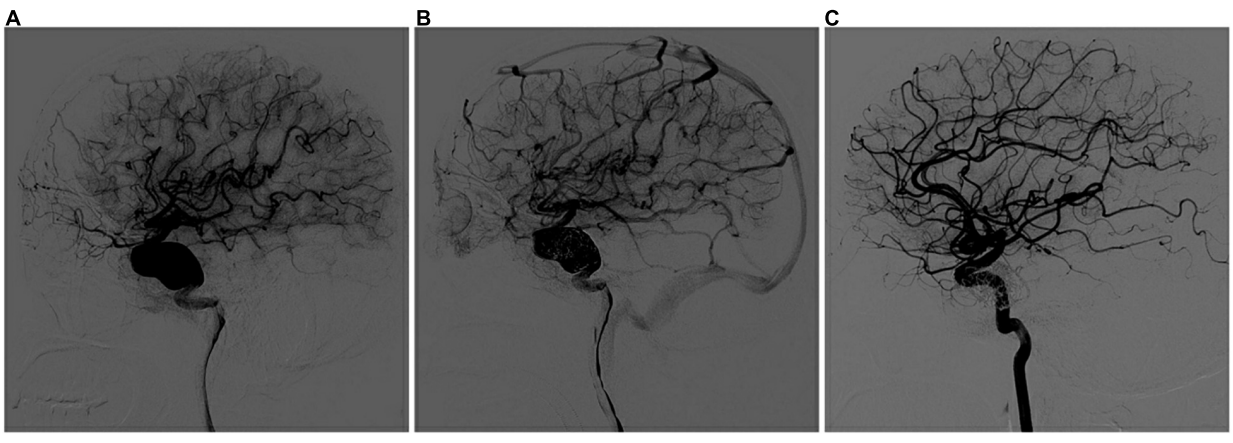

FIGURE 1 | Multi-PEDs for the treatment of a fusiform aneurysm (telescope technique). **(A)** Digital subtraction angiography (DSA) identified a fusiform aneurysm with a proximal diameter of 4.87 mm and a distal diameter of 4.38 mm in the internal carotid artery before operation. **(B)** After three pipeline embolization devices (4.5 mm × 35 mm/5 mm × 35 mm/5 mm × 30 mm) telescoped, DSA showed blood flow retention in the aneurysm, and no abnormalities were found in the branches or distal vessels. **(C)** Complete occlusion was seen at the 3-month DSA follow-up examination.

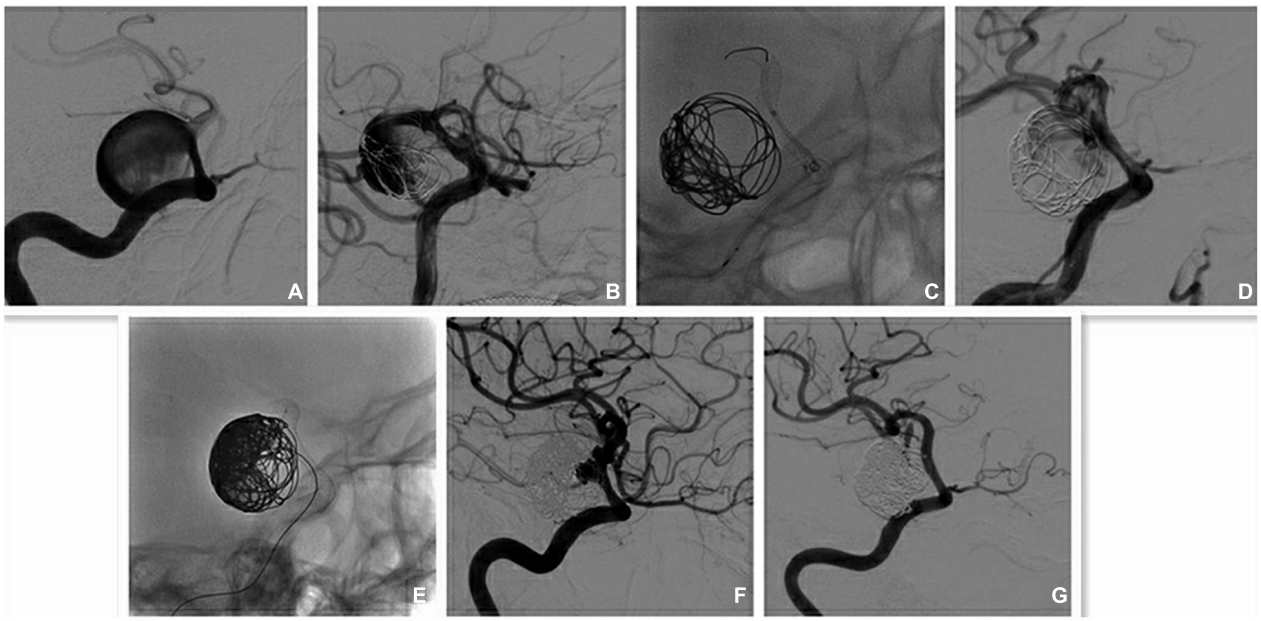

FIGURE 2 | Multi-PEDs for the treatment of a giant aneurysm (overlap technique). **(A)** Digital subtraction angiography (DSA) identified a large aneurysm with jet-sign at the narrow neck in the internal carotid artery (ICA) before operation. The proximal diameter and distal diameter were 4.55 and 3.77 mm, respectively. **(B)** The jet-sign is decreased slightly after the implantation of a pipeline embolization device (PED; 4.25 mm × 35 mm) and coil embolization. **(C)** The second PED (4.5 mm × 18 mm) was overlapped within the first one to cover the neck. **(D)** The ejection (jet-sign) is decreased largely after the implantation of two PEDs and coil embolization. **(E)** More coil was used to fill the entrance area of the sac. **(F)** DSA shows that the aneurysm was nearly occluded a week after operation. **(G)** The aneurysm is completely occluded, and the patency of the parent arteries is satisfactory at the 3-month DSA follow-up examination.

angles between inflow and outflow vessels, or greatly varying diameters, telescoping short and small PEDs are also an option to avoid poor opening or wall attachment during operation.

In addition, the application of a single PED assisted with coil embolization in the treatment of ruptured intracranial aneurysms has also been reported, and the short-term occlusion rate and incidence of complications are acceptable. Although the risks were higher than those of unruptured aneurysms, all occurred during the perioperative period (Chalouhi et al., 2015; Lin et al., 2015; Mokin et al., 2018). Nevertheless, there remains a 16% risk of aneurysm recurrence and re-rupture, particularly for blood blister-like aneurysms (Ji et al., 2017; Zhu et al., 2018). Thus, a multi-PED technique might be a promising option for this type of aneurysm.

Operation Strategies and Skills of Multiple Pipeline Embolization Devices

Strategies for using multi-PEDs include telescoping and overlapping techniques, with or without coil embolization. The detailed operations are as follows:

For telescoping, the first point is that the selection of the longest length and diameter should be larger than the anchoring zone. The first PED should be anchored firmly and for a sufficient length in the outflow vessel to ensure stability. Thus, the first PED achieves good opening and wall apposition. It should not be displaced when the second PED is pushed and pulled within the first PED. The diameter of the second PED should not be smaller than that of the first. When releasing the second PED, our experience is that it is necessary to ensure that the distal part of the second PED should overlap the first PED by 1/2 to 1/3 of its length. Thus, the second PED can cross the neck of the aneurysm safely along the small curve and be anchored stably in the proximal normal inflow vessel. If the system is not anchored stably, the third PED must be considered in the previous steps. As for the release, the first PED is implanted from distal to proximal and is released *in situ* or in slightly distant vessels. In other words, the distal part of the PED should be anchored in the normal outflow vessels with sufficient length, and the proximal part is then released into the inflow vessel or sac. When releasing the second PED, the stent catheter passes through the first deployed PED along the middle support wire of the conveying stent and is then deployed. The release of the second PED is mostly *in situ*, within the former PED, and a push release is mostly used. Once the PEDs cover the whole neck and after the final release of the last PED, intra-arterial rotational angiography (VasoCT, Philips Healthcare) or dynamic CT angiography (Dyna CT, Siemens Healthcare) is performed to identify whether the PEDs are opened well and have achieved good wall attachment, before coil embolization; otherwise, post-operative adjustment with guidewire and balloon application is the next step. To increase the stability of the multi-PEDs for patients with large/giant aneurysms, the embolization microcatheter is prepositioned in the sac, in parallel with the stent catheter in a 7F guiding sheath, in advance.

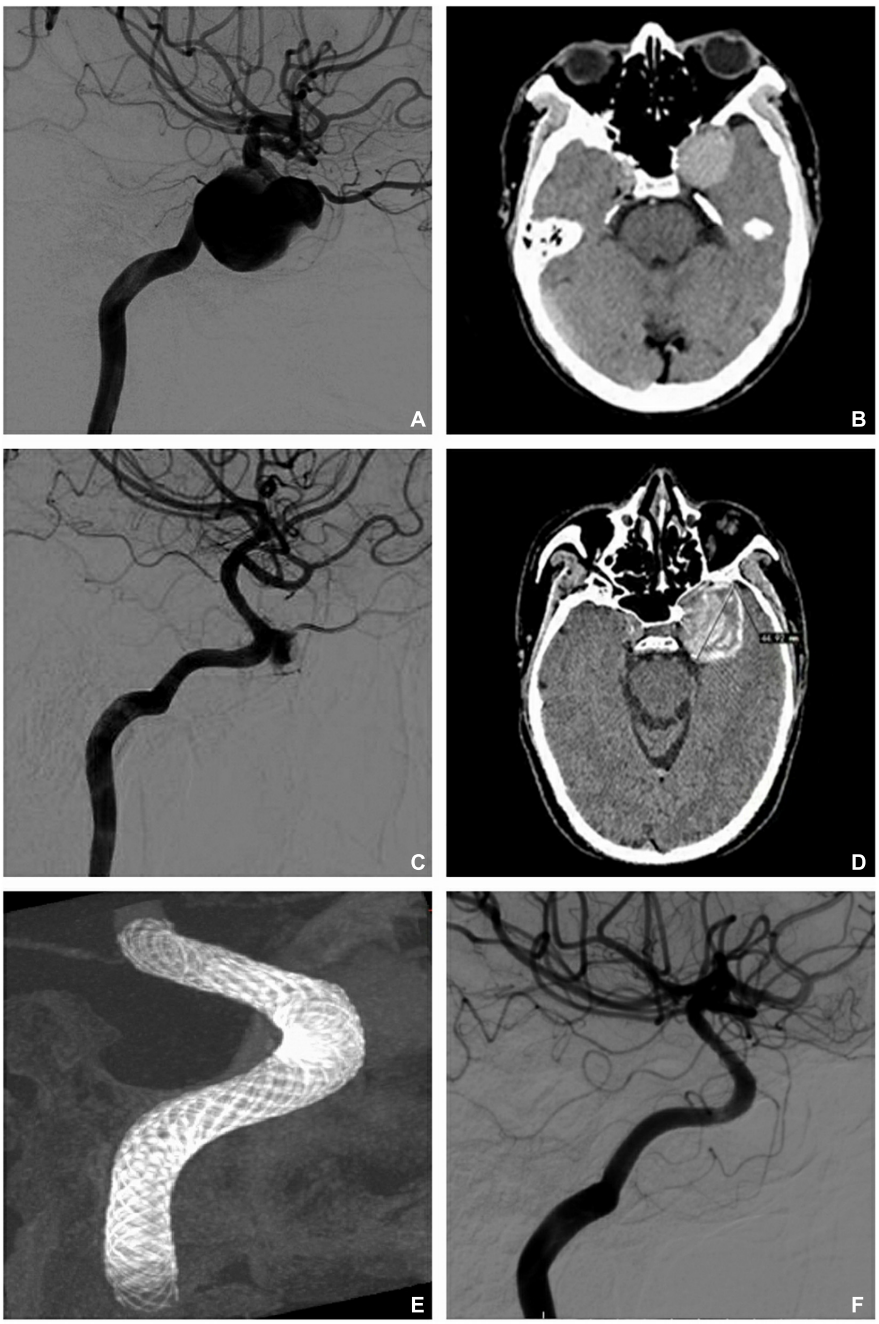

FIGURE 3 | Retreatment for unoccluded aneurysms (telescope and overlap techniques). **(A)** Digital subtraction artery (DSA) identified a giant aneurysm with a proximal diameter of 4.33 mm and a distal diameter of 3.93 mm in the internal carotid artery before operation. **(B)** Computed tomography (CT) revealed the maximum diameter of the aneurysm as 32 mm before operation. **(C)** DSA showed no occlusion after the implantation of two telescoped pipeline embolization devices (PEDs; 4.75 × 35 mm/4.75 × 30 mm) for 36 months. **(D)** CT shows that the sac enlarged over 36 months (maximum diameter = 45 mm). **(E)** Vaso-CT demonstrates the reconstruction after another two PEDs (4.5 mm × 30 mm/4.5 mm × 20 mm) overlapped at the neck of the aneurysm. **(F)** Complete occlusion is seen at 10 months after retreatment with the two overlapping PEDs.

After angiography confirms that the PED system completely covers the neck, the sac is filled with the coil to support the stability of the PEDs and promote thrombosis (Bender et al., 2018). Generally, a size larger than the diameter of the sac is selected, although the packing density is not crucial. More contact between the coil and PED at the neck is important for achieving better support and diversion. If the sac does not support the coil, the PED is pushed against the large curve, facilitating release. Simultaneously, concurrent insertion of more PEDs is possible.

The overlapping of PEDs is not complicated, and the operation is similar to that of a normal stent. Because the PED is fully visible, the proximal and distal positions and the opening and wall attachment can be clearly recognized under fluoroscopy or angiography. The overlapping technique entails deployment of a longer and a shorter PED. The longer stent is deployed first. It should be noted that the first PED must be as long as possible to cover the neck and be stably placed, so that the PED catheter can pass through it safely. The second PED is shorter (covering only the neck), but the diameter is equal to that of the first PED. The shorter stent is deployed within the lumen of the longer stent.

There are several challenges in the implantation of a PED. When multi-PEDs are implanted, there are more risks. One of the most difficult situations is the loss of the distal outflow vessel after the first PED is released. At this point, the only option is to use a microcatheter and microguidewire to find the back outflow vessel using biplane fluoroscopy. A somewhat soft and thin microcatheter can be selected to reach far from the outflow vessel and is then exchanged for a slightly harder microguidewire or catheter. Alternatively, the stent catheter or intermediate catheter can be introduced after anchoring with a balloon or stent. Moreover, poor opening and wall attachment may occur when the path is tortuous. In such a case, a balloon or balloon-expanding stent can be applied when the multi-PED system is stable. Otherwise, retreatment is an option in the second stage. For complications of thrombosis or microembolism, a moderate dose of tirofiban can be administered intraoperatively in addition to dual antiplatelet therapy.

This study has potential limitations. First, this is a retrospective observational study based on a small sample size. There are therefore subject to biases and confounding that may have influenced our results. Second, clinical results may be influenced by the differences in treatment strategies and experiences at different centers. Third, much longer follow-up and larger sample sizes need to be used to assess the effectiveness of multi-PED implantation. In addition, multicenter prospective studies need to be designed in the future for the study.

CONCLUSION

The use of multi-PEDs is safe and effective for the treatment of aneurysms in the anterior circulation, but is not recommended for those in the posterior circulation. Implantation of multi-PEDs could be considered for large-scale fusiform aneurysms, large/giant saccular aneurysms with a jet-sign after PED implantation, as salvage for failed PED treatment, and in cases where the diameter of the parent artery varies greatly.

DATA AVAILABILITY STATEMENT

The raw data supporting the conclusions of this article will be made available by the authors, without undue reservation.

ETHICS STATEMENT

The study was approved by the Ethics Committee of The First Affiliated Hospital of Zhengzhou University (KY 2018-098-02). The patients/participants provided their written informed consent to participate in this study.

AUTHOR CONTRIBUTIONS

FF carried out the studies, participated in collecting data, and drafted the manuscript. SG performed the statistical analysis and participated in its design. All authors contributed to the article and approved the submitted version.

REFERENCES

Becske, T., Kallmes, D. F., Saatci, I., McDougall, C. G., Szikora, I., Lanzino, G., et al. (2013). Pipeline for uncoilable or failed aneurysms: results from a multicenter clinical trial. *Radiology* 267, 858–868. doi: 10.1148/radiol.13120099

Bender, M. T., Jiang, B., Campos, J. K., Lin, L.-M., Beaty, N., Vo, C. D., et al. (2018). Single-stage flow diversion with adjunctive coiling for cerebral aneurysm: outcomes and technical considerations in 72 cases. *J. Neurointerv. Surg.* 10, 843–850. doi: 10.1136/neurintsurg-2017-013739

Brinjikji, W., Lanzino, G., Cloft, H., Siddiqui, A., Boccardi, E., Cekirge, S., et al. (2016). Risk factors for ischemic complications following Pipeline Embolization Device treatment of intracranial aneurysms: results from the IntrePED study. *Am. J. Neuroradiol.* 37, 1673–1678. doi: 10.3174/ajnr.A4807

Chalouhi, N., Tjoumakaris, S., Phillips, J., Starke, R., Hasan, D., Wu, C., et al. (2014). A single pipeline embolization device is sufficient for treatment of intracranial aneurysms. *Am. J. Neuroradiol.* 35, 1562–1566. doi: 10.3174/ajnr.A3957

Chalouhi, N., Zanaty, M., Whiting, A., Tjoumakaris, S., Hasan, D., Ajiboye, N., et al. (2015). Treatment of ruptured intracranial aneurysms with the pipeline embolization device. *Neurosurgery* 76, 165–172. doi: 10.1227/NEU.0000000000000586

Crobeddu, E., Lanzino, G., Kallmes, D. F., and Cloft, H. J. (2013). Marked decrease in coil and stent utilization following introduction of flow diversion technology. *J. Neurointerv. Surg.* 5, 351–353. doi: 10.1136/neurintsurg-2012-010320

Damiano, R. J., Tutino, V. M., Paliwal, N., Ma, D., Davies, J. M., Siddiqui, A. H., et al. (2017). Compacting a single flow diverter versus overlapping flow diverters for intracranial aneurysms: a computational study. *Am. J. Neuroradiol.* 38, 603–610. doi: 10.3174/ajnr.A5062

El-Chalouhi, N., Jabbour, P. M., Tjoumakaris, S. I., Starke, R. M., Dumont, A. S., Liu, H., et al. (2014). Treatment of large and giant intracranial aneurysms: cost comparison of flow diversion and traditional embolization strategies. *World Neurosurg.* 82, 696–701. doi: 10.1016/j.wneu.2013.02.089

Griessenauer, C. J., Ogilvy, C. S., Adeeb, N., Dmytriw, A. A., Foreman, P. M., Shallwani, H., et al. (2018). Pipeline embolization of posterior circulation aneurysms: a multicenter study of 131 aneurysms. *J. Neurosurg.* 130, 923–935. doi: 10.3171/2017.9.JNS171376

Griffin, A., Lerner, E., Zuchowski, A., Zomorodi, A., Gonzalez, L. F., and Hauck, E. F. (2021). Flow diversion of fusiform intracranial aneurysms. *Neurosurg. Rev.* 44, 1471–1478. doi: 10.1007/s10143-020-01332-0

Heit, J. J., Telischak, N. A., Do, H. M., Dodd, R. L., Steinberg, G. K., and Marks, M. P. (2017). Pipeline embolization device retraction and foreshortening after internal carotid artery blister aneurysm treatment. *Interv. Neuroradiol.* 23, 614–619. doi: 10.1177/1591019917722514

Ji, T., Guo, Y., Huang, X., Xu, B., Xu, K., and Yu, J. (2017). Current status of the treatment of blood blister-like aneurysms of the supraclinoid internal carotid artery: a review. *Int. J. Med. Sci.* 14, 390–402. doi: 10.7150/ijms.17979

Kwolek, C. J., Jaff, M. R., Leal, J. I., Hopkins, L. N., Shah, R. M., Hanover, T. M., et al. (2015). Results of the ROADSTER multicenter trial of transcarotid stenting with

dynamic flow reversal. *J. Vasc. Surg.* 62, 1227–1234.e1. doi: 10.1016/j.jvs.2015.04.460.

Lin, N., Brouillard, A. M., Keigher, K. M., Lopes, D. K., Binning, M. J., Liebman, K. M., et al. (2015). Utilization of Pipeline embolization device for treatment of ruptured intracranial aneurysms: US multicenter experience. *J. Neurointerv. Surg.* 7, 808–815. doi: 10.1136/neurintsurg-2014-011320

Meng, H., Tutino, V., Xiang, J., and Siddiqui, A. (2014). High WSS or low WSS? Complex interactions of hemodynamics with intracranial aneurysm initiation, growth, and rupture: toward a unifying hypothesis. *Am. J. Neuroradiol.* 35, 1254–1262. doi: 10.3174/ajnr.A3558

Mokin, M., Chinea, A., Primiani, C. T., Ren, Z., Kan, P., Srinivasan, V. M., et al. (2018). Treatment of blood blister aneurysms of the internal carotid artery with flow diversion. *J. Neurointerv. Surg.* 10, 1074–1078. doi: 10.1136/neurintsurg-2017-013701

Mona, M., Yan, B., Dowling, R. J., and Mitchell, P. J. (2013). Current status of pipeline embolization device in the treatment of intracranial aneurysms: a review. *World Neurosurg.* 80, 829–835. doi: 10.1016/j.wneu.2012.09.023

Nelson, P., Lylyk, P., Szikora, I., Wetzel, S., Wanke, I., and Fiorella, D. (2011). The pipeline embolization device for the intracranial treatment of aneurysms trial. *Am. J. Neuroradiol.* 32, 34–40. doi: 10.3174/ajnr.A2421

Niimi, H., Kawano, Y., and Sugiyama, I. (1984). Structure of blood flow through a curved vessel with an aneurysm. *Biorheology* 21, 603–615. doi: 10.3233/bir-1984-21418

Oishi, H., Teranishi, K., Yatomi, K., Fujii, T., Yamamoto, M., and Arai, H. (2018). Flow diverter therapy using a pipeline embolization device for 100 unruptured large and giant internal carotid artery aneurysms in a single center in a Japanese population. *Neurol. Med. Chir.* 58, 461–476. doi: 10.2176/nmc.oa.2018-0148

O'kelly, C., Krings, T., Fiorella, D., and Marotta, T. (2010). A novel grading scale for the angiographic assessment of intracranial aneurysms treated using flow diverting stents. *Interv. Neuroradiol.* 16, 133–137. doi: 10.1177/159101991001600204

Wang, X. A. M., Moullaali, T. J., Li, Q., Berge, E., Robinson, T. G., Lindley, R., et al. (2020). Utility-weighted modified rankin scale scores for the assessment of stroke outcome pooled analysis of 20 000+patients. *Stroke* 51, 2411–2417. doi: 10.1161/STROKEAHA.119.028523

Zhu, D., Yan, Y., Zhao, P., Duan, G., Zhao, R., Liu, J., et al. (2018). Safety and efficacy of flow diverter treatment for blood blister–like aneurysm: a systematic review and meta-analysis. *World Neurosurg.* 118, e79–e86. doi: 10.1016/j.wneu.2018.06.123

Conflict of Interest: The authors declare that the research was conducted in the absence of any commercial or financial relationships that could be construed as a potential conflict of interest.

Publisher's Note: All claims expressed in this article are solely those of the authors and do not necessarily represent those of their affiliated organizations, or those of the publisher, the editors and the reviewers. Any product that may be evaluated in this article, or claim that may be made by its manufacturer, is not guaranteed or endorsed by the publisher.

frontiers | Frontiers in Aging Neuroscience

ORIGINAL RESEARCH
published: 05 July 2022
doi: 10.3389/fnagi.2022.785661

Three-Dimensional High-Resolution Magnetic Resonance Imaging for the Assessment of Cervical Artery Dissection

Xianjin Zhu[1], Yi Shan[2,3], Runcai Guo[4], Tao Zheng[3], Xuebin Zhang[4], Zunjing Liu[3] and Kunpeng Liu[5]**

[1] Department of Neurology, Beijing Friendship Hospital, Capital Medical University, Beijing, China, [2] Graduate School of Peking Union Medical College, Beijing, China, [3] Department of Neurology, China-Japan Friendship Hospital, Beijing, China, [4] Department of Radiology, China-Japan Friendship Hospital, Beijing, China, [5] Department of Anesthesiology, Peking University International Hospital, Beijing, China

OPEN ACCESS

Edited by:
Gaiqing Wang,
Third People's Hospital of Hainan Province, China

Reviewed by:
Qing Huang,
Central South University, China
Hang Jin,
First Affiliated Hospital of Jilin University, China
Qi Yang,
Capital Medical University, China

***Correspondence:**
Zunjing Liu
liuzunjing@163.com
Kunpeng Liu
liukunpeng@pkuih.edu.cn

Specialty section:
This article was submitted to Neurocognitive Aging and Behavior, a section of the journal Frontiers in Aging Neuroscience

Received: 29 September 2021
Accepted: 09 June 2022
Published: 05 July 2022

Citation:
Zhu X, Shan Y, Guo R, Zheng T, Zhang X, Liu Z and Liu K (2022) Three-Dimensional High-Resolution Magnetic Resonance Imaging for the Assessment of Cervical Artery Dissection. Front. Aging Neurosci. 14:785661. doi: 10.3389/fnagi.2022.785661

Background and Purpose: Diagnosing cervical artery dissection (CAD) is still a challenge based on the current radiographic criteria. This study aimed to assess the value of three-dimensional high-resolution magnetic resonance imaging (3D HRMRI) in the detection of the signs of CAD and its diagnosis.

Materials and Methods: Patients with CAD from January 2016 to January 2021 were recruited from our 3D HRMRI database. The signs of dissection (intramural hematomas, intimal flap, double lumen), length and location of the dissection, thickness of the intramural hematoma, intraluminal thrombus, and percentage of dilation of the outer contour of the dissection on 3D HRMRI were assessed.

Results: Fourteen patients with 16 CADs, including 12 carotid CADs and 4 vertebral CADs, were finally diagnosed in this study. On 3D HRMRI, intramural hematomas were detected in 13/16 (81.3%) lesions with high sensitivity (100%) and high specificity (100%). Intimal flaps were found in 9/16 (56.3%) lesions with moderate sensitivity (64.3%) and high specificity (88.9%). Double lumen signs were observed in 4/16 (25.0%) lesions with high sensitivity (80.0%) and high specificity (100%). In addition, concomitant intraluminal thrombus were detected in 4/16 (25.0%) lesions with high sensitivity (80.0%) and high specificity (100%). The mean length of dissection was (25.1 ± 13.7) mm. The mean thickness of the intramural hematoma was (4.3 ± 2.3) mm. The mean percentage of dilation for the outer contour of the dissection was (151.3 ± 28.6)%.

Conclusion: The 3D HRMRI enables detection of the dissecting signs, such as intramural hematoma, intimal flap, double lumen, and intraluminal thrombus with high sensitivity and specificity, suggesting a useful, and non-invasive tool for definitively diagnosing CAD.

Keywords: cervical artery dissection, intimal flap, high resolution magnetic resonance image, intramural hematoma, double lumen

INTRODUCTION

Cervical arterial dissection (CAD), involving the extracranial carotid or vertebral artery, is an important cause of stroke (Debette and Leys, 2009) with the major mechanism being artery-to-artery embolism (Morel et al., 2012) associated with intimal damage and microthrombosis (Wu et al., 2019). Optimum treatment of CAD strongly relies on the accuracy of the diagnosis (Markus et al., 2019). The difficulties in the diagnosis of CAD have been well-documented in many previous studies (Robertson and Koyfman, 2017; Markus et al., 2019). Its clinical symptoms are often non-specific (Gallerini et al., 2019). Digital subtraction angiography (DSA), which was regarded as the gold standard for luminal imaging before magnetic resonance imaging (MRI), is no longer recommended for the diagnosis of CAD, not only because of its invasive nature but also because it lacks the ability to visualize the vessel wall (Debette and Leys, 2009). Computed tomography angiography (CTA) and MR angiography (MRA) are non-invasive techniques for assessing CAD (Caplan, 2008; Provenzale, 2009) but these modalities also focus on the luminal characteristics without providing enough information on the vessel wall (Debette and Leys, 2009). Doppler sonography is another non-invasive technique for assessing carotid atherosclerotic plaque (Lyu et al., 2020; Goudot et al., 2021) and for diagnosing CAD sometimes (Caplan, 2008; Robertson and Koyfman, 2017) but it should only be considered as a screening tool due to its operator dependence and poor diagnostic yield (Debette and Leys, 2009). Understanding the pathognomonic vessel wall radiological features of CAD, such as a double lumen, intimal flap, and intramural hematoma, is of utmost importance in making the definitive diagnosis (Debette and Leys, 2009).

Currently, MRI has become the first-line diagnostic modality for CAD (Debette and Leys, 2009). High-resolution MRI (HRMRI) has been used in the previous studies because it offers good visualization of the arterial wall (Yin, 2017; Zhao and Zhu, 2021) making it possible to detect the features of arterial dissection with greater sensitivity (Eliasziw et al., 1994; Bachmann et al., 2007; Saam et al., 2009; Qiao et al., 2011, 2016; Hunter et al., 2012; Machet et al., 2013; Yamada et al., 2016; Zhu et al., 2016, 2020; Coppenrath et al., 2017; McNally et al., 2018; Huang et al., 2019). This technique often involves black blood two-dimensional (2D) fast spin echo (FSE) sequences that rely mostly on double inversion recovery preparation or pre-regional saturation pulses to null the blood signal (Saam et al., 2009; Hunter et al., 2012; Machet et al., 2013; Coppenrath et al., 2017; Yin, 2017). The limitations of this technique include having a limited number of slices due to time constraints and anisotropic spatial resolution with low spatial resolution in the slice-select direction (Qiao et al., 2011; Zhu et al., 2016; Yin, 2017). It could be challenging to radiologically diagnose CAD using 2D HRMRI because of the features of the cervical carotid or vertebral artery, such as the variability of the dissecting length and the characteristics of the signals on MRI, the tortuous course of the lesions, adjacent veins, the smaller caliber of the vertebral artery, and the presence of an intraluminal thrombus (Debette and Leys, 2009; Morel et al., 2012).

Recently, three-dimensional (3D) HRMRI with variable flip-angle refocusing pulse sequence was introduced. In contrast to 2D HRMRI, 3D HRMRI has many advantages such as a higher signal–to-noise ratio, a larger coverage, and reduced scanning time (Qiao et al., 2011). Furthermore, 3D HRMRI could acquire isotropic volumetric datasets with sub-millimeter voxel size, which could enable multiplanar reconstruction for a more global assessing of vessel wall (Zhu et al., 2020). This 3D HRMRI technique has been used to image carotid and intracranial arterial walls for the evaluation of atherosclerotic plaque and intracranial dissecting aneurysms (Qiao et al., 2016; Zhu et al., 2016, 2020) and it may be also suitable for detecting the signs of dissection in the cervical carotid or vertebral artery.

MATERIALS AND METHODS

Patient Selection

We reviewed our HRMRI database for patients with CAD diagnosed using imaging techniques from January 2016 to January 2021. Considering no widely recognized golden standard available for the diagnosis of CAD nowadays, a definitive diagnosis of CAD was made when any pathognomonic sign of dissection (double lumen, intimal flap, and intramural hematoma) was detected at least one imaging modality such as MRA, CTA, DSA, or 3D HRMRI. Diffusion-weighted imaging (DWI) and HRMRI were performed simultaneously. This observational cross-sectional study was approved by our local institutional ethics committee. The demographics, clinical findings, imaging data, and risk factors—such as hypertension, hyperlipidemia, diabetes mellitus, and cigarette smoking—were noted.

Imaging Protocol

All MR examinations were performed with a 3T MRI scanner (Ingenia; Philips Healthcare, Nederland) using a 20-channel integrated head/neck coil. 3D HRMRI was acquired using a pre- and post-contrast black blood technique called volumetric isotropic turbo spin-echo acquisition (VISTA). The parameters were as follows: repetition time/echo time = 800/21 ms, field of view = 180 × 180, matrix = 300 × 300, NEX = 1, and slice thickness = 0.6 mm; the voxel volume was 0.6 mm × 0.6 mm × 0.6 mm on the T1-weighted image (T1WI). The post-contrast T1WI was obtained 5 min after gadolinium injection (0.1 mmol/kg of gadopentetate dimeglumine, Magnevist, Berlin, Germany) with the same parameters as pre-contrast T1WI.

High-Resolution Magnetic Resonance Imaging Assessment

Initially, two trained readers with more than 5 years of experience in reading HRMR images and blinded to the clinical information and DWI of the patients assessed for the signs of dissection, such as intramural hematoma, intimal flap, double lumen, and intraluminal thrombus on the VISTA images. Analytical data were used to calculate the interobserver variability. The differences between the two observers were solved by consensus.

Intramural hematoma was defined as the detection of crescent-shaped, intermediate-to-high signal intensity within the arterial wall on pre-contrast T1WI (**Figures 1–3**; Wu et al., 2019; Zhu et al., 2020). Furthermore, signal intensity alterations were classified as homogenous or heterogeneous (Wu et al., 2019; Zhu et al., 2020). Intraluminal thrombus was defined as hyperintense filling on pre-contrast T1W images (Wu et al., 2019) and an intimal flap was defined as an abnormal curvilinear or

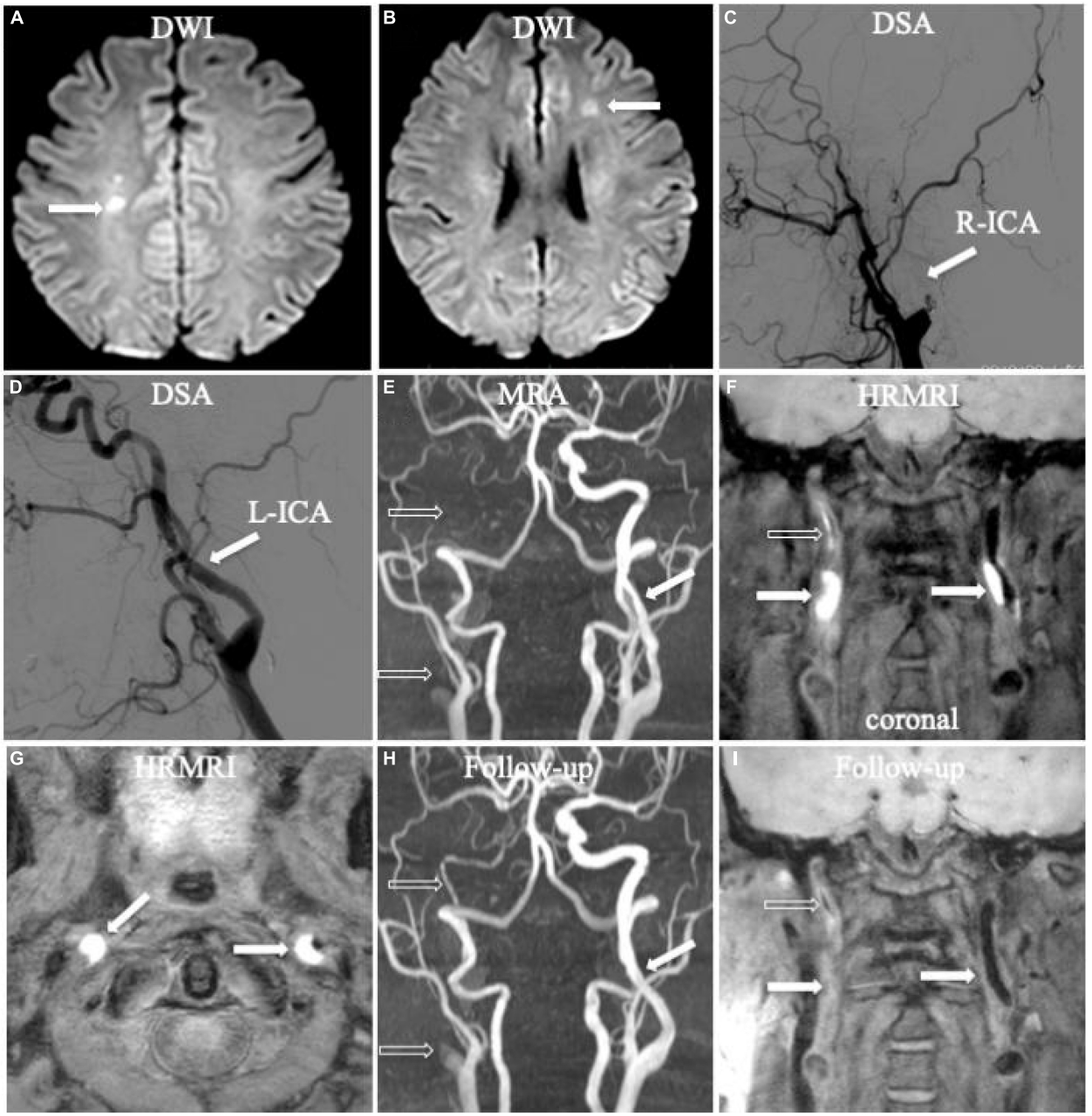

FIGURE 1 | Bilateral acute ischemic stroke associated with dissection in the internal carotid arteries (ICA) bilaterally. Diffusion-weighted imaging (DWI) showed acute ischemic stroke in bilateral hemispheres (**A,B**, arrow). Digital subtraction angiography (DSA) only showed occlusion in the right ICA (**C**, arrow) and mild irregular stenosis in the left ICA (**D**, arrow) without any direct dissecting signs. Initial magnetic resonance angiography (MRA) displayed occlusion (**E**, empty arrow) in the right ICA and mild irregular stenosis in the left ICA (**E**, arrow), similar as the founding on DSA. Initial coronal T1-weighted high-resolution magnetic resonance imaging (HRMRI) demonstrated a T1-hyperintense intramural hematoma (**F**, arrow) in the proximal C1 segments of the ICA bilaterally and a T1-hyperintense intraluminal thrombus in the middle and distal right ICA (**F**, empty arrow). Transverse HRMRI presented with typical crescent-shaped intramural hematomas (**G**, arrow). Follow-up MRA showed partial recanalization in the middle and distal right ICA (**H**, empty arrow) and a nearly normal lumen in the left ICA (**H**, arrow). Follow-up coronal HRMRI exhibited disappearance of the T1-hyperintense intramural hematoma (**I**, arrow) in the ICA bilaterally and T1-hyperintense intraluminal thrombus (**I**, empty arrow) in the right ICA.

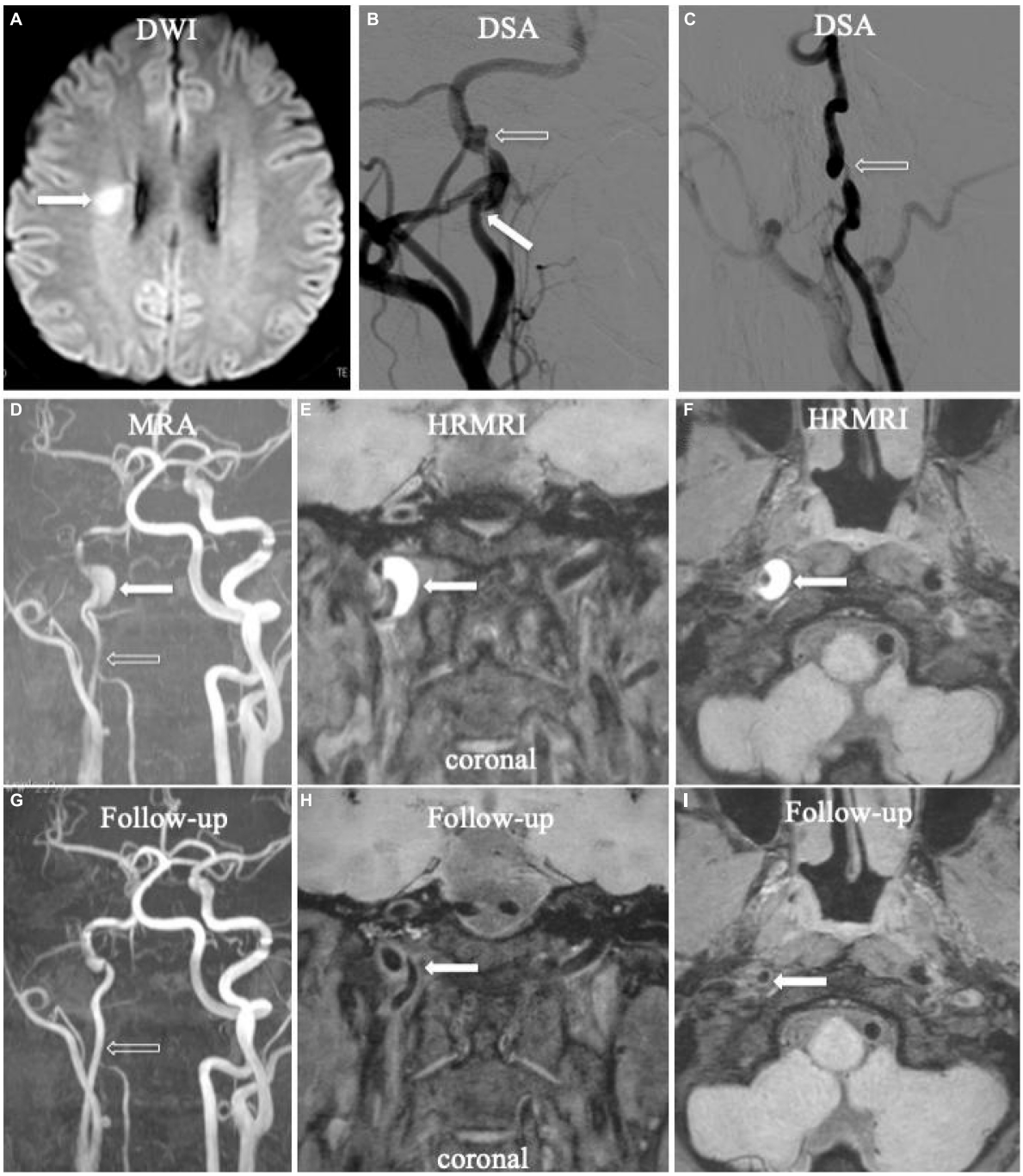

FIGURE 2 | Acute ischemic stroke (**A**, arrow) in the territory of the right ICA. Digital subtraction angiography (DSA) showed aneurysmal dilation with focal stenosis (**B,C**, empty arrow) and suspicious intimal flap (**B**, arrow) in the right ICA. Initial MRA displayed tapered stenosis (**D**, empty arrow) and a suspicious hematoma (**D**, arrow). Initial HRMRI showed an intramural hematoma on the T1-weighted coronal (**E**, arrow) and transverse image (**F**, arrow). Follow-up MRA (**G**, arrow) showed partial recanalization on the affected arterial lumen. The intramural hematoma had disappeared on follow-up T1-weighted coronal (**H**, arrow) and transverse (**I**, arrow) HRMRI.

linear structure separating a true lumen from a false lumen (Zhu et al., 2020). To distinguish the intimal flap from the inflow artifact that usually appears at the center portion of the lumen, we considered a linear structure as an intimal flap that extended to the arterial sidewall on pre- and/or post-contrast T1W images (Wu et al., 2019; Zhu et al., 2020). The double-lumen sign was defined as two jets of flow void within one vessel on MRI (Wu et al., 2019; Zhu et al., 2020).

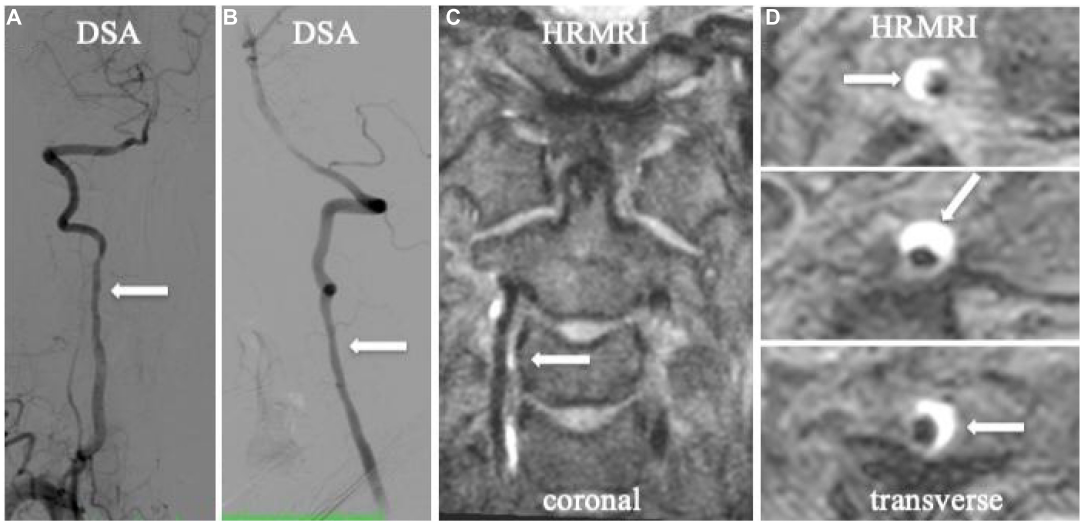

FIGURE 3 | Spiral intramural hematoma in the patient with vertebral artery dissection. Digital subtraction angiography (DSA) showed irregularly mild stenosis without any dissecting signs on anteroposterior and lateral projections (**A,B**, arrow). T1-weighted HRMRI showed an spiral intramural hematoma in the right vertebral artery in the coronal (**C**, arrow) and transverse planes (**D**, arrow).

TABLE 1 | Clinical characteristics of the patients with cervical artery dissection.

Patient no.	Symptoms	Risk factors	NIHSS	mRS
1	Headache	-	0	0
2	Recurrent dizziness	Hyperlipidemia	0	0
3	Left lower extremity weakness and numbness	Smoking	2	1
4	Left upper extremity weakness and numbness	-	3	1
5	Left upper extremity weakness and slurring of speech	Smoking	3	1
6	Recurrent dizziness	Smoking	0	0
7	Recurrent dizziness and headache	-	0	0
8	Right extremity weakness and slurring of speech	-	3	1
9	Slurring of speech and facial palsy	History of trauma	3	1
10	Right hand weakness and slurring of speech	History of trauma	3	1
11	Dizziness	-	0	0
12	Right side weakness	-	1	1
13	Left side weakness and slurring of speech	Hypertension, smoking	3	1
14	Recurrent dizziness	Hypertension, diabetes mellitus, smoking	1	1

NIHSS, National Institutes of Health Stroke Scale; mRS, modified Rankin Scale.

The stenosis degree at the most stenotic site of the true lumen was defined as (1-lesion luminal diameter/reference luminal diameter) × 100%, according to the North American Symptomatic Carotid Endarterectomy Trial criteria (Eliasziw et al., 1994). The degree of stenosis was graded as no or mild stenosis (<50%), moderate stenosis (50–69%), and severe stenosis or occlusion (70–100%). Enlargement of the outer contour of dissection was assessed using the following formula: percentage of dilation = $D_{dilatation}/D_{normal} \times 100$ (Itabashi et al., 2014). The $D_{dilatation}$ was defined as the maximum diameter of the outer contour of the lesions and D_{normal} as the outer diameter of the nearest normal segment proximal to the lesions. If the proximal segment was not available, the outer diameter of the nearest normal segment distal to the lesions was substituted. To assess interobserver variability, the two readers independently measured the $D_{dilatation}$ and D_{normal} of all the lesions.

Statistical Analysis

Continuous variables were summarized as mean ± standard deviation (*SD*). Categorical variables were presented as percentages. The Cohen's k coefficient was computed to quantify the interobserver agreement for detecting intramural hematoma, intimal flap, double lumen, intraluminal thrombus, and the heterogeneous signal intensity of the intramural hematoma. A value of $k > 0.75$ was used to indicate a high level of agreement, and $0.40 \leq k \leq 0.75$ denoted moderate agreement. Intraclass correlation coefficient (ICC) was used to determine interobserver agreement for the measurements of the length of dissection, thickness of intramural hematoma, and percentage

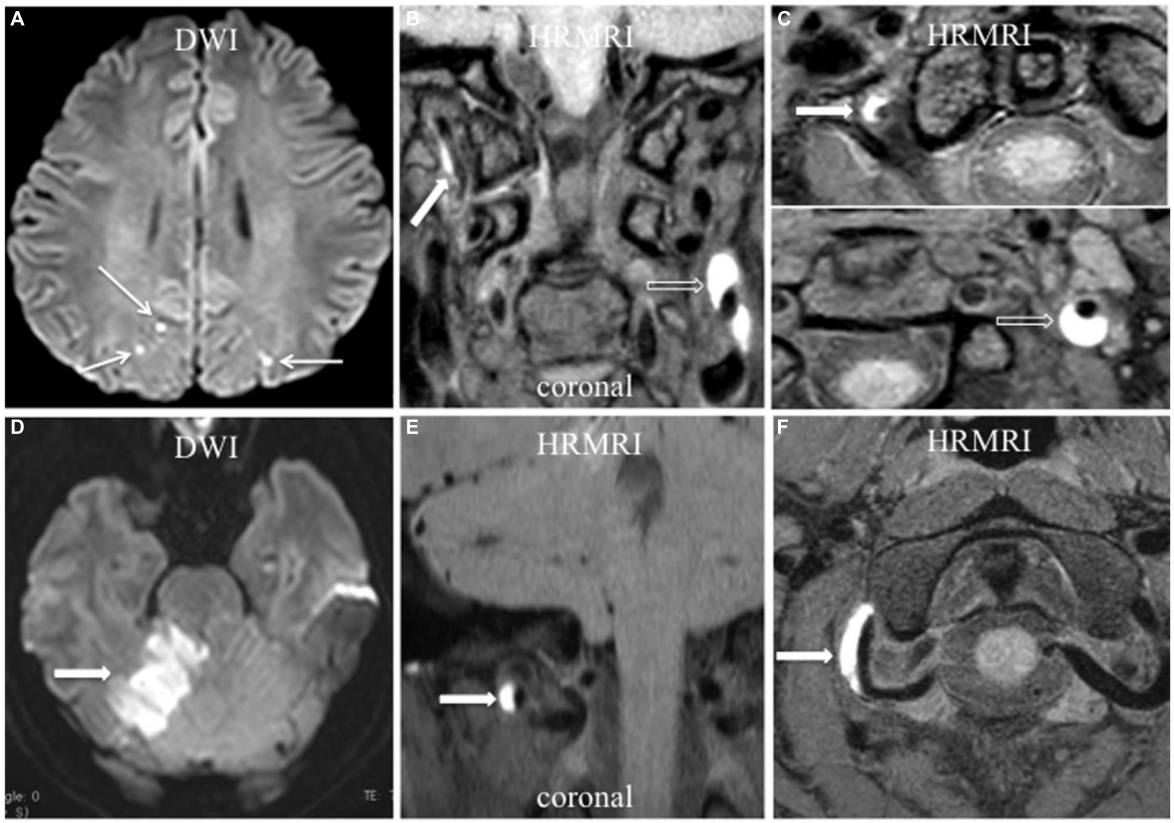

FIGURE 4 | Acute ischemic stroke associated with vertebral artery dissection. **(A–C)** Multiple acute ischemic stroke lesions in the parietooccipital junction bilaterally (**A**, arrow) with dissection in the right vertebral artery and left ICA. T1-weighted HRMRI showed an intramural hematoma in the right vertebral artery (**B,C**, arrow) and left ICA (**B,C**, empty arrow) in the coronal and transverse planes. **(D–F)** Acute ischemic stroke in the right cerebellum (**D**, arrow) with V3 segment dissection of the right vertebral artery. T1-weighted HRMRI showed an intramural hematoma in the right vertebral artery in the coronal (**E**, arrow), and transverse (**F**, arrow) planes.

TABLE 2 | Signs of dissection on high-resolution magnetic resonance imaging (HRMRI) for individual patients and lesions.

Patient no.	Lesion location	Initial HRMRI			Follow-up HRMRI	
		Intramural hematoma	Intimal flap	Double lumen	Lumen	Intramural hematoma
1	LICA	Y	Y	N	-	-
	RVA	Y	N	N	-	-
2	RICA	Y	N	N	-	-
3	RICA	Y	N	N	Partial recanalization	Reduced
	LICA	Y	N	N	Complete recanalization	Disappeared
4	RICA	Y	Y	N	-	-
5	RICA	Y	Y	Y	Partial recanalization	Disappeared
6	RVA	Y	N	N	Complete recanalization	Disappeared
7	RVA	Y	N	N	-	-
8	LICA	N	Y	Y	-	-
9	LICA	Y	Y	N	Complete recanalization	Disappeared
10	LICA	Y	Y	N	Complete recanalization	Disappeared
11	RICA	Y	N	N	Complete recanalization	Disappeared
12	RVA	Y	Y	Y	-	-
13	LICA	N	Y	Y	-	-
14	RICA	N	Y	N	-	-

LICA, left internal carotid artery; RICA, right internal carotid artery; RVA, right vertebral artery; Y, yes; N, no; HRMRI, high-resolution magnetic resonance imaging.

of dilation. The SPSS 20 (SPSS, Inc., Chicago, IL) was used for the statistical analysis. All reported p-values were 2-sided, and p-values < 0.05 were considered significant.

RESULTS

Patients

A total of 14 patients with 16 CADs (6 men and 8 women) were enrolled in this study, including 7 patients who presented with acute ischemic stroke and 7 patients without acute ischemic stroke but with neurological symptoms (**Table 1**). The mean age was 43.9 ± 10.9 years. Among the 14 patients, 9 patients presented with unilateral internal carotid arteries (ICA) dissections (64.3%), 3 with unilateral vertebral dissections (21.4%), 2 with multiple dissections (14.3%)—including 1 patient with bilateral ICA dissection and 1 with unilateral ICA and vertebral dissection. Of the 16 lesions [12 lesions (75.0%) in the extracranial carotid artery, 4 lesions (25.0%) in the extracranial vertebral artery] (**Figure 2**), dissections caused no or mild stenosis in 6 lesions, moderate stenosis in 4 lesions, and severe stenosis or occlusion in 6 lesions. The risk factors included hypertension (n = 2, 14.3%), hyperlipidemia (n = 1, 7.1%), diabetes mellitus (n = 1, 7.1%), smoking (n = 5, 35.7%), and a history of trauma to the neck within the previous 28 days (n = 2, 14.3%).

Interobserver Agreement

The interobserver agreement was high for the identification of intramural hematomas (k = 0.818), intimal flaps (k = 0.871), and the double lumen sign (k = 0.846); it was moderate for identifying intraluminal thrombi (k = 0.714); and it was high for the measurements of the length of dissection (ICC = 0.919), thickness of intramural hematoma (ICC = 0.994), and percentage of dilation (ICC = 0.919).

High-Resolution Magnetic Resonance Imaging Assessment

On 3D HRMRI, intramural hematomas were identified in 13 lesions (81.3%) in 11 patients (**Figures 1**–**4**) with the sensitivity 100% and the specificity 100%. Among the 11 patients, 6 presented with unilateral ICA intramural hematomas, 3 with unilateral vertebral intramural hematomas, 1 with bilateral ICA intramural hematomas, and 1 with unilateral ICA and vertebral intramural hematomas. Of the 13 lesions with intramural hematomas, 7 (53.8%) showed heterogeneous signal intensity. The mean thickness of the intramural hematomas was (4.3 ± 2.3) mm. Intraluminal thrombi were found in four ICA dissections (25.0%) of four patients (sensitivity 80.0%, specificity 100%) (**Figures 1**–**4**).

On 3D HRMRI, the intimal flap was detected in nine lesions (56.3%) in nine patients (sensitivity 64.3%, specificity 88.9%), including eight intimal flaps in unilateral ICA of eight patients and an intimal flap in unilateral vertebral dissection of one patient. A double lumen was detected in four lesions (25.0%) in four patients (sensitivity 80.0%, specificity 100%), including three unilateral ICA dissections in three patients and one vertebral dissection in one patient (**Table 2**).

In total, three signs of dissection were detected in 2 lesions, two signs in 7 lesions, and one sign in 7 lesions on 3D HRMRI. The mean length of dissection was (25.1 ± 13.7) mm. The mean percentage of dilation for the outer contour of the dissection was (151.3 ± 28.6%).

Follow-up 3D HRMRI was performed in six patients with seven lesions (mean 204.8 ± 109.9 days) (**Figures 1**, **2**). On follow-up 3D HRMRI, intramural hematoma disappearance was found in 6/7 lesions (85.7%), including luminal complete recanalization in 5/7 lesions (71.4%) and luminal partial recanalization in 1/7 lesions (14.3%). For one lesion (14.3%), the intramural hematoma was reduced and became an intermediate signal intensity with luminal partial recanalization (**Table 2**).

DISCUSSION

This study showed that 3D HRMRI with pre- and post-contrast T1-weighted images was useful for investigating the pathognomonic radiological features of cervical dissection, such as intramural hematoma, intimal flap, double lumen, and intraluminal thrombus with high sensitivity and specificity, thus allowing the definitive diagnosis of dissection.

Intramural hematoma was the most specific sign of CAD (carotid or vertebral), with the typical imaging manifestation of crescent-shaped intermediate-to-high signal intensity surrounding a lumen within the arterial wall on a pre-contrast T1-weighted image. In this study, intramural hematoma was the most frequent sign of dissection detected on 3D HRMRI, with a positive rate of 81.3%. Intramural hematomas were best revealed in the subacute or early chronic stage with high signal intensity; however, after 2 months, most of them became isointense and became difficult to recognize on MR images (Habs et al., 2011). The disappearance of intramural hematomas with regression of dissection has been found in over 80% of cases at radiological follow-up, and the mean time for the arterial lumen to return to normal is approximately 3 months (Morel et al., 2012). In this study, intramural hematomas disappeared in 6/7 lesions (85.7%) at 3D HRMRI follow-up with complete or partial recanalization.

Intraluminal thrombi might play a major role in the pathogenesis of stroke, with the radiological characteristics of an intraluminal filling defect within the lumen on MRA (Yamada et al., 2016) or a hyper-intense filling defect within the lumen on pre-contrast T1W images (McNally et al., 2018). An intraluminal thrombus can be detected on the dissecting site (Markus et al., 2019) or the distal segment of the dissecting vessel (McNally et al., 2018). The 3D HRMRI could provide large coverage and a high signal-to-noise ratio and improve the ability to assess intraluminal thrombi in dissecting vessels.

An intimal flap, with or without a double lumen, was also regarded as a reliable diagnostic finding for CAD (Debette and Leys, 2009). However, it is a subtle sign, and it is only seen in a minority of cases. We found that the intimal flap could be well identified on the post-contrast HRMR T1-weighted images—it manifested as an enhanced curvilinear or linear structure

(Debette and Leys, 2009). Detection of the double-lumen sign relied on the identification of blood products in the false lumen (Morel et al., 2012). An entry-exit-type dissection with a communication between the true and false lumen would provide a constant flow of blood through the false lumen, resulting in a signal flow-void similar to that of the true lumen on MRI (Mizutani et al., 2001). In contrast, another type of dissection without a communication between the true and false lumen often has an intramural hematoma in the false lumen, with various signal intensities according to the hemorrhagic stage on MRI (Habs et al., 2011; Zhu et al., 2020).

Vertebral CADs were less commonly reported than carotid CADs in previous studies (Babo von et al., 2013; Traenka et al., 2017). One of the main reasons for the accurate diagnosis of vertebral CAD is the small size of the vertebral arteries and the influence of bony structures (Debette and Leys, 2009). With the increased use of MRI, vertebral CAD is more frequently reported. The 3D HRMRI could be useful in cases of suspected vertebral CAD or multiple lesions (**Figure 3**).

High-resolution magnetic resonance imaging has been used to reveal the arterial structure for detecting the signs of dissection, mainly with 2D acquisition (Machet et al., 2013; Yin, 2017). However, the reliable identification of arterial dissection by 2D images might be impaired by the lower spatial resolution in the slice-select direction and the limited anatomic coverage (Yin, 2017). Multiple CADs were found in 13–16% of cases, which emphasized the significance of broad coverage imaging. Compared with 2D imaging, 3D HRMRI enables the coverage of a larger volume of cervical arteries and can provide isotropic reconstructed images (Bachmann et al., 2007; Yamada et al., 2016; McNally et al., 2018; Huang et al., 2019). It has the advantage of evaluating the complex anatomy of artery dissections, especially in cases with multiple lesions.

Our study had several limitations. First, it only included a small number of subjects, which may limit the generalizability of the results. Second, not all imaging follow-up findings were available. Finally, the diagnosis was not confirmed by histological examination. Further studies with more cases and follow-up information are needed to assess the sensitivity and specificity of 3D HRMRI, and reveal the imaging changes in 3D HRMRI findings.

CONCLUSION

The 3D HRMRI enables a larger anatomical coverage with high isotropic spatial resolution and high reproducibility to reliably assess the signs of dissection—such as intramural hematoma, intimal flap, double lumen, and a concomitant intraluminal thrombus with high sensitivity and specificity—suggesting a useful and non-invasive tool for definitively diagnosing CAD.

DATA AVAILABILITY STATEMENT

The original contributions presented in this study are included in the article/supplementary material, further inquiries can be directed to the corresponding authors.

ETHICS STATEMENT

The studies involving human participants were reviewed and approved by the Ethics Committee of clinical trials of drugs or devices in China-Japan Friendship Hospital. The patients/participants provided their written informed consent to participate in this study. Written informed consent was obtained from the individual(s) for the publication of any potentially identifiable images or data included in this article.

AUTHOR CONTRIBUTIONS

XJZ: manuscript writing, analysis, interpretation of results, and editing. YS: manuscript writing, analysis, data acquisition, and participant recruitment. ZL and KL: research design, interpretation of results, and manuscript writing and editing. RG, TZ, and XBZ: data acquisition, participant recruitment, image processing, and editing. All authors contributed to the manuscript and approved the submitted version.

FUNDING

This study was supported by the National Natural Science Foundation of China (Grant No: 52073310) and Elite Medical Professionals Project of China-Japan Friendship Hospital (Gant No: ZRJY2021 - BJ03).

ACKNOWLEDGMENTS

We gratefully acknowledge all the authors of this manuscript for their assistance with data acquisition, participant recruitment, image processing, and logistics.

REFERENCES

Babo von, M., De Marchis, G. M., Sarikaya, H., Stapf, C., Buffon, F., et al. (2013). Differences and similarities between spontaneous dissections of the internal carotid artery and the vertebral artery. *Stroke* 44, 1537–1542. doi: 10.1161/STROKEAHA.113.001057

Bachmann, R., Nassenstein, I., Kooijman, H., Dittrich, R., Stehling, C., Kugel, H., et al. (2007). High-resolution magnetic resonance imaging (MRI) at 3.0 tesla in the short-term follow-up of patients with proven cervical artery dissection. *Invest. Radiol.* 42, 460–466. doi: 10.1097/01.rli.0000262758.98098.d6

Caplan, L. R. (2008). Dissections of brain-supplying arteries. *Nat. Clin. Pract. Neurol.* 4, 34–42. doi: 10.1038/ncpneuro0683

Coppenrath, E., Lenz, O., Sommer, N., Lummel, N., Linn, J., Treitl, K., et al. (2017). Clinical significance of intraluminal contrast enhancement in patients with spontaneous cervical artery dissection: a black-blood mri study. *Fortschr. Röntgenstr.* 189, 624–631. doi: 10.1055/s-0043-104632

Debette, S., and Leys, D. (2009). Cervical-artery dissections: predisposing factors, diagnosis, and outcome. *Lancet Neurol.* 8, 668–678. doi: 10.1016/S1474-4422(09)70084-5

Eliasziw, M., Smith, R. F., Singh, N., Holdsworth, D. W., Fox, A. J., and Barnett, H. J. (1994). Further comments on the measurement of carotid stenosis from angiograms. North American Symptomatic Carotid Endarterectomy Trial (NASCET) Group. *Stroke* 25, 2445–2449. doi: 10.1161/01.str.25.12.2445

Gallerini, S., Marsili, L., Bartalucci, M., Marotti, C., Chiti, A., and Marconi, R. (2019). Headache secondary to cervical artery dissections: practice pointers. *Neurol. Sci.* 40, 613–615. doi: 10.1007/s10072-018-3576-y

Goudot, G., Sitruk, J., Jimenez, A., Julia, P., Khider, L., Alsac, J.-M., et al. (2021). Carotid Plaque vulnerability assessed by combined shear wave elastography and ultrafast doppler compared to histology. *Transl. Stroke Res.* 13, 100–101. doi: 10.1007/s12975-021-00920-6

Habs, M., Pfefferkorn, T., Cyran, C. C., Grimm, J., Rominger, A., Hacker, M., et al. (2011). Age determination of vessel wall hematoma in spontaneous cervical artery dissection:A multi-sequence 3T Cardiovascular Magnetic resonance study. *J. Cardiovasc. Magn. Reson.* 13:76. doi: 10.1186/1532-429X-13-76

Huang, R. J., Lu, Y., Zhu, M., Zhu, J. F., and Li, Y. G. (2019). Simultaneous non-contrast angiography and intraplaque haemorrhage (SNAP) imaging for cervical artery dissections. *Clin. Radiol.* 74, e1–e817. doi: 10.1016/j.crad.2019.06.018

Hunter, M. A., Santosh, C., Teasdale, E., and Forbes, K. P. (2012). High-resolution double inversion recovery black-blood imaging of cervical artery dissection using 3T MR Imaging. *AJNR Am. J. Neuroradiol.* 33, E133–E137. doi: 10.3174/ajnr.A2599

Itabashi, R., Mori, E., Furui, E., Sato, S., Yazawa, Y., Kawata, K., et al. (2014). A dilated surface appearance on basiparallel anatomic scanning-magnetic resonance imaging is a useful tool for the diagnosis of spontaneous vertebral artery dissection in lateral medullary infarction. *J. Stroke Cerebrovasc. Dis.* 235, 805–810. doi: 10.1016/j.jstrokecerebrovasdis.2013.07.003

Lyu, Q., Tian, X., Ding, Y., Yan, Y., Huang, Y., Zhou, P., et al. (2020). Evaluation of carotid plaque rupture and neovascularizationby contrast-enhanced ultrasound imaging: an exploratory study based on histopathology. *Transl. Stroke Res.* 12, 49–56. doi: 10.1007/s12975-020-00825-w

Machet, A., Fonseca, A. C., Oppenheim, C., Touze, E., Meder, J. F., Mas, J. L., et al. (2013). Does anticoagulation promote mural hematoma growth or delayed occlusion in spontaneous cervical artery dissections. *Cerebrovasc. Dis.* 35, 175–181. doi: 10.1159/000346592

Markus, H. S., Levi, C., King, A., Madigan, J., Norris, J., and Investigators, F. T. C. A. D. I. S. S. C. (2019). Antiplatelet therapy vs anticoagulation therapy in cervical artery dissection: the cervical artery dissection in stroke study (CADISS) randomized clinical trial final results. *JAMA Neurol.* 76, 657–664.18-9 doi: 10.1001/jamaneurol.2019.0072

McNally, J. S., Hinckley, P. J., Sakata, A., Eisenmenger, L. B., Kim, S.-E., De Havenon, A. H., et al. (2018). Magnetic resonance imaging and clinical factors associated with ischemic stroke in patients suspected of cervical artery dissection. *Stroke* 49, 2337–2344. doi: 10.1161/STROKEAHA.118.021868

Mizutani, T., Kojima, H., Asamoto, S., and Miki, Y. (2001). Pathological mechanism and three-dimensional structure of cerebral dissecting aneurysms. *J. Neurosurg.* 94, 712–717. doi: 10.3171/jns.2001.94.5.0712

Morel, A., Naggara, O., Touzé, E., Raymond, J., Mas, J. L., Meder, J. F., et al. (2012). Mechanism of ischemic infarct in spontaneous cervical artery dissection. *Stroke* 43, 1354–1361. doi: 10.1161/STROKEAHA.111.643338

Provenzale, J. M. (2009). MRI and MRA for evaluation of dissection of craniocerebral arteries: lessons from the medical literature. *Emerg. Radiol.* 16, 185–193. doi: 10.1007/s10140-008-0770-x

Qiao, Y., Anwar, Z., Intrapiromkul, J., Liu, L., Zeiler, S. R., Leigh, R., et al. (2016). Patterns and implications of intracranial arterial remodeling in stroke patients. *Stroke* 47, 434–440. doi: 10.1161/STROKEAHA.115.009955

Qiao, Y., Steinman, D. A., Qin, Q., Etesami, M., Schär, M., Astor, B. C., et al. (2011). Intracranial arterial wall imaging using three-dimensional high isotropic resolution black blood MRI at 3.0 Tesla. *J. Magn. Reson. Imaging* 34, 22–30. doi: 10.1002/jmri.22592

Robertson, J. J., and Koyfman, A. (2017). Extracranial cervical artery dissections. *Emerg. Med. Clin. North Am.* 35, 727–741. doi: 10.1016/j.emc.2017.06.006

Saam, T., Raya, J. G., Cyran, C. C., Bochmann, K., Meimarakis, G., Dietrich, O., et al. (2009). High resolution carotid black-blood 3T MR with parallel imaging and dedicated 4-channel surface coils. *J. Cardiovasc. Magn. Reson.* 11:64. doi: 10.1186/1532-429X-11-41

Traenka, C., Dougoud, D., Simonetti, B. G., Metso, T. M., Debette, S., Pezzini, A., et al. (2017). Cervical artery dissection in patients =60 years: often painless, few mechanical triggers. *Neurology* 88, 1313–1320. doi: 10.1212/WNL.0000000000003788

Wu, Y., Wu, F., Liu, Y., Fan, Z., Fisher, M., Li, D., et al. (2019). High-resolution magnetic resonance imaging of cervicocranial artery dissection. *Stroke* 50, 3101–3107. doi: 10.1161/STROKEAHA.119.026362

Yamada, S., Ohnishi, H., Takamura, Y., Takahashi, K., Hayashi, M., Kodama, Y., et al. (2016). Diagnosing intra-cranial and cervical artery dissection using MRI as the initial modality. *J. Clin. Neurosci.* 33, 177–181. doi: 10.1016/j.jocn.2016.03.038

Yin, Y.-C. C. A. X. (2017). A high-resolution MRI study of relationship between remodeling patterns and ischemic stroke in patients with atherosclerotic middle cerebral artery stenosis. *Front. Aging Neurosci.* 9:140. doi: 10.3389/fnagi.2017.00140

Zhao, H., and Zhu, Y. Z. A. C. (2021). Intracranial atherosclerotic plaque characteristics and burden associated with recurrent acute stroke: a 3D quantitative vessel wall MRI Study. *Front. Aging Neurosci.* 13:706544. doi: 10.3389/fnagi.2021.706544

Zhu, X., Qiu, H., Hui, F. K., Zhang, Y., Liu, Y.-E., Man, F., et al. (2020). Practical value of three-dimensional high resolution magnetic resonance vessel wall imaging in identifying suspicious intracranial vertebrobasilar dissecting aneurysms. *BMC Neurol.* 20:199. doi: 10.1186/s12883-020-01779-0

Zhu, X.-J., Wang, W., and Liu, Z.-J. (2016). High-resolution magnetic resonance vessel wall imaging for intracranial arterial stenosis. *Chin. Med. J.* 129, 1363–1368. doi: 10.4103/0366-6999.182826

Conflict of Interest: The authors declare that the research was conducted in the absence of any commercial or financial relationships that could be construed as a potential conflict of interest.

The reviewer QY declared a shared parent affiliation with the authors, XJZ to the handling editor at the time of review.

frontiers | Frontiers in Aging Neuroscience

MINI REVIEW
published: 07 July 2022
doi: 10.3389/fnagi.2022.921809

Neurofilament Light Chain: A Candidate Biomarker of Perioperative Stroke

Xiaoting Zhang[1†], Huixian Wang[1†], Li Li[2], Xiaoming Deng[1] and Lulong Bo[1]*

[1] Faculty of Anesthesiology, Changhai Hospital, Naval Medical University, Shanghai, China, [2] Department of Anesthesiology, Affiliated Beijing Friendship Hospital, Capital Medical University, Beijing, China

Perioperative stroke is defined as a brain infarction of ischemic or hemorrhagic etiology that occurs during surgery or within 30 days after surgery. However, identifying perioperative stroke is challenging. Thus, the discovery and validation of neurological biomarkers for perioperative stroke are urgently needed. Neurofilament forms part of the neuronal cytoskeleton and is exclusively expressed in neurons. After disease-related neuroaxonal damage occurs, neurofilament light chain protein is released into the cerebrospinal fluid and blood. Blood neurofilament light chain has recently been shown to serve as a potential marker of interest during the perioperative period. Therefore, the aim of the present review was to give an overview of the current understanding and knowledge of neurofilament light chain as a potential biomarker of perioperative stroke.

Keywords: perioperative, stroke, neurofilament light chain, expression, biomarker

OPEN ACCESS

Edited by:
Yu-Min Kuo,
National Cheng Kung University, Taiwan

Reviewed by:
Tian Zhang,
First Affiliated Hospital of Zhengzhou University, China
Li Tan,
Fudan University, China
Kai Zhang,
The Affiliated Hospital of Xuzhou Medical University, China

***Correspondence:**
Lulong Bo
bartbo@smmu.edu.cn

† These authors have contributed equally to this work and share first authorship

Specialty section:
This article was submitted to Neuroinflammation and Neuropathy, a section of the journal Frontiers in Aging Neuroscience

Received: *16 April 2022*
Accepted: *14 June 2022*
Published: *07 July 2022*

Citation:
Zhang X, Wang H, Li L, Deng X and Bo L (2022) Neurofilament Light Chain: A Candidate Biomarker of Perioperative Stroke. Front. Aging Neurosci. 14:921809. doi: 10.3389/fnagi.2022.921809

INTRODUCTION

With the development of an aging population, surgical case volumes have gradually increased annually. Compared with other perioperative complications, perioperative stroke is a potentially devastating, and relatively under-recognized neurological complication of surgery with high mortality and morbidity. The incidence of perioperative stroke varies among different types of surgical procedures and populations. It is approximately 0.1–1.9% in patients undergoing non-cardiac or non-neurological surgery, compared to 1.9–9.7% in patients undergoing high-risk cardiovascular or neurological surgery (Al-Hader et al., 2019). Compared to community-onset stroke, perioperative stroke is a serious medical emergency, represents a significant public health burden, and usually has unfavorable outcomes (Benesch et al., 2021).

Based on the guidelines of the Society for Neuroscience in Anesthesiology and Critical Care, perioperative stroke is defined as a brain infarction of ischemic or hemorrhagic etiology that occurs during surgery or within 30 days after surgery (Vlisides et al., 2020). Perioperative stroke can develop intraoperatively or postoperatively after recovery from anesthesia (Vlisides et al., 2020). However, identifying perioperative stroke is sometimes challenging due to its pathogenesis is multifactorial. The evaluation of neurological outcome of patients can sometimes be affected by the residual effects of anesthetic agents and medications, certain underlying metabolic causes, and symptoms related to cerebral irritation such as delirium and agitation (Misal et al., 2016).

Many risk factors have been identified and associated with perioperative stroke such as age, previous stroke, male sex, obesity, diabetes mellitus, atrial fibrillation, hypertension, smoking, physical inactivity, and acute stress (Nagre, 2018). Several screening tools for stroke have been available for the postoperative period such as the modified National Institutes of Health Stroke Scale

Abbreviations: CSF, cerebrospinal fluid; EVT, endovascular thrombectomy; NfH, neurofilament heavy chain; NfL, neurofilament light chain; NfM, neurofilament medium chain.

(mNIHSS), although its validity has not been verified in surgical populations (Sun et al., 2016). Thus, the prevention, early identification, and proper management of perioperative stroke are of vital importance.

A biomarker is a defined characteristic that is measured as an indicator of normal, biological, pathogenic processes, or responses to an exposure or intervention (Califf, 2018). Considerable interest exists in reliable neurological biomarkers with the hope that they will improve the accuracy of differential diagnosis and prognostic assessment, as well as predict the severity of the adverse outcomes of perioperative stroke. Thus, the discovery and validation of neurological biomarkers for perioperative stroke are urgently needed, which will be useful for subsequent clinical management.

Neurofilament forms the neuronal cytoskeleton and is exclusively expressed in neurons. After disease-related neuroaxonal damage occurs, neurofilament light chain (NfL) protein is released into the cerebrospinal fluid (CSF) and, to a smaller extent, in the peripheral blood (Khalil et al., 2018; Uphaus et al., 2019). Accumulating evidence has illustrated that NfL changes more significantly in the occurrence and development of various nervous system diseases, which indicates that NfL is an emerging marker of neuronal and axonal injury, and thus has important significance for the diagnosis and prognosis of various diseases (Teunissen et al., 2022). Blood levels of NfL has recently been shown to serve as a potentially interesting marker during the perioperative period. Therefore, the aim of the present review was to give an overview on the current knowledge and understanding of NfL as a potential biomarker of perioperative stroke.

STRUCTURE, FUNCTION, AND MEASUREMENT OF NEUROFILAMENT LIGHT CHAIN

Neurofilament heteropolymers are major cytoskeletal components of axons. They are responsible for axoplasmic transport, thereby maintaining the normal morphology of neurons and the elasticity of nerve fibers, preventing their breakage, and promoting the radial growth of axons (Lee et al., 1993). A neurofilament is composed of an NfL, a neurofilament medium chain (NfM), and a neurofilament heavy chain (NfH). The C-terminal of the NfM and NfH has 483 amino acids and 676 amino acids, respectively; therefore, the molecular weight of NfL is far less than that of NfM and NfH, which is 68, 150, and 190–210 kDa, respectively (Yuan et al., 2012).

NfL is the only neurofilament protein that can self-assemble functional fibers. Moreover, the abnormal expression of NfL and the mutation of human NfL gene can cause a variety of diseases. A large number of clinical and experimental studies (Barro et al., 2020; Biernacki et al., 2022) have illustrated that the level of NfL changes more significantly in the occurrence and development of various nervous system diseases. This finding suggests that NfL is a molecular marker of neuronal and axonal injury, which has important guiding significance for the diagnosis and prognosis of a variety of neurological disorders.

NfL has emerged as a biomarker candidate for neurodegenerative pathology in a number of neurological diseases. Under pathological conditions, the amount of NfL released depends on the severity of axon injury and is released into peripheral blood at a low concentration. With the development and progress of immunoassay technology, remarkable progress has been made in the detection of NfL (Thebault et al., 2021). Accurate measurement of its concentration can help in the understanding of the development of many diseases. CSF sampling is clinically a traumatic examination, and CSF samples are not easy to obtain as are peripheral blood samples. Previous detection methods have primarily used enzyme-linked immunosorbent assay to determine the concentration of NfL in CSF. Since the concentration of NfL in blood is only 1/40 of the content of CSF, the sensitivity of the ELISA assay is not enough and it is difficult to meet the requirements when used in the detection of blood NfL. With the introduction of third-generation electrochemiluminescence technology, the analytical sensitivity has been greatly improved (Zanut et al., 2020). In recent years, the latest generation of single-molecule array (SiMoA) technology allows the recognition resolution of ultra-high molecular signal and the detection of single molecule through digital signal output form. It is convenient for the wide application of blood NfL detection for clinical and experimental use. With the advent of SiMoA technology, reliable quantification of low NfL concentrations in the peripheral blood became available (Kuhle et al., 2016). This cutting-edge technique facilitated the comprehensive study of this protein as a diagnostic and prognostic marker in various acute and chronic neurological disorders.

Factors other than neuroaxonal damage may also contribute to the increase in blood NfL is important to highlight. NfL increases in normal aging, paralleled by a higher variability in the elderly population. Thus, correctly interpreting this marker on an individual level is difficult. Some evidence also suggests that blood NfL may be influenced by body mass index, blood volume, and renal function. Koini et al. (2021) explored factors influencing the blood NfL concentration by analyzing a large set of demographic, lifestyle, and clinical variables in a normal aging cohort that included 327 neurologically inconspicuous individuals. Their results showed that age was, by far, the most important factor influencing blood NfL concentration, which was primarily driven by individuals $\geq$ 60 years. In individuals $\geq$ 60 years, age, blood volume, renal function, and high density lipoprotein were associated with blood NfL levels, although at a much lower scale to influence blood NfL. Body mass index independently predicted blood NfL in individuals aged 38–60 years (Koini et al., 2021). A speculation is that the increase in blood NfL in a normal aging cohort was associated with brain volume loss over time, thereby supporting the notion that other factors beyond normal aging may also contribute to the increase in blood NfL concentrations in older individuals (i.e., $>$ 60 years; Khalil et al., 2020).

NfL is a sensitive but non-specific marker of brain injury. Fohner et al. explored the association of blood NfL and magnetic resonance imaging (MRI) findings in older adults.

Their longitudinal cohort study included two cranial MRI scans conducted approximately 5 years apart and assessed for white matter hyperintensities and infarcts. Among older adults without a history of stroke, higher blood NfL concentration was associated with the covert MRI findings of vascular brain injury, especially the burden of white matter hyperintensities and its worsening (Fohner et al., 2022).

NEUROFILAMENT LIGHT CHAIN AND PERIOPERATIVE STROKE

For surgical patients, especially those at high risk of stroke, the early detection of perioperative stroke will greatly benefit the patient's perioperative prognosis and functional outcomes (Ko, 2018). Patients with symptoms of transient ischemic attacks and clinical signs of stroke constitute only a small fraction of patients experiencing perioperative stroke. Perioperative stroke can occur in the forms of overt or covert stroke, with the latter being dominant; therefore, many patients with perioperative stroke are not identified or detected in time. Diffusion-weighted MRI has high sensitivity and specificity in relevant changes in brain imaging. However, this method is time-consuming, expensive, and of limited value for repeated monitoring, which may limit its clinical use. Several neurological biomarkers have been identified and their use during the perioperative period has been explored. More in-depth studies of neurological biomarkers may help to identify patients at high risk of perioperative stroke, including neurological impairment and vulnerability.

Learning from previous studies on biomarkers of community-onset stroke is worthwhile and can provide hints for identifying biomarkers for perioperative stroke. A series of studies (Pedersen et al., 2019; Pekny et al., 2021) indicate that blood NfL levels are increased in the acute phase after stroke and peak during the initial 3 months. A few studies (Stokowska et al., 2021) have demonstrated that blood NfL can serve as a predictor of functional improvement in the late phase after stroke. Patients with higher blood NfL, compared to patients with lower blood NfL, had a 1.71 times higher risk of poor functional outcomes during follow-up after ischemic stroke (Liu et al., 2020). A recent review summarized the findings of recent literature exploring the blood NfL level in the acute and post-acute phase after stroke (Pekny et al., 2021). Blood NfL also serves as a predictor of adaptive neural plasticity and functional improvement in the late phase after stroke. A conclusion is that high blood NfL levels in the acute phase after stroke can predict unfavorable outcomes. However, previous studies have rarely evaluated the role of NfL in perioperative periods, especially its role in perioperative stroke.

Chen et al. (2021) found that blood NfL predicts the outcomes in stroke patients receiving endovascular thrombectomy (EVT). Their study included 60 patients receiving EVT for acute ischemic stroke with large vessel occlusion type and focused on changes in the levels of blood NfL, GFAP, tau, and ubiquitin carboxyl-terminal esterase L1 before EVT, immediately after EVT, and 24 h after EVT. Higher blood NfL levels before, immediately after EVT, and 24 h after EVT were associated death or disability at 90 days.

Rahmig et al. (2021) in their prospective study analyzed blood NfL levels in patients undergoing EVT for anterior circulation large vessel occlusion. The blood NfL level was serially measured before EVT and at 30 min, 6 h, 12 h, 24 h, 48 h, and 7 days after EVT. No differences existed among the serial blood NfL levels in the first 12 h post-EVT; however, a constant increase was observed afterward. Serum NfL may complement clinical and imaging predictors of treatment response and functional outcome in stroke patients undergoing EVT for anterior circulation large vessel occlusion (Rahmig et al., 2021).

Alifier et al. (2020) found that patients who had cardiac surgery had higher blood NfL levels than did patients who underwent other operations and that patients who experienced cardiopulmonary bypass had even higher levels. Their results indicated that blood NfL levels may guide the development of surgical procedures to minimize neuronal damage and may be used in longitudinal clinical studies to evaluate the relationship of surgery with future neurocognitive impairment. Saller et al. (2019) observed a sharp postoperative increase in blood NfL in cardiac surgery patients with cardiopulmonary bypass with the highest levels occurring in patients with delirium. A speculation is that surgery or trauma can induce a neuroinflammatory response and microglia activation, thereby eventually leading to neuronal damage. Thus, blood NfL may be of benefit to identify cardiac surgery patients at risk of delirium and to detect individuals with the postoperative emergence of delirium.

A recent study (Zhang et al., 2021) indicated that the median blood NfL level of patients with an acute type A aortic dissection who had a stroke 12 h after surgery was nearly double that of patients who did not have a stroke postoperatively. Patients with stroke had a higher baseline value than did non-stroke patients. Their study interestingly did not find changes in S100β protein or in neuron-specific enolase in patients with stroke. To the best of our knowledge, the Zhang study was the first to evaluate the role of blood NfL as an early and sensitive biomarker for predicting perioperative stroke, particularly 12 h after surgery. Thus, further studies are needed to validate whether the blood NfL can be used as a biomarker for postoperative stroke.

Whether blood NfL is better than other biomarkers such as S100 and neuron-specific enolase in the prediction and prognosis of perioperative stroke would also be interesting to know. No study has perioperatively compared blood NfL and other biomarkers, although the findings from studies on community-onset stroke could provide valuable insights. The area under the curve of blood NfL for the prediction of cardiovascular events and functional outcome 90 days after acute ischemic stroke has been reported as significantly higher than that of S100, N-terminal pro-brain natriuretic peptide, atrial natriuretic peptide, and fatty acid–binding proteins (Uphaus et al., 2019). A recent study (Chen et al., 2021) reported that blood NfL, tau, and glial fibrillary acidic protein increased over time in patients after EVT in anterior circulation stroke. Blood tau and glial fibrillary acidic protein levels peaked at 24–72 h and were lower at 3 months after stroke, whereas blood NfL levels continued to increase at 3 months, which

makes it a promising biomarker for prognostic prediction after stroke.

Covert strokes represent brain infarcts that are not recognized acutely because of unappreciated, subtle, or misclassified manifestations but are detected on brain imaging. Covert stroke is more common than overt stroke in the non-operative setting, which raises the possibility that covert strokes may occur after non-cardiac surgery. The NeuroVISION study (Mrkobrada et al., 2019) was a prospective cohort study conducted in 12 academic centers in nine countries. In the study, 1114 patients aged 65 years or older who underwent in-hospital, elective, non-cardiac surgery were included and underwent brain MRI after surgery. The NeuroVISION study demonstrated that 7% of patients had a perioperative covert stroke, which was associated with an increased risk of perioperative delirium and cognitive decline at 1 year (Mrkobrada et al., 2019). However, the availability of MRI scanners may limit the immediate evaluation of underlying perioperative stroke. Casey et al. found that postoperative delirium, occurred at least once during the postoperative periods of 1–4 days, is associated with a greater rise in NfL on postoperative day 1 than in participants who did not have delirium (Casey et al., 2020).

The Casey study suggests that the incidence of perioperative covert stroke is relatively high and may have been underestimated previously. It also identified a link between perioperative covert stroke and cognitive decline in surgical populations. Thus, research aimed at determining whether postoperative delirium is the manifestation form of perioperative covert stroke is attracting increasing research interest. If appropriate biomarkers are available, patients at risk can be timely screened and accurately assessed preoperatively, thereby allowing for a more accurate and desirable anesthesia plan.

Recent data exploring the potential role of covert perioperative stroke in postoperative delirium and cognitive function have opened up a whole new range of research area (Cui et al., 2020). Evaluating the neurological condition of postoperative patients is usually difficult because of sedation or mechanical ventilation and because moving these patients may be inappropriate. Thus, a promising and potential biomarker reflecting brain damage will be of great value and provide valuable information to help in the clinical management of patients.

The Successful Aging after Elective Surgery Study examined the association of the levels of plasma NfL, total tau, glial fibrillary acid protein, and ubiquitin carboxyl-terminal hydrolase L1 with delirium, delirium severity, and cognitive performance in older adults without dementia who are undergoing major elective surgery (Fong et al., 2020). The results indicated that patients with delirium had higher NfL levels postoperatively. Patients with the highest preoperative or postoperative day 2 blood NfL levels were more likely to develop into delirium. Elevated blood NfL at 1 month after surgery was associated with delirium and greater cognitive decline. These findings suggest that blood NfL may be useful as a biomarker for predicting the risk of delirium and long-term cognitive decline and, once confirmed, would provide pathophysiological insights and new evidence on neuroaxonal injury after delirium (Fong et al., 2020).

Results from the Cerebrospinal Fluid and Preclinical Alzheimer Cognitive Trajectory (CAPACITY) and the Assessment and Review of Cognition, Alzheimer's Disease, and Inflammation in Elderly Patients After Hospital Intervention (ARCADIAN) studies found that the mean blood NfL increased postoperatively to a maximal level at 48 h (Evered et al., 2018). Tau levels also increased significantly from baseline with a peak increase at 6 h postoperatively, after which they declined but remained elevated for at least 48 h. A significant and rapid increase in blood NfL and tau occurred in response to anesthesia and surgery, regardless of the type of anesthesia or surgery. The changes in blood NfL reflect an acute response to the precipitating event of anesthesia and surgery, which may be more similar to acute traumatic brain injury. These findings indicate that general anesthesia and surgical procedures exert acute response to neuronal injury on the central nervous system, which has enlightenment for neurological outcomes and for the mechanisms underlying general anesthesia (Evered et al., 2018).

CONCLUSION AND FUTURE DIRECTIONS

Recognition of perioperative stroke is often difficult, particularly in the early stages. Perioperative stroke can present with only impaired consciousness and is usually in the differential diagnosis of delayed emergence after general anesthesia. A large knowledge gap remains with regard to perioperative stroke. The identification of reliable and effective biomarkers for perioperative stroke is an urgent and challenging task in clinical practice. Clinicians are more inclined to choose more effective and affordable screening methods for perioperative stroke, other than MRI scans.

An ideal biomarker should be accurate, non-invasive, and inexpensive. It should be easily measured in a standardized manner with a sensitivity and specificity of at least 80%. An important factor is that clinical management strategies could be determined, based on biomarker levels. Studies evaluating the role of perioperative NfL remain insufficient, although NfL levels measured during the perioperative period shows potential in identifying patients at risk of perioperative stroke, postoperative delirium, and cognitive dysfunction. Also worth considering is that the blood NfL level, as a biomarker of neuronal injury, which universally occurs after damage to nervous system, will increase in various neurological diseases. Nevertheless, blood NfL cannot be used to differentiate between diseases without the aid of clinical examinations and other laboratory and imaging studies. Furthermore, to understand the dynamics of blood NfL perioperatively, as well as its maximum serum concentration and half-life in blood, is of great significance. No clear answer to these questions exist. This issue needs to be clarified by further research.

To conclude, the measurement of blood NfL levels in clinical practice provides a relatively simple and quantitative method

to measure neuronal damage. Future studies will better define its optimal use in clinical practice, including the establishment of its reference range and a more complete understanding of the regulating mechanism responsible for the release of NfL in perioperative stroke.

AUTHOR CONTRIBUTIONS

XZ, HW, and LB contributed to the search and assessment of the available literature, and wrote the manuscript. LL and XD helped to revise the manuscript to the final form. All authors contributed to the article and approved the submitted version.

FUNDING

This work was supported by the Shanghai Science and Technology Committee Rising-Star Program (Shanghai, China; grant number: 19QA1408500) and the "234 Discipline Construction Climbing Plan" of the Changhai Hospital, Naval Medical University (Shanghai, China; grant number: 2020YXK053).

ACKNOWLEDGMENTS

We would like to thank Editage (www.editage.com) for English language editing.

REFERENCES

Al-Hader, R., Al-Robaidi, K., Jovin, T., Jadhav, A., Wechsler, L. R., and Thirumala, P. D. (2019). The incidence of perioperative stroke: estimate using state and national databases and systematic review. *J. Stroke* 21, 290–301. doi: 10.5853/jos.2019.00304

Alifier, M., Olsson, B., Andreasson, U., Cullen, N. C., Czyzewska, J., Jakubow, P., et al. (2020). Cardiac surgery is associated with biomarker evidence of neuronal damage. *J. Alzheimers Dis.* 74, 1211–1220. doi: 10.3233/JAD-191165

Barro, C., Chitnis, T., and Weiner, H. L. (2020). Blood neurofilament light: a critical review of its application to neurologic disease. *Ann. Clin. Transl. Neurol.* 7, 2508–2523. doi: 10.1002/acn3.51234

Benesch, C., Glance, L. G., Derdeyn, C. P., Fleisher, L. A., Holloway, R. G., Messe, S. R., et al. (2021). Perioperative neurological evaluation and management to lower the risk of acute stroke in patients undergoing noncardiac, nonneurological surgery: a scientific statement from the american heart Association/American stroke association. *Circulation* 143, e923–e946. doi: 10.1161/CIR.0000000000000968

Biernacki, T., Kokas, Z., Sandi, D., Füvesi, J., Fricska-Nagy, Z., Faragó, P., et al. (2022). Emerging biomarkers of multiple sclerosis in the blood and the CSF: a focus on neurofilaments and therapeutic considerations. *Int. J. Mol. Sci.* 23:3383. doi: 10.3390/ijms23063383

Califf, R. M. (2018). Biomarker definitions and their applications. *Exp. Biol. Med.* 243, 213–221. doi: 10.1177/1535370217750088

Casey, C. P., Lindroth, H., Mohanty, R., Farahbakhsh, Z., Ballweg, T., Twadell, S., et al. (2020). Postoperative delirium is associated with increased plasma neurofilament light. *Brain* 143, 47–54. doi: 10.1093/brain/awz354

Chen, C. H., Chu, H. J., Hwang, Y. T., Lin, Y. H., Lee, C. W., Tang, S. C., et al. (2021). Plasma neurofilament light chain level predicts outcomes in stroke patients receiving endovascular thrombectomy. *J. Neuroinflammation* 18:195. doi: 10.1186/s12974-021-02254-4

Cui, Q., Wang, D., Zeng, M., Dong, J., Jin, H., Hu, Z., et al. (2020). Association of postoperative covert stroke and cognitive dysfunction among elderly patients undergoing non-cardiac surgery: protocol for a prospective cohort study (PRECISION study). *BMJ Open* 10:e034657.

Evered, L., Silbert, B., Scott, D. A., Zetterberg, H., and Blennow, K. (2018). Association of changes in plasma neurofilament light and tau levels with anesthesia and surgery: results from the CAPACITY and ARCADIAN studies. *JAMA Neurol.* 75, 542–547. doi: 10.1001/jamaneurol.2017.4913

Fohner, A. E., Bartz, T. M., Tracy, R. P., Adams, H., Bis, J. C., Djousse, L., et al. (2022). Association of serum neurofilament light chain concentration and MRI findings in older adults: the cardiovascular health study. *Neurology* 98, e903–e911. doi: 10.1212/WNL.0000000000013229

Fong, T. G., Vasunilashorn, S. M., Ngo, L., Libermann, T. A., Dillon, S. T., Schmitt, E. M., et al. (2020). Association of plasma neurofilament light with postoperative delirium. *Ann. Neurol.* 88, 984–994. doi: 10.1002/ana.25889

Khalil, M., Pirpamer, L., Hofer, E., Voortman, M. M., Barro, C., Leppert, D., et al. (2020). Serum neurofilament light levels in normal aging and their association with morphologic brain changes. *Nat. Commun.* 11:812. doi: 10.1038/s41467-020-14612-6

Khalil, M., Teunissen, C. E., Otto, M., Piehl, F., Sormani, M. P., Gattringer, T., et al. (2018). Neurofilaments as biomarkers in neurological disorders. *Nat. Rev. Neurol.* 14, 577–589. doi: 10.1038/s41582-018-0058-z

Ko, S. B. (2018). Perioperative stroke: pathophysiology and management. *Korean J. Anesthesiol.* 71, 3–11. doi: 10.4097/kjae.2018.71.1.3

Koini, M., Pirpamer, L., Hofer, E., Buchmann, A., Pinter, D., Ropele, S., et al. (2021). Factors influencing serum neurofilament light chain levels in normal aging. *Aging* 13, 25729–25738. doi: 10.18632/aging.203790

Kuhle, J., Barro, C., Andreasson, U., Derfuss, T., Lindberg, R., Sandelius, Å, et al. (2016). Comparison of three analytical platforms for quantification of the neurofilament light chain in blood samples: ELISA, electrochemiluminescence immunoassay and Simoa. *Clin. Chem. Lab. Med.* 54, 1655–61. doi: 10.1515/cclm-2015-1195

Lee, M. K., Xu, Z., Wong, P. C., and Cleveland, D. W. (1993). Neurofilaments are obligate heteropolymers in vivo. *J. cell Biology.* 122, 1337–1350. doi: 10.1083/jcb.122.6.1337

Liu, D., Chen, J., Wang, X., Xin, J., Cao, R., and Liu, Z. (2020). Serum neurofilament light chain as a predictive biomarker for ischemic stroke outcome: a systematic review and meta-analysis. *J. Stroke Cerebrovasc. Dis.* 29:104813. doi: 10.1016/j.jstrokecerebrovasdis.2020.104813

Misal, U. S., Joshi, S. A., and Shaikh, M. M. (2016). Delayed recovery from anesthesia: a postgraduate educational review. *Anesth. Essays Res.* 10, 164–172. doi: 10.4103/0259-1162.165506

Mrkobrada, M., Chan, M. T. V., Cowan, D., Campbell, D., Wang, C. Y., Torres, D., et al. (2019). Perioperative covert stroke in patients undergoing non-cardiac surgery (NeuroVISION): a prospective cohort study. *Lancet* 394, 1022–1029. doi: 10.1016/S0140-6736(19)31795-7

Nagre, A. S. (2018). Perioperative stroke - Prediction. Prevention, and Protection. *Indian J. Anaesth.* 62, 738–742. doi: 10.4103/ija.IJA_292_18

Pedersen, A., Stanne, T. M., Nilsson, S., Klasson, S., Rosengren, L., Holmegaard, L., et al. (2019). Circulating neurofilament light in ischemic stroke: temporal profile and outcome prediction. *J. Neurol.* 266, 2796–2806. doi: 10.1007/s00415-019-09477-9

Pekny, M., Wilhelmsson, U., Stokowska, A., Tatlisumak, T., Jood, K., and Pekna, M. (2021). Neurofilament light chain (NfL) in Blood-A biomarker predicting unfavourable outcome in the acute phase and improvement in the late phase after stroke. *Cells* 10:1537. doi: 10.3390/cells10061537

Rahmig, J., Akgün, K., Simon, E., Gawlitza, M., Hartmann, C., Siepmann, T., et al. (2021). Serum neurofilament light chain levels are associated with stroke severity and functional outcome in patients undergoing endovascular therapy for large vessel occlusion. *J. Neurol. Sci.* 429:118063. doi: 10.1016/j.jns.2021.118063

Saller, T., Petzold, A., Zetterberg, H., Kuhle, J., Chappell, D., von Dossow, V., et al. (2019). A case series on the value of tau and neurofilament protein levels to predict and detect delirium in cardiac surgery patients. *Biomed. Pap. Med. Fac. Univ. Palacky Olomouc Czech. Repub.* 163, 241–246. doi: 10.5507/bp.2019.043

Stokowska, A., Bunketorp Käll, L., Blomstrand, C., Simrén, J., Nilsson, M., Zetterberg, H., et al. (2021). Plasma neurofilament light chain levels predict improvement in late phase after stroke. *Eur. J. Neurol.* 28, 2218–2228. doi: 10.1111/ene.14854

Sun, Z., Yue, Y., Leung, C. C., Chan, M. T., and Gelb, A. W. (2016). Clinical diagnostic tools for screening of perioperative stroke in general surgery: a systematic review. *Br. J. Anaesth.* 116, 328–338. doi: 10.1093/bja/aev452

Teunissen, C. E., Verberk, I., Thijssen, E. H., Vermunt, L., Hansson, O., Zetterberg, H., et al. (2022). Blood-based biomarkers for Alzheimer's disease: towards clinical implementation. *Lancet Neurol.* 21, 66–77. doi: 10.1016/S1474-4422(21)00361-6

Thebault, S., Booth, R. A., Rush, C. A., MacLean, H., and Freedman, M. S. (2021). Serum neurofilament light chain measurement in MS: hurdles to clinical translation. *Front. Neurosci.* 15:654942. doi: 10.3389/fnins.2021.654942

Uphaus, T., Bittner, S., Groschel, S., Steffen, F., Muthuraman, M., Wasser, K., et al. (2019). NfL (Neurofilament light chain) levels as a predictive marker for Long-Term outcome after ischemic stroke. *Stroke* 50, 3077–3084. doi: 10.1161/STROKEAHA.119.026410

Vlisides, P. E., Moore, L. E., Whalin, M. K., Robicsek, S. A., Gelb, A. W., Lele, A. V., et al. (2020). Perioperative care of patients at high risk for stroke during or after non-cardiac, non-neurological surgery: 2020 guidelines from the society for neuroscience in anesthesiology and critical care. *J. Neurosurg. Anesth.* 32, 210–226. doi: 10.1097/ANA.0000000000000686

Yuan, A., Rao, M. V., Veeranna, and Nixon, R. A. (2012). Neurofilaments at a glance. *J. Cell Sci.* 125, 3257–3263. doi: 10.1242/jcs.104729

Zanut, A., Fiorani, A., Canola, S., Saito, T., Ziebart, N., Rapino, S., et al. (2020). Insights into the mechanism of coreactant electrochemiluminescence facilitating enhanced bioanalytical performance. *Nat. Commun.* 11:2668. doi: 10.1038/s41467-020-16476-2

Zhang, K., Wang, Z., Zhu, K., Dong, S., Pan, X., Sun, L., et al. (2021). Neurofilament light chain protein is a predictive biomarker for stroke after surgical repair for acute type a aortic dissection. *Front Cardiovasc. Med.* 8:754801. doi: 10.3389/fcvm.2021.754801

Conflict of Interest: The authors declare that the research was conducted in the absence of any commercial or financial relationships that could be construed as a potential conflict of interest.

Publisher's Note: All claims expressed in this article are solely those of the authors and do not necessarily represent those of their affiliated organizations, or those of the publisher, the editors and the reviewers. Any product that may be evaluated in this article, or claim that may be made by its manufacturer, is not guaranteed or endorsed by the publisher.

frontiers | Frontiers in Aging Neuroscience

ORIGINAL RESEARCH
published: 11 July 2022
doi: 10.3389/fnagi.2022.885680

DNA Methylation of Patatin-Like Phospholipase Domain-Containing Protein 6 Gene Contributes to the Risk of Intracranial Aneurysm in Males

Shengjun Zhou[1,2], Junjun Zhang[1], Chenhui Zhou[1,2], Fanyong Gong[1], Xueli Zhu[3], Xingqiang Pan[4], Jie Sun[1], Xiang Gao[1]* and Yi Huang[1,2,5]**

[1]Department of Neurosurgery, Ningbo First Hospital, Ningbo, China, [2]Key Laboratory of Precision Medicine for Atherosclerotic Diseases of Zhejiang Province, Ningbo, China, [3]Department of Ultrasound, Ningbo First Hospital, Ningbo, China, [4]Ningbo Center for Disease Control and Prevention, Ningbo, China, [5]Medical Research Center, Ningbo First Hospital, Ningbo, China

OPEN ACCESS

Edited by:
Li Li,
Capital Medical University, China

Reviewed by:
Jia Cheng,
Zhongshan Hospital of Xiamen University, China
Fan Xia,
Sichuan University, China

***Correspondence:**
Jie Sun
nbyysj@sina.com
Xiang Gao
qinyuecui@163.com
Yi Huang
huangy102@gmail.com

Specialty Section:
This article was submitted to Neuroinflammation and Neuropathy, a section of the journal Frontiers in Aging Neuroscience

Received: *28 February 2022*
Accepted: *17 June 2022*
Published: *11 July 2022*

Citation:
Zhou S, Zhang J, Zhou C, Gong F, Zhu X, Pan X, Sun J, Gao X and Huang Y (2022) DNA Methylation of Patatin-Like Phospholipase Domain-Containing Protein 6 Gene Contributes to the Risk of Intracranial Aneurysm in Males. Front. Aging Neurosci. 14:885680. doi: 10.3389/fnagi.2022.885680

Objective: This study is aimed to investigate the contribution of patatin-like phospholipase domain-containing protein 6 (*PNPLA6*) DNA methylation to the risk of intracranial aneurysm (IA) in the Han Chinese population.

Methods: A total of 96 age- and sex-matched participants were recruited to evaluate *PNPLA6* methylation *via* bisulfite pyrosequencing. The *PNPLA6* mRNA expression in the plasma was determined using real-time quantitative reverse transcription-polymerase chain reaction. Human primary artery smooth muscle cells (HPCASMC) were used for the in vitro function study.

Results: *PNPLA6* methylation was significantly higher in patients with IA than in healthy controls ($p < 0.01$). Sex group analysis showed that this correlation appeared in the male group ($p < 0.01$) but not in the female group ($p > 0.05$). *PNPLA6* methylation was significantly associated with age in all participants ($r = 0.306$, $p = 0.003$) and in the control group ($r = 0.377$, $p = 0.008$) but not in the IA group ($r = 0.127$, $p = 0.402$). Furthermore, the *PNPLA6* mRNA expression significantly decreased in patients with IA than that in the controls ($p = 0.016$). *PNPLA6* expression was significantly inversely correlated with elevated DNA methylation in participants ($r = -0.825$, $p < 0.0001$). In addition, *PNPLA6* transcription was significantly enhanced following treatment with 5-aza-2'-deoxycytidine methylation inhibitor in HPCASMC.The receiver operating characteristic analyses of curves showed that the *PNPLA6* mean methylation [area under the curve (AUC) = 0.74, $p < 0.001$] and mRNA expression (AUC = 0.86, $p < 0.001$) could have a diagnostic value for patients with IA.

Conclusion: Although future functional experiments are required to test our hypothesis, our study demonstrated that *PNPLA6* methylation and mRNA expression were significantly associated with the risk of IA; thus, they show potential for use in the early diagnosis of IA.

Keywords: PNPLA6, DNA methylation, mRNA expression, age, intracranial aneurysms

INTRODUCTION

Intracranial aneurysm (IA) is a common cerebrovascular disease with an extremely high mortality (Lu et al., 2021). Its incidence is greater than 7% in the Chinese population aged >35 years old (Li et al., 2013). IA is a complex disease with genetic and environmental risk factors (Bakker et al., 2020; Lu et al., 2021). Tobacco and alcohol consumption, high-fat diet, age, sex, and other factors can increase the risk of IA by affecting the expression of related genes (Bakker et al., 2020; Wang et al., 2021). However, the mechanisms underlying IA pathogenesis are not yet fully understood.

DNA methylation often occurs in cytosine-phosphate-guanine (CpG) dinucleotide sequences in the mammalian genome (Moore et al., 2013). Its levels can be influenced by external factors, which can alter DNA stability, as well as its ability to interact with proteins (Zocher et al., 2021). It can regulate the expression of numerous genes, and aberrant gene methylation plays a vital role in the development of multiple diseases (Deng et al., 2019). In addition, DNA methylation and the binding of its effector proteins to methylated DNA are essential for vascular function and development (Rao et al., 2011). DNA methylation may also participate in the development of IA by regulating the expression of genes involved in inflammatory reactions, cell function, and cell signal transduction (Yu et al., 2017).

Patatin-like phospholipase domain-containing protein 6 (*PNPLA6*) is a phospholipase that deacetylates intracellular phosphatidylcholine to produce glycerophosphatidylcholine (Richardson et al., 2013). *PNPLA6* is located on human chromosome 19p13.2, which contains 37 exons and multiple mutation sites (Richardson et al., 2020). *PNPLA6* mutations are associated with many diseases (Sen et al., 2020; Wu et al., 2021) and are involved in several disorders in adult organisms and embryos (Emekli et al., 2021; Suchowersky et al., 2021). The content of the *PNPLA6* in the brain plays an important role in the balance of brain function. Loss of *PNPLA6* activity leads to abnormally elevated levels of phosphatidylcholine in the brain and damages the secretory pathway in neurons (Pamies et al., 2014b). *PNPLA6* has also been associated with chorioretinal dystrophy (Dogan et al., 2021), Parkinson's syndrome (Sen et al., 2020), and nerve lesions (Richardson et al., 2020). *PNPLA6* likely participates in the development of neural and vascular systems in living organisms (Moser et al., 2004; Chang and Wu, 2010). Silencing the expression of *PNPLA6* causes a series of changes in functional pathways, which eventually leads to lesions in cerebrovascular system (Pamies et al., 2014a,b). IA is a cerebrovascular disease in which the walls of cerebral arteries are abnormally prominent. However, the investigation into the association between *PNPLA6* and pathological changes in arterial vessels is lacking.

In this study, we hypothesized that *PNPLA6* DNA methylation contributes to IA risk. We aimed to test the association between *PNPLA6* DNA methylation and IA in Han Chinese individuals. We also investigated the relationships among *PNPLA6* mRNA, DNA methylation, and age in homogeneous samples.

MATERIALS AND METHODS

Sample Collection

A total of 96 age- and sex-matched individuals were recruited from the Ningbo First Hospital for the case-control study. The participants' clinical data including age, triglycerides (TG), total cholesterol (TC), high-density lipoprotein (HDL), and low-density lipoprotein (LDL) were reported in previous studies (Wang et al., 2021). The case group was diagnosed using cerebral angiography or magnetic resonance imaging. The control group was composed of healthy subjects. Those with cardiovascular and cerebrovascular, severe liver and kidney, and other diseases were excluded. All study protocols were approved by the Ethics Committee of Ningbo First Hospital. Peripheral blood was collected from participants and coagulated at 4°C and 3,000 rpm for 15 min. The upper plasma and peripheral blood mononuclear cells were carefully aspirated for subsequent experiments.

Pyrosequencing Assay

An automatic nucleic acid extractor (Lab-Aid 820, Xiamen, China) was used to extract DNA from peripheral blood mononuclear cells. The DNA was subjected to quality control using a NanoDrop 2000 spectrophotometer (Thermo Fisher Scientific Inc., MA, USA). Bisulfite transformation was performed using an Epi Tech DNA bisulfite kit (Qiagen, Hilden, Germany). DNA methylation levels were measured using a PyroMark Q96 ID System (Qiagen). Five CpG dinucleotides on the fragment (GRCh37/hg19, Chr19: 7, 615, 203–7, 615, 727) with *PNPLA6* were chosen to measure methylation levels. Polymerase chain reaction (PCR) amplification primers were designed using the PyroMark Assay Design software v2.0.1.15 (Qiagen). The sequences of the PCR primers were as follows: forward primer, 5′-Biotin-GGATTTGGGGGTGGTTAGA-3′; reverse primer, 5′- TACTCCCCCACCAACTCCTTCT-3′; and sequencing primer, 5′-ACCAACTCCTTCTTAC-3′.

Quantitative Real-Time (qRT)-PCR

Among the included samples, 18 IA patients (nine males and nine females) and 18 sex-age-matched controls (nine males and nine females) were selected for RNA expression detection. Total RNA was isolated from plasma using TRIzol reagent (Invitrogen, CA, USA) and then reverse transcribed into cDNA using a high-capacity cDNA reverse transcription kit (Applied Biosystems, CA, USA). qRT-PCR amplification was performed on a LightCycler 480 system (Roche, Mannheim, Germany) by using an SYBR Green Master Mix kit (TaKaRa, Dalian, China). The transcription of *PNPLA6* was normalized to that of *ACTB*. The primer sequences for *PNPLA6* (Zhong et al., 2018) and *ACTB* (Cheng et al., 2022) were as follows: *PNPLA6* (forward) 5′-CCAAGAGTTCCGGCTGTCA-3′, (reverse) 5′-CACAATGAGGATGCAGTCGG-3′; ACTB (forward) 5′-AGCACAGAGCCTCGCCTT-3′, (reverse) 5′-CATCATCCATGGTGAGCTGG-3′.

Cell Culture and 5-Aza-2'-Deoxycytidine Treatment

Human primary artery smooth muscle cells (HPCASMC; http://www.atcc.org/Products/All/PCS-100-021.aspx) were used for the in vitro studies. Cells were cultured at a density of 1×10^6 cells/well in 6-well plates using Dulbecco's modified eagle's medium (DMEM) with 10% fetal bovine serum (FBS) and penicillin/streptomycin (Invitrogen, MA, USA) at 37°C for 24 h. The medium was changed every 6–8 h. 5-aza-2'-deoxycytidine (AZA) was used to examine the potential regulatory role of DNA methylation in *PNPLA6* gene transcription. Cells were treated with three different concentrations of AZA (0.5, 1.0, and 2.0 μM), and RNA was collected three days later for gene expression assays.

Statistical Analyses

Statistical and figure analyses were performed using GraphPad Prism version 8.0 (La Jolla, CA, USA). The DNA methylation levels between the two groups were compared using paired statistical tests and presented as violin plots. Power and sample size calculation software (Nashville, TN, USA) was used for the power analysis. Correlations between mRNA expression, DNA methylation, age, TG, TC, HDL, and LDL were analyzed using Pearson's correlation test. A receiver operating characteristic (ROC) curve was used to evaluate the sensitivity of *PNPLA6* methylation in IA diagnosis. A two-sided $p < 0.05$ was considered significant.

RESULTS

A total of 48 subjects with IA (24 males and 24 females, mean age: 48.08 ± 5.69 years) and 48 controls (24 males and 24 females, mean age: 46.63 ± 6.04 years, $p > 0.05$) were recruited. The clinical information including TG, TC, HDL, and LDL was presented in our previous study (Wang et al., 2021) and was not statistically different between IA and control groups ($p > 0.05$). The five selected CpG dinucleotides on the fragment (GRCh37/hg19, Chr19: 7, 615, 203–7, 615, 727) with *PNPLA6* in the methylation assay are shown in **Figure 1**. The DNA methylation levels in the five CpG dinucleotides significantly correlated with each other in all participants (**Figure 2**, $p < 0.01$). There were no significant associations between *PNPLA6* methylations and clinical data such as TG, TC, HDL, and LDL (**Figure 2**, $p > 0.05$). *PNPLA6* methylation was significantly higher in patients with IA than in healthy controls (CpG1, $p = 0.016$, CpG2, $p = 0.040$, CpG3, $p = 0.018$, CpG4, $p = 0.003$ and mean methylation, $p = 0.016$, **Figure 3A**). Power analysis showed that the CpGs methylation had more than 80% power to detect the significant associations based on the nominal type I error rate of 0.01. Sex group analysis showed that this correlation only appeared in the male group (CpG1, $p = 0.001$, CpG2, $p < 0.001$, CpG3, $p = 0.006$, CpG4, $p = 0.003$, CpG5, $p = 0.034$ and mean methylation, $p = 0.002$, **Figure 3B**) but not in the female group (CpG1–5 and mean methylation, $p > 0.05$, **Figure 3C**). Subsequent sex comparison analysis showed no sex difference between the control (CpG1–5 and mean methylation, $p > 0.05$, **Figure 3D**) and IA groups (CpG1–5 and mean methylation, $p > 0.05$, **Figure 3E**). The comparison of the ruptured aneurysms revealed no differences in *PNPLA6* methylation between the ruptured IA and unruptured IA groups (CpG1–5 and mean methylation, $p > 0.05$, **Figure 3F**).

Correlation tests were performed to analyze the relationship between *PNPLA6* methylation and age. The results showed that *PNPLA6* methylation was significantly associated with age in all participants (mean methylation: $r = 0.306$, $p = 0.003$, **Figure 4A**) and the control group (mean methylation: $r = 0.377$, $p = 0.008$, **Figure 4B**) but not the IA group ($r = 0.127$, $p = 0.402$, **Figure 4C**). Furthermore, *PNPLA6* mRNA expression significantly decreased in patients with IA compared with that in the controls ($p = 0.016$, **Figure 5A**). Moreover, *PNPLA6* expression was significantly inversely correlated with elevated DNA methylation in participants ($r = -0.825$, $p < 0.001$, **Figure 5B**). In addition, the results of methylase inhibitor AZA treatment of HPCASMC showed that the *PNPLA6* gene expression in cells treated with AZA at a concentration of 1.0 μM was significantly higher than that in the control group ($p = 0.037$, **Figure 5C**).

ROC curves were used to evaluate the *PNPLA6* diagnostic value in patients with IA. The area under the curve (AUC) of *PNPLA6* mRNA expression was 0.86 (95% CI, 0.74–0.98, $p < 0.001$), and *PNPLA6* mean methylation was 0.74 (95% CI, 0.60–0.88; $p < 0.001$; **Figure 6**).

DISCUSSION

In the present study, we aimed to explore the association between *PNPLA6* methylation and the risk of IA. First, our results showed that plasma *PNPLA6* expression was much lower in patients with IA than in controls. Second, *PNPLA6* methylation levels were significantly higher in patients with IA than in controls, and these differences were found only in male patients. Third, *PNPLA6* methylation was inversely associated with *PNPLA6* mRNA expression in the study participants. Fourth, DNA methylation may serve an important role in the regulation of *PNPLA6* transcription in HPCASMC. Fifth, *PNPLA6* DNA methylation and mRNA expression levels had diagnostic value in patients with IA. Lastly, *PNPLA6* methylation was significantly associated with age in all participants and in the control group but not in the IA group.

The PNPLA6 protein is mainly located on the surface of the cytoplasmic endoplasmic reticulum, and concentrated in the neurons of the brain, placenta, kidney, and vascular (Richardson et al., 2013). *PNPLA6* expression is strongly associated with nervous system integrity and maintenance (Sogorb et al., 2016). *Pnpla6* silencing significantly alters the formation of the respiratory tube and nervous system (Winrow et al., 2003) and impairs vasculogenesis and placental vasculature in a mouse model (Moser et al., 2004). *PNPLA6* overexpression significantly promotes the migration and tube formation of human umbilical vein endothelial cells (HUVECs) (Li et al., 2021), and *PNPLA6* short hairpin RNA (shRNA) inhibits the migration and tube formation of HUVECs (Li et al., 2021). In the current study,

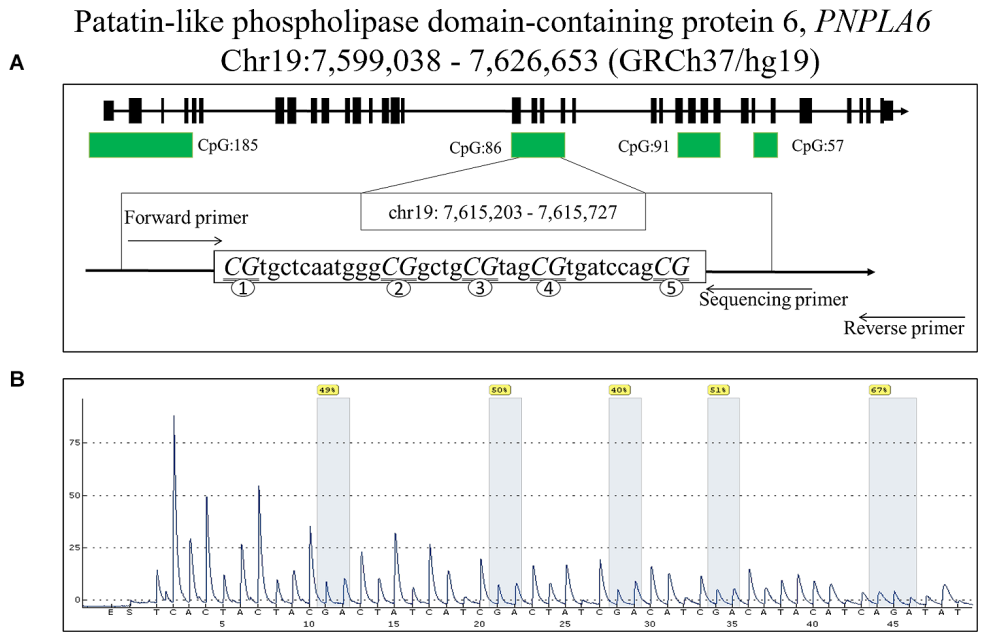

FIGURE 1 | The locations and analysis of the five CpGs in *PNPLA6* gene. **(A)** The locations of the five CpGs in *PNPLA6* gene. **(B)** Representative sequencing analysis of five methylation sites.

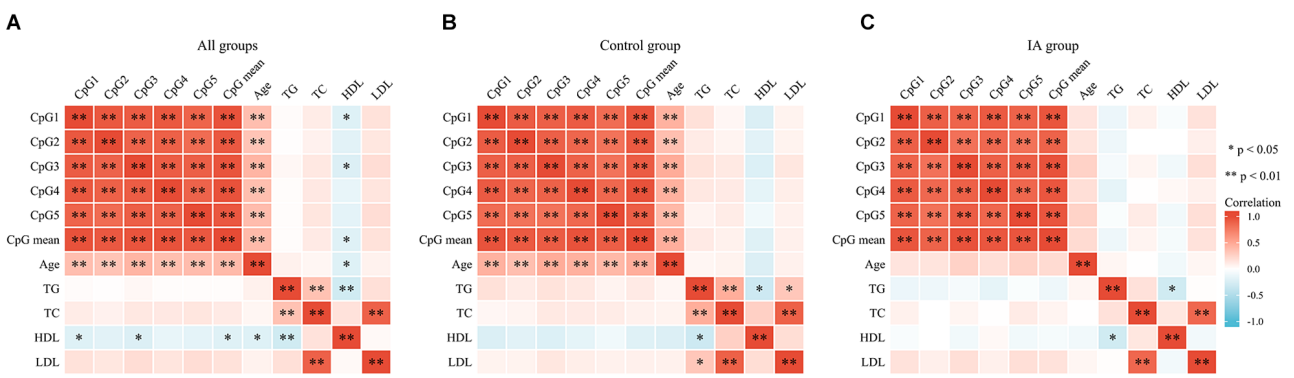

FIGURE 2 | The correlations among GpGs methylation and clinical data in different subgroups. **(A)** The correlation analysis in all groups. **(B)** The correlation analysis in the control group. **(C)** The correlation analysis in IA group. The correlations among the five CpGs methylation were analyzed using Pearson's correlation test, $^{**}p < 0.01$; $^{*}p < 0.05$.

the results showed that the level of *PNPLA6* expression was much lower in patients with IA than in the controls possibly because of the lower *PNPLA6* expression in patients with IA than in the controls, consequently, the risk of angiogenic lesions increases.

Studies have shown that DNA methylation influences the development of many diseases by regulating gene expression (He et al., 2022; Zhu et al., 2022). In the development of cerebrovascular disease, DNA methylation may trigger lesions by altering the expression levels of genes related to vasoconstriction or vasoproliferation, which in turn affects changes in the levels of proteins related to vascular stability (He et al., 2022). DNA methylation is closely associated with the risk of IA (Nikkola et al., 2015; Zhou et al., 2017; Shafeeque et al., 2020; Wang et al., 2021). Kim et al.'s study (Kim et al., 2022) showed that different genes with DNA methylation can be useful biomarkers for the accurate diagnosis of delayed cerebral ischemia after aneurysmal subarachnoid hemorrhage. DNA methylation participates in IA development possibly by modulating the expression of genes involved in immune and inflammatory reactions, cell signal transduction, and vascular stability (Yu et al., 2017). In other aneurysm-related diseases, Toghill et al.'s study (Toghill et al., 2018) found that *SMYD2* gene promoter methylation may be involved in the pathobiological

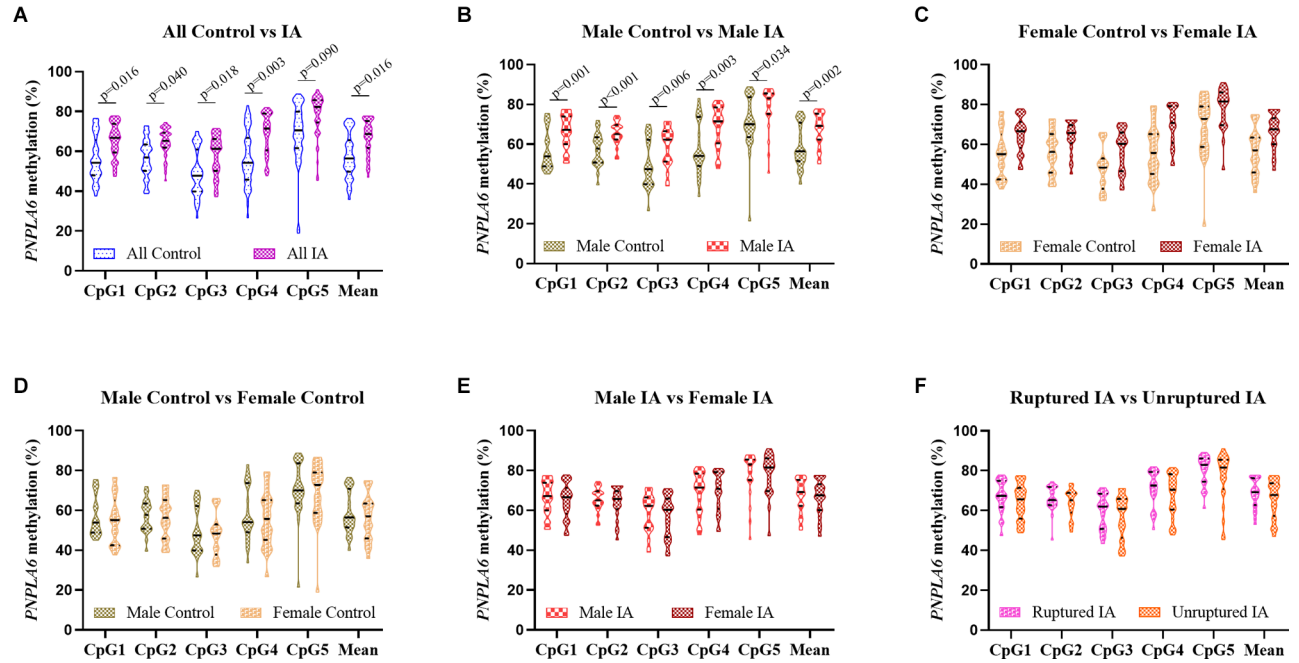

FIGURE 3 | Comparison of the five GpGs methylation levels in different subgroups. **(A)** The comparison between controls and IAs in males and females. **(B)** The comparison between controls and IAs in males. **(C)** The comparison between controls and IAs in females. **(D)** The comparison between males and females in the control group. **(E)** The comparison between males and females in the IA group. **(F)** The comparison between ruptured IA and unruptured IA. Data were represented as mean ± SD.

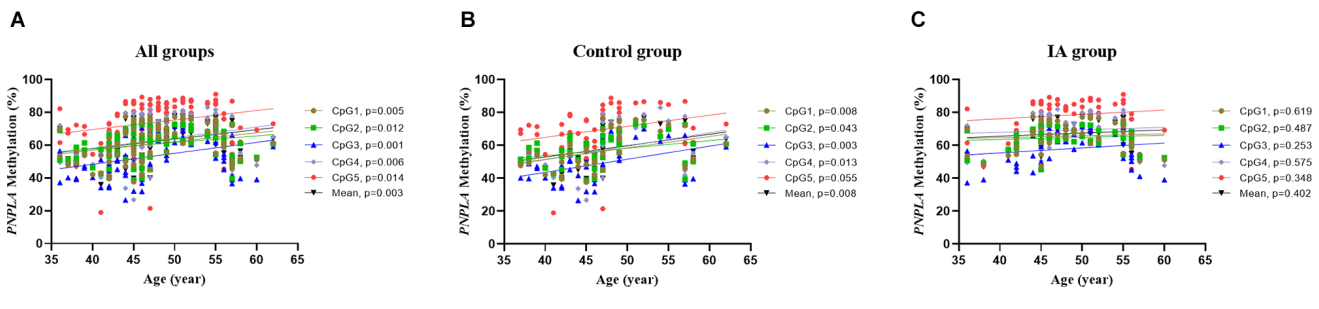

FIGURE 4 | The relationship between *PNPLA6* methylations and age in different subgroups. **(A)** The relationship analysis in all participants. **(B)** The relationship analysis in the control group. **(C)** The relationship analysis in the IA group.

development of abdominal aortic aneurysm by reducing *SMYD2* gene expression. In the present study, the cell experiments showed that DNA methylase inhibitor significantly upregulated *PNPLA6* transcription levels in the HPCASMC, which suggested that DNA methylation may serve an important role in the regulation of *PNPLA6* transcription. The clinical results suggested that *PNPLA6* methylation levels were significantly higher in patients with IA than in controls, and *PNPLA6* expression was inversely associated with *PNPLA6* methylation in the study participants. Thus, *PNPLA6* methylation may increase the risk of IA by regulating its mRNA expression. Moreover, ROC analyses revealed that *PNPLA6* DNA methylation and mRNA expression levels have a potential diagnostic value for IA.

Sex dichotomous effects and age are implicated in the risk factors of IA and many gene methylation rates (Vlak et al., 2011; Unnikrishnan et al., 2019; Li and Liu, 2021). The prevalence of IA and the risk of aneurysmal rupture in females are higher than those in males (Zuurbier et al., 2022). DNA methylation also shows strong sex-specific differences when individuals are exposed to harsh environments (Curtis et al., 2020). Recent studies had shown that multiple gene methylation was associated with gender differences in cardiovascular and cerebrovascular diseases (Asllanaj et al., 2020). Qin et al.'s study (Qin et al., 2019) showed that hypermethylation of ATP-binding cassette G1 gene was significantly associated with carotid intima–media thickness in males. Wang et al.'s study (Wang et al., 2016) suggested that sex modulates the interaction

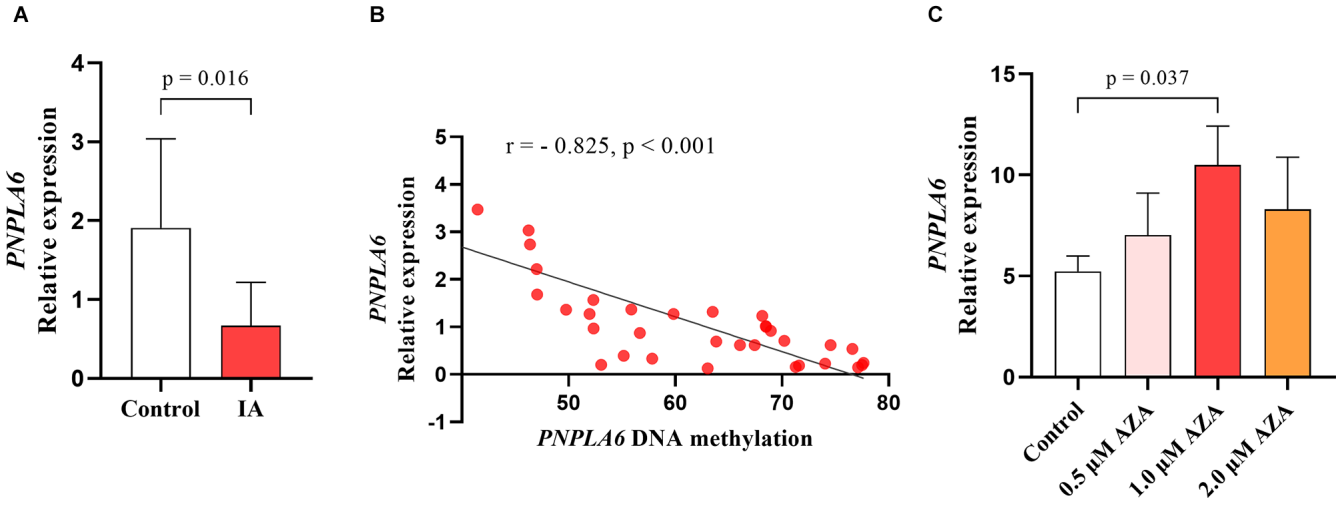

FIGURE 5 | The significant association between *PNPLA6* mRNA expression and DNA methylation. **(A)** *PNPLA6* mRNA expression was much lower in IAs than in healthy controls. **(B)** The *PNPLA6* expression was significantly associated with DNA methylation in all individuals. **(C)** The changes of *PNPLA6* expression in the cell lines treated with AZA.

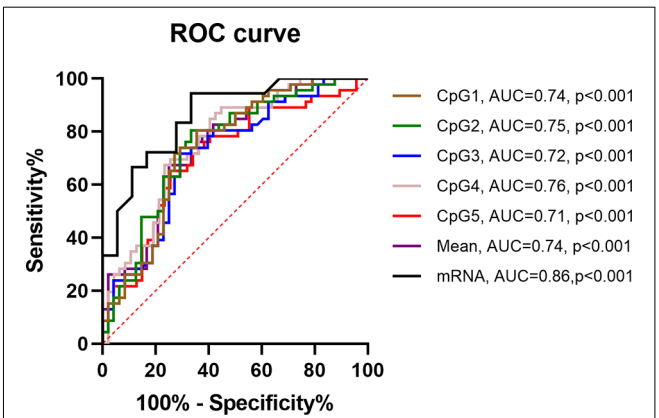

FIGURE 6 | ROC curves of *PNPLA6* DNA methylation in IA patients. ROC, receiver operating characteristic. AUC, area under the curve.

of *NOS1AP* promoter DNA methylation in patients with IA. Our results revealed that *PNPLA6* methylation occurred only in male patients with IA but not in females. In humans, DNA methylation levels are strongly associated with age (Horvath and Raj, 2018). The DNA methylation levels of different genes may gradually increase or decrease with age in healthy humans (Sen et al., 2016). Furthermore, DNA methylation can be used to predict chronological age (Noroozi et al., 2021). In the present study, *PNPLA6* DNA methylation levels gradually increased with age in the healthy controls but not in the patients with IA possibly because of DNA methylation disorders caused by vascular damage in patients with IA.

Our study had some limitations. First, only five GpGs on the fragment (chr19: 7, 615, 203–7, 615, 727) were selected to represent *PNPLA6*. Therefore, more CpGs analysis should be included in future studies. Second, although the subjects included in this study were sex- and age-matched, we cannot exclude those other factors including surgical treatment, medication, dietary habits, and cellular heterogeneity that may affect methylation differences. Third, although this study had great statistical power, the sample size included in this study was relatively small, more sample tests for DNA methylation and gene expression should be conducted in the future to confirm our findings. Fourth, only the DNA methylation and mRNA expression of the *PNPLA6* gene were studied in this study, and changes in protein levels would be more helpful in revealing its relationship to the pathogenesis of IA. Fifth, a candidate study was performed but a mechanistic investigation *in vitro*, in silico, or *in vivo* are needed to further verify and validate the results.

CONCLUSION

Although future functional experiments are required to test our hypothesis, our findings suggest that *PNPLA6* methylation may contribute to an increased risk of IA in males by regulating its mRNA expression. Thus, *PNPLA6* methylation and mRNA expression have the potential for use in the early diagnosis of IA.

DATA AVAILABILITY STATEMENT

The raw data supporting the conclusions of this article will be made available by the authors, without undue reservation.

ETHICS STATEMENT

The studies involving human participants and all study protocols were reviewed and approved by the Ethics Committee of Ningbo

First Hospital. The patients/participants provided their written informed consent to participate in this study.

AUTHOR CONTRIBUTIONS

XG and JS contributed to the conception and design of the study. SZ, JZ, CZ, and FG organized the database and experiments. XZ and XP performed the statistical analysis. SZ and YH wrote the first draft of the manuscript. All authors contributed to the article and approved submitted version.

FUNDING

This study was supported by the grants from the Zhejiang Provincial Natural Science Foundation of China (LY22H090001), Medicine and Health Science and Technology Projects of Zhejiang Province (2022KY305, 2022KY322), National Natural Science Foundation of China (82101354), Ningbo Health Branding Subject Fund (PPXK2018-04), Ningbo Science and Technology Innovation 2025 Major Project (2019B10105), and Key Laboratory of Precision Medicine for Atherosclerotic Diseases of Zhejiang Province (2022E10026).

REFERENCES

Asllanaj, E., Zhang, X., Ochoa Rosales, C., Nano, J., Bramer, W. M., Portilla-Fernandez, E., et al. (2020). Sexually dimorphic DNA-methylation in cardiometabolic health: a systematic review. *Maturitas* 135, 6–26. doi: 10.1016/j.maturitas.2020.02.005

Bakker, M. K., Van Der Spek, R. A. A., Van Rheenen, W., Morel, S., Bourcier, R., Hostettler, I. C., et al. (2020). Genome-wide association study of intracranial aneurysms identifies 17 risk loci and genetic overlap with clinical risk factors. *Nat. Genet.* 52, 1303–1313. doi: 10.1038/s41588-020-00725-7

Chang, P. A., and Wu, Y. J. (2010). Neuropathy target esterase: an essential enzyme for neural development and axonal maintenance. *Int. J. Biochem. Cell Biol.* 42, 573–575. doi: 10.1016/j.biocel.2009.12.007

Cheng, Y. W., Chuang, Y. C., Huang, S. W., Liu, C. C., and Wang, J. R. (2022). An auto-antibody identified from phenotypic directed screening platform shows host immunity against EV-A71 infection. *J. Biomed. Sci.* 29:10. doi: 10.1186/s12929-022-00794-2

Curtis, S. W., Gerkowicz, S. A., Cobb, D. O., Kilaru, V., Terrell, M. L., Marder, M. E., et al. (2020). Sex-specific DNA methylation differences in people exposed to polybrominated biphenyl. *Epigenomics* 12, 757–770. doi: 10.2217/epi-2019-0179

Deng, G. X., Xu, N., Huang, Q., Tan, J. Y., Zhang, Z., Li, X. F., et al. (2019). Association between promoter DNA methylation and gene expression in the pathogenesis of ischemic stroke. *Aging (Albany NY)* 11, 7663–7677. doi: 10.18632/aging.102278

Dogan, M., Eroz, R., and Ozturk, E. (2021). Chorioretinal dystrophy, hypogonadotropic hypogonadism and cerebellar ataxia: Boucher-Neuhauser syndrome due to a homozygous (c.3524C>G (p.Ser1175Cys)) variant in PNPLA6 gene. *Ophthalmic Genet.* 42, 276–282. doi: 10.1080/13816810.2021.1894461

Emekli, A. S., Samanci, B., Simsir, G., Hanagasi, H. A., Gurvit, H., Bilgic, B., et al. (2021). A novel PNPLA6 mutation in a Turkish family with intractable Holmes tremor and spastic ataxia. *Neurol. Sci.* 42, 1535–1539. doi: 10.1007/s10072-020-04869-6

He, S., Ye, X., Duan, R., Zhao, Y., Wei, Y., Wang, Y., et al. (2022). Epigenome-wide association study reveals differential methylation sites and association of gene expression regulation with ischemic moyamoya disease in adults. *Oxid. Med. Cell Longev.* 2022:7192060. doi: 10.1155/2022/7192060

Horvath, S., and Raj, K. (2018). DNA methylation-based biomarkers and the epigenetic clock theory of ageing. *Nat. Rev. Genet.* 19, 371–384. doi: 10.1038/s41576-018-0004-3

Kim, B. J., Youn, D. H., Chang, I. B., Kang, K., and Jeon, J. P. (2022). Identification of differentially-methylated genes and pathways in patients with delayed cerebral ischemia following subarachnoid hemorrhage. *J. Korean Neurosurg. Soc.* 65, 4–12. doi: 10.3340/jkns.2021.0035

Li, M. H., Chen, S. W., Li, Y. D., Chen, Y. C., Cheng, Y. S., Hu, D. J., et al. (2013). Prevalence of unruptured cerebral aneurysms in Chinese adults aged 35 to 75 years: a cross-sectional study. *Ann. Intern. Med.* 159, 514–521. doi: 10.7326/0003-4819-159-8-201310150-00004

Li, Y., and Liu, F. (2021). DNA methylation reshapes sex development in zebrafish. *Genomics Proteomics Bioinform.* 19, 44–47. doi: 10.1016/j.gpb.2021.01.002

Li, M., Shen, X., Liu, H., Yang, B., Lu, S., Tang, M., et al. (2021). Reduced neuropathy target esterase in pre-eclampsia suppresses tube formation of HUVECs via dysregulation of phospholipid metabolism. *J. Cell. Physiol.* 236, 4435–4444. doi: 10.1002/jcp.30160

Lu, J., Li, M., Burkhardt, J. K., Zhao, Y., Li, Y., Chen, X., et al. (2021). Unruptured giant intracranial aneurysms: risk factors for mortality and long-term outcome. *Transl. Stroke Res.* 12, 593–601. doi: 10.1007/s12975-020-00861-6

Moore, L. D., Le, T., and Fan, G. (2013). DNA methylation and its basic function. *Neuropsychopharmacology* 38, 23–38. doi: 10.1038/npp.2012.112

Moser, M., Li, Y., Vaupel, K., Kretzschmar, D., Kluge, R., Glynn, P., et al. (2004). Placental failure and impaired vasculogenesis result in embryonic lethality for neuropathy target esterase-deficient mice. *Mol. Cell. Biol.* 24, 1667–1679. doi: 10.1128/MCB.24.4.1667-1679.2004

Nikkola, E., Laiwalla, A., Ko, A., Alvarez, M., Connolly, M., Ooi, Y. C., et al. (2015). Remote ischemic conditioning alters methylation and expression of cell cycle genes in aneurysmal subarachnoid hemorrhage. *Stroke* 46, 2445–2451. doi: 10.1161/STROKEAHA.115.009618

Noroozi, R., Ghafouri-Fard, S., Pisarek, A., Rudnicka, J., Spolnicka, M., Branicki, W., et al. (2021). DNA methylation-based age clocks: from age prediction to age reversion. *Ageing Res. Rev.* 68:101314. doi: 10.1016/j.arr.2021.101314

Pamies, D., Bal-Price, A., Fabbri, M., Gribaldo, L., Scelfo, B., Harris, G., et al. (2014a). Silencing of PNPLA6, the neuropathy target esterase (NTE) codifying gene, alters neurodifferentiation of human embryonal carcinoma stem cells (NT2). *Neuroscience* 281, 54–67. doi: 10.1016/j.neuroscience.2014.08.031

Pamies, D., Vilanova, E., and Sogorb, M. A. (2014b). Functional pathways altered after silencing Pnpla6 (the codifying gene of neuropathy target esterase) in mouse embryonic stem cells under differentiation. *In vitro Cell. Dev. Biol. Anim.* 50, 261–273. doi: 10.1007/s11626-013-9691-4

Qin, X., Li, J., Wu, T., Wu, Y., Tang, X., Gao, P., et al. (2019). Overall and sex-specific associations between methylation of the ABCG1 and APOE genes and ischemic stroke or other atherosclerosis-related traits in a sibling study of Chinese population. *Clin. Epigenetics* 11:189. doi: 10.1186/s13148-019-0784-0

Rao, X., Zhong, J., Zhang, S., Zhang, Y., Yu, Q., Yang, P., et al. (2011). Loss of methyl-CpG-binding domain protein 2 enhances endothelial angiogenesis and protects mice against hind-limb ischemic injury. *Circulation* 123, 2964–2974. doi: 10.1161/CIRCULATIONAHA.110.966408

Richardson, R. J., Fink, J. K., Glynn, P., Hufnagel, R. B., Makhaeva, G. F., and Wijeyesakere, S. J. (2020). Neuropathy target esterase (NTE/PNPLA6) and organophosphorus compound-induced delayed neurotoxicity (OPIDN). *Adv. Neurotoxicol.* 4, 1–78. doi: 10.1016/bs.ant.2020.01.001

Richardson, R. J., Hein, N. D., Wijeyesakere, S. J., Fink, J. K., and Makhaeva, G. F. (2013). Neuropathy target esterase (NTE): overview and future. *Chem. Biol. Interact.* 203, 238–244. doi: 10.1016/j.cbi.2012.10.024

Sen, K., Finau, M., and Ghosh, P. (2020). Bi-allelic variants in PNPLA6 possibly associated with Parkinsonian features in addition to spastic paraplegia phenotype. *J. Neurol.* 267, 2749–2753. doi: 10.1007/s00415-020-10028-w

Sen, P., Shah, P. P., Nativio, R., and Berger, S. L. (2016). Epigenetic mechanisms of longevity and aging. *Cell* 166, 822–839. doi: 10.1016/j.cell.2016.07.050

Shafeeque, C. M., Sathyan, S., Saradalekshmi, K. R., Premkumar, S., Allapatt, J. P., and Banerjee, M. (2020). Methylation map genes can be critical in determining the methylome of intracranial aneurysm patients. *Epigenomics* 12, 859–871. doi: 10.2217/epi-2019-0280

Sogorb, M. A., Pamies, D., Estevan, C., Estevez, J., and Vilanova, E. (2016). Roles of NTE protein and encoding gene in development and neurodevelopmental toxicity. *Chem. Biol. Interact.* 259, 352–357. doi: 10.1016/j.cbi.2016.07.030

Suchowersky, O., Ashtiani, S., Au, P. B., Mcleod, S., Estiar, M. A., Gan-Or, Z., et al. (2021). Hereditary spastic paraplegia initially diagnosed as cerebral palsy. *Clin. Parksonism Relat. Disord.* 5:100114.. doi: 10.1016/j.prdoa.2021.100114

Toghill, B. J., Saratzis, A., Freeman, P. J., Sylvius, N., Collaborators, U., and Bown, M. J. (2018). SMYD2 promoter DNA methylation is associated with abdominal aortic aneurysm (AAA) and SMYD2 expression in vascular smooth muscle cells. *Clin. Epigenetics* 10:29. doi: 10.1186/s13148-018-0460-9

Unnikrishnan, A., Freeman, W. M., Jackson, J., Wren, J. D., Porter, H., and Richardson, A. (2019). The role of DNA methylation in epigenetics of aging. *Pharmacol. Ther.* 195, 172–185. doi: 10.1016/j.pharmthera.2018.11.001

Vlak, M. H., Algra, A., Brandenburg, R., and Rinkel, G. J. (2011). Prevalence of unruptured intracranial aneurysms, with emphasis on sex, age, comorbidity, country and time period: a systematic review and meta-analysis. *Lancet Neurol.* 10, 626–636. doi: 10.1016/S1474-4422(11)70109-0

Wang, Z., Zhao, J., Sun, J., Nie, S., Li, K., Gao, F., et al. (2016). Sex-dichotomous effects of NOS1AP promoter DNA methylation on intracranial aneurysm and brain arteriovenous malformation. *Neurosci. Lett.* 621, 47–53. doi: 10.1016/j.neulet.2016.04.016

Wang, Z., Zhou, S., Zhao, J., Nie, S., Sun, J., Gao, X., et al. (2021). Tobacco smoking increases methylation of polypyrimidine tract binding protein 1 promoter in intracranial aneurysms. *Front. Aging Neurosci.* 13:688179. doi: 10.3389/fnagi.2021.688179

Winrow, C. J., Hemming, M. L., Allen, D. M., Quistad, G. B., Casida, J. E., and Barlow, C. (2003). Loss of neuropathy target esterase in mice links organophosphate exposure to hyperactivity. *Nat. Genet.* 33, 477–485. doi: 10.1038/ng1131

Wu, S., Sun, Z., Zhu, T., Weleber, R. G., Yang, P., Wei, X., et al. (2021). Novel variants in PNPLA6 causing syndromic retinal dystrophy. *Exp. Eye Res.* 202:108327. doi: 10.1016/j.exer.2020.108327

Yu, L., Wang, J., Wang, S., Zhang, D., Zhao, Y., Wang, R., et al. (2017). DNA methylation regulates gene expression in intracranial aneurysms. *World Neurosurg.* 105, 28–36. doi: 10.1016/j.wneu.2017.04.064

Zhong, T., Chen, J., Ling, Y., Yang, B., Xie, X., Yu, D., et al. (2018). Down-regulation of neuropathy target esterase in preeclampsia placenta inhibits human trophoblast cell invasion via modulating MMP-9 levels. *Cell. Physiol. Biochem.* 45, 1013–1022. doi: 10.1159/000487296

Zhou, S., Gao, X., Sun, J., Lin, Z., and Huang, Y. (2017). DNA methylation of the PDGFD gene promoter increases the risk for intracranial aneurysms and brain arteriovenous malformations. *DNA Cell Biol.* 36, 436–442. doi: 10.1089/dna.2016.3499

Zhu, H., Wang, X., Meng, X., Kong, Y., Li, Y., Yang, C., et al. (2022). Selenium supplementation improved cardiac functions by suppressing DNMT2-mediated GPX1 promoter DNA methylation in AGE-induced heart failure. *Oxid. Med. Cell. Longev.* 2022:5402997. doi: 10.1155/2022/5402997

Zocher, S., Overall, R. W., Lesche, M., Dahl, A., and Kempermann, G. (2021). Environmental enrichment preserves a young DNA methylation landscape in the aged mouse hippocampus. *Nat. Commun.* 12:3892. doi: 10.1038/s41467-021-23993-1

Zuurbier, C. C. M., Molenberg, R., Mensing, L. A., Wermer, M. J. H., Juvela, S., Lindgren, A. E., et al. (2022). Sex difference and rupture rate of intracranial aneurysms: an individual patient data meta-analysis. *Stroke* 53, 362–369. doi: 10.1161/STROKEAHA.121.035187

Conflict of Interest: The authors declare that the research was conducted in the absence of any commercial or financial relationships that could be construed as a potential conflict of interest.

Publisher's Note: All claims expressed in this article are solely those of the authors and do not necessarily represent those of their affiliated organizations, or those of the publisher, the editors and the reviewers. Any product that may be evaluated in this article, or claim that may be made by its manufacturer, is not guaranteed or endorsed by the publisher.

frontiers | Frontiers in Aging Neuroscience

ORIGINAL RESEARCH
published: 18 July 2022
doi: 10.3389/fnagi.2022.897611

Machine Learning Prediction Models for Postoperative Stroke in Elderly Patients: Analyses of the MIMIC Database

Xiao Zhang[1†], Ningbo Fei[2†], Xinxin Zhang[1], Qun Wang[1] and Zongping Fang[1]*

[1] Department of Anesthesiology and Perioperative Medicine, Xijing Hospital, Fourth Military Medical University, Xi'an, China, [2] Department of Orthopedics and Traumatology, The Duchess of Kent Children's Hospital at Sandy Bay, The University of Hong Kong, Hong Kong, Hong Kong SAR, China

Objective: With the aging of populations and the high prevalence of stroke, postoperative stroke has become a growing concern. This study aimed to establish a prediction model and assess the risk factors for stroke in elderly patients during the postoperative period.

Methods: ML (Machine learning) prediction models were applied to elderly patients from the MIMIC (Medical Information Mart for Intensive Care)-III and MIMIC-VI databases. The SMOTENC (synthetic minority oversampling technique for nominal and continuous data) balancing technique and iterative SVD (Singular Value Decomposition) data imputation method were used to address the problem of category imbalance and missing values, respectively. We analyzed the possible predictive factors of stroke in elderly patients using seven modeling approaches to train the model. The diagnostic value of the model derived from machine learning was evaluated by the ROC curve (receiver operating characteristic curve).

Results: We analyzed 7,128 and 661 patients from MIMIC-VI and MIMIC-III, respectively. The XGB (extreme gradient boosting) model got the highest AUC (area under the curve) of 0.78 (0.75–0.81), making it better than the other six models, Besides, we found that XGB model with databalancing was better than that without data balancing. Based on this prediction model, we found hypertension, cancer, congestive heart failure, chronic pulmonary disease and peripheral vascular disease were the top five predictors. Furthermore, we demonstrated that hypertension predicted postoperative stroke is much more valuable.

Conclusion: Stroke in elderly patients during the postoperative period can be reliably predicted. We proved XGB model is a reliable predictive model, and the history of hypertension should be weighted more heavily than the results of laboratory tests to prevent postoperative stroke in elderly patients regardless of gender.

Keywords: stroke, machine learning, prediction model, post-operative, MIMIC database

OPEN ACCESS

Edited by:
Yujie Chen,
Army Medical University, China

Reviewed by:
Iqram Hussain,
Seoul National University, South Korea
Jinlong Liu,
Zhejiang University, China

****Correspondence:***
Zongping Fang
zongping03@163.com

† These authors have contributed equally to this work and share first authorship

Specialty section:
This article was submitted to Neuroinflammation and Neuropathy, a section of the journal Frontiers in Aging Neuroscience

Received: *16 March 2022*
Accepted: *13 June 2022*
Published: *18 July 2022*

Citation:
Zhang X, Fei N, Zhang X, Wang Q and Fang Z (2022) Machine Learning Prediction Models for Postoperative Stroke in Elderly Patients: Analyses of the MIMIC Database. Front. Aging Neurosci. 14:897611. doi: 10.3389/fnagi.2022.897611

INTRODUCTION

Stroke, also called cerebrovascular accident, includes the neurological pathology of the brain arteries that can result from ischemia or hemorrhage (Boursin et al., 2018). Stoke ranks as the second-leading cause of mortality and disability worldwide behind ischemic heart disease and thereby become a major health-related challenge (Merino, 2014; Sirsat et al., 2020). Stroke also gives approximately 16,000,000 individuals worldwide various motor and cognitive impairments, which are often unavoidable sequelae in stroke patients. These sequelae greatly aggravate the social and family burden (Di Carlo, 2009). People with advanced age, surgery patients and ICU patients are at high risk of stroke (Mantz et al., 2010; Biteker et al., 2014; Dong et al., 2017). Consequently, it's urgent to establish an advanced model that can help to predict and diagnose stroke. The early correct detection of stroke will lay a solid foundation to efficiently prevent and treat stroke and will greatly improve the prognosis of surgery. A prediction model is a practicable way to achieve the above goals and several attempts have been made (Maravic-Stojkovic et al., 2014; Khattar et al., 2016; Dunham et al., 2017; Sporns et al., 2017; Zhou et al., 2020). However, there is still a demand for models that can predict stroke in elderly patients after surgery.

Machine Learning (ML), as a mature and scientific modeling method, is attracting more attention than traditional modeling approaches such as the Cox proportional hazard model. ML is a pivotal part of artificial intelligence (AI), it can achieve self-optimization by learning complex structure with numerous variables and data (Bi et al., 2019). So far, ML has wide application in several fields, including search engines, sales and marketing, and autonomous driving (Deo, 2015; Jiang et al., 2017; Handelman et al., 2018; Connor, 2019), as well as medical diagnostics and clinical research (Heo et al., 2019; Saber et al., 2019; Sirsat et al., 2020). During the past few decades, several studies were conducted on the improvement of stroke diagnosis using ML, most of them obtained satisfying results, which would be of great value in early prognosis of stroke (Asadi et al., 2016; Cox et al., 2016; Bacchi et al., 2020; Wu and Fang, 2020). For example, the electromyography (EMG) based muscular activity monitoring system, electroencephalography (EEG) based neuronal firing activity monitoring system and electrocardiogram (ECG) based monitoring system have been applied into the early identification and prognosis of stroke, which are also beneficial to post-stroke rehabilitation (Robinson et al., 2003; Hussain and Park, 2020, 2021a,b).

We obtained our data from two public clinical databases, which contains rich and complete clinical data. In the practice of machine learning modeling, we utilized not only subjects from MIMIC-VI for internal validation but also samples from the MIMIC-III database for further external testing. The goal of the present study is to introduce a prediction model for postoperative stroke in elderly patients. We applied seven machine learning method in this research combined with iterative SVD data imputation and SMOTENC method, which would deliver an accurate and quick prediction outcome. Based on our results, the perioperative patients with high risk of stroke could be found and treated as early as possible, which would shed new light on the prevention of stroke.

MATERIALS AND METHODS

Database and Study Design

We obtained our data from two publicly available retrospective multigranular clinical databases, MIMIC-III and MIMIC-VI, which are high-quality database of admitted patients from 2000 to 2014 and from 2014 to 2018, respectively. They have large samples with comprehensive clinical information. The 80% percent of the samples from MIMIC-VI, chosen randomly, were

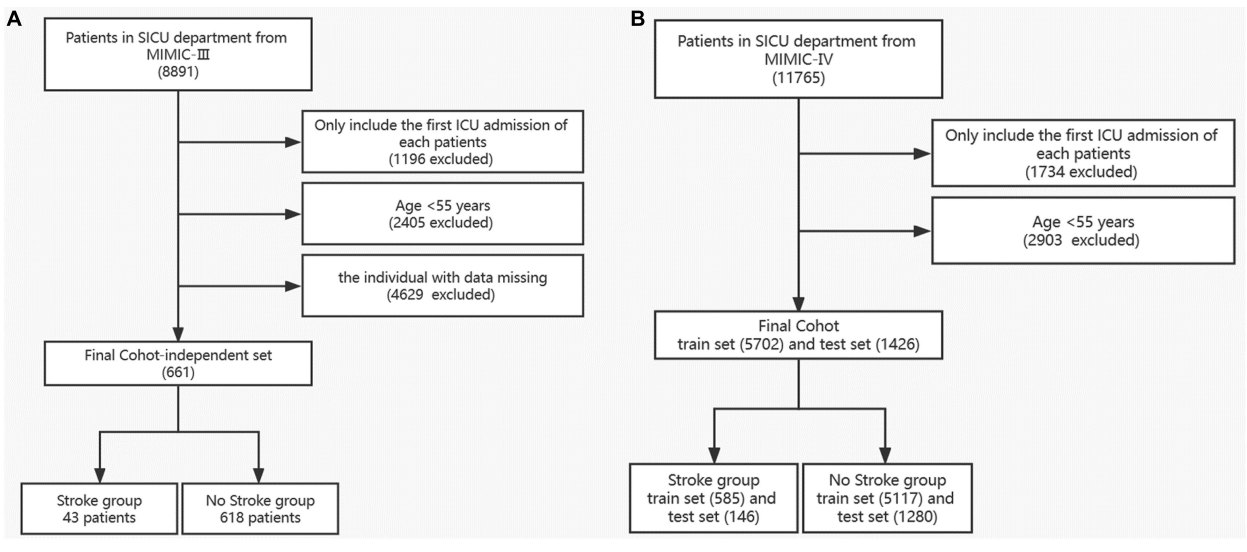

FIGURE 1 | Flow diagram of the selection process of patients in MIMIC III **(A)** and MIMIC VI **(B)**.

regarded as the development set, and the remaining 20% were regarded as the validation set. Besides, the samples from MIMIC-III were applied as an independent testing set to further evaluate the applicability of the established models and predictors.

Subjects and Outcomes

In this study, subjects who were admitted to the SICU (surgery intensive care unit) with age > 55 years were selected. All these patients should include vital signs, complications and laboratory results. As shown in **Figure 1**, subjects younger than 55 years were excluded. Missing values of enrolled individuals in MIMIC-VI were filled with the iterative SVD data imputation method. Only patients with complete data in MIMIC-III were kept. We finally screened 661 patients from MIMIC-III and 7,128 patients from MIMIC-VI into the study. Incidence of stroke was used as the outcome measure. Then we separated patients into the stroke group and non-stroke group based on their diagnosis in the hospital.

We select predictors according to what features chosen in the previous research (Heo et al., 2019; Sirsat et al., 2020; Wu and Fang, 2020), as well as our clinical experience. Predictors with missing data more than 30% in MIMIC-III and MIMIC-VI, such as bicarbonate, were excluded. The predictors included (a) demographic information: age, sex, ethnicity and BMI index; (b) comorbidities: peripheral vascular disease, hypertension, chronic pulmonary disease, diabetes, renal disease, liver disease, peptic ulcer disease, sepsis, congestive heart failure, cancer, and rheumatic disease; (c) the first-day laboratory results in the ICU: the mean level of glucose; the lowest and mean levels of Spo_2, the lowest and highest levels of anion gap, albumin, bilirubin total, creatinine, hematocrit, hemoglobin, WBC (white blood cells), lactate, platelets, potassium, PTT (partial thromboplastin time), PT (prothrombin time), INR (international normalized ratio), and BUN (blood urea nitrogen); and (e) the first-day vital signs in the ICU: the highest and mean levels of heart rate, SBP (systolic blood pressure), DBP (diastolic blood pressure), and MBP (mean blood pressure) (Dunham et al., 2017; Wu and Fang, 2020; Bolourani et al., 2021).

We extracted the target subjects with all of the above information and outcome measures *via* navicat premium12 software. Data cleaning was completed by Stata software after the data extraction. Firstly, individuals who met the exclusion criteria were excluded. Secondly, the extreme values and outliers were deleted. For data in MIMIC- VI, we excluded subjects with missing values accounting for more than 5% of the predictive features. Imputation method

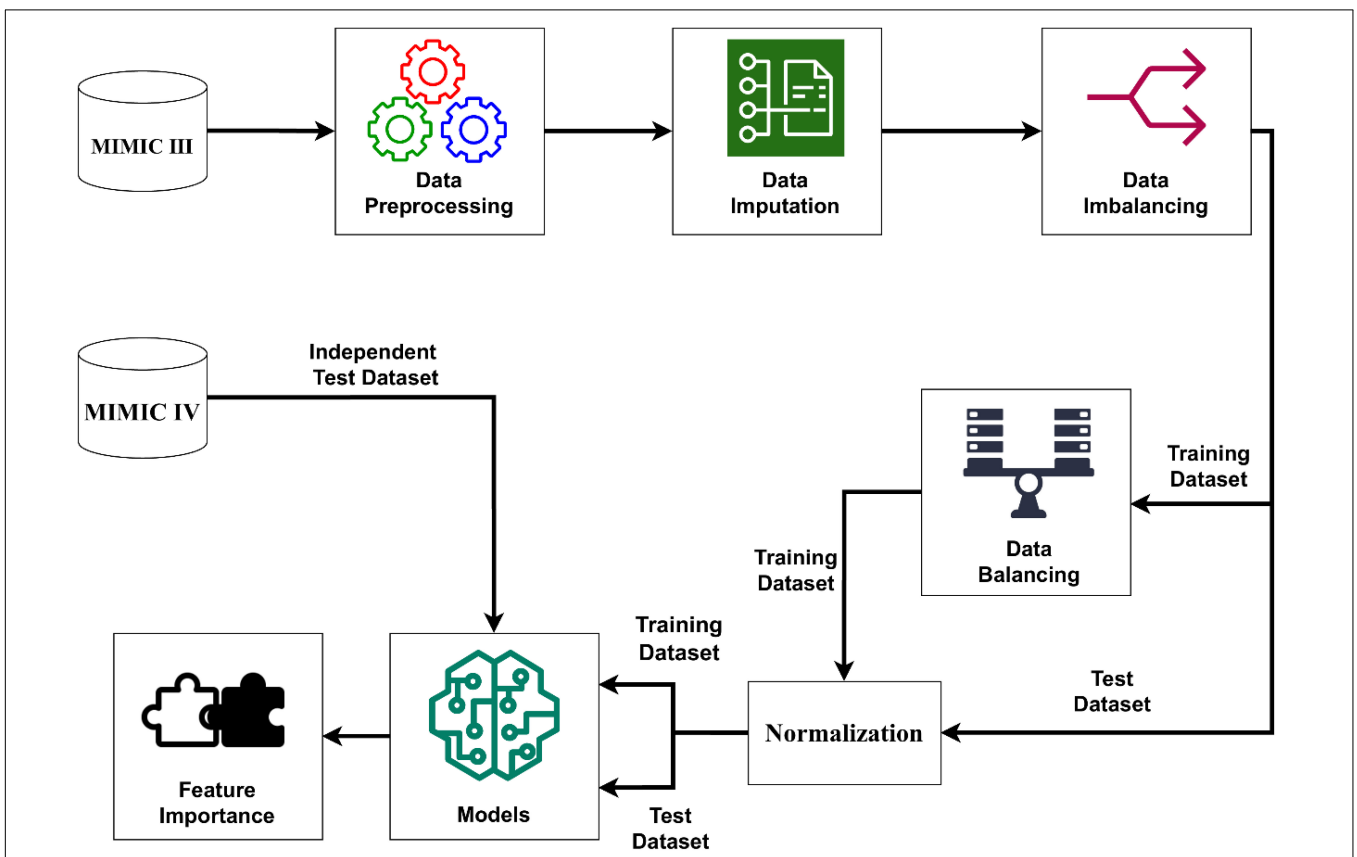

FIGURE 2 | Schematic illustration to the performance of the stroke prediction model. The SMOTENC balancing technique was applied to training dataset before establishing the model due to the imbalanced ratio of non-stroke to stroke patients in this work. After the normalization of data was completed, we applied seven machine learning methods to train and test models with the training dataset, test dataset and the independent test dataset. Finally, we can get model-based importance of features.

TABLE 1 | Characteristics of stroke and non-stroke patients in the training and validation sets of the MIMIC-IV database.

Variables	Total (*n* = 7,128)	Non-stroke (*n* = 6,397)	Stroke (*n* = 731)	*P*
Demographic characteristics				
Age, mean ± *SD*	72.3 ± 10.4	72.1 ± 10.4	74.0 ± 10.5	<0.001
Gender, female *n* (%)	3,426 (48.1)	3,082 (48.2)	344 (47.1)	0.584
Race, *n* (%)				0.039
Asian, *n* (%)	222 (3.1)	193 (3)	29 (4)	0.198
Black, *n* (%)	592 (8.3)	538 (8.4)	54 (7.4)	0.38
White, *n* (%)	5,083 (71.3)	4,584 (71.7)	499 (68.3)	0.06
Other, *n* (%)	1,231 (17.3)	1,082 (16.9)	149 (20.4)	0.022
BMI, mean ± *SD*	1300.8 ± 85503.1	1404.9 ± 90219.6	389.4 ± 7628.6	0.761
Comorbidities				
CHF, *n* (%)	1,483 (20.8)	1,399 (21.9)	84 (11.5)	<0.001
PVD, *n* (%)	927 (13.0)	858 (13.4)	69 (9.4)	0.003
Hypertension, *n* (%)	2,794 (39.2)	2,278 (35.6)	516 (70.6)	<0.001
CPD, *n* (%)	1,712 (24.0)	1,595 (24.9)	117 (16)	<0.001
Diabetes, *n* (%)	2,070 (29.0)	1,879 (29.4)	191 (26.1)	0.074
Renal_disease, *n* (%)	1,349 (18.9)	1,267 (19.8)	82 (11.2)	<0.001
Liver_disease, *n* (%)	844 (11.8)	817 (12.8)	27 (3.7)	<0.001
PUD, *n* (%)	204 (2.9)	201 (3.1)	3 (0.4)	<0.001
Cancer, *n* (%)	1,405 (19.7)	1,322 (20.7)	83 (11.4)	<0.001
Rheumatic_disease, *n* (%)	259 (3.6)	245 (3.8)	14 (1.9)	0.012
Sepsis, *n* (%)	3,033 (42.6)	2,773 (43.3)	260 (35.6)	<0.001
Laboratory results				
Spo2_min, mean ± *SD*	91.8 ± 7.1	91.8 ± 6.7	92.1 ± 9.6	0.383
Spo2_mean, mean ± *SD*	96.8 ± 2.6	96.8 ± 2.5	97.0 ± 3.2	0.14
Aniongap_min, mean ± *SD*	13.5 ± 3.3	13.4 ± 3.4	13.8 ± 2.6	0.004
Aniongap_max, mean ± *SD*	16.2 ± 4.3	16.3 ± 4.4	16.0 ± 3.1	0.182
Albumin_min, mean ± *SD*	3.3 ± 0.5	3.3 ± 0.5	3.6 ± 0.4	<0.001
Albumin_max, mean ± *SD*	3.4 ± 0.5	3.4 ± 0.5	3.7 ± 0.4	<0.001
Glucose_mean, mean ± *SD*	140.5 ± 49.0	140.6 ± 48.5	139.8 ± 53.5	0.679
Potassium_min, mean ± *SD*	3.8 ± 0.4	3.8 ± 0.4	3.7 ± 0.3	<0.001
Potassium_max, mean ± *SD*	4.1 ± 0.5	4.1 ± 0.5	3.9 ± 0.4	<0.001
Bilirubin_total_min, median (IQR)	0.8 (0.4, 1.6)	0.9 (0.4, 1.6)	0.8 (0.4, 1.2)	<0.001
Bilirubin_total_max, median (IQR)	1.0 (0.4, 1.9)	1.0 (0.4, 2.0)	0.8 (0.4, 1.4)	<0.001
Creatinine_min, median (IQR)	0.9 (0.7, 1.2)	0.9 (0.7, 1.2)	0.8 (0.7, 1.1)	0.002
Creatinine_max, median (IQR)	1.0 (0.8, 1.4)	1.0 (0.8, 1.5)	0.9 (0.8, 1.2)	<0.001
Lactate_min, median (IQR)	1.5 (1.2, 1.9)	1.5 (1.2, 1.9)	1.4 (1.2, 1.7)	<0.001
Lactate_max, median (IQR)	2.0 (1.4, 2.9)	2.1 (1.4, 2.9)	1.9 (1.4, 2.4)	<0.001
Platelets_min, median (IQR)	193.0 (141.0, 253.0)	192.0 (139.0, 254.0)	196.0 (157.0, 246.5)	0.12
Platelets_max, median (IQR)	218.0 (165.0, 285.0)	218.0 (163.0, 287.0)	216.0 (171.0, 273.0)	0.816
Ptt_min, median (IQR)	28.3 (25.0, 32.6)	28.4 (25.2, 33.1)	26.8 (23.6, 30.0)	<0.001
Ptt_max, median (IQR)	30.5 (26.5, 40.2)	30.8 (26.7, 42.0)	28.6 (24.9, 33.3)	<0.001
Inr_min, median (IQR)	1.2 (1.1, 1.4)	1.2 (1.1, 1.4)	1.1 (1.0, 1.2)	<0.001
Inr_max, median (IQR)	1.2 (1.1, 1.6)	1.2 (1.1, 1.7)	1.1 (1.1, 1.4)	<0.001
Pt_min, median (IQR)	13.0 (11.7, 15.1)	13.1 (11.7, 15.3)	12.3 (11.4, 13.6)	<0.001
Pt_max, median (IQR)	13.8 (12.1, 18.8)	13.9 (12.1, 19.3)	13.0 (11.8, 15.5)	<0.001
Bun_min, median (IQR)	18.0 (12.0, 26.2)	18.0 (13.0, 27.0)	16.0 (12.0, 21.0)	<0.001
Bun_max, median (IQR)	20.0 (15.0, 31.0)	21.0 (15.0, 32.0)	19.0 (15.0, 24.0)	<0.001
Wbc_min, median (IQR)	9.3 (6.8, 12.6)	9.3 (6.8, 12.7)	9.2 (7.1, 11.9)	0.951
Wbc_max, median (IQR)	11.7 (8.6, 15.9)	11.8 (8.6, 16.1)	11.1 (8.7, 14.5)	<0.001
Vital signs				
TP_mean, mean ± *SD*	100.8 ± 20.3	101.3 ± 20.5	96.9 ± 18.4	<0.001
HR_max, mean ± *SD*	82.4 ± 15.0	82.8 ± 15.2	78.5 ± 12.8	<0.001
HR_mean, mean ± *SD*	153.9 ± 23.3	152.8 ± 23.3	164.2 ± 21.2	<0.001

(Continued)

TABLE 1 | Continued

Variables	Total (*n* = 7,128)	Non-stroke (*n* = 6,397)	Stroke (*n* = 731)	*P*
Sbp_max, mean ± *SD*	123.5 ± 17.4	122.5 ± 17.4	132.3 ± 14.4	<0.001
Sbp_mean, mean ± *SD*	88.0 ± 20.2	87.7 ± 20.2	90.9 ± 19.4	<0.001
Dbp_max, mean ± *SD*	62.6 ± 10.7	62.3 ± 10.8	64.8 ± 10.1	<0.001
Dbp_mean, mean ± *SD*	106.6 ± 24.0	106.1 ± 24.1	110.6 ± 22.5	<0.001
Mbp_max, mean ± *SD*	79.5 ± 11.0	79.1 ± 11.1	83.0 ± 9.8	<0.001
Mbp_mean, mean ± *SD*	36.9 ± 0.6	36.8 ± 0.6	36.9 ± 0.6	<0.001

Continuous variables are presented as the median and interquartile range (IQR). Count data are presented as numbers and percentages. Severe respiratory failure, severe coagulation failure, severe liver failure, severe cardiovascular failure, severe central nervous failure, and severe renal failure refer to the scores of the specific organ or system that scored 4 in the SOFA scheme. The definition of the medical condition was based on the ICD-9 code. A mean, minimum, or maximum parameter refers to the mean, the highest, or the lowest level of the parameter on the first day of ICU admission. CHF, congestive heart failure; PVD, peripheral vascular disease; CPD, chronic pulmonary disease; PUD, chronic pulmonary disease; Spo2, finger pulse oxygen saturation; ptt, partial thromboplastin time; INR, international normalized ratio; pt, prothrombin time; BUN, blood urea nitrogen; wbc, white blood cells; TP, temperature; HR, heart rate; sbp, systolic blood pressure; dbp, diastolic blood pressure; mbp, mean blood pressure.

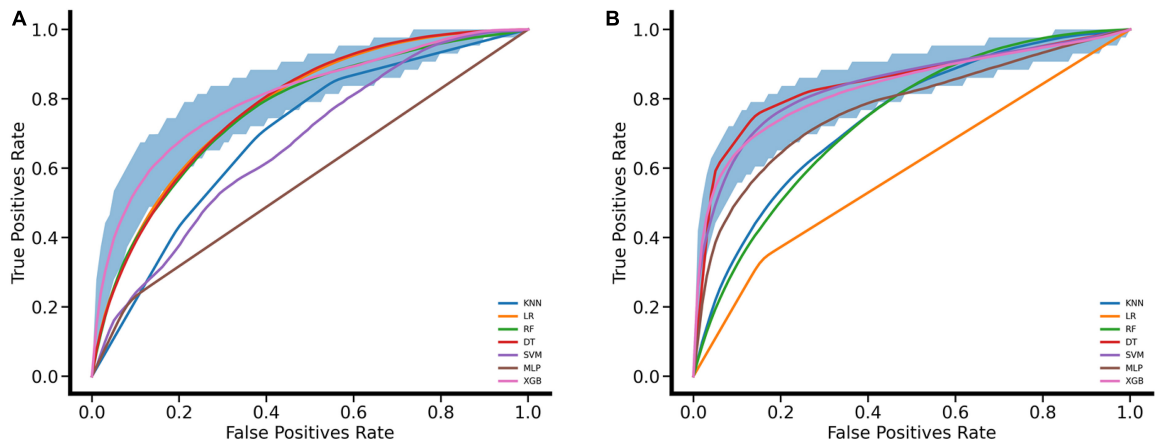

FIGURE 3 | Performance evaluation for seven machine learning algorithms with ROC curves. **(A)** ROC curves were drawn for the validation set based on MIMIC VI performed by leaving 20% as a testing set and using the rest for the training set. **(B)** ROC curves were drawn for the independent testing set based on MIMIC III. The mean ROC curve of XGB is shown in pink and its corresponding 95% confidence interval is shown in deep blue.

TABLE 2 | Performance of machine learning methods in different data sets.

		Accuracy	Sensitivity	Specificity	AUC
The validating set	KNN	0 0.59 (0.47–0.65)	0.75 (0.65–0.9)	0.57 (0.43–0.64)	0.69 (0.66–0,73)
	LR	0.68 (0.55–0.79)	0.71 (0.55–0.86)	0.67 (0.51–0.82)	0.75 (0.71–0.78)
	RF	0.69 (0.56–0.79)	0.74 (0.6–0.88)	0.69 (0.53–0.81)	0.78 (0.74–0.81)
	DT	0 0.79 (0.77–0.81)	0.34 (0.26–0.41)	0.84 (0.82–0.87)	0.59 (0.55–0.63)
	SVM	0.69 (0.59–0.78)	0.75 (0.62–0.86)	0.68 (0.56–0.8)	0.76 (0.73–0.8)
	MLP	0.64 (0.52–0.76)	0.75 (0.58–0.89)	0.63 (0.47–0.78)	0.74 (0.7–0.77)
	XGB	0.68 (0.57–0.78)	0.77 (0.63–0.9)	0.67 (0.53–0.8)	0.78 (0.75–0.81)
The independenttesting set	KNN	0.82 (0.72–0.87)	0.98 (0.97–0.99)	0.25 (0.16–0.31)	0.84 (0.81–0.88)
	LR	0.81 (0.68–0.9)	0.95 (0.94–0.96)	0.13 (0.1–0.2)	0.67 (0.65–0.69)
	RF	0.88 (0.79–0.93)	0.97 (0.96–0.98)	0.33 (0.2–0.49)	0.84 (0.8–0.87)
	DT	0.87 (0.84–0.89)	0.94 (0.94–0.95)	0.15 (0.09–0.24)	0.57 (0.51–0.63)
	SVM	0.87 (0.78–0.92)	0.96 (0.95–0.97)	0.26 (0.17–0.38)	0.77 (0.74–0.81)
	MLP	0.84 (0.75–0.91)	0.97 (0.96–0.98)	0.24 (0.16–0.35)	0.8 (0.76–0.84)
	XGB	0.87 (0.78–0.93)	0.97 (0.96–0.98)	0.3 (0.19–0.45)	0.83 (0.79–0.87)

was used to handle with the missing values. For data in MIMIC- III, we merely keep variables with complete values, which was treated as an independent validation set. Therefore, the subsets were established for the final analyses. The process of establishing models was well illustrated in **Figure 2**.

Statistical Analysis

We compared the characteristics above between the stroke group and the non-stroke group, also between the development cohort and validation cohort. Differences in normally distributed data are described as mean ± *SD* (standard deviation) and were compared by the Students' *t*-test, while differences in non-normal data are described as median and IQR (interquartile range) and were compared by a non-parametric test. Differences in rate and constituent ratio data are presented as numbers and percentages, and they were compared with the chi-squared test or a non-parametric test.

The missing values of the training set and the verification set in the MIMIC-VI database were reasonably filled in with the iterative SVD data imputation method (Troyanskaya et al., 2001; Di Lena et al., 2019). The results of previous literature suggested that machine learning methods with data balancing methods had better performance in stroke prediction compared with imbalanced data (Wu and Fang, 2020). And in this research, a variant of SMOTE called SMOTE-NC is applied in this research to solve the problem of category imbalance because of the categorical features. All classifiers are trained with an equal number of training samples per class through oversampling (Pears et al., 2014; Bolourani et al., 2021).

In this article, several kinds of classifiers are used in machine learning methods to classify strokes. We used a Python library called Scikit-learn to build our classifier. This Python package provides several classification algorithms and is a powerful and useful open-source machine learning toolkit. The details of performing the stroke prediction model are shown in **Figure 2**. We employed 7 machine learning algorithms including KNN (k-nearest neighbor), SVM (support vector machine), MLP (multilayer perceptron), LR (logistic regression), DT (decision tree), RF (random forest) and XGBoost (extreme gradient boosting) to establish a stroke prediction model with the training set. The hyperparameters which we used in 7 machine learning algorithms came from default setting in scikit-learn package. Eg: The hyperparameter of KNN is k and the default setting in scikit-learn is "k = 3," which was used in this study. The performance of the models was weighed by the AUROC (area under the receiver operating characteristic curves) (Zhou et al., 2020). For the best-performing model, the importance of the predictors was evaluated and computed with the information gain. SAS 9.4, R software 3.6.1, and MATLAB 9.9 were used for statistical analyses.

RESULTS

Patient Characteristics

With the data obtained from the common database, we finally identified 7,128 and 661 patients from MIMIC-VI and MIMIC-III, respectively. The screening process is shown in **Figure 1**. Predictors with too much missing data, such as bicarbonate, were excluded. In the current research, we ultimately included 51 predictors. The age, vital signs and partial laboratory results are shown as mean and *SD*; other laboratory results are shown as median and IQR. Sex, race, and comorbidities are shown as number and percentage. Patients in the MIMIC-VI database were divided into stroke group (n = 731) and non-stroke group (n = 6,397). Their baseline characteristics are shown in **Table 1**. The stroke group subjects were older (74.0 ± 10.5 vs. 72.1 ± 10.4) and had a higher incidence of hypertension. Additionally, both the stroke group and the non-stroke group were similar in BMI and sex distribution. Patients in the MIMIC-VI database were randomly separated into training and validation sets at a ratio of 8:2, while the MIMIC-III database made up the independent testing set. Patients with stroke in the training set, validation set and independent testing set accounted for 10.3, 10.2, and 6.51%, respectively. The training cohort included 5,117 non-stroke subjects and 585 stroke subjects. The validation cohort had 1,280 non-stroke subjects and 146 stroke subjects. The independent testing cohort had 618 non-stroke subjects and 43 stroke subjects. Patients in the training and validation cohorts were similar in demographic characteristics, the incidence of various comorbidities, laboratory results and vital signs, as shown in **Supplementary Table 1**. For the independent testing set, constituted by data from MIMIC-VI database, the population included was quite different, and only patients with complete values were included, which is a requirement of an independent testing cohort. The characteristics of patients in the independent testing set were shown in **Supplementary Table 2**.

Prediction Models

The process of performing the stroke prediction model was illustrated in **Figure 2**. Due to the imbalanced ratio of non-stroke to stroke patients in this work, the SMOTENC balancing technique was applied to training dataset before establishing the model. After normalization of data was completed, we applied KNN, SVM, MLP, LR, DT, RF, and XGBoost machine learning algorithms to train with the training dataset, and to test models with testing dataset and the independent testing dataset. The ROC curves of all seven models applied to the testing dataset and the independent testing dataset are given in **Figure 3**. The mean AUC values of 7 models in the validation cohort were 0.69, 0.76, 0.74, 0.75, 0.59, 0.78, and 0.78, respectively. Take the ROC curves into consideration, the XGB model performed best, with higher accuracy, sensitivity, specificity, and AUC values, they are 0.68 (0.57–0.78), 0.77 (0.63–0.9), 0.67 (0.53–0.8), 0.78 (0.75–0.81), respectively (**Table 2**). Due to the differences between the populations included in the database, the proportion of stroke patients and data characteristics of the independent testing cohort were distinct from those of the training set and validation set. Not surprisingly, we found the XGB model performed best in the independent testing set (**Table 2**). The accuracy, sensitivity, specificity, and AUC values of XGB model are 0.87 (0.78–0.93), 0.97 (0.96–0.98), 0.3 (0.19–0.45), 0.83 (0.79–0.87) respectively.

Finally, we can get model-based importance of features, we present the importance of the predictors in the XGB model in **Figure 4**. The top five predictors were hypertension, cancer, congestive heart failure, chronic pulmonary disease and peripheral vascular disease (with importance values of 0.275, 0.104, 0.080, 0.063, and 0.054, respectively). The confusion matrix

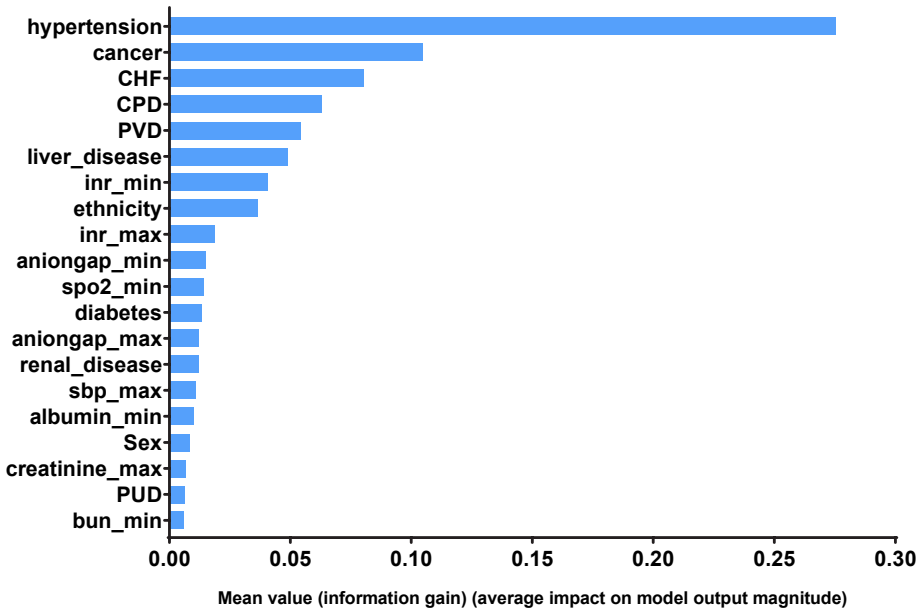

FIGURE 4 | Significance of the predictors in the XGB model. The 20 variables with the highest relative importance are measured by the amount the variable reduced the information gain. CHF, congestive heart failure; CPD, chronic pulmonary disease; PVD, peripheral vascular disease; inr, international normalized ratio; spo2, Finger pulse oxygen saturation; sbp, systolic blood pressure; PUD, chronic pulmonary disease; bun, blood urea nitrogen.

of the XGB model is presented in **Table 3**, which represents the predicted values vs. actual values for the validating and independent testing cohorts.

DISCUSSION

In this study, we aimed to establish suitable model to recognize the possible stroke in elderly patients undergoing surgery and characterize the critical predictors of post-operative stroke. Nowadays, machine learning has been widely used in establishing disease prediction model.

With the help of ML methods, we found that the incidence of stroke in elderly patients undergoing surgery was associated with various clinical features. The XGB model performed best among the KNN, SVM, MLP, LR, DT, RF, and XGB models in our study. We identified hypertension, cancer, congestive heart failure, chronic pulmonary disease and peripheral vascular disease as predictors that were most associated with stroke.

Similar to our study, a study conducted using data from the Chinese Longitudinal Healthy Longevity Study built a stroke prediction model in elderly patients aged more than 60 years (Wu and Fang, 2020). It used SMOTH to deal with imbalanced data and selected important predictors as inputs in three machine learning methods. However, due to the different sources of patients and models, they found that sex, LDLC (low-density lipoprotein cholesterol), GLU (blood glucose), hypertension, and UA (uric acid) were the top five predictors in their RF model.

Compared with other studies, ours have certain strengths. This is the first study to establish stroke prediction models focused on elderly patients undergoing surgery by using an advanced machine learning method. We used several different methods to impute data (KNN, SoftImpute, IterativeImputer, IterativeSVD) and deal with imbalanced data (SMOTENC, ADASYN, BorderlineSMOTE, KMeansSMOTE, SVMSMOTE). Finally, we chose IterativeSVD and SMOTENC according to the AUC values. We utilized not only subjects from MIMIC-III for internal validation but also samples from the MIMIC-VI database for further external testing of the seven machine learning models.

Our study also has some limitations. First, relying on the results, we can only prevent stoke as much as possible, but cannot identify the stroke. The physiological signals like EMG, EEG, and ECG based monitoring system may have a chance to early identify stroke, which is also helpful to post-stroke treatment (Robinson et al., 2003; Hussain and Park, 2020, 2021a,b). Second, there were a certain number of missing values. We abandoned some potential confounding variables for having too many missing data, which is unavoidable in retrospective studies. Third, there were many variables involved, and the excessive variables increased the difficulty of model construction and the accuracy of the established models. Therefore further study about the effect

TABLE 3 | Confusion matrix of the XGBoost model.

		Predicted: non-stroke	Predicted: stroke
The validating set	Actual: non-stroke	988	292
	Actual: stroke	52	94
The independent testing set	Actual: non-stroke	572	46
	Actual: stroke	19	24

of the strongest stroke predictors that we screened out should be carried out in the future.

CONCLUSION

Our results showed that hypertension, cancer, congestive heart failure, chronic pulmonary disease and peripheral vascular disease might be closely associated with stroke in SICU elderly patients. The XGBoost model performs better than the KNN, SVM, MLP, LR, DT, and RF models in our study. In order to prevent stroke of elderly patients in SICU, we need to pay attention to their comorbidities more than other laboratory features, especially maintaining stable blood pressure. However, further additional verifications are necessary to examine the generalization of our models and predictors.

DATA AVAILABILITY STATEMENT

Publicly available datasets were analyzed in this study. This data can be found here: https://mimic.mit.edu/.

ETHICS STATEMENT

Medical Information Mart for Intensive Care (MIMIC) is a large, freely-available medical database consisting of deidentified data from patients who were admitted to the critical care units of the Beth Israel Deaconess Medical Center. The consent was obtained at the beginning of data collection. Therefore, the ethical approval statement and the need for informed consent were jumped in this manuscript, which were not required for this study in accordance with the national legislation and the institutional requirements.

AUTHOR CONTRIBUTIONS

ZF, QW, and XZ made contributions to the conception and design of the work. XZ extracted the data from the MIMIC-III and MIMIC-VI databases. NF and XXZ participated in processing the data and the statistical analysis. XZ and NF finished the first draft, they contributed equally to this work and shared first authorship. All authors had revised the manuscript and approved the final edition.

FUNDING

This work was supported the National Natural Science Foundation of China (no. 82171322) to ZF.

ACKNOWLEDGMENTS

We are extremely grateful to my husband Xiuquan Wu for his consolation and constructive comments on the draft.

SUPPLEMENTARY MATERIAL

The Supplementary Material for this article can be found online at: https://www.frontiersin.org/articles/10.3389/fnagi.2022.897611/full#supplementary-material

REFERENCES

Asadi, H., Kok, H. K., Looby, S., Brennan, P., O'Hare, A., and Thornton, J. (2016). Outcomes and Complications After Endovascular Treatment of Brain Arteriovenous Malformations: A Prognostication Attempt Using Artificial Intelligence. *World Neurosurg.* 96, 562.e–569.e. doi: 10.1016/j.wneu.2016.09.086

Bacchi, S., Zerner, T., Oakden-Rayner, L., Kleinig, T., Patel, S., and Jannes, J. (2020). Deep Learning in the Prediction of Ischaemic Stroke Thrombolysis Functional Outcomes: A Pilot Study. *Acad. Radiol.* 27:e19–e23. doi: 10.1016/j.acra.2019.03.015

Bi, Q., Goodman, K. E., Kaminsky, J., and Lessler, J. (2019). What is Machine Learning? A Primer for the Epidemiologist. *Am. J. Epidemiol.* 188, 2222–2239. doi: 10.1093/aje/kwz189

Biteker, M., Kayatas, K., Türkmen, F. M., and Mısırlı, C. H. (2014). Impact of perioperative acute ischemic stroke on the outcomes of noncardiac and nonvascular surgery: a single centre prospective study. *Can. J. Surg.* 57, E55–E61. doi: 10.1503/cjs.003913

Bolourani, S., Brenner, M., Wang, P., McGinn, T., Hirsch, J. S., Barnaby, D., et al. (2021). A Machine Learning Prediction Model of Respiratory Failure Within 48 Hours of Patient Admission for COVID-19: Model Development and Validation. *J. Med. Internet Res.* 23, e24246. doi: 10.2196/24246

Boursin, P., Paternotte, S., Dercy, B., Sabben, C., and Maïer, B. (2018). [Semantics, epidemiology and semiology of stroke]. *Soins* 63, 24–27. doi: 10.1016/j.soin.2018.06.008

Connor, C. W. (2019). Artificial Intelligence and Machine Learning in Anesthesiology. *Anesthesiology* 131, 1346–1359. doi: 10.1097/aln.0000000000002694

Cox, A. P., Raluy-Callado, M., Wang, M., Bakheit, A. M., Moore, A. P., and Dinet, J. (2016). Predictive analysis for identifying potentially undiagnosed post-stroke spasticity patients in United Kingdom. *J. Biomed. Inform.* 60, 328–333. doi: 10.1016/j.jbi.2016.02.012

Deo, R. C. (2015). Machine Learning in Medicine. *Circulation* 132, 1920–1930. doi: 10.1161/circulationaha.115.001593

Di Carlo, A. (2009). Human and economic burden of stroke. *Age Ageing* 38, 4–5. doi: 10.1093/ageing/afn282

Di Lena, P., Sala, C., Prodi, A., and Nardini, C. (2019). Missing value estimation methods for DNA methylation data. *Bioinformatics* 35, 3786–3793. doi: 10.1093/bioinformatics/btz134

Dong, Y., Cao, W., Cheng, X., Fang, K., Zhang, X., Gu, Y., et al. (2017). Risk Factors and Stroke Characteristic in Patients with Postoperative Strokes. *J. Stroke Cerebrovasc. Dis.* 26, 1635–1640. doi: 10.1016/j.jstrokecerebrovasdis.2016.12.017

Dunham, A. M., Grega, M. A., Brown, C.H.t, McKhann, G. M., Baumgartner, W. A., and Gottesman, R. F. (2017). Perioperative Low Arterial Oxygenation Is Associated With Increased Stroke Risk in Cardiac Surgery. *Anesth. Analg.* 125, 38–43. doi: 10.1213/ane.0000000000002157

Handelman, G. S., Kok, H. K., Chandra, R. V., Razavi, A. H., Lee, M. J., and Asadi, H. (2018). eDoctor: machine learning and the future of medicine. *J. Intern. Med.* 284, 603–619. doi: 10.1111/joim.12822

Heo, J., Yoon, J. G., Park, H., Kim, Y. D., Nam, H. S., and Heo, J. H. (2019). Machine Learning-Based Model for Prediction of Outcomes in Acute Stroke. *Stroke* 50, 1263–1265. doi: 10.1161/strokeaha.118.024293

Hussain, I., and Park, S. J. (2020). HealthSOS: Real-Time Health Monitoring System for Stroke Prognostics. *IEEE Access* 8, 213574–213586. doi: 10.1109/access.2020.3040437

Hussain, I., and Park, S. J. (2021a). Big-ECG: Cardiographic Predictive Cyber-Physical System for Stroke Management. *IEEE Access* 9, 123146–123164. doi: 10.1109/access.2021.3109806

Hussain, I., and Park, S. J. (2021b). Prediction of Myoelectric Biomarkers in Post-Stroke Gait. *Sensors* 21:5334. doi: 10.3390/s21165334

Jiang, F., Jiang, Y., Zhi, H., Dong, Y., Li, H., Ma, S., et al. (2017). Artificial intelligence in healthcare: past, present and future. *Stroke Vasc. Neurol.* 2, 230–243. doi: 10.1136/svn-2017-000101

Khattar, N. K., Friedlander, R. M., Chaer, R. A., Avgerinos, E. D., Kretz, E. S., Balzer, J. R., et al. (2016). Perioperative stroke after carotid endarterectomy: etiology and implications. *Acta Neurochir.* 158, 2377–2383. doi: 10.1007/s00701-016-2966-2

Mantz, J., Dahmani, S., and Paugam-Burtz, C. (2010). Outcomes in perioperative care. *Curr. Opin. Anaesthesiol.* 23, 201–208. doi: 10.1097/ACO.0b013e328336aeef

Maravic-Stojkovic, V., Lausevic-Vuk, L. J., Obradovic, M., Jovanovic, P., Tanaskovic, S., Stojkovic, B., et al. (2014). Copeptin level after carotid endarterectomy and perioperative stroke. *Angiology* 65, 122–129. doi: 10.1177/0003319712473637

Merino, J. G. (2014). Clinical stroke challenges: A practical approach. *Neurol. Clin. Pract.* 4, 376–377. doi: 10.1212/cpj.0000000000000082

Pears, R., Finlay, J., and Connor, A. M. (2014). Synthetic Minority Over-sampling TEchnique(SMOTE) for Predicting Software Build Outcomes. *Comput. Sci.* 1508–2806. doi: 10.48550/arXiv.1407.2330

Robinson, T. G., Dawson, S. L., Eames, P. J., Panerai, R. B., and Potter, J. F. (2003). Cardiac baroreceptor sensitivity predicts long-term outcome after acute ischemic stroke. *Stroke* 34, 705–712. doi: 10.1161/01.Str.0000058493.94875.9f

Saber, H., Somai, M., Rajah, G. B., Scalzo, F., and Liebeskind, D. S. (2019). Predictive analytics and machine learning in stroke and neurovascular medicine. *Neurol. Res.* 41, 681–690. doi: 10.1080/01616412.2019.1609159

Sirsat, M. S., Ferme, E., and Camara, J. (2020). Machine Learning for Brain Stroke: A Review. *J. Stroke Cerebrovasc. Dis.* 29:105162. doi: 10.1016/j.jstrokecerebrovasdis.2020.105162

Sporns, P. B., Hanning, U., Schwindt, W., Velasco, A., Buerke, B., Cnyrim, C., et al. (2017). Ischemic Stroke: Histological Thrombus Composition and Pre-Interventional CT Attenuation Are Associated with Intervention Time and Rate of Secondary Embolism. *Cerebrovasc. Dis.* 44, 344–350. doi: 10.1159/000481578

Troyanskaya, O., Cantor, M., Sherlock, G., Brown, P., Hastie, T., Tibshirani, R., et al. (2001). Missing value estimation methods for DNA microarrays. *Bioinformatics* 17, 520–525. doi: 10.1093/bioinformatics/17.6.520

Wu, Y., and Fang, Y. (2020). Stroke Prediction with Machine Learning Methods among Older Chinese. *Int. J. Environ. Res. Public Health* 17:1828. doi: 10.3390/ijerph17061828

Zhou, Q., Zhu, C., Shen, Z., Zhang, T., Li, M., Zhu, J., et al. (2020). Incidence and potential predictors of thromboembolic events in epithelial ovarian carcinoma patients during perioperative period. *Eur. J. Surg. Oncol.* 46, 855–861. doi: 10.1016/j.ejso.2020.01.026

Conflict of Interest: The authors declare that the research was conducted in the absence of any commercial or financial relationships that could be construed as a potential conflict of interest.

Publisher's Note: All claims expressed in this article are solely those of the authors and do not necessarily represent those of their affiliated organizations, or those of the publisher, the editors and the reviewers. Any product that may be evaluated in this article, or claim that may be made by its manufacturer, is not guaranteed or endorsed by the publisher.

frontiers | Frontiers in Aging Neuroscience

TYPE Original Research
PUBLISHED 25 July 2022
DOI 10.3389/fnagi.2022.905453

OPEN ACCESS

EDITED BY
Gaiqing Wang,
The Third People's Hospital of Hainan Province, China

REVIEWED BY
Yuanli Zhao,
Beijing Tiantan Hospital, Capital Medical University, China
Shengxiang Liang,
Fujian University of Traditional Chinese Medicine, China

*CORRESPONDENCE
Xi Sun
3021064@nyist.edu.cn
Dezhi Kang
kdz99988@vip.sina.com

†These authors have contributed equally to this work and share first authorship

SPECIALTY SECTION
This article was submitted to Neurocognitive Aging and Behavior, a section of the journal Frontiers in Aging Neuroscience

RECEIVED 27 March 2022
ACCEPTED 30 June 2022
PUBLISHED 25 July 2022

CITATION
Chen F, Kang Y, Yu T, Lin Y, Dai L, Yu L, Wang D, Sun X and Kang D (2022) Altered functional connectivity within default mode network after rupture of anterior communicating artery aneurysm.
Front. Aging Neurosci. 14:905453.
doi: 10.3389/fnagi.2022.905453

Altered functional connectivity within default mode network after rupture of anterior communicating artery aneurysm

Fuxiang Chen[1,2,3†], Yaqing Kang[4†], Ting Yu[1,2,3†], Yuanxiang Lin[1,2,3], Linsun Dai[1,2,3], Lianghong Yu[1,2,3], Dengliang Wang[1,2,3], Xi Sun[5*] and Dezhi Kang[1,2,3*]

[1]Department of Neurosurgery, The First Affiliated Hospital, Neurosurgery Research Institute, Fujian Medical University, Fuzhou, China, [2]Department of Neurosurgery, Binhai Branch of National Regional Medical Center, The First Affiliated Hospital, Fujian Medical University, Fuzhou, China, [3]First Affiliated Hospital, Fujian Provincial Institutes of Brain Disorders and Brain Sciences, Fujian Medical University, Fuzhou, China, [4]Department of Radiology, The First Affiliated Hospital of Fujian Medical University, Fuzhou, China, [5]School of Information Engineering, Nanyang Institute of Technology, Nanyang, China

Background: Rupture of anterior communicating artery (ACoA) aneurysm often leads to cognitive impairment, especially memory complaints. The medial superior frontal gyrus (SFGmed), a node of the default mode network (DMN), has been extensively revealed to participate in various cognitive processes. However, the functional connectivity (FC) characteristics of SFGmed and its relationship with cognitive performance remain unknown after the rupture of the ACoA aneurysm.

Methods: Resting-state functional MRI (fMRI) and cognitive assessment were acquired in 27 eligible patients and 20 controls. Seed-based FC between unilateral SFGmed and the rest of the brain was calculated separately, and then compared their intensity differences between the two groups. Furthermore, we analyzed the correlation between abnormal FC and cognitive function in patients with ruptured ACoA aneurysm.

Results: Cognitive impairment was confirmed in 51.9% of the patients. Compared with the controls, patients suffering from ruptured ACoA aneurysm exhibited a similar FC decline between each side of SFGmed and predominant nodes within DMN, including the precuneus, angular gyrus, cingulate cortex, left hippocampus, left amygdala, left temporal pole (TPO), and left medial orbitofrontal cortex (mOFC). Besides, significantly decreased FC of left SFGmed and left insula, right middle temporal gyrus (MTG), as well as right mOFC, were also found. In addition, only enhanced insular connectivity with right SFGmed was determined, whereas increased FC of the left SFGmed was not observed. Correlation analyses showed that lower total cognitive performance or stronger subjective memory complaints were related to reduced connectivity in the SFGmed and several cortical regions such as the angular gyrus and middle cingulate cortex (MCC).

Conclusion: Our results suggest that patients with ruptured ACoA aneurysm exist long-term cognitive impairment and intrinsic hypoconnectivity of cognition-related brain regions within DMN. Deactivation of DMN may be a potential neural mechanism leading to cognitive deficits in these patients.

KEYWORDS

anterior communicating artery aneurysm, subarachnoid hemorrhage, cognitive impairment, resting-state fMRI, functional connectivity, default mode network

Introduction

Aneurysmal subarachnoid hemorrhage (aSAH) is a life-threatening cerebrovascular disease with high mortality and morbidity, and 40% of them are due to rupture of anterior communicating artery (ACoA) aneurysm (Weir et al., 2002). Long-term cognitive impairments have been reported in approximately half of the survivors suffering from ruptured ACoA aneurysm (Martinaud et al., 2009), throwing a heavy burden to patients and their families because of insufficient awareness and limited therapeutic strategies. Currently, functional brain network-directed neuromodulation has shown great promise in various cognitive disorders, including poststroke dementia (Liu et al., 2019; Gimbel et al., 2021; Kolskår et al., 2021; Clancy et al., 2022). However, the neural mechanisms of impaired cognitive function have not been fully elucidated in patients after the rupture of an ACoA aneurysm, which undoubtedly restricts future potential therapeutic applications.

In recent years, neuroimaging studies with respect to cognitive deficits after aSAH have drawn increasing attention, but almost concentrated on structural brain changes, especially subcortical white matter (Yeo et al., 2012; Jang and Kim, 2015; Fragata et al., 2017a,b, 2018). For example, by analyzing brain diffusion tensor imaging (DTI) data in acute and subacute stages of aSAH, Fragata et al. (2017a,b, 2018) found that DTI parameters can early predict the occurrence of delayed cerebral ischemia and functional outcome. There were also some studies that unravel the central mechanisms of brain injury *via* the acquisition of DTI in the chronic stage, including consciousness deficit (Jang and Kim, 2015), motor weakness (Yeo et al., 2012), and cranial nerve damage following aSAH (Seo et al., 2015). Additionally, in comparison with subjects suffering from an unruptured aneurysm, microstructural white matter abnormalities were determined in patients with aSAH and that was linked with their cognitive impairment at 3 months after ictus (Reijmer et al., 2018). Collectively, DTI findings of these aSAH studies provide a necessary structural basis for further functional network research.

Resting-state functional MRI (fMRI) is an important non-invasive technique for the evaluation of brain networks and demonstrated to reliably reflect the spontaneous neural activity of the human brain (Egorova et al., 2018). As a result, investigators are greatly interested in using resting-state fMRI to explore the neural mechanism of cognitive impairment and evaluate the therapeutic effect of neuromodulation (Siegel et al., 2016). It is generally known that working memory and executive function are most susceptible to being impaired in patients with aSAH. Pathogenesis has been investigated *via* resting-state functional connectivity (FC) in a few studies (Maher et al., 2015; Mikell et al., 2015; Su et al., 2018). Compared with healthy controls, the authors discovered that there is multiple seed-based FC strength decline in the aSAH group, including the left parahippocampal gyrus, the left inferior temporal gyrus, and the left thalamus. Besides, abnormal cerebral FC of patients was significantly correlated with their poor memory performance (Su et al., 2018). Another study concerning executive function demonstrated that cognition-impaired patients with aSAH exhibit increased frontoparietal connectivity (Maher et al., 2015). These studies shed light on the brain network mechanisms underlying cognitive dysfunction after aSAH to some extent. But notably, locations of ruptured aneurysm were highly heterogeneous in the abovementioned studies, which undoubtedly cause different patterns of structural brain damage and functional network changes from the start. Additionally, hydrocephalus and epileptic seizure are common complications secondary to the rupture of ACoA aneurysm that may also result in long-term cognitive decline (Taufique et al., 2016; Neifert et al., 2021). Hence, these major confounding factors should be considered for a more accurate understanding of the characteristic brain network changes associated with cognitive dysfunction in patients with aSAH and provide the most precise brain network-directed treatments in the future.

Spontaneous subarachnoid hemorrhage in the anterior interhemispheric cistern on CT images is an important radiographic feature for the diagnosis of the ruptured ACoA aneurysm. It is also a contributing factor leading to frontal cortex structure and function damage, especially disruption in the medial gyri, including the subcallosal gyrus, anterior cingulate gyrus, and rectal gyrus, which have been identified in previous anatomical studies and were demonstrated to be responsible for the later developed cognitive impairment

involving extensive domains (Martinaud et al., 2009; Beeckmans et al., 2020; Mugikura et al., 2020). In addition, SFGmed lesions detected by structural MRI due to the rupture of ACoA aneurysm were also discovered in correlation with cognitive executive deficit and task coordination deficit (Martinaud et al., 2009). Furthermore, imaging studies have suggested that the medial superior frontal gyrus (SFGmed) plays an important role in a variety of cognitive processes (Pan et al., 2021). As reported in various neuropsychiatric disorders with cognitive deficits, abnormal functional brain connectivity of SFGmed with several cognition-related nodes within the default mode network (DMN) was discovered (Qiu et al., 2021; Xu et al., 2021), including precuneus, amygdala, and anterior and posterior cingulate gyrus (Pan et al., 2021; Nagahama et al., 1999; Xu et al., 2021). But as far as we know, SFGmed-based resting-state FC has not been investigated in patients with aSAH caused by ACoA aneurysm rupture.

Hence, we separately defined bilateral SFGmed as the region of interest (ROI) and then used seed-based resting-state FC analysis to explore the features of cognition-related brain network in patients with aSAH caused by the rupture of ACoA aneurysm. We hypothesized that the decline of SFGmed-based FC strength in patients with aSAH due to ruptured ACoA aneurysm as compared to healthy controls, and abnormalities of some network features were related to their cognitive performance.

Materials and methods

Subjects

We recruited patients with aSAH who were hospitalized in our department. The inclusion criteria were: (1) aSAH due to the rupture of ACoA aneurysm; (2) aSAH history of more than 6 months; (3) age range from 35 to 70 years old; and (4) cognitive function intact before the aSAH onset. The exclusion criteria included: (1) history of stroke or neuropsychiatric diseases; (2) occurrence of delayed cerebral ischemia or epileptic seizure during hospitalization; and (3) appearance of hydrocephalus secondary to aSAH. The severity of aSAH at admission was rated using the Hunt–Hess scale (1). Healthy controls matched for age, gender, and level of education were consecutively enrolled in the local community. All the participants were right-handed. This study was approved by the Local Ethics Committee of the First Affiliated Hospital of Fujian Medical University. All the participants provided written informed consent.

Magnetic resonance imaging acquisition

All the MRI data were collected using the same 3.0 T Siemens Imaging Scanner (Siemens Medical Solutions, Germany). Foam padding and earplugs were used to restrict head motion and minimize scanner noise. Subjects were instructed to stay awake with their eyes closed and to think of nothing during resting-state fMRI acquisition. Functional data were obtained using an echo-planar imaging sequence with the following parameters: 50 slices, thickness/gap = 3.4/0 mm, repetition time (TR) = 3,000 ms, echo time (TE) = 30 ms, flip angle = 90°, field of view = 240 mm × 240 mm, matrix = 80 × 80, and voxel size = 3.0 mm^3 × 3.0 mm^3 × 3.4 mm^3. A total of 205 time points were collected for each subject and the resting-state data were acquired over 10 min. The T1-weighted images were acquired in the following parameters: TR = 2,300 ms, TE = 3.09 ms, flip angle = 9°, 192 sagittal slices, thickness = 1 mm, spaced = 0.5 mm, acquisition matrix = 256 × 256, field of view = 256 mm × 240 mm, and voxel size = 1.0 mm^3 × 1.0 mm^3 × 1.0 mm^3. In addition, all the participants were scanned with T2-weighted images to exclude morphological abnormalities.

Neuropsychological assessment

A neuropsychological test was carried out after MRI acquisition by two researchers who were blinded to this study. As previously reported, the Subjective Memory Complaints Questionnaire (SMCQ) was adopted to measure subjective memory problems in general and daily living, and the SMCQ score of 6 or above was assigned as a diagnostic threshold (Kim et al., 2021). Besides, all the participants were instructed to accomplish the Montreal Cognitive Assessment (MoCA), consisting of several cognitive domains such as memory, attention, visuospatial, and executive functions. Cognitive impairment was defined as the MoCA total score of less than 26 according to previously reported (Wong et al., 2012).

Data processing

All the fMRI data were processed using Data Processing Assistant for Resting-State fMRI (DPARSF).[1] First, the fMRI data were preprocessed. The data preprocessing was referred to the previous research (Chao-Gan and Yu-Feng, 2010), including: (1) slice timing; (2) head motion correction; (3) normalizing to the Montreal Neurological Institute (MNI) space (voxel size: 2 mm^3 × 2 mm^3 × 2 mm^3); (4) smoothing by 8 mm full width at half maximum; (5) linear detrending; (6) bandpass temporal filtering (0.01–0.08 Hz); and (7) regressing out nuisance covariates (Friston 24 head motion parameters, whiter matter signal, and cerebrospinal fluid signal).

Then, binary masks of left SFGmed and right SFGmed were chosen to set as seed regions. Time courses from all the voxels

1 http://www.restfmri.net

within each seed were averaged and used as reference time courses. The Pearson's correlation coefficient was calculated between the time courses of each reference and voxel, and then underwent Fisher's z-score transformation. FC maps of the two regions were established and then analyzed in SPM12 using the ANOVA model for calculating the difference between group-level functional maps. Brain regions were considered significant within a threshold of $p < 0.05$ after the false discovery rate corrected for multiple comparisons and cluster size > 50.

Statistical analysis

Between-group statistics were performed by using the SPSS software version 20.0. Demographic and clinical characteristics differences between the groups were compared by using an independent two-sample *t*-test and the chi-squared test. For non-parametric data, the Mann–Whitney *U*-test was used. A two-tailed Pearson's correlation analysis was used to obtain the correlations between the FC values of the significant brain regions and the MoCA/SMCQ scores. The statistical significance threshold was set to $p < 0.05$.

Results

Demographic and clinical characteristics of the participants

Twenty-seven patients after rupturing of ACoA aneurysm and 20 healthy controls were enrolled for fMRI scans and cognitive assessment between April 2020 and March 2021. One patient and one control were excluded due to excessive head motion. The demographic and clinical characteristics of the remaining subjects are shown in Table 1. The Hunt–Hess scale for the majority of patients (25/26) at admission was grade 1–3, and the size of the aneurysm was almost small than 10 mm. There was no significant difference in age, gender, or years of education between the two groups. In addition, the MoCA and SMCQ scores were lower in patients with aSAH than in healthy controls ($p < 0.01$). Moreover, cognitive impairment was found in 51.9% (14/27) of all the patients with ruptured ACoA aneurysm, and subjective memory complaints in 44.4% (12/27) of patients.

TABLE 1 Clinical characteristics of the patients with ruptured ACoA aneurysm and healthy controls.

	Patients with ruptured ACoA aneurysm	Healthy controls	*P*-value
Age (year)	57.3 ± 9.8	53.3 ± 7.2	0.12
Gender (male/female)	15/11	10/9	0.77
Education (years)	9.1 ± 4.3	9.4 ± 4.1	0.623
Hunt-Hess on admission			
1	7	–	
2	16	–	
3	2	–	
4	1	–	
Size of aneurysm			
≤5 mm	12	–	
5–10 mm	13	–	
>10 mm	1	–	
Aneurysm treatment			
Coiling	8	–	
Clipping	18	–	
Interval between aSAH and MRI acquirement (month)	23.9 ± 13.4	–	
MoCA	23.88 ± 5.37	29.42 ± 0.84	<0.01
SMCQ	4.16 ± 3.88	0.11 ± 0.32	<0.001

The values were represented with mean ± standard deviation. aSAH, aneurysmal subarachnoid hemorrhage; ACoA, anterior communicating artery; MRI, magnetic resonance imaging; MoCA, Montreal Cognitive Assessment; SMCQ, Subjective Memory Complaints Questionnaire.

Comparisons of functional connectivity strength between the two groups

The seed-based FC analyses showed similar alternations in the brain network of bilateral SFGmed. Specifically, when the left SFGmed was defined as the ROI, a reduction in FC was found in the left temporal pole (TPO), left hippocampus, left amygdala, left insula, and right middle temporal gyrus (MTG), as well as the bilateral precuneus, bilateral angular gyrus, bilateral medial orbitofrontal cortex (mOFC), bilateral anterior cingulate cortex (ACC), bilateral middle cingulate cortex (MCC), and bilateral posterior cingulate cortex (PCC) in the aSAH group in comparison with the healthy controls. However, significantly increased functional brain connectivity of left SFGmed was not observed (Figure 1 and Table 2). Similarly, decreased functional brain connectivity in the bilateral precuneus, bilateral angular gyrus, and bilateral cingulate cortex was also uncovered when the right SFGmed was chosen as another ROI. In addition, we also found a decline in FC strength between the right SFGmed and left TPO, as well as right SFGmed and left mOFC. Conversely, compared with healthy controls, hyperconnectivity between right SFGmed and right insula was revealed in patients with ruptured ACoA aneurysm (Figure 2 and Table 3).

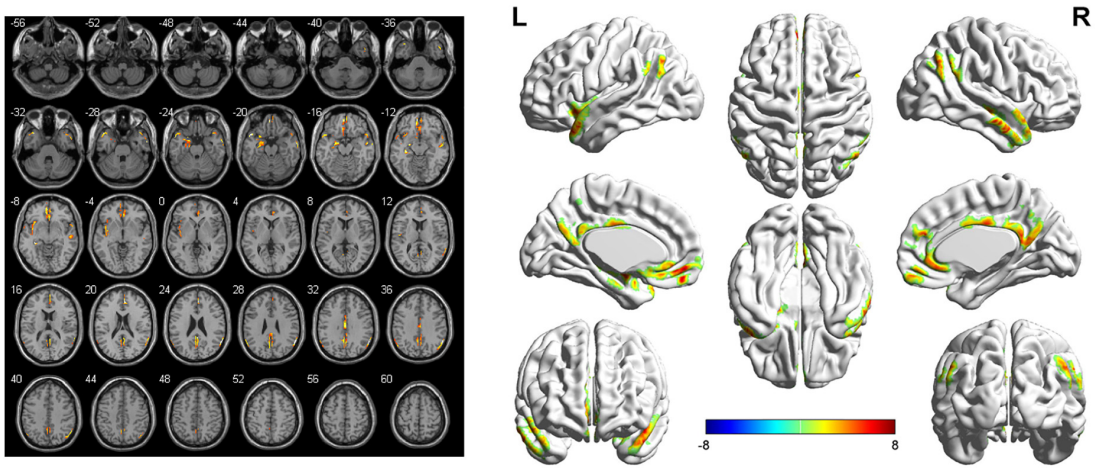

FIGURE 1
Left-side SFGmed-based resting-state functional connectivity analysis between patients with ruptured ACoA aneurysm and healthy controls. Results were displayed in 2D **(left)** and 3D **(right)**, respectively. The color bar represents T-scores. Brain regions labeling with color indicate decreased functional connectivity in patients with ruptured ACoA aneurysm as compared to the healthy controls. The threshold for displaying was set to $p < 0.05$, false discovery rate corrected, and cluster size > 50. Details of these color regions are given in Table 2. SFGmed, medial superior frontal gyrus; ACoA, anterior communicating artery; L, left; R, right.

TABLE 2 Brain regions showing significant decreased left SFGmed-based functional connectivity in the aSAH group as compared to the healthy controls.

Brain region	Number of voxels	PeakMNI coordinates			Peak *T*-value
		X	Y	Z	
Right middle temporal gyrus	103	60	0	−26	8.13
Left temporal pole	127	−50	16	−20	8.99
Left hippocampus/left amygdala	235	−34	−30	−8	10.47
Left insula	192	−26	12	−22	8.27
Medial orbitofrontal cortex/anterior cingulate cortex	466	−4	52	−12	9.28
Right temporal pole	50	52	16	−18	5.25
Precuneus/posterior cingulate cortex	367	2	−44	24	7.87
Right angular	140	60	−58	28	11.91
Left angular	56	−50	−64	40	6.08
Middle cingulate cortex	99	2	−16	32	6.69

SFGmed, medial superior frontal gyrus; aSAH, aneurysmal subarachnoid hemorrhage; MNI, Montreal Neurological Institute.

Correlations between functional connectivity strength and cognitive performance in the aneurysmal subarachnoid hemorrhage group

We also used correlation analysis to investigate whether the resting-state FC strength of the bilateral SFGmed seeds was associated with cognitive or memory performance. In patient with rupture of ACoA aneurysm, positive correlations between MoCA total score and left SFGmed-left ACC, right SFGmed-right MCC, as well as right SFGmed-left MCC FC strength were discovered ($r = 0.435$, $r = 0.393$, and $r = 0.441$, respectively). As shown in Figure 3, we also found negative correlations between the SMCQ scores and FC strength of right SFGmed-right MCC, right SFGmed-left MCC, and right SFGmed-right angular gyrus ($r = -0.488$, $r = -0.4$, and $r = -0.408$, respectively). In addition, the decreased FC strength between left SFGmed and right angular gyrus, as well as right MCC was significantly correlated with the increased score of the SMCQ ($r = -0.411$ and $r = -0.486$, respectively).

Discussion

To the best of our knowledge, this is the first study to explore alterations in the resting-state functional brain connectivity

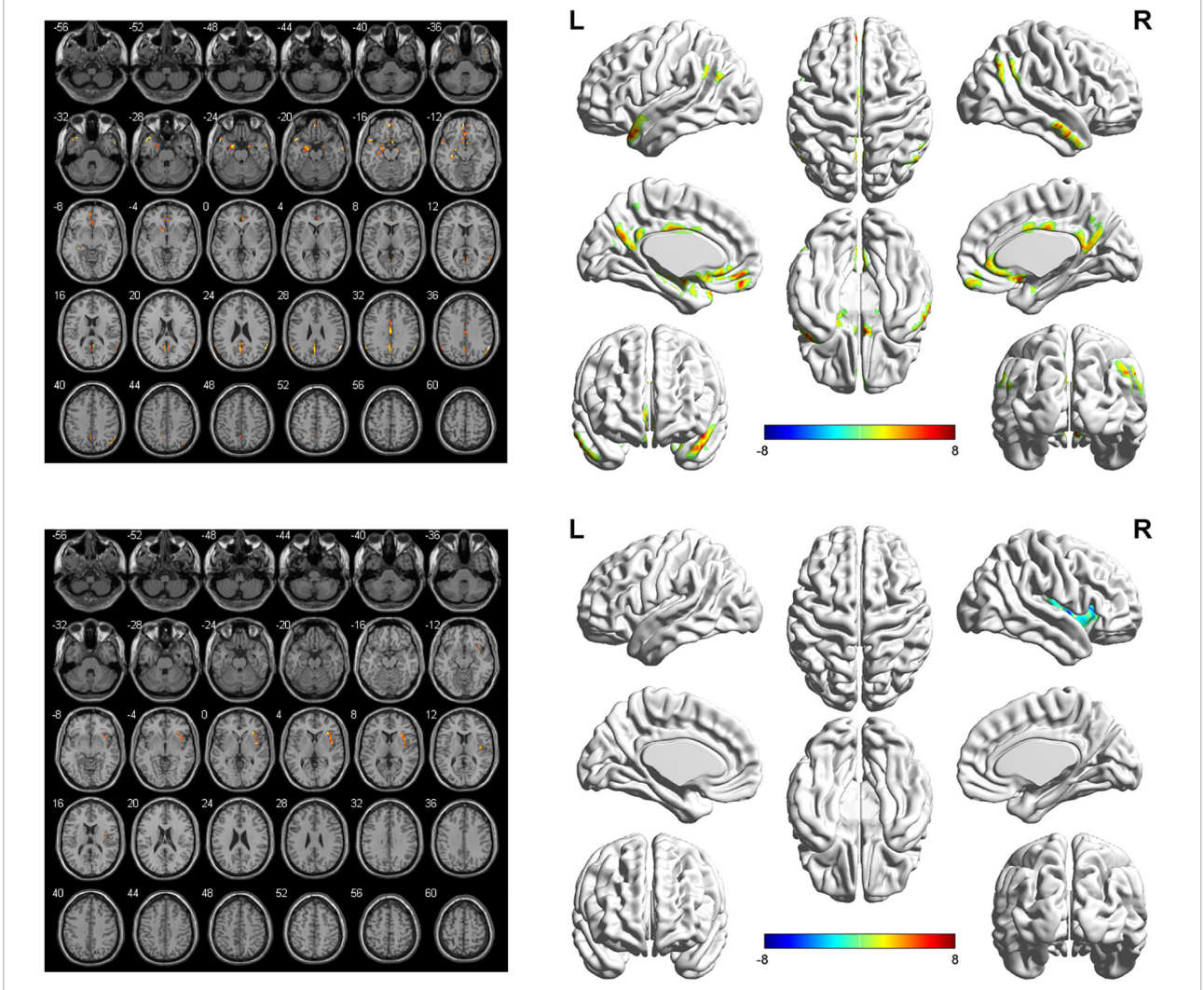

FIGURE 2
Right-side SFGmed-based resting-state functional connectivity analysis between patients with ruptured ACoA aneurysm and healthy controls. Results were represented in 2D (left) and 3D (right), respectively. The color bar represents T-scores. Brain regions labeling with color indicate decreased **(top panel)** or increased functional connectivity **(bottom panel)** in patients with ruptured ACoA aneurysm as compared to the healthy controls. The threshold for displaying was set to $p < 0.05$, false discovery rate corrected, and cluster size > 50. Details of these color regions are given in **Table 2**. SFGmed, medial superior frontal gyrus; ACoA, anterior communicating artery; L, left; R, right.

of the SFGmed-based in patients with ruptured ACoA aneurysm as compared to the controls. The correlation between functional network changes and cognitive performance was also investigated. The current study primarily revealed decreased strength of FC between SFGmed and predominant brain regions within DMN, including the bilateral precuneus, bilateral angular gyrus, bilateral cingulate cortex, temporal cortex, and limbic system in patients after the rupture of ACoA aneurysm relative to healthy controls. Resting hypoconnectivity between some of the abovementioned brain regions such as SFGmed-right MCC, SFGmed-angular gyrus, and right SFGmed-left MCC was found to be significantly correlated with the MoCA and SMCQ scores, which have been widely demonstrated to participate in various cognitive deficits. Consistent with our hypothesis, our findings indicate a decline of extensive FC strength in cognition-related brain regions following the rupture of an ACoA aneurysm.

Cognitive dysfunction caused by neurodegenerative diseases has been an emphase by researchers around the world. In recent years, increasing attention has been paid to stroke-related cognitive deficits, which are mainly due to the high incidence of vascular stroke. Cognitive dysfunction is common in patients with aSAH due to ruptured ACoA aneurysm, no matter undergoing surgical clipping or endovascular coiling (Beeckmans et al., 2020). In this study, half (14/27) of the patients developed cognitive impairment approximately 2 years after the rupture of the ACoA aneurysm. Moreover, most of

TABLE 3 Brain regions showing significant differences of the right SFGmed-based functional connectivity in the aSAH group as compared to the healthy controls.

Brain region	Number of voxels	PeakMNI coordinates			Peak *T*-value
		X	Y	Z	
Left temporal pole	114	−50	14	−26	8.27
Left hippocampus/left amygdala	213	−34	−30	−8	8.38
Left medial orbitofrontal cortex	58	−4	50	−14	8.12
Anterior cingulate cortex	67	4	12	−16	6.96
Precuneus/posterior cingulate cortex	262	−2	−60	28	6.63
Right angular	93	60	−56	28	10.00
Left angular	54	−60	−56	30	6.90
Middle cingulate cortex	70	−2	−14	30	5.82
Right insula	138	40	0	0	−6.50

SFGmed, medial superior frontal gyrus; aSAH, aneurysmal subarachnoid hemorrhage; MNI, Montreal Neurological Institute.

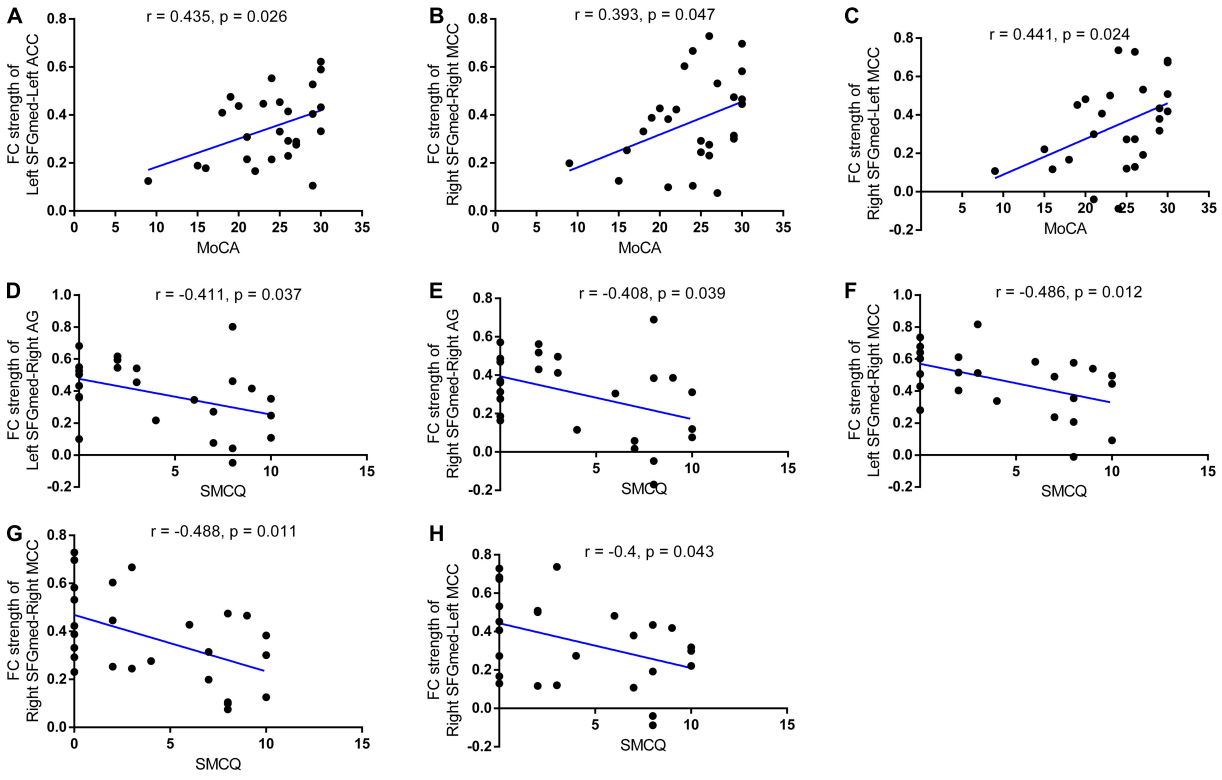

FIGURE 3
Correlations between functional connectivity strength and cognitive performance in patients with ruptured ACoA aneurysm. Positive correlations between the MoCA scores and left SFGmed-left ACC **(A)**, right SFGmed-right MCC **(B)**, as well as right SFGmed-left MCC **(C)** connectivity strength were discovered in patients with ruptured ACoA aneurysm. Negative correlations between the SMCQ scores and left SFGmed-right AG **(D)**, right SFGmed-right AG **(E)**, left SFGmed-right MCC **(F)**, right SFGmed-right MCC **(G)**, and right SFGmed-left MCC **(H)** connectivity strength were displayed in patients with ruptured ACoA aneurysm. ACoA, anterior communicating artery; SFGmed, medial superior frontal gyrus; AG, angular gyrus; MoCA, Montreal Cognitive Assessment; ACC, anterior cingulate cortex; MCC, middle cingulate cortex; SMCQ, Subjective Memory Complaints Questionnaire.

them belong to the Hunt–Hess scale grade of 1–3, i.e., low-grade aSAH. But conversely, another study involvement of 126 similar subjects existed only 22.2% of cognitive impairments (Ma et al., 2021). This discrepancy is likely due to the use of different cognitive assessment scales. In their study, the Modified Telephone Interview for Cognitive Status was adopted

with the disadvantage of not being able to assess the cognitive function of subjects face-to-face, suggesting a possibility of subjective judgments. However, the present study employed a more widely used and valid MoCA scale (Wong et al., 2014). Subjective memory complaints were recognized as the most common domain of cognitive deficits described in patients with aSAH. Therefore, the SMCQ was also used in this study to assess subjective memory problems. Consistent with the results of the MoCA, subjective memory complaints were determined in 44.4% (12/27) of all the participants. On the other hand, the smaller size of patients with a ruptured history of ACoA aneurysm collected in our study may be another non-negligible factor.

Cognitive rehabilitation is necessary for many patients suffering from ruptured ACoA aneurysms, but the essential prerequisite is to grasp the exact neural mechanism of cognitive impairment. As reported in previous fMRI studies, abnormalities of frontoparietal executive network (Maher et al., 2015), frontal networks (Mikell et al., 2015), as well as the mirror neuron system (Plata-Bello et al., 2017) were discovered in patients with aSAH as compared to the control group. Besides, the altered connection properties were also associated with clinical dysfunction or cognitive manifestation. The distribution of aneurysms leading to aSAH varied in these studies, and even patients with intracranial hemorrhage were included. The homogeneity of patients is known to be importance for exploring the brain network mechanism of cognitive dysfunction, including the location of the ruptured aneurysm. The main advantage of this study is that only patients with ruptured ACoA aneurysm were included. What is more, confounding factors contributing to cognitive decline such as hydrocephalus and epileptic seizure were excluded. Therefore, the results of the present study may be more reliable to some extent.

Compared to the healthy controls, patients who survived the rupture of ACoA aneurysm exhibited a decline in resting-state FC between SFGmed and wide brain regions. Furthermore, the distribution of these cortical and subcortical brain regions with hypoconnectivity was basically similar, no matter which side of SFGmed was set as ROI, mainly including temporal cortex, mOFC, bilateral angular gyrus, bilateral cingulate cortex, bilateral precuneus, and limbic cortex (left hippocampus and left amygdala). Notably, the majority of these brain regions are known for vital components of the DMN, which is a well-established intrinsic large-scale brain network responsible for various cognitive processes such as recollection, imagination, semantic and episodic memory, and conceptual processing (Hsu et al., 2016; Smallwood et al., 2021). Substantial evidence has demonstrated that dysregulation, especially the deactivation of the DMN, is linked with many kinds of neuropsychiatric disorders, including stroke (Veldsman et al., 2018; Kolskår et al., 2021). In a matched case–control study, patients with poststroke cognitive impairment were observed to affect the DMN more frequently compared with controls (Lim et al., 2014). Structural evidence for DMN involvement comes from another study showing that correlations in the rate of atrophy within the DMN are more extensive after ischemic stroke (Veldsman et al., 2018). What is more, cognitive recovery in patients suffering stroke achieved from non-invasive treatment strategies was demonstrated to be associated with higher activation of nodes within DMN such as precuneus, PCC, temporal cortex, medial prefrontal gyrus, and angular gyrus (Batista et al., 2019; Kolskår et al., 2021). In addition, previous studies have suggested that the human DMN can be divided into two subsystems and a midline core region according to different responses to multifarious cognitive tasks. Among them, the medial temporal lobe subsystem consisting of the amygdala and hippocampus is linked with memory and emotional processes. Another subsystem mainly containing the temporoparietal cortex is associated with language and social cognition. Consistent with previous results, our findings of resting-state FC and correlation analyses are mainly located in the cognition-related subsystems of DMN (Robin et al., 2015; Hsu et al., 2016). Taken together, the decreased connection between nodes within the DMN is probably a central mechanism for cognitive impairment in patients with ruptured ACoA aneurysm.

Compared with healthy controls, the FC between SFGmed and insula was decreased in the left hemisphere, whereas increased in the right hemisphere in patients suffering from ruptured ACoA aneurysm. The insular cortex is involved in a variety of functions such as sensory stimuli and cognitive and emotional processing. Therefore, hypoconnectivity between the left SFGmed and left insular may be an intrinsic manifestation of cognitive impairment. The functional imaging studies have suggested that there exists abundant interinsular connectivity in physiological state. As a result, once the activity of left-sided insula is decreased, the contralateral insular cortex may play a compensatory role to limit the functional loss. This speculation is supported by a recent study of unilateral tumor infiltration of the insula whether dynamically modulates the FC of the contralesional one (Almairac et al., 2021). The potential functional plasticity in patients after a ruptured ACoA aneurysm also informs brain network-directed therapy.

There are several limitations to our study. First, cognitive function consists of multiple domains such as executive function, memory, attention, and visuospatial abilities. Although the MoCA and the SMCQ are widely considered suitable for the assessment of total cognitive impairment and subjective memory complaints, scales for other cognitive domains preferably also need to be evaluated. Second, the SFGmed can be separated into the supplementary motor areas and the pre-supplementary motor areas. Evidence suggested that they play important roles in motor and cognitive control, respectively. To better characterize the features of seed-based

resting-state FC in patients after the rupture of the ACoA aneurysm, functional subdivisions of the SFGmed may be deserved. Third, we tried to minimize the effect of confounding factors on cognitive function, so the exclusion criteria for the present study included epileptic seizure during hospitalization and hydrocephalus at follow-up. In addition, we only recruited patients following rupture of ACoA aneurysm at our center in a relatively short period of time. As a result, a small group of eligible ACoA patients was included in our study. Studies with a larger sample size should be designed in the future to achieve a stronger conclusion.

In summary, the present study put forward evidence of a decline of FC between SFGmed and widespread brain regions in patients with ruptured ACoA aneurysm. Most of the cortical hypoconnectivity is mainly located in DMN, which has been correlated with poststroke cognitive deficits. Our findings implicate that decreased intrinsic connectivity within DMN may account for cognitive impairment following the rupture of ACoA aneurysm, which we hope will contribute to future translational therapy options after aSAH.

Data availability statement

The original contributions presented in the study are included in the article/supplementary material, further inquiries can be directed to the corresponding author/s.

Ethics statement

The studies involving human participants were reviewed and approved by the Local Ethics Committee of the First Affiliated Hospital of Fujian Medical University. The patients/participants provided their written informed consent to participate in this study.

Author contributions

FC and DK conceived and designed the experiments. FC drafted the manuscript. DK revised the manuscript. YK performed the MRI scanning. TY and YL assessed the cognitive function. FC, DK, TY, YK, YL, LY, DW, and LD helped to collect patients and healthy controls. FC and XS participated in data processing and statistical analysis. All authors have read and approved the final version of the manuscript.

Funding

This study was supported by grants from the National Natural Science Foundation of China (81901338, 81870930, and 82171327), the Youth Project of Fujian Provincial Health (2019-1-39), the Joint Funds for the Innovation of Science and Technology, Fujian Province (2018Y9085), and the Technology Platform Construction Project of Fujian Province (2021Y2001).

Conflict of interest

The authors declare that the research was conducted in the absence of any commercial or financial relationships that could be construed as a potential conflict of interest.

Publisher's note

All claims expressed in this article are solely those of the authors and do not necessarily represent those of their affiliated organizations, or those of the publisher, the editors and the reviewers. Any product that may be evaluated in this article, or claim that may be made by its manufacturer, is not guaranteed or endorsed by the publisher.

References

Almairac, F., Deverdun, J., Cochereau, J., Coget, A., Lemaitre, A., Moritz-Gasser, S., et al. (2021). Homotopic redistribution of functional connectivity in insula-centered diffuse low-grade glioma. *Neuroimage Clin.* 29:102571. doi: 10.1016/j.nicl.2021.102571

Batista, A., Bazán, P., Conforto, A., Martin, M., Simon, S., Hampstead, B., et al. (2019). Effects of mnemonic strategy training on brain activity and cognitive functioning of left-hemisphere ischemic stroke patients. *Neural Plast.* 2019:4172569. doi: 10.1155/2019/4172569

Beeckmans, K., Crunelle, C., Van den Bossche, J., Dierckx, E., Michiels, K., Vancoillie, P., et al. (2020). Cognitive outcome after surgical clipping versus endovascular coiling in patients with subarachnoid hemorrhage due to ruptured anterior communicating artery aneurysm. *Acta Neurol. Belg.* 120, 123–132.

Chao-Gan, Y., and Yu-Feng, Z. (2010). DPARSF: a matlab toolbox for "Pipeline" data analysis of resting-state fMRI. *Front. Syst. Neurosci.* 4:13. doi: 10.3389/fnsys.2010.00013

Clancy, K., Andrzejewski, J., You, Y., Rosenberg, J., Ding, M., and Li, W. (2022). Transcranial stimulation of alpha oscillations up-regulates the default mode network. *Proc. Natl. Acad. Sci. U.S.A.* 119:e2110868119. doi: 10.1073/pnas.2110868119

Egorova, N., Cumming, T., Shirbin, C., Veldsman, M., Werden, E., and Brodtmann, A. (2018). Lower cognitive control network connectivity in stroke participants with depressive features. *Transl. Psychiatry* 7:4. doi: 10.1038/s41398-017-0038-x

Fragata, I., Alves, M., Papoila, A. L., Ferreira, P., Nunes, A. P., Moreira, N. C., et al. (2018). Prediction of clinical outcome in subacute subarachnoid hemorrhage using diffusion tensor imaging. *J. Neurosurg.* [Epub ahead of print]. doi: 10.3171/2017.10.JNS171793

Fragata, I., Alves, M., Papoila, A. L., Nunes, A. P., Ferreira, P., Canto-Moreira, N., et al. (2017a). Early prediction of delayed ischemia and functional outcome in acute subarachnoid hemorrhage: role of diffusion

tensor imaging. *Stroke* 48, 2091–2097. doi: 10.1161/STROKEAHA.117.016811

Fragata, I., Canhao, P., Alves, M., Papoila, A. L., and Canto-Moreira, N. (2017b). Evolution of diffusion tensor imaging parameters after acute subarachnoid haemorrhage: a prospective cohort study. *Neuroradiology* 59, 13–21. doi: 10.1007/s00234-016-1774-y

Gimbel, S., Ettenhofer, M., Cordero, E., Roy, M., and Chan, L. (2021). Brain bases of recovery following cognitive rehabilitation for traumatic brain injury: a preliminary study. *Brain Imaging Behav.* 15, 410–420. doi: 10.1007/s11682-020-00269-8

Hsu, L., Liang, X., Gu, H., Brynildsen, J., Stark, J., Ash, J., et al. (2016). Constituents and functional implications of the rat default mode network. *Proc. Natl. Acad. Sci. U.S.A.* 113, E4541–E4547. doi: 10.1073/pnas.1601485113

Jang, S. H., and Kim, H. S. (2015). Aneurysmal subarachnoid hemorrhage causes injury of the ascending reticular activating system: relation to consciousness. *AJNR Am. J. Neuroradiol.* 36, 667–671. doi: 10.3174/ajnr.A4203

Kim, J., Shin, E., Han, K., Park, S., Youn, J., Jin, G., et al. (2021). Efficacy of smart speaker-based metamemory training in older adults: case-control cohort study. *J. Med. Internet Res.* 23:e20177. doi: 10.2196/20177

Kolskår, K., Richard, G., Alnaes, D., Dørum, E., Sanders, A., Ulrichsen, K., et al. (2021). Reliability, sensitivity, and predictive value of fMRI during multiple object tracking as a marker of cognitive training gain in combination with tDCS in stroke survivors. *Hum. Brain Mapp.* 42, 1167–1181. doi: 10.1002/hbm.25284

Lim, J., Kim, N., Jang, M., Han, M., Kim, S., Baek, M., et al. (2014). Cortical hubs and subcortical cholinergic pathways as neural substrates of poststroke dementia. *Stroke* 45, 1069–1076. doi: 10.1161/STROKEAHA.113.004156

Liu, J., Zhang, B., Wilson, G., Kong, J., and Alzheimer's Disease Neuroimaging Initiative (2019). New perspective for non-invasive brain stimulation site selection in mild cognitive impairment: based on meta- and functional connectivity analyses. *Front. Aging Neurosci.* 11:228. doi: 10.3389/fnagi.2019.00228

Ma, N., Feng, X., Wu, Z., Wang, D., and Liu, A. (2021). Cognitive impairments and risk factors after ruptured anterior communicating artery aneurysm treatment in low-grade patients without severe complications: a multicenter retrospective study. *Front. Neurology.* 12:613785. doi: 10.3389/fneur.2021.613785

Maher, M., Churchill, N. W., de Oliveira Manoel, A. L., Graham, S. J., Macdonald, R. L., and Schweizer, T. A. (2015). Altered resting-state connectivity within executive networks after aneurysmal subarachnoid hemorrhage. *PLoS One* 10:e0130483. doi: 10.1371/journal.pone.0130483

Martinaud, O., Perin, B., Gérardin, E., Proust, F., Bioux, S., Gars, D., et al. (2009). Anatomy of executive deficit following ruptured anterior communicating artery aneurysm. *Eur. J. Neurol.* 16, 595–601.

Mikell, C. B., Banks, G. P., Frey, H. P., Youngerman, B. E., Nelp, T. B., Karas, P. J., et al. (2015). Frontal networks associated with command following after hemorrhagic stroke. *Stroke* 46, 49–57. doi: 10.1161/STROKEAHA.114.007645

Mugikura, S., Mori, N., Kikuchi, H., Mori, E., Takahashi, S., and Takase, K. (2020). Relationship between decreased cerebral blood flow and amnesia after microsurgery for anterior communicating artery aneurysm. *Ann. Nucl. Med.* 34, 220–227. doi: 10.1007/s12149-020-01436-z

Nagahama, Y., Okada, T., Katsumi, Y., Hayashi, T., Yamauchi, H., Sawamoto, N., et al. (1999). Transient neural activity in the medial superior frontal gyrus and precuneus time locked with attention shift between object features. *Neuroimage* 10, 193–199. doi: 10.1006/nimg.1999.0451

Neifert, S., Chapman, E., Martini, M., Shuman, W., Schupper, A., Oermann, E., et al. (2021). Aneurysmal Subarachnoid Hemorrhage: the Last Decade. *Transl. Stroke Res.* 12, 428–446.

Pan, Y., Liu, Z., Xue, Z., Sheng, Y., Cai, Y., Cheng, Y., et al. (2021). Abnormal network properties and fiber connections of DMN across major mental disorders: a probability tracing and graph theory study. *Cereb. Cortex.* [Epub ahead print]. doi: 10.1093/cercor/bhab405

Plata-Bello, J., Modrono, C., Acosta-Lopez, S., Perez-Martin, Y., Marcano, F., Garcia-Marin, V., et al. (2017). Subarachnoid hemorrhage and visuospatial and visuoperceptive impairment: disruption of the mirror neuron system. *Brain Imaging Behav.* 11, 1538–1547. doi: 10.1007/s11682-016-9609-3

Qiu, X., Lu, S., Zhou, M., Yan, W., Du, J., Zhang, A., et al. (2021). The relationship between abnormal resting-state functional connectivity of the left superior frontal gyrus and cognitive impairments in youth-onset drug-Naïve Schizophrenia. *Front. Psychiatry* 12:679642. doi: 10.3389/fpsyt.2021.679642

Reijmer, Y. D., van den Heerik, M. S., Heinen, R., Leemans, A., Hendrikse, J., de Vis, J. B., et al. (2018). Microstructural white matter abnormalities and cognitive impairment after aneurysmal subarachnoid hemorrhage. *Stroke* 49, 2040–2045. doi: 10.1161/STROKEAHA.118.021622

Robin, J., Hirshhorn, M., Rosenbaum, R., Winocur, G., Moscovitch, M., and Grady, C. (2015). Functional connectivity of hippocampal and prefrontal networks during episodic and spatial memory based on real-world environments. *Hippocampus* 25, 81–93. doi: 10.1002/hipo.22352

Seo, Y. S., Chang, C. H., Jung, Y. J., and Jang, S. H. (2015). Injury of the oculomotor nerve after aneurysmal subarachnoid hemorrhage: diffusion tensor tractography study. *Am. J. Phys. Med. Rehabil.* 94, e51–e52. doi: 10.1097/PHM.0000000000000270

Siegel, J. S., Ramsey, L. E., Snyder, A. Z., Metcalf, N. V., Chacko, R. V., Weinberger, K., et al. (2016). Disruptions of network connectivity predict impairment in multiple behavioral domains after stroke. *Proc. Natl. Acad. Sci. U.S.A.* 113, E4367–E4376.

Smallwood, J., Bernhardt, B., Leech, R., Bzdok, D., Jefferies, E., and Margulies, D. (2021). The default mode network in cognition: a topographical perspective. *Nat. Rev. Neurosci.* 22, 503–513.

Su, J., E, T., Guo, Q., Lei, Y., and Gu, Y. (2018). Memory deficits after aneurysmal subarachnoid hemorrhage: a functional magnetic resonance imaging study. *World Neurosurg.* 111, e500–e506.

Taufique, Z., May, T., Meyers, E., Falo, C., Mayer, S., Agarwal, S., et al. (2016). Predictors of poor quality of life 1 year after subarachnoid hemorrhage. *Neurosurgery* 78, 256–264.

Veldsman, M., Curwood, E., Pathak, S., Werden, E., and Brodtmann, A. (2018). Default mode network neurodegeneration reveals the remote effects of ischaemic stroke. *J. Neurol. Neurosurg. Psychiatry* 89, 318–320. doi: 10.1136/jnnp-2017-315676

Weir, B., Disney, L., and Karrison, T. (2002). Sizes of ruptured and unruptured aneurysms in relation to their sites and the ages of patients. *J. Neurosurg.* 96, 64–70. doi: 10.3171/jns.2002.96.1.0064

Wong, G. K., Lam, S., Ngai, K., Wong, A., Mok, V., Poon, W. S., et al. (2012). Evaluation of cognitive impairment by the Montreal cognitive assessment in patients with aneurysmal subarachnoid haemorrhage: prevalence, risk factors and correlations with 3 month outcomes. *J. Neurol. Neurosurg. Psychiatry* 83, 1112–1117.

Wong, G. K., Lam, S. W., Wong, A., Mok, V., Siu, D., Ngai, K., et al. (2014). Early MoCA-assessed cognitive impairment after aneurysmal subarachnoid hemorrhage and relationship to 1-year functional outcome. *Transl. Stroke Res.* 5, 286–291. doi: 10.1007/s12975-013-0284-z

Xu, Y., Zhang, X., Xiang, Z., Wang, Q., Huang, X., Liu, T., et al. (2021). Abnormal functional connectivity between the left medial superior frontal Gyrus and amygdala underlying abnormal emotion and premature ejaculation: a resting state fMRI Study. *Front. Neurosci.* 15:704920. doi: 10.3389/fnins.2021.704920

Yeo, S. S., Choi, B. Y., Chang, C. H., Kim, S. H., Jung, Y. J., and Jang, S. H. (2012). Evidence of corticospinal tract injury at midbrain in patients with subarachnoid hemorrhage. *Stroke* 43, 2239–2241. doi: 10.1161/STROKEAHA.112.661116

frontiers | Frontiers in Aging Neuroscience

TYPE Original Research
PUBLISHED 28 July 2022
DOI 10.3389/fnagi.2022.942438

OPEN ACCESS

EDITED BY
Gaiqing Wang,
The Third People's Hospital of Hainan Province, China

REVIEWED BY
Ruili Wei,
Zhejiang University School of Medicine, China
Han Zhao,
Second Affiliated Hospital and Yuying Children's Hospital of Wenzhou Medical University, China

*CORRESPONDENCE
Bo Wu
dragonwb@126.com

†These authors have contributed equally to this work and share first authorship

SPECIALTY SECTION
This article was submitted to Neurocognitive Aging and Behavior, a section of the journal Frontiers in Aging Neuroscience

RECEIVED 12 May 2022
ACCEPTED 30 June 2022
PUBLISHED 28 July 2022

CITATION
Ye C, Kwapong WR, Tao W, Lu K, Pan R, Wang A, Liu J, Liu M and Wu B (2022) Alterations of optic tract and retinal structure in patients after thalamic stroke.
Front. Aging Neurosci. 14:942438.
doi: 10.3389/fnagi.2022.942438

Alterations of optic tract and retinal structure in patients after thalamic stroke

Chen Ye†, William Robert Kwapong†, Wendan Tao, Kun Lu, Ruosu Pan, Anmo Wang, Junfeng Liu, Ming Liu and Bo Wu*

Department of Neurology, West China Hospital, Sichuan University, Chengdu, China

Objectives: To investigate the association between degeneration of retinal structure and shrinkage of the optic tract in patients after thalamic stroke.

Materials and methods: Patients with unilateral thalamic stroke were included. Structural magnetic resonance imaging (MRI) and optical coherence tomography (OCT) were performed to obtain parameters of optic tract shrinkage (lateral index) and retina structural thickness (retinal nerve fiber layer, RNFL; peripapillary retinal nerve fiber layer, pRNFL; ganglion cell-inner plexiform layer, GCIP), respectively. Visual acuity (VA) examination under illumination was conducted using Snellen charts and then converted to the logarithm of the minimum angle of resolution (LogMAR). We investigated the association between LI and OCT parameters and their relationships with VA.

Results: A total of 33 patients and 23 age-sex matched stroke-free healthy controls were enrolled. Patients with thalamic stroke showed altered LI compared with control participants (P = 0.011) and a significantly increased value of LI in the subgroup of disease duration more than 6 months (P = 0.004). In these patients, LI were significantly associated with pRNFL thickness (β = 0.349, 95% confidence interval [CI]: 0.134–0.564, P = 0.002) after adjusting for confounders (age, sex, hypertension, diabetes, dyslipidemia, and lesion volume). LI and pRNFL were both significantly associated with VA in all patients (LI: β = −0.275, 95% CI: −0.539 to −0.011, P = 0.041; pRNFL: β = −0.023, 95% CI: −0.046 to −0.001, P = 0.040) and in subgroup of disease duration more than 6 months (LI: β = −0.290, 95% CI: −0.469 to −0.111, P = 0.002; pRNFL: β = −0.041, 95% CI: −0.065 to −0.017, P = 0.003).

Conclusion: Shrinkage of the optic tract can be detected in patients with thalamic stroke, especially after 6 months of stroke onset. In these patients, the extent of optic tract atrophy is associated with pRNFL thickness, and they are both related to visual acuity changes.

KEYWORDS

thalamic stroke, retinal structure, optic tract, retrograde degeneration, MRI, OCT

Introduction

The last few decades have seen a substantial increase in research identifying alterations in retinal structure and microvasculature after stroke (Park et al., 2013; Wang et al., 2014; Zhang et al., 2020; Kwapong et al., 2021). It is suggested that the retina can act as a novel and non-invasive imaging marker with potential diagnostic and clinical significance in neurological diseases (Cabrera DeBuc et al., 2017; Mutlu et al., 2017; Kwapong et al., 2018). Thinning of the retinal nerve fiber layer (RNFL) and ganglion cell layer (GCL)-inner plexiform layer (GCIPL) has been consistently documented in previous reports (Park et al., 2013; Zhang et al., 2020; Kashani et al., 2021; Snyder et al., 2021; Ye et al., 2022) in most cerebrovascular disorders. These reports suggest retinal neurodegeneration reflects cerebral neurodegeneration, and this mechanism may occur simultaneously. Importantly, prior reports (Ong et al., 2015; Mutlu et al., 2017; Chua et al., 2021) suggested that the retinal sublayer thicknesses reflect the cerebral microstructure (white matter and gray matter microstructure). The brain and retina share many characteristics, including similar microvasculature, embryology, and precise neuronal cell layers; axons from the optic nerve form a direct link, through the optic head, between the retina and the brain, thus, it is suggested that damage in the brain is associated with retinal thinning (especially for peripapillary RNFL and macular GCL) (Cabrera DeBuc et al., 2017; Kwapong et al., 2018; Mutlu et al., 2018).

As the central hub of the brain, the thalamus plays an important role in relaying sensory information to and from the cerebral cortex (Bogousslavsky et al., 1988). Notably, projections from the visual cortex are *via* the thalamus, emphasizing its importance in vision. Thalamic stroke accounts for 3–4% of ischemic stroke and is associated with neuro-ophthalmic deficits (Bogousslavsky et al., 1988; AdamsJr., Bendixen et al., 1993; Schmahmann, 2003). Impaired visual acuity and oculomotor deficits have been reported in a series of studies (AdamsJr., Bendixen et al., 1993; Rorden and Brett, 2000; Weidauer et al., 2004; Moon et al., 2021). Notably, neuro-ophthalmic deficits after a thalamic injury can also lead to a great disease burden and serious disability affecting everyday activities (Moon et al., 2021). Previous reports focused on cerebral changes associated with thalamic stroke (Chen et al., 2016; Conrad et al., 2022), while very less is known about the retinal changes and their association with the cerebral changes.

Magnetic resonance imaging (MRI) studies conducted on visual system-damaged subjects have revealed objective signs of shrinkage of optic tract (OT) volume and denoted it as the lateral index (LI) (Bridge et al., 2011; Cowey et al., 2011; Millington et al., 2014). The degeneration of OT, known as transsynaptic retrograde degeneration (TRD), may have an impact on the recovery effect from visual restoration training in cortical blindness subjects and indicates interindividual variability of relatable therapy (Fahrenthold et al., 2021). As the thalamus is the relay center and is involved in visual processing, we hypothesize that damage to the thalamus may result in the disruption of connections in the visual tract, especially the optic tract (OT), which may cause retrograde degeneration of the optic nerve, resulting in retinal changes. Exploring the correlations between retinal thicknesses and brain structural changes in thalamic stroke may give insights into the mechanism underlying visual disturbances and neurodegeneration during the disease cascade and ultimately benefit treatments for these patients.

Therefore, this study aimed to investigate the association between retinal thickness and structural OT indicators in thalamic stroke, and we further explored their relationships with clinical visual features in these patients.

Materials and methods

Study population

Patients with first-ever unilateral thalamic stroke who visited the Department of Neurology, West China Hospital, Sichuan University, were consecutively enrolled from 2020 to 2022. During the same study period, age-sex matched healthy control participants who had no history of neurological diseases and vascular risks were recruited from voluntary persons dwelling in native communities. Patients were included in the study if they (1) had a clinical diagnosis of first-ever unilateral thalamic stroke confirmed by experienced neurologists and MRI examinations; (2) completed an OCT retinal imaging scan and a structural brain MRI examination; and (3) provided written informed consent. The exclusion criteria of our patients were as follows: (1) diagnosed with diabetic retinopathy or other retinal diseases; (2) glaucoma; (3) pacemaker or other contraindications for MRI examinations; (4) a history of stroke or any other pathological conditions of neurological diseases; and (5) poor MRI or OCT imaging qualities. Control participants were included if they met the following criteria: (1) aged 18 years or older; (2) could undergo and cooperate with retinal and MR imaging; (3) had no history of cerebrovascular diseases, neurodegenerative diseases, or any other kind of central nervous system illness; and (4) no history of retinal diseases or ophthalmic abnormalities that could affect the retinal structure/microvasculature.

Demographic and clinical information were collected in a standardized format, including sex, age, and risk factors for cerebrovascular disease (history of hypertension, diabetes, and dyslipidemia). Time since stroke onset (months) and National Institute of Health Stroke Scale (NIHSS) scores were also documented. Since it has been well recognized that the process of TRD is time-dependent (usually occurring significantly from 3 to 7 months to the first few years maximally) (Jindahra et al.,

2012), along with the expansion course of poststroke visual deficit, which becomes steady after 6 months (Cavanaugh and Huxlin, 2017; Wang et al., 2017; Saionz et al., 2020), in the following analysis we divided our patients into two subgroups: Group 1 (≤ 6 months) and Group 2 (>6 months). Visual acuity (VA) under illumination was completed for each eye using Snellen charts by an experienced neuro-ophthalmologist (WK) and later converted to the logarithm of the minimum angle of resolution (LogMAR). Standardized neurological examinations, including eye movement and visual field, were conducted by senior neurology residents (CY and KL) under the guidance of an experienced neurologist (BW). Written informed consent was obtained from each participant or their legal guardians, and approval of our project was obtained from the Ethics Committee of West China Hospital of Sichuan University [No. 2020 (922)].

Magnetic resonance imaging acquisition and obtaining of optic tract volume and lateral index within each subject

All participants enrolled in this study underwent structural MRI examination (3D-T1 weighted image, brain volume sequence, and BRAVO) using a 3.0 T MR scanner (SIGNA^{TM} Premier, GE Medical Systems) with the 48-channel head coil, with parameters as follows: repetition time (TR)/echo time (TE) = 7.2/3.0 ms; field of view = 256 × 256 mm; matrix = 256 × 256; slice thickness = 1.0 mm, a total of 152 slices with no gap; flip angle = 12°. Routine clinical sequences including diffusion-weighted images (DWI), T2-weighted images, and fluid-attenuated inversion recovery (FLAIR) images were also acquired. Head motion and scanner noise was reduced using comfortable foam padding and earplugs.

Optic tract volume (OT) measurements and lateral index (LI) calculating methods were adapted from previously published reports (Bridge et al., 2011; Millington et al., 2014; Fahrenthold et al., 2021) based on the intensity values of the T1-weighted images. First, structural MRI images were reoriented and resampled in standard space (1 mm) using FMRIB software library (FSL) image analysis software[1] to make the optic tract parallel to the anterior-posterior axis so that the effects of individual head orientations in the scanner were minimized. Second, equal-sized masks were hand-drawn on the two sides of optic tracts in each slice of processed MRI images (planes parallel and perpendicular to the OT), starting from the third slice posterior to the origin of the optic chiasm and continuing until the OT was unable to be discerned from surrounding tissues, as shown in **Figure 1**. The ipsilateral OT (iOT) and contralateral OT (cOT) were stratified according to the location of the stroke lesion in the patient group, while it was described as right or left OT (rOT and lOT) in the control group. Third, under Fahrenthold et al.'s study (Fahrenthold et al., 2021), we built an intensity threshold filter, ranging from 5 to 95% of the maximal brightness values of T1-weighted signals, to obtain the number of voxels in the masks as the OT volume. Then we performed the calculation of each subject's lateral index (LI) using the following formulas: LI = (iOT–cOT)/(iOT + cOT) in patients and LI = (rOT–lOT)/(rOT + lOT) in controls. By doing so, only voxels containing most of the white matter were included in the analysis.

We also measured the stroke lesion volume by drawing lesion masks manually on the structural MR images with the combination of DWI and FLAIR images using MRIcron (Rorden and Brett, 2000). Then lesion volumes were obtained by the volume of interest (VOI, cm^3). Two trained neurologists (C.Y. and W.D.T.) were engaged in the MRI processing and measurements blinded to clinical information, and an experienced neurologist (B.W.) was consulted when disagreement occurred. The inter-rater agreement was good with an intraclass correlation coefficient (ICC) of 0.80 for LI and 0.83 for lesion volume.

Optical coherence tomography examination

Swept-source optical coherence tomography (SS-OCT, VG 200, SVision Imaging Limited, Luoyang, China) was used to image the structure of the retina by an experienced neuro-ophthalmologist (WK). The specifications of the OCT tool have been well described in our previous report (Ye et al., 2022). As shown in **Figure 2**, the peripapillary retinal nerve fiber layer (pRNFL) was done using the optic nerve head protocol with a scanning range covering a circle with a diameter of 3.45 mm focused on the optic disc. Structural OCT imaging of the macula was done with 18 radial scan lines focused on the fovea. Automatic segmentation of the retinal nerve fiber layer (RNFL) and ganglion cell-inner plexiform layer (GCIPL) was done with a built-in algorithm in the OCT tool. Average thicknesses of the RNFL (measured in μm) and GCIPL (measured in μm) in a 3 × 3 mm area around the fovea were used in this study.

Statistical analysis

Continuous variables with a normal distribution were expressed as mean ± standard deviation (SD), while those with skewed distribution were expressed as medians and interquartile ranges (IQR). Categorical variables are presented as frequencies and percentages. Participants' demographic and clinical variables were assessed using a chi-square test for categorical variables and an independent sample *t*-test

1 http://www.fmrib.ox.ac.uk/fsl

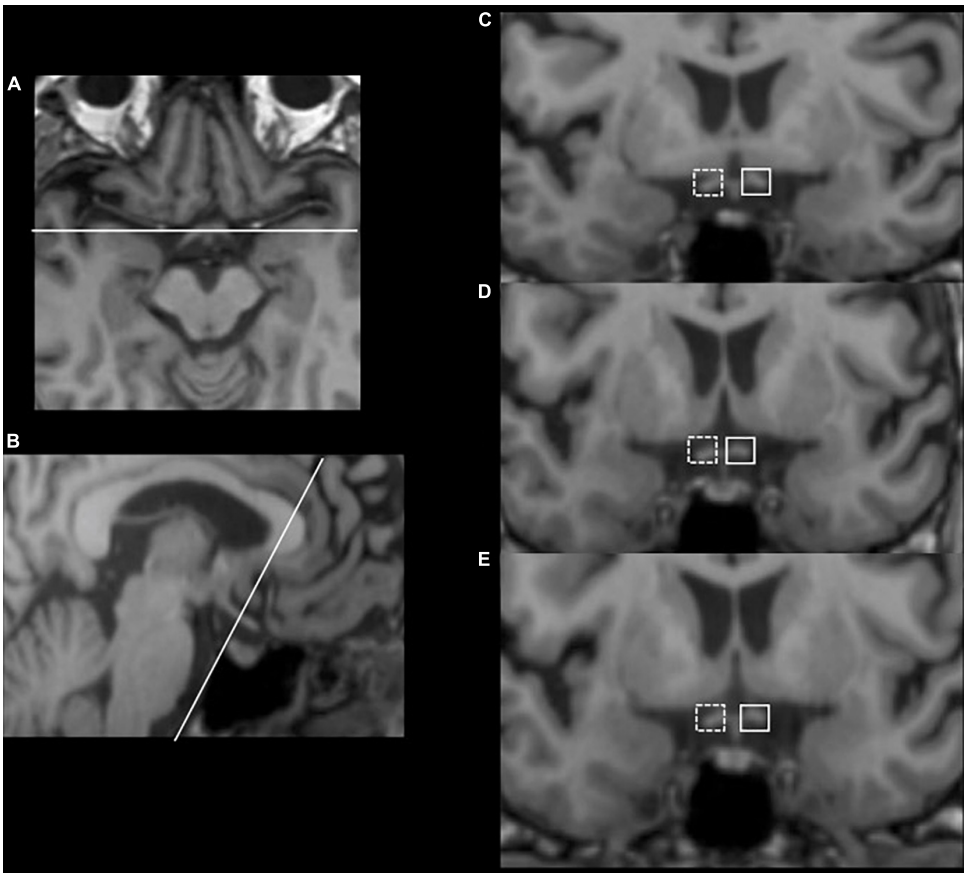

FIGURE 1
Illustration of optic tract measurements with an example from a 56-year-old female thalamus stroke patient. Consecutive **(C–E)** coronal slices, which have been resliced and reoriented to be perpendicular to the OT **(B)**, were obtained starting with three slices posterior to the beginning of the optic chiasm **(A)**. Equal-sized masks were hand-drawn on the two sides of optic tracts in each slice, with the solid border as the contralateral side and the dashed border as the ipsilateral side.

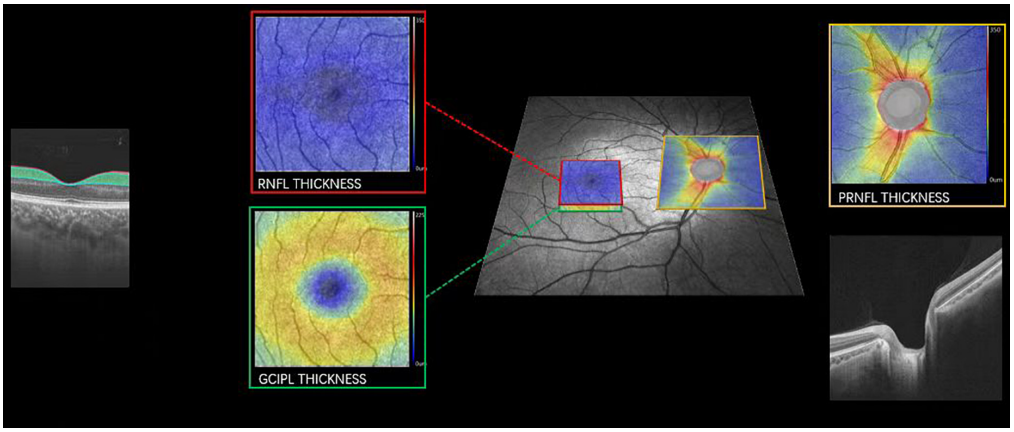

FIGURE 2
Imaging of pRNFL, RNFL, and GCIPL thickness. Representative image focusing on the macula (red and green box) and optic nerve (yellow box) with the corresponding cross-sectional view of the retina. pRNFL, peripapillary retinal nerve fiber layer; RNFL, retinal nerve fiber layer; GCIPL, the ganglion cell and inner plexiform layer. A color map of the OCT structural thickness was shown to indicate the thickness. Warm colors indicate a thick structure, while cold colors indicate a thin structure.

TABLE 1 Baseline demographic and clinical characteristics of all included subjects.

Characteristics	Thalamic stroke (n = 35)	Controls (n = 23)	P
Age, years	59.8 ± 10.7	57.9 ± 7.5	0.449
Gender (males), n (%)	27 (77.1)	17 (73.9)	0.779
Hypertension, n (%)	19 (54.2)	–	
Diabetes, n (%)	10 (28.6)	–	
Dyslipidemia, n (%)	5 (14.3)	–	
Stroke type		–	
Ischemic, n (%)	32 (91.43)		
Hemorrhagic, n (%)	3 (8.57)		
Lesion location		–	
Left, n (%)	17 (48.57)		
Right, n (%)	18 (51.43)		
Duration, months	7.0 (0.2 to 44)	–	
≤ 6 months, n (%)	13 (37.1)	–	
>6 months, n (%)	22 (62.9)	–	
NIHSS score	1 (1 to 2)	–	
Lesion volume, cm^3	0.14 (0.06 to 0.54)	–	
VA, LogMAR	0.24 ± 0.21	0.01 ± 0.08	< **0.001**

NIHSS, National Institute of Health Stroke Scale; VA: visual acuity. Values in bold indicate $P < 0.05$.

or non-parametric test for continuous variables. Multilinear regression was performed to assess the associations among OT parameters and retina structural parameters, and VA, LogMAR while adjusting for confounding factors (age, sex, hypertension, diabetes, dyslipidemia, and lesion volume) with β coefficient and 95% confidence interval (95% CI). All data were analyzed using SPSS (version 23; SPSS, Chicago, United States) and GraphPad Prism (version 9.3.0; GraphPad Software, San Diego, United States), and a two-sided $P<0.05$ was considered statistically significant.

Results

Baseline demographic and clinical characteristics

A total of 33 patients with first-ever thalamic stroke (27 men, mean age = 59.8 ± 10.7 years) and 23 age-sex matched healthy control participants (17 men, mean age = 57.9 ± 7.5 years) were enrolled in this study. In the thalamic stroke group, 19 patients had a history of hypertension, 10 had diabetes, and 5 had dyslipidemia. The baseline demographic and clinical characteristics are shown in Table 1. None of the control participants had a history of hypertension, diabetes, and dyslipidemia. For stroke type, 32 had an ischemic stroke while 3 had a hemorrhagic stroke; 18 patients had right-sided stroke lesions and 17 were left-sided. The median NIHSS score of patients with thalamic stroke was 1 (IQR, 1–2), and the median disease duration since stroke onset was 7.0 (IQR, 0.2–44) months, of which 13 (37.1%) were less than or equal to 6 months and 22 (62.9%) were greater than 6 months. No significant visual fields and oculomotor deficits were observed in this study, but the visual acuity (VA, LogMAR) of the patients' group was worse than that of control participants (0.24 ± 0.21 vs. 0.01 ± 0.08, $P < 0.001$). The stroke lesion volume was 0.14 (IQR, 0.06–0.54) cm^3. There was no significant difference (P = 0.052) in the visual acuity between patients with left thalamic stroke (0.26 ± 0.21) and patients with right thalamic stroke (0.17 ± 0.14).

All the patients underwent SS-OCT imaging and 67 eyes (33 eyes on the ipsilateral side and 34 eyes on the contralateral side; three eyes were excluded due to poor cooperation and bad image quality) were included in this study, divided into two groups based on the disease duration: Group 1, ≤ 6 months; and Group 2, >6 months. No significant differences were found in the retinal structural parameters (pRNFL, RNFL, and GCIPL thickness) and VA between Group 1 and Group 2 (all $P>0.05$). Details are displayed in Supplementary Table 1.

Optic tract parameters in patients with thalamic stroke and comparisons to control participants

As shown in Figure 3 (details in Supplementary Table 2), ipsilateral optic tract volume (iOT) was 189.51 ± 47.51 and the contralateral side (cOT) was 174.80 ± 39.18 in patients with thalamic stroke, while right-side optic tract volume was 169.26 ± 31.49 and the left side was 167.17 ± 31.30 in control participants. No significant differences were found when comparing patients to control participants (all $P>0.05$). Optic tract lateral index (LI) differed significantly among these different groups (P = 0.006). When compared with control participants (0.002, IQR −0.006 to 0.015), all thalamic stroke groups showed a prominently increased LI value of 0.021 (IQR, 0.007 to 0.078) with P = 0.011. Notably, the LI of Group 2 (0.031, IQR 0.01–0.135) was significantly greater than that in the control group (P = 0.004). Although not reaching statistical significance (P = 0.183), Group 1 showed a decreased median LI value (0.015, IQR −0.091 to 0.61) compared with Group 2.

Associations between LI and retina structural parameters in patients with thalamic stroke

Associations between LI and retina structural parameters (pRNFL, RNFL, and GCIPL thickness) were assessed in

TABLE 2 Associations between LI and retina structural parameters in patients with thalamic stroke.

	All			Group 1 (≤ 6 months)			Group 2 (>6 months)		
	β	95% CI	*P*	β	95% CI	*P*	β	95% CI	*P*
pRNFL, μm	0.238	−0.028 to 0.505	0.078	0.028	−0.095 to 0.151	0.626	0.349	0.134 to 0.564	**0.002**
RNFL, μm	−0.009	−0.272 to 0.255	0.948	−0.077	−0.233 to 0.079	0.297	−0.005	−0.209 to 0.199	0.962
GCIPL, μm	0.038	−0.225 to 0.301	0.775	−0.065	−0.271 to 0.141	0.499	0.011	−0.201 to 0.223	0.917

Adjusted for age, gender, vascular risks (hypertension, diabetes, and dyslipidemia), and lesion volume. pRNFL, peripapillary retinal nerve fiber layer; RNFL, retinal nerve fiber layer; GCIPL, the ganglion cell and inner plexiform layer. Values in bold indicate $P < 0.05$.

patients with thalamic stroke, as shown in Table 2. After adjusting for confounders (age, gender, vascular risk factors [i.e., hypertension, diabetes, and dyslipidemia], and lesion volume), LI had no significant association with pRNFL, RNFL, and GCIPL (all $P>0.05$) in the patients' group and Group 1 (≤ 6 months). In patients with duration >6 months (Group 2), LI was significantly associated with pRNFL (β = 0.349, 95% CI 0.134–0.564, P = 0.002). However, no statistically significant associations were found in RNFL (P = 0.962) and GCIPL (P = 0.917) with LI in this group.

Associations of LI and retina structural parameters with visual acuity, logarithm of the minimum angle of resolution (LogMAR) in patients with thalamic stroke

We further explored the associations of LI and retinal structural parameters with visual acuity (VA, LogMAR) in patients with thalamic stroke, respectively. As shown in Table 3, LI and pRNFL thickness were both significantly correlated with VA in all patients after adjusting for confounding factors (LI: β = −0.275, 95% CI −0.539 to −0.011, P = 0.041; pRNFL: β = −0.023, 95% CI −0.046 to −0.001, P = 0.040). Particularly, in Group 2 of disease duration of more than 6 months, these adjusted associations remained statistically significant (LI: β = −0.290, 95% CI −0.469 to −0.111, P = 0.002; pRNFL: β = −0.041, 95% CI −0.065 to −0.017, P = 0.003).

Discussion

Our current report builds upon our previous report on retinal neurodegeneration following thalamic infarction (Ye et al., 2022) and the fundamental observations that such retrograde transsynaptic neurodegeneration after visual pathway insult follows a distinct time course and pattern (Jindahra et al., 2012; Saionz et al., 2020; Fahrenthold et al., 2021). This study showed that the LI value, which indicates the shrinkage extent of the optic tract (Bridge et al., 2011; Millington et al., 2014; Fahrenthold et al., 2021), altered distinctly compared with age-sex matched stroke-free controls. Particularly, it increased significantly in the group with a disease duration of more than 6 months. In such patients, LI was significantly associated with pRNFL thickness. Besides, both the LI and pRNFL were significantly related to the subject's visual acuity (VA, LogMAR). To the best of our knowledge, this study is the first to explore the optic tract changes in patients with thalamic stroke and investigate their associations with retinal structural parameters by combining MRI and OCT techniques.

Previous reports showed that transsynaptic retrograde neurodegeneration (TRD) after post-thalamic visual area (occipital lobe) stroke was high after the first few years and fairly stable over the years (Cowey et al., 2011; Jindahra et al., 2012; Meier et al., 2015; Schneider et al., 2019). In our previous report (Ye et al., 2022), thalamic infarction patients with a duration of more than 6 months also showed a thinner retinal structure compared to patients with a duration of fewer than 6 months. These findings suggest that retinal degeneration follows a clear-cut time sequence, i.e., retrograde degeneration is progressive and becomes steady over time. Moreover, a well-established MRI technique has been used to reveal the detectable phenomenon of OT shrinkage in chronic hemianopia or cortical-blindness patients (Bridge et al., 2011; Millington et al., 2014). In this study, compared with controls, profound changes in LI were detected in patients with thalamic stroke, especially in patients with a duration of more than 6 months. In line with Cowey et al.'s findings (Cowey et al., 2011), the mechanism can be explained as disruption of networks within the visual tract and triggering of retrograde degeneration in the visual processing projections resulting from damage to the thalamus (particularly the lateral geniculate nucleus, LGN), a key structure involved in visual processing. Specifically, it has been suggested to lead to direct retrograde degeneration in the optic tract volume (Bridge et al., 2011; Millington et al., 2014).

Furthermore, following the TRD time course, significant correlations were found between LI and pRNFL thickness in patients with thalamic stroke with a duration of more than 6 months. Lesions involved in the visual pathway and the following retrograde degeneration may ultimately result in structural changes in the retina (Jindahra et al., 2009). Besides,

TABLE 3 Associations between LI and retina structural parameters with VA, LogMAR in patients with thalamic stroke, respectively.

	All			Group 1 (≤ 6 months)			Group 2 (>6 months)		
	β	95% CI	*P*	β	95% CI	*P*	β	95% CI	*P*
LI	−0.275	−0.539 to −0.011	**0.041**	0.086	−0.170 to 0.342	0.470	−0.290	−0.469 to −0.111	**0.002**
pRNFL, μm	−0.023	−0.046 to −0.001	**0.040**	0.001	−0.075 to 0.077	0.968	−0.041	−0.065 to −0.017	**0.003**
RNFL, μm	−0.010	−0.217 to 0.197	0.923	−0.276	−0.868 to 0.317	0.286	0.068	−0.196 to 0.333	0.588
GCIPL, μm	−0.017	−0.053 to 0.019	0.334	−0.030	−0.151 to 0.092	0.557	−0.013	−0.058 to 0.032	0.547

Adjusted for age, gender, vascular risks (hypertension, diabetes, and dyslipidemia), and lesion volume. VA: visual acuity, LogMAR. pRNFL: peripapillary retinal nerve fiber layer; RNFL: retinal nerve fiber layer; GCIPL: the ganglion cell and inner plexiform layer. Values in bold indicate $P < 0.05$.

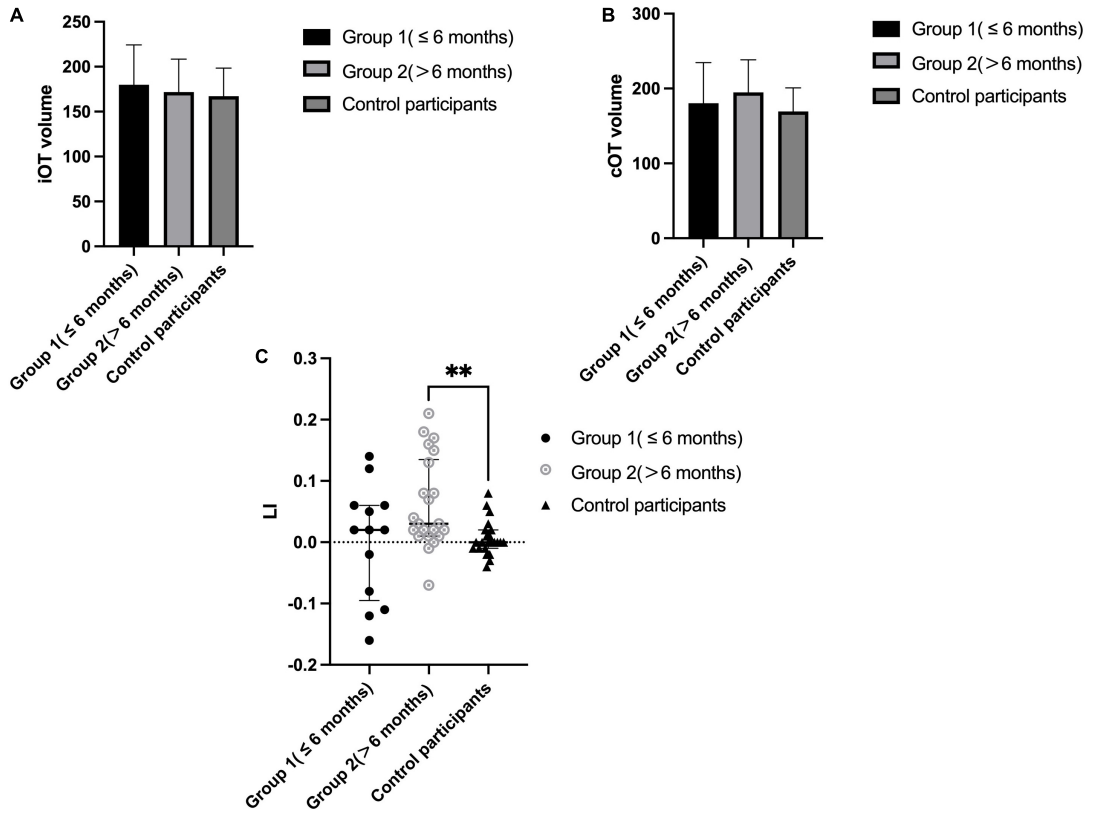

FIGURE 3
Optic tract parameters in patients with thalamic stroke and comparison to control participants. **(A)**: Ipsilateral OT volume (voxel numbers) in Group 1 (≤ 6 months) and Group 2 (>6 months) patients and control participants (right side); **(B)**: Contralateral OT volume (voxel numbers) in Group 1 (≤ 6 months) and Group 2 (>6 months) patients and control participants (left side); **(C)**: LI in Group 1 (≤ 6 months) and Group 2 (>6 months) patients and control participants; $^{**}P < 0.05$.

large to subtle changes in the visual-related structures have been reported in patients with thalamic disorders (Agarwal et al., 2011; Pula and Yuen, 2017), and significant relationships have been found between altered retinal thickness and volumetric changes in the thalamus area (Mutlu et al., 2018). Recently, by combining structural and functional MR techniques, Conrad et al. found radiological evidence of white matter volume loss following thalamic infarction and revealed its implications for cortical areas involved in sensory and ocular function (Conrad et al., 2022). Given the fact that pRNFL (located around the optic nerve head) can characterize the global ganglion cell axonal integrity and directly connect to the brain (Saidha et al., 2013) and can represent the most proximal part of the visual projection pathway (Jimenez et al., 2014), pRNFL might be more sensitive to damage in the visual pathway. Thus, it is plausible to suggest that shrinkage of the optic tract after thalamic stroke was correlated to retinal neurodegeneration, and LI can be considered an imaging marker of neurodegeneration in thalamic stroke. Future studies with larger sample sizes of homogenous patients are needed to validate our hypothesis.

Visual complaints have been reported in patients with thalamic stroke (Roth et al., 2016; Hwang et al., 2017), implicating structural changes in the retina and the presence of axonal damage along the visual pathway. Previous reports have shown patients with thalamic stroke have vision-related problems, which impose a heavy disease burden affecting daily activities (Bogousslavsky et al., 1988; Rorden and Brett, 2000; Schmahmann, 2003; Li et al., 2018; Moon et al., 2021). Notably, we showed that LI and pRNFL thickness significantly correlated with visual acuity in patients with thalamic stroke and patients with a duration of more than 6 months. Since LI (Mehra and Moshirfar, 2022) and pRNFL (Lim et al., 2019; Rajabi et al., 2019) play significant roles in vision, it is conceivable to suggest that LI atrophy and pRNFL thinning may be associated with reduced visual acuity in patients with thalamic stroke, and they should be taken into account in treatment decisions for such patients. Apart from visual restoration training and compensatory therapy strategies, effective therapeutic options are still lacking in such patient groups (Sahraie et al., 2016; Cavanaugh and Huxlin, 2017; Fahrenthold et al., 2021). It may result from the highly individualized heterogeneity and variability that exist in the efficacy of such treatments (Saionz et al., 2020; Fahrenthold et al., 2021). Thus, it is important to accurately identify subjects who may benefit from these therapeutic options. Particularly, in addition to routine secondary prevention treatments of cerebrovascular diseases, there is still a lack of individualized treatment and evaluation indicators for stroke patients with specific and distinct clinical syndromes. It has been clarified that the existence and extent of retrograde degeneration of the neural pathway disease involved can impact interventional and natural recovery effects (Millington et al., 2014; Fahrenthold et al., 2021). This study illustrates some significant alterations in retinal structure and optic tract after thalamic stroke and explores their correlations with damage to the brain and time effects. These findings may highlight the potential of combining these two markers for disease assessment and response to therapy in these patients and suggest the need for research on related interventions.

Surprisingly, in this study, the pRNFL in patients with thalamic stroke was more sensitive to vision loss and optic tract shrinkage than the macular RNFL and GCIPL. The pRNFL is located around the optic nerve head (second cranial nerve), which plays a significant role in vision; thus, pRNFL changes may be sensitive to visual changes and *vice versa* as previously reported (Lin et al., 2018; Wagner et al., 2020). The optic tract consists of white matter microstructure (Rokem et al., 2017; Caffarra et al., 2021), which has been reported to be associated with the pRNFL thickness (Ong et al., 2015; Mutlu et al., 2017). Besides, axons from the eye to the brain leave through the optic nerve head (pRNFL) to the brain *via* the optic tract (Raz and Levin, 2014). Taken together, we suggest that pRNFL thickness in patients with thalamic stroke may be sensitive to neurodegeneration (axonal damage) and visual loss.

Our study has some limitations. First, the observational cross-sectional study design is a limitation in our study; thus, an interpretation of the causal relationship seen in our study could not be made. Second, no symptoms of the visual field or oculomotor deficits occurred, which diminished the clinical interest and expandability to some extent; however, as a type of ischemic stroke with a lower proportion, a 10-year cohort study only found out 11.7% of thalamic insulted patients who developed prominent neuro-ophthalmologic manifestations (Moon et al., 2021). Further investigations with larger samples are needed in the future. Third, we were not able to conduct a detailed analysis of the subtypes of patients with thalamic stroke (i.e., at different time points). Long-term follow-up cohort studies with data on dynamic changes are needed in the future.

Conclusion

Shrinkage of the optic tract can be detected in patients with thalamic stroke, especially after 6 months of stroke onset. In these patients, the extent of optic tract atrophy correlated with pRNFL thickness, and they were both associated with visual acuity changes. The findings of our study emphasize the importance of further research into combining retinal imaging and MR imaging markers for disease assessment and ultimately help to guide individualized treatment choices. Longitudinal studies with a greater sample size are needed to validate our hypotheses in the future.

Data availability statement

The raw data supporting the conclusions of this article will be made available by the authors, without undue reservation.

Ethics statement

The studies involving human participants were reviewed and approved by the Ethics Committee of West China Hospital, Sichuan University [No. 2020(922)]. The patients/participants provided their written informed consent to participate in this study.

Author contributions

BW: study concept and design. CY, WK, WT, JL, RP, KL, and AW: data acquisition. CY and WK: data analysis and interpretation and drafting the manuscript. ML: resources. BW: study supervision. BW and WK: critical review of the manuscript. All authors contributed to the article and approved the submitted version.

Funding

This study was supported by the 1.3.5 project for disciplines of excellence (ZYGD18009) and Clinical Research Incubation Project (2020HXFH012), West China Hospital, Sichuan University, the Technology Innovation R&D Project of Chengdu Science and Technology Bureau (2021-YF05- 01325-SN), and the National Natural Science Foundation of China (81870937, 82071320, and 81901199).

Conflict of interest

The authors declare that the research was conducted in the absence of any commercial or financial relationships that could be construed as a potential conflict of interest.

Publisher's note

Supplementary material

The Supplementary Material for this article can be found online at: https://www.frontiersin.org/articles/10.3389/fnagi.2022.942438/full#supplementary-material

References

Adams, H. P. Jr., Bendixen, B. H., Kappelle, L. J., Biller, J., Love, B. B., Gordon, D. L., et al. (1993). 'Classification of subtype of acute ischemic stroke. Definitions for use in a multicenter clinical trial. TOAST. Trial of Org 10172 in Acute Stroke Treatment. *Stroke* 24, 35–41. doi: 10.1161/01.str.24.1.35

Agarwal, P., Gupta, S., Jindal, S., Pathak, S. B., and Biswas, R. (2011). Visual hemifield loss in thalamic hematoma. *Ann. Neurosci.* 18, 177–178. doi: 10.5214/ans.0972.7531.111812

Bogousslavsky, J., Regli, F., and Uske, A. (1988). 'Thalamic infarcts: clinical syndromes, etiology, and prognosis'. *Neurology* 38, 837–848. doi: 10.1212/WNL.38.6.837

Bridge, H., Jindahra, P., Barbur, J., and Plant, G. T. (2011). 'Imaging Reveals Optic Tract Degeneration in Hemianopia'. *Invest. Ophthalmol. Vis. Sci.* 52, 382–388. doi: 10.1167/iovs.10-5708

Cabrera DeBuc, D., Somfai, G. M., and Koller, A. (2017). Retinal microvascular network alterations: potential biomarkers of cerebrovascular and neural diseases. *Am. J. Physiol. Heart Circ. Physiol.* 312, H201–H212. doi: 10.1152/ajpheart.00201.2016

Caffarra, S., Joo, S. J., Bloom, D., Kruper, J., Rokem, A., and Yeatman, J. D. (2021). 'Development of the visual white matter pathways mediates development of electrophysiological responses in visual cortex'. *Hum. Brain Mapp.* 42, 5785–5797. doi: 10.1002/hbm.25654

Cavanaugh, M. R., and Huxlin, K. R. (2017). 'Visual discrimination training improves Humphrey perimetry in chronic cortically induced blindness'. *Neurology* 88, 1856–1864. doi: 10.1212/WNL.0000000000003921

Chen, L., Luo, T., Lv, F., Shi, D., Qiu, J., Li, Q., et al. (2016). 'Relationship between hippocampal subfield volumes and memory deficits in patients with thalamus infarction'. *Eur. Arch. Psychiat. Clin. Neurosci.* 266, 543–555. doi: 10.1007/s00406-015-0654-5

Chua, S. Y. L., Lascaratos, G., Atan, D., Zhang, B., Reisman, C., Khaw, P. T., et al. (2021). 'Relationships between retinal layer thickness and brain volumes in the UK Biobank cohort'. *Eur. J. Neurol.* 28, 1490–1498. doi: 10.1111/ene.14706

Conrad, J., Habs, M., Ruehl, R. M., Bogle, R., Ertl, M., Kirsch, V., et al. (2022). 'White matter volume loss drives cortical reshaping after thalamic infarcts'. *Neuroimage Clin.* 33:102953. doi: 10.1016/j.nicl.2022.102953

Cowey, A., Alexander, I., and Stoerig, P. (2011). 'Transneuronal retrograde degeneration of retinal ganglion cells and optic tract in hemianopic monkeys and humans'. *Brain* 134, 2149–2157. doi: 10.1093/brain/awr125

Fahrenthold, B. K., Cavanaugh, M. R., Jang, S., Murphy, A. J., Ajina, S., Bridge, H., et al. (2021). 'Optic Tract Shrinkage Limits Visual Restoration After Occipital Stroke'. *Stroke* 52, 3642–3650. doi: 10.1161/STROKEAHA.121.034738

Hwang, K., Bertolero, M. A., Liu, W. B., and D'Esposito, M. (2017). 'The Human Thalamus Is an Integrative Hub for Functional Brain Networks'. *J. Neurosci.* 37, 5594–5607. doi: 10.1523/JNEUROSCI.0067-17.2017

Jimenez, B., Ascaso, F. J., Cristobal, J. A., and Lopez del Val, J. (2014). Development of a prediction formula of Parkinson disease severity by optical coherence tomography. *Mov. Disord.* 29, 68–74. doi: 10.1002/mds.25747

Jindahra, P., Petrie, A., and Plant, G. T. (2009). 'Retrograde trans-synaptic retinal ganglion cell loss identified by optical coherence tomography'. *Brain* 132, 628–634. doi: 10.1093/brain/awp001

Jindahra, P., Petrie, A., and Plant, G. T. (2012). 'The time course of retrograde trans-synaptic degeneration following occipital lobe damage in humans'. *Brain* 135, 534–541. doi: 10.1093/brain/awr324

Kashani, A. H., Asanad, S., Chan, J. W., Singer, M. B., Zhang, J., Sharifi, M., et al. (2021). 'Past, present and future role of retinal imaging in neurodegenerative disease'. *Prog. Retin. Eye Res.* 83:100938. doi: 10.1016/j.preteyeres.2020.100938

Kwapong, W. R., Yan, Y., Hao, Z., and Wu, B. (2021). 'Reduced Superficial Capillary Density in Cerebral Infarction Is Inversely Correlated With the NIHSS Score'. *Front. Aging Neurosci.* 13:626334. doi: 10.3389/fnagi.2021.626334

Kwapong, W. R., Ye, H., Peng, C., Zhuang, X., Wang, J., Shen, M., et al. (2018). 'Retinal Microvascular Impairment in the Early Stages of Parkinson's Disease'. *Invest. Ophthalmol. Vis. Sci.* 59, 4115–4122. doi: 10.1167/iovs.17-23230

Li, S., Kumar, Y., Gupta, N., Abdelbaki, A., Sahwney, H., Kumar, A., et al. (2018). 'Clinical and Neuroimaging Findings in Thalamic Territory Infarctions: A Review'. *J. Neuroimag.* 28, 343–349. doi: 10.1111/jon.12503

Lim, H. B., Shin, Y. I., Lee, M. W., Park, G. S., and Kim, J. Y. (2019). 'Longitudinal Changes in the Peripapillary Retinal Nerve Fiber Layer Thickness of Patients With Type 2 Diabetes'. *JAMA Ophthalmol.* 137, 1125–1132. doi: 10.1001/jamaophthalmol.2019.2537

Lin, P. W., Chang, H. W., Lin, J. P., and Lai, I. C. (2018). 'Analysis of peripapillary retinal nerve fiber layer and inner macular layers by spectral-domain optical coherence tomography for detection of early glaucoma'. *Int. J. Ophthalmol.* 11, 1163–1172.

Mehra, D., and Moshirfar, M. (2022). "Neuroanatomy, Optic Tract," in *StatPearls*, ed. Erin Hughes and Gerson Rubio Treasure Island: StatPearls Publishing.

Meier, P. G., Maeder, P., Kardon, R. H., and Borruat, F. X. (2015). 'Homonymous ganglion cell layer thinning after isolated occipital lesion: macular OCT demonstrates transsynaptic retrograde retinal degeneration'. *J. Neuroophthalmol.* 35, 112–116. doi: 10.1097/WNO.0000000000000182

Millington, R. S., Yasuda, C. L., Jindahra, P., Jenkinson, M., Barbur, J. L., Kennard, C., et al. (2014). 'Quantifying the pattern of optic tract degeneration

in human hemianopia'. *J. Neurol. Neurosurg. Psychiat.* 85, 379–386. doi: 10.1136/jnnp-2013-306577

Moon, Y., Eah, K. S., Lee, E. J., Kang, D. W., Kwon, S. U., Kim, J. S., et al. (2021). 'Neuro-ophthalmologic features and outcomes of thalamic infarction: a single-institutional 10-year experience'. *J. Neuroophthalmol.* 41, 29–36. doi: 10.1097/WNO.0000000000000864

Mutlu, U., Bonnemaijer, P. W. M., Ikram, M. A., Colijn, J. M., Cremers, L. G. M., Buitendijk, G. H. S., et al. (2017). 'Retinal neurodegeneration and brain MRI markers: the Rotterdam Study'. *Neurobiol. Aging* 60, 183–191. doi: 10.1016/j.neurobiolaging.2017.09.003

Mutlu, U., Ikram, M. K., Roshchupkin, G. V., Bonnemaijer, P. W. M., Colijn, J. M., Vingerling, J. R., et al. (2018). 'Thinner retinal layers are associated with changes in the visual pathway: a population-based study'. *Hum. Brain Mapp.* 39, 4290–4301. doi: 10.1002/hbm.24246

Ong, Y. T., Hilal, S., Cheung, C. Y., Venketasubramanian, N., Niessen, W. J., Vrooman, H., et al. (2015). 'Retinal neurodegeneration on optical coherence tomography and cerebral atrophy'. *Neurosci. Lett.* 584, 12–16. doi: 10.1016/j.neulet.2014.10.010

Park, H. Y., Park, Y. G., Cho, A. H., and Park, C. K. (2013). 'Transneuronal retrograde degeneration of the retinal ganglion cells in patients with cerebral infarction'. *Ophthalmology* 120, 1292–1299. doi: 10.1016/j.ophtha.2012.11.021

Pula, J. H., and Yuen, C. A. (2017). 'Eyes and stroke: the visual aspects of cerebrovascular disease'. *Stroke Vasc. Neurol.* 2, 210–220. doi: 10.1136/svn-2017-000079

Rajabi, M. T., Ojani, M., Riazi Esfahani, H., Tabatabaei, S. Z., Rajabi, M. B., and Hosseini, S. S. (2019). 'Correlation of peripapillary nerve fiber layer thickness with visual outcomes after decompression surgery in subclinical and clinical thyroid-related compressive optic neuropathy'. *J. Curr. Ophthalmol.* 31, 86–91. doi: 10.1016/j.joco.2018.11.003

Raz, N., and Levin, N. (2014). 'Cortical and white matter mapping in the visual system-more than meets the eye: on the importance of functional imaging to understand visual system pathologies'. *Front. Integr. Neurosci.* 8:68. doi: 10.3389/fnint.2014.00068

Rokem, A., Takemura, H., Bock, A. S., Scherf, K. S., Behrmann, M., Wandell, B. A., et al. (2017). 'The visual white matter: the application of diffusion MRI and fiber tractography to vision science'. *J. Vis.* 17:4. doi: 10.1167/17.2.4

Rorden, C., and Brett, M. (2000). 'Stereotaxic display of brain lesions'. *Behav. Neurol.* 12, 191–200. doi: 10.1155/2000/421719

Roth, M. M., Dahmen, J. C., Muir, D. R., Imhof, F., Martini, F. J., and Hofer, S. B. (2016). 'Thalamic nuclei convey diverse contextual information to layer 1 of visual cortex'. *Nat. Neurosci.* 19, 299–307. doi: 10.1038/nn.4197

Sahraie, A., Smania, N., and Zihl, J. (2016). 'Use of NeuroEyeCoach to Improve Eye Movement Efficacy in Patients with Homonymous Visual Field Loss'. *Biomed. Res. Int.* 2016:5186461. doi: 10.1155/2016/5186461

Saidha, S., Sotirchos, E. S., Oh, J., Syc, S. B., Seigo, M. A., Shiee, N., et al. (2013). 'Relationships between retinal axonal and neuronal measures and global central nervous system pathology in multiple sclerosis'. *JAMA Neurol.* 70, 34–43. doi: 10.1001/jamaneurol.2013.573

Saionz, E. L., Tadin, D., Melnick, M. D., and Huxlin, K. R. (2020). 'Functional preservation and enhanced capacity for visual restoration in subacute occipital stroke'. *Brain* 143, 1857–1872. doi: 10.1093/brain/awaa128

Schmahmann, J. D. (2003). 'Vascular syndromes of the thalamus'. *Stroke* 34, 2264–2278.

Schneider, C. L., Prentiss, E. K., Busza, A., Matmati, K., Matmati, N., Williams, Z. R., et al. (2019). 'Survival of retinal ganglion cells after damage to the occipital lobe in humans is activity dependent'. *Proc. Biol. Sci.* 286:20182733. doi: 10.1098/rspb.2018.2733

Snyder, P. J., Alber, J., Alt, C., Bain, L. J., Bouma, B. E., Bouwman, F. H., et al. (2021). 'Retinal imaging in Alzheimer's and neurodegenerative diseases'. *Alzheimers Dem.* 17, 103–111. doi: 10.1002/alz.12179

Wagner, F. M., Hoffmann, E. M., Nickels, S., Fiess, A., Munzel, T., Wild, P. S., et al. (2020). 'Peripapillary retinal nerve fiber layer profile in relation to refractive error and axial length: results from the gutenberg health study'. *Transl. Vis. Sci. Technol.* 9:35. doi: 10.1167/tvst.9.9.35

Wang, D., Li, Y., Wang, C., Xu, L., You, Q. S., Wang, Y. X., et al. (2014). 'Localized retinal nerve fiber layer defects and stroke'. *Stroke* 45, 1651–1656.

Wang, V., Saionz, E., Cavanaugh, M., and Huxlin, K. (2017). 'Natural progression of perimetric visual field defects after V1 stroke'. *J. Vision* 17, 51–52.

Weidauer, S., Nichtweiss, M., Zanella, F. E., and Lanfermann, H. (2004). 'Assessment of paramedian thalamic infarcts: MR imaging, clinical features and prognosis'. *Eur. Radiol.* 14, 1615–1626. doi: 10.1007/s00330-004-2303-7

Ye, C., Kwapong, W. R., Tao, W., Lu, K., Pan, R., Wang, A., et al. (2022). 'Characterization of macular structural and microvascular changes in thalamic infarction patients: a swept-source optical coherence tomography–angiography study'. *Brain Sci.* 12:518. doi: 10.3390/brainsci12050518

Zhang, Y., Shi, C., Chen, Y., Wang, W., Huang, S., Han, Z., et al. (2020). 'Retinal structural and microvascular alterations in different acute ischemic stroke subtypes'. *J. Ophthalmol.* 2020:8850309. doi: 10.1155/2020/8850309

frontiers | Frontiers in Aging Neuroscience

TYPE Original Research
PUBLISHED 03 August 2022
DOI 10.3389/fnagi.2022.808415

OPEN ACCESS

EDITED BY
Li Li,
Capital Medical University, China

REVIEWED BY
Zhen-Ni Guo,
First Affiliated Hospital of Jilin University, China
Marta Rubiera,
Vall d'Hebron University Hospital, Spain
Tamra Ranasinghe,
Wake Forest Baptist Medical Center, United States

*CORRESPONDENCE
Xudong Pan
drpan022@163.com

SPECIALTY SECTION
This article was submitted to Neurocognitive Aging and Behavior, a section of the journal Frontiers in Aging Neuroscience

RECEIVED 03 November 2021
ACCEPTED 01 July 2022
PUBLISHED 03 August 2022

CITATION
Zhang M, Wang K, Xie L and Pan X (2022) Short-term Montreal Cognitive Assessment predicts functional outcome after endovascular therapy. *Front. Aging Neurosci.* 14:808415. doi: 10.3389/fnagi.2022.808415

Short-term Montreal Cognitive Assessment predicts functional outcome after endovascular therapy

Meng Zhang, Kun Wang, Linlin Xie and Xudong Pan*

Department of Neurology, The Affiliated Hospital of Qingdao University, Qingdao, China

Background: The previous studies have shown that cognition in patients 4–8 weeks after stroke can predict early functional outcomes after stroke. The analyses of data from the REVASCAT trial proved that stent thrombectomy improves post-morbid wiring test outcomes in patients with AIS compared with drug therapy. However, few studies focus on the relationship between cognitive impairment and functional outcomes in patients undergoing endovascular treatment.

Methods: A total of 647 participants registered from stroke centers. Stroke severity was evaluated by National Institutes of Health stroke scale (NIHSS). The functional status was estimated by modified Rankin scale (mRS). The cognitive impairment was assessed by trained neurologists at 14 (±4) and 90 (±7) days after stroke onset using the Montreal Cognitive Assessment (MoCA). A MoCA score of less than 26 was considered post-stroke cognitive impairment (PSCI).

Results: A total of 120 Patients who underwent endovascular therapy were included. The PSCI group had higher levels of age, men, educational status, atrial fibrillation, smoking, alcoholism, Alberta Stroke Program Early CT (ASPECT) score of the anterior circulation, and OTP time than the non-PSCI group ($p < 0.05$). In contrast, the 14-day MoCA score, 14-day NIHSS score, 3-month MoCA score, 3-month NIHSS score, 3-month mRS score, and 3-month EQ5D score were lower in those PSCI patients. The risk predictors of PSCI were age, sex, educational level, atrial fibrillation, smoking, alcoholism, ASPECT Score (anterior circulation), 14-day MoCA score, and 14-day NIHSS score. There were strong relationships between 3-month NIHSS and MoCA ($r = -0.483$, $p < 0.001$). Receiver operating characteristic (ROC) curve indicated that 14-day MoCA score, memory, abstraction, visuospatial/executive functions, attention, and language, played a significant role to predict PSCI [area under the curve (AUC) > 0.7]. It had predictive value for the 14-day visuospatial/executive functions to predict 3-month functional outcomes.

Conclusion: Early application of the MoCA in different cognitive regions could predict the PSCI and future functional outcomes, which is necessary to screen high-risk patients with poor prognosis and conduct an early intervention.

KEYWORDS

post-stroke cognitive impairment (PSCI), endovascular therapy, functional outcome, risk factors, MoCA

Introduction

Stroke is the second leading cause of death worldwide and is estimated to affect more than 13.7 million people each year (GBD 2019 Stroke Collaborators, 2021). A common complication after stroke is cognitive impairment. More than half of stroke patients will have varying degrees of cognitive impairment in the acute phase and the recovery period from 3 to 6 months after stroke (Levine et al., 2015). Cognitive impairment is closely related to stroke patients' physical recovery and independent living ability (Gottesman and Hillis, 2010). The severe cognitive impairment will increase the risk of death, harming the prognosis of stroke patients (Zheng et al., 2019). Some studies showed that the impact of cognitive dysfunction on quality of life was much higher than physical dysfunction (Zheng et al., 2019). So far, post-stroke cognitive impairment (PSCI) has become an international research hotspot. Early identification and management of high-risk populations with PSCI are essential topics to be solved.

Endovascular therapy (EVT) has been shown to improve functional outcomes and physical disability of patients who suffered from acute ischemic stroke (AIS) (Campbell et al., 2017). The previous analyses of data from the REVASCAT trial have shown that stent thrombectomy improves trail-making test performance in patients with AIS compared with drug therapy, especially in patients with a good functional outcome (López-Cancio et al., 2017). Other studies showed that cognition in patients 4–8 weeks after stroke could predict early functional outcomes after stroke (Zietemann et al., 2018; Li et al., 2020). However, few studies focus on the relationship between cognitive impairment and functional outcomes in patients undergoing endovascular therapy. Besides, recognizing the significance of individual cognitive domain after stroke has not been paid much attention in the existing studies.

So we investigated the risk factors for cognitive impairment and the relationship between various cognitive domains and functional outcomes after endovascular therapy in stroke patients. We aim to find a decision-making tool that is relatively effective and convenient for screening high-risk patients with poor prognoses and conducting early intervention after EVT.

Abbreviations: PSCI, post-stroke cognition impairment; IQR, inter quartile range; BMI, body mass index; CHD, coronary heart disease; AF, atrial fibrillation; TIA, transient ischemic attack; mRS, modified Rankin scale; NIHSS, National Institutes of Health Stroke Scale; ASPECT, Alberta Stroke Program Early CT; OCSP, Oxfordshire Community Stroke Project; TACI, total anterior circulation infarct; PACI, partial anterior circulation infarct; POCI, posterior circulation infarct; LACI, lacunar infarct; IV tPA, intravenous tissue type plasminogen activator; EVT, endovascular therapy; OTD, onset to door; OTP, onset to puncture; OTR, onset to revascularization; TICI, thrombolysis in cerebral infarction; MoCA, Montreal Cognitive Assessment; EQ5D, EurolQol five dimensions questionnaire.

Participants and methods

Study population

In our prospective hospital-based cohort study, 647 participants registered from stroke centers in Qingdao and Beijing, China, from July 2018 to September 2020. The local ethics committees authorized our research protocol. All patients or legal guardians obtained written informed consent before participation. Patients who underwent EVT in the stroke centers were included based on the evidence-based guidelines from the American Heart Association/American Stroke Association (AHA/ASA) (Powers et al., 2019). According to the intraoperative situation, endovascular therapy can be used in the following ways: stent thrombectomy, catheter aspiration, intra-arterial thrombolysis, balloon angioplasty, permanent stenting, etc. Exclusion criteria: (1) with consciousness disorder, severe aphasia, or hemiplegia, unable to complete the neuropsychological test; (2) other neurological diseases known to cause cognitive impairment (such as brain trauma, brain tumors, encephalitis, epilepsy, and multiple sclerosis); (3) suffering from severe diseases of the heart, lung, liver, kidney, autoimmune disease, diseases of the endocrine and blood systems, or severe malnutrition; (4) have a history of mental illness; (5) history of cognitive impairment or dementia; (6) modified Rankin scale (mRS) score $\geq$ 3 and unable to take care of themselves; (7) Refused to undergo relevant imaging examination or refused to undergo endovascular therapy.

Assessment of baseline characteristics

The data of baseline characteristics were collected: age, sex, body mass index (BMI), educational level, previous medical history, smoking and alcohol use, blood pressure, blood glucose, etc; auxiliary examination: electrocardiograph (ECG) and head computerized tomography (CT), computerized tomography angiography (CTA), computed tomography perfusion imaging (CTP), digital subtraction angiography (DSA), etc; treatment: admission National Institutes of Health stroke scale (NIHSS) score, onset to door (OTD) time, onset to puncture (OTP) time, onset to revascularization (OTR) time, anesthetic mode, operation procedure, etc. Ischemic stroke subtypes were classified by the Oxfordshire Community Stroke Project (OCSP) (Paci et al., 2011). Alberta Stroke Program Early Computed Tomography Score (ASPECTS) was used to evaluate infarction severity (Naito et al., 2015). Thrombolysis in cerebral infarction (TICI) was used to assess the degree of recanalization; TICI grade 2B or 3 is considered successful after EVT (Jang et al., 2020). History of smoking and drinking was defined as smoking at least one cigarette per day and the alcohol consumption $>$ 168 g/week, currently or previously (Li et al., 2021).

Assessment of cognitive outcome

Trained neurologists assessed cognitive impairment at 14 ($\pm$4) and 90 ($\pm$7) days after stroke onset using the Montreal Cognitive Assessment (MoCA). The MoCA score includes the following 7 aspects: visuospatial/executive functions, orientation, attention, memory, abstraction language, and naming (Nasreddine et al., 2005). With the consent and cooperation of the subjects, face-to-face evaluations are conducted by the physician in a quiet room, and the scores are recorded. The overall score of the scale was 30, with higher scores associated with better cognitive function, and the MoCA score increased by 1 point when ischemic stroke patients had less than 12 years of education (Folstein et al., 1975). A MoCA score of less than 26 at 90 ($\pm$7) days after stroke onset was considered to have PSCI through face-to-face interviews (Lees et al., 2014). Mild PSCI was defined by MoCa $\geq$ 19, and severe PSCI was defined by MoCA $<$ 19 (Li et al., 2020).

Assessment of functional outcome

All the AIS patients were followed for 3 months. The stroke severity was assessed by NIHSS. The mRS score was used to estimate the functional state. The mRS $<$ 3 was considered to have a good functional prognosis. The mRS $\geq$ 3 was considered to have a poor functional prognosis (Tu et al., 2018). EurolQol five dimensions questionnaire (EQ5D) was used to assess the patient's multidimensional physical and mental health (Rangaraju et al., 2017).

Statistical analysis

The measurement data are presented as mean $\pm$ *SD* or median (interquartile range). Enumeration data were presented as frequencies (percentages). Independent *t*-test and Wilcoxon (Mann–Whitney) test were used to analyze the measurement data according to the appropriate condition. Enumeration data were analyzed by Pearson χ^2 or Fisher exact test. Independent *t*-test and Wilcoxon (Mann–Whitney) test were used to analyze the measurement data according to the appropriate condition. Univariable and multivariable logistic regression analyses were used to identify the independent predictive factors of PSCI and 3-month outcomes. Receiver operating characteristic (ROC) curves evaluated the predictive ability of the MoCA score for PSCI and functional outcome. The 3-month MoCA and NIHSS score association was assessed by the Spearman correlation analysis. The SPSS 26.0 statistical software was used for statistical processing and analysis. The $p < 0.05$ was considered statistically significant.

Results

Baseline characteristics

Approximately 253 of all the AIS patients were treated with EVT. A total of 122 patients were included in the initial analysis (75 patients did not have available MoCA scores, 54 patients were lost during follow-up, and 2 died). A total of 120 patients were incorporated into the final analysis (2 were missing MoCA items) (**Figure 1**). Reasons for incomplete MoCA score include aphasia, uncooperation, coma, loss of follow-up, isolation due to COVID-19, death, etc.

Table 1 summarized the baseline characteristics of the participants. A total of 120 patients, such as 73 PSCI and 47 non-PSCI, were studied. The significant differences were found in the vascular risk factors, auxiliary examination, and treatment (**Table 1**). The median age of EVT subjects was 63 years. Approximately 65.0% of them were men. The PSCI group was older, had more men, and had a lower level of education compared to the non-PSCI group ($p < 0.05$). They had a higher incidence of atrial fibrillation, smoking, and drinking. Besides, the ASPECT score of the anterior circulation and OTP time in the PSCI group were higher than the non-PSCI group ($p < 0.05$). Meanwhile, the cognitive state (the 14-day MoCA score and 3-month MoCA score), the functional status (14-day NIHSS score, 3-month NIHSS score, 3-month mRS score, and 3-month EQ5D score), were worse in those PSCI patients. The two groups did not differ in other baseline characteristics ($p > 0.05$).

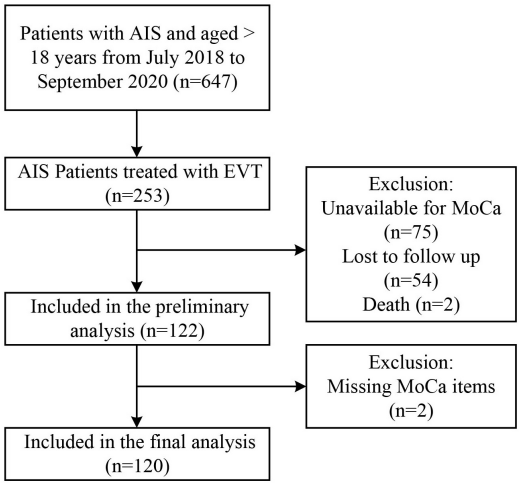

FIGURE 1
Flowchart of study participants.

The risk factors associated with cognitive impairment

The univariate logistic regression analysis was used to found the predictive factors. Age, sex, educational level, atrial fibrillation, smoking, alcoholism, ASPECT score (anterior circulation), 14-day MoCA score, and 14-day NIHSS score were screened out to be the risk factors for PSCI. Then, those predictive factors were included in a multivariate logistic regression analysis. The results showed that the independent indictors of PSCI were the 14-day MoCA and NIHSS score (Table 2) after adjusting for age, sex, and educational level. Patients with higher 14-day MoCA score had a 1.750-fold (95% CI 1.649–1.865, $p < 0.001$, Table 2) higher risk of PSCI. Similarly, those with higher 14-day NIHSS score had a 1.186-fold (95% CI 1.033–1.363, $p < 0.001$, Table 2) higher risk of PSCI. Furthermore, hypertension, diabetes mellitus, coronary heart disease, atrial fibrillation, dyslipidemia, previous TIA/stroke, smoking, alcoholism, and admission NIHSS score were adjusted on this basis. And the 14-day MoCA and NIHSS score were finally considered as the independent indicators of PSCI.

The correlation between 3-month Montreal Cognitive Assessment and National Institutes of Health stroke scale score

The relationships were observed between the 3-month NIHSS and MoCA scores ($r = -0.483$, $p < 0.001$, Figure 2). The PSCI group was further divided into the mild PSCI (MoCA $\geq$ 19) and severe PSCI (MoCA $<$ 19). The results showed that the MoCA (such as scores in different cognitive domains) and 3-month EQ5D score of 3-month were significantly lower in the severe PSCI group compared to the mild group. While the 3-month NIHSS and mRS scores were substantially higher (Table 3 and Figure 3).

After a 3-month follow-up, a total of 120 patients treated with EVT were divided into two groups according to the different mRS scores. Approximately 20 of them experienced poor functional outcomes. The 3-month MoCA scores (such as visuospatial/executive functions, attention, memory, naming, and orientation) and the 3-month EQ5D scores of these subjects were lower than the patients who had good outcomes ($p < 0.05$, Table 4). While 3-month NIHSS and mRS scores were higher ($p < 0.05$, Table 4). There were no statistically significant differences in the abstraction and language score between the two groups ($p > 0.05$, Table 4).

The predictive value of Montreal Cognitive Assessment score for post-stroke cognitive impairment and functional outcome

The 14-day MoCA scores (such as scores of different cognitive domains) were analyzed by ROC (Figure 4 and Table 5). The results suggested that 14-day MoCA score, memory, abstraction, visuospatial/executive functions, attention, and language, especially for memory, played a significant role to predict PSCI [area under the curve (AUC) > 0.7]. The AUC of 14-day MoCA score was 0.868 [95% CI (0.792–0.944), $p < 0.001$].

Univariate logistic regression analysis was used to found the predictive factors of 3-month functional outcomes. After adjusting for the vascular risk factors (such as age, sex, educational level, hypertension, diabetes mellitus, coronary heart disease, atrial fibrillation, dyslipidemia, previous TIA/stroke, smoking, and alcoholism), that is to say, those risk factors were included in the multivariate logistic regression analysis. The results showed that the independent indictors of 3-month functional outcomes were visuospatial/executive functions. Patients with lower 14-day visuospatial/executive functions score had a 1.498-fold (95% CI 1.040–2.158, $p = 0.03$) higher risk of poor outcomes. Furthermore, the ROC curve was used to evaluate the predictive value of 14-day visuospatial/executive functions for 3-month functional outcome. The results suggested that it had predictive value for the 14-day visuospatial/executive functions to predict 3-month functional outcomes (AUC > 0.7). The AUC was 0.706 [95% CI (0.553–0.860), $p = 0.009$, Figure 5]. The cut-off valve was 2 with 77.4% sensitivity and 68.7% specificity.

10.3389/fnagi.2022.808415

TABLE 1 Baseline demographics and clinical data of all participants.

Variable	All (n = 120)	PSCI (n = 73)	Non-PSCI (n = 47)	P-value[a]
Age, years (median, IQR)	**63** (16)	**66** (15)	**57** (20)	**0.004***
Male (%)	**65.0%**	**42.5%**	**23.4%**	**0.033***
BMI (kg/m^2) (median, IQR)	24 (4)	24 (4)	25 (5)	0.179
Educational Level, < 6 years (%)	**32.9%**	**57.7%**	**18.2%**	**0.021***
Hypertension (%)	45%	46.6%	42.6%	0.666
Diabetes mellitus (%)	7.5%	8.2%	6.4%	0.709
CHD (%)	6.7%	8.2%	4.3%	0.395
Dyslipidemia (%)	3.3%	4.1%	2.1%	0.555
AF (%)	**12.5%**	**19.2%**	**2.1%**	**0.006***
Previous TIA/stroke (%)	17.5%	17.8%	17.0%	0.912
Smoking (%)	**39.8%**	**52.2%**	**31.9%**	**0.029***
Alcoholism (%)	**40.5%**	**56.5%**	**30.0%**	**0.004***
Previous mRS score (median, IQR)	0 (0)	0 (0)	0 (0)	0.368
Admission systolic pressure (median, IQR)	140 (30)	140 (32)	140 (33)	0.455
Admission diastolic pressure (median, IQR)	85 (19)	83 (20)	86 (19)	0.282
Admission NIHSS score (median, IQR)	12 (7)	12 (5)	11 (8)	0.351
ASPECT score				
Anterior circulation	**9** (2)	**8** (3)	**9** (2)	**0.017***
Posterior circulation	10 (0)	10 (0)	10 (0)	0.720
OCSP classification (%)				0.772
TACI	47.5%	47.9%	46.8%	
PACI	40.0%	41.1%	38.3%	
POCI	11.7%	9.6%	14.9%	
LACI	0.8%	1.4%	0	
IV tPA + EVT (%)	53.3%	46.6%	63.8%	0.807
OTD time (median, IQR)	109 (121)	116 (134)	100 (98)	0.103
OTP time (median, IQR)	**245** (128)	**265** (148)	**235** (126)	**0.022***
OTR time (median, IQR)	319 (147)	328 (203)	305 (118)	0.068
Anesthetic mode (%)				0.110
General anesthesia	34.2%	39.7%	25.5%	
Local anesthesia	65.8%	60.3%	74.5%	
Operation procedure (%)				
Stent thrombectomy	65.8%	67.1%	63.8%	0.710
Intra-arterial thrombolysis	22.5%	19.2%	27.7%	0.277
Catheter aspiration	32.5%	35.6%	27.7%	0.364
Balloon angioplasty	21.7%	21.9%	21.3%	0.934
Permanent stening	15.8%	13.7%	19.1%	0.425
TICI > 2a	92.5%	90.4%	95.7%	0.177
14-day MoCA score (median, IQR)	**22** (15)	**16** (12)	**28** (4)	**< 0.001***
14-day NIHSS score (median, IQR)	**1** (5)	**3** (5)	**1** (4)	**0.005***
3-month MoCA score (median, IQR)	**24** (9)	**21** (10)	**29** (3)	**< 0.001***
3-month NIHSS score (median, IQR)	**0** (2)	**1** (3)	**0** (1)	**0.003***
3-month mRS score (median, IQR)	**1** (1)	**1** (2)	**1** (1)	**0.003***
3-month EQ5D score (median, IQR)	**95** (13)	**93** (18)	**95** (9)	**0.017***

PSCI, post-stroke cognition impairment; IQR, inter quartile range; BMI, body mass index; CHD, coronary heart disease; AF, atrial fibrillation; TIA, transient ischemic attack; mRS, modified Rankin scale; NIHSS, National Institute of Health Stroke Scale; ASPECT, Alberta Stroke Program Early CT; OCSP, Oxfordshire Community Stroke Project; TACI, total anterior circulation infarct; PACI, partial anterior circulation infarct; POCI, posterior circulation infarct; LACI, lacunar infarct; IV tPA, intravenous tissue type plasminogen activator; EVT, endovascular therapy; OTD, onset to door; OTP, onset to puncture; OTR, onset to revascularization; TICI, thrombolysis in cerebral infarction; MoCA, Montreal Cognitive Assessment; EQ5D, EurolQol five dimensions questionnaire.

[a]Chi-square and Mann–Whitney U test were applied for comparing the proportions and medians.

*$P < 0.05$ was considered statistically significant, and the bold values are also included.

TABLE 2 Univariate analysis and multivariate analysis of predictors of post-stroke cognitive impairment (PSCI).

	Odds ratio	95% CI	*P*-value
Univariate analysis			
Age	1.050	1.016–1.084	0.003*
Sex	2.416	1.065–5.481	0.035*
Educational Level	1.923	1.252–2.956	0.003*
AF	10.915	1.384–86.075	0.023*
Smoking	2.324	1.085–4.978	0.030*
Alcoholism	3.033	1.397–6.586	0.005*
ASPECT Score (anterior circulation)	0.675	0.489–0.930	0.016*
14-day MoCA score	1.781	1.705–1.865	< 0.001*
14-day NIHSS score	1.143	1.027–1.273	0.014*
Multivariate analysis[a]			
14-day MoCA score	1.750	1.649–1.865	< 0.001*
14-day NIHSS score	1.186	1.033–1.363	0.016*
Multivariate analysis[b]			
14-day MoCA score	1.735	1.614–1.881	0.001*
14-day NIHSS score	1.237	1.045–1.464	0.013*

PSCI, post-stroke cognition impairment; CI, confidence interval; AF, atrial fibrillation; ASPECT, Alberta Stroke Program Early CT; MoCA, Montreal Cognitive Assessment; NIHSS, National Institute of Health Stroke Scale.

[a]Adjusted for age, sex, educational level.

[b]Adjusted for age, sex, educational level, hypertension, diabetes mellitus, coronary heart disease, atrial fibrillation, dyslipidemia, previous TIA/stroke, smoking, alcoholism, admission NIHSS score.

*$P < 0.05$ were considered statistically significant.

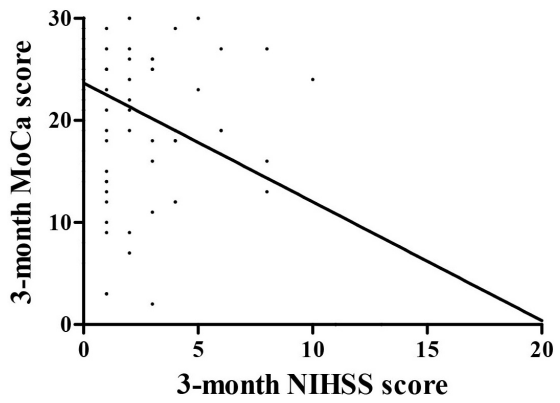

FIGURE 2
Correlation between 3-month MoCa and NIHSS score.

Discussion

This prospective cohort study demonstrated the relationship between PSCI and functional outcomes in patients undergoing endovascular therapy. The PSCI group had higher levels of age, men, educational status, atrial fibrillation, smoking, alcoholism, ASPECT score of anterior circulation, and OTP time compared to non-PSCI group ($p < 0.05$). In contrast, the 14-day MoCA score, 14-day NIHSS score, 3-month MoCA score, 3-month NIHSS score, 3-month mRS score, and 3-month EQ5D score were lower in those PSCI patients. The risk predictors of PSCI were age, sex, educational level, atrial fibrillation, smoking, alcoholism, ASPECT Score (anterior circulation), 14-day MoCA score, and 14-day NIHSS score. There was a strong relationship between 3-month NIHSS and MoCA score ($r = -0.483$, $p < 0.001$). The ROC curve indicated that 14-day MoCA score, memory, abstraction, visuospatial/executive functions, attention, and language, played a significant role to predict PSCI (AUC > 0.7). It had predictive value for the 14-day visuospatial/executive functions to predict 3-month functional outcomes.'

Cognitive function refers to the various conscious mental activities of human beings in the state of awakening, which is the function of the brain to perform higher activities. The cognitive function consists of multiple cognitive domains, such as attention, calculation, memory, orientation, executive ability, and language. The multiple cognitive domain impairment is called cognitive dysfunction (Levine et al., 2015). The incidence of cognitive dysfunction after stroke is high. The incidence rates reported vary from study to study because of the criteria used to define cognitive dysfunction and the chosen tools. The research from Hachinski et al. (2006) showed that 64% of stroke patients had some degree of cognitive impairment, and about one-third of them would develop dementia. Another study found that 91.5% of patients without dementia had at least one cognitive domain impairment after an ischemic stroke, while 73.4% had multiple cognitive domain impairments (Jaillard et al., 2009).

TABLE 3 The 3-month score of included PSCI patients.

Variable	Mild ($n = 10$)	Severe ($n = 33$)	*P*-value[a]
Visuospatial/executive functions (median, IQR)	3 (2)	1 (2)	< 0.001*
Attention (median, IQR)	5 (3)	2 (4)	< 0.001*
Abstraction (median, IQR)	1 (2)	0 (1)	< 0.001*
Memory (median, IQR)	2 (3)	0 (1)	< 0.001*
Language (median, IQR)	3 (1)	0 (2)	< 0.001*
Naming (median, IQR)	3 (0)	2 (2)	< 0.001*
Orientation (median, IQR)	6 (0)	5 (6)	< 0.001*
3-month MoCA score (median, IQR)	23 (3)	12 (12)	< 0.001*
3-month NIHSS score (median, IQR)	0 (2)	2 (3)	0.001*
3-month mRS score (median, IQR)	1 (1)	2 (2)	0.001*
3-month EQ5D score (median, IQR)	95 (10)	83 (33)	0.001*

IQR, interquartile range; PSCI, post-stroke cognition impairment; MoCA, Montreal Cognitive Assessment; NIHSS, National Institute of Health Stroke Scale; mRS, modified Rankin scale; EQ5D, EurolQol five dimensions questionnaire.

[a]Mann–Whitney *U* test was applied to compare the proportions and median values between groups.

*$P < 0.05$ were considered statistically significant.

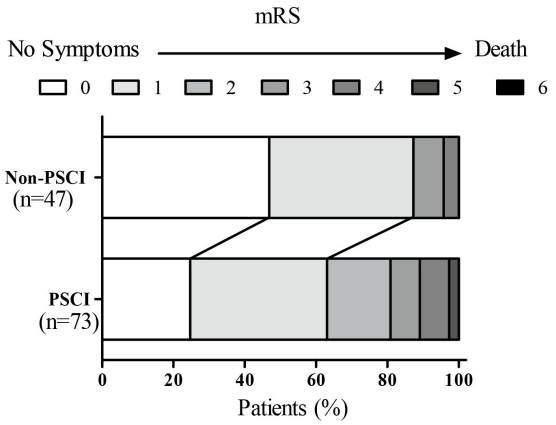

FIGURE 3
mRS score in non-PSCI and PSCI groups.

TABLE 4 The 3-month score according to the functional outcomes.

Variable	Good (n = 100) (mRS < 3)	Poor (n = 20) (mRS ≥ 3)	P-value[a]
Visuospatial /executive functions (median, IQR)	4 (3)	2 (4)	0.006*
Attention (median, IQR)	6 (2)	4 (6)	0.016*
Abstraction (median, IQR)	2 (2)	1 (2)	0.113*
Memory (median, IQR)	3 (4)	2 (4)	0.048*
Language (median, IQR)	3 (1)	2 (3)	0.053*
Naming (median, IQR)	3 (1)	3 (3)	0.011*
Orientation (median, IQR)	6 (0)	6 (5)	0.003*
3-month MoCA score (median, IQR)	24 (10)	19 (24)	0.017*
3-month NIHSS score (median, IQR)	0 (1)	6 (7)	< 0.001*
3-month mRS score (median, IQR)	1 (1)	4 (1)	< 0.001*
3-month EQ5D score (median, IQR)	95 (10)	60 (43)	< 0.001*

IQR, inter quartile range; MoCA, Montreal Cognitive Assessment; NIHSS, National Institute of Health Stroke Scale; mRS, modified Rankin scale; EQ5D, EurolQol five dimensions questionnaire.
[a]Mann–Whitney U test were applied for comparing the proportions and medians values between groups.
*$P < 0.05$ were considered statistically significant.

Cognitive dysfunction after stroke not only directly affects patients' self-care ability in daily life but also seriously affects their active coordination ability in the rehabilitation of motor, sensory, swallowing, and other functional disorders, which leads to the decline of patients' quality of life and survival time. Therefore, the PSCI has become a hotspot of stroke-related research and intervention worldwide.

In the early stage of acute cerebral artery occlusion, the ischemic lesion can directly affect the cognitive function of patients, and the blood perfusion of the tissue around the core infarction area is significantly reduced. Thus, the metabolic rate of brain tissue and the excitability of nerve cells decrease, which can aggravate cognitive function impairment (Pantoni and Salvadori, 2021). With endovascular therapy, blood flow will be restored to the tissues around the core infarct area, thereby improving partial cognitive function, which proves that cerebral ischemia can lead to cognitive dysfunction on the other hand.

The MoCA was developed by Nasreddine et al. (2005) by combining extensive clinical experience with certain cognitive items and scoring criteria in the Minimum Mental State Examination (MMSE). Several studies have shown that the sensitivity of the MoCA scale in the test of mild vascular cognitive impairment is much higher than that of MMSE, which is conducive to the early diagnosis of vascular cognitive impairment and the timely prevention of vascular dementia (VD) (Wen et al., 2008). Therefore, MoCA was used to assess the subjects' cognitive function in this study. The previous studies have found that the risk factors for PSCI include education level, sex, age, alcohol, blood glucose, stroke type, ischemic location, etc. (Alexandrova and Danovska, 2016; He et al., 2018; Ward et al., 2018). Advanced age was a significant predictor of cognitive impairment after cerebral infarction, and our study also reached the same conclusion. The mechanism may be that the accumulation of amyloid protein and the concentration of total amyloid-beta (Aβ) were promoted in elderly stroke patients who tended to have more basic diseases and poorer vascular foundation, which led to the impairment of cognitive function.

Chronic alcohol use is associated with cognitive decline, ranging from mild impairment to severe and irreversible dementia (Ridley et al., 2013), which may be attributed to the decreased cell density in the prefrontal cortex (Charlton et al., 2019). Meanwhile, several studies have reported impaired cognitive flexibility following chronic alcohol exposure. Alcohol exposure can lead to impairments in decision-making, suggesting that these impairments can exist both as risk factors for and consequences of excessive drinking (McMurray et al., 2016; Schindler et al., 2016; Boutros et al., 2017; Salling et al., 2018) and this is consistent with our research results.

Diabetes is also a risk factor for predicting the occurrence of PSCI. Studies have found that endothelial dysfunction and microvascular damage caused by diabetes can cause cognitive dysfunction or dementia by damaging the blood–brain barrier (Tamura et al., 2017). High education is also an essential factor affecting cognitive function (Das et al., 2013; Kessels et al., 2017). The higher the level of education, the better the cognitive reserve, which can increase the synaptic connections of brain cells, reduce the damage to cognitive function by brain injury, and thus reduce the prevalence of PSCI

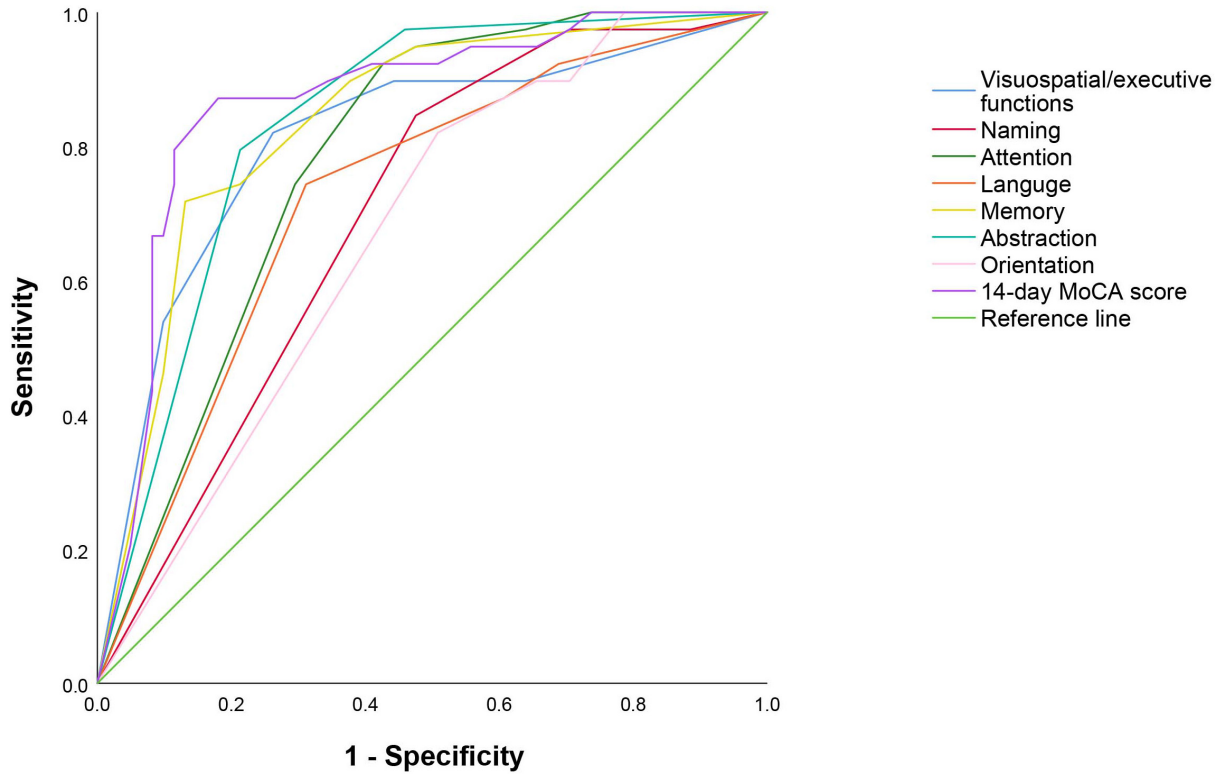

FIGURE 4
Receiver operating characteristic curve on predicting PSCI.

TABLE 5 Receiver operating characteristic analysis of PSCI.

	AUC	95% CI	Cut-off value	Sensitivity	Specificity	*P*-value
14-day MoCA score	0.868	0.792–0.944	22	0.872	0.820	< 0.001*
Memory	0.838	0.758–0.919	3	0.718	0.869	< 0.001*
Abstraction	0.836	0.757–0.915	1	0.795	0.787	< 0.001*
Visuospatial/executive functions	0.811	0.720–0.903	3	0.821	0.738	< 0.001*
Attention	0.782	0.693–0.871	4	0.925	0.574	< 0.001*
Language	0.727	0.626–0.828	2	0.744	0.689	< 0.001*
Naming	0.699	0.597–0.801	2	0.846	0.525	< 0.001*
Orientation	0.670	0.566–0.775	5	0.821	0.492	0.004*

AUC, area under the curve; CI, confidence interval; MoCA, Montreal Cognitive Assessment; PSCI, post-stroke cognitive impairment.
*$P < 0.05$ were considered statistically significant.

(Mohd Zulkifly et al., 2016; Robitaille et al., 2018). At the same time, the severity of stroke is related to PSCI, and the NIHSS score is a critical evaluation index reflecting stroke severity. The higher the NIHSS score, the more sites and larger areas of intracranial ischemic damage, leading to cognitive impairment.

Alberta Stroke Program Early Computed Tomography Score is mainly used to evaluate the severity of cerebral infarction, and the lower the score is, the larger the infarct area (Yoo et al., 2016). Low baseline ASPECTS was closely associated with poor neurological outcomes after endovascular treatment and even with increased mortality after endovascular treatment. Stroke patients with ASPECTS higher than 6 had good outcomes with endovascular therapy, while patients with ASPECTS lower than 4 had poor outcomes (Desilles et al., 2017). The results of univariate regression analysis in this study showed that the ASPECTS score of anterior circulation was also a risk factor for cognitive impairment. However, due to the limited sample size, it lacked more detailed stratified analysis, follow-up observation, and etiological mechanism research. Our findings provide only theoretical support for future scientific research.

Many clinical studies, such as MR CLEAN, ESCAPE, and EXTEND-IA, SWIFT-PRIME, have shown that the rate of good

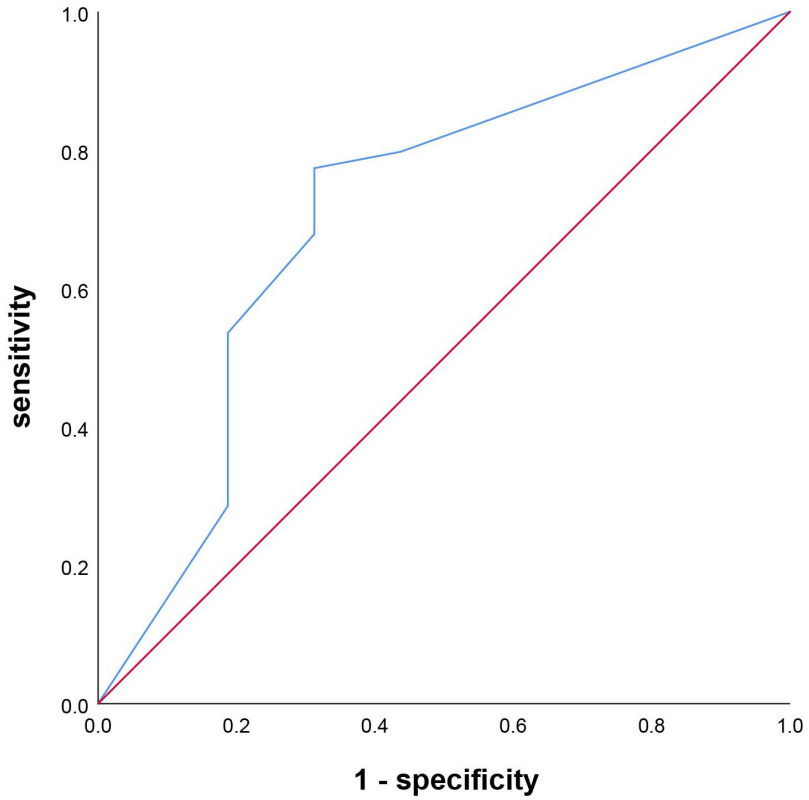

FIGURE 5
Receiver operating characteristic curve on predicting 3-month functional outcomes.

outcomes in patients receiving endovascular therapy decreases with increasing onset-to-puncture time (OTP) (Prabhakaran et al., 2015). In addition, there was a significant correlation between prognosis and onset-to-reperfusion time (OTR) (Goyal et al., 2011). Our results showed that OTP time was also associated with cognitive impairment after stroke. We believe both are related to reperfusion, contributing to more functional recovery of ischemic brain tissue.

The previous studies have shown that early MoCA test results can predict long-term functional recovery after stroke (Zietemann et al., 2018). Our results also support the above views: there was a strong relationship between 3-month MoCA and NIHSS score (r = –0.483, p < 0.001). The ROC curve indicated that the 14-day MoCA score had an excellent predictive value for PSCI. Especially, memory was the best predictor of functional outcome in 3 months. However, Li et al. (2019) found that patients with mild ischemic stroke had multiple cognitive domains impaired, of which executive function was the most commonly impaired cognitive domain. Besides, the previous studies also found that the memory function of stroke patients was significantly reduced, and there were significant obstacles in both immediate and delayed recall (Graham et al., 2004). Given that the degree of cognitive impairment varies depending on the location of the infarction, we speculate that the differences in results may be related to the study population, different screening methods, different assessment criteria, and limited sample size.

Our study focused on the relationship between cognition and functional outcome after endovascular therapy. It suggested that early cognitive function was the valuable predictor of PSCI and functional outcome at 3 months. Given the convenience and high sensitivity for mild cognitive impairment of MoCA, we recommend the early application of MoCA after endovascular treatment, which will be conducive to screening high-risk patients with poor prognoses and conducting early intervention for clinicians.

We also recognize the existence of limitations in our study. First, the number of participants is relatively small in our retrospective research. Therefore, the results need to be verified by a large sample perspective study. Second, we excluded patients with aphasia and other serious diseases, which may cause an underestimate of the practical occurrence rate of PSCI. Third, we did not analyze the influence of size and location of infarct lesions on cognitive function. Forth, TICI score was used instead of the eTICI score which includes TICI 2c as well due to the limitation of the conditions at that time (Goyal et al., 2014). Finally, although commonalities dominate the cognitive structure, differences in race, language, and culture will still

affect the universality of scales, especially for tests like MoCA that require certain educational background. Therefore, it is far from enough to rely on translation and introduction in the future. We also look forward to the emergence of more local authoritative scales.

Conclusion

This prospective cohort study demonstrated that cognition was strongly associated with functional outcomes after endovascular treatment. Short-term cognitive outcomes, assessed by MoCA, could predict PSCI and future functional outcomes. The early application of the MoCA score in different cognitive regions after EVT, will contribute to screening high-risk patients with poor prognoses so that the clinicians could implement interventions as early as possible.

Data availability statement

The original contributions presented in this study are included in the article/supplementary material, further inquiries can be directed to the corresponding author.

Ethics statement

The studies involving human participants were reviewed and approved by the Ethical Committee of the Affiliated Hospital of Qingdao University and Ethical Committee of the Beijing Tiantan Hospital. The patients/participants provided their written informed consent to participate in this study. Written informed consent was obtained from the individual(s) for the publication of any potentially identifiable images or data included in this article.

Author contributions

MZ analyzed the patients' data and was the major contributor in writing the manuscript. KW and LX were responsible for gathering and organizing data. XP provided support for research design and draft writing, and were responsible for draft revision. All authors read and approved the final and revised manuscript.

Conflict of interest

The authors declare that the research was conducted in the absence of any commercial or financial relationships that could be construed as a potential conflict of interest.

Publisher's note

All claims expressed in this article are solely those of the authors and do not necessarily represent those of their affiliated organizations, or those of the publisher, the editors and the reviewers. Any product that may be evaluated in this article, or claim that may be made by its manufacturer, is not guaranteed or endorsed by the publisher.

References

Alexandrova, M. L., and Danovska, M. P. (2016). Cognitive impairment one year after ischemic stroke: Predictorsand dynamics of significant determinants. *Turk. J. Med. Sci.* 46, 1366–1373. doi: 10.3906/sag-1403-29

Boutros, N., Der-Avakian, A., Markou, A., and Semenova, S. (2017). Effects of early life stress and adolescent ethanol exposure on adult cognitive performance in the 5-choice serial reaction time task in Wistar male rats. *Psychopharmacology* 234, 1549–1556. doi: 10.1007/s00213-017-4555-3

Campbell, B. C. V., Mitchell, P. J., Davis, S. M., and Donnan, G. A. (2017). The long-term benefits of endovascular therapy. *Lancet Neurol.* 16, 337–338. doi: 10.1016/S1474-4422(17)30079-0

Charlton, A. J., May, C., Luikinga, S. J., Burrows, E. L., Hyun Kim, J., Lawrence, A. J., et al. (2019). Chronic voluntary alcohol consumption causes persistent cognitive deficits and cortical cell loss in a rodent model. *Sci. Rep.* 9:18651. doi: 10.1038/s41598-019-55095-w

Das, S., Paul, N., Hazra, A., Ghosal, M., Ray, B. K., Banerjee, T. K., et al. (2013). Cognitive dysfunction in stroke survivors: A community-based prospective study from Kolkata, India. *J. Stroke Cerebrovasc. Dis.* 22, 1233–1242. doi: 10.1016/j.jstrokecerebrovasdis.2012.03.008

Desilles, J. P., Consoli, A., Redjem, H., Coskun, O., Ciccio, G., smajda, s., et al. (2017). successful reperfusion with mechanical thrombectomy is associated with reduced disability and mortality in patients with pretreatment diffusion-weighted imaging-alberta stroke program early computed tomography score =6. *Stroke* 48, 963–969. doi: 10.1161/STROKEAHA.116.015202

Folstein, M. F., Folstein, S. E., and McHugh, P. R. (1975). "Mini-mental state". A practical method for grading the cognitive state of patients for the clinician. *J. Psychiatr. Res.* 12, 189–198. doi: 10.1016/0022-3956(75)90026-6

GBD 2019 Stroke Collaborators (2021). Global, regional, and national burden of stroke and its risk factors, 1990-2019: A systematic analysis for the Global Burden of Disease Study 2019. *Lancet Neurol.* 20, 795–820. doi: 10.1016/S1474-4422(21)00252-0

Gottesman, R. F., and Hillis, A. E. (2010). Predictors and assessment of cognitive dysfunction resulting from ischaemic stroke. *Lancet Neurol.* 9, 895–905. doi: 10.1016/S1474-4422(10)70164-2

Goyal, M., Fargen, K. M., Turk, A. S., Mocco, J., Liebeskind, D. S., Frei, D., et al. (2014). 2C or not 2C: Defining an improved revascularization grading scale and the need for standardization of angiography outcomes in stroke trials. *J. Neurointerv. Surg.* 6, 83–86. doi: 10.1136/neurintsurg-2013-010665

Goyal, M., Menon, B. K., Coutts, S. B., Hill, M. D., Demchuk, A. M., Penumbra Pivotal Stroke Trial Investigators, et al. (2011). Effect of baseline CT scan appearance and time to recanalization on clinical outcomes in endovascular thrombectomy of acute ischemic strokes. *Stroke* 42, 93–97. doi: 10.1161/STROKEAHA.110.594481

Graham, N. L., Emery, T., and Hodges, J. R. (2004). Distinctive cognitive profiles in Alzheimer's disease and subcortical vascular dementia. *J. Neurol. Neurosurg. Psychiatry* 75, 61–71.

Hachinski, V., Iadecola, C., Petersen, R. C., Breteler, M. M., Nyenhuis, D. L., Black, S., et al. (2006). National institute of neurological disorders and stroke-canadian stroke network vascular cognitive impairment harmonization standards. *Stroke* 37, 2220–2241. doi: 10.1161/01.STR.0000237236.88823.47

He, M., Wang, J., Liu, N., Xiao, X., Geng, S., Meng, P., et al. (2018). Effects of blood pressure in the early phase of ischemic stroke and stroke subtype on poststroke cognitive impairment. *Stroke* 49, 1610–1617. doi: 10.1161/STROKEAHA.118.020827

Jaillard, A., Naegele, B., Trabucco-Miguel, S., LeBas, J. F., and Hommel, M. (2009). Hidden dysfunctioning in subacute stroke. *Stroke* 40, 2473–2479. doi: 10.1161/STROKEAHA.108.541144

Jang, K. M., Nam, T. K., Ko, M. J., Choi, H. H., Kwon, J. T., Park, S. W., et al. (2020). Thrombolysis in cerebral infarction grade 2C or 3 represents a better outcome than 2B for endovascular thrombectomy in acute ischemic stroke: A network meta-analysis. *World Neurosurg.* 136, e419–e439. doi: 10.1016/j.wneu.2020.01.020

Kessels, R. P., Eikelboom, W. S., Schaapsmeerders, P., Maaijwee, N. A., Arntz, R. M., van Dijk, E. J., et al. (2017). Effect of formal education on vascular cognitive impairment after stroke: A meta-analysis and study in young-stroke patients. *J. Int. Neuropsychol. Soc.* 23, 223–238. doi: 10.1017/S1355617716001016

Lees, R., Selvarajah, J., Fenton, C., Pendlebury, S. T., Langhorne, P., Stott, D. J., et al. (2014). Test accuracy of cognitive screening tests for diagnosis of dementia and multidomain cognitive impairment in stroke. *Stroke* 45, 3008–3018. doi: 10.1161/STROKEAHA.114.005842

Levine, D. A., Galecki, A. T., Langa, K. M., Unverzagt, F. W., Kabeto, M. U., Giordani, B., et al. (2015). Trajectory of cognitive decline after incident stroke. *JAMA* 314, 41–51. doi: 10.1001/jama.2015.6968

Li, H. Q., Wang, X., Wang, H. F., Zhang, W., Song, J. H., Chi, S., et al. (2021). Dose-response relationship between blood pressure and intracranial atherosclerotic stenosis. *Atherosclerosis* 317, 36–40. doi: 10.1016/j.atherosclerosis.2020.12.004

Li, J., Wang, J., Wu, B., Xu, H., Wu, X., Zhou, L., et al. (2020). Association between early cognitive impairment and midterm functional outcomes among Chinese acute ischemic stroke patients: A longitudinal study. *Front. Neurol.* 11:20. doi: 10.3389/fneur.2020.00020

Li, J., You, S. J., Xu, Y. N., Yuan, W., Shen, Y., Huang, J. Y., et al. (2019). Cognitive impairment and sleep disturbances after minor ischemic stroke. *Sleep Breath.* 23, 455–462. doi: 10.1007/s11325-018-1709-4

López-Cancio, E., Jovin, T. G., Cobo, E., Cerdá, N., Jiménez, M., Gomis, M., et al. (2017). Endovascular treatment improves cognition after stroke: A secondary analysis of REVASCAT trial. *Neurology* 88, 245–251. doi: 10.1212/WNL.0000000000003517

McMurray, M. S., Amodeo, L. R., and Roitman, J. D. (2016). Consequences of adolescent ethanol consumption on risk preference and orbitofrontal cortex encoding of reward. *Neuropsychopharmacology* 41, 1366–1375. doi: 10.1038/npp.2015.288

Mohd Zulkifly, M. F., Ghazali, S. E., Che Din, N., Singh, D. K., and Subramaniam, P. (2016). A review of risk factors for cognitive impairment in stroke survivors. *TheScientificWorldJournal* 2016:3456943. doi: 10.1155/2016/3456943

Naito, T., Takeuchi, S., and Arai, N. (2015). Exclusion of isolated cortical swelling can increase efficacy of baseline alberta stroke program early CT score in the prediction of prognosis in acute ischemic stroke patients treated with thrombolysis. *J. Stroke Cerebrovasc. Dis.* 24, 2754–2758. doi: 10.1016/j.jstrokecerebrovasdis.2015.08.006

Nasreddine, Z. S., Phillips, N. A., Bédirian, V., Charbonneau, S., Whitehead, V., Collin, I., et al. (2005). The montreal cognitive assessment, MoCA: A brief screening tool for mild cognitive impairment. *J. Am. Geriatr. Soc.* 53, 695–699. doi: 10.1111/j.1532-5415.2005.53221.x

Paci, M., Nannetti, L., D'Ippolito, P., and Lombardi, B. (2011). Outcomes from ischemic stroke subtypes classified by the Oxfordshire community stroke project: A systematic review. *Eur. J. Phys. Rehabil. Med.* 47, 19–23.

Pantoni, L., and Salvadori, E. (2021). Location of infarcts and post-stroke cognitive impairment. *Lancet Neurol.* 20, 413–414. doi: 10.1016/S1474-4422(21)00107-1

Powers, W. J., Rabinstein, A. A., Ackerson, T., Adeoye, O. M., Bambakidis, N. C., Becker, K., et al. (2019). Guidelines for the early management of patients with acute ischemic stroke: 2019 update to the 2018 guidelines for the early management of acute ischemic stroke: A guideline for healthcare professionals from the American Heart Association/American Stroke Association. *Stroke* 50, e344–e418. doi: 10.1161/STR.0000000000000211

Prabhakaran, S., Ruff, I., and Bernstein, R. A. (2015). Acute stroke intervention: A systematic review. *JAMA* 313, 1451–1462. doi: 10.1001/jama.2015.3058

Rangaraju, S., Haussen, D., Nogueira, R. G., Nahab, F., and Frankel, M. (2017). Comparison of 3-month stroke disability and quality of life across modified rankin scale categories. *Interv. Neurol.* 6, 36–41. doi: 10.1159/000452634

Ridley, N. J., Draper, B., and Withall, A. (2013). Alcohol-related dementia: An update of the evidence. *Alzheimers Res. Ther.* 5:3. doi: 10.1186/alzrt157

Robitaille, A., van den Hout, A., Machado, R. J. M., Bennett, D. A., Ðukić, I., Deary, I. J., et al. (2018). Transitions across cognitive states and death among older adults in relation to education: A multistate survival model using data from six longitudinal studies. *Alzheimers Dement.* 14, 462–472. doi: 10.1016/j.jalz.2017.10.003

Salling, M. C., Skelly, M. J., Avegno, E., Regan, S., Zeric, T., Nichols, E., et al. (2018). Alcohol consumption during adolescence in a mouse model of binge drinking alters the intrinsic excitability and function of the prefrontal cortex through a reduction in the hyperpolarization-activated cation current. *J. Neurosci.* 38, 6207–6222. doi: 10.1523/JNEUROSCI.0550-18.2018

Schindler, A. G., Soden, M. E., Zweifel, L. S., and Clark, J. J. (2016). Reversal of alcohol-induced dysregulation in dopamine network dynamics may rescue maladaptive decision-making. *J. Neurosci.* 36, 3698–3708. doi: 10.1523/JNEUROSCI.4394-15.2016

Tamura, Y., Kimbara, Y., Yamaoka, T., Sato, K., Tsuboi, Y., Kodera, R., et al. (2017). White matter hyperintensity in elderly patients with diabetes mellitus is associated with cognitive impairment, functional disability, and a high glycoalbumin/glycohemoglobin ratio. *Front. Aging Neurosci.* 9:220. doi: 10.3389/fnagi.2017.00220

Tu, W. J., Qiu, H. C., Cao, J. L., Liu, Q., Zeng, X. W., Zhao, J. Z., et al. (2018). Decreased concentration of irisin is associated with poor functional outcome in ischemic stroke. *Neurotherapeutics* 15, 1158–1167. doi: 10.1007/s13311-018-0651-2

Ward, R., Valenzuela, J. P., Li, W., Dong, G., Fagan, S. C., Ergul, A., et al. (2018). Poststroke cognitive impairment and hippocampal neurovascular remodeling: The impact of diabetes and sex. *Am. J. Physiol. Heart Circ. Physiol.* 315, H1402–H1413. doi: 10.1152/ajpheart.00390.2018

Wen, H. B., Zhang, Z. X., Niu, F. S., and Li, L. (2008). [The application of Montreal cognitive assessment in urban Chinese residents of Beijing]. *Zhonghua Nei Ke Za Zhi* 47, 36–39.

Yoo, A. J., Berkhemer, O. A., Fransen, P. S. S., van den Berg, L. A., Beumer, D., Lingsma, H. F., et al. (2016). Effect of baseline alberta stroke program early CT Score on safety and efficacy of intra-arterial treatment: A subgroup analysis of a randomised phase 3 trial (MR CLEAN). *Lancet Neurol.* 15, 685–694. doi: 10.1016/S1474-4422(16)00124-1

Zheng, F., Yan, L., Zhong, B., Yang, Z., and Xie, W. (2019). Progression of cognitive decline before and after incident stroke. *Neurology* 93, e20–e28. doi: 10.1212/WNL.0000000000007716

Zietemann, V., Georgakis, M. K., Dondaine, T., Müller, C., Mendyk, A. M., Kopczak, A., et al. (2018). Early MoCA predicts long-term cognitive and functional outcome and mortality after stroke. *Neurology* 91, e1838–e1850. doi: 10.1212/WNL.0000000000006506

frontiers | Frontiers in Aging Neuroscience

TYPE Original Research
PUBLISHED 14 November 2022
DOI 10.3389/fnagi.2022.935934

OPEN ACCESS

EDITED BY
Li Li,
Department of Anesthesiology, Affiliated Beijing Friendship Hospital, Capital Medical University, China

REVIEWED BY
Shun Ishibashi,
Jichi Medical University, Japan
Cheng Ni,
Chinese Academy of Medical Sciences and Peking Union Medical College, China

*CORRESPONDENCE
Ziqing Hei
heiziqing@sina.com
Chulian Gong
gongchl@mail.sysu.edu.cn

SPECIALTY SECTION
This article was submitted to Neurocognitive Aging and Behavior, a section of the journal Frontiers in Aging Neuroscience

RECEIVED 04 May 2022
ACCEPTED 27 October 2022
PUBLISHED 14 November 2022

CITATION
Chen C, Wen Q, Ma C, Li X, Huang T, Ke J, Gong C and Hei Z (2022) Hypertriglyceridemia is associated with stroke after non-cardiac, non-neurological surgery in the older patients: A nested case-control study.
Front. Aging Neurosci. 14:935934.
doi: 10.3389/fnagi.2022.935934

Hypertriglyceridemia is associated with stroke after non-cardiac, non-neurological surgery in the older patients: A nested case-control study

Chaojin Chen[1], Qianyu Wen[2], Chuzhou Ma[3], Xiaoyue Li[1], Tengchao Huang[4], Jie Ke[5], Chulian Gong[1]* and Ziqing Hei[1]*

[1]Department of Anesthesiology, The Third Affiliated Hospital of Sun Yat-sen University, Guangzhou, Guangdong, China, [2]Big Data and Artificial Intelligence Center, The Third Affiliated Hospital of Sun Yat-sen University, Guangzhou, Guangdong, China, [3]Department of Anesthesiology, Shantou Central Hospital, Shantou, Guangdong, China, [4]Department of Neurosurgery, Third Affiliated Hospital of Sun Yat-sen University, Guangzhou, Guangdong, China, [5]Guangzhou AID Cloud Technology Co., Ltd, Guangzhou, Guangdong, China

Introduction: Geriatric postoperative stroke is a rare but serious complication after surgery. The association between hypertriglyceridemia and postoperative stroke remains controversial, especially in older patients undergoing non-cardiac, non-neurological surgery. The study aims to address this clinical dilemma.

Materials and methods: We conducted a nested case-control study among 9601 aged patients undergoing non-cardiac non-neurological surgery from October 2015 to 2021. A total of 22 positive cases were matched for the surgical type and time, to 88 control patients by a ratio of 1:4. The effect of hypertriglyceridemia on the occurrence of postoperative stroke within 30 days after surgery was estimated using conditional logistic regression analysis by adjusting to various potential confounders.

Results: A total of 22 cases developed ischemia stroke after surgery, and compared with the non-stroke group, they had more postoperative ICU admission, longer postoperative hospitalization and higher total cost (all $p < 0.05$), and more patients were presenting with preoperative hypertriglyceridemia [8 (36.4%) *vs.* 15 (17.0%), $p = 0.045$]. There was a significant association between hypertriglyceridemia and postoperative stroke, with adjusted odds ratios of 6.618 (95% *CI* 1.286, 34.064) ($p = 0.024$). The above results remained robust in the sensitivity analyses.

Conclusion: Among older patients undergoing non-cardiac and non-neurological surgery, hypertriglyceridemia was associated with significant increased risk of postoperative stroke.

KEYWORDS

elderly patients, hypertriglyceridemia, postoperative stroke, non-cardiac non-neurological surgery, sensitivity analysis

Introduction

Postoperative stroke is a rare but serious postoperative complication associated with high disability and fatality rates. The incidence of postoperative stroke was approximately 0.01–1% in patients undergoing non-cardiac, non-neurological procedures (Mashour et al., 2011, 2014) and even up to 9–10% in patients undergoing difficult heart surgery and neurosurgery (Vlisides and Mashour, 2016; Mrkobrada et al., 2019). However, the 30-day mortality rates in patients who experience postoperative stroke ranged from 21 to 26%, which were 8 times greater than those without postoperative stroke (Mashour et al., 2011; Wang et al., 2019; Benesch et al., 2021). Meanwhile, patients with postoperative stroke also have longer hospital stay and higher risk of being discharged to long-term care facilities (Lindberg and Flexman, 2021). Notably, perioperative covert stroke was reported to occur in up to 7% of the older patients undergoing non-cardiac, non-neurological surgery (Mrkobrada et al., 2019). As the population ages, age of patients undergoing surgery has been increasing, the geriatric stroke after surgery represents a significant public health burden worldwide and early prediction and intervention help to improve the postoperative outcomes of the older patients (Minhas et al., 2020).

Multiple studies have reported the risk factors for postoperative stroke in patients undergoing non-cardiac, non-neurological surgery, including dyslipidemia, overweight and obesity, and metabolic syndrome (Kernan et al., 2014). Whereas, to our knowledge, few study is focusing on the older populations (van Lier et al., 2009; Bahrainwala et al., 2011; Dong et al., 2017; Kwon et al., 2021). Compared with hypercholesterolemia which is tightly associated with stroke (Sacco et al., 2008), hypertriglyceridemia is another type of dyslipidemia that received lesser attention, as its role in stroke remains controversial (Kivioja et al., 2018). On one way, patients with hypertriglyceridemia were also reported to have a significantly increased risk of incident ischemic stroke (Toth et al., 2018; Wang et al., 2018). On the other way, Anxin Wang and his colleague did not observe any significant association between triglycerides variability and ischemic or hemorrhagic stroke (Wang et al., 2020). In another nested case-control study which enrolled 5475 patients with ischemic stroke, 4776 patients with intracerebral hemorrhage, and 6290 control patients, it was demonstrated that hypertriglyceridemia were weakly correlated with ischemic stroke risk (Sun et al., 2019). To our knowledge, whether preoperative hypertriglyceridemia is associated with postoperative stroke in the older patients receiving non-cardiac, non-neurological procedures has not been reported.

To explore the risk factors for postoperative stroke in older patients undergoing non-cardiac, non-neurological surgery, we conducted a nested case-control study using a large retrospective cohort in our center, and found that hypertriglyceridemia is associated with stroke after non-cardiac, non-neurological surgery in the older patients, which enable early intervention to improve their postoperative outcomes.

Materials and methods

Study design

The current study was designed as a nested case-control study in a large retrospective cohort of older patients undergoing non-cardiac and non-neurosurgical surgery. The local hospital ethics committee (The Third Affiliated Hospital of Sun Yat-sen University) approved the study protocol [No. (2019)02-609-02]. No formal informed permission was required because patients were not subjected to investigational actions and unidentifiable patient information was derived from electric health records (EHR).

Study population

All patients over 65 yrs old who underwent inpatient surgical procedures in our center from April 2015 to 2021 were included. Patients with any of the following conditions were excluded: (1) patients undergoing cardiac or neurosurgical procedures, including surgeries of major arteries such as aneurisms of thoracic aorta, (2) patients with preoperative stroke or stroke occurred beyond 30 days after surgery.

Selection of cases and controls

Postoperative stroke is defined as a brain infarction of ischemic or hemorrhagic etiology that occurs within 30 days

after surgery (Leary and Varade, 2020). Positive cases were patients with a new focal neurologic impairment of cerebral origin that lasts more than 24 h, or a computed tomography [CT] hemorrhage (Ferrara, 2020). The diagnosis of stroke was made by a neurologist and an anesthesiologist who reviewed all the EHR. Notably, positive cases included diagnoses established solely on clinical grounds (i.e., without CT abnormalities). Cases (with stroke) and controls (without stroke) were matched on type and time of surgery. For every patient with postoperative stroke, four control patients were selected who underwent the same surgery during the same period (as close as possible to the surgical date of the case) but did not experience a postoperative stroke. A ratio of 1:4 is known to yield the best results taking into account the effort to collect the information of the controls (Zhou et al., 2021). When an identical type of surgery was not available, a patient who had the most similar procedure was chosen as a control.

Data collection

Based on previous literature, the clinical data related to demographics, detailed medical histories or perioperative variables associated with postoperative stroke were collected from the EHR system according to our earlier report (Chen et al., 2022). Demographic characteristics related to older patients including age, gender, and body mass index (BMI). Preoperative comorbidity include hypertension, diabetes, cerebrovascular disorders, carotid stenosis, coronary heart disease, atrial fibrillation, renal insufficiency, systemic lupus erythematosus (SLE), chronic obstructive pulmonary disease (COPD), history of drinking and smoking, hemodialysis and intubation before surgery. Preoperative mediations include β blocker, anticoagulant and antiplatelet agents. Preoperative laboratory findings included hemoglobin (HGB), hematocrit (HCT), platelets (PLT), monocyte, neutrophil (NEUT), high sensitivity C reactive protein (hsCRP), creatinine, blood urea nitrogen (BUN), estimated glomerular filtration rate (GFR), uric acid (UA), glucose (GLU), gamma-glutamyl transpeptidase (GGT), alanine transaminase (ALT), aspartate aminotransferase (AST), total bilirubin (TBILI), indirect bilirubin (IBILI), total cholesterol (TC), high-density lipoprotein cholesterol (HDL-C), low-density lipoprotein cholesterol (LDL-C), triglycerides, thrombin time (TT), activated partial thromboplastin time (APTT), international normalized ratio (INR), and fibrinogen. Intraoperative variables included administration of dexmedetomidine, parecoxib sodium, flurbiprofen axetil, dexamethasone, metylprednisolon, furosemide and mannitol, intraoperative infusion of crystal, colloid and red blood cell (RBC), volume of blood loss and urine output, and duration of surgery. Postoperative outcomes were also collected, including intensive care unit (ICU) admission, postoperative hospitalization, total cost and in-hospital death.

Potential confounders

As the normal range of triglycerides was 0.34–1.92 mmol/L in our hospital, the hypertriglyceridemia was defined as triglycerides concentration > 1.92 mmol/L. Variables potentially confounding the association between hypertriglyceridemia and postoperative stroke were predefined based on existing literature, clinical experience and our available EHR system, including age, gender, hypertension, diabetes, concentration of fibrinogen, and duration of surgery.

Statistical analysis

Differences in clinical characteristics between the positive cases and controls were compared using the Student's *t*-test for continuous variables which were normally distributed, and the non-parametric Kruskall-Wallis test was used for continuous variables with non-normal distribution. Categorical variables were compared using the Pearson chi-square test or the Fisher exact test. Conditional logistic regression analysis was conducted to estimate association between hypertriglyceridemia and postoperative stroke (Arfè et al., 2016; Glanz et al., 2018). We adjusted for different number of potential confounders in the conditional logistic regression, based on the event per variable (EPV), our experience and the data integrity. The odds ratio (OR) and 95% confidence intervals (CI) were calculated, respectively (Zhang et al., 2019; Zhao et al., 2021).

Several sensitivity analyses were performed to evaluate the robustness of the association between hypertriglyceridemia and postoperative stroke. We analyzed whether the association would change if individuals who underwent liver transplantation were removed. We reanalyzed the association if individuals who underwent carotid endarterectomy were removed. Given the possible impact of anesthesia type on postoperative stroke, we evaluated the association between hypertriglyceridemia and postoperative stroke in those patients with general anesthesia. All analyses were performed using R (release 2.13.1; R Foundation for Statistical Computing, Vienna, Austria).

Results

Of the 9601 initially screened patients in the cohort, 577 patients received cardiac or neurosurgical surgery and 460 patients had stroke before surgery or beyond 30 days after surgery were excluded. Among the 8564 patients, 22 patients (0.26%) were diagnosed as postoperative stroke within 30 days after surgery. After excluding 8454 patients with missing data or did not match the stroke group by surgery and time, a total of 22 eligible cases and 88 successfully matched controls were finally included in the study (**Figure 1**).

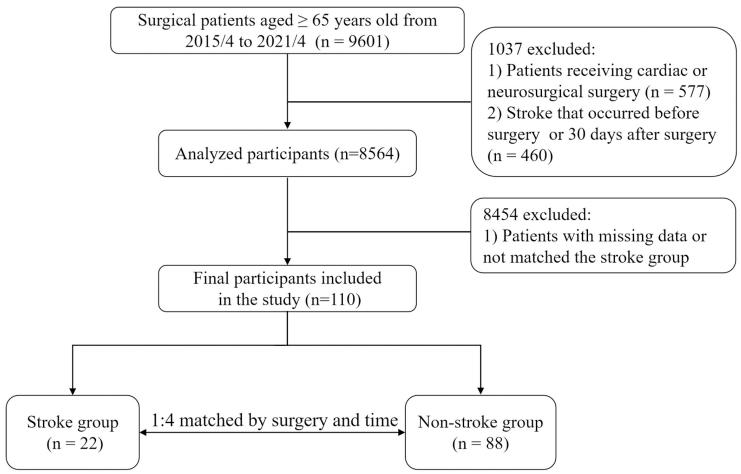

FIGURE 1
Study flowchart. The stroke diagnosis of each patient, both in the case and control groups, was re-confirmed by a neurologist and an anesthesiologist.

Characteristics of the study population

In the study, we found all the 22 cases were diagnosed as ischemia stroke and all the stroke occurred within 21 days after surgery (**Supplementary Table 1**). Among the 110 patients (22 cases and 88 controls), the median age was 70 (67–75) years and 68 (61.8%) were men. Patients in the two groups were comparable in age [70 (67–74) *vs.* 72 (68–76), $p = 0.564$, **Table 1**], gender [52 (59.1%) men *vs.* 16 (72.7%) men, $p = 0.239$] and BMI [23 (21.1–25.5) *vs.* 24.8 (22.2–26.7), $p = 0.115$, **Table 1**].

Compared with the control group, more patients in the stroke group were presenting with hypertriglyceridemia [8 (36.4%) *vs.* 15 (17.0%), $p = 0.045$], while other preoperative variables including the comorbidities (hypertension, diabetes, cerebrovascular disorders, carotid stenosis, coronary heart disease, atrial fibrillation, renal insufficiency, SLE and COPD), administration of β blockers, anticoagulant and antiplatelet agents, other lipid indexes (TC, HDL-C, LDL-C) and other laboratory variables showed no significant differences between groups (all $p > 0.05$). The intraoperative characteristics of the 110 cases including medication, transfusion and duration of surgery were basically balanced (all $p > 0.05$, **Table 2**).

Prognosis of the study population

Compared with the control group, the stroke group had higher incidence of postoperative ICU admission [2 (9.1%) *vs.* 0 (0), $p = 0.039$; **Table 3**], longer postoperative hospitalization [19 (8, 25) *vs.* 7 (4, 12), $p < 0.001$; **Table 3**] and higher total cost [85060 (52524, 165378) yuan *vs.* 57586 (37592, 96905) yuan, $p < 0.001$; **Table 3**]. Meanwhile, the overall mortality was zero in the study.

Risk of stroke after non-cardiac, non-neurological surgery in the older patients

There were 8 (36.4%) and 15 (17.0%) patients had preoperative hypertriglyceridemia in the stroke and the control groups, respectively. The crude analysis showed a 4.71-fold [95% *CI* (1.13, 19.63), $p = 0.0331$] increased risk of postoperative stroke in patients with elevated triglycerides. After adjusting only for matched covariates (age, gender, fibrinogen, hypertension, diabetes and duration of surgery), we observed an increased risk of stroke in patients presenting with preoperative hypertriglyceridemia, compared with those who did not [OR 7.46, 95% *CI* (1.35, 41.22), $p = 0.0211$; **Table 4**]. Meanwhile, we found that after adjusting for two to eight confounders like age, gender, fibrinogen, hypertension, diabetes, duration of surgery and medications like β blockers and antiplatelet agents, preoperative hypertriglyceridemia was significantly associated with postoperative stroke (**Supplementary Table 2**). However, if we increased to 11 confounders and made the EPV to be 2, we found no significant increased risk of stroke between patients presenting with preoperative hypertriglyceridemia and those who did not ($P > 0.05$).

Sensitivity analyses

We conducted three sensitivity analyses to account for observed confounders (**Figure 2**). First, the result remained robust after excluding patients undergoing liver transplantation whose conditions and operations were much more complicated than others. Compared with patients with triglyceride ≤ 1.92, those with triglyceride > 1.92 had a higher risk of stroke

TABLE 1 Preoperative characteristics of patients between two groups.

Variable	All patients	Postoperative stroke		*P* value
		No (*n* = 88)	Yes (*n* = 22)	
Demographics				
Age	70 (67;75)	70 (67;74)	72 (68;76)	0.564
Gender				0.239
Female	42 (38.2%)	36 (40.9%)	6 (27.3%)	
Male	68 (61.8%)	52 (59.1%)	16 (72.7%)	
BMI	23.4 (21.3;26)	23 (21.1;25.5)	24.8 (22.2;26.7)	0.115
Preoperative comorbidity				
Hypertension				0.764
No	38 (34.5%)	31 (35.2%)	7 (31.8%)	
Yes	72 (65.5%)	57 (64.8%)	15 (68.2%)	
Diabetes				0.592
No	80 (72.7%)	65 (73.9%)	15 (68.2%)	
Yes	30 (27.3%)	23 (26.1%)	7 (31.8%)	
Cerebrovascular disorders				1
Yes	0 (0)	0	0	
No	110 (100%)	88 (100%)	22 (100%)	
Carotid stenosis				1
Yes	0 (0)	0	0	
No	110 (100%)	88 (100%)	22 (100%)	
Coronary heart disease				1
Yes	0 (0)	0	0	
No	110 (100%)	88 (100%)	22 (100%)	
Atrial fibrillation				1
Yes	4 (3.6%)	3 (3.4%)	1 (4.5%)	
No	106 (96.4%)	85 (96.6%)	21 (95.5%)	
Renal insufficiency				1
Yes	0 (0)	0 (0)	0 (0)	
No	110 (100%)	88 (100%)	22 (100%)	
SLE				1
Yes	0 (0)	0 (0)	0 (0)	
No	110 (100%)	88 (100%)	22 (100%)	
COPD				1
Yes	10 (9.1%)	8 (9.1%)	2 (9.1%)	
No	100 (90.9%)	80 (90.9%)	20 (90.9%)	
Smoking				0.854
Yes	73 (84.9%)	61 (85.9%)	12 (80.0%)	
No	13 (15.1%)	10 (14.1%)	3 (20.0%)	
Drinking				0.712
Yes	78 (91.8%)	66 (93.0%)	12 (85.7%)	
No	7 (8.24%)	5 (7.04%)	2 (14.3%)	
Hemodialysis				0.2
Yes	1 (0.9%)	0 (0)	1 (4.5%)	
No	109 (99.1%)	88 (100%)	21 (95.5%)	
Intubation				0.361
Yes	2 (1.8%)	1 (1.1%)	1 (1.8%)	
No	108 (98.2%)	87 (98.9%)	21 (98.2%)	
Preoperative medication				
β blockers				0.326
Yes	17 (15.5%)	12 (13.6%)	5 (22.7%)	
No	93 (84.5%)	76 (86.4%)	17 (77.3%)	
Anticoagulant agents				1
Yes	0 (0)	0 (0)	0 (0)	
No	110 (100%)	88 (100%)	22 (100%)	
Antiplatelet agents				1
Yes	3 (2.7%)	3 (3.4%)	0 (0)	
No	107 (97.3%)	85 (96.6%)	22 (100%)	
Preoperative laboratory variables				
HGB	127 (114;135)	127.5 (114.3;135)	124 (104;135)	0.244
HCT	0.37 (0.06)	0.37 (0.06)	0.35 (0.06)	0.121
PLT	216 (79.3)	221 (81.9)	194 (65.4)	0.106
Monocyte	0.5 (0.39;0.68)	0.48 (0.39;0.655)	0.61 (0.32;0.83)	0.289
NEUT	4.25 (2.83;6.01)	4.23 (2.65;6.00)	4.40 (3.32;7.80)	0.542
hsCRP	5.15 (3.45;7.4)	5.25 (3.45;7.37)	4.56 (4.41;7.91)	0.766
Creatinine	74 (61.75;95.25)	72 (61.25;94.5)	81 (61.9;105.5)	0.342
BUN	5.62 (4.47;7.2)	5.62 (4.46;7.39)	5.605 (4.81;6.95)	0.917
Estimated GFR	75.7 (19.8)	75.9 (18.7)	75.0 (23.8)	0.894
UA	351 (108)	350 (103)	357 (127)	0.822
GLU	5.47 (4.98;6.44)	5.49 (4.90;6.30)	5.27 (5.08;6.65)	0.881
GGT	25 (16;49)	24 (16;45.25)	39 (17.75;68.25)	0.12
ALT	16 (12;24)	17 (13;23)	14.5 (10.75;28.5)	0.728
AST	21 (16;29)	21 (16;29)	20 (14;27.25)	0.766
TBILI	10.35 (7.74;15.2)	10.5 (7.8;15.2)	9.67 (7.57;15.6)	0.962
IBILI	6.6 (4.98;9.85)	6.6 (5;9.7)	6.3 (4.2;10.3)	0.84
Triglycerides	1.12 (0.8; 1.59)	1.05 (0.79; 1.54)	1.36 (0.82; 2.42)	0.103
Triglycerides categories				0.045
≤1.92	87 (79.1%)	73 (83.0%)	14 (63.6%)	
>1.92	23 (20.9%)	15 (17.0%)	8 (36.4%)	
TC	4.61 (1.13)	4.55 (1.10)	4.83 (1.21)	0.349
TC				0.367
≤5.7	92 (83.6%)	75 (85.2%)	17 (77.3%)	
>5.7	18 (16.4%)	13 (14.8%)	5 (22.7%)	
HDL-C	1.04 (0.31)	1.05 (0.30)	1.03 (0.35)	0.839
LDL-C	2.88 (0.95)	2.87 (0.96)	2.89 (0.92)	0.936
TT	13.3 (12.6;14.18)	13.3 (12.6;14.18)	13.25 (12.43;14.1)	0.914
APTT	37.3 (34.3;39.6)	37.1 (33.8;40.1)	37.85 (35.08;39.33)	0.644
INR	1 (0.94;1.1)	1 (0.94;1.11)	1.01 (0.922;1.07)	0.641
Fibrinogen	3.72 (2.94;4.66)	3.67 (3.02;4.61)	4.21 (2.75;5.28)	0.48

Data was expressed as "median (IQR)", "mean (SD)" or "N (%)"; BMI, Body Mass Index; SLE, systemic lupus erythematosus; HGB, Hemoglobin; HCT, Hematocrit; PLT, Platelets; NEUT, neutrophil; hs-CRP, high sensitivity C-reactive protein; BUN, Blood Urea Nitrogen; GFR, Glomerular Filtration Rate; UA, Uric Acid; GLU, Glucose; GGT, Gamma-Glutamyl Transpeptidase; ALT, Alanine aminotransferase; AST, Aspartate aminotransferase; TBILI, Total bilirubin; IBILI, Indirect bilirubin; TC, Total cholesterol; HDL-C, High-density lipoprotein cholesterol; LDL-C, Low-density lipoprotein cholesterol; TT, Thrombin time; APTT, Activated partial thromboplastin time; INR, International normalized ratio.

TABLE 2 Intraoperative characteristics of patients between two groups.

Variable	All patients	Postoperative stroke		*P* value
		No (*n* = 88)	Yes (*n* = 22)	
Intraoperative mediation				
Dexmedetomidine				0.762
Yes	37 (33.6%)	29 (33.0%)	8 (36.4%)	
No	73 (66.4%)	59 (67.0%)	14 (63.6%)	
Parecoxib Sodium				0.516
Yes	29 (26.4%)	22 (25.0%)	7 (31.8%)	
No	81 (73.6%)	66 (75.0%)	15 (68.2%)	
Flurbiprofen axetil				0.405
Yes	33 (30.0%)	28 (31.8%)	5 (22.7%)	
No	77 (70.0%)	60 (68.2%)	17 (77.3%)	
Dexamethasone				0.214
Yes	10 (9.1%)	10 (11.4%)	0 (0)	
No	100 (90.9%)	78 (88.6%)	22 (100%)	
Metylprednisolon				1
Yes	18 (16.4%)	14 (15.9%)	4 (18.2%)	
No	92 (83.6%)	74 (84.1%)	18 (81.8%)	
Furosemide				0.12
Yes	16 (14.5%)	10 (11.4%)	6 (27.3%)	
No	94 (85.5%)	78 (88.6%)	16 (72.7%)	
Mannitol				1
Yes	0 (0)	0 (0)	0 (0)	
No	110 (100%)	88 (100%)	22 (100%)	
Intraoperative transfusion				
Crystal	700 (200;1237.5)	700 (200;1200)	1000 (450;1800)	0.141
Colloid	500 (500;500)	500 (500;500)	500 (375;500)	0.22
RBC	0 (0;0)	0 (0;0)	0 (0;0)	0.457
Blood loss (ml)	50 (20;100)	50 (20;100)	50 (30;200)	0.259
Urine output (ml)	300 (100;700)	300 (100;750)	275 (100;650)	0.894
Duration of surgery	115 (66;195)	118.5 (64.75;195)	90 (67;290)	0.480

Data was expressed as "median (IQR)", "mean (SD)" or "N (%)"; RBC, Red blood cell count.

TABLE 3 Outcomes of patients between two groups.

Variable	All patients	Postoperative stroke		*P* value
		No (*n* = 88)	Yes (*n* = 22)	
ICU admission				0.039
Yes	2 (1.8%)	0 (0)	2 (9.1%)	
No	108 (98.2%)	88 (100%)	20 (90.9%)	
Postoperative hospitalization	8 (4;16)	7 (4;12)	19 (8;25)	0.001
Total cost	60625 (380623; 100391)	57586 (37592; 96905)	85060 (52524; 165378)	0.007
In-hospital death	0 (0)	0 (0)	0 (0)	1

TABLE 4 Relationship of hypertriglyceridemia with the risk of postoperative stroke in older patients undergoing non-cardiac non-neurosurgery procedures.

	Crude		Adjusted	
	OR (95% CI)	*P*-value	OR (95% CI)	*P*-value
Triglycerides				
≤1.92	Ref		Ref	
>1.92	4.71 (1.13,19.63)	0.033	7.46 (1.35, 41.22)	0.021
Age(yr)	1.01 (0.93, 1.10)	0.762	1.02 (0.92, 1.12)	0.739
Gender (male)				
Female	Ref		Ref	
Male	1.90 (0.66, 5.41)	0.232	1.76 (0.57, 5.38)	0.324
Fibrinogen	1.03 (0.77, 1.37)	0.841		
Hypertension				
No	Ref		Ref	
Yes	1.29 (0.47, 3.53)	0.616	1.64 (0.51, 5.26)	0.408
Diabetes				
No	Ref		Ref	
Yes	1.33 (0.47, 3.81)	0.586	0.92 (0.29, 2.95)	0.889
Duration of surgery	1.00(0.99,1.01)	0.192		

Adjusted for age, gender, fibrinogen, hypertension, diabetes and duration of surgery at baseline.

[aOR 9.35, 95% CI (1.41, 49.49), p = 0.019]. In addition, we reanalyzed the data after excluding patients undergoing carotid endarterectomy. The risk of stroke was significantly increased in the multivariable model [aOR 7.26, 95% *CI* (1.24, 45.45), p = 0.028]. After excluding the patients undergoing regional anesthesia, the hypertriglyceridemia was still associated with increased risk of stroke [aOR 9.66, 95% CI (1.33, 70.27), p = 0.025].

Discussion

In this nested case-control study among the older patients undergoing non-cardiac, non-neurological surgery, we found that 0.257% of the older patients suffered from a perioperative ischemia stroke, which prolonged postoperative hospital stay and increased the total hospitalization charges. Moreover, we found preoperative hypertriglyceridemia was associated with 7.46-fold increased risk of postoperative stroke after adjusting for confounding variables including age, gender, hypertension, diabetes, fibrinogen and duration of surgery.

To our knowledge, the incidence of postoperative stroke in the study was consistent with early reports in patients undergoing non-cardiac, non-neurological procedures (Mashour et al., 2011, 2014). Moreover, this was the first study to show the clinical association between hypertriglyceridemia and the probability of postoperative stroke in older patients receiving non-cardiac, non-neurological surgery. Hypertriglyceridemia

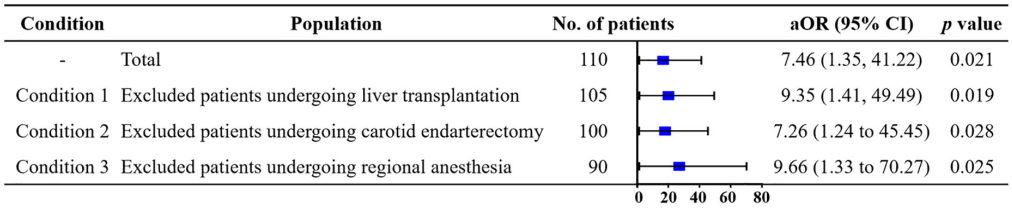

FIGURE 2
Sensitivity analysis by adjusted for certain confounders.

is generally caused by defects in triglyceride metabolism in the older population and manifests as increased levels of plasma triglyceride (Bhatt et al., 2019). Although hypertriglyceridemia has been reported to be correlated with the increased risk of ischemic stroke according to large clinical trials (Cui and Naikoo, 2019; Gu et al., 2019), its role in stroke remains controversial and few study focuses on postoperative stroke (Glasser et al., 2016; Holmes et al., 2018). For instance, a longitudinal observational cohort study showed that in patients receiving conventional statin therapy, no significant difference was found in the incidence of non-fatal strokes between the hypertriglyceridemia group and the normal triglyceride group (HR, 1.09; 95% CI, 0.89 to 1.33; $p = 0.42$) (Nichols et al., 2018). In another population-based cohort study, researchers enrolled 961 patients with ischemic stroke and 1403 patients without ischemic stroke, and found no significant association between hypertriglyceridemia and ischemic stroke (aOR, 1.19; 95% CI, 0.94 to 1.53) (Kivioja et al., 2018). In the current nested case-control study, we included 22 older patients with postoperative stroke and matched them on type and time of surgery by a ratio of 1:4. Finally, the conditional logistic regression analysis showed that hypertriglyceridemia maintained an independent relationship with postoperative stroke in fully adjusted models, and the sensitivity analyses yielded similar results.

Triglyceride molecules are the primary means of storing and transporting fatty acids in the cells and in the plasma. Fatty acids are eliminated by oxidation within the hepatocyte or by secretion into the plasma through triglyceride-rich very low-density lipoproteins (VLDL). It is shown that with the increase of age, the activity of lipoprotein lipase and LDL receptor decrease, the levels of VLDL increase, which further increases the level of triglycerides in the plasma (Alves-Bezerra and Cohen, 2017; Johnson and Stolzing, 2019). We think hypertriglyceridemia may increase the risk of postoperative stroke by promoting atherosclerosis in the older patients (Peng et al., 2017). Firstly, hypertriglyceridemia may theoretically cause subendothelial retention of remnant particles and elicitation of endothelial dysfunction, to establish chronic inflammation in the cerevascular (Liang et al., 2022). Secondly, hypertriglyceridemia may cause hyperviscosity and promote thrombosis through a procoagulant effect involved in the disturbance of both blood coagulation and fibrinolysis, and led to postoperative stroke. Notably, the current results revealed that lipid-lowering and triglyceride reduction measures might help to prevent perioperative ischemic stroke in older patients with preoperative hypertriglyceridemia (Bhatt et al., 2019).

To further confirm the association between preoperative hypertriglyceridemia and postoperative stroke, we tried to enroll more variables potentially confounding the association between hypertriglyceridemia and postoperative stroke, include most of the demographic characteristics, preoperative comorbidity, mediations, laboratory results and intraoperative variables. However, the rule of EPV is taken into consideration in the sample size requirement of logistic regression (Peduzzi et al., 1996). Although EPV values are preferably 10 or greater, there are still several important potential confounders need to be adjusted in the study, including age, gender, hypertension, diabetes, concentration of fibrinogen and duration of surgery. As a result, the current EPV is relaxed as almost 5 samples per predictor (Vittinghoff and McCulloch, 2007). Meanwhile, the current results showed that after adjusting for 11 potentially confounding variables and relaxing the EPV to 2, no significant increased risk of stroke was found between patients presenting with preoperative hypertriglyceridemia and those who did not. The results are interesting and we think this might be attributed to the small sample size and EPV value in this condition.

Limitations of the study

The study has several limitations. First of all, we did not collect the duration of hypertriglyceridemia in the patients and whether the triglyceride concentration level was positively correlated with the severity of stroke need to be further explored. Secondly, due to the retrospective observational design, the results lack information of preoperative and postoperative medications like lipid-lowering agents, blood pressure-lowering agents and glucose-lowering agents *etc.* In terms of agents for hypertriglyceridemia, lipid-lowering agents like omega 3 PUFA may increase bleeding events, while fibrates may increase thrombotic events. Therefore, the drug information is important to interpret the results and further studies are needed to explore and elucidate the role of preoperative and postoperative medications in the development and prognosis of postoperative

stroke. Thirdly, the sample size and the positive cases were small and this limited our subgroup analysis to further explore the association between hypertriglyceridemia and postoperative stroke in different kinds of older patients, as well as the effects between different levels of hypercholesterolemia and hypertriglyceridemia in the current study. Fourthly, we did not explore whether hypertriglyceridemia is also a risk factor for other postoperative vascular events like deep vein thrombosis (DVT) and ischemic heart diseases, and further studies are needed to explore it. Finally, although we considered many confounders, the intraoperative hypotension was not correctly recorded in our database and residual confounders such as different test methods in different years might interfere with our findings.

Conclusion

Among the older patients undergoing non-cardiac, non-neurological surgery, preoperative hypertriglyceridemia is associated with increased risk of postoperative stroke. The study findings are limited by potential confounders due to retrospective observational design and further prospective randomized clinical trials are needed to validate the finding.

Data availability statement

The raw data supporting the conclusions of this article will be made available by the authors, without undue reservation.

Ethics statement

The studies involving human participants were reviewed and approved by Ethics Committee of the Third Affiliated Hospital of Sun Yat-sen University. Written informed consent for participation was not required for this study in accordance with the national legislation and the institutional requirements.

Author contributions

CC, CG, and ZH: conception and design. CC, QW, CM, XL, TH, JK, and CG: acquisition of data. CC, QW, and CM: analysis and interpretation of data. CC, QW, CM, XL, TH, JK, CG, and ZH: writing, review, and/or revision of the manuscript. CC and ZH: study supervision. All authors contributed to the article and approved the submitted version.

Funding

This study was supported partly by the National Natural Science Foundation of China (Grant Nos. 81974296 and 82102297), Natural Science Foundation of Guangdong Province (Grant Nos. 2019A1515110020 and 2022A1515012603), the Fundamental Research Funds for the Central Universities of China (Grant No. 22qntd3401), and Young Talent Support Project of Guangzhou Association for Science and Technology (Grant No. QT20220101257).

Conflict of interest

Author JK was employed by Guangzhou AID Cloud Technology Co., Ltd.

The remaining authors declare that the research was conducted in the absence of any commercial or financial relationships that could be construed as a potential conflict of interest.

Publisher's note

All claims expressed in this article are solely those of the authors and do not necessarily represent those of their affiliated organizations, or those of the publisher, the editors and the reviewers. Any product that may be evaluated in this article, or claim that may be made by its manufacturer, is not guaranteed or endorsed by the publisher.

Supplementary material

The Supplementary Material for this article can be found online at: https://www.frontiersin.org/articles/10.3389/fnagi.2022.935934/full#supplementary-material

References

Alves-Bezerra, M., and Cohen, D. E. (2017). Triglyceride metabolism in the liver. *Compr. Physiol.* 8, 1–8. doi: 10.1002/cphy.c170012

Arfè, A., Scotti, L., Varas-Lorenzo, C., Nicotra, F., Zambon, A., Kollhorst, B., et al. (2016). Non-steroidal anti-inflammatory drugs and risk of heart failure in four European countries: Nested case-control study. *BMJ* 354:i4857. doi: 10.1136/bmj.i4857

Bahrainwala, Z. S., Grega, M. A., Hogue, C. W., Baumgartner, W. A., Selnes, O. A., McKhann, G. M., et al. (2011). Intraoperative hemoglobin levels and

transfusion independently predict stroke after cardiac operations. *Ann. Thorac. Surg.* 91, 1113–1118. doi: 10.1016/j.athoracsur.2010.12.049

Benesch, C., Glance, L. G., Derdeyn, C. P., Fleisher, L. A., Holloway, R. G., Messe, S. R., et al. (2021). Perioperative neurological evaluation and management to lower the risk of acute stroke in patients undergoing noncardiac, nonneurological surgery: A scientific statement from the american heart association/american stroke association. *Circulation* 143:e923–e946. doi: 10.1161/CIR.0000000000000968

Bhatt, D. L., Steg, P. G., Miller, M., Brinton, E. A., Jacobson, T. A., Ketchum, S. B., et al. (2019). Cardiovascular risk reduction with icosapent ethyl for hypertriglyceridemia. *N. Engl. J. Med.* 380, 11–22. doi: 10.1056/NEJMoa1812792

Chen, C., Chen, X., Chen, J., Xing, J., Hei, Z., Zhang, Q., et al. (2022). Association between preoperative hs-crp/albumin ratio and postoperative sirs in elderly patients: A retrospective observational cohort study. *J. Nutr. Health Aging* 26, 352–359. doi: 10.1007/s12603-022-1761-4

Cui, Q., and Naikoo, N. A. (2019). Modifiable and non-modifiable risk factors in ischemic stroke: A meta-analysis. *Afr. Health Sci.* 19, 2121–2129. doi: 10.4314/ahs.v19i2.36

Dong, Y., Cao, W., Cheng, X., Fang, K., Zhang, X., Gu, Y., et al. (2017). Risk factors and stroke characteristic in patients with postoperative strokes. *J. Stroke Cerebrovasc. Dis.* 26, 1635–1640. doi: 10.1016/j.jstrokecerebrovasdis.2016.12.017

Ferrara, A. (2020). Computed tomography in stroke diagnosis, assessment, and treatment. *Radiol. Technol.* 91:447CT–462CT.

Glanz, J. M., Newcomer, S. R., Daley, M. F., DeStefano, F., Groom, H. C., Jackson, M. L., et al. (2018). Association between estimated cumulative vaccine antigen exposure through the first 23 months of life and non-vaccine-targeted infections from 24 through 47 months of age. *JAMA* 319, 906–913. doi: 10.1001/jama.2018.0708

Glasser, S. P., Mosher, A., Howard, G., and Banach, M. (2016). What is the association of lipid levels and incident stroke? *Int. J. Cardiol.* 220, 890–894. doi: 10.1016/j.ijcard.2016.06.091

Gu, X., Li, Y., Chen, S., Yang, X., Liu, F., Li, Y., et al. (2019). Association of lipids with ischemic and hemorrhagic stroke: A prospective cohort study among 267 500 Chinese. *Stroke* 50, 3376–3384. doi: 10.1161/STROKEAHA.119.026402

Holmes, M. V. I., Millwood, Y., Kartsonaki, C., Hill, M. R., Bennett, D. A., Boxall, R., et al. (2018). Lipids, lipoproteins, and metabolites and risk of myocardial infarction and stroke. *J. Am. Coll. Cardiol.* 71, 620–632. doi: 10.1016/j.jacc.2017.12.006

Johnson, A. A., and Stolzing, A. (2019). The role of lipid metabolism in aging, lifespan regulation, and age-related disease. *Aging Cell* 18:e13048. doi: 10.1111/acel.13048

Kernan, W. N., Ovbiagele, B., Black, H. R., Bravata, D. M., Chimowitz, M. I., Ezekowitz, M. D., et al. (2014). Guidelines for the prevention of stroke in patients with stroke and transient ischemic attack: A guideline for healthcare professionals from the american heart association/american stroke association. *Stroke* 45, 2160–2236. doi: 10.1161/STR.0000000000000024

Kivioja, R., Pietila, A., Martinez-Majander, N., Gordin, D., Havulinna, A. S., Salomaa, V., et al. (2018). Risk factors for early-onset ischemic stroke: A case-control study. *J. Am. Heart Assoc.* 7:e009774. doi: 10.1161/JAHA.118.009774

Kwon, S., Kim, T. J., Choi, E. K., Ahn, H. J., Lee, E., Lee, S. R., et al. (2021). Predictors of ischemic stroke for low-risk patients with atrial fibrillation: A matched case-control study. *Heart Rhythm* 18, 702–708. doi: 10.1016/j.hrthm.2021.01.016

Leary, M. C., and Varade, P. (2020). Perioperative stroke. *Curr. Neurol. Neurosci. Rep.* 20:12. doi: 10.1007/s11910-020-01033-7

Liang, H. J., Zhang, Q. Y., Hu, Y. T., Liu, G. Q., and Qi, R. (2022). Hypertriglyceridemia: A neglected risk factor for ischemic stroke? *J. Stroke* 24, 21–40. doi: 10.5853/jos.2021.02831

Lindberg, A. P., and Flexman, A. M. (2021). Perioperative stroke after non-cardiac, non-neurological surgery. *BJA Educ.* 21, 59–65. doi: 10.1016/j.bjae.2020.09.003

Mashour, G., Moore, L., Lele, A., Robicsek, S., and Gelb, A. (2014). Perioperative care of patients at high risk for stroke during or after non-cardiac, non-neurologic surgery: Consensus statement from the society for neuroscience in anesthesiology and critical care*. *J. Neurosurg. Anesthesiol.* 26, 273–285. doi: 10.1097/ana.0000000000000087

Mashour, G., Shanks, A., and Kheterpal, S. (2011). Perioperative stroke and associated mortality after noncardiac, nonneurologic surgery. *Anesthesiology* 114, 1289–1296. doi: 10.1097/ALN.0b013e318216e7f4

Minhas, J. S., Rook, W., Panerai, R. B., Hoiland, R. L., Ainslie, P. N., Thompson, J. P., et al. (2020). Pathophysiological and clinical considerations in the perioperative care of patients with a previous ischaemic stroke: A multidisciplinary narrative review. *Br. J. Anaesth.* 124, 183–196. doi: 10.1016/j.bja.2019.10.021

Mrkobrada, M., Chan, M. T. V., Cowan, D., Campbell, D., Wang, C. Y., Torres, D., et al. (2019). Perioperative covert stroke in patients undergoing non-cardiac surgery (NeuroVISION): A prospective cohort study. *Lancet* 394, 1022–1029. doi: 10.1016/s0140-6736(19)31795-7

Nichols, G. A., Philip, S., Reynolds, K., Granowitz, C. B., and Fazio, S. (2018). Increased cardiovascular risk in hypertriglyceridemic patients with statin-controlled LDL cholesterol. *J. Clin. Endocrinol. Metab.* 103, 3019–3027. doi: 10.1210/jc.2018-00470

Peduzzi, P., Concato, J., Kemper, E., Holford, T. R., and Feinstein, A. R. (1996). A simulation study of the number of events per variable in logistic regression analysis. *J. Clin. Epidemiol.* 49, 1373–1379. doi: 10.1016/s0895-4356(96)00236-3

Peng, J., Luo, F., Ruan, G., Peng, R., and Li, X. (2017). Hypertriglyceridemia and atherosclerosis. *Lipids Health Dis.* 16:233. doi: 10.1186/s12944-017-0625-0

Sacco, R. L., Diener, H. C., Yusuf, S., Cotton, D., Ounpuu, S., Lawton, W. A., et al. (2008). Aspirin and extended-release dipyridamole versus clopidogrel for recurrent stroke. *N. Engl. J. Med.* 359, 1238–1251. doi: 10.1056/NEJMoa0805002

Sun, L., Clarke, R., Bennett, D., Guo, Y., Walters, R. G., Hill, M., et al. (2019). Causal associations of blood lipids with risk of ischemic stroke and intracerebral hemorrhage in Chinese adults. *Nat. Med.* 25, 569–574. doi: 10.1038/s41591-019-0366-x

Toth, P., Granowitz, C., Hull, M., Liassou, D., Anderson, A., and Philip, S. (2018). High triglycerides are associated with increased cardiovascular events, medical costs, and resource use: A real-world administrative claims analysis of statin-treated patients with high residual cardiovascular risk. *J. Am. Heart Assoc.* 7:e008740. doi: 10.1161/jaha.118.008740

van Lier, F., Schouten, O., van Domburg, R. T., van der Geest, P. J., Boersma, E., Fleisher, L. A., et al. (2009). Effect of chronic beta-blocker use on stroke after noncardiac surgery. *Am. J. Cardiol.* 104, 429–433. doi: 10.1016/j.amjcard.2009.03.062

Vittinghoff, E., and McCulloch, C. E. (2007). Relaxing the rule of ten events per variable in logistic and cox regression. *Am. J. Epidemiol.* 165, 710–718. doi: 10.1093/aje/kwk052

Vlisides, P., and Mashour, G. A. (2016). Perioperative stroke. *Can. J. Anaesth.* 63, 193–204. doi: 10.1007/s12630-015-0494-9

Wang, A., Li, H., Yuan, J., Zuo, Y., Zhang, Y., Chen, S., et al. (2020). Visit-to-visit variability of lipids measurements and the risk of stroke and stroke types: A prospective cohort study. *J. Stroke* 22, 119–129. doi: 10.5853/jos.2019.02075

Wang, H., Li, S., Bai, J., and Wang, D. (2019). Perioperative acute ischemic stroke increases mortality after noncardiac, nonvascular, and non-neurologic surgery: A retrospective case series. *J. Cardiothorac. Vasc. Anesth.* 33, 2231–2236. doi: 10.1053/j.jvca.2019.02.009

Wang, W., Shen, C., Zhao, H., Tang, W., Yang, S., Li, J., et al. (2018). A prospective study of the hypertriglyceridemic waist phenotype and risk of incident ischemic stroke in a Chinese rural population. *Acta Neurol. Scand.* 138, 156–162. doi: 10.1111/ane.12925

Zhang, X. P., Gao, Y. Z., Chen, Z. H., Chen, M. S., Li, L. Q., Wen, T. F., et al. (2019). An eastern hepatobiliary surgery hospital/portal vein tumor thrombus scoring system as an aid to decision making on hepatectomy for hepatocellular carcinoma patients with portal vein tumor thrombus: A multicenter study. *Hepatology* 69, 2076–2090. doi: 10.1002/hep.30490

Zhao, B. C., Lei, S. H., Yang, X., Zhang, Y., Qiu, S. D., Liu, W. F., et al. (2021). Assessment of prognostic value of intraoperative oliguria for postoperative acute kidney injury: A retrospective cohort study. *Br. J. Anaesth.* 126, 799–807. doi: 10.1016/j.bja.2020.11.018

Zhou, F., Liu, C., Ye, L., Wang, Y., Shao, Y., Zhang, G., et al. (2021). The relative contribution of plasma homocysteine levels vs. traditional risk factors to the first stroke: A nested case-control study in rural China. *Front. Med.* 8:727418. doi: 10.3389/fmed.2021.727418

Frontiers in
Aging Neuroscience

Explores the mechanisms of central nervous system aging and age-related neural disease

The third most-cited journal in the field of geriatrics and gerontology, with a focus on understanding the mechanistic processes associated with central nervous system aging.

Discover the latest Research Topics

See more →

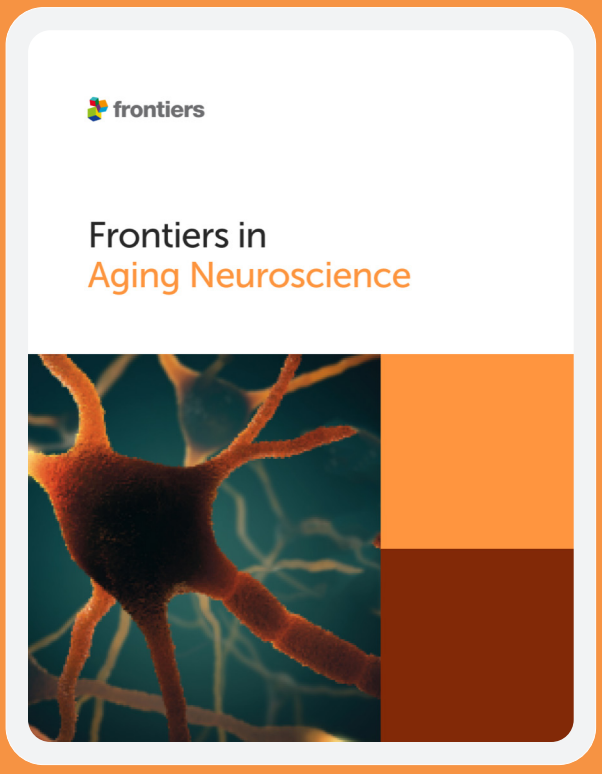

Frontiers

Avenue du Tribunal-Fédéral 34
1005 Lausanne, Switzerland
frontiersin.org

Contact us

+41 (0)21 510 17 00
frontiersin.org/about/contact